

Photoinduced Electron Transfer Reactions of Organic Anions

Dissertation

Zur Erlangung des Doktorgrades der Naturwissenschaften

(Dr. rer. nat.)

an der Fakultät für Chemie und Pharmazie

der Universität Regensburg



vorgelegt von

Matthias Schmalzbauer

aus Maxhütte-Haidhof

2020

The experimental work has been carried out between November 2016 and April 2020 under the supervision of Prof. Dr. Burkhard König at the University of Regensburg, Institute of Organic Chemistry.

Date of submission: 23.06.2020

Date of colloquium: 05.08.2020

Board of examiners:	Prof. Dr. Joachim Wegener	(chair)
	Prof. Dr. Burkhard König	(1 st referee)
	Prof. Dr. Oliver Reiser	(2 nd referee)
	Prof. Dr. Patrick Nürnberger	(examiner)

„Fantasie ist wichtiger als Wissen, denn Wissen ist begrenzt.“

Albert Einstein 1879-1955

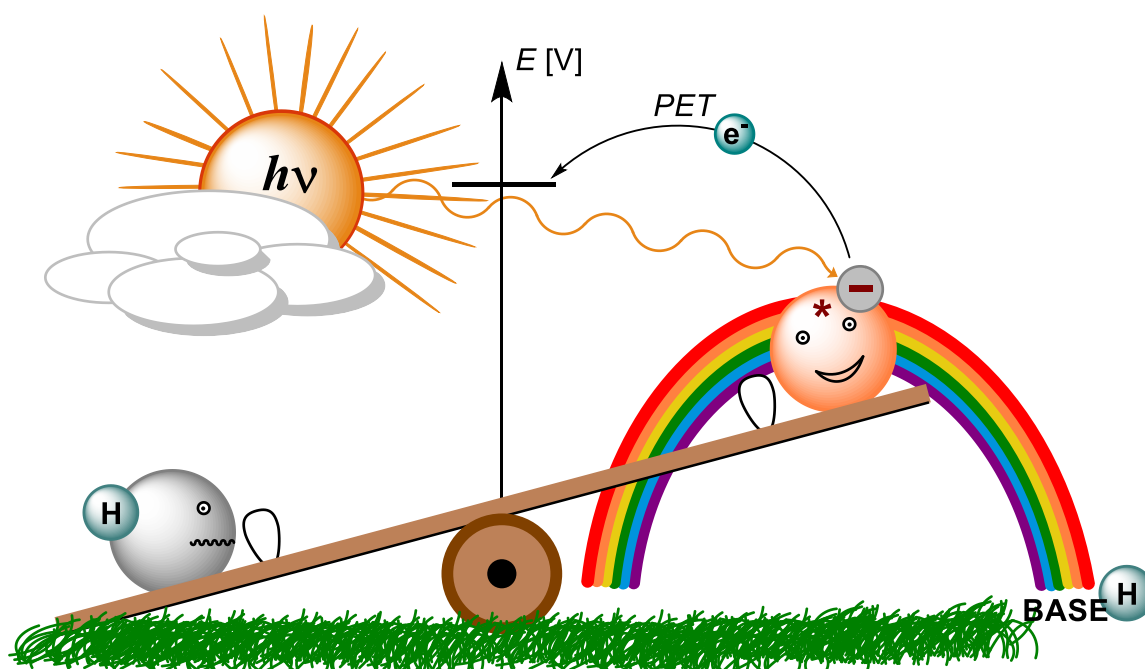
TABLE OF CONTENTS

1	EXCITED STATE ANIONS IN ORGANIC TRANSFORMATIONS	1
1.1	Introduction	3
1.2	Organic Anions as Photocatalysts	10
1.3	Organic Anions as Photochemical Reagents	24
1.4	Inorganic Anions	40
1.5	Summary and Outlook.....	43
1.6	References.....	44
2	ANTHRAQUINONES AS PHOTOREDOX CATALYSTS FOR THE REDUCTIVE ACTIVATION OF ARYL HALIDES	49
2.1	Introduction	51
2.2	Results and Discussion.....	53
2.3	Conclusion	59
2.4	Experimental Part.....	60
2.5	References.....	73
3	UTILIZING EXCITED STATE ORGANIC ANIONS FOR PHOTOREDOX CATALYSIS: ACTIVATION OF (HETERO)ARYL CHLORIDES BY VISIBLE LIGHT-ABSORBING 9-ANTHROLATE ANIONS	77
3.1	Introduction	79
3.2	Results and Discussion.....	81
3.3	Conclusion	94
3.4	Experimental Part.....	95
3.5	References.....	129

4	REDOX-NEUTRAL PHOTOCATALYTIC C–H CARBOXYLATION OF ARENES AND STYRENES WITH CO₂	133
4.1	Introduction.....	135
4.2	Results and Discussion	137
4.3	Conclusion	148
4.4	Experimental Part.....	149
4.5	References.....	208
5	SUMMARY	217
6	ZUSAMMENFASSUNG	223
7	APPENDIX	229
7.1	Abbreviations	229
7.2	NMR Spectra Chapter 2	232
7.3	Appendix Chapter 3	244
7.4	NMR Spectra Chapter 4	286
7.5	Curriculum Vitae	341
8	DANKSAGUNG	347

CHAPTER 1

1 Excited State Anions in Organic Transformations



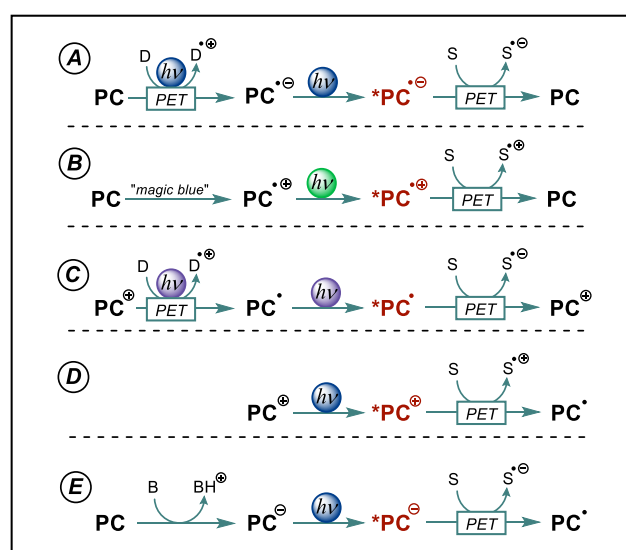
Matthias Schmalzbauer and Michela Marcon wrote the manuscript. Burkhard König supervised the project.

Abstract

Utilizing light is a smart way to fuel chemical transformations as it allows to selectively focus the energy on certain molecules. Many reactions involving electronically excited species proceed *via* open-shell intermediates enabling novel and unique routes to expand the hitherto used synthetic toolbox in organic chemistry. The direct conversion of non-prefunctionalized, less activated compounds is a highly desirable goal to pave the way towards a more sustainable and atom-economic chemistry. Photoexcited closed-shell anions have been shown to reach extreme potentials in single electron transfer reactions and reveal unusual excited state reactivity. It is therefore surprising, that their use as reagent or as photocatalyst is limited to a few examples. In this chapter, we briefly discuss the characteristics of anionic photochemistry, highlight pioneering work and show recent progress which has been made by utilizing photoexcited anionic species in organic synthesis.

1.1 Introduction

During the last decade, impressive progress has been made in the field of synthetic photoredox catalysis and many novel transformations, which were previously inaccessible, have been developed. Photoexciting a molecule changes the electron distribution in the molecular orbitals resulting in both, increased oxidizing- and reducing abilities of the excited species compared to the ground state. These excited state redox properties can be fine-tuned by attaching electron donating or withdrawing substituents.^[1–3] Up to now, a variety of photocatalysts have been reported which are often classified regarding their composition into polypyridyl transition metal complexes,^[4] organic dyes^[5] or polyoxometalates^[6] (POMs). In addition, heterogenous organic semiconductors were successfully employed as photocatalysts.^[7] Their intrinsic photophysical properties like excited state redox potential, absorption of light or the excited state lifetime define the scope and limitations of chemical reactions. Further expansion towards ever more challenging transformations required new concepts and catalytic approaches to provide the necessary activation energy.



Scheme 1-1. Photochemical approaches leading to excited reactive intermediates with extreme redox potentials (red) allowing to convert non-activated substrates (S).

Apart from commonly used neutral organic dyes, molecules with a charged or an open-shell ground state or both were found to significantly increase achievable excited state potentials and allowed to widen the substrate scope for photoinduced electron transfer (PET) reactions (Scheme 1-1). Several organic dyes form stable and colored radical anions *via* PET in presence

of a suitable sacrificial donor and hence, a subsequent second excitation of such species is possible (see Scheme 1-1, A).^[8–11] The photochemistry of excited radical anions allowed to convert (hetero)aryl halides in coupling reactions and has been subject of several reviews.^[12–15] In contrast, the formation of super-oxidants has been reported upon photoexcitation of stable phenothiazine radical cations (see Scheme 1-1, B).^[16] Furthermore, electron transfer from photoexcited doublet states of neutral radicals has been studied.^[17–21] Very recently, the acridine radical was found to act as an extremely potent photo-reductant upon excitation with blacklight (see Scheme 1-1, C).^[22] Although enabling high redox potentials, the photochemistry of excited open-shell species suffers from short lifetimes which are usually in the picosecond range.^[22–24]

Photoreactions using catalytic amounts of closed-shell cations were found to be synthetically very useful (Scheme 1-1, D). The pioneering work of Fukuzumi and co-workers^[25] paved the way for plenty of publications using the cationic donor-acceptor dyad 9-mesityl-10-methylacridinium perchlorate and further functionalized derivatives as strongly oxidizing photocatalysts.^[5,26–29] Moreover, a new benchmark regarding the excited state potential was set by using pyrylium-, quinolinium- or diazapyrenium salts as extremely powerful photooxidants.^[5] Surprisingly, in contrast to the wealth of reports dealing with photoexcited cations, the photochemistry of closed-shell anions received far less attention although it constitutes the logically equivalent (Scheme 1-1, E). In this chapter, we briefly summarize key spectroscopic and electrochemical properties of organic anions and provide an overview of the versatile photochemistry of anionic species with a special focus on recent advances of organic anions used as photocatalysts or as reagents.

1.1.1 Spectroscopic Properties of Organic Anions

The chemistry of molecules excited by light is initiated by the absorption of a photon and thus, we will start with discussing the peculiarities of the absorption spectra for closed-shell anions. Compared to their neutral precursors, organic anions usually experience a significant bathochromic shift in their absorption spectra and pronounced absorption bands can be attributed to π, π^* transitions. The narrowed gap between HOMO and LUMO causing the red-shift can be primarily explained by the increased shielding of the core due to an imbalance of charges. The strength of the electric field is reduced and electrons in the HOMO sense much weaker attracting forces. As a result, the spatial distribution of electrons becomes more diffuse

as if the conjugation length is extended.^[30,31] The absorption of organic anions is also affected by size and nature of the counteranion, solvent polarity and ion pairing effects in solution. In non-polar or weakly polar solvents, contact ion pairs are formed and the properties of the anionic species are strongly influenced by the character of the counteranion. In contrast, the increased solubility of ions in polar solvents induced by aligning molecular dipoles causes solvent-separated or free ion pairs and the mutual ionic interaction is diminished. In general, an increase in solvent polarity and/or ionic radius of the counteranion results in a bathochromic shift of the absorption, which can be attributed to a destabilization of the ground state ion pair. This destabilization effect is less pronounced in the excited state.^[30,32] (Figure 1-1).

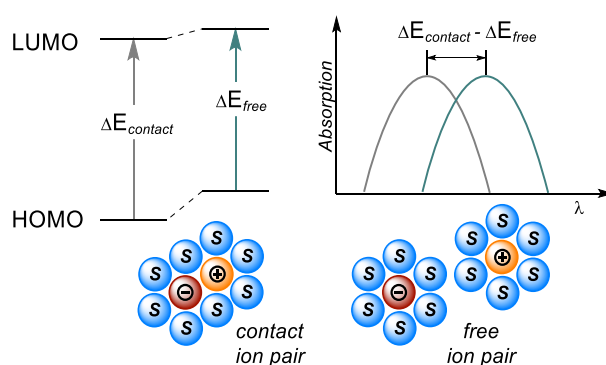
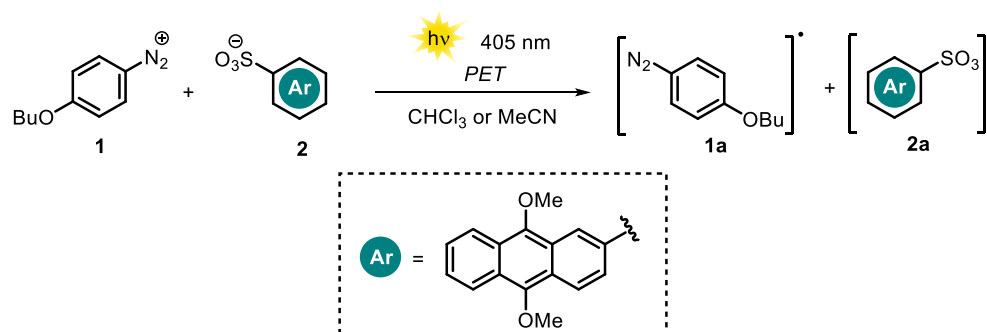


Figure 1-1. Energetic destabilization of the ground state of a free ion pair in polar solvent compared to the contact ion pair in non-polar solvent and influence on the absorption spectrum.

Similarly, the emission of excited organic anions is usually influenced by solvent polarity and counteranion. The fluorescence decay of sodium β -naphtholate was studied in different solvents.^[33] For polar protic and polar aprotic solvents, a mono-exponential fluorescence decay was observed. However, in polar protic MeOH the fluorescence lifetime was remarkably decreased and the emission spectrum was blue-shifted compared to polar protic DMF or DMSO, which the authors attribute to a stabilization of the anion ground state caused by strong solvent hydrogen bonding. In weakly polar THF contact ion pairs and solvent separated ion pairs of β -naphtholate and Na^+ coexist and cause a bi-exponential fluorescence decay due to varying fluorescence lifetimes. Upon addition of crown-ether to the system, a mono-exponential decay was recorded suggesting that sodium cations are complexed and the ion pairs formed with naphtholate are rather solvent separated. Owing to the lack of ground state

stabilization in solvent separated or free ion pairs, lifetimes similar to experiments in polar aprotic solvents were found in presence of crown-ether.



Scheme 1-2. The rate of photoinduced electron transfer is influenced by the solvent polarity: fast in CHCl_3 (tight pair), slow in MeCN (loose pair)

The nature of ion pairing might also affect the efficiency of bimolecular electron transfer processes. Tamaoki and co-workers studied the quantum yield for the photodissociation of a benzene diazonium salt **1** with 1,8-dimethoxyanthracene-3-sulfonate (**2**) being the visible-light absorbing counteranion (Scheme 1-2).^[34] The photodecomposition of the benzene diazonium cation **1** initiated by PET from the excited anion was found to be six-times higher in CHCl_3 compared to MeCN. The difference in reactivity of the diazonium salt between the solvents was explained by the different nature of ion pairs formed. The weakly polar solvent CHCl_3 promotes a fast reaction due to the close proximity of **1** and **2** in a tight ion pair. Solvent separated loose ion pairs in polar MeCN allowed to measure a distinct fluorescence lifetime. Upon excitation the anionic donor needs to encounter a cationic acceptor in polar media to trigger the photodecomposition and hence increased lifetimes are recorded. For a more comprehensive discussion of ion-pairing and solvent effects, we refer to several excellent reports.^[32,33,35–37]

1.1.2 Photoinduced Electron Transfer

Electron transfer reactions from electronically excited states of molecules are among the earliest photochemical reactions reported.^[38] Photoexcited molecules exhibit increased reduction and oxidation potentials compared to their ground state and the resulting excited state potentials can be estimated according to the free enthalpy change of a PET by measuring

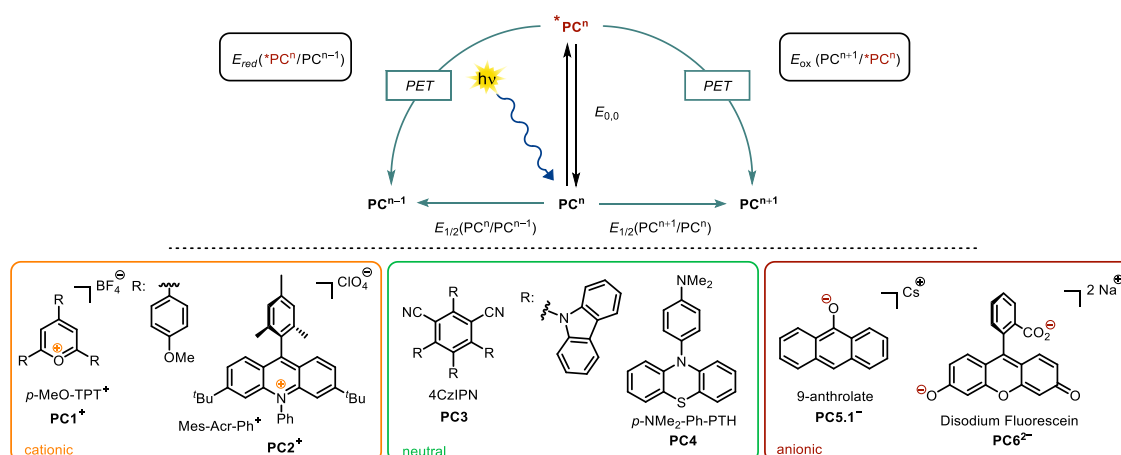


Figure 1-2. Diagram of ground and excited state potentials of a photocatalyst (top); representatives of cationic, neutral and anionic organic photocatalyst (bottom).

the ground state potentials $E_{1/2}$ and the transition energy $E_{0,0}$ (Figure 1-2).^[39] For polar organic solvents, the electrostatic work term contributes only little to the free enthalpy change and is frequently omitted.^[5]

Table 1-1. Ground state and excited state redox potentials of cationic, neutral and anionic photocatalysts represented in Figure 1-2 and the corresponding transition energy.

Entry	PC^n	$E_{1/2}(PC^n/PC^{n-1})$	$E_{red}(^*PC^n/PC^{n-1})$	$E_{1/2}(PC^{n+1}/PC^n)$	$E_{ox}(PC^{n+1}/^*PC^n)$	$E_{0,0}$ [eV]
1 ^[5]	$PC1^+$	- 0.50 ^a	+ 1.84	-	-	2.34 ^b
2 ^[3]	$PC2^+$	- 0.59 ^c	+ 2.08	-	-	2.67
3 ^[1]	$PC3$	- 1.24 ^d	+ 1.43	+ 1.49 ^d	- 1.18	2.67
4 ^[2]	$PC4$	-	-	+ 0.57 ^d	- 2.5	3.1
5 ^[53]	$PC5.1^-$	-	-	- 0.34 ^{d,e}	- 2.65	2.31
6 ^[54]	$PC6^{2-}$	-	-	+ 0.87 ^f	- 1.55	2.42

Potentials are reported *vs.* SCE. Transition energy $E_{0,0}$ was determined from the intersection of normalized absorption and emission spectra ^a Potential recorded *vs.* NHE and converted to SCE by subtracting 0.141 V; ^b Determined from the highest energy emission maximum; ^c Potential recorded *vs.* Ag/AgCl and converted to SCE by subtracting 0.03 V; ^d Potential recorded *vs.* Fc^+/Fc and converted to SCE by adding 0.38 V; ^e Potential was measured in dry degassed DMSO with excess of CS_2CO_3 ; ^f Potential was measured in MeOH containing NaOH (0.1 mM) against Ag/AgCl and referenced to SCE by conversion.

Literally, the last decade has been a very exciting time in terms of photochemistry and many novel chemical transformations have been developed which complement the available synthetic toolbox. Depending on the type of photocatalyst used (ionic or neutral), specific reactions can be triggered. Among other cationic dyes, the photoexcited pyrylium- or

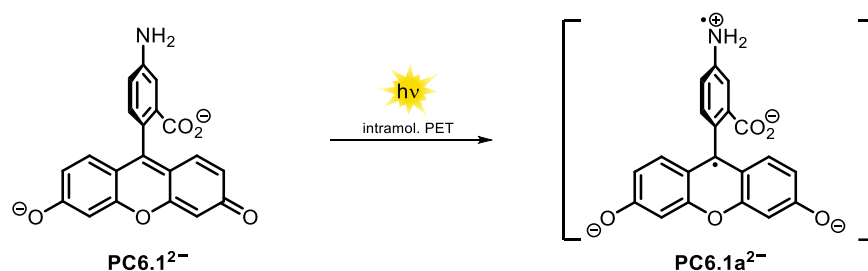
acridinium salts (*e.g.* **PC1**⁺ and **PC2**⁺, Figure 1-2) are strong oxidants in their excited states and found widespread synthetic applications.^[5,40–47] In contrast, the photochemistry of the non-charged donor-acceptor dyad **PC3** covers a broad electrochemical range. Bearing a versatile excited-state reduction and oxidation potential, it is often used to replace precious and toxic Ru- or Ir-polypyridyl complexes.^[1,48] However, to convert less activated substrates *via* reduction, the frontiers need to be pushed towards more negative potentials. Recently, it was shown that photoexcited, electron-rich N-arylphenothiazines (*e.g.* **PC4**) act as very strong reductants. However, as these compounds do not absorb in the visible range, UV light is necessary for excitation. A large Stokes shift was found and results in a high transition energy (*cf.*, Table 1-1, Entry 4).^[2] PET from a neutral excited donor (^{*}D) to a neutral ground state acceptor (A) causes a charge separation resulting in a pair of radical ions. In contrast, the PET from an anionic donor to a neutral acceptor can be considered as a charge shift generating products that are free of electrostatic attraction and expected to diffuse freely (Scheme 1-3). Hence, the lost channel of a back-electron transfer (BET) which would regenerate the initial non-excited status quo is less competitive in a charge-shift process.^[49]



Scheme 1-3. Charge separation with neutral donor (left) and charge shift with anionic donor (right).

An anionic molecule is considered as a superior electron donor compared to its neutral parent. Both repulsion between electrons and the shielding from the nucleus are increased. As a consequence, the excess negative charge facilitates the removal of an electron. Experimentally, this becomes apparent when solvated electrons are expelled from organic anions in a biphotonic process using energy-rich UV light^[50] in glassy matrices (77 K) or pulsed high-energy lasers^[51,52] in alkaline aqueous solution. Working with visible-light LEDs and in common organic solvents however, renders the photo-ejection of an electron unlikely to occur and hence under these conditions electron transfer reactions are promoted. We recently demonstrated, that 9-anthrone and its derivatives are easily deprotonated in presence of carbonate base to form colored anions (*e.g.* **PC5.1**⁻, Figure 1-2) which upon visible-light excitation turn into remarkably strong reductants.^[53] Cyclic voltammetry measurements in alkaline DMSO revealed, that the anionic ground state is already a good reductant as the excess charge is removed easily due to resonance stabilization of the resulting radical. In sharp contrast, the dianion of fluorescein **PC6**²⁻ shows a significantly decreased tendency towards

electrochemical oxidation in alkaline MeOH and hence, the resulting excited state oxidation potential is only moderate (*cf.*, Table 1-1, Entry 5-6).^[54] Furthermore, it was reported that fluorescein-type dianions are reduced upon photoexcitation in presence of triethanolamine or even phenol to form semi-reduced radical dianions.^[55–57] Walt and co-workers attached an amino group on the benzoate scaffold of the fluorescein and found that the fluorescence quantum yield of **PC6.1²⁻** dropped by almost a factor of 60. They explained this observation by an intramolecular PET from the nitrogen lone pair to the fluorescein scaffold (Scheme 1-4).



Scheme 1-4. Intramolecular PET from the amino group causing self-quenching of the fluorescence.

A similar fluorescence quantum yield with respect to unsubstituted fluorescein (**PC6²⁻**) was however recorded, after adjusting the pH of the solution to a value around the pK_a of the aromatic amine. Upon protonation of the amine, the nitrogen lone pair is no longer available for intramolecular PET resulting in increased fluorescence.^[58] In 1991, Soumilion *et al.* showed that the fluorescence of the excited anion of the xanthene dye resorufin is quenched in presence of 2-naphtholate and the formation of a radical dianion of resorufin was proposed.^[49] The moderate reducing abilities of negatively charged xanthenes (*e.g.* **PC6²⁻**) can be explained by an overwhelming contribution of the electron-deficient conjugated system to the overall electronic properties. Thus, to obtain strongly reducing excited anions, a facile single electron oxidation is crucial (*cf.*, Table 1-1, Entry 5-6 show similar values for $E_{0,0}$ but differ significantly in their ground state and excited state oxidation potentials).

Excited anionic species are also utilized in key photochemical steps in biology. For instance, in an ATP-driven process the excited oxyluciferin anion causes the bioluminescence of fireflies.^[59] Moreover, phototrophic organisms show locomotory movement upon stimulus of light. The Photoactive Yellow Protein (PYP) encloses the anionic *trans-para*-coumaric acid as blue-light photoreceptor. Subsequent *trans-cis* isomerization of the excited chromophore induces a conformational change of the protein leading to a biological signal transduction.^[60] The enzyme-mediated repair of photodamaged DNA is another well-known example dealing

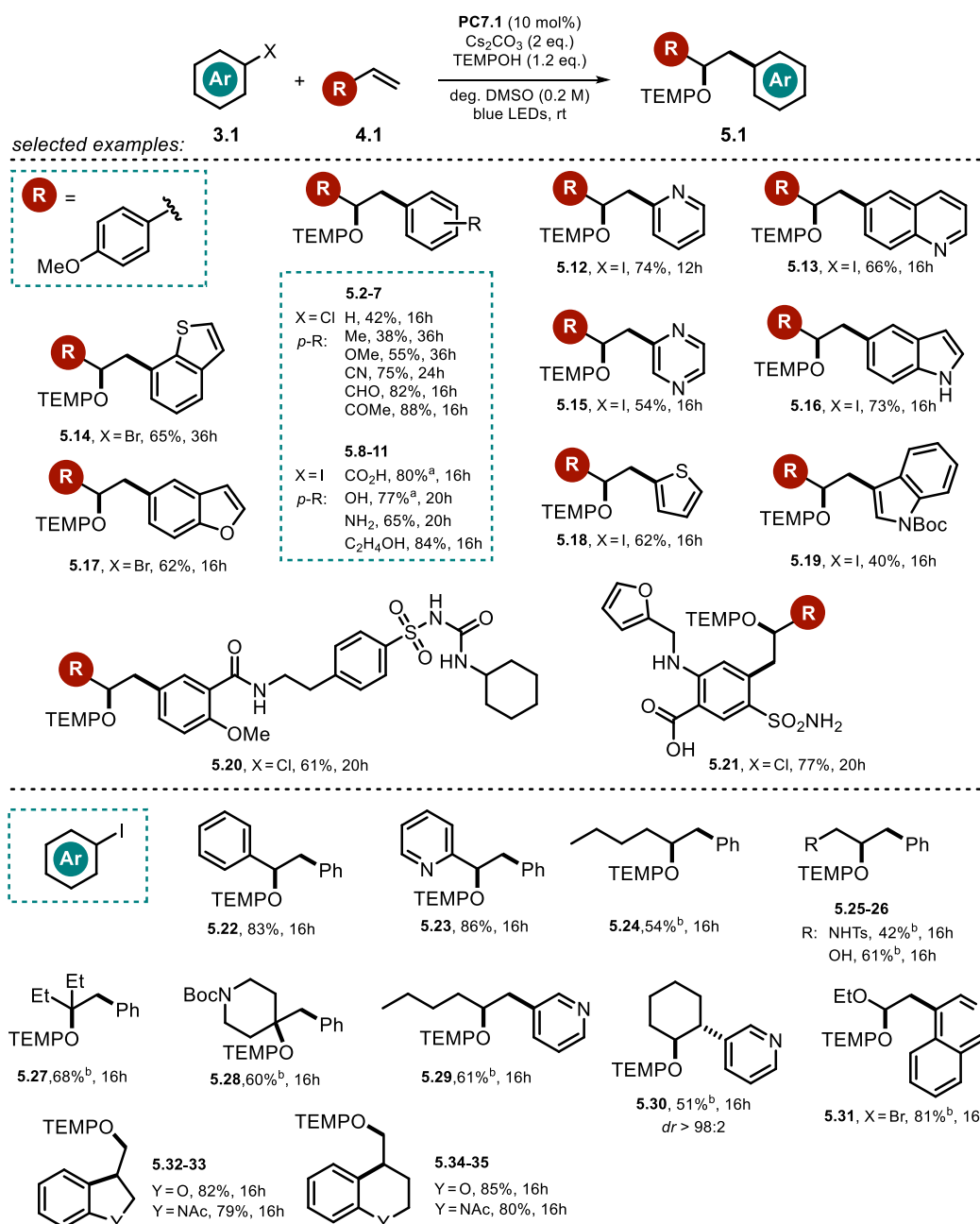
with excited anions in living cells. A crucial step is the photoinduced electron transfer from the excited cofactor flavin adenine dinucleotide (FADH⁻) which provides an electron for the light-driven repair catalyzed by photolyases.^[61,62] We are sure that, inspired by nature and the herein presented examples, the photochemistry of closed-shell anions will be further developed towards the generation of ever stronger light-activated reductants. The herein discussed reactions are divided by the role of the excited anion in the reaction mechanism: as catalyst for a certain conversion on the one side and as light-activated substrate or reagent on the other. In addition, a short overview is provided dealing with photoexcited anionic metal complexes and other light-activated inorganic anions.

1.2 Organic Anions as Photocatalysts

1.2.1 Phenolate Catalyzed Oxyarylation of Olefins with Aryl Halides

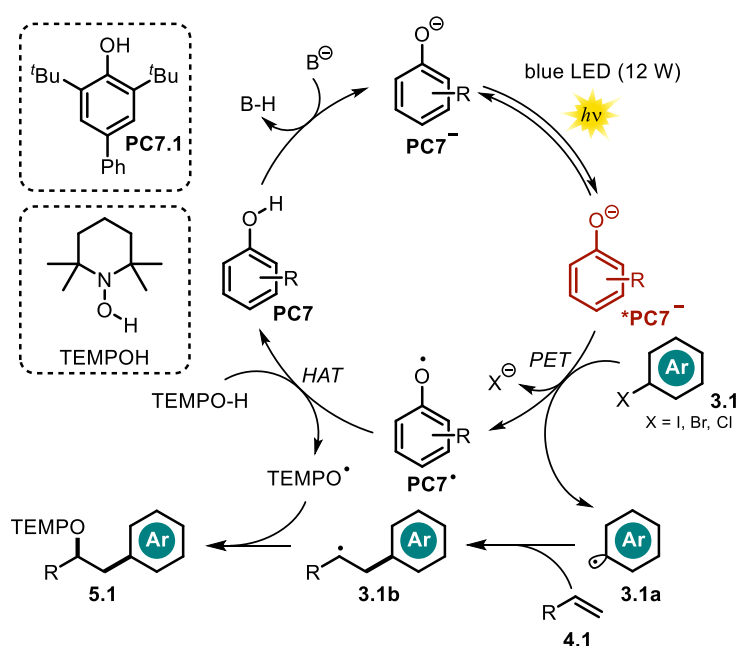
The low pK_a value of phenols, caused by the charge stabilizing effect of the benzene ring, allows facile deprotonation in presence of base to afford the phenolate, which is able to undergo photochemical reactions under visible light irradiation. Xia and co-workers examined several 4-phenylphenol derivatives as potential photocatalysts for the visible-light oxyarylation of olefins upon photoreduction of aryl halides (Scheme 1-5).^[63] 4-Phenylphenol **PC7.1** bearing bulky tert-butyl groups adjacent to the phenolic alcohol (see Scheme 1-6) showed the highest catalytic efficiency and the corresponding oxyarylated product **5.2** formed with iodobenzene, 4-methoxystyrene and TEMPOH could be isolated in good yield. Remarkably, the estimated excited state oxidation potential of **PC7.1**^{-*} ($E_{ox}^* = -3.16$ V *vs.* SCE) also allowed to convert more inert and electron rich aryl bromides and chlorides in presence of 4-methoxystyrene. Following the developed procedure, the authors present a broad scope of tolerated (hetero)aryl bromides and iodides including polyaromatic hydrocarbons, pyridines, indoles, quinolines, thiophen, thianaphthene and benzofuran. The reaction scope of tolerated olefins comprises various styrenes, aliphatic olefins, allylic sulfonamide and alcohol derivatives, enol ethers as well as 1,1- and 1,2- disubstituted olefins. In addition, the method allowed for intramolecular cyclization reactions using aryl iodides and for the late-stage modification of pharmaceuticals. Noteworthy, the use of TEMPOH as H-atom donor and radical trap seems to be crucial due to the weak nature of the O–H bond and the high stability of the aminoxyl radical formed.

The proposed reaction mechanism involves the deprotonation of the phenol **PC7** by base and a PET from the photoexcited **PC7**^{*} to the aryl halide **3.1**. Upon cleavage of the halide anion, the resulting aryl radical is trapped by the olefin **4.1** causing a carbon centered radical **3.1b**. Hydrogen atom transfer between the oxidized species of the catalyst and TEMPOH recovers



Scheme 1-5. Scope of the oxyarylation reaction of olefins with aryl halides and TEMPOH. ^a With 3 equiv. of Cs₂CO₃; ^b With 3 equiv. of olefin.

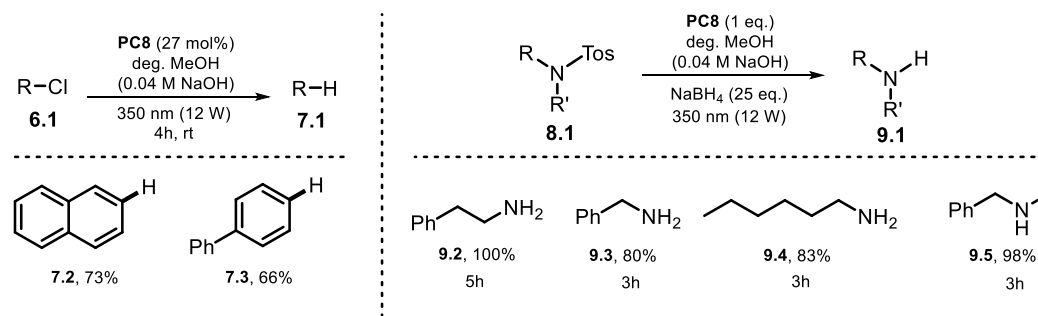
PC7 and forms the stable radical **TEMPO[•]**. The oxyarylation product **5.1** is formed upon radical-radical coupling (Scheme 1-6). The formation of a ground-state electron donor acceptor complex (EDA) between phenolate anion and aryl halide was excluded by UV-vis experiments. Fluorescence quenching experiments and isolated TEMPO trapping-adducts of the aryl radical intermediate support the mechanistic hypothesis. Moreover, a radical clock experiment suggests the formation of a benzylic radical whereas intramolecular trapping experiments disprove the involvement of a benzylic carbocation formed upon oxidation of the radical.



Scheme 1-6. Proposed mechanism for the phenolate catalyzed oxyarylation of olefins *via* the generation of aryl radicals.

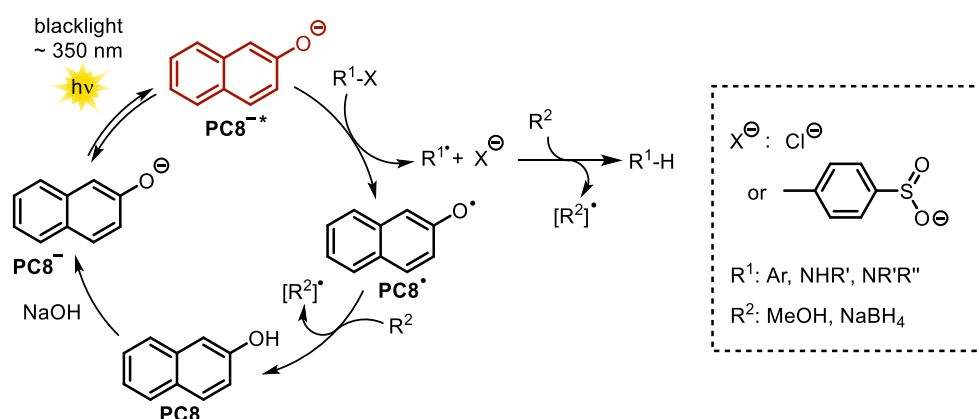
1.2.2 Naphtholate Catalyzed Dehalogenation and Detosylation

The first studies of the photochemical behavior of 2-naphtholate anion **PC8⁻** date back to 1989, when the counteranion, temperature and solvent were systematically evaluated regarding effects on the luminescence lifetime and the absorption and emission maxima.^[64] In the same year Soumilion and co-workers demonstrated the application of the naphtholate anion in the photocatalyzed defunctionalization of 2-chloronaphthalene and 4-chlorobiphenyl (**6.2-3**) in



Scheme 1-7. Scope of the dechlorination (left) and the desulfonylation reactions (right).

degassed, alkaline MeOH (Scheme 1-7).^[65] This concept was further extended in a heterogeneous approach where 2-hydroxynaphthoic acid was covalently anchored to a silica surface *via* amidation reaction. The efficiency in dechlorination reactions however was significantly decreased.^[66] The substrate scope was later on broadened to mono- and dichloronitrobenzenes.^[67] In addition, naphtholate was shown to catalyze the detosylation of sulfonamides in presence of excess $NaBH_4$ as terminal reductant (Scheme 1-7).^[68] Following this procedure, 2-phenylethylamine (**9.2**) and *N*-methylbenzylamine (**9.5**) were obtained in quantitative yield starting from the respective sulfonamides. Although a stoichiometric amount of 2-naphthol (**PC8**) was utilized, the catalyst is efficiently regenerated.

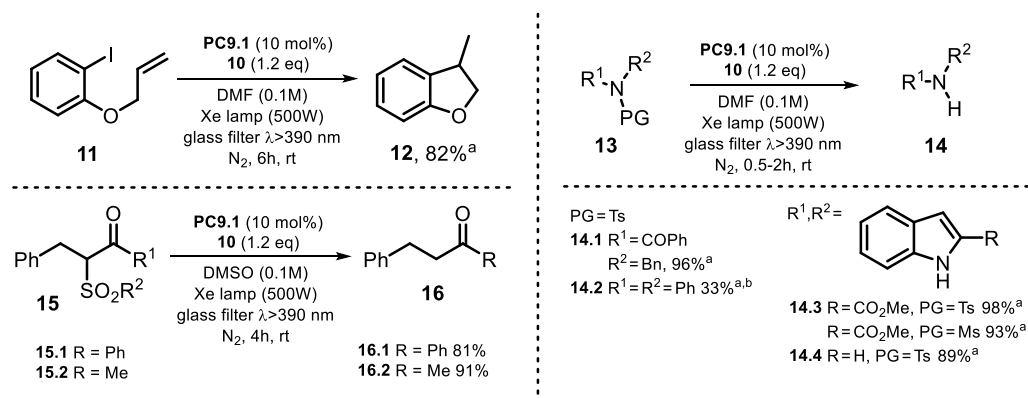


Scheme 1-8. Proposed photocatalytic cycle for the naphtholate anion.

The proposed reaction mechanism suggests the deprotonation of **PC8** to form the naphtholate **PC8⁻**. Upon excitation with blacklight the photoexcited state of **PC8^{-*}** is oxidatively quenched by either aryl chloride or sulfonamide which causes the formation of **PC8[•]** and an arene radical anion. After cleavage of the respective anionic leaving group (Cl^- or $4-Me(C_6H_4)SO_2^-$) an aryl- or nitrogen centered radical is formed respectively. Abstraction of a hydrogen atom from the solvent affords the defunctionalized arene. The *N*-centered radical converts to the amine *via*

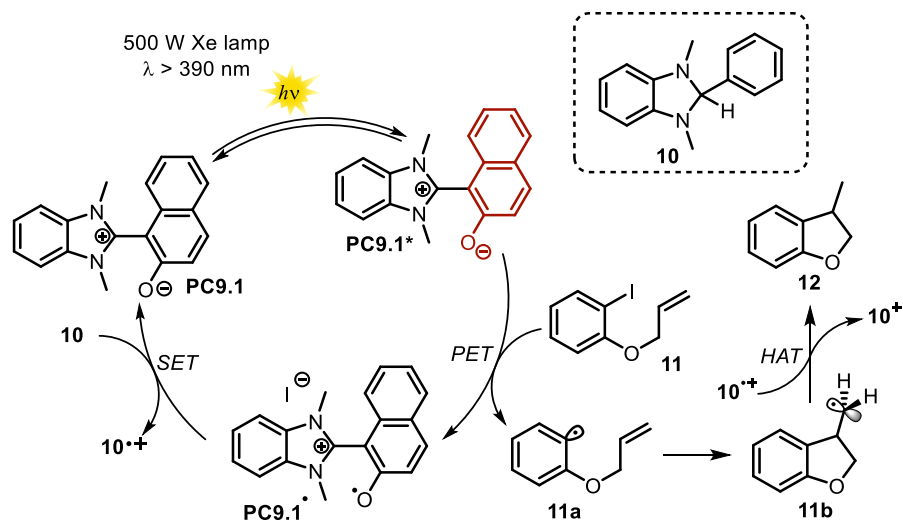
H-atom abstraction from either the solvent or NaBH₄. To close the catalytic cycle, **PC8*** is transformed to **PC8** *via* hydrogen atom abstraction from the solvent or NaBH₄ followed by subsequent deprotonation (Scheme 1-8).

Recently, a zwitterionic visible-light-absorbing benzimidazolium naphtholate **PC9.1** was successfully employed in photocatalytic deiodination and desulfonylation reactions in presence of a combined electron and hydrogen atom donor **10**.^[69] The cationic benzimidazolium moiety can be considered as separated from the naphtholate, due to the tilted structure that prevents π -conjugation. The photocatalytic activity was studied using different solvents with attributed Lewis-basic or Lewis-acidic character estimated by donor and acceptor numbers. The authors concluded that Lewis-basic solvents cause tight interaction with the Lewis-acidic benzimidazolium moiety whereas the electronic properties of Lewis-basic naphtholate anion are less governed, resulting in an increased electron donating ability. The best results (see Scheme 1-9) were found using DMF as solvent. Utilizing 10 mol% of catalyst **PC9.1** and 1.2 eq. of **10** enabled the formation of cyclized **12** in 82% yield. A lower catalyst loading of only 1 mol% resulted in full conversion of the iodoarene **11** however, the product yield was lowered (69%). In addition to the cyclization of iodoarene, the photocatalytic reactivity was demonstrated based on reductive desulfonylation of tertiary sulfonamides **13** and β -ketosulfones **15**. The respective secondary amines and desulfonylated ketones were obtained in good yields.



Scheme 1-9. Cyclization of iodoarene and scope of desulfonylation. ^a NMR yields; ^b DMSO, 6 h.

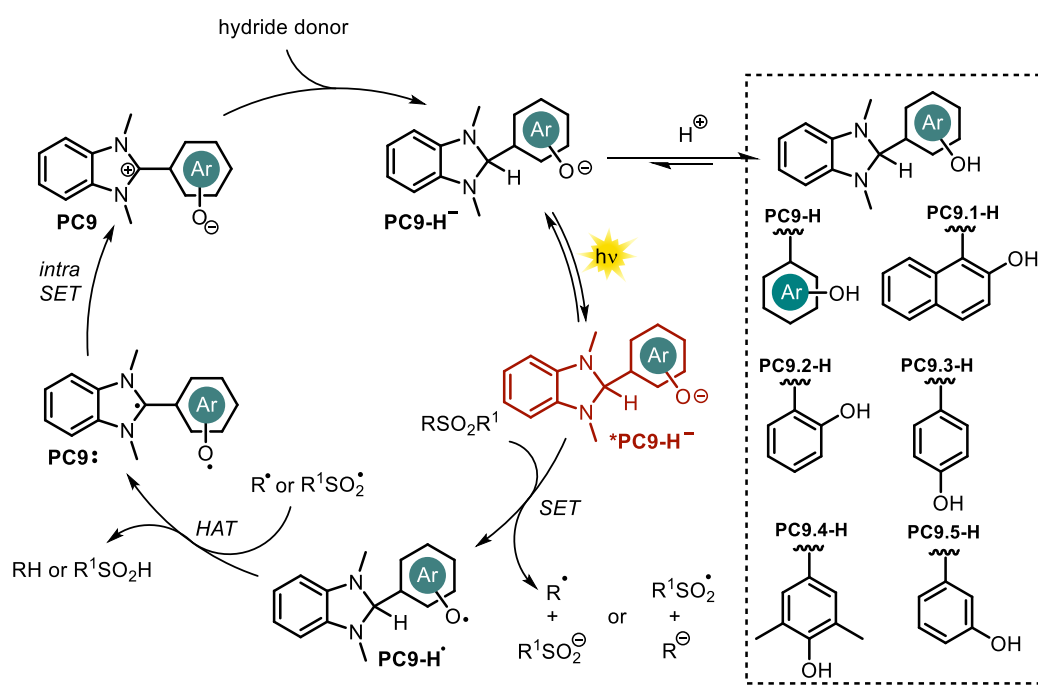
The proposed photocatalytic cycle is depicted in Scheme 1-10. Upon photoexcitation ($\lambda > 390$ nm), the zwitterionic excited state catalyst **PC9.1*** ($E_{ox}^* = -2.08$ v. SCE) reduces **11**



Scheme 1-10. Proposed catalytic cycle for the radical cyclization of iodoarene in presence of photoexcited benzimidazolium naphtholate.

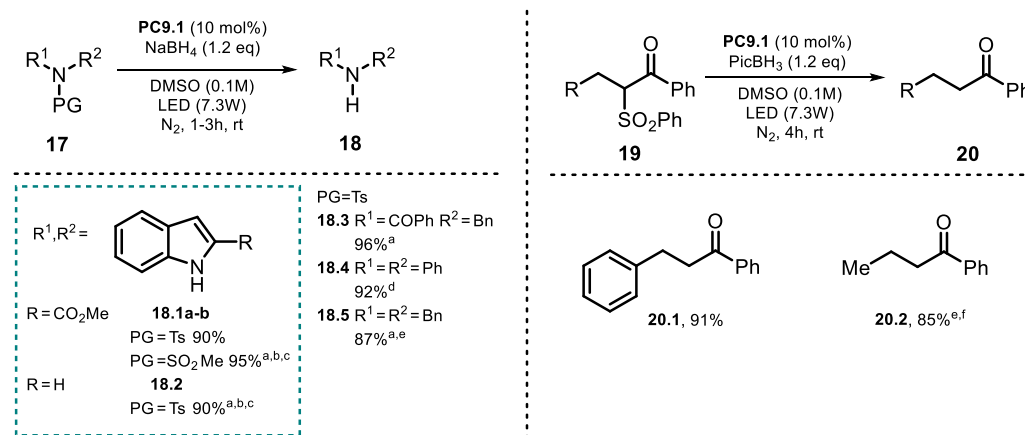
via PET. Subsequent cleavage of iodide followed by fast 5-exo-trig cyclization affords the primary radical **11b**. The oxidized photocatalyst **PC9.1'** is regenerated in presence of a sacrificial reductant **10** ($E_{1/2} = +0.34$ V *vs.* SCE) *via* single electron transfer to give the radical cation **10•+** which acts as hydrogen atom donor to form **12** and in turn is converted to the cation **10+**. In presence of other terminal reductants *e.g.* Hantzsch ester ($E_{1/2} = +0.93$ V) no product was formed as the higher ground state oxidation potential renders an electron transfer towards **PC9.1'** endergonic.

In a previously published work, photoexcited 1,3-dimethyl-2-hydroxynaphthyl-benzimidazoline (**PC9.1'**) was found to convert *N*-sulfonamides and *N*-sulfonylamines into the respective desulfonylated products.^[70] Based on these results, Hasegawa *et al.* further developed the catalytic system depicted in Scheme 1-10 by utilizing the *in situ* reduction of betaine **PC9** in presence of readily available boron hydride donors to generate the anionic species **PC9-H⁻**.^[71]



Scheme 1-11. Proposed photocatalytic cycle for the desulfonation reported by Hasegawa *et al.*

In addition to the reported electron donor and hydrogen atom donor abilities of the benzimidazoline scaffold (*cf.*, Scheme 1-10, **10**),^[70] the resulting benzimidazoline aryloxides **PC9-H** are equipped with a photo-redox active unit, the aryloxide moiety. Reductant, H-atom donor and photocatalyst are thus combined in one molecule. Various benzimidazoline aryloxides **PC9.1-H** - **PC9.5-H** (Scheme 1-11) were synthesized and characterized regarding their spectroscopic and electronic properties.^[71] The calculated excited state oxidation potential for **PC9.1-H** ($E_{ox}^* = -2.71$ V *vs.* SCE) was found to be significantly enhanced compared to the zwitterionic species **PC9.1**, allowing the conversion of less activated substrates. The elaborated protocol was used for the reductive desulfonation of *N*-sulfonylindoles, -amides, -amines, and α -sulfonyl ketones, affording the unprotected secondary amines as well as the α -defunctionalized ketones in good to excellent yield (Scheme 1-12).

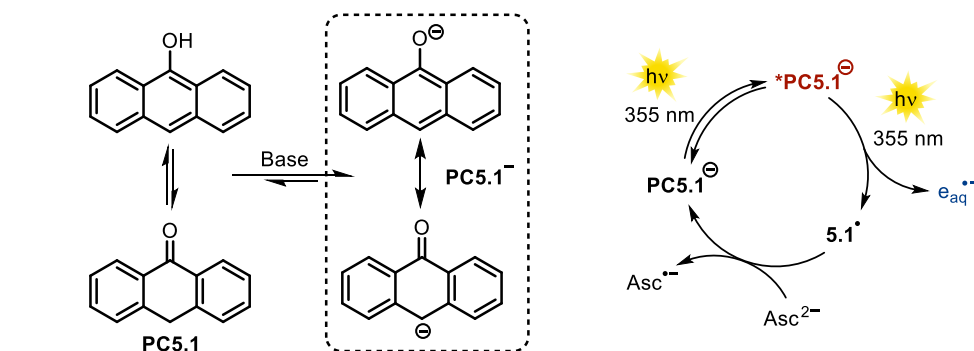


Scheme 1-12. Scope of the desulfonylation. ^a NMR yield; ^b DMF; ^c Xe lamp (500 W), glass filter >390 nm; ^d 24 h; ^e 2×LED (10.8 W), 48 h; ^f Cs₂CO₃ (1 eq.).

For the desulfonylation of α -carbonyls, a less reactive hydride donor PicBH₃ was used to avoid the direct reduction of the carbonyl group. Remarkably, utilizing the developed photocatalytic protocol allowed to convert diphenylsulfonamide (**17.5**) and dibenzylsulfonamide (**17.5**) almost quantitatively in 24 and 48 hours, respectively although both substrates exhibit a challenging reduction potential (> -2 V *vs.* SCE). All synthesized catalysts **PC9** were successfully tested in the desulfonylation of **17.3a** but the betaine **PC9.1** showed superior catalytic activity. Changing the light-source from a xenon lamp (500 W, $\lambda > 390$ nm) to a white LED (7.3 W) affords comparable product yields, but the reaction time increased. No product was formed in the absence of catalyst **PC9.1** and only traces were found in absence of hydride donor or light. Regarding the mechanism, the authors propose the *in-situ* formation of **PC9-H⁻** via nucleophilic attack of a hydride on the benzimidazolium moiety of **PC9**. Excitation with either Xe lamp or white LED renders the catalyst a strong photo-reductant and allows PET onto the substrate. The open-shell fragment formed upon N-S or C-S bond-rupture abstracts a hydrogen atom from the photocatalyst **PC9'** which is turned into a biradical **PC9:** and upon intramolecular single electron transfer the benzimidazolium **PC9** is regenerated. Eventually, a hydride transfer activates the catalyst for another catalytic cycle. The acidic hydroxy group on the aryl oxide is easily deprotonated and allows to employ directly the benzimidazoline **PC9-H** instead of the betaine **PC9** as catalyst. In that case, the addition of base (sodium carbonate or butoxide) increased the reaction efficiency significantly, indicating the facile deprotonation of **PC9-H**.

1.2.3 Anthrolate Catalyzed Generation of Hydrated Electrons

Goez and co-workers thoroughly investigated the potential use of anionic 9-anthrolate (**PC5.1**[−]) as a sustainable source for hydrated electrons which are ejected upon laser irradiation.^[51] Hydrated electrons are among the strongest reductants^[72–74] and are capable to directly reduce molecular nitrogen^[75] or carbon dioxide^[76]. Approaches to liberate solvated electrons photochemically often rely on high-energetic and harmful UV-C light. Notably, pulsed 355 nm UV-A laser irradiation of **PC5.1**[−] in alkaline aqueous media afforded hydrated electrons *via* a biphotonic photoionization pathway. The first photon generates the excited anionic species (S₁ state) and the absorption of another photon within the excited state lifetime of **PC5.1**[−]* stimulates photo-ejection of a hydrated electron. The catalytic cycle is closed in presence of the ascorbate dianion, which acts as sacrificial reductant recovering the catalyst from its oxidized species **PC5.1**[•] (Scheme 1-13). The sequence of photoionization and regeneration could be repeated several times until the system was exhausted. At the same time, the initial concentration of the catalyst could be regenerated, indicating the robustness of anthrolate **PC5.1**[−] against an attack of the exceptionally reducing solvated electron. Despite its minute molar absorption coefficient at the wavelength used for exciting the system, the ascorbate dianion was found to slightly contribute in generating hydrated electrons.



Scheme 1-13. The photocatalytic generation of hydrated electrons by Goez and co-workers.

A follow-up work of the Goez group^[52] focused on the direct photoionization of the ascorbate dianion in absence of catalyst by applying a 355 nm laser pulse. A possible application of solvated electrons generated in this way was demonstrated based on the efficient dechlorination of chloroacetate as a generic pollutant in waste water detoxification.

1.2.4 Activation of Aryl Chlorides with 9-Anthrolate

Recently, the photochemical properties and synthetic applications of a series of 9-anthrone derivatives were studied in our group and the corresponding anions were found to reach remarkable excited-state oxidation potentials.^[53] In solution, anthrone **PC5.1** is in equilibrium with its enolic form and is easily deprotonated to give the visible light-absorbing anthrolate **PC5.1⁻**. The most efficient catalysts examined in that work are depicted in Figure 1-3. These photocatalysts were proved successful in catalyzing the C–H arylation reaction of several (hetero)aryl chlorides with electron-rich (hetero)arenes, isocyanides, phosphite and B₂pin₂ (Scheme 1-14).

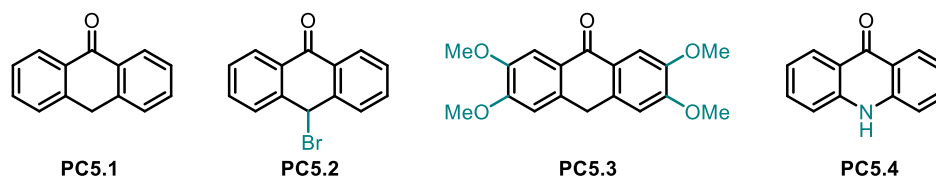
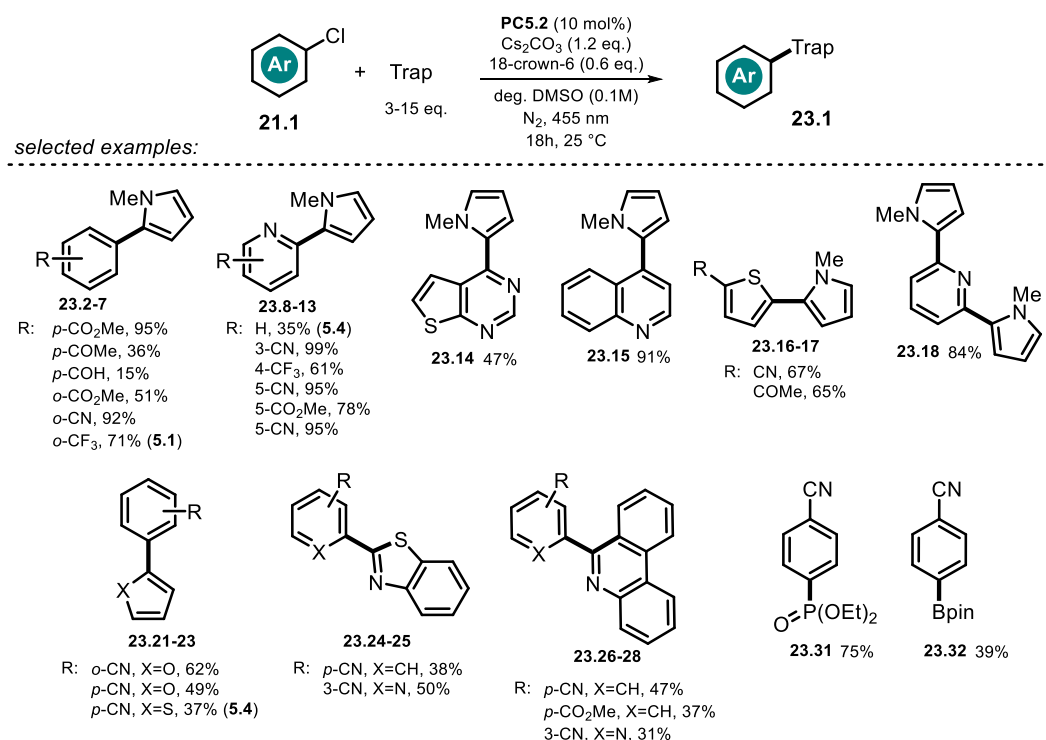


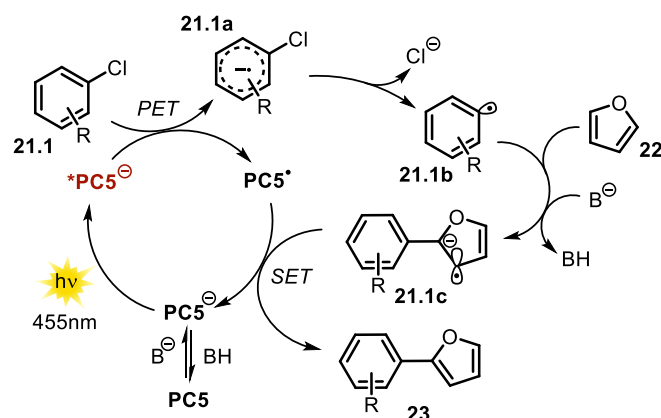
Figure 1-3. 9-Anthrone-based photocatalysts reported by König and co-workers.

In presence of base, anthrone **PC5** is deprotonated, which causes a red-shift in the absorption spectrum with a new distinct absorption band arising in the visible range. Upon excitation with blue LED light, the strongly reducing excited anion **PC5^{-*}** is formed (*cf.*, Table 1-1, Entry 5 for **PC5.1⁻**). Exceeding the reduction potential of the aryl chloride, oxidative quenching of the excited catalyst would form an arene radical anion **21.1a** and the open-shell anthrone **PC5[•]**. A subsequent mesolytic bond cleavage gives rise to a reactive aryl radical, which is trapped by an electron rich arene **22**. In alkaline media, the bicyclic radical intermediate gets deprotonated to afford the radical anion **21.1c**. The catalytic cycle is closed *via* electron transfer from **21.1c** to **PC5[•]** (Scheme 1-15). Time-resolved luminescence quenching experiments of the excited photocatalyst **PC5.1⁻** with various tolerated aryl chlorides shortened the lifetime whereas unsuccessful aryl chlorides caused no quenching. TEMPO trapping experiments confirmed the formation of aryl radical **21.1b** and bicyclic radical **21.1c**. Remarkably, in contrast to other photocatalyzed procedures for aryl halide activation^[8–11,22,77] no sacrificial electron donor (*e.g.* DIPEA) was necessary and the scope of aryl chlorides as well as tolerated radical trapping reagents could be broadened. In the model reaction, the catalyst loading was lowered to 5 mol% (92% yield) which indicates a turn-over number greater than 18. In accordance with



Scheme 1-14. Scope of the C–H arylation of (hetero)arenes using pyrroles, isocyanides, phosphite and B₂pin₂ as trapping reagents. For some substrates, other catalyst derivatives were used as stated in parenthesis behind the entry.

recently reported photocatalyzed C–H arylation procedures^[9–11,77], it was found that excess of the trapping agent is crucial for the reaction outcome, as a stoichiometric amount with reference to the aryl halide resulted in significantly decreased product yield.

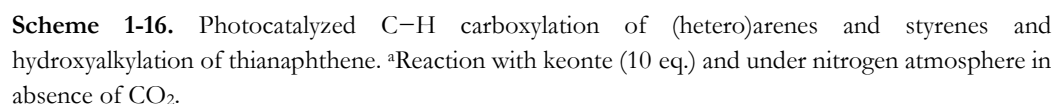


Scheme 1-15. Proposed mechanism of the photocatalyzed C–H arylation in presence of 9-anthrone.

Anthrolates **PC5**[−] are converted in presence of oxygen yielding the corresponding anthraquinones, thus reactions were run under inert atmosphere. Noteworthy, acridanone (**PC5.4**) afforded the desired arylation product **23.2** in good yield (83%) in non-degassed solvent and in presence of air, indicating a decreased tendency towards reaction with oxygen.

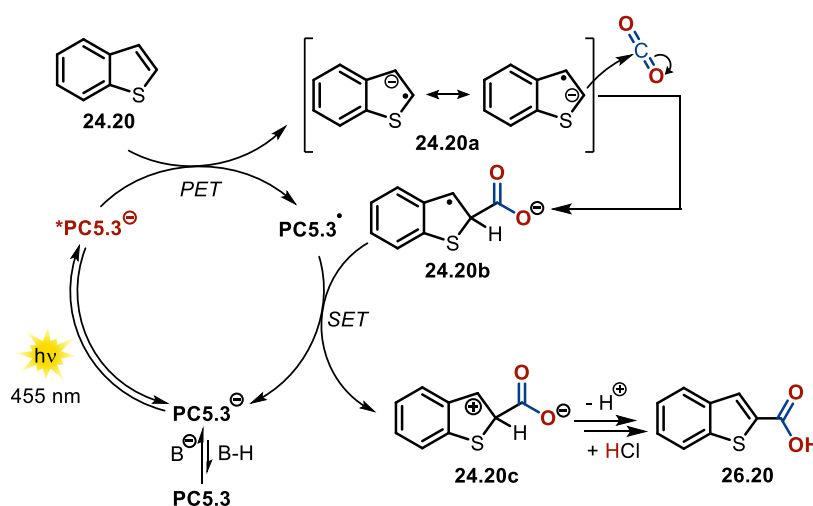
1.2.5 Anthrolate Catalyzed C–H Carboxylation of (Hetero)arenes and Styrenes with CO₂

Very recently, the visible-light absorbing strong photoreductant tetramethoxyanthrolate **PC5.3**[−] ($E_{ox}^* = -2.92$ V *vs.* SCE) was utilized to achieve the photocatalytic direct reduction of (hetero)arenes and styrenes to their respective radical anions.^[78] The associated nucleophilic character of such electron rich species was exploited in C–H carboxylation reactions with gaseous CO₂ affording the aromatic carboxylic- and cinnamic acids in moderate to excellent yields. Among others, non-prefunctionalized naphthalenes, thiophenes, furans, indoles, pyrazoles and styrenes are converted to the corresponding carboxylic acids under exceptionally mild reaction conditions (Scheme 1-16). An examined gram scale carboxylation of 2-cyanothiophene **26.9** illustrates the ease of scaling the reaction up. Moreover, a late-stage C–H carboxylation of a Boc-protected thiophene analogue of propranolol **26.31** is demonstrated following this procedure. Besides CO₂, ketones were found to convert to the corresponding tertiary alcohols following the same approach. Noteworthy, similar transformations usually require stoichiometric amounts of reactive organolithium reagents and are conducted under low temperature (−78 °C). Thus, a former protection of labile functional groups is often required leading to a multi-step synthesis.^[79–81] The regioselectivity of the carboxylation reaction can be predicted by theoretical means. In contrast to the organometallic-mediated carboxylation, the reported photocatalyzed, redox-neutral insertion of CO₂ into non-activated sp²-hybridized C–H bonds benefits from increased regioselectivity giving rise to only one regioisomer (**26.18** & **26.25**).



In presence of base, **PC5.3** is in equilibrium with the anionic form, which in contrast to the neutral species shows distinct absorption in the visible range. Excitation with a blue LED generates the excited state of the anionic catalyst **PC5.3**^{−*} which acts as a remarkably strong photo-reductant. Upon SET, benzothiophene **24.20** is reduced to the resonance stabilized radical anion **24.20a**. Subsequent nucleophilic attack affords the carboxylate **24.20b**. Closure of the catalytic cycle is proposed by an electron transfer to regenerate the active catalyst and to form the zwitterionic species **24.20c** which upon re-aromatization and acidic work-up converts to the desired carboxylated product **26.20** (Scheme 1-17). An alternate pathway *via* direct H-atom abstraction from **24.20b** caused by the open-shell species **PC5.3**[•] is also conceivable. In both cases, the gain in energy through re-aromatization of the compound is considered as the driving force to close the catalytic cycle. The mechanistic hypothesis was supported by time-resolved luminescence quenching experiments of the catalyst **PC5.3**^{−*} in

presence of (hetero)arenes and styrenes. Tolerated substrates shortened the excited-state lifetime of the photocatalyst and linear Stern-Volmer plots could be developed. Although the direct reduction of CO_2 ($E_{1/2} = -2.21 \text{ V vs. SCE}$)^[82] by the excited catalyst is thermodynamically feasible, a DMSO solution saturated with carbon dioxide was found to scarcely affect the excited state lifetime. Examined substrates that showed quenching of the photoexcited state of the catalyst, however failed to give the respective carboxylic acids are considered to exhibit insufficient nucleophilicity when present as radical anions and thus do not react with carbon dioxide. In addition, deuterium labelling experiments of **24.21** in presence of D_2O and tBuOD respectively, caused the incorporation of deuterium into the reactive C-2 position, supporting the assumption of a basic radical anion intermediate.

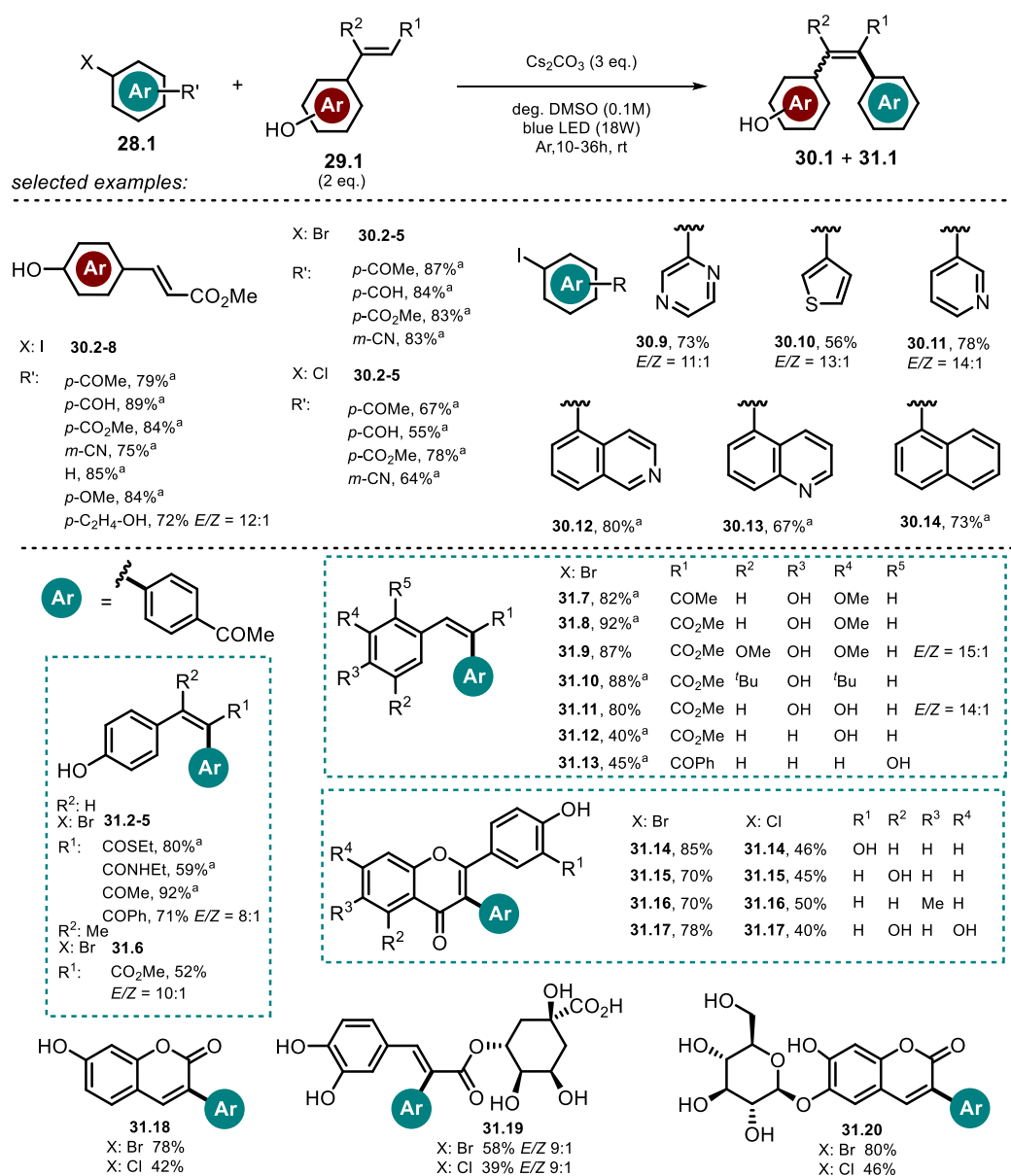


Scheme 1-17. Proposed reaction mechanism for the redox-neutral, photocatalyzed carboxylation of (hetero)arenes and styrenes utilizing **PC5.3** as strong photo-reductant.

1.3 Organic Anions as Photochemical Reagents

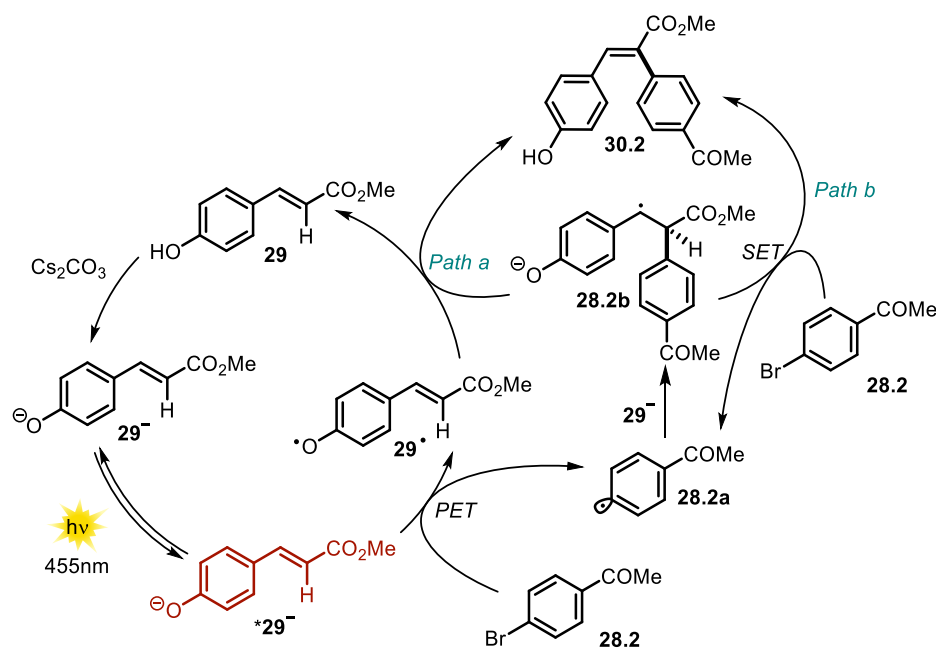
1.3.1 Excited State Phenolate as Photo-reductant

Recently, Xia and co-workers made use of the remarkable excited state potential of the vinylphenolate **29** ($E_{ox}^* = -2.48$ V *vs.* SCE) in a Heck-type arylation reaction promoted by blue LED light.^[83] The synthetic utility was demonstrated based on the arylation of methyl 4-hydroxycinnamates **30.2-14** with various (hetero)aryl halides (Scheme 1-18).



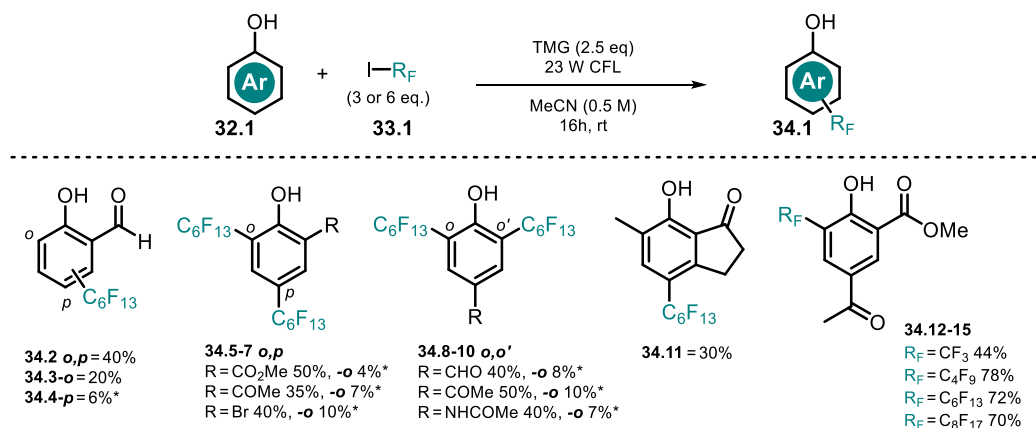
Scheme 1-18. Substrate scope of the Heck-type arylation reaction reported by Xia and co-workers; ^a $E/Z > 19:1$.

In addition, other derivatives of cinnamic acid (**31.2-13**, **31.19**), and flavonoids (**31.16-18**, **31.20**) were shown to react smoothly *via* the generated aryl radical to afford the respective arylation products in moderate to good yields. Remarkably, as the proposed mechanistic cycle is redox-neutral, no sacrificial electron donor is necessary. Besides electron deficient aryl iodides, the scope includes electron rich as well as electron neutral derivatives. In contrast, arylation products formed with less activated aryl bromides and chlorides are only shown with activated, electron deficient arenes. The *E/Z* ratios of the formed arylation products are high for most of the isolated compounds. The mild reaction conditions allowed to convert complex, biologically active substrates like chlorogenic acid, esculin and scutellarin. Upon deprotonation of the phenolic OH group, the absorption spectrum of **29** in DMSO is shifted towards longer wavelength and enables direct excitation of the phenolate **29⁻** with blue light. From the photoexcited state **29^{-*}** (Scheme 1-19), an electron transfer to the aryl halide **28.2** is feasible and subsequent cleavage of bromide forms the reactive aryl radical **28.2a**, which preferentially couples to electron rich species like the vinylphenolate **29⁻**. The resulting radical anion **28.2b** is assumed to either initiate a radical chain mechanism by reducing another equivalent of **28.2** and yielding the desired Heck-type arylation product **30.2** (*Path b*), or is converted to the former *via* direct hydrogen atom transfer or electron transfer to the phenoxy radical **29[•]** followed by proton shift (*Path a*).



Scheme 1-19. Proposed reaction mechanisms for the photochemical Heck-type arylation of vinylphenols.

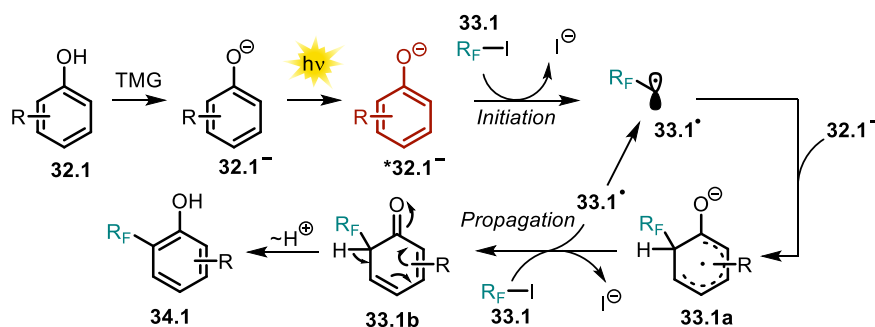
Melchiorre and co-workers have recently demonstrated how phenolate can elicit the generation of perfluoroalkyl radicals *via* single electron transfer.^[84] Photoredox-catalysis was demonstrated as a suitable approach to generate fluorinated radicals (R_F^\bullet) under mild, catalytic conditions. The developed method allows for the direct perfluoroalkylation and trifluoromethylation of phenols bearing electron withdrawing substituents **34.2-15** (Scheme 1-20). In presence of the non-nucleophilic base 1,1,3,3-tetramethylguanidine (TMG) the absorption spectrum of salicylaldehyde (**32.2**) is red-shifted and no change was observed upon addition of the perfluoroalkyl iodide **33**, excluding the formation of a ground state EDA complex. The base-induced bathochromic shift allowed for the use of a CFL bulb as light source. Using a 300 W Xe lamp with cut-off filter ($\lambda > 385$ nm) still allowed to form the product however in slightly decreased yield. The proposed mechanism of this transformation (Scheme 1-21) starts with a SET from the photoexcited phenolate **32.1⁻** to **33.1**. Subsequent reductive cleavage of iodine gives rise to a perfluoroalkyl radical **33.1[•]**.



Scheme 1-20. Scope of the perfluoroalkylation of substituted phenols. Minor positional isomers estimated by crude ¹⁹F-NMR are marked with (*). 6 eq. of alkylating agent **33.1** were used for products **34.7-10**.

In the bond-forming step, the radical is trapped by the ground-state phenolate yielding a cyclohexadienyl radical **33.1a** which propagates the reaction by reducing another equivalent of **33.1** *via* SET. Subsequent proton shift affords the alkylated phenol **34.1**. Stern-Volmer quenching studies of the phenolate in presence of alkyl iodide support the mechanistic proposal. For *o*-substituted phenols, the perfluoroalkylation proceed with moderate regioselectivity giving rise to *o*-, *p*-monoalkylated and *o,p*-dialkylated products whereas *p*-substituted phenols caused the formation of *o,o'*-dialkylated products. Monitoring the product distribution over the reaction time revealed that *o*- and *p*-alkylated products are formed as

intermediates and are further converted to bifunctionalized *ortho,para*-adducts. Non-substituted or methoxy-substituted phenols as well as nitrophenols failed to convert. Employing phenol **32.12** bearing electron withdrawing groups in *ortho* and *para* position afforded the mono-alkylated product as sole isomer. The demonstrated scope of perfluoroalkyl iodides comprises C₈, C₆, C₄ and C₁ chains (**34.12-15**).

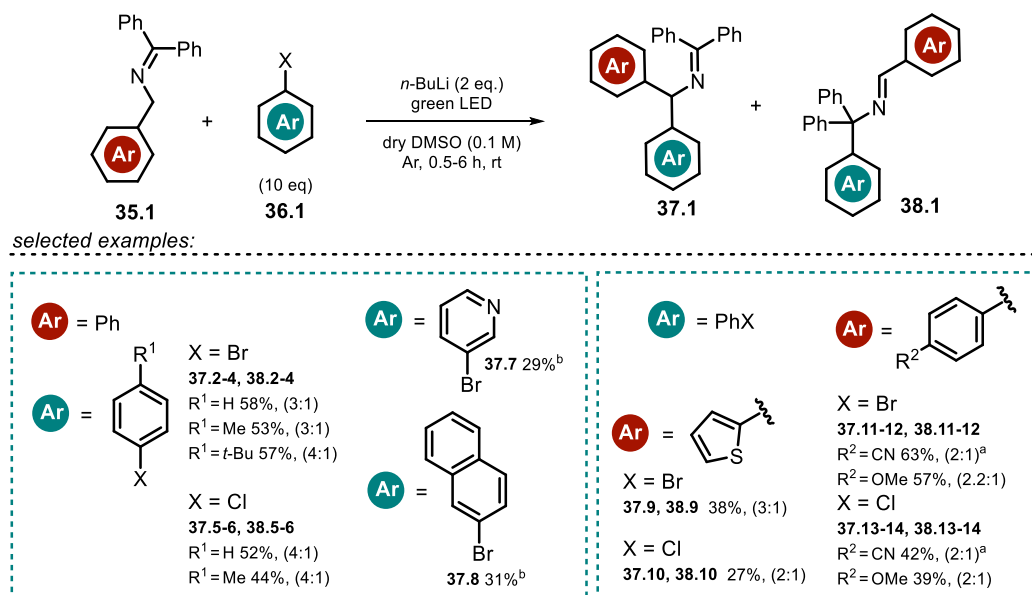


Scheme 1-21. Light-triggered perfluoroalkylation of phenolates bearing an electron withdrawing substituent by Melchiorre and co-workers. For simplicity, only the *ortho*-alkylation pathway is shown.

1.3.2 Visible-Light promoted Arylation of Azaallyl Anions

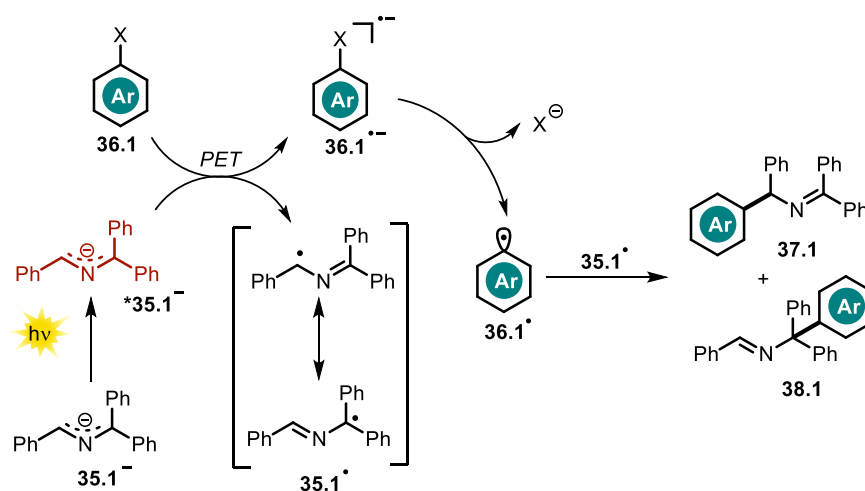
Chruma and co-workers demonstrated how irradiation of the colored azaallyl anion **35.1⁻** with visible light notably increases its excited state oxidation potential.^[85] In presence of strong bases (pK_a conjugated acid > 32), the formed 2-azaallyl anion acts as super-electron-donor in the dark^[86] and had been successfully employed in the functionalization of non-activated aryl iodides and tertiary alkyl halides.

The accessible substrate scope could be extended by employing visible light causing enhanced reduction potentials and allowed for the conversion of non-activated bromo- and chloro-(hetero)arenes, which are present in large excess regarding to **35.1**. The regioselectivity of the arylation reaction is moderate and product mixtures of **37.1** and **38.1** are usually obtained (Scheme 1-22).



Scheme 1-22. Scope of the light mediated azaallyl anion coupling with aryl halides. Ratio (37:38) of the formed regioisomers is given. ^a Blue light; ^b The other regioisomer was not isolated.

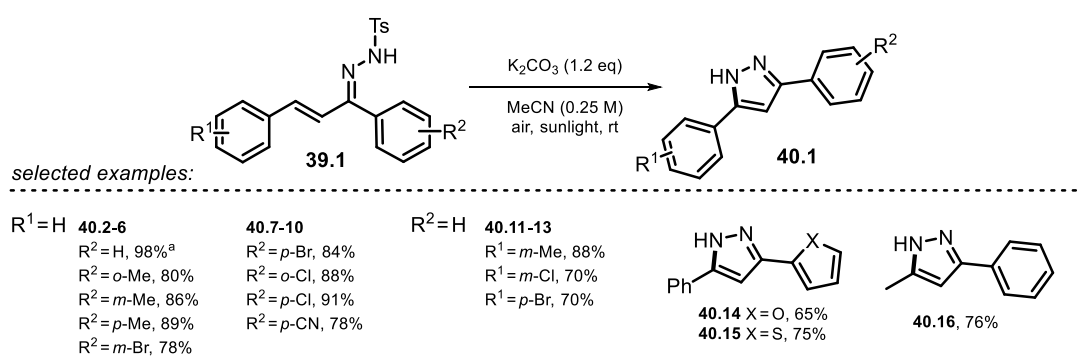
The authors propose an electron transfer from the excited state azaallyl anion **35.1^{-*}** to the aryl halide **36.1**. After cleavage of the C-X bond, a reactive transient aryl radical is formed which reacts with the stabilized azaallyl radical **35.1[•]** to form the arylation products (Scheme 1-23).



Scheme 1-23. Arylation of 2-azaallyl anions with non-activated aryl halides.

1.3.3 Synthesis of Pyrazoles *via* Irradiation of *N*-centered Hydrazone Anions

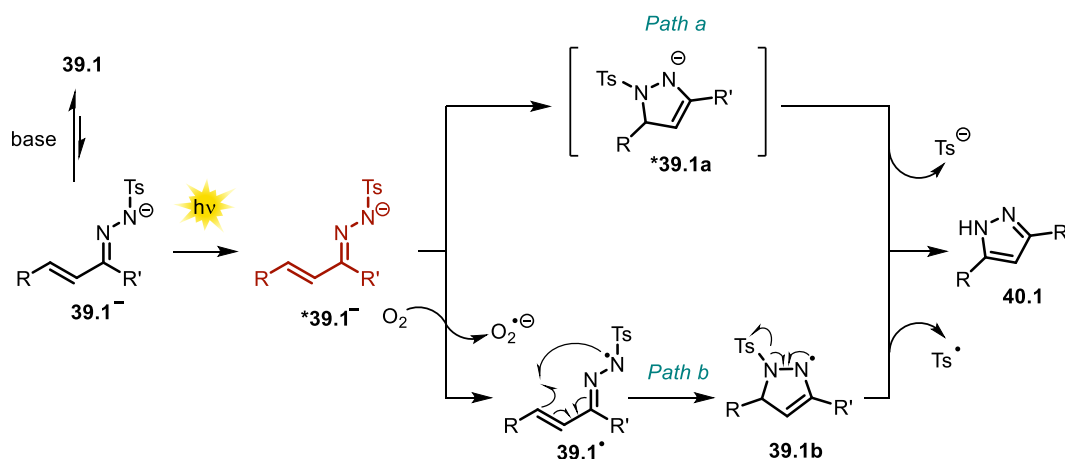
Zhu and co-workers reported a series of substituted hydrazones **39.1** which are able to undergo cyclization in presence of base affording pyrazole derivatives **40.1** mediated by sunlight.^[87] The UV-vis spectrum of the anionic hydrazone exhibits a significant red-shift compared to the neutral parent, enabling the use of visible-light to accomplish the cyclization reaction. Selected examples of formed pyrazoles are depicted in Scheme 1-24.



Scheme 1-24. Selected examples of the formed pyrazoles *via* irradiation of *N*-centered hydrazone anions.

^a Scaled up to 20 mmol reaction.

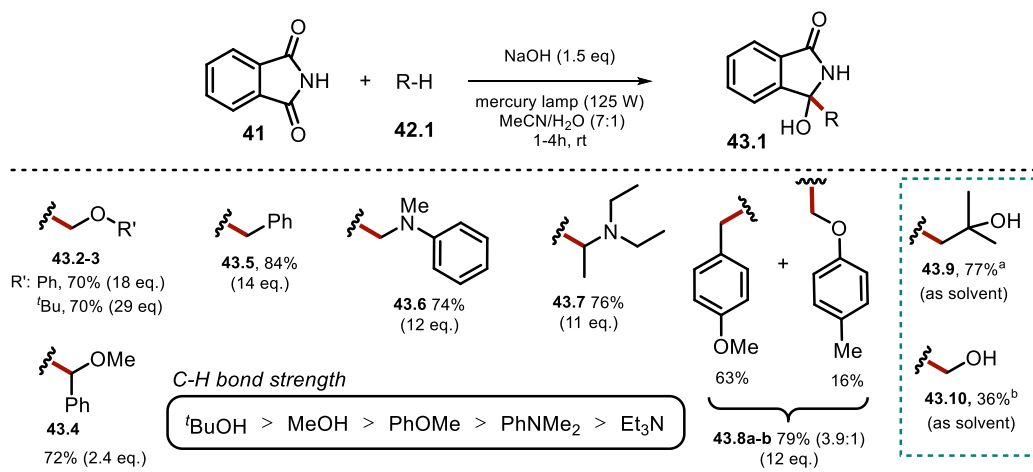
The authors propose two possible mechanistic pathways (Scheme 1-25): Deprotonated **39.1**[−] gets photoexcited and undergoes either direct anionic cyclization to **39.1a** (*Path a*) or is oxidized by O₂ to afford the *N*-centered radical **39.1**[•] (*Path b*) which upon intramolecular radical cyclization followed by cleavage of a tosyl radical yields the pyrazole **40.1**. Decreased yield is obtained when conducting the reaction under N₂ atmosphere or in presence of the radical trap TEMPO, indicative for the latter mechanistic proposal. Notably, the reactions were also shown to operate in water, however resulted in decreased yields.



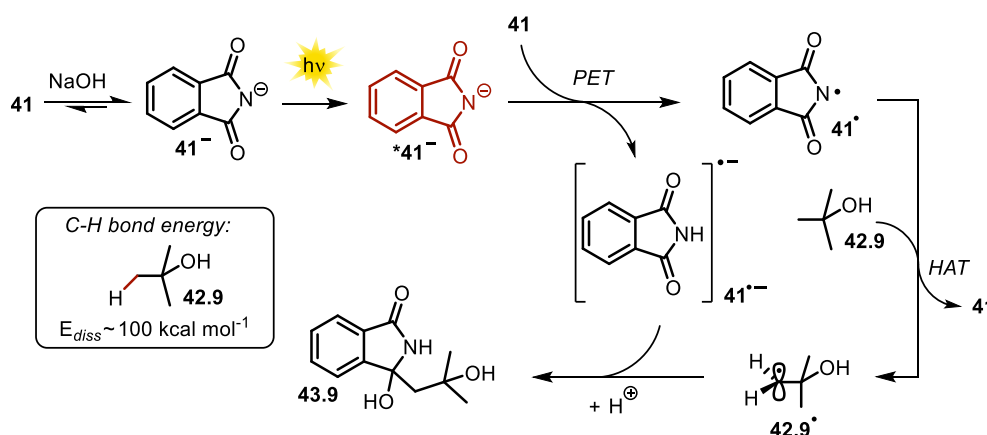
Scheme 1-25. Proposed photoinduced reaction mechanism towards pyrazole formation.

1.3.4 Utilizing Phthalimide Anions for H-Atom Abstraction

Already in 1988 the exceptionally high ability of the excited phthalimide anion **41⁻** to abstract hydrogen atoms from alcoholic solutions was recognized.^[88] This procedure was further developed and could be extended to ethers, alkylbenzenes and amines affording the reductive addition products with phthalimide (Scheme 1-26).^[89] The use of 4-methylanisole afforded a product mixture (**43.8a-b**) as H-atom abstraction is possible from the methoxy group or in benzylic position. In alkaline solution, phthalimide **41** is in equilibrium with its conjugate base **41⁻**. The photoinduced electron transfer from **41^{-*}** to ground-state phthalimide is a thermodynamically favorable process. Thus, the authors propose the phthalimidyl radical **41[•]** as the hydrogen atom abstracting intermediate which evolves from the excited anion **41^{-*}** upon PET towards phthalimide **41**. Remarkably, the electrophilic radical **41[•]** is able to activate C–H bonds possessing high bond dissociation energies (e.g. ^tBuOH, $E_{\text{diss}} = 100 \pm 2 \text{ kcal}\cdot\text{mol}^{-1}$)^[90] and upon hydrogen abstraction, phthalimide **41** and the alkyl radical **42.9[•]** are formed. Radical-radical coupling between the phthalimide radical anion **41^{-•}** and the carbon-centered radical **42.9[•]** affords the addition product **43.9** (Scheme 1-27).



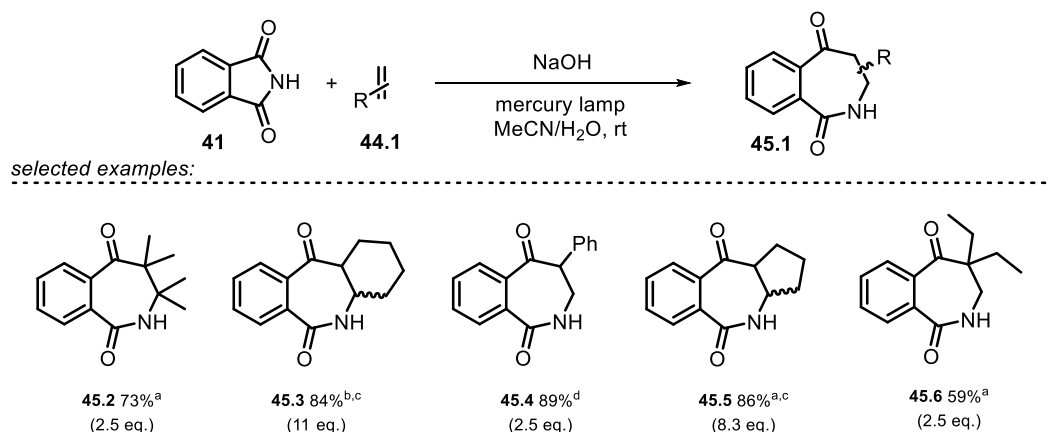
Scheme 1-26. Light-triggered reductive alkylation of phthalimide. Yields are given on consumed phthalimide. Equivalents used of the hydrogen atom donor are given in brackets. ^a Deviation from reaction conditions: **41** (13.6 mmol), NaOH (16 mL, 1M), ^tBuOH (150 mL), mercury lamp (125 W), 5h; ^b Deviation from reaction conditions: **41** (13.6 mmol), NaOH (10 mL, 1M), MeOH (160 mL), mercury lamp (125 W), 1h.



Scheme 1-27. Light-mediated C-H abstraction and radical addition to phthalimide radical anion initiated by the phthalimide radical.

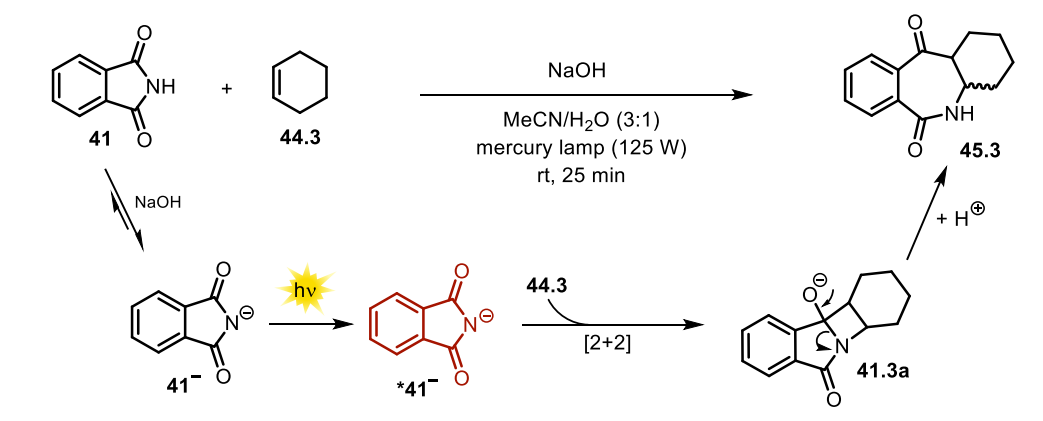
1.3.5 Photocycloadditions of Phthalimide and Saccharin Anion

The formation of [2]benzazepine-1,5-dione derivatives **45.1** *via* [2+2] photocycloaddition using phthalimide **41** was previously limited to electron poor non-cyclic alkenes due to competing excited state electron transfer reactions.^[91,92] Suau and co-workers thus mitigated the oxidizing strength by employing the anionic sodium phthalimide **41**[−] and obtained efficient, regiocontrolled photocycloaddition with a broader range of alkenes being tolerated (Scheme 1-28).



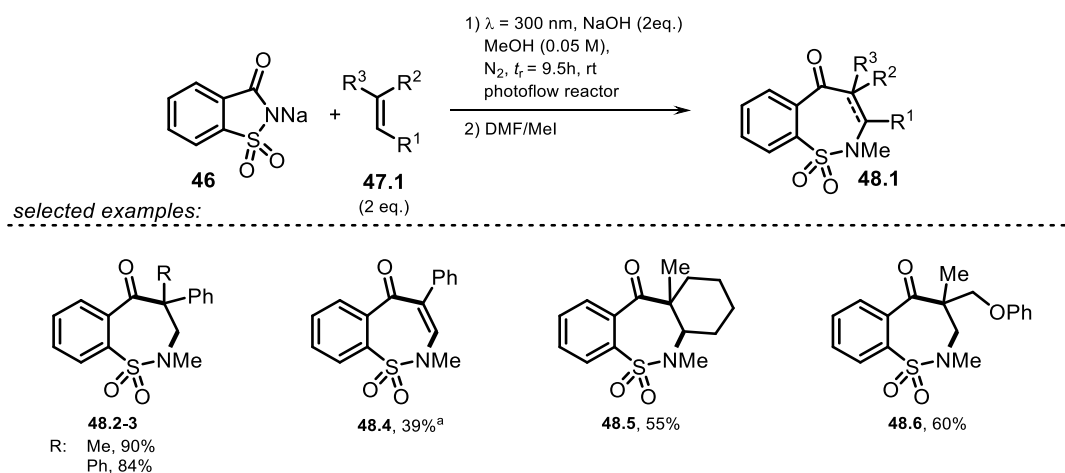
Scheme 1-28. [2+2] photocycloaddition of excited phthalimide anion with alkenes. ^a **41** (6.8 mmol), NaOH (8 mL, 1M, 1.2 eq.), MeCN/H₂O (160 mL, 7:1), 0.5 h, 125 W mercury lamp; ^b **41** (6.8 mmol), NaOH (pH≈10), MeCN/H₂O (7:1), 0.5 h, 125 W mercury lamp; ^c mixture of *cis*- and *trans*-**45** was obtained; ^d **41** (6.8 mmol), NaOH (10.2 mL, 1M, 1.5 eq.), MeCN/H₂O (7:1), 2 h, 400 W mercury lamp.

In contrast to the neutral species, **41**[−] shows significant fluorescence emission which was effectively quenched upon alkene addition indicating that the singlet excited state **41**^{−*} is the reactive intermediate. The [2+2] cycloaddition of photoexcited phthalimide anion to double bonds is a stereospecific process yielding the ring expanded *cis*-**45.1** adduct. Epimerization caused by the alkaline media affords a mixture of *cis*- and *trans*-**45.1** (Scheme 1-29).



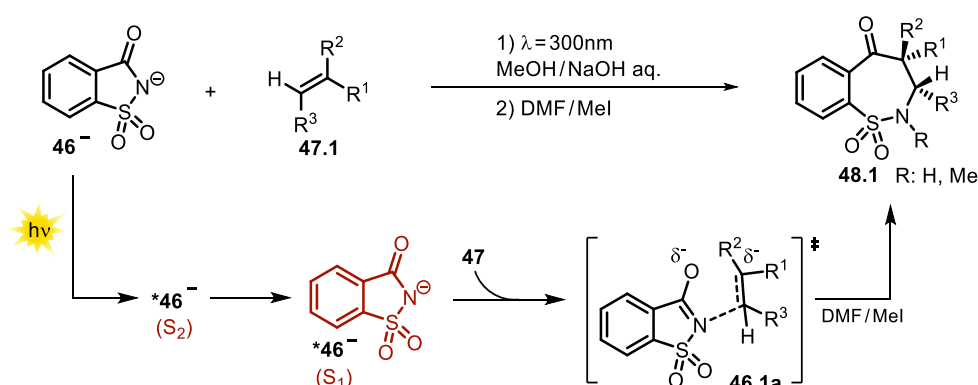
Scheme 1-29. Proposed mechanism for the [2+2] photocycloaddition of phthalimide anion with cyclohexene.

The photoexcited saccharin anion **46** was recently found to show similar reactivity towards alkenes which was utilized in regioselective ring expansion reactions giving benzosultams **48.2-6** (Scheme 1-30) starting from the cheap and commercially available sweetener saccharin.^[93]



Scheme 1-30. Selected examples of isolated benzosultams upon ring expansion with alkenes. Reaction conditions: Photoflow reactor 0.75 mm internal diameter. ^a phenylacetylene was used.

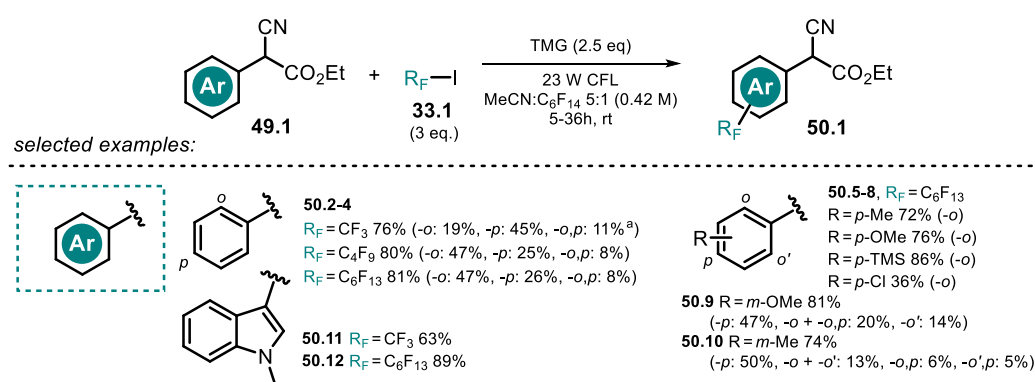
Remarkably, common approaches to form benzo-fused seven-membered sultam derivatives are multistep reactions and rely on the use of toxic organotin hydride^[94] or expensive Pd catalyst^[95]. A mechanism was proposed based on experimental and computational studies, suggesting the prevailing population of the S₂ state upon irradiation of the saccharin anion **46**[−]. The computed data indicate a fast deactivation into the first singlet state. Presumably, the key step towards benzosultam formation is a nucleophilic attack of the nitrogen of the excited state saccharin anion to the alkene. Moreover, no evidence for an azetidine intermediate (*cf.*, **41.3a** Scheme 1-29) resulting from [2+2] cycloaddition of saccharin and alkene was found neither in experiment nor in computational analysis. The C-C bond formation between carbonyl group and alkene is expected to occur in the ground state. Regioselectivity is gained due to the kinetic preference of the nucleophilic nitrogen atom to attack at the terminal, sterically less hindered side (Scheme 1-31).



Scheme 1-31. Proposed reaction mechanism for the light-promoted formation of benzosultams.

1.3.6 Organic Anions involved in Donor-Acceptor Complexes

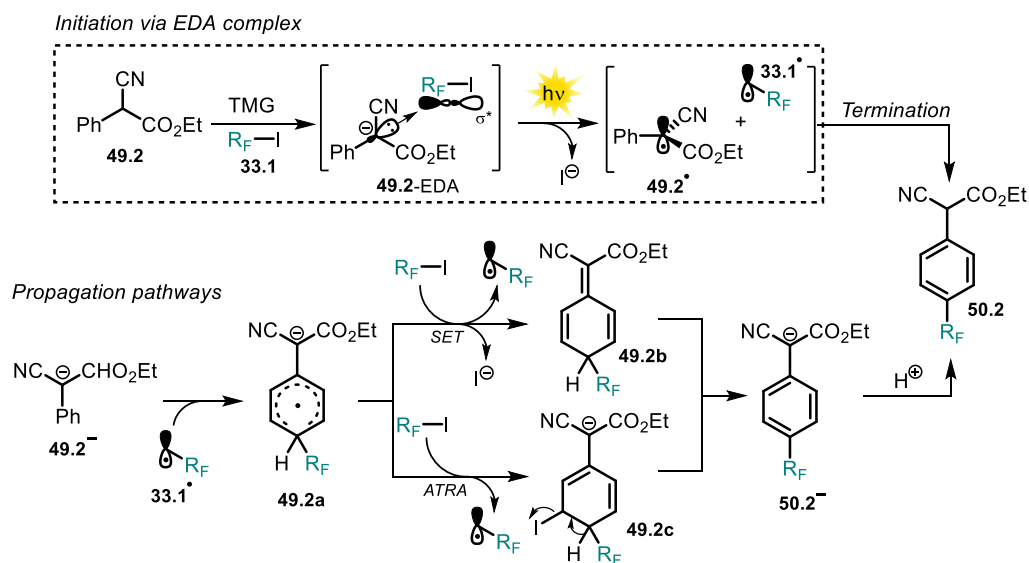
Organic anions are also reported to form ground state electron donor-acceptor (EDA) complexes with electron deficient species usually accompanied by the appearance of a new red-shifted charge-transfer absorption band. During the last years, EDA photochemistry has become increasingly popular. Among others, we highlight herein three examples to demonstrate the concept of organic anions participating in EDA complex formation. For a more detailed study we refer to recent excellent reviews.^[96,97] The aromatic perfluoroalkylation of α -cyano arylacetates **49.1** developed by Melchiorre and co-workers^[98] is mediated by visible light (CFL 23 W) although neither enolate **49.1**⁻ nor perfluoroalkyl iodide **33.1** or TMG show absorbance in that range of light. Mixing all the reagents together however results in a colored solution featured by a strong bathochromic shift in the absorption spectrum indicating the formation of an EDA complex. Irradiation of *p*-substituted substrates allowed to perfluoroalkylate α -cyano arylacetates selectively in *ortho* position. A mixture of regioisomers was obtained when *m/o*-substituted substrates were employed. In accordance with the proposed homolytic aromatic substitution (HAS) pathway lower yields were obtained with electron deficient arenes. Following the developed protocol, the substrate scope could be extended to heteroarenes and ketones (Scheme 1-32). Control experiments revealed that the formed product inhibits the reaction as the product enolate **50.1**⁻ outperforms the absorbance of the EDA complex. This issue was addressed by utilizing a biphasic system consisting of tetradecafluorohexane and MeCN, which allowed higher yield and shortened the reaction time.



Scheme 1-32. Selected examples of perfluoroalkylation of (hetero)arenes. ^a Yield determined by ¹⁹F-NMR.

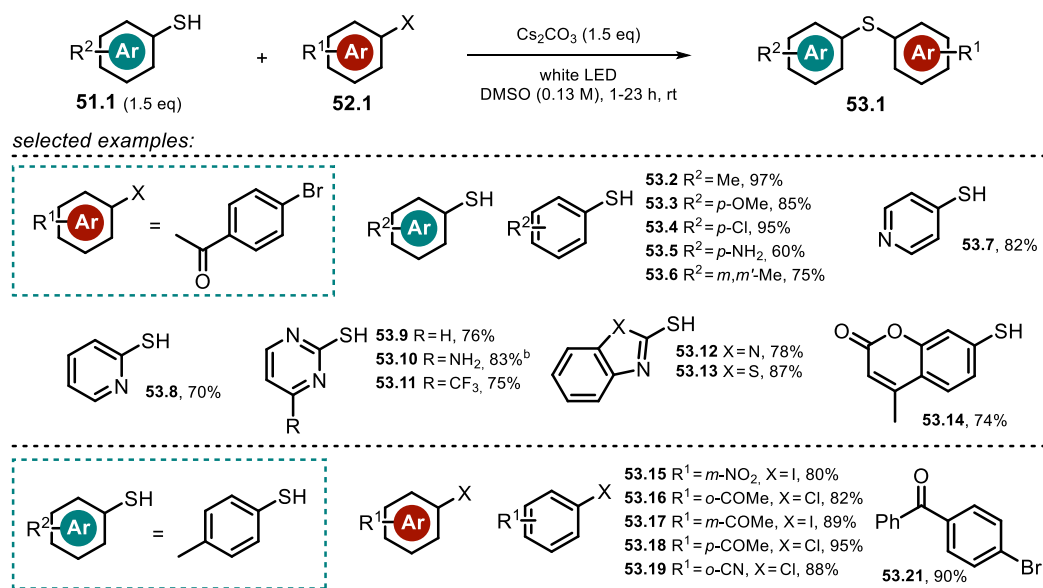
The radical chain reaction is initiated by the base promoted formation of the EDA complex **49.2**-EDA which absorbs visible light and releases a radical pair upon reductive cleavage of

iodine, consisting of benzylic radical **49.2[•]** and perfluoroalkyl radical **33.1[•]**. The electron rich enolate **49.2⁻** reacts with the alkyl radical *via* HAS to afford the radical anion intermediate **49.2a^{•-}**. Chain propagation is assumed either by SET affording **49.2b** or *via* atom-transfer radical addition (ATRA) followed by cleavage of HI (**49.2c**). Reaction work-up yields the perfluoroalkylated product **50.2**. Termination of the radical chain is possible upon direct radical-radical coupling of **49.2[•]** and **33.1[•]** (Scheme 1-33).



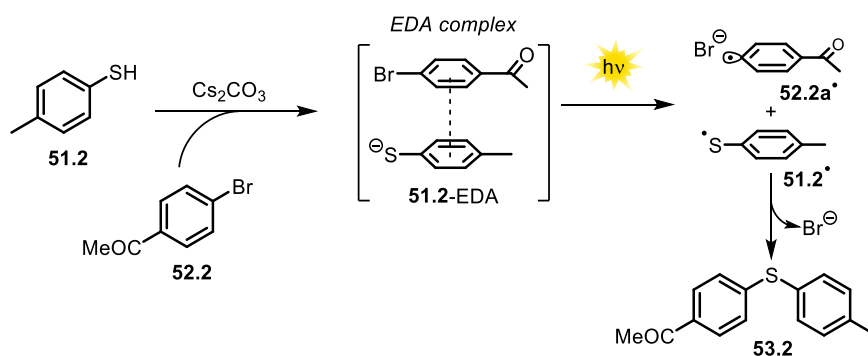
Scheme 1-33. Proposed reaction mechanism for the perfluoroalkylation of α -cyano arylacetates involving the formation of a visible-light absorbing EDA complex.

The Miyake group made use of the EDA complex formed between an electron rich thiolate anion **51.1⁻** and aryl halides **52.1** to afford a broad scope of aromatic thioethers.^[99] The protocol allowed to convert both electron rich and poor thiophenols under visible-light irradiation and in presence of cesium carbonate (Scheme 1-34). Remarkably, tolerated aryl halides are not limited to activated, electron-deficient arenes, as thioethers were formed with iodobenzene and toluene, however a prolonged reaction time was required (20-24 h).



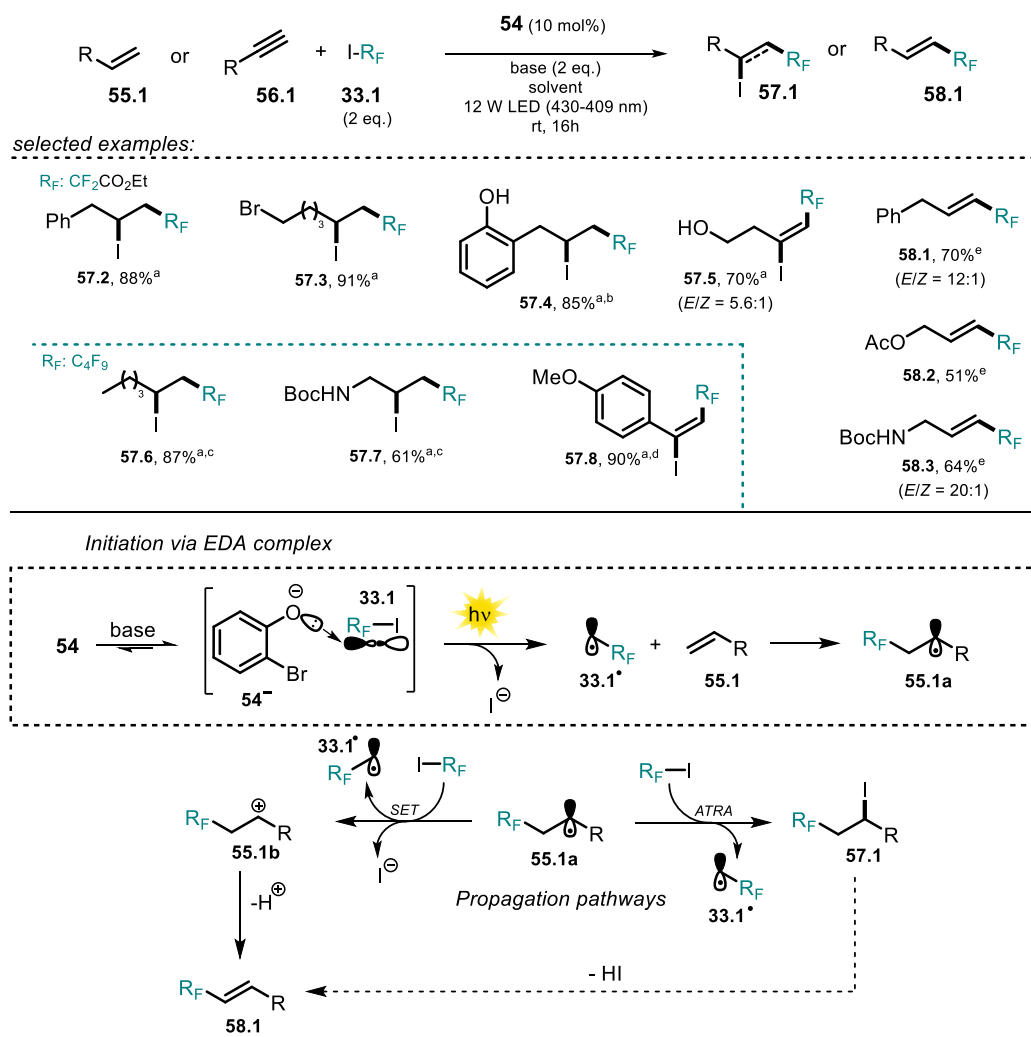
Scheme 1-34. Selected examples for the thiolation of aryl halides. ^a 50 mmol scale. ^b Cs₂CO₃ (2 eq.).

Very fast reactions (1 h) were obtained when electron deficient aryl halides and electron rich thiophenols were coupled. In addition, benzylic halides revealed to convert similarly. Following the developed protocol allowed for the mild and efficient late-stage functionalization of pharmaceutically active compounds. The formation of an EDA complex **51.2**-EDA between thiophenolate **51.2**[−] and aryl halide **52.2** was confirmed by UV-vis spectroscopy and TD-DFT calculations. The arising charge-transfer absorption band allows for visible-light excitation initiating the reaction with an electron transfer from the thiolate anion to the aryl halide followed by cleavage of the halide anion. The formed thiyl- and aryl radical combine to afford the C-S cross-coupled product **53.2** (Scheme 1-35).



Scheme 1-35. Proposed reaction mechanism for the C-S cross-coupling reaction of thiophenols and aryl halides *via* the formation of a visible-light absorbing EDA complex.

Based on the perfluoroalkylation of alkenes and alkynes it was recently shown, that the anionic counterpart involved in the EDA complex formation can be utilized catalytically.^[100] In presence of base, 2-bromophenol (**54**) was found to promote the visible light-mediated 1,2-addition of fluoroalkyl iodides to alkenes and alkynes. Noteworthy, although a significant amount of product was formed in the reaction of allylbenzene **55.2** and ethyl iododifluoroacetate **33.2** in absence of phenol catalyst, the yield could be doubled using a catalytic amount of **54**. The use of a more polar solvent gave rise to Heck-type coupling products. Allylphenols, acting themselves as catalyst, could be converted to either the addition product **57.1** or the coupling product **58.1** without adding catalyst **54**. Initiation of the reaction is proposed to occur *via* EDA complex formation between phenolate **54**⁻ and alkylating reagent **33.1**. The photoexcited EDA complex causes the formation of radical **33.1**[•] which reacts with the olefin **55.1** to yield the radical intermediate **55.1a**. Depending on the reaction media, either abstraction of an iodine atom from **33.1** affords the addition product **57** or SET with **33.1** gives rise to the cationic intermediate **55.1b** which forms the Heck-type product **58.1** upon deprotonation (Scheme 1-36).

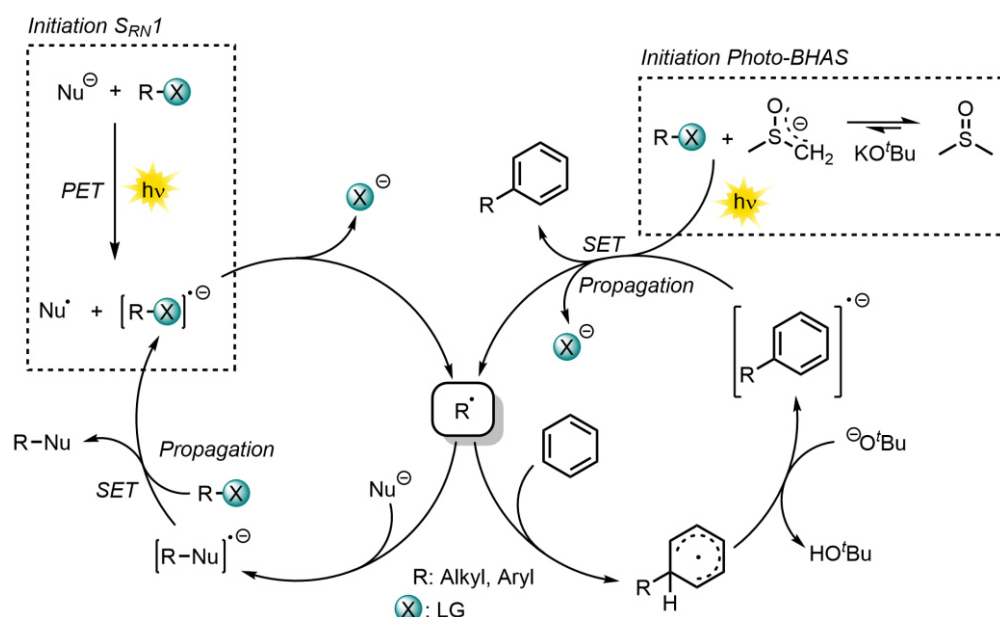


Scheme 1-36. Selected examples for fluoroalkylation of alkenes and alkynes affording addition products or Heck-type coupling products (top) ^a Using KOAc (2 eq) in DCE; ^b without **54** in dioxane; ^c Cs₂CO₃ instead of KOAc; ^d K₂CO₃ instead of KOAc; ^e Using K₂CO₃ (2 eq.) in DMSO; Proposed reaction mechanism for the visible light-promoted fluoroalkylation using 2-bromophenol as catalyst (bottom).

1.3.7 Organic Anions promoting the Radical-Nucleophilic Substitution (S_{RN}1) Reaction

In the course of S_{RN}1 reactions, radicals and radical anions are formed as intermediates and chain mechanisms are likely to occur. Proposed for the first time in the 1960s,^[101,102] the reaction affords nucleophilic substitution on aromatic and aliphatic compounds and tolerates a wide scope of nucleophiles and substrates.^[103] Initiation is commonly achieved by photoinduced electron transfer from an electron-rich anionic nucleophile and an electron-poor

acceptor leading to the open-shell nucleophile Nu^\bullet and a radical anion. EDA complex formations between nucleophile and substrate are reported and allow to initiate $\text{S}_{\text{RN}}1$ reactions by using less-energetic light.^[96] Upon mesolytic bond-cleavage the resulting radical R^\bullet is trapped by the nucleophile and forms a radical anion. A single electron transfer from the radical anion $[\text{R-Nu}]^{\bullet-}$ to the acceptor R-X affords the desired substitution product along with another radical anion $[\text{R-X}]^{\bullet-}$, which allows the propagation of the chain reaction (Scheme 1-37) provided that this SET is thermodynamically favorable.



Scheme 1-37. General reaction mechanism for the radical-nucleophilic substitution ($\text{S}_{\text{RN}}1$) reaction and for the photoinitiated base-promoted homolytic aromatic substitution reaction (photo-BHAS).

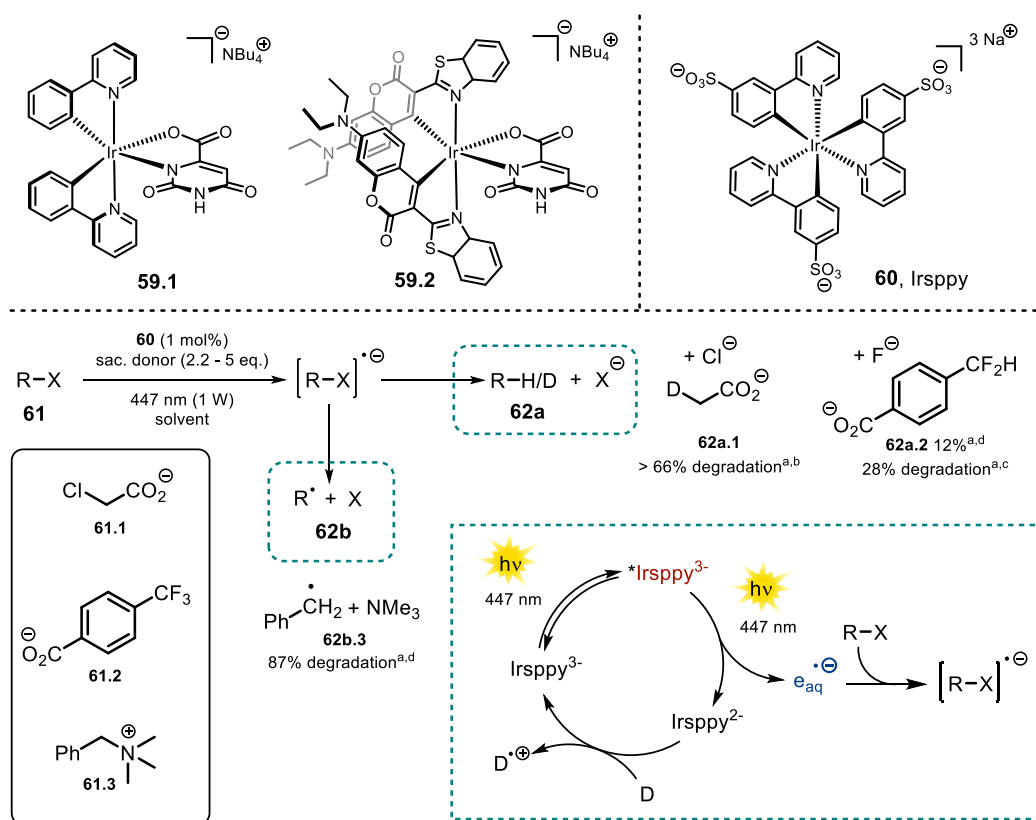
Closely related to the concept of the light-induced $\text{S}_{\text{RN}}1$ reaction is the photoinitiated base-promoted homolytic aromatic substitution reaction (photo-BHAS) affording C–H arylated products starting from aryl or alkyl halides in presence of a strong base (*e.g.* KO^tBu or NaH). The reactive intermediate R^\bullet is proposed to add to the arene forming an aromatic radical which is converted into the respective radical anion by deprotonation and eventually gives the arylated product upon SET to propagate the chain reaction. In absence of further additives, it has recently been shown that the dimsyl anion can be excited by visible light and plays a pivotal role for initiating the reaction (see Scheme 1-36).^[104] The initiation of the BHAS reaction was also reported by other photo-activation modes *e.g.* through PET from an iridium sensitizer to R-X or upon light-excitation of an *in-situ* formed photosensitive complex between KO^tBu and phenanthroline.^[105,106] Non-nucleophilic bases are commonly employed to avoid the competing

$S_{RN}1$ reaction pathway. Light-mediated substitutions following the $S_{RN}1$ reaction with organic anions as nucleophiles have been studied extensively and were subject of recent reviews^[32,103,107-111] and thus will not be further discussed herein.

1.4 Inorganic Anions

1.4.1 Transition Metal Complexes

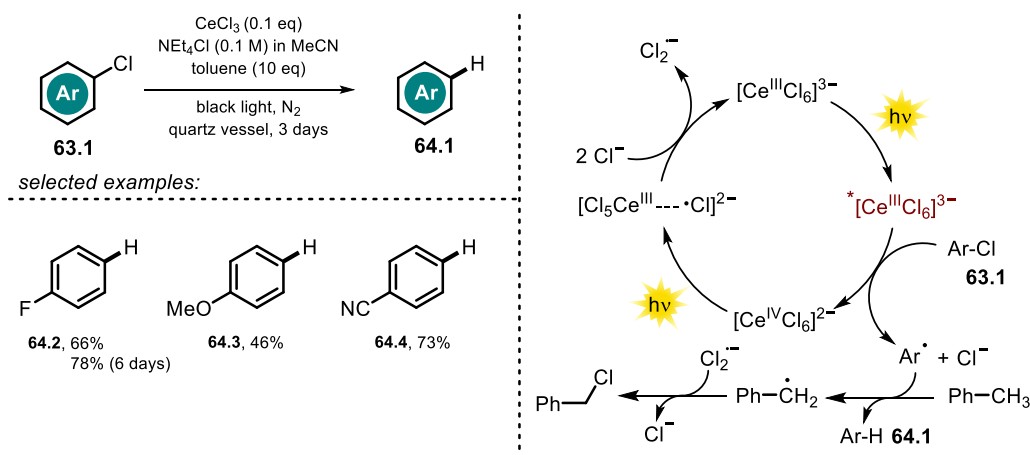
Transition-metal complexes like the Ru(II) polypyridine or the cyclometalated Ir(III) found widespread applications in photocatalysis, as they are photostable, show tunable redox potentials and excited state lifetimes are usually durable.



Scheme 1-38. Negatively charged iridium complexes (top); Irppy catalyzed degradation of pollutants (center); ^a Conversion was determined by crude NMR; ^b Reaction conditions: Chloroacetate **61.1** (12.5 mM), NaHAsc (2.2 eq.) in D_2O (3 mL), 4h; ^c Reaction conditions: Trifluoromethyl arene **61.2** (15 mM), TEOA (5 eq.) in H_2O (16 mL), 4h; ^d Reaction conditions: benzyltrimethylammonium salt **61.3** (10 mM), TEOA (5 eq.) in D_2O (3 mL), 3h. Proposed catalytic cycle for the generation of hydrated electrons (bottom right).

In contrast to neutral complexes like *fac*-Ir(ppy)₃ or cationic metal-based sensitizers [*e.g.* Ru(bpy)₃²⁺, Ir(ppy)₂(dtbbpy)⁺], anionic transition-metal complexes have been less explored, which might be attributed to photodecomposition with monodentate anionic ligands^[112] and the shortage of more stable dianionic ancillary ligands available. Godbert and co-workers were able to synthesize and characterize the anionic iridium complex **59.1** with a dianionic orotate ligand (Scheme 1-38, top).^[113] Later on, the complex was modified by exchanging the 2-phenylpyridine ligands with coumarin-derived ligands (**59.2**), to increase the visible-light absorption. The authors successfully demonstrated the use of **59.2** in visible-light-driven H₂ generation which resembled the first example of a photoinduced electron transfer using an anionic Ir(III) sensitizer.^[114] Based on the well-established *fac*-Ir(ppy)₃, Wenger and co-workers utilized a trisulfonated analogue **60** (Scheme 1-38, top), which renders the sensitizer water-soluble and negatively charged, to generate hydrated electrons.^[115] A potential use of hydrated electrons in waste water treatment was demonstrated by the degradation of chloroacetate and benzyltrimethylammonium salt. In addition, the defluorination of trifluoromethylbenzoate is possible in presence of such a strong reductant (Scheme 1-38, **62a.1-2**). The catalytic cycle is depicted in Scheme 1-38 (bottom right). The photocatalyst is excited with a 447 nm collimated diode laser. Remarkably, the absorption of a second photon stimulates the ejection of the electron within the lifetime ($\approx 1.6 \mu\text{s}$) of the excited sensitizer. The photocatalyst is then regenerated by either sodium ascorbate or triethanolamine acting as sacrificial electron donors. Compared to the neutral *fac*-Ir(ppy)₃, the excited state oxidation potential of the anionic sensitizer **60** (-1.89 V vs. SCE) was found to be slightly increased.

The trianionic hexachlorocerate(III) [Ce^{III}Cl₆]³⁻ was proven to be effective in the reductive dehalogenation of aryl halides **63.1** using UVA light (Scheme 1-39).^[116] This species is stable to air and moisture and can be generated *in-situ* by mixing CeCl₃ and NEt₄Cl in acetonitrile. Blacklight irradiation causes a metal centered excited state ($E_{ox}^* \approx -3 \text{ V vs. SCE}$)^[117,118], enabling the PET to the aryl halide along with oxidation to Ce^{IV}. Interestingly, the reaction could also be performed with a catalytic amount of CeCl₃, owing to the complementary oxidative photochemistry of [Ce^{IV}Cl₆]²⁻ (Scheme 1-39, right).^[119] The addition of toluene as the terminal reductant allowed to close the catalytic cycle.



Scheme 1-39. Scope of the CeCl_3 catalyzed defunctionalization of aryl halides by the *in-situ* formation of $[\text{Ce}^{\text{III}}\text{Cl}_6]^{3-}$ and conceivable mechanism of the reaction.

In a follow-up work, the developed catalytic protocol was utilized for the photoinduced Miyaura borylation of aryl bromides and chlorides. Schelter and co-workers used bis(pinacolato)diboron which functioned as both borylation reagent and terminal reductant.^[120]

1.4.2 Polyoxometalates

Polyoxometalates are a class of widely studied inorganic compounds which find application in many fields as photocatalysts. Well-known representatives are the decatungstates.^[121] Despite being negatively charged, these compounds are reported to act as strong oxidants from their excited state. This rare feature might be explained analogously to what was discussed for fluorescein (*vide supra*). Tungsten is present in a high oxidation state (+V) while the negative charge is centered on the oxygen atoms of the cluster, rendering the metal center highly electron poor and prone to reduction. Upon photoexcitation, a ligand to metal charge transfer ($\text{O} \rightarrow \text{M}$) is proposed, generating a relaxed excited state cluster $[\text{W}_{10}\text{O}_{32}]^{4-*}$ which is easily reduced ($E_{red}^* = +2.44 \text{ V vs. SCE}$)^[122]. Besides electron transfer reactions, excited decatungstate is well known for its ability to abstract hydrogen atoms from non-activated $\text{C}(\text{sp}^3)\text{-H}$ bonds. A few examples are known where polyoxometalates equipped with binding sites on the cluster shell or in presence of co-catalysts participate in photoreductive CO_2 activation or H_2 generation.^[6]

1.4.3 Sulfite Anions used in Photoreactions

A couple of examples are present in literature on the ability of sulfite anion to generate hydrated electrons upon irradiation. The method was successfully applied for the photodegradation of hazardous halogenated pollutants as monochloroacetic acid^[123] and perfluorooctanesulfonate.^[124] However, the excitation is obtained with harmful high-energetic UV light and the efficiency suffers in more complex media due to light attenuation by scattering or competing absorption of other organic compounds including the solvent.

1.5 Summary and Outlook

Organic anions and light are a perfect combination to achieve challenging synthetic transformations, as either reagent or photocatalysts. Compared to a corresponding neutral molecule, the absorption spectrum of the negatively charged anion usually exhibits a bathochromic shift and often fluorescence is exclusively observed for the anionic species. This allows photochemical conversions with less energetic light, in many cases visible light. Fluorescence quenching studies enable the verification of interactions between substrates and the excited chromophore. The seminal work of Soumillion and co-workers in this field and their excellent review^[32] demonstrated early the potential of organic anions as strong photoreductants in the dechlorination of arenes and the desulfonylation of sulfonamides using excited 2-naphtholate. In addition to the use of anions as photocatalysts, excited anions found applications as strong reductants to activate a reaction partner *via* PET followed by a subsequent conversion of both open-shell intermediates. Examples are the arylation of azaallylanions or the Heck-type arylation of vinylphenols. Photoexcited organic anions allow cyclization reactions yielding pyrazoles or participate in ring-expanding reactions. Moreover, organic anions serve as potent electron rich donor molecules for the formation of light-absorbing EDA complexes.

Overall, the use of organic anions as cheap and sustainable photocatalysts harbors enormous potential for applications in synthetic organic chemistry. We observe an increasing research interest in applying photoexcited anions in synthesis and hope that this review will stimulate more contributions to this yet underexplored emerging field, which holds promise for many more exciting applications in organic synthesis.

1.6 References

- [1] E. Speckmeier, T. G. Fischer, K. Zeitler, *J. Am. Chem. Soc.* **2018**, *140*, 15353–15365.
- [2] F. Speck, D. Rombach, H. A. Wagenknecht, *Beilstein J. Org. Chem.* **2019**, *15*, 52–59.
- [3] A. Joshi-Pangu, F. Lévesque, H. G. Roth, S. F. Oliver, L. C. Campeau, D. Nicewicz, D. A. DiRocco, *J. Org. Chem.* **2016**, *81*, 7244–7249.
- [4] C. K. Prier, D. A. Rankic, D. W. C. MacMillan, *Chem. Rev.* **2013**, *113*, 5322–5363.
- [5] N. A. Romero, D. A. Nicewicz, *Chem. Rev.* **2016**, *116*, 10075–10166.
- [6] C. Streb, *Dalt. Trans.* **2012**, *41*, 1651–1659.
- [7] I. Ghosh, J. Khamrai, A. Savateev, N. Shlapakov, M. Antonietti, B. König, *Science* **2019**, *365*, 360–366.
- [8] I. Ghosh, T. Ghosh, J. I. Bardagi, B. König, *Science* **2014**, *346*, 725–728.
- [9] I. Ghosh, B. König, *Angew. Chem. Int. Ed.* **2016**, *55*, 7676–7679.
- [10] J. I. Bardagi, I. Ghosh, M. Schmalzbauer, T. Ghosh, B. König, *Eur. J. Org. Chem.* **2018**, *2018*, 34–40.
- [11] M. Neumeier, D. Sampedro, M. Májek, V. A. de la Peña O'Shea, A. Jacobi von Wangelin, R. Pérez-Ruiz, *Chem. Eur. J.* **2018**, *24*, 105–108.
- [12] M. Majek, A. Jacobi Von Wangelin, *Acc. Chem. Res.* **2016**, *49*, 2316–2327.
- [13] I. Ghosh, L. Marzo, A. Das, R. Shaikh, B. König, *Acc. Chem. Res.* **2016**, *49*, 1566–1577.
- [14] I. Ghosh, *Phys. Sci. Rev.* **2019**, *4*, 20170185, doi: <https://doi.org/10.1515/psr-2017-0185>.
- [15] C. S. Wang, P. H. Dixneuf, J. F. Soulé, *Chem. Rev.* **2018**, *118*, 7532–7585.
- [16] J. A. Christensen, B. T. Phelan, S. Chaudhuri, A. Acharya, V. S. Batista, M. R. Wasielewski, *J. Am. Chem. Soc.* **2018**, *140*, 5290–5299.
- [17] D. Weir, J. C. Scaiano, *Chem. Phys. Lett.* **1986**, *128*, 156–159.
- [18] A. Samanta, K. Bhattacharyya, P. K. Das, P. V. Kamat, D. Weir, G. L. Hug, *J. Phys. Chem.* **1989**, *93*, 3651–3656.
- [19] J. C. Scaiano, M. Tanner, D. Weir, *J. Am. Chem. Soc.* **1985**, *107*, 4396–4403.
- [20] L. J. Johnston, *Chem. Rev.* **1993**, *93*, 251–266.
- [21] B. R. Arnold, J. C. Scaiano, W. G. McGimpsey, *J. Am. Chem. Soc.* **1992**, *114*, 9978–9982.
- [22] I. A. MacKenzie, L. Wang, N. P. R. Onuska, O. F. Williams, K. Begam, A. M. Moran, B. D. Dunietz, D. A. Nicewicz, *Nature* **2020**, *580*, 76–80.
- [23] D. Gosztola, M. P. Niemczyk, W. Svec, A. S. Lukas, M. R. Wasielewski, *J. Phys. Chem. A* **2000**, *104*, 6545–6551.
- [24] J. Haimerl, I. Ghosh, B. König, J. Vogelsang, J. M. Lupton, *Chem. Sci.* **2019**, *10*, 681–687.
- [25] S. Fukuzumi, K. Ohkubo, T. Suenobu, *Acc. Chem. Res.* **2014**, *47*, 1455–1464.
- [26] T. Hering, T. Slanina, A. Hancock, U. Wille, B. König, *Chem. Commun.* **2015**, *51*, 6568–6571.
- [27] B. Zilate, C. Fischer, C. Sparr, *Chem. Commun.* **2020**, *56*, 1767–1775.
- [28] K. A. Margrey, D. A. Nicewicz, *Acc. Chem. Res.* **2016**, *49*, 1997–2006.
- [29] Q. Xu, B. Zheng, X. Zhou, L. Pan, Q. Liu, Y. Li, *Org. Lett.* **2020**, *22*, 1692–1697.
- [30] M. A. Fox, *Chem. Rev.* **1979**, *79*, 253–273.
- [31] A. H. Zimmerman, R. Gygas, J. I. Brauman, *J. Am. Chem. Soc.* **1978**, *100*, 5595–5597.
- [32] J.-P. Soumilion, *Top. Curr. Chem.* **1993**, *168*, 93–141.
- [33] J. P. Soumilion, P. Vandereecken, M. Van Der Auweraer, F. C. De Schryver, A. Schanck, *J. Am. Chem. Soc.* **1989**, *111*, 2217–2225.
- [34] N. Tamaoki, Y. Takahashi, T. Yamaoka, *J. Chem. Soc. Chem. Commun.* **1994**, 1749–1750.
- [35] J. Smid, *Angew. Chem. Int. Ed.* **1972**, *11*, 112–127.

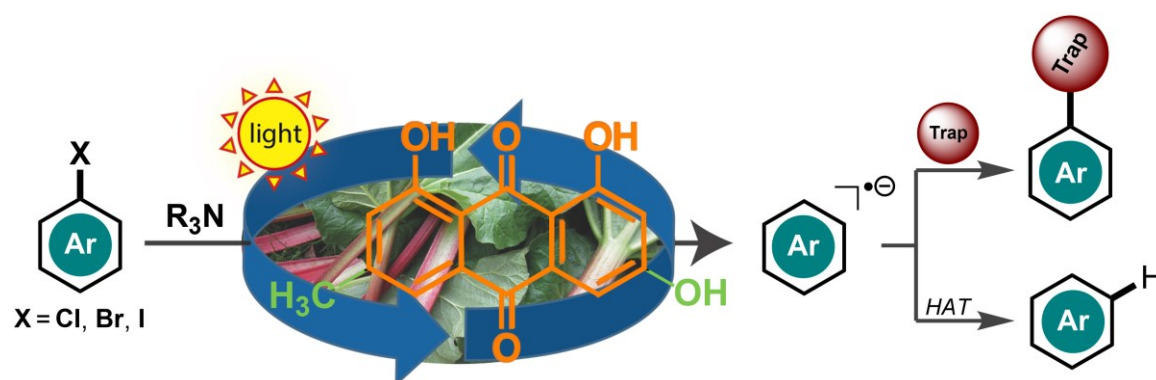
- [36] M. J. Kaufman, S. Gronert, D. A. Bors, A. Streitwieser, *J. Am. Chem. Soc.* **1987**, *109*, 602–603.
- [37] Y. Marcus, G. Hefter, *Chem. Rev.* **2006**, *106*, 4585–4621.
- [38] H. D. Roth, *Top. Curr. Chem.* **1990**, *156*, 1–19.
- [39] D. Rehm, A. Weller, *Isr. J. Chem.* **1970**, *8*, 259–271.
- [40] P. D. Morse, T. M. Nguyen, C. L. Cruz, D. A. Nicewicz, *Tetrahedron* **2018**, *74*, 3266–3272.
- [41] E. Alfonzo, F. S. Alfonso, A. B. Beeler, *Org. Lett.* **2017**, *19*, 2989–2992.
- [42] K. Wang, L. G. Meng, L. Wang, *Org. Lett.* **2017**, *19*, 1958–1961.
- [43] K. Tu, T. Xu, L. Zhang, Z. Cheng, X. Zhu, *RSC Adv.* **2017**, *7*, 24040–24045.
- [44] T. Krappitz, K. Jovic, F. Feist, H. Frisch, V. P. Rigoglioso, J. P. Blinco, A. J. Boydston, C. Barner-Kowollik, *J. Am. Chem. Soc.* **2019**, *141*, 16605–16609.
- [45] J. Li, Z. Liu, S. Wu, Y. Chen, *Org. Lett.* **2019**, *21*, 2077–2080.
- [46] P. D. Morse, D. A. Nicewicz, *Chem. Sci.* **2015**, *6*, 270–274.
- [47] H. T. Qin, S. W. Wu, J. L. Liu, F. Liu, *Chem. Commun.* **2017**, *53*, 1696–1699.
- [48] Y. Y. Loh, K. Nagao, A. J. Hoover, D. Hesk, N. R. Rivera, S. L. Colletti, I. W. Davies, D. W. C. MacMillan, *Science* **2017**, *358*, 1182–1187.
- [49] B. Legros, P. Vandereecken, J. P. Soumillion, *J. Phys. Chem.* **1991**, *95*, 4752–4761.
- [50] E. Vander Donckt, J. Nasielski, P. Thiry, *J. Chem. Soc. D* **1969**, 1249–1250.
- [51] C. Kerzig, M. Goetz, *Phys. Chem. Chem. Phys.* **2015**, *17*, 13829–13836.
- [52] M. Brautzsch, C. Kerzig, M. Goetz, *Green Chem.* **2016**, *18*, 4761–4771.
- [53] M. Schmalzbauer, I. Ghosh, B. König, *Faraday Discuss.* **2019**, *215*, 364–378.
- [54] X. F. Zhang, I. Zhang, L. Liu, *Photochem. Photobiol.* **2010**, *86*, 492–498.
- [55] K. Hashimoto, T. Kawai, T. Sakata, *Chem. Lett.* **1983**, *12*, 709–712.
- [56] E. F. Zwicker, L. I. Grossweiner, *J. Phys. Chem.* **1963**, *67*, 549–555.
- [57] L. I. Grossweiner, E. F. Zwicker, *J. Chem. Phys.* **1961**, *34*, 1411–1417.
- [58] C. Munkholm, D. R. Parkinson, D. R. Walt, *J. Am. Chem. Soc.* **1990**, *112*, 2608–2612.
- [59] T. O. Baldwin, *Structure* **1996**, *4*, 223–228.
- [60] K. J. Hellingwerf, J. Hendriks, T. Gensch, *J. Phys. Chem. A* **2003**, *107*, 1082–1094.
- [61] S. Faraji, A. Dreuw, *Annu. Rev. Phys. Chem.* **2014**, *65*, 275–292.
- [62] W. Lee, G. Kodali, R. J. Stanley, S. Matsika, *Chem. Eur. J.* **2016**, *22*, 11371–11381.
- [63] K. Liang, Q. Liu, L. Shen, X. Li, D. Wei, L. Zheng, C. Xia, *Chem. Sci.* **2020**, doi: <https://doi.org/10.1039/D0SC02160A>.
- [64] J. P. Soumillion, P. Vandereecken, M. Van Der Auweraer, F. C. De Schryver, A. Schanck, *J. Am. Chem. Soc.* **1989**, *111*, 2217–2225.
- [65] J. P. Soumillion, P. Vandereecken, F. C. De Schryver, *Tetrahedron Lett.* **1989**, *30*, 697–700.
- [66] M. Ayadim, J. P. Soumillion, *Tetrahedron Lett.* **1996**, *37*, 381–384.
- [67] A. H. Dwivedi, U. Pande, *J. Photochem. Photobiol. A* **2003**, *154*, 303–309.
- [68] J. F. Art, J. P. Kestemont, J. P. Soumillion, *Tetrahedron Lett.* **1991**, *32*, 1425–1428.
- [69] E. Hasegawa, N. Izumiya, T. Miura, T. Ikoma, H. Iwamoto, S. Y. Takizawa, S. Murata, *J. Org. Chem.* **2018**, *83*, 3921–3927.
- [70] E. Hasegawa, Y. Nagakura, N. Izumiya, K. Matsumoto, T. Tanaka, T. Miura, T. Ikoma, H. Iwamoto, K. Wakamatsu, *J. Org. Chem.* **2018**, *83*, 10813–10825.
- [71] E. Hasegawa, T. Tanaka, N. Izumiya, T. Kiuchi, Y. Ooe, H. Iwamoto, S. Y. Takizawa, S. Murata, *J. Org. Chem.* **2020**, *85*, 4344–4353.
- [72] J. H. Baxendale, *Radiation Res. Suppl.* **1964**, *4*, 139.
- [73] E. J. Hart, *Surv. Prog. Chem.* **1969**, *5*, 129–184.

- [74] G. V. Buxton, C. L. Greenstock, W. P. Heiman, A. B. Ross, *J. Phys. Chem. Ref. Data* **1988**, *17*, 513–886.
- [75] D. Zhu, L. Zhang, R. E. Ruther, R. J. Hamers, *Nat. Mater.* **2013**, *12*, 836–841.
- [76] L. Zhang, D. Zhu, G. M. Nathanson, R. J. Hamers, *Angew. Chem. Int. Ed.* **2014**, *53*, 9746–9750.
- [77] I. Ghosh, R. S. Shaikh, B. König, *Angew. Chem. Int. Ed.* **2017**, *56*, 8544–8549.
- [78] M. Schmalzbauer, T. D. Svejstrup, F. Fricke, P. Brandt, M. J. Johansson, G. Bergonzini, B. König, **2020**, doi: <https://doi.org/10.26434/chemrxiv.12485786.v1>.
- [79] S. Mahboobi, S. Dove, A. Sellmer, M. Winkler, E. Eichhorn, H. Pongratz, T. Ciossek, T. Baer, T. Maier, T. Beckers, *J. Med. Chem.* **2009**, *52*, 2265–2279.
- [80] H. Liu, H. Tang, D. Yang, Q. Ji, *Chinese J. Pharm.* **2011**, *42*, 641–644.
- [81] M. Raghu, J. Grover, S. S. V. Ramasastry, *Chem. Eur. J.* **2016**, *22*, 18316–18321.
- [82] E. Lamy, L. Nadjo, J. M. Saveant, *J. Electroanal. Chem.* **1977**, *78*, 403–407.
- [83] K. Liang, T. Li, N. Li, Y. Zhang, L. Shen, Z. Ma, C. Xia, *Chem. Sci.* **2020**, *11*, 2130–2135.
- [84] G. Filippini, M. Nappi, P. Melchiorre, *Tetrahedron* **2015**, *71*, 4535–4542.
- [85] Q. Wang, M. Poznik, M. Li, P. J. Walsh, J. J. Chruma, *Adv. Synth. Catal.* **2018**, *360*, 2854–2868.
- [86] M. Li, S. Berritt, L. Matuszewski, G. Deng, A. Pascual-Escudero, G. B. Panetti, M. Poznik, X. Yang, J. J. Chruma, P. J. Walsh, *J. Am. Chem. Soc.* **2017**, *139*, 16327–16333.
- [87] T. Zhang, Y. Meng, J. Lu, Y. Yang, G. Q. Li, C. Zhu, *Adv. Synth. Catal.* **2018**, *360*, 3063–3068.
- [88] R. S. Suarez, R. G. Segura, *Tetrahedron Lett.* **1988**, *29*, 1071–1074.
- [89] C. Sánchez-Sánchez, E. Pérez-Inestrosa, R. García-Segura, R. Suau, *Tetrahedron* **2002**, *58*, 7267–7274.
- [90] Y. R. Luo, *Comprehensive Handbook of Chemical Bond Energies*, CRC Press, **2007**.
- [91] K. Maruyama, Y. Kubo, *J. Org. Chem.* **1985**, *50*, 1426–1435.
- [92] R. Suau, C. Sánchez-Sánchez, R. García-Segura, E. Pérez-Inestrosa, *Eur. J. Org. Chem.* **2002**, 1903–1911.
- [93] F. N. Figueroa, A. A. Heredia, A. B. Peñéñory, D. Sampedro, J. E. Argüello, G. Oksdath-Mansilla, *J. Org. Chem.* **2019**, *84*, 3871–3880.
- [94] A. K. Ganguly, S. S. Alluri, D. Caroccia, D. Biswas, C. H. Wang, E. Kang, Y. Zhang, A. T. McPhail, S. S. Carroll, C. Burlein, et al., *J. Med. Chem.* **2011**, *54*, 7176–7183.
- [95] D. K. Rayabarapu, A. Zhou, K. O. Jeon, T. Samarakoon, A. Rolfe, H. Siddiqui, P. R. Hanson, *Tetrahedron* **2009**, *65*, 3180–3188.
- [96] C. G. S. Lima, T. D. M. Lima, M. Duarte, I. D. Jurberg, M. W. Paixão, *ACS Catal.* **2016**, *6*, 1389–1407.
- [97] G. E. M. Crisenza, D. Mazzarella, P. Melchiorre, *J. Am. Chem. Soc.* **2020**, *142*, 5461–5476.
- [98] M. Nappi, G. Bergonzini, P. Melchiorre, *Angew. Chem. Int. Ed.* **2014**, *53*, 4921–4925.
- [99] B. Liu, C. H. Lim, G. M. Miyake, *J. Am. Chem. Soc.* **2017**, *139*, 13616–13619.
- [100] E. Zhu, X. X. Liu, A. J. Wang, T. Mao, L. Zhao, X. Zhang, C. Y. He, *Chem. Commun.* **2019**, *55*, 12259–12262.
- [101] N. Komblum, R. E. Michel, R. C. Kerber, *J. Am. Chem. Soc.* **1966**, *88*, 5662–5663.
- [102] G. A. Russell, W. C. Danen, *J. Am. Chem. Soc.* **1966**, *88*, 5663–5665.
- [103] R. A. Rossi, A. B. Pierini, A. B. Peñéñory, *Chem. Rev.* **2003**, *103*, 71–167.
- [104] M. E. Budén, J. I. Bardagí, M. Puiatti, R. A. Rossi, *J. Org. Chem.* **2017**, *82*, 8325–8333.
- [105] Y. Cheng, X. Gu, P. Li, *Org. Lett.* **2013**, *15*, 2664–2667.
- [106] Z. Xu, L. Gao, L. Wang, M. Gong, W. Wang, R. Yuan, *ACS Catal.* **2015**, *5*, 45–50.

- [107] R. A. Rossi, J. F. Guastavino, M. E. Budén, „Radical-Nucleophilic Aromatic Substitution“, in *Arene Chemistry: Reaction Mechanisms and Methods for Aromatic Compounds* (Ed.: J. Mortier), John Wiley & Sons, Inc., New Jersey, **2015**, pp. 243–268.
- [108] J. I. Bardagí, M. E. Budén, R. A. Rossi, *Targets Heterocycl. Syst.* **2016**, *20*, 247–282.
- [109] M. E. Budén, S. E. Martín, R. A. Rossi, „Recent Advances in the Photoinduced Radical Nucleophilic Substitution Reactions“, in *CRC Handbook of Organic Photochemistry and Photobiology* (Eds.: A. Griesbeck, M. Oelgemöller, F. Ghetti), CRC Press, Boca Raton, **2012**, pp. 347–368.
- [110] A. B. Peñeñory, J. E. Argüello, „Aromatic and Heteroaromatic Substitution by $S_{RN}1$ and S_N1 Reactions“, in *Handbook of Synthetic Photochemistry* (Eds.: A. Albini, M. Fagnoni), Wiley-VCH, Weinheim, **2010**, pp. 319–351.
- [111] A. Studer, D. P. Curran, *Nat. Chem.* **2014**, *6*, 765–773.
- [112] M. K. Nazeeruddin, R. Humphry-Baker, D. Berner, S. Rivier, L. Zuppiroli, M. Graetzel, *J. Am. Chem. Soc.* **2003**, *125*, 8790–8797.
- [113] A. Ionescu, E. I. Szerb, Y. J. Yadav, A. M. Talarico, M. Ghedini, N. Godbert, *Dalton Trans.* **2014**, *43*, 784–789.
- [114] S. Y. Takizawa, R. Kano, N. Ikuta, S. Murata, *Dalton Trans.* **2018**, *47*, 11041–11046.
- [115] C. Kerzig, X. Guo, O. S. Wenger, *J. Am. Chem. Soc.* **2019**, *141*, 2122–2127.
- [116] H. Yin, Y. Jin, J. E. Hertzog, K. C. Mullane, P. J. Carroll, B. C. Manor, J. M. Anna, E. J. Schelter, *J. Am. Chem. Soc.* **2016**, *138*, 16266–16273.
- [117] Potential is reported *vs.* the Fc^+/Fc couple and was converted against SCE by adding +380 mV (see ref.^[118]).
- [118] V. V. Pavlishchuk, A. W. Addison, *Inorganica Chim. Acta* **2000**, *298*, 97–102.
- [119] L. L. Costanzo, S. Pistarà, G. Condorelli, *J. Photochem.* **1983**, *21*, 45–51.
- [120] Y. Qiao, Q. Yang, E. J. Schelter, *Angew. Chem. Int. Ed.* **2018**, *57*, 10999–11003.
- [121] D. Ravelli, M. Fagnoni, T. Fukuyama, T. Nishikawa, I. Ryu, *ACS Catal.* **2018**, *8*, 701–713.
- [122] V. De Waele, O. Poizat, M. Fagnoni, A. Bagno, D. Ravelli, *ACS Catal.* **2016**, *6*, 7174–7182.
- [123] X. Li, J. Ma, G. Liu, J. Fang, S. Yue, Y. Guan, L. Chen, X. Liu, *Environ. Sci. Technol.* **2012**, *46*, 7342–7349.
- [124] Y. Gu, W. Dong, C. Luo, T. Liu, *Environ. Sci. Technol.* **2016**, *50*, 10554–10561.

CHAPTER 2

2 Anthraquinones as Photoredox Catalysts for the Reductive Activation of Aryl Halides



This chapter has been published in: J. I. Bardagí, I. Ghosh, M. Schmalzbauer, T. Ghosh, B. König *Eur. J. Org. Chem.* **2018**, 34-40. – Reproduced with permission from John Wiley and Sons.

The experiments have been carried out in cooperation with Javier I. Bardagí, Indrajit Ghosh and Tamal Ghosh. M. Schmalzbauer isolated a part of the compounds (**3c**, **e**, **g**, **h**, **m**) presented in Figure 2-2, assisted J.I.B. and I.G. in mechanistic investigations and revised the manuscript and the Experimental Part.

Abstract

Quinones are ubiquitous in nature and are found as structural motif of natural products or redox mediator in biological electron transfer processes. While their oxidation properties have already been widely used in chemical and photochemical reactions, applications of quinones in reductive photoredox catalysis are less explored. In this chapter we report the visible-light photoreduction of aryl halides (Ar-X ; where $\text{X} = \text{Cl}, \text{Br}, \text{I}$) by 1,8-dihydroxyanthraquinone. The resulting aryl radical anions fragment into halide anions and aryl radicals, which are converted in hydrogen abstraction or C–C bond forming reactions. The active photocatalyst is generated *in-situ* from 1,8-dihydroxyanthraquinone by photoinduced single electron reduction to form the radical anion or *via* subsequent protonation and further reduction (or *vice versa*) to yield the semiquinone anion. Succeeding visible-light excitation of the anthraquinone radical anion or semiquinone anion converts them into very potent single electron donors. A plausible mechanism of the reaction is proposed based on control experiments and spectroscopic observations.

2.1 Introduction

The use of visible light for the generation of reactive intermediates in organic transformations has many advantages, and the growing interest in catalytic, visible-light-mediated transformations over the last decade demonstrates the feasibility of the approach.^[1-9] Ru- and Ir-based coordination complexes have received enormous attention because of their excellent visible-light-harvesting properties, modest to high oxidation and reduction potentials, relatively long excited-state lifetimes and reasonably good chemical- and photo-stabilities under oxidative and reductive conditions.^[2] In addition, considerable efforts have been made to develop catalytic and metal-free versions by using organic dyes,^[8,10-14] such as eosin Y^[10,11] or rhodamine derivatives^[13,14] and organic heterogeneous photocatalysts^[15] for synthetic transformations.

Quinones^[8,16-17] occur in nature and are known for their excellent electron accepting and hydrogen-abstracting abilities.^[16,18] Not surprisingly, different quinone derivatives have been used for photooxidative transformations under visible light.^[19-22] Fukuzumi reported the photoredox catalytic conversion of benzene to phenol with 2,3-dichloro-5,6-dicyano-*p*-benzoquinone (DDQ) under visible-light irradiation.^[23] Itoh and subsequently Yuan reported the trifluoromethylations of arenes and heteroarenes with anthraquinone-2-carboxylic acid^[24] and DDQ,^[25] respectively. In addition, Itoh reported the synthesis of carboxylic acids from their respective methyl aromatics with 2-chloroanthraquinone.^[26] Recently, Brasholz disclosed cascade dehydrogenation/ 6π -cyclization/oxidation reactions of 1-(nitromethyl)-2-aryltetrahydroisoquinolines in the presence of 1-aminoanthraquinone to obtain tetracyclic 12-nitroindolo[2,1-*d*]isoquinoline products.^[19] Similarly, the same group also reported an intermolecular version with 1,5-diaminoanthraquinone as a photocatalyst for the synthetic transformations of *N*-aryl-tetrahydroisoquinolines and nitromethane to prepare the same product.

Anthraquinone (**Aq**) and its derivatives (Figure 2-1 A) form colored radical anions upon single-electron reduction [see Figure 2-1 B for the absorption spectra of the electrochemically generated radical anion of 1,8-dihydroxyanthraquinone (**Aq-OH**)]. The radical anions of anthraquinones possess moderate reduction potentials in their ground state [*e.g.*, $E^0(\text{Aq}/\text{Aq}^{\cdot-})$ and $E^0(\text{Aq-OH}/\text{Aq-OH}^{\cdot-})$ are -0.82 V and -0.55 V *vs.* SCE, respectively]^[27] and can be accessed electrochemically, chemically, or through photoinduced electron transfer (PET) pro-

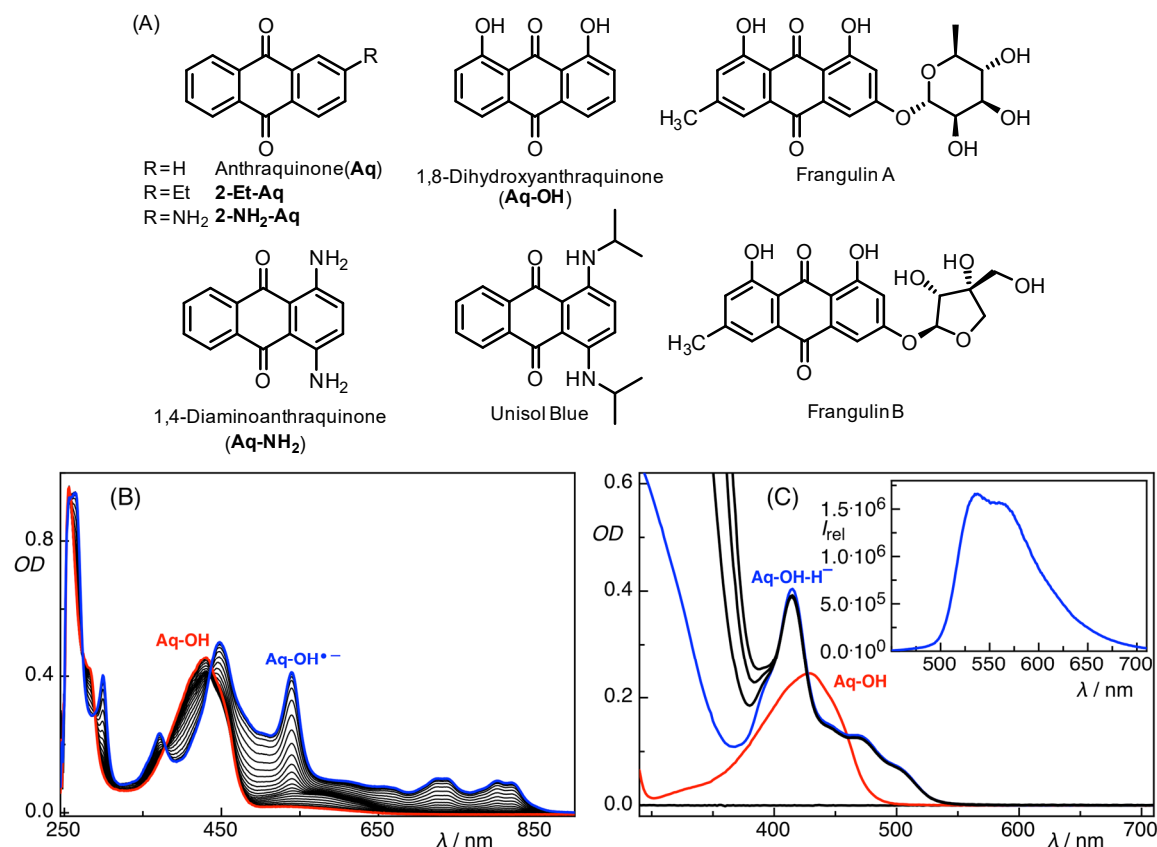


Figure 2-1. (A) Chemical structures of anthraquinone derivatives investigated herein. (B) Spectroelectrochemistry of **Aq-OH** in deaerated DMF. (C) Formation of the 1,8-dihydroxyanthraquinone semiquinone anion (**Aq-OH-H⁻**) in the presence of Na₂S₂O₄.^[40] In the inset, the luminescence spectrum (λ_{ex} = 427 nm) of **Aq-OH-H⁻** is shown. For the formation of the radical anion and the semiquinone anion of **Aq-OH** upon photoirradiation in the presence of Et₃N, see Figure 2-3.

cesses in the presence of a suitable electron donor under an inert atmosphere (see Figure 2-3 A). Eggs^[28] as well as Lund and Eriksen^[29] showed that the excited states of colored radical anions of **Aq** (or in general quinone derivatives, see ref.^[28]) are powerful reductants and can transfer electrons to organic substrates with extremely negative reduction potentials (*e.g.*, 1,2-dibromobenzene, an aryl halide substrate with a reduction potential of -1.88 V *vs.* SCE).^[28] Although the radical anions of quinone derivatives are common intermediates in natural and synthetic photochemical energy storage,^[16,30] they have not yet been applied as photocatalysts for reductive transformations. As the excited states of radical anions act as powerful reductants,^[12-13,28-29,31] we envisioned that anthraquinone derivatives could be employed for the photoredox catalytic reduction of aryl halide substrates, including challenging aryl chlorides, to obtain aryl radicals for metal-free dehalogenation reactions^[12,32-35] or for synthetically important carbon-carbon^[12,32,36-38] bond-forming reactions. Such catalytic photoredox methods^[12-13,32-39] are valuable alternatives to well-established transition-metal-based activation

techniques. Herein, we report the use of 1,8-dihydroxyanthraquinone as a photocatalyst to forge new C–C bonds starting from bench-stable aryl halides under visible-light irradiation.

2.2 Results and Discussion

We began our investigations with methyl 2-bromobenzoate (**1a**) as a test substrate and 1,8-dihydroxyanthraquinone as photoredox catalyst. A mixture of **1a**, **Aq-OH** (10 mol%) and Et₃N (1.0 equiv., as a sacrificial electron donor and hydrogen atom donor, see below) was irradiated in *N,N*-dimethylformamide (DMF) with a blue light-emitting diode

Table 2-1. Control reactions and optimization of the photoredox catalytic reduction conditions with methyl 2-bromobenzoate (**1a**) as a test substrate.^a

Entry	Donor (equiv.)	Catalyst (mol%)	Conditions	Yield [%] (conversion, %) ^b
<i>Control reactions</i>				
1	Et ₃ N (1.0)	Aq-OH (10)	455 nm, 24 h	61 (80)
2	Et ₃ N (1.0)	Aq-OH (10)	455 nm, 48 h	74 (90)
3	-	-	455 nm, 48 h	0 (1) ^c
4	Et ₃ N (1.0)	-	455 nm, 48 h	≥ 1 (2) ^c
5	-	Aq-OH (10)	455 nm, 48 h	13 (24)
6	Et ₃ N (1.0)	Aq-OH (10)	Dark , 48 h	0 (0) ^c
7	Et ₃ N (1.0)	Aq-OH (10)	455 nm, 48 h	9 (11) ^d
<i>Optimization of the reaction condition</i>				
8	Et ₃ N (1.0)	Aq-OH (2)	455 nm, 24 h	47 (58)
9	Et ₃ N (1.0)	Aq-OH (5)	455 nm, 24 h	44 (54)
10	Et ₃ N (0.7)	Aq-OH (10)	455 nm, 24 h	47 (64)
<i>Different anthraquinone derivatives</i> ^e				
11	Et ₃ N (1.0)	Aq (10)	455 nm, 24 h	35 (62)
12	Et ₃ N (1.0)	2-Et-Aq (10)	455 nm, 24 h	34 (62)
13	Et ₃ N (1.0)	2-NH₂-Aq (10)	455 nm, 24 h	48 (76)
14	Et ₃ N (1.0)	Aq-NH₂ (10)	455 nm, 24 h	6 (18)
15	Et ₃ N (1.0)	Unisol Blue (10)	455 nm, 24 h	3 (16)
16	Et ₃ N (1.0)	Frangulin (10)	455 nm, 24 h	58 (74)

^a Reactions were performed under nitrogen with **1a** in DMF (1.0 mL) with a blue LED ($\lambda_{\text{Ex}} = 455 \pm 15$ nm, See Experimental Part for the reaction setup); ^b Calculated from GC-FID analysis (error *ca.* $\pm 5\%$) by the internal-standard method (see Experimental Part for details). The substrate conversion is shown in parenthesis; ^c The yield is below the GC quantification limit; ^d The reaction was performed with 4-bromoanisole as substrate; ^e See Figure 2-1 A for chemical structures.

(LED, $\lambda_{\text{ex}} = 455 \pm 15$ nm) for 24 h. Methyl benzoate (**2a**) was obtained in 61% yield (Table 2-1, Entry 1).^[41] Continuous irradiation of the same reaction mixture for 48 h gave **2a** in 74% yield along with *ca.* 90% substrate conversion. Control experiments with the omission of each of the individual catalytic components confirmed, that the photocatalyst, electron donor, and most importantly light irradiation are necessary for the dehalogenation reactions to occur (Table 2-1, Entry 1-6). Among the other derivatives of anthraquinone, including Unisol Blue, which is used for microscopy, **Aq-OH** was selected for further experiments because of the better product yield (*cf.*, Entry 1 and 11-15). Naturally occurring Frangulin A/B, which are derivatives of 1,8-dihydroxyanthraquinone, perform as well as **Aq-OH** (Entry 16); therefore, this core structure has superior catalytic performance.

After the optimization of the reaction conditions (see Table 2-1, Entry 1-2 and 8-10), which required the simple mixing of aryl halides, commercially available inexpensive **Aq-OH**, Et₃N, and photoirradiation with blue LEDs under nitrogen, the scope of the method was explored with different aryl halide substrates. Good-to-excellent photoreduction yields (up to 87%) were obtained with aryl bromide substrates possessing different functional groups, for example, -CN, -CO₂Me (*-o*, *-m*, and *-p*), -CHO, -COMe, and -CONH₂ (see Figure 2-2) which highlights the mild reaction conditions employed. Using bromobenzene resulted in poor product yield indicative for its very challenging reduction potential. The yield increased with iodobenzene as the substrate (25%); the reduction of 4-iodotoluene proceeded in 27% yield, and the reduction of 4'-iodoacetophenone proceeded in 60% yield. Aryl chloride substrates with suitable reduction potentials (*e.g.*, 2-chlorobenzonitrile) could also be activated by this catalytic method. However, aryl halide substrates with very high reduction potentials (*e.g.*, 4-bromoanisole) could not be activated effectively for synthetically useful transformations and demonstrate the limitations of the substrate scope. The photoredox catalytic SET dehalogenation reactions proceed *via* a radical mechanism, as strongly supported by the experimental results and recent reports.^[32,42] Additionally, reaction mixtures containing 4'-bromoacetophenone and 2-bromobenzonitrile were irradiated in the presence of 1,1-diphenylethylene, which is a radical scavenger,^[43-44] and the coupling products **3n** and **3o** + **3p** were obtained in 42% and 58% isolated yields (see Figure 2-2 and the Experimental Part for further details). These results provide further evidence for the radical nature of the reaction.

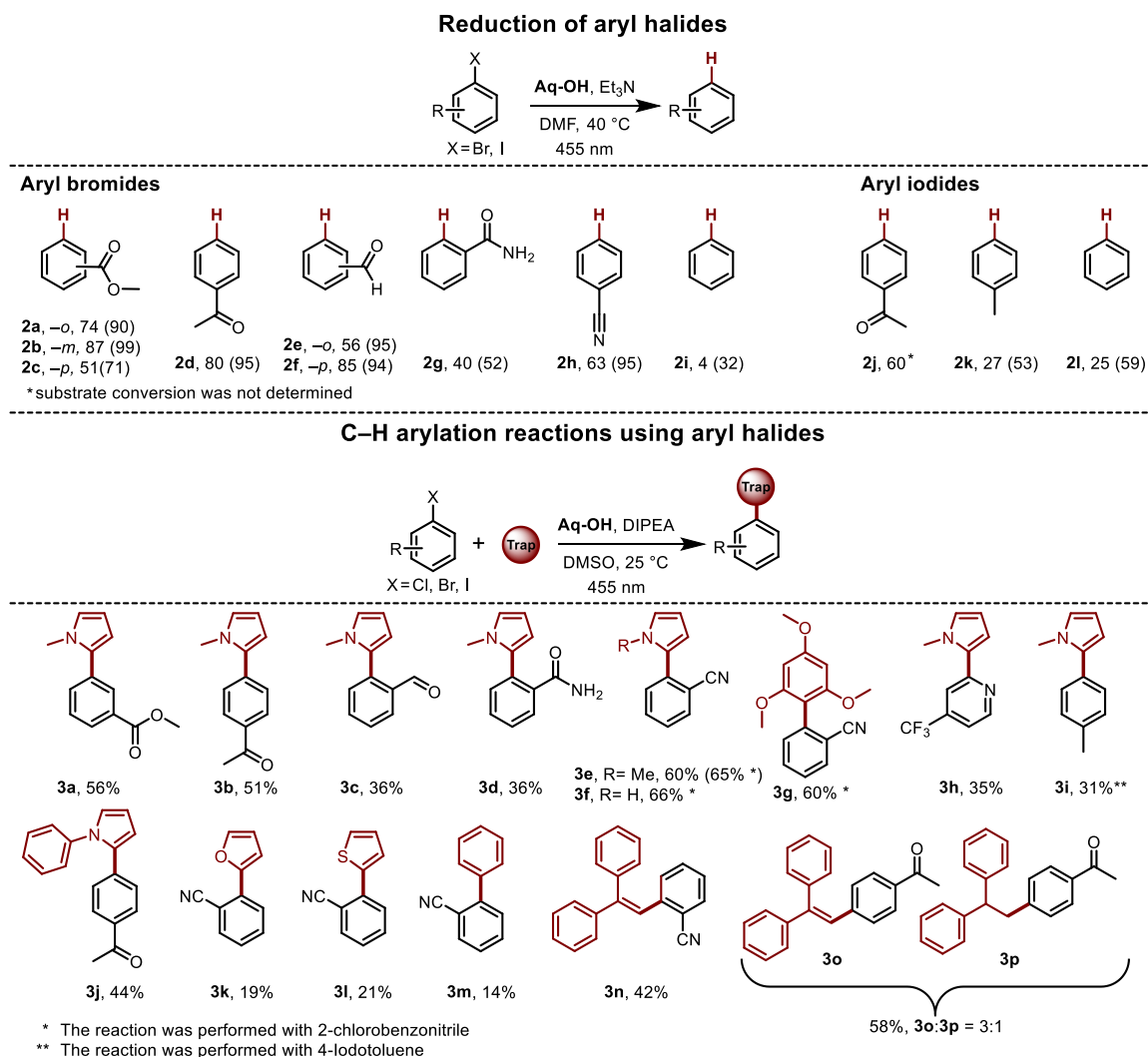
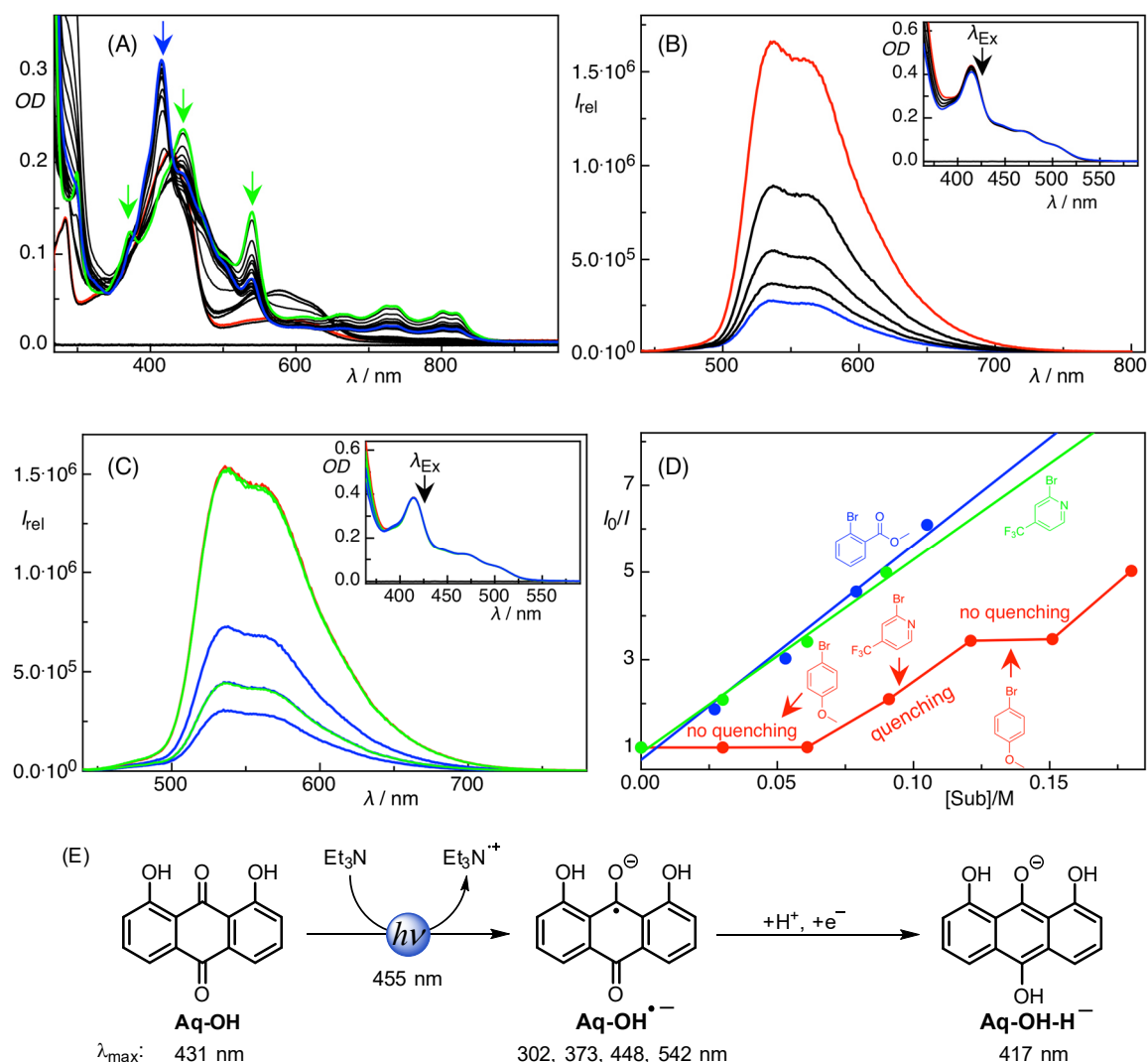


Figure 2-2. Yields for photoredox catalytic reductions and C–C bond forming reactions with aryl halide substrates (Ar–X; X = I, Br, Cl). For the photoreduction reactions, the substrate conversions after 48 h are shown in parentheses (also see the Experimental Part).

We explored the photoredox catalytic generation of aryl radicals from their respective halides for C–C bond-forming reactions with arenes, heteroarenes, and unsaturated double bonds. The main challenge in this case, is the competing hydrogen atom abstraction by the reactive aryl radicals either from the radical cation of the amine or from the solvent. This undesired side-reaction causes the formation of the defunctionalized substrate and was also observed for other photoredox catalytic C–H arylation reactions of aryl halides.^[12–13,32,36–38] However, when a reaction mixture containing 2-bromobenzonitrile, **Aq-OH**, *N,N*-diisopropylethylamine (DIPEA) and benzene was irradiated with blue LEDs, the desired product **3m** was obtained in 14% yield.^[45] Similarly, when furan and thiophene were introduced as the radical trapping reagents, the desired products **3k** and **3l** were obtained in useful yields. Note that thiophene

and furan efficiently trap aryl radicals under photoredox conditions in redox-neutral reactions, in which the excited state of the photocatalyst transfers an electron to the aryl radical precursor and no sacrificial electron donor is necessary (*e.g.*, the photoredox catalytic generation of aryl radicals from their respective diazonium salts).^[11,32]



However, they consistently fail to trap aryl radicals generated from the respective aryl halides under other reported photoredox catalytic conditions. For instance, it has recently been reported that thiophene and furan fail to trap 2-benzothiazole radicals generated through SET from the respective bromides under photoredox catalytic conditions in the presence of *fac*-Ir(ppy)₃ (ppy = 2-phenylpyridine) and R₃N as an electron donor.^[36] The reason for this is still unclear and needs further detailed investigations. The **Aq-OH** photoredox catalytic system enables the C–H arylation of thiophene and furan, albeit in low isolated yields of *ca.* 20%. When 1,3,5-trimethoxybenzene, a substituted arene, was used as a trapping reagent for the 2-cyanophenyl radical, the desired product was obtained in 60% isolated yield. For pyrrole derivatives as trapping reagents, the C–H arylated products were isolated in moderate-to-good yields. Notably, also unprotected pyrrole reacts smoothly with the aryl radicals. All investigated heterocycles (*i.e.*, furan, thiophene, and pyrrole derivatives) were selectively arylated at the 2-position (*cf.*, Figure 2-2). The C–H functionalization reaction of 1,1-diphenylethylene with 2-bromobenzonitrile gave **3n** in 42% yield. 4'-Bromoacetophenone gave a mixture of **3o** and **3p** in 58% isolated yield and this result confirmed that both the hydrogen atom abstraction and the oxidation reaction occur after the aryl radical addition step (see Figure S2-3). The C–H arylation reactions were also effective for aryl chlorides as the precursors of the aryl radicals. Utilizing 2-chlorobenzonitrile resulted in the formation of **3e–3g** in good isolated yields.

The presence of different photo- and redox-active species (including all intermediates in the reaction mixture) under the synthetic reaction conditions and the challenges of performing spectroscopic and electrochemical experiments under non-idealized reaction conditions do not allow us to report a complete mechanism. However, on the basis of previous reports^[28–29,32,42] and spectroscopic investigations (see Figures 2-1 and 2-3 and the Experimental Part), a proposed mechanism is depicted in Figure 2-4. The reaction did not yield any photoreduction products (see Table 2-1, Entry 6) or C–H arylated products in the dark. No luminescence quenching of **Aq-OH** in presence of **1a** indicates that the excited state of **Aq-OH** is not responsible for the initiation of the SET to the aryl halides (Figure S2-1). Upon visible-light excitation, the excited state of **Aq-OH** is quenched by Et₃N to generate the radical anion **Aq-OH^{•-}** (and the radical cation of Et₃N, *i.e.*, Et₃N^{•+}) which forms the semiquinone, **Aq-OH-H⁻**, through protonation and successive reduction (or *vice versa* through consecutive or coupled steps). The presence of both **Aq-OH^{•-}** and **Aq-OH-H⁻** species was confirmed by

the irradiation of a mixture of **Aq-OH** and Et₃N under nitrogen in DMF and dimethyl sulfoxide (DMSO, see Figures 2-3 A and S2-2). Notably, the electron transfer from the ground-state radical anion of anthraquinone or the semiquinone anion to the aryl halide substrates is thermodynamically unlikely owing to their intrinsically low ground-state potentials (*cf.*, $E^0(\text{Aq-OH}/\text{Aq-OH}^{\bullet-}) \approx -0.5 \text{ V vs. SCE}$ and ref.^[46]).

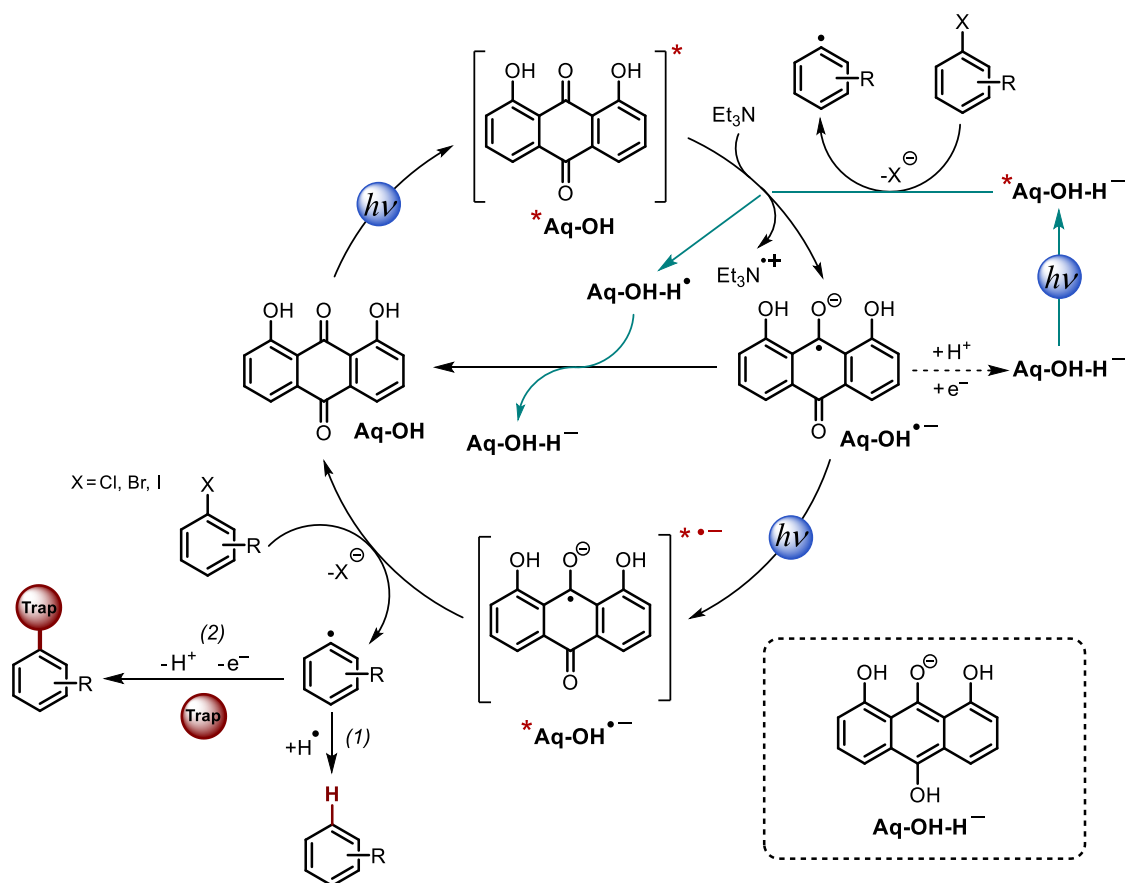


Figure 2-4. Proposed mechanism for the photoredox catalytic cycle for the photoreduction of aryl halides and C–C bond-forming reactions with suitable trapping reagents.

The semiquinone anion **Aq-OH-H[−]** could be generated chemically in the presence of Na₂S₂O₄ under nitrogen atmosphere (see Figure 2-1) and showed luminescence.^[40,47] The absorption spectrum of **Aq-OH-H[−]** did not change upon addition of **1a**, but the **Aq-OH-H[−]** luminescence was significantly quenched (Figure 2-3). The luminescence of **Aq-OH-H[−]** was also quenched in the presence of 2-bromo-4-(trifluoromethyl)pyridine (another investigated substrate), but no significant change was observed when 4-bromoanisole (a substrate that is difficult to activate under the photoredox catalytic conditions) was added. A competitive quenching experiment (see Figure 2-3), in which 2-bromo-4-(trifluoromethyl)pyridine and 4-

bromoanisole were added alternately, gave the expected luminescence responses [*i.e.*, when 4-bromoanisole was added the luminescence remained unaltered, but the luminescence was quenched when 2-bromo-4-(trifluoromethyl)pyridine was added to the same solution]. Thus, we propose an electron transfer from the photoexcited radical anion **Aq-OH^{•-}** to the investigated aryl halide. Previous work^[28-29] on the luminescence quenching of the excited state of **Aq^{•-}** by aryl halides supports this assumption. Initiated by the SET to aryl halides (Ar-X, X = Cl, Br, and I), the generated radical anion subsequently fragments to yield aryl radicals that either (1) abstract a hydrogen atom from the radical cation of R₃N (*i.e.*, Et₃N^{•+} or DIPEA^{•+}) or from the solvent molecules (in this case, DMF or DMSO) to yield the reduction product or (2) react with (hetero)arenes or unsaturated double bonds to yield the corresponding C-C coupling products after oxidation and release of a proton (Figure 2-4). Gas chromatography-mass spectrometry (GC-MS) analysis of the crude product mixture confirmed the formation of diethylamine (see Figure S2-3). During the photoreaction, **Aq-OH** degrades. Such bleaching is often observed in photoredox catalytic reactions with organic dyes^[44] or transition-metal photocatalysts.^[48] In addition, the formation of substituted **Aq-OH** from a reaction with the aryl radicals was observed.^[49] These photoproducts can continue to participate in the photoredox transformations.^[50]

2.3 Conclusion

Radical anions and semiquinone anions of anthraquinones, a class of quinoid compounds, gain sufficient redox energy under visible-light irradiation to perform synthetically challenging reductive transformations. 1,8-Dihydroxyanthraquinone (**Aq-OH**) forms its colored radical anion and semiquinone anion upon visible-light irradiation in the presence of R₃N under nitrogen atmosphere. The radical anion and the semiquinone anion are excited by visible light and transfer a single electron to aryl halides, which react in dehalogenation or C-C bond forming reactions. We believe that the described results will pave the way to a broader use of commercially available and inexpensive anthraquinone derivatives in synthetic photoredox catalysis for reductive transformations.

2.4 Experimental Part

2.4.1 General Information

Aryl halides, investigated anthraquinone-derivatives and Unisol Blue were commercially available and used without further purification unless otherwise stated. Spectroscopic grade DMF and DMSO were dried with 3 Å molecular sieves following a reported procedure.^[51] Thin-layer chromatography was performed using silica gel plates 60 F254: Visualization was accomplished with short wavelength UV light (254 nm) and near UV light (366 nm) sources. Standard flash chromatography was performed on a Biotage® Isolera™ Spektra automated with high performance flash purification system using silica gel of particle size 40–63 µm or a reverse column (specification: Biotage® SNAP KP-C18-HS). ¹H- and ¹³C-NMR spectra were recorded on Bruker Avance spectrometers (300 MHz and 75 MHz or 400 MHz and 101 MHz) in CDCl₃ or DMSO-d₆ solution with internal solvent signal as reference (7.26 and 77.0, 2.50 and 39.4, respectively). Proton NMR data are reported as follows: chemical shift (ppm), multiplicity (s = singlet, d = doublet, t = triplet, q = quartet, quint = quintet, sext = sextet, hept = heptet, dd = doublet of doublets, ddd = doublet of doublets of doublets, td = triplet of doublets, qd = quartet of doublets, m = multiplet, br. s. = broad singlet), coupling constants (Hz) and numbers of protons. Data for ¹³C-NMR are reported in terms of chemical shift and no special nomenclature is used for equivalent carbons. High resolution mass spectra (HRMS) were obtained from the central analytic mass spectrometry facilities of the Faculty of Chemistry and Pharmacy, Regensburg University and are reported according to the IUPAC recommendations 2013. Gas chromatography (GC) and gas chromatography coupled to low-resolution mass spectrometry (GC-MS) analysis were performed using a capillary column (length: 30 m; diam. 0.25 mm; film: 0.25 µm) using He gas as carrier. GC was equipped with an FID detector. GC-MS was performed on 5975 MSD single quadrupole detector. Reduction products were identified by comparing with authentic samples (GC-FID and GC-MS). Quantification of reduction products was performed by GC-FID by the internal standard method. UV-Vis and fluorescence measurements were performed with Agilent Cary 100 UV–Vis spectrophotometer and Horiba FluoroMax-4 spectrofluorometer, respectively. Electrochemical studies were carried out under argon atmosphere. The measurements were performed in dimethylformamide (DMF) containing 0.1 M tetra-*n*-butylammonium tetrafluoroborate using ferrocene/ferrocenium (Fc/Fc⁺) as an internal reference. A glassy carbon electrode (working electrode), platinum wire counter electrode, and Ag quasi-reference

electrode were employed. Spectroelectrochemical studies were carried out in an optically transparent thin layer electrochemical cell (OTTLE). Photoirradiation experiments were followed by UV-vis spectroscopy and performed in a fluorescence cuvette with a stirring bar and a blue LED ($\lambda = 455 \text{ nm}$ ($\pm 15 \text{ nm}$)) was used at a right angle with respect to the UV-vis detector. Photoreduction and C–H arylation reactions were performed with 455 nm LEDs (OSRAM Oslon SSL 80 royal-blue LEDs ($\lambda = 455 \text{ nm}$ ($\pm 15 \text{ nm}$)), 3.5 V, 700 mA).

2.4.2 General Procedures

2.4.2.1 General procedure for the photoreduction of aryl halides (Method A)

In a 5 mL snap vial equipped with a magnetic stirring bar, the respective aryl halide (0.1 mmol, 1.0 equiv) and catalyst (0.01 mmol, 0.10 equiv.) were dissolved in dry DMF (total volume of the solution 1.0 mL) and the resulting mixture was degassed (2 \times) with a syringe needle. Triethylamine (0.10 mmol, 1.0 equiv.) was added under N₂ and the reaction mixture was irradiated through the plane bottom side of the snap vial at 40 °C with a LED ($\lambda = 455 \text{ nm}$). The reaction progress was monitored by GC-FID analysis. The yields of the reduction products were determined from GC measurements with appropriate internal standards.

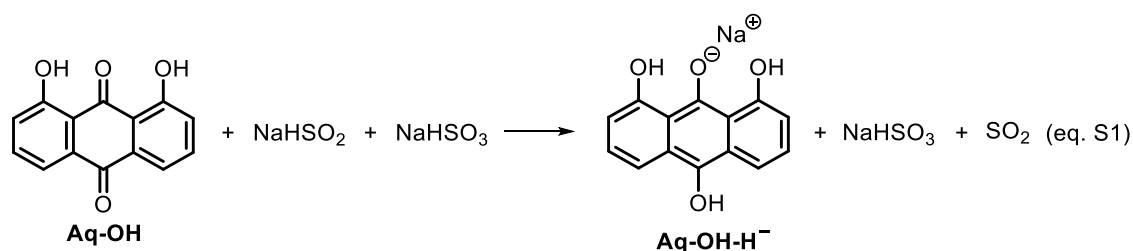
2.4.2.2 General procedure for C–H arylation reactions (Method B)

In a 5 mL snap vial equipped with a magnetic stirring bar, the aryl halide (0.2 mmol, 1.0 equiv.) and **Aq-OH** (0.02 mmol, 0.1 equiv) were dissolved in dry DMSO (total volume of the solution 1.0 mL), and the resulting mixture was degassed with a syringe needle. DIPEA (0.20–0.40 mmol, 1–2 equiv.) and the corresponding trapping reagent (4.0–6.0 mmol, 20–30 equiv.) were added under N₂ and the reaction mixture was irradiated through the plane bottom side of the snap vial at 25 °C with a blue LED ($\lambda = 455 \text{ nm}$) for the time reported. The reaction progress was monitored by GC analysis until full conversion was obtained or the reaction slowed down significantly. For work-up, one of the two following procedures was used: (1) The reaction mixture was transferred into a separating funnel and distilled water (10 mL) and brine (2 mL) were added. The resulting mixture was extracted with ethyl acetate (3 \times 10 mL). The combined organic layers were dried over MgSO₄, filtered and concentrated *in vacuo*. Silica gel (*ca.* 1.0 g) was added to prepare the dry load for column chromatography. (2) The reaction mixture was transferred into a flask and DMSO was partially evaporated (*ca.* 0.5 mL) under

reduced pressure. Ethyl acetate (10 mL) and silica gel (*ca.* 1.0 g) were added to prepare the dry load for column chromatography. In both methods, purification was achieved by flash column chromatography with petrol ether/ethyl acetate as the eluent.

2.4.3 Supporting Spectroscopic Investigations

Preparation of 1,8-dihydroxyanthraquinone semiquinone anion (Aq-OH-H⁻) for spectroscopic investigations: In a 15 mL snap vial, a concentrated solution (*ca.* 0.01 M) of 1,8-dihydroxy-9,10-anthraquinone (**Aq-OH**) was prepared in DMSO or DMF. From this solution, a dilute solution of *ca.* 2.5×10^{-5} M was prepared and degassed by syringe needle. The dilute solution was poured in a cuvette with a septum screw cap and degassed again by syringe needle. Formation of semiquinone anion **Aq-OH-H⁻** was performed in the cuvette by addition (*ca.* 10 μ L) of freshly prepared (used within *ca.* 10–20 mins) aqueous solution of Na₂S₂O₄ (*ca.* 0.1 M) according to eq. S1.



Preparation of aqueous solution of Na₂S₂O₄: In a 10 mL snap vial, Na₂S₂O₄ (260 mg) was weighed in and degassed by syringe needle. Then degassed water (15 mL) was added by syringe and the solution was used immediately.

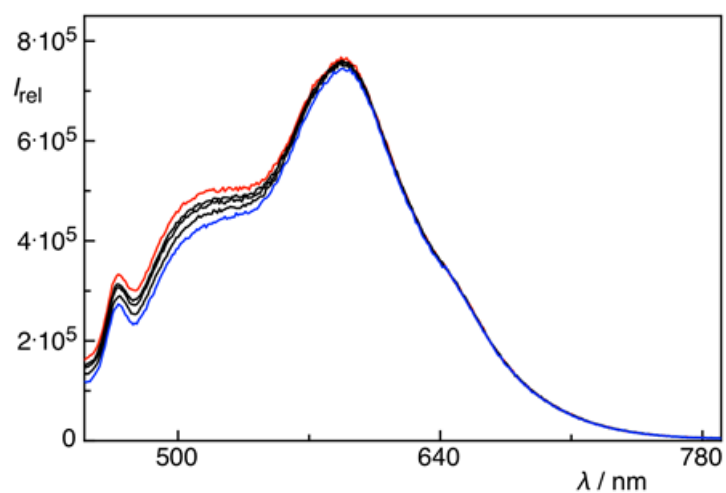


Figure S2-1. Changes in the fluorescence spectra of 1,8-dihydroxyanthraquinone (**Aq-OH**) upon successive addition of methyl 2-bromobenzoate (**1a**, test substrate).

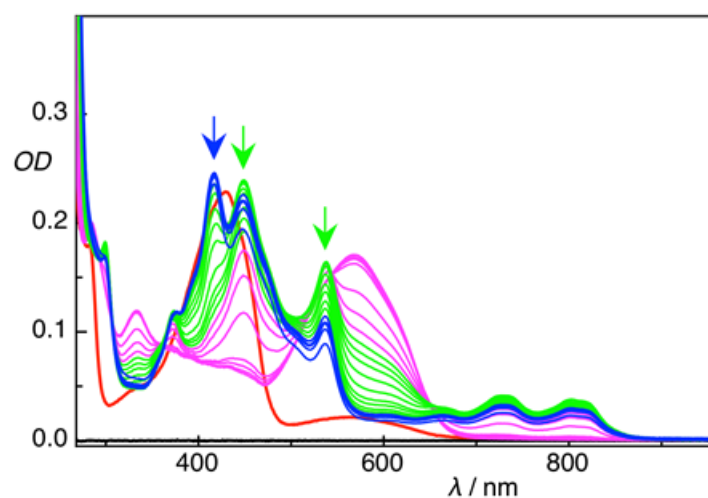


Figure S2-2. Changes in the absorption spectra of **Aq-OH** (red) upon addition of Et_3N , and successive photoirradiation ($\lambda_{\text{Ex}} = 455 \pm 15 \text{ nm}$) in DMSO under nitrogen atmosphere. The green and blue arrows indicate the absorption maxima of **Aq-OH** $^{\bullet-}$ and **Aq-OH-H** $^{\bullet-}$ respectively.

2.4.4 Detailed proposed Mechanism

A detailed proposed mechanism for the photocatalyzed dehalogenation and C–H arylation of aryl halides in presence of 1,8-dihydroxyanthraquinone as catalyst is depicted in Figure S2-3.

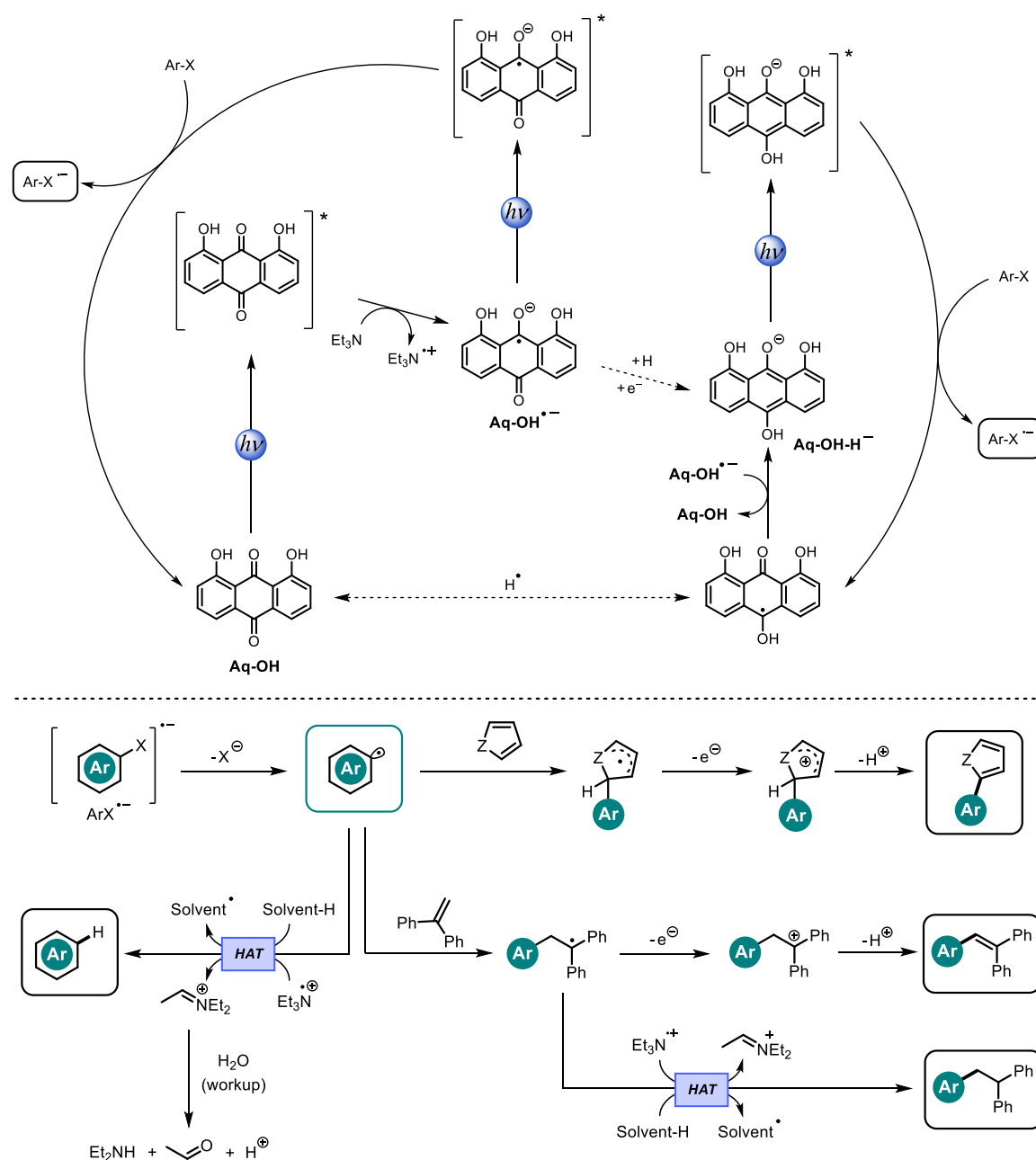
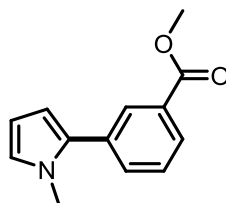


Figure S2-3. Detailed catalytic cycle proposed for the Aq-OH-catalyzed photoreduction of aryl halides and C–H arylation reactions using aryl halides.

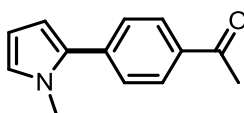
2.4.5 Characterization of the Products

Methyl 3-(1-methyl-1*H*-pyrrol-2-yl)benzoate (3a)

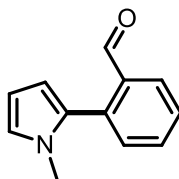


The compound was prepared according to the general procedure using methyl 3-bromobenzoate (44.6 mg, 0.2 mmol, 1 equiv.), 1,8-dihydroxy-9,10-anthraquinone (4.8 mg, 0.02 mmol, 10 mol%), *N*-methylpyrrole (0.36 mL, 4 mmol, 20 equiv.) and diisopropylethylamine (70 μ L, 0.4 mmol, 2 equiv.). 90% conversion was obtained after 62 h. Method B(1) was used for work-up. Colorless oil. **¹H-NMR** (300 MHz, CDCl₃): 8.09 (t, *J* = 1.6 Hz, 1H), 7.98 – 7.95 (m, 1H), 7.61 – 7.58 (m, 1H), 7.47 (t, *J* = 7.7 Hz, 1H), 6.75 – 6.74 (m, 1H), 6.29 (dd, *J* = 3.6, 1.5 Hz, 1H), 6.23 – 6.21 (m, 1H), 3.94 (s, 3H), 3.69 (s, 3H). **¹³C-NMR** (75 MHz, CDCl₃) δ 167.0, 133.6, 133.5, 132.9, 130.3, 129.5, 128.5, 127.7, 124.24, 109.3, 108.0, 52.2, 35.2. Data is in accordance with literature.^[12]

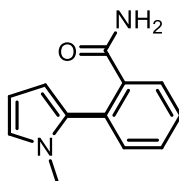
4-(1-Methyl-1*H*-pyrrol-2-yl)acetophenone (3b)



The compound was prepared according to the general procedure using 4-bromoacetophenone (40.4 mg, 0.2 mmol, 1 equiv.), 1,8-dihydroxy-9,10-anthraquinone (4.8 mg, 0.02 mmol, 10 mol%), *N*-methylpyrrole (0.36 mL, 4 mmol, 20 equiv.) and diisopropylethylamine (70 μ L, 0.4 mmol, 2 equiv.). Full conversion was obtained after 96 h. Method B(2) was used for work-up. Yellow oil. **¹H-NMR** (300 MHz, CDCl₃): δ 7.99 (d, *J* = 8.5 Hz, 2H), 7.50 (d, *J* = 8.5 Hz, 2H), 6.78 – 6.77 (m, 1H), 6.35 (dd, *J* = 3.6, 1.8 Hz, 1H), 6.23 (dd, *J* = 3.5, 2.8 Hz, 1H), 3.73 (s, 3H), 2.63 (s, 3H). **¹³C-NMR** (75 MHz, CDCl₃): δ 197.6, 137.9, 134.9, 133.4, 128.6, 128.0, 125.3, 110.2, 108.4, 35.5, 26.6. Data is in accordance with literature.^[12]

2-(1-Methyl-1*H*-pyrrol-2-yl)benzaldehyde (3c)


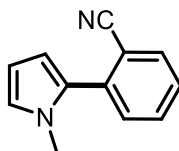
The compound was prepared according to the general procedure using 2-bromobenzaldehyde (36.4 mg, 0.2 mmol, 1 equiv.), 1,8-dihydroxy-9,10-anthraquinone (4.8 mg, 0.02 mmol, 10 mol%), *N*-methylpyrrole (0.36 mL, 4 mmol, 20 equiv.) and diisopropylethylamine (70 μ L, 0.4 mmol, 2 equiv.). Full conversion was obtained after 48 h. Method B(1) was used for work-up. Yellow oil (compound gets dark brown with exposition to air). **¹H-NMR** (300 MHz, CDCl₃) δ 9.93 (d, J = 0.6 Hz, 1H), 8.02 (dd, J = 7.8, 1.0 Hz, 1H), 7.63 (td, J = 7.5, 1.4 Hz, 1H), 7.51 – 7.41 (m, 2H), 6.81 – 6.80 (m, 1H), 6.27 – 6.25 (m, 1H), 6.20 (dd, J = 3.6, 1.8 Hz, 1H), 3.52 (s, 3H). **¹H-NMR** (400 MHz, DMSO-*d*₆) δ 9.83 (d, J = 0.6 Hz, 1H), 7.89 (dd, J = 7.7, 0.8 Hz, 1H), 7.73 (td, J = 7.5, 1.5 Hz, 1H), 7.59 – 7.52 (m, 2H), 6.99 – 6.96 (m, 1H), 6.16 (dd, J = 3.5, 2.7 Hz, 1H), 6.11 (dd, J = 3.6, 1.8 Hz, 1H), 3.52 (s, 3H). **¹³C-NMR** (101 MHz, DMSO-*d*₆) δ 191.9, 136.0, 134.5, 133.5, 131.4, 127.9, 127.8, 127.1, 124.8, 113.0, 107.6, 34.3. **HRMS** (EI): calculated for M⁺ C₁₂H₁₁NO⁺ 185.0835; found 185.0836.

2-(1-Methyl-1*H*-pyrrol-2-yl)benzamide (3d)


The compound was prepared according to the general procedure using 2-bromobenzamide (42.6 mg, 0.2 mmol, 1 equiv.), 1,8-dihydroxy-9,10-anthraquinone (4.8 mg, 0.02 mmol, 10 mol%), *N*-methylpyrrole (0.36 mL, 4 mmol, 20 equiv.) and diisopropylethylamine (70 μ L, 0.4 mmol, 2 equiv.). 80% conversion was obtained after 96 h. Method B(2) was used for work-up. Yellow solid. **¹H-NMR** (300 MHz, CDCl₃) δ 8.08 – 8.05 (m, 1H), 7.56 – 7.47 (m, 2H), 7.39 – 7.33 (m, 1H), 6.77 (t, J = 2.1 Hz, 1H), 6.23 – 6.20 (m, 2H), 5.67 (bs, 1H, NH), 5.55 (bs, 1H, NH), 3.37 (s, 3H).

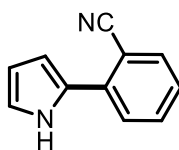
¹³C-NMR (75 MHz, CDCl₃) δ 169.9, 134.1, 132.0, 131.4, 131.2, 131.1, 130.1, 128.7, 123.7, 108.9, 108.1, 34.2. **HRMS** (ESI): calculated for [M+H]⁺ C₁₂H₁₃N₂O⁺ 201.1022; found 201.1026.

2-(1-Methyl-1*H*-pyrrol-2-yl)benzonitrile (3e)

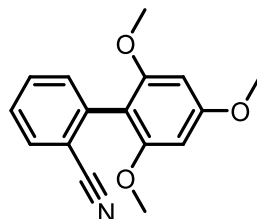


The compound was prepared according to the general procedure using 2-bromobenzonitrile (36.4 mg, 0.2 mmol, 1 equiv.), 1,8-dihydroxy-9,10-anthraquinone (4.8 mg, 0.02 mmol, 10 mol%), *N*-methylpyrrole (0.36 mL, 4 mmol, 20 equiv.) and diisopropylethylamine (35 μL, 0.2 mmol, 1 equiv.). Full conversion was obtained after 16 h. Method B(2) was used for work-up. White solid. **¹H-NMR** (300 MHz, CDCl₃): δ 7.75–7.73 (m, 1H), 7.64 – 7.59 (m, 1H), 7.45 – 7.38 (m, 2H), 6.81 – 6.79 (m, 1H), 6.41 (dd, *J* = 3.7, 1.7 Hz, 1H), 6.25 (dd, *J* = 3.7, 2.7 Hz, 1H), 3.62 (s, 3H). **¹³C-NMR** (75 MHz, CDCl₃): δ 135.8, 132.5, 131.3, 129.8, 128.9, 126.4, 123.8, 117.6, 111.8, 110.4, 107.3, 33.8. Data is in accordance with literature.^[52]

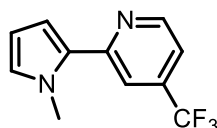
2-(1*H*-Pyrrol-2-yl)benzonitrile (3f)



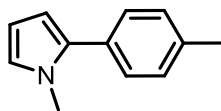
The compound was prepared according to the general procedure using 2-chlorobenzonitrile (13.7 mg, 0.1 mmol, 1 equiv.), 1,8-dihydroxy-9,10-anthraquinone (2.4 mg, 0.01 mmol, 10 mol%), pyrrole (0.15 mL, 2 mmol, 20 equiv.) and diisopropylethylamine (35 μL, 0.2 mmol, 2 equiv.). Full conversion was obtained after 24 h. For isolation four identical reaction were combined. Method B(2) was used for work-up. Brown solid. **¹H-NMR** (300 MHz, DMSO-*d*₆) δ 11.52 (s, 1H), 7.85 – 7.78 (m, 1H), 7.74 – 7.67 (m, 2H), 7.35 (ddd, *J* = 7.9, 6.0, 2.6 Hz, 1H), 7.02 (td, *J* = 2.7, 1.5 Hz, 1H), 6.85 (ddd, *J* = 3.7, 2.7, 1.4 Hz, 1H), 6.23 (dt, *J* = 3.6, 2.5 Hz, 1H). **¹³C-NMR** (75 MHz, DMSO-*d*₆) δ 135.6, 134.4, 133.4, 127.3, 126.4, 126.1, 121.3, 119.5, 109.6, 109.5, 106.5. Data is in accordance with literature.^[53]

2-(2,4,6-Trimethoxybenzen-1-yl)benzonitrile (3g)


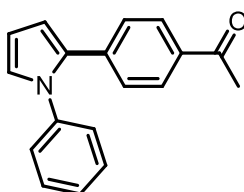
The compound was prepared according to the general procedure using 2-chlorobenzonitrile (13.7 mg, 0.1 mmol, 1 equiv.), 1,8-dihydroxy-9,10-anthraquinone (2.4 mg, 0.02 mmol, 10 mol%), 1,3,5-trimethoxybenzene (336 mg, 2 mmol, 20 equiv.) and diisopropylethylamine (35 μ L, 0.2 mmol, 2 equiv.). Full conversion was obtained after 24 h. Method B(1) was used for work-up. Yellow solid. **¹H-NMR** (300 MHz, CDCl₃) δ 7.70 (dd, J = 7.7, 0.8 Hz, 1H), 7.58 (td, J = 7.8, 1.4 Hz, 1H), 7.41 – 7.34 (m, 2H), 6.23 (s, 2H), 3.87 (s, 3H), 3.75 (s, 6H). **¹³C-NMR** (75 MHz, CDCl₃) δ 162.0, 158.4, 138.9, 132.7, 132.7, 132.0, 127.1, 119.1, 114.9, 108.7, 91.0, 55.9, 55.5. Data is in accordance with literature.^[38]

2-(1-Methyl-1*H*-pyrrol-2-yl)-4-(trifluoromethyl)pyridine (3h)


The compound was prepared according to the general procedure using 2-bromopyridine (44.5 mg, 0.2 mmol, 1 equiv.), 1,8-dihydroxy-9,10-anthraquinone (4.8 mg, 0.02 mmol, 10 mol%), *N*-methylpyrrole (0.36 mL, 4 mmol, 20 equiv.) and diisopropylethylamine (70 μ L, 0.4 mmol, 2 equiv.). Full conversion was obtained after 48h. Method B(1) was used for work-up. Yellow oil. **¹H-NMR** (300 MHz, CDCl₃) δ 8.70 (d, J = 5.1 Hz, 1H), 7.74 (s, 1H), 7.26 (dd, J = 5.2, 1.0 Hz 1H), 6.82 – 6.76 (m, 1H), 6.71 (dd, J = 3.9, 1.8 Hz, 1H), 6.22 (dd, J = 3.9, 2.6 Hz, 1H), 4.03 (s, 3H). **¹³C-NMR** (75 MHz, CDCl₃) δ 153.8, 149.6, 138.6 (q, J^{C-F} = 33.7 Hz), 131.1, 127.8, 123.0 (q, J^{C-F} = 273.1 Hz), 116.6 (q, J^{C-F} = 3.8 Hz), 115.2 (q, J^{C-F} = 3.4 Hz), 112.2, 108.2, 37.4. **¹⁹F-NMR** (282 MHz, CDCl₃) δ -65.52. **HRMS** (EI): calculated for M⁺ C₁₁H₁₀F₃N₂O⁺ 226.0710; found 226.0704.

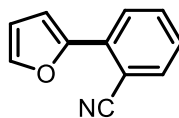
1-Methyl-2-(4-tolyl)-1*H*-pyrrole (3i)

The compound was prepared according to the general procedure using 4-iodotoluene (44.1 mg, 0.2 mmol, 1 equiv.), 1,8-dihydroxy-9,10-anthraquinone (4.8 mg, 0.02 mmol, 10 mol%), *N*-methylpyrrole (0.36 mL, 4 mmol, 20 equiv.) and diisopropylethylamine (70 μ L, 0.4 mmol, 2 equiv.). 80% conversion was obtained after 120 h. Method B(1) was used for work-up. Colorless oil. **¹H-NMR** (300 MHz, CDCl₃) δ 7.62 (dd, J = 7.5, 1.1 Hz, 1H), 7.52 (td, J = 7.5, 1.5 Hz, 1H), 7.46 – 7.37 (m, 2H), 6.76 – 6.75 (m, 1H), 6.23 – 6.21 (m, 1H), 6.14 (dd, J = 3.5, 1.6 Hz, 1H), 3.42 (s, 3H), 1.93 (s, 3H). Data is in accordance with literature.^[54]

4-(1-Methyl-1*H*-pyrrol-2-yl)acetophenone (3j)

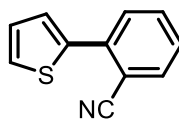
The compound was prepared according to the general procedure using 4-bromoacetophenone (40.0 mg, 0.2 mmol, 1 equiv.), 1,8-dihydroxy-9,10-anthraquinone (4.8 mg, 0.02 mmol, 10 mol%), 1-phenylpyrrole (570 mg, 4 mmol, 20 equiv.) and diisopropylethylamine (70 μ L, 0.4 mmol, 2 equiv.). Full conversion was obtained after 96 h. Method B(2) was used for work-up. Pale yellow solid. **¹H-NMR** (300 MHz, CDCl₃) δ 7.81 – 7.78 (m, 2H), 7.34 (t, J = 5.2 Hz, 3H), 7.21 – 7.17 (m, 4H), 6.99 (dd, J = 2.7, 1.7 Hz, 1H), 6.57 (dd, J = 3.6, 1.7 Hz, 1H), 6.40 (dd, J = 3.5, 3.0 Hz, 1H), 2.55 (s, 3H). Data is in accordance with literature.^[55]

2-(Furan-2-yl)benzonitrile (3k)

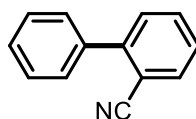


The compound was prepared according to the general procedure using 2-bromobenzonitrile (19.4 mg, 0.1 mmol, 1 equiv.), 1,8-dihydroxy-9,10-anthraquinone (2.4 mg, 0.01 mmol, 10 mol%), furan (220 μ L, 3.0 mmol, 30 equiv.) and diisopropylethylamine (35 μ L, 0.2 mmol, 2 equiv.). Full conversion was obtained after 24h. Method B(2) was used for work-up. **¹H-NMR** (300 MHz, CDCl₃) δ 7.90 (d, J = 8.1 Hz, 1H), 7.70 (d, J = 7.7 Hz, 1H), 7.65 – 7.59 (m, 1H), 7.56 (d, J = 1.4 Hz, 1H), 7.36 – 7.31 (m, 2H), 6.57 (dd, J = 3.5, 1.7 Hz, 1H). Data is in accordance with literature.^[56]

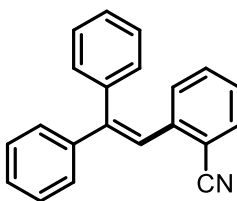
2-(Thiophen-2-yl)benzonitrile (3l)



The compound was prepared according to the general procedure using 2-bromobenzonitrile (18.7 mg, 0.1 mmol, 1 equiv.), 1,8-dihydroxy-9,10-anthraquinone (2.4 mg, 0.01 mmol, 10 mol%), thiophene (240 μ L, 3.0 mmol, 30 equiv.) and diisopropylethylamine (35 μ L, 0.2 mmol, 2 equiv.). Full conversion was obtained after 24h. Method B(2) was used for work-up. **¹H-NMR** (300 MHz, CDCl₃) δ 7.70 (d, J = 8.2 Hz, 1H), 7.60 – 7.52 (m, 3H), 7.40 (dd, J = 5.1, 1.1 Hz, 1H), 7.34 (ddd, J = 7.7, 6.8, 2.0 Hz, 1H), 7.12 (dd, J = 5.1, 3.7 Hz, 1H). Data is in accordance with literature.^[57]

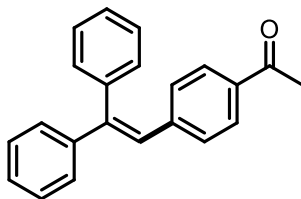
[1,1'-Biphenyl]-2-carbonitrile (3m)

The compound was prepared according to the general procedure using 2-bromobenzonitrile (37.9 mg, 0.2 mmol, 1 equiv.), 1,8-dihydroxy-9,10-anthraquinone (4.8 mg, 0.02 mmol, 10 mol%), benzene (540 μ L, 6.1 mmol, 30 equiv.) and diisopropylethylamine (70 μ L, 0.4 mmol, 2 equiv.). Full conversion was obtained after 24 h. Method B(1) was used for work-up. **¹H-NMR** (300 MHz, CDCl₃) δ 7.79 – 7.76 (m, 1H), 7.65(td, J = 7.7, 1.4 Hz, 1H), 7.59 – 7.42 (m, 7H). Data is in accordance with literature.^[57]

2-(2,2-Diphenylvinyl)benzonitrile (3n)

The compound was prepared according to the general procedure using 2-bromobenzonitrile (37.9 mg, 0.2 mmol, 1 equiv.), 1,8-dihydroxy-9,10-anthraquinone (4.8 mg, 0.02 mmol, 10 mol%), 1,1-diphenylethylene (176 μ L, 1.0 mmol, 5 equiv.) and diisopropylethylamine (35 μ L, 0.2 mmol, 1 equiv.). Full conversion was obtained after 24 h. Method B(2) was used for work-up. **¹H-NMR** (300 MHz, CDCl₃) δ 7.61 (dd, J = 6.3, 2.9 Hz, 1H), 7.38 – 7.15 (m, 13H), 6.94 – 6.90 (m, 1H). Data is in accordance with literature.^[58]

4-(2,2-Diphenylvinyl)acetophenone (**3o**)



The compound was prepared according to the general procedure using 4-bromoacetophenone (20.8 mg, 0.1 mmol, 1 equiv.), 1,8-dihydroxy-9,10-anthraquinone (2.4 mg, 0.01 mmol, 10 mol%), 1,1-diphenylethylene (176 μ L, 1.0 mmol, 10 equiv.) and diisopropylethylamine (35 μ L, 0.2 mmol, 2 equiv.). Full conversion was obtained after 96 h. Method B(2) was used for work-up. White solid. **¹H-NMR** (300 MHz, CDCl₃) δ 7.72 (d, J = 8.4 Hz, 2H), 7.36 – 7.33 (m, 8H), 7.21 – 7.17 (m, 2H), 7.09 (d, J = 8.3 Hz, 2H), 6.99 (s, 1H), 2.53 (s, 3H). Data is in accordance with literature.^[59]

2.4.6 NMR Spectra

The corresponding NMR spectra of the compounds **3a-o** are included in the Appendix (see section 7.2).

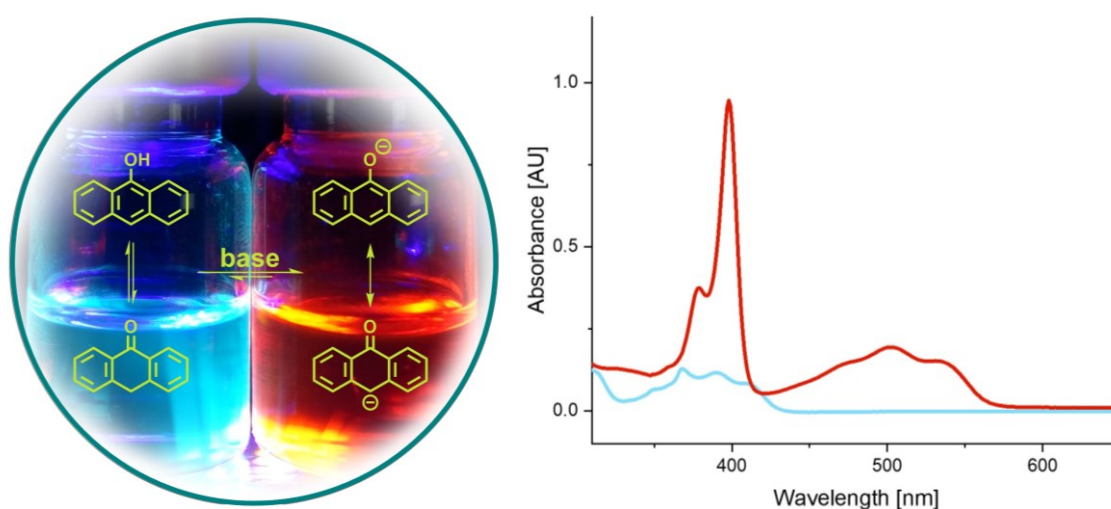
2.5 References

- [1] D. A. Nicewicz, D. W. C. MacMillan, *Science* **2008**, *322*, 77–80.
- [2] C. K. Prier, D. A. Rankic, D. W. C. MacMillan, *Chem. Rev.* **2013**, *113*, 5322–5363.
- [3] C. Stephenson, T. Yoon, *Acc. Chem. Res.* **2016**, *49*, 2059–2060.
- [4] B. König, *Eur. J. Org. Chem.* **2017**, 1979–1981.
- [5] T. P. Yoon, M. A. Ischay, J. N. Du, *Nat. Chem.* **2010**, *2*, 527–532.
- [6] M. H. Shaw, J. Twilton, D. W. C. MacMillan, *J. Org. Chem.* **2016**, *81*, 6898–6926.
- [7] J. M. R. Narayanam, C. R. J. Stephenson, *Chem. Soc. Rev.* **2011**, *40*, 102–113.
- [8] N. A. Romero, D. A. Nicewicz, *Chem. Rev.* **2016**, *116*, 10075–10166.
- [9] For an example of the use of quantum dots in visible-light photoredox transformations, see A. Pal, I. Ghosh, S. Sapra, B. König, *Chem. Mater.* **2017**, *29*, 5225–5231.
- [10] M. Neumann, S. Földner, B. König, K. Zeitler, *Angew. Chem. Int. Ed.* **2011**, *50*, 951–954.
- [11] D. P. Hari, B. König, *Chem. Commun.* **2014**, *50*, 6688–6699.
- [12] I. Ghosh, T. Ghosh, J. I. Bardagi, B. König, *Science* **2014**, *346*, 725–728.
- [13] I. Ghosh, B. König, *Angew. Chem. Int. Ed.* **2016**, *55*, 7676–7679.
- [14] A. Das, I. Ghosh, B. König, *Chem. Commun.* **2016**, *52*, 8695–8698.
- [15] F. Z. Su, S. C. Mathew, L. Möhlmann, M. Antonietti, X. C. Wang, S. Blechert, *Angew. Chem. Int. Ed.* **2011**, *50*, 657–660.
- [16] N. El-Najjar, H. Gali-Muhtasib, R. A. Ketola, P. Vuorela, A. Urtti, H. Vuorela, *Phytochem. Rev.* **2011**, *10*, 353–370.
- [17] H. Nohl, W. Jordan, R. J. Youngman, *Adv. Free Radical Biol. Med.* **1986**, *2*, 211–279.
- [18] J. M. Lü, S. V. Rosokha, I. S. Neretin, J. K. Kochi, *J. Am. Chem. Soc.* **2006**, *128*, 16708–16719.
- [19] F. Rusch, L.-N. Unkel, D. Alpers, F. Hoffmann, M. Brasholz, *Chem. Eur. J.* **2015**, *21*, 8336–8340.
- [20] S. Lerch, L.-N. Unkel, M. Brasholz, *Angew. Chem. Int. Ed.* **2014**, *53*, 6558–6562.
- [21] N. Tada, Y. Ikebata, T. Nobuta, S. I. Hirashima, T. Miura, A. Itoh, *Photochem. Photobiol. Sci.* **2012**, *11*, 616–619.
- [22] C. W. Kee, K. F. Chin, M. W. Wong, C. H. Tan, *Chem. Commun.* **2014**, *50*, 8211–8214.
- [23] K. Ohkubo, A. Fujimoto, S. Fukuzumi, *J. Am. Chem. Soc.* **2013**, *135*, 5368–5371.
- [24] L. Cui, Y. Matusaki, N. Tada, T. Miura, B. Uno, A. Itoh, *Adv. Synth. Catal.* **2013**, *355*, 2203–2207.
- [25] B. Chang, H. G. Shao, P. Yan, W. Z. Qiu, Z. G. Weng, R. S. Yuan, *ACS Sustain. Chem. Eng.* **2017**, *5*, 334–341.
- [26] N. Tada, K. Hattori, T. Nobuta, T. Miura, A. Itoh, *Green Chem.* **2011**, *13*, 1669–1671.
- [27] R. M. Wightman, J. R. Cockrell, R. W. Murray, J. N. Burnett, S. B. Jones, *J. Am. Chem. Soc.* **1976**, *98*, 2562–2570.
- [28] B. R. Eggins, P. K. J. Robertson, *J. Chem. Soc. Faraday Trans.* **1994**, *90*, 2249–2256.
- [29] P. Nalleborg, H. Lund, J. Eriksen, *Tetrahedron Lett.* **1985**, *26*, 1773–1776.
- [30] A. R. Cook, L. A. Curtiss, J. R. Miller, *J. Am. Chem. Soc.* **1997**, *119*, 5729–5734.
- [31] D. Gosztola, M. P. Niemczyk, W. Svec, A. S. Lukas, M. R. Wasielewski, *J. Phys. Chem. A* **2000**, *104*, 6545–6551.
- [32] I. Ghosh, L. Marzo, A. Das, R. Shaikh, B. König, *Acc. Chem. Res.* **2016**, *49*, 1566–1577.
- [33] J. D. Nguyen, E. M. D’Amato, J. M. R. Narayanam, C. R. J. Stephenson, *Nat. Chem.* **2012**, *4*, 854–859.
- [34] H. Kim, C. Lee, *Angew. Chem. Int. Ed.* **2012**, *51*, 12303–12306.
- [35] E. H. Discekici, N. J. Treat, S. O. Poelma, K. M. Mattson, Z. M. Hudson, Y. D. Luo, C. J. Hawker, J. R. de Alaniz, *Chem. Commun.* **2015**, *51*, 11705–11708.

- [36] A. Arora, J. D. Weaver, *Org. Lett.* **2016**, *18*, 3996–3999.
- [37] S. O. Poelma, G. L. Burnett, E. H. Discekici, K. M. Mattson, N. J. Treat, Y. D. Luo, Z. M. Hudson, S. L. Shankel, P. G. Clark, J. W. Kramer, C. J. Hawker, J. R. de Alaniz, *J. Org. Chem.* **2016**, *81*, 7155–7160.
- [38] I. Ghosh, R. S. Shaikh, B. König, *Angew. Chem. Int. Ed.* **2017**, *56*, 8544–8549.
- [39] M. Majek, U. Faltermeier, B. Dick, R. Pérez-Ruiz, A. Jacobi von Wangelin, *Chem. Eur. J.* **2015**, *21*, 15496–15501.
- [40] For the chemical generation of the semiquinone anion, we recommend that a fresh $\text{Na}_2\text{S}_2\text{O}_4$ solution is prepared under an inert atmosphere. See the Experimental Part for details.
- [41] See the Experimental Part for the photochemical reaction setup and general procedures.
- [42] C. Costentin, M. Robert, J. M. Savéant, *J. Am. Chem. Soc.* **2004**, *126*, 16051–16057.
- [43] W. Liu, H. Cao, H. Zhang, H. Zhang, K. H. Chung, C. A. He, H. B. Wang, F. Y. Kwong, A. W. Lei, *J. Am. Chem. Soc.* **2010**, *132*, 16737–16740.
- [44] A. Graml, I. Ghosh, B. König, *J. Org. Chem.* **2017**, *82*, 3552–3560.
- [45] For the C–H arylation reactions, the use of DMSO as the solvent and DIPEA as the sacrificial electron donor provided better chemical yields.
- [46] The electrochemical experiments reported in ref.^[27] indicate that $E^0(\text{Aq-OH-H}^+/\text{Aq-OH-H}^-) < -0.5 \text{ V vs. SCE}$.
- [47] Note that the absorption maxima of Aq-OH-H^- , generated in the presence of $\text{Na}_2\text{S}_2\text{O}_4$, are consistent with the reported values.^[27]
- [48] J. J. Devery III, J. J. Douglas, J. D. Nguyen, K. P. Cole, R. A. Flowers, C. R. J. Stephenson, *Chem. Sci.* **2015**, *6*, 537–541.
- [49] Under the photoredox catalytic reactions conditions, the substitution products were identified by HPLC and HPLC–MS analysis.
- [50] The role of such photoproducts in determining the kinetics or chemical yield is currently unclear.
- [51] D. B. G. Williams, M. Lawton, *J. Org. Chem.* **2010**, *75*, 8351–8354.
- [52] D. T. Gryko, O. Vakuliuk, D. Gryko, B. Koszarna, *J. Org. Chem.* **2009**, *74*, 9517–9520.
- [53] M. Alešković, N. Basarić, K. Mlinarić-Majerski, *J. Heterocycl. Chem.* **2011**, *48*, 1329–1335.
- [54] F. Bilodeau, M. C. Brochu, N. Guimond, K. H. Thesen, P. Forgione, *J. Org. Chem.* **2010**, *75*, 1550–1560.
- [55] J. Roger, H. Doucet, *Adv. Synth. Catal.* **2009**, *351*, 1977–1990.
- [56] D. Wu, Z. X. Wang, *Org. Biomol. Chem.* **2014**, *12*, 6414–6424.
- [57] J. R. Naber, S. L. Buchwald, *Adv. Synth. Catal.* **2008**, *350*, 957–961.
- [58] M. J. Wu, L. M. Wei, C. F. Lin, S. P. Leou, L. L. Wei, *Tetrahedron* **2001**, *57*, 7839–7844.
- [59] G. J. Quinteros, P. M. Uberman, S. E. Martín, *Eur. J. Org. Chem.* **2015**, 2698–2705.

CHAPTER 3

3 Utilizing Excited State Organic Anions for Photoredox Catalysis: Activation of (Hetero)aryl Chlorides by visible light-absorbing 9-Anthrolate Anions



This chapter has been published in: M. Schmalzbauer, I. Ghosh, B. König, *Faraday Discuss.* **2019**, 215, 364-378. – Reproduced by permission of The Royal Society of Chemistry.

M. Schmalzbauer designed the catalytic system, optimized the reaction, carried out all the experimental work and wrote the manuscript with input from all of the authors. B. König supervised the project and is corresponding author.

Abstract

The tricyclic aromatic ketone 9-anthrone and its derivatives are under basic conditions in equilibrium with their corresponding anionic forms. Unlike the neutral species, the 9-anthrolate anions can be excited by blue LED light, which turns them into strong photoreductants and thus, are able to initiate photoinduced electron transfer (PET) reactions. To demonstrate the synthetic applicability of the catalytic system, various (hetero)aryl chlorides were converted in C-C and C-Het bond-forming reactions yielding the corresponding arylation products in moderate to excellent yield. The reactions proceed under very mild conditions without the need for a sacrificial electron donor. Besides 9-anthrone, other closely related derivatives were synthesized and investigated concerning their ability to catalyze demanding reductive transformations. Based on spectroscopic findings and radical trapping experiments a conceivable mechanism is proposed.

3.1 Introduction

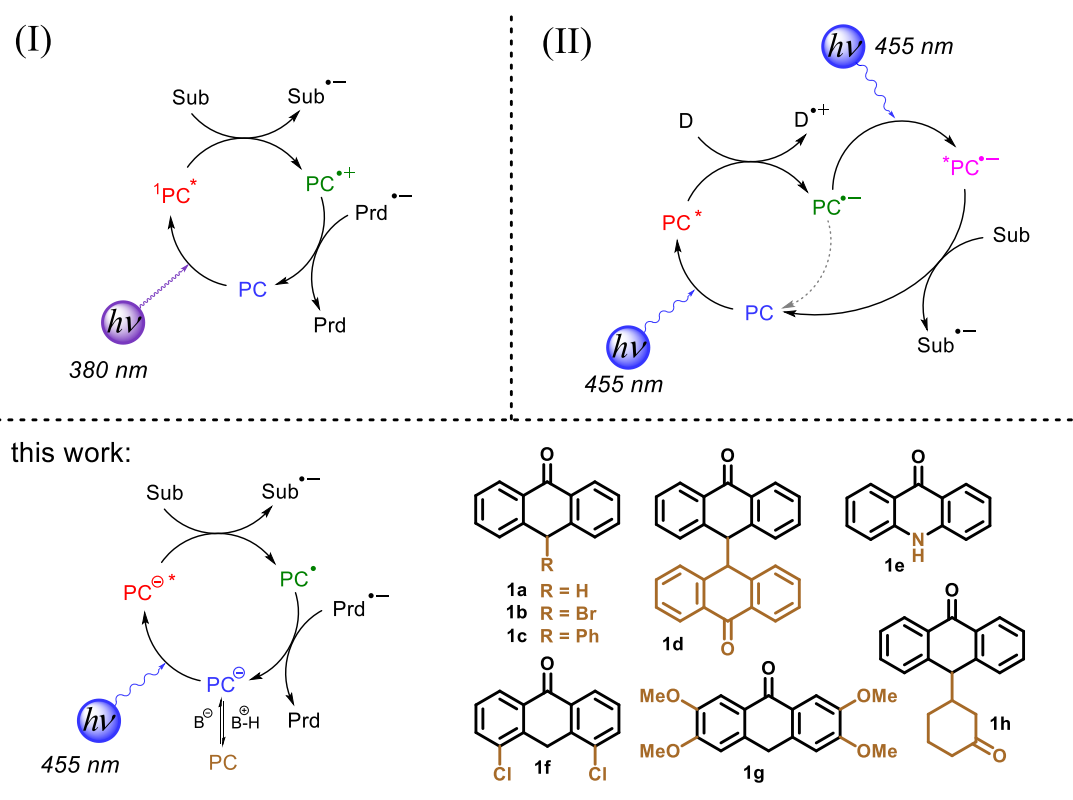
Within the past few years, photoredox catalysis evolved into a versatile tool in organic synthesis. In that course, the photoreduction of aryl halides to generate highly reactive aryl radicals has emerged as a valuable transition-metal-free alternative to the well-established Pd- and Rh-catalyzed C–H activation chemistry.^[1–8] The formation of complex molecules starting from cheap, readily available and bench-stable starting materials has always been an important request in synthetic organic chemistry. Among (hetero)aryl halides, in particular chloroarenes can be considered as such reagents and thus, approaches to activate the C(sp²)–Cl bond are of great interest. However, converting (hetero)aryl chlorides to forge new bonds upon mesolytic cleavage is still challenging, as the bond-dissociation energy (*e.g.* Ar–Cl; BDE = 407 kJ·mol^{–1}) is high and reduction potentials are usually difficult to reach using commonly employed photocatalysts.^[2,9,10] To expand the accessible substrate scope in photoredox chemistry towards less activated molecules, the development of photocatalytic systems with stronger reducing power is required. In this context, several synthetically useful, mild and transition-metal-free strategies have recently been reported and among others, two are discussed in here.

(I) Using a photocatalyst with large S1←S0 band gap: the group of de Alaniz showed that activated aryl chlorides can be reduced by using 10-phenylphenothiazine (PTH) which possesses a very large S1←S0 band gap and is therefore able to convert high energy photons into redox equivalents ($\lambda_{\text{ex}} = 380 \text{ nm}$, $\lambda_{\text{em}} = 445 \text{ nm}$; $E_{\text{ox}}^* = -2.1 \text{ V vs. SCE}$).^[11]

Very recently a modified carbazole scaffold was reported to act as a strong reductant ($E_{\text{ox}}^* \approx -2.75 \text{ V vs. SCE}$),^[2] which converted both unactivated aryl and alkyl chlorides (using UVA-LEDs) to their corresponding dechlorinated products in good yields. However, C–C bond-forming reactions with less activated aryl chlorides and electron rich pyrroles (or benzene) were achieved only in low yields. Altering the reaction conditions to elevated temperature (90 °C), high excess of trapping reagent and by using an inorganic base instead of a typical amine electron donor, DIPEA, led to slightly improved yields of C–H arylated products.

(II) Consecutive photoinduced electron transfer (conPET) process: recently, our group demonstrated that the reduction power of a photocatalyst can be easily enhanced by using the energy of two photons in one catalytic cycle. Perylene diimide (PDI) was used as a photocatalyst and the excitation of the ground state radical anion (PDI^{•–}, generated *in-situ via* a

photoinduced electron transfer process, Scheme 3-1) led to the formation of a strongly reducing doublet excited state (*i.e.*, $\text{PDI}^{\bullet-}$) capable of activating acceptor substituted aryl halides for C–H arylation reactions.^[12] In this effort, we also demonstrated that the use of rhodamine 6G under very similar reaction conditions allows for activating electron rich aryl bromides in C–C bond-forming reactions.^[13,14] However, only a few examples of aryl chlorides are discussed and electron rich pyrrole derivatives or isocyanides were mainly used as trapping reagents.



Scheme 3-1. Overview of discussed activation strategies: (I) Using a photocatalyst with large $\text{S}_1 \leftarrow \text{S}_0$ band gap; (II) Two-photon-process (conPET); (bottom) concept for excitation of visible light-absorbing organic anions and the structures of the herein examined photocatalysts.

In this work we report a series of visible-light absorbing anionic ground state photocatalysts **1** (Scheme 3-1) that act as strong reducing agents from their photoexcited states. We got inspired by literature reports in which the excited states of cationic organic dyes, such as 9-mesityl-10-methylacridinium perchlorate or triphenylpyrylium tetrafluoroborate, have been utilized frequently as powerful single electron accepting photocatalysts.^[15–17] We envisioned that photoexcited anions of organic molecules accordingly may act as very strong electron donors. Additionally, intermediates of a PET between excited anionic donor and neutral ground state

acceptor are free of electrostatic attraction resulting in an accelerated separation of the radical pair and hence, could decrease the rate of back electron transfer (BET) events to render reactions more efficient.^[18,19] To the best of our knowledge, organic anions are a barely explored class of photoredox catalysts^[20–22] and thus, we examined 9-anthrolate and some derivatives as visible light-absorbing anionic photocatalysts which enable the activation of several aryl and heteroaryl chlorides *via* a photoinduced electron transfer process for C(sp²)–C and C(sp²)–heteroatom bond-forming reactions.

3.2 Results and Discussion

In solution, 9-anthrone (**1a**) is present in a tautomeric equilibrium and the keto-enol ratio strongly depends on the hydrogen bonding ability of the solvent. A value of $K_{\text{enol}} = 1.6 \pm 1$ in DMSO is reported for **1a**, *i.e.* both forms are coexistent in considerable amount.^[23] Hence, a gain in energy due to aromatic stabilization by forming the enol 9-anthrole is less pronounced compared to phenol. Furthermore, resonance stabilization of 9-anthrolate **2a** is pivotal for the distinct acidity of **1a**.^[24–26] Under basic conditions 9-anthrone is known to get deprotonated^[27] (*cf.*, ¹H-NMR spectra, Figure 3-1) and the resulting anionic species possesses an altered absorption spectrum with a prominent maximum around 400 nm and a new broad absorption band in the visible region ranging from 410 to 560 nm (Figure 3-1).^[22] Thus, working in alkaline solution allows for the photoexcitation of 9-anthrolate (**2a**) with blue LED (455 nm) light. To our delight, the examined enolate **2a** turned out to be emissive, which allowed us to record its emission spectrum and to determine the luminescence lifetime ($\tau = 18.7$ ns, see Experimental Part) of the chromophore in a time-dependent experiment. Additional data regarding photophysical and electrochemical properties of considered anthrone derivatives, including compound **1b**, which has been used almost exclusively for synthetic reactions, are provided in the Experimental Part.

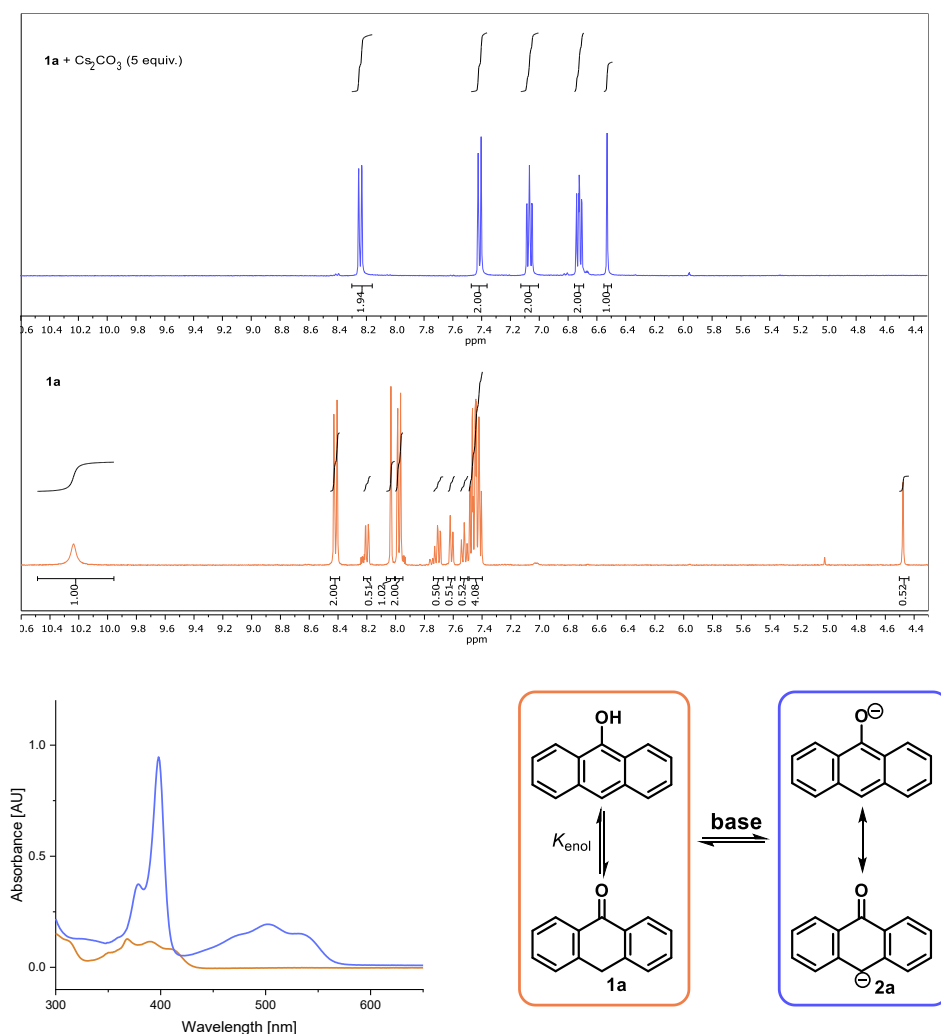


Figure 3-1. (top) Stacked $^1\text{H-NMR}$ spectra in presence (blue) and absence (orange) of base. Integration over signals suggests the formation of the anion in presence of base; (bottom) UV-Vis spectra of 9-anthrone (**1a**, 50 μM) in absence (orange) and presence (blue) of Cs_2CO_3 . Spectra were recorded in a gastight quartz cuvette (10×10 mm) under N_2 atmosphere in dry degassed DMSO.

3.2.1 Screening of Catalysts

With these spectroscopic data in hand, we began our synthetic investigations using methyl 4-chlorobenzoate **3a** (0.1 mmol) as model substrate, *N*-methylpyrrole **4a** (1.5 mmol) as trapping reagent, which has recently been reported to trap aryl radicals efficiently, and catalytic amounts of **1a-h** (10 mol% w.r.t. **3a**). To activate the chromophore, caesium carbonate was added as base and reactions were carried out under nitrogen atmosphere as anthrolate anions **2** are prone to oxidation in presence of air.^[28] The yield of coupling product **5a** was determined by calibrated GC-FID analysis with biphenyl as internal standard. All anthrone derivatives (**1a-1h**,

see Scheme 3-1 for the respective chemical structures) investigated herein, were effective in catalyzing the model reaction and the desired product was obtained in moderate to good yields (Table 3-1, Entry 1-8).

Table 3-1. Catalyst screening and control reactions.

Entry	PC	Conversion ^a [%]	Yield ^a [%]
1	1a	85	66
2	1b	91	77
3	1c	78	64
4	1d	100	79
5	1e	100	81
6	1f	69	54
7	1g	100	84
8	1h	85	65
9 ^b	1b	15	0
10 ^c	1b	6	6
11 ^d	-	47	22

Reaction conditions: A mixture containing of substrate **3a** (0.1 mmol), catalyst **1** (10 mol% w.r.t. **3a**) and Cs₂CO₃ (0.2 mmol) was dissolved in dry, degassed DMSO (1 mL) in a sealed snap vial equipped with stirring bar and under N₂ atmosphere. **4a** (1.5 mmol) was added *via* syringe needle. While stirring the reaction was exposed to LED light (455 nm) for 18 hours; ^a Yield and conversion were determined by calibrated GC-FID analysis with internal standard method; ^b reaction was examined in the dark; ^c reaction in absence of Cs₂CO₃; ^d reaction without catalyst.

When **1a** was used as photocatalyst, the desired C–H arylated product was obtained in 66% yield. Other derivatives such as **1c** and **1h** gave very similar yields, and product formation dropped slightly when **1f** was used as a photocatalyst. It is worth mentioning here, that the intention behind synthesizing the compounds **1c** and **1h** was to introduce steric hindrance into the 10-position of the molecule bearing a bulky phenyl or cyclohexanone residue. Nicewicz *et al.* reported that Mes-Acr-Me⁺ and its reduced radical species are shielded by the sterically demanding mesityl group against nucleophilic and radical addition and thus diminish the bleaching of the dye.^[17] However, no enhancement in catalytic activity could be noticed

compared to the unsubstituted 9-anthrone. Efforts to synthesize 10-mesityl-9-anthrone remained unsuccessful. The use of 10-bromo-9-anthrone (**1b**) as photocatalyst increased the product yield to 77% and showed an enhanced selectivity towards the desired coupling product (*cf.*, Table 3-1, Entry 1-2). Other employed anthrone derivatives for example the dimer of anthrone **1d** or the nitrogen analogue **1e**, gave very similar yields with respect to **1b**. The highest yield of 84% was obtained by using the electron rich tetramethoxy anthrone **1g** (Entry 7) however, it is not commercially available and is typically prepared in a three-step synthesis. Hence, we continued using **1b**, which is easily obtained from the commercially available 9-anthrone *via* bromination, for further reaction optimization and synthetic investigations. The control reactions in the dark (Entry 9) or in the absence of base (Entry 10) gave no or only traces of the product **5a**. Interestingly, a detectable amount of product (22%, Entry 11) was formed when the reaction mixture was irradiated only in presence of Cs₂CO₃ (2.0 equiv.). Very recently, Rossi *et al.* proposed the formation of a dimsyl anion as a key intermediate in the initiation step of photoinduced base-promoted homolytic aromatic substitution reactions (*cf.*, Section 1.3.7, Chapter 1).^[29] According to their report, strong bases such as KO^tBu or NaH can facilitate electron transfer reactions in DMSO under visible-light irradiation. However, the authors have also reported that the use of Cs₂CO₃ or K₂CO₃ did not allow for substrate conversion and hence may not be able to generate dimsyl anions. To get more insights, the reaction progress was monitored in absence and presence of **1b** by GC-FID (Table S3-1, Experimental Part). The obtained results indicate an induction period with almost no detectable amount of product formed within the first hours and only little substrate conversion after 2 hours of irradiation. After 4 hours, a small amount of product was formed, however, the reaction rate in presence of **1b** was significantly faster accompanied by higher selectivity towards **5a**.^[30]

3.2.2 Optimization of the Reaction Conditions

The polarity of the solvent seems to play a crucial role as the product formation was observed in aprotic polar solvents such as DMSO, DMF or MeCN, whereas no substrate conversion was detected in less polar methylene chloride. Among the aprotic polar solvents, DMSO was found to be the most suitable one under our reaction conditions. Therefore, the optimization reactions were carried out in DMSO under nitrogen atmosphere using **1b** as a photocatalyst,^[31] **3a** as the model substrate and **4a** as trapping reagent and were examined in the presence of a

broad range of inorganic or organic bases and additive. The results are summarized in Table 3-2.

Table 3-2. Optimization of the reaction conditions.

Entry	1b [mol%]	Base [equiv.]	Additive [equiv.]	Time [h]	Yield^a [%]
1	10	2 (Cs ₂ CO ₃)	-	18	77 (91)
2	10	1 (Cs ₂ CO ₃)	-	18	47 (79)
3	10	1.2 (Cs ₂ CO ₃)	0.6 (18c6)	18	95 ^b
4	5	1.2 (Cs ₂ CO ₃)	0.6 (18c6)	18	92 (98)
5	20	1.2 (Cs ₂ CO ₃)	0.6 (18c6)	18	88 (94)
6	10	2 (Li ₂ CO ₃)	-	18	0 (0)
7	10	2 (Na ₂ CO ₃)	-	18	4 (13)
8	10	2 (K ₂ CO ₃)	-	18	47 (53)
9	10	2 (K ₃ PO ₄)	-	18	46 (70)
10	10	2 (NaAsc)	-	18	2 (2)
11	10	1.2 (TMG)	-	18	42 (63)
12	10	1.2 (DBU)	-	18	35 (65)
13	10	1.2 (DABCO)	-	18	0 (0)
14	10	1.2 (Cs ₂ CO ₃)	0.6 (18c6)	10	79 (88)
15 ^c	10	1.2 (Cs ₂ CO ₃)	0.6 (18c6)	18	8 (31)
16 ^d	10	1.2 (Cs ₂ CO ₃)	0.6 (18c6)	18	30 (51)
17 ^e	10	1.2 (Cs ₂ CO ₃)	0.6 (18c6)	18	34 (59)
18 ^{e,f}	10	1.2 (Cs ₂ CO ₃)	0.6 (18c6)	18	83 (100)

Reaction conditions: A mixture containing of substrate **3a** (0.1 mmol), catalyst **1b**, Cs₂CO₃ and additive was dissolved in dry, degassed DMSO (1 mL) in a sealed snap vial equipped with stirring bar and under N₂ atmosphere. **4a** (1.5 mmol) was added *via* syringe needle. While stirring the reaction was exposed to LED light (455 nm); ^a yields were determined by calibrated GC-FID analysis with internal standard method, numbers in parenthesis refer to the conversion of **3a**; ^b isolated yield; ^c 1 equiv. of **4a** was used; ^d green LED (535 nm) was used as irradiation source, however radiant flux is lowered by a factor of 8 compared to blue LED (see Experimental Part); ^e reactions were run in air; ^f catalyst **1c** was used.

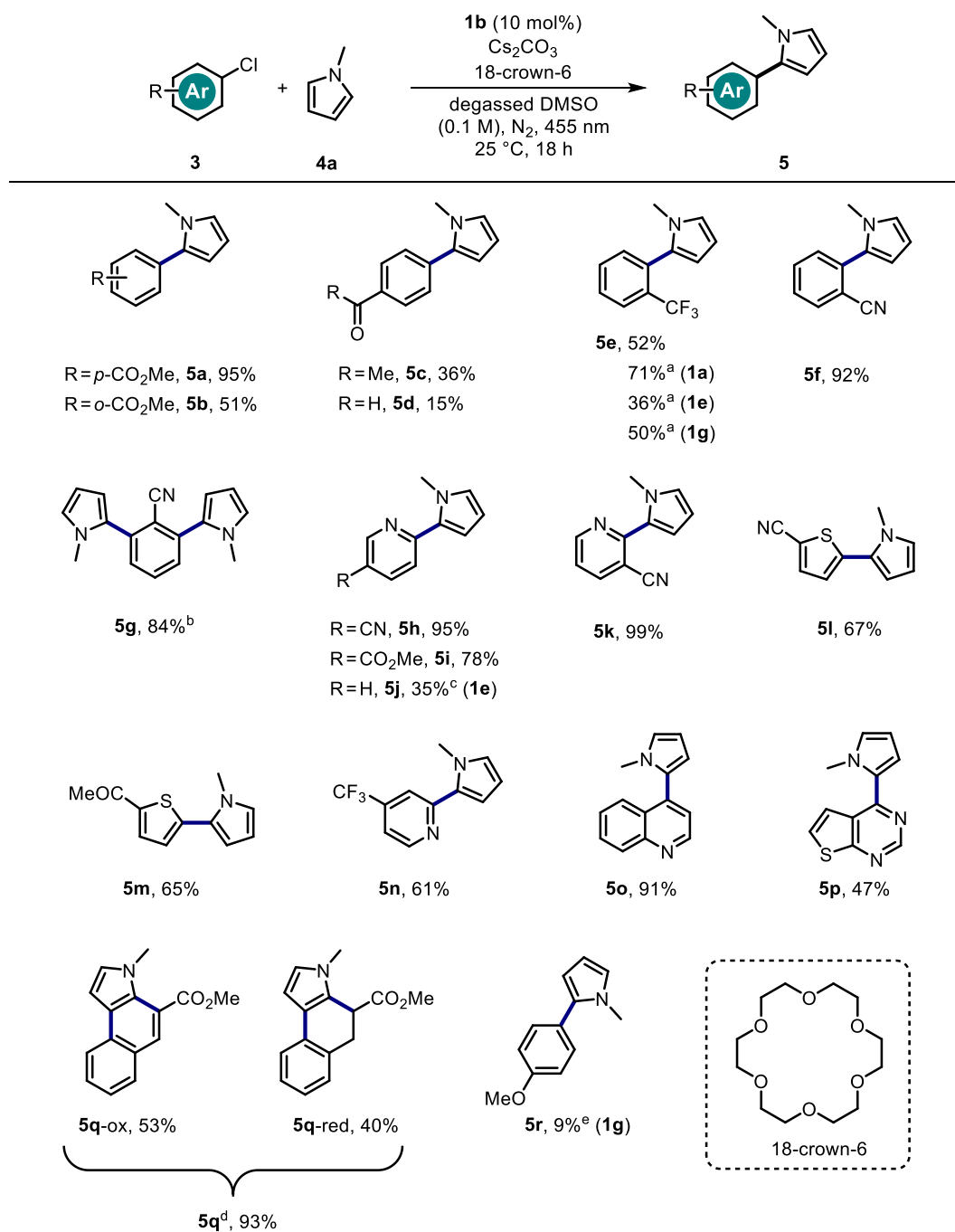
Interestingly, the use of Li₂CO₃ did not allow product formation (Table 3-2, Entry 6), however, detectable amounts of product were obtained when Na₂CO₃ or sodium ascorbate (NaAsc)

were used as bases (Entry 7 and 10). The product yield increased in reasonable amount in the presence of K_2CO_3 or K_3PO_4 (Entry 8–9). Under similar reaction conditions, the use of Cs_2CO_3 led to 77% product formation. Employing strong non-nucleophilic organic bases, such as tetramethylguanidine (TMG) or 1,8-diazabicyclo[5.4.0]undec-7-ene did not increase the yield of the desired product, although they are completely soluble in DMSO. The weaker amine base triethylenediamine (DABCO) resulted in no product formation (Entry 11-13).

With respect to the amount of base: it is not only necessary to activate the catalyst, but furthermore to neutralize the HCl formed in the course of the reaction. Hence, lowering the amount of Cs_2CO_3 to only one equivalent with reference to **3a**, caused a decrease in product yield to 47% (Entry 2). Carbonates are poorly soluble in DMSO. However, adding crown ether (18-crown-6, *cf.*, Table 3-3) increases both solubility and reactivity of the carbonate base in DMSO and the product could be isolated in excellent yield (95%). Simultaneously, it allowed to reduce the amount of base to 1.2 equivalents (Table 3-2, Entry 3). Under these reaction conditions, a doubling of the catalyst loading to 20 mol% had a detrimental effect on the reaction outcome but a catalyst loading as low as 5 mol% resulted in only slightly decreased yield (*cf.*, Entry 3-5). The product yield and substrate conversion dropped however significantly, when we tried to employ *N*-methylpyrrole (**4a**) in stoichiometric amount (for further details see Table S3-2 in the Experimental Part).^[32] From the recorded UV-vis spectrum of **1b** in presence of base (Figure S3-2, Experimental Part) it is evident, that excitation should also occur with less-energetic and more economical light sources. To provide evidence, we examined a reaction using a weak green light LED (535 nm, Entry 16) which also resulted in product formation. Anthrolate anions **2** are known to get oxidized in presence of air. However, acridanone **1e**, the oxidized acridine, is less reactive towards oxygen in alkaline media. Reactions in air revealed a significant decrease in product yield using catalyst **1b**, whereas a remarkably catalytic activity was found for acridanone (**1e**) even under non-inert atmosphere (Entry 17-18).

3.2.3 Scope of Chlorinated Substrates for C–H Arylation

Under the optimized reaction conditions (Table 3-2, Entry 3), a range of aryl and biologically important heteroaryl chlorides could be effectively converted in coupling reactions. The isolated yields are summarized in Table 3-3.

Table 3-3. Scope of (hetero)aryl chlorides.

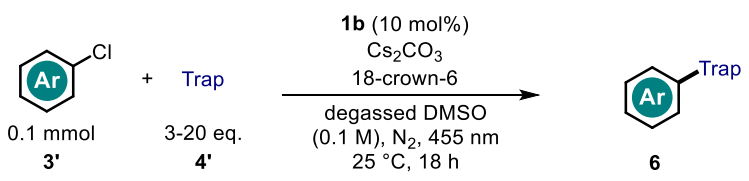
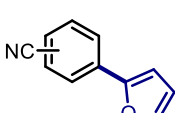
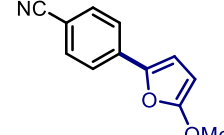
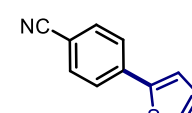
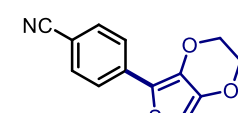
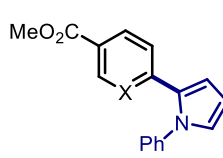
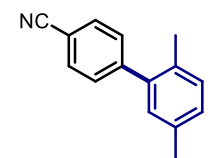
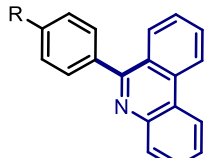
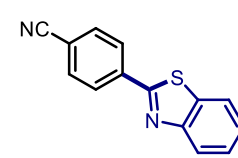
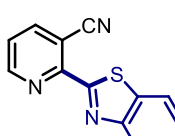
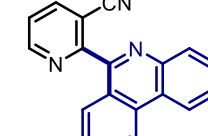
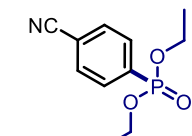
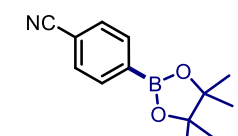
Reaction conditions: A mixture containing of substrate **3** (0.1 mmol), catalyst **1b** (10 mol% w.r.t. **3**) crown ether (0.06 mmol) and Cs₂CO₃ (0.12 mmol) in a sealed snap vial equipped with stirring bar and under N₂ atmosphere, was dissolved in dry, degassed DMSO (1 mL) and **4a** (1.5 mmol) was added *via* syringe needle. While stirring, the reaction was exposed to LED light (455 nm) for 18 hours from the plane bottom side of the vial; ^a Catalyst **1** given in parenthesis was used instead of **1b**. ^b Only the disubstituted product was obtained; ^c 2.0 mmol **4a**, 0.2 mmol Cs₂CO₃, 0.1 mmol crown ether and 20 mol% **1e** were used. Reaction was irradiated for 24 h. ^d Methyl (*Z*)- α -chlorocinnamate was used as substrate and products **5q-ox** and **5q-red** could be isolated separately. ^e Catalyst **1g** (15 mol% w.r.t. **3**) and slightly increased amount of Cs₂CO₃ (2.0 mmol) were used. The reaction was irradiated for 41 h.

When **4a** is used as a trapping reagent, the direct C–H arylated products using methyl chlorobenzoates (**5a** and **5b**) were obtained in 95% and 51% isolated yield. 2-Chlorobenzonitrile was readily converted to give the desired biaryl **5f** in excellent 92%. Interestingly, 2,6-dichlorobenzonitrile (**3g**) gave the twofold arylated product in 84% isolated yield with excellent selectivity towards the difunctionalized product.^[33] Our developed reaction conditions allowed for the activation of 2-chlorobenzotrifluoride (**3e**), which was found to be challenging (for CV measurements see Experimental Part). Nevertheless, the C–H arylation product **5e** could be isolated in 52% yield. Notably, when employing catalyst **1a** the isolated yield could be increased reasonably to 71% (Table 3-3, **5e**). 4-chloroacetophenone (**3c**) and 4-chlorobenzaldehyde (**3d**) possess very similar reduction potentials with respect to methyl benzoate **3a**^[34] however, are less tolerated and give the corresponding coupling products in reasonable to low 36% and 15% yield.^[35] Arylated heteroarenes constitute an important structural motif in material and pharmaceutical sciences due to their optoelectronic and biological properties.^[36,37] Hence, we were pleased to see that arylated derivatives of 3-cyanopyridine are formed in excellent 95% and 99% yield (**5h**, **5k**). The presence of an electron withdrawing group attached to the pyridine ring facilitates the product formation however, under slightly altered reaction conditions (see Table 3-3, **5j**) we were also able to transform unsubstituted 2-chloropyridine ($E_{\text{red}} = -2.40$ V *vs.* SCE, see Experimental Part). Chlorinated thiophenes, trifluoromethylpyridine and chloroquinoline gave the desired products in 65%-67%, 61% and 91% isolated yield respectively. Chloroquinoline **3o** gave the arylated product in excellent yield. The chlorinated thienopyrimidine is also useful as a substrate providing **5p** in 47% yield. Notably, the heteroarene-functionalized thienopyrimidines have been shown to possess a variety of interesting biological properties.^[38] Our photocatalytic protocol also allows cascade bond forming processes providing interesting tricyclic compounds, for example **5q**, in almost quantitative yield. Notably, such cascade reactions were previously reported by Reiser and co-workers,^[39,40] using vinyl halides as the precursors for vinyl radicals. A poor yield of the C–H arylated product **5r** was obtained in presence of catalyst **1g** which can be attributed to the very low reduction potential of 4-chloroanisole ($E_{\text{red}} = -2.88$ V *vs.* SCE) and thus, defines the limitation of the method.^[5]

3.2.4 Scope of Tolerated Trapping Reagents

Depending on the aryl halide employed, the arylation reactions with **4a** led to product formation in poor to excellent yields. From previous work it is known that electron deficient aryl radicals react readily with electron rich counterparts.^[6,12,41]

Table 3-4. Scope of suitable trapping agents.

			
 <p>p-CN, 6a, 49%^a o-CN, 6b, 62%^b</p>	 <p>6c, 21% (24h)</p>	 <p>6d, 34% (24h) 16%^c (1a) 37%^c (1e) 28%^c (1g)</p>	 <p>6e, 33% (24h)</p>
 <p>X=C, 6f, 41%^d (22h) X=N, 6g, 48%^d (22h)</p>	 <p>6h, 15% (24h)</p>	 <p>R=CN, 6i, 47%^e R=CO₂Me, 6j, 37%^f</p>	 <p>6k, 38%^e</p>
 <p>6l, 50%^f</p>	 <p>6m, 31%^f</p>	 <p>6n, 75%</p>	 <p>6o, 39%^g</p>

Reaction conditions: A mixture containing of substrate **3'** (0.1 mmol), catalyst **1b** (10 mol% w.r.t. **3'**) crown ether (0.06 mmol) and Cs₂CO₃ (0.12 mmol) in a sealed snap vial equipped with stirring bar and under N₂ atmosphere, was dissolved in dry, degassed DMSO (1 mL). Trapping agent **4'** (1.5 mmol) was added *via* syringe needle (liquids) or before sealing the snap vial (solids). While stirring, the reaction was exposed to LED light (455 nm) for 18 hours (unless otherwise stated) from the plane bottom side of the vial; ^a 2.0 mmol of furan was used; ^b Cs₂CO₃ (0.3 mmol), perylene (0.01 mmol) and DIPEA (50 mol%) were used; ^c Catalyst **1** given in parenthesis was used instead of **1b**. ^d **4'f** (1.0 mmol), Cs₂CO₃ (0.3 mmol) and DIPEA (25 mol%) were used; ^e isocyanide (0.5 mmol) was used; ^f isocyanide (0.3 mmol) was used; ^g compound was not isolated, yield determined by crude NMR with internal standard method.

Furthermore, isocyanides are reported to react with aryl radicals.^[14,42] In contrast to activation strategy (II) mentioned in the introductory part, no sacrificial electron donor is necessary under the reaction conditions discussed in this work. Hence, excluding sacrificial electron donors like tertiary amines, which are efficient H-atom donors once oxidized to their radical cations, might throttle the predominant side reaction causing the dehalogenated, reduced substrate. We envisioned that this enables the use of less reactive agents as coupling partners, *i.e.* furans, thiophenes or even benzenes. C–H arylation reactions of furan and thiophene using aryl sulfonyl chlorides^[43] or aryl diazonium salts^[44] are well known and the desired heterocyclic products could be obtained in good yields. However, it has been realized that such heteroarenes are poor trapping reagents under reductive reaction conditions (typically in the presence of a sacrificial electron donor) using (hetero)aryl bromides or chlorides as substrates. Consequently, photoredox catalytic protocols to functionalize furan or thiophene using aryl halides are barely reported.^[6] Interestingly, that has also been realized when the amine donor was used in sub-stoichiometric amount.^[45] To our delight, the developed catalytic protocol allows for a variety of heteroarene functionalization: For example, when furan was used as trapping reagent the C–H arylated products were isolated in 49% and 62% yields respectively (**6a,6b**).^[46] Similarly, thiophene (**6d**) or alkoxy-substituted heteroarenes (**6c, 6e**) gave the desired products in moderate yield. Compound **6d** was also obtained when other derivatives of catalyst **1** were employed. In case of 1-phenylpyrrole (**4'f**) the excess amount of trapping agent was reduced (10 eq. w. r. to **3**). The corresponding coupling products (**6f, 6g**) nonetheless could be isolated in reasonable yield. Aromatic hydrocarbons, such as benzene, mesitylene, or *p*-xylene gave the corresponding C–H arylated product (example **6h**), however a low substrate conversion was observed. Recently, efficient trapping and cascade cyclization of aryl radicals with isocyanobiphenyls and 2-isocianoaryl thioethers were reported.^[14,42] Hence, isocyanides **4'i** and **4'k** were synthesized and reactions with several aryl chlorides were examined.^[47] The corresponding coupling products **6i-6m** could be isolated in moderate to good yield. Furthermore, aryl phosphonate **6n** was obtained in good yield when triethyl phosphite was used as trapping reagent and in addition, the pinacol ester of the aryl boronic acid **6o** was formed in the presence of bis(pinacolato)diboron.

3.2.5 Mechanistic Investigations

Excited state interactions (*e.g.* single electron transfer) between the luminescent catalyst molecule and a quencher cause a decrease in emission intensity and excited-state lifetime. Therefore, a steady state and time-resolved fluorescence titration was performed to elucidate the mechanism of the discussed reaction. The spectroscopic investigations were performed

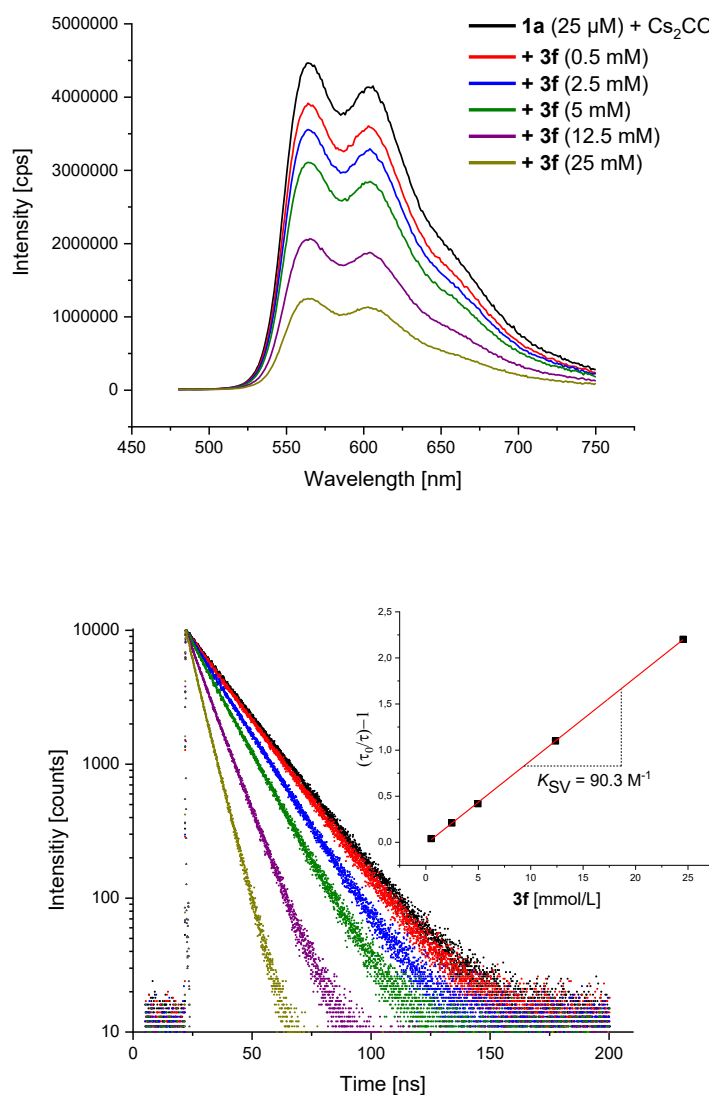
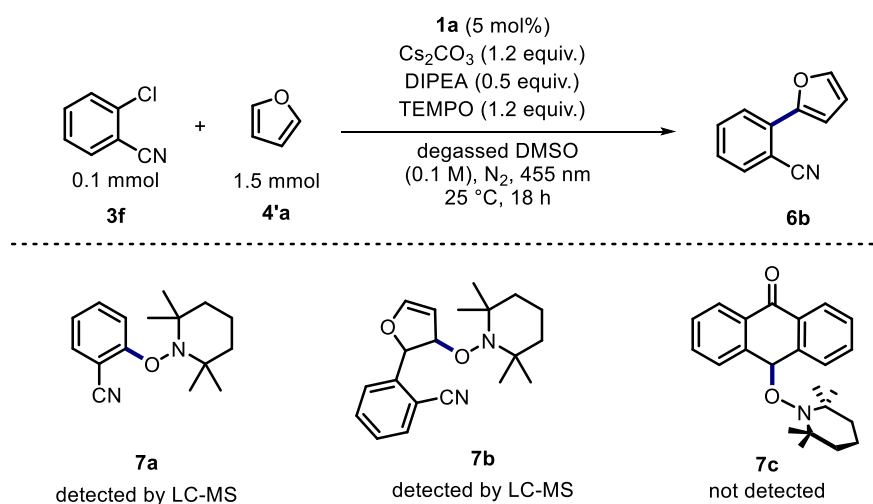


Figure 3-2. (top) Steady-state luminescence quenching of **1a** in presence of base. Superimposed emission spectra at different concentrations of **3f**; (bottom) time-resolved luminescence quenching of **1a** in presence of base. Stacked luminescence decays at different concentrations of **3f**; inset: Stern-Volmer plot of the time-resolved experiment.

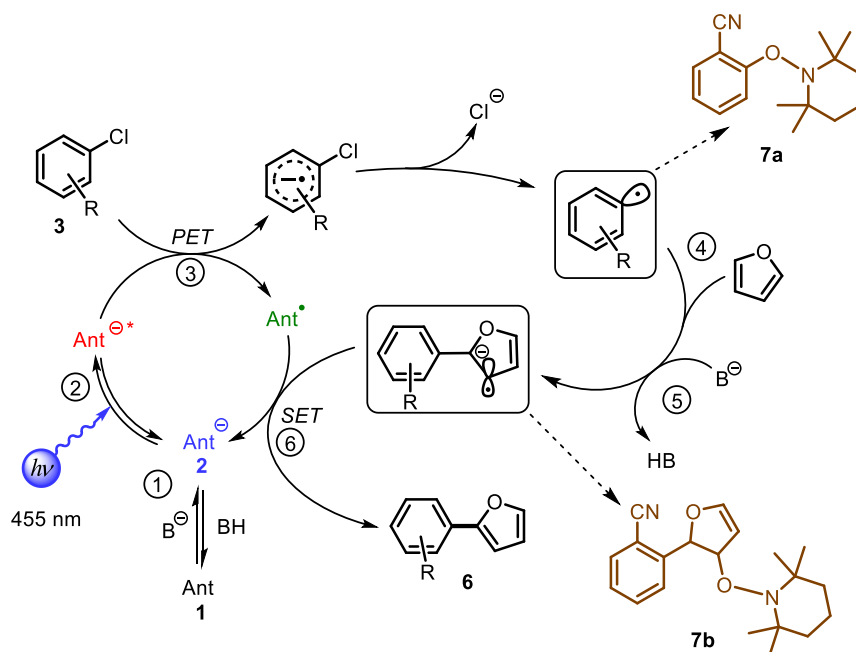
using **1a** in presence of a base as fluorophore and 2-chlorobenzonitrile (**3f**, $E_{\text{red}} = -2.01$ V *vs.* SCE) as an emission quencher. Notably, the compound **3f** was easily activated in the presence of **1b** to afford the desired coupling product with **4a** in 92% isolated yield (*cf.*, Table 3-3, **5f**). Hence, it is also expected to quench the excited state of anion **2a** *via* an electron transfer process. The steady-state fluorescence titration experiment revealed a decrease of emission intensity upon addition of the substrate **3f** (Figure 3-2, top). Moreover, in the time-resolved study a decline in the excited state lifetime was observed. A Stern-Volmer analysis revealed a linear correlation indicating a dynamic quenching of the excited **2a** by the aryl chloride **3f**. In a control experiment, no quenching, neither in the steady-state nor in the time-resolved experiment, was found when 2-chloroanisole (Figure S3-5 A, Experimental Part) was added. Chloroanisole exhibits a very negative reduction potential of -2.83 V *vs.* SCE and remains inert both, in C–H arylation reactions and in the quenching experiment in presence of catalyst **1a**. However, a humble conversion of 4-chloroanisole in presence of the strong photoreductant **1g** was found (*cf.*, Table 3-3, **5r**).



Scheme 3-2. (top) Reaction conditions for the TEMPO radical trapping experiment; (bottom) structural proposals for detected and expected adducts.

Next, we identified radical intermediates in the reaction mixture by trapping experiments (Scheme 3-2). The persistent radical TEMPO is known to trap other radicals efficiently to form stable adducts, which can be detected by mass analysis. Adding TEMPO (1.2 equiv.) to the reaction mixture of 2-chlorobenzonitrile (**3f**), furan (**4'a**) and catalyst **1a** led, besides the coupling product **6b**, to detectable amounts of TEMPO adducts, which could be assigned to structures **7a** and **7b** by LCMS analysis. These findings support the hypothesis of an initial

formed aryl radical (*cf.*, Scheme 3-2, **7a**) and the subsequent radical reaction with the present (hetero)arene (*cf.*, **7b**). In a control experiment examined in the dark, no TEMPO adducts could be detected, indicating the photochemical nature of this transformation.



Scheme 3-3. Proposed photocatalytic mechanism based on experimental findings.

Based on the results obtained in spectroscopic measurements and radical trapping experiments we propose the following mechanism (Scheme 3-3) for the photocatalyzed coupling reaction of (hetero)aryl chlorides with hetero(arenes). The visible light-absorbing catalyst **2** is in an acid base equilibrium with the neutral non-absorbing pre-catalyst **1** (**1**). UV-vis absorption and luminescence spectroscopy revealed, that **2** is photoexcited by blue light (**2**). Emission quenching studies showed that the excited state of **2a** interacts with suitable substrates. We propose a single electron transfer from the photoexcited anion **2a**^{*} to the (hetero)aryl chloride (**3**) to form a radical anion of the substrate **3**. Upon mesolytic cleavage, the reactive aryl radical intermediate is released, which is trapped by the (hetero)arene (**4**) to give a bicyclic radical intermediate. Walton recently showed that radicals adjacent to certain functional groups cause a remarkable increase in acidity. Moreover, cyclohexadienyl type radicals formed after addition of a radical to an (hetero)aromatic ring exhibit an enhanced acidity caused by the neighboring radical.^[48,49] Hence, such compounds are easily deprotonated in presence of base (**5**) to form a radical anion intermediate. Regeneration of the oxidized catalyst by single electron transfer (SET) from the radical anion intermediate provides the desired product **6** and closes the

catalytic cycle (6). The formation of the aryl radical as well as the bicyclic radical intermediate were confirmed by TEMPO trapping experiments (see Scheme 3-2, **7a** and **7b**).

3.3 Conclusion

A novel photocatalytic concept based on photoexcitation of an organic anionic ground state catalyst is reported. Instead of using high-energy light sources or accumulating the energy of two photons (conPET), we could show, that an initial chemical activation (*i.e.* deprotonation) of a ground state molecule followed by subsequent photoexcitation generates a strong anionic reducing agent, featuring a remarkably long excited state lifetime. The reaction methodology was used to activate a variety of aryl chlorides and the corresponding C–H arylation or coupling products were obtained in moderate to excellent yield. Furthermore, the reaction operates under very mild reaction conditions and avoids the use of sacrificial electron donor molecules, which are typically required in conPET processes. Thus, the reported metal-free protocol allows efficient C–C or C–Het bond-forming reactions while using bench-stable (hetero)aryl chlorides and many applications in organic synthesis can be envisaged.

3.4 Experimental Part

3.4.1 General Information

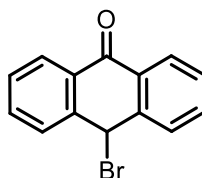
¹H-NMR: The following spectra were measured either on a Bruker Avance 300 (300 MHz) or on a Bruker Avance 400 (400 MHz). The chemical shifts are given in the unit δ (ppm) relative to chloroform (CDCl₃, 7.26 ppm) or dimethyl sulfoxide (DMSO-d₆, 2.50 ppm). The coupling constant (J) is given in Hertz (Hz). Definition of the signals: s = singlet, bs = broad singlet, d = doublet, t = triplet, q = quartet, m = multiplet. The integral above a certain signal displays the relative amount of hydrogen nuclei. **¹³C-NMR:** The following spectra were measured either on a Bruker Avance 300 (75.5 MHz) or on a Bruker Avance 400 (100.6 MHz). The chemical shifts are given in the unit δ (ppm) relative to chloroform (CDCl₃, 77.16 ppm) or dimethyl sulfoxide (DMSO-d₆, 39.52 ppm). ¹³C-NMR resonance assignment was aided using DEPT 135 techniques (DEPT = distortion less enhancement by polarization transfer) to distinguish CH₂ groups from CH and CH₃ groups and to assign quaternary carbons (C_q). **¹⁹F-NMR:** Isolated products containing fluorine were analyzed by fluorine NMR and spectra were measured on a Bruker Avance 300 (282.4 MHz). **³¹P-NMR:** Isolated products containing phosphorus were analyzed by phosphorus NMR and spectra were measured on a Bruker Avance 400 (162 MHz). **¹¹B-NMR:** Isolated products containing boron were analyzed by boron NMR on a Bruker Avance 400 (128 MHz). **Gas chromatography (GC)** measurements were performed on an Agilent Intuvo 9000 GC system coupled to a FID unit. The system was equipped with a capillary column (HP-5ms UI, length 30 m, diam. 0.25 mm, film 0.25 μ m) and worked with H₂ as carrier gas. GC program: The initial temperature of the GC was set to 40 °C and kept for 1.5 minutes. Subsequently, the oven temperature was increased at a rate of 25 °C/min. until reaching 280 °C, which was maintained for 3 min. Then, temperature was further increased (42 °C/min) until reaching 300 °C and final temperature was hold for 5 minutes. Injector temperature was set to 280 °C and temperature of the detecting unit to 310 °C. A split ratio of 30:1 (split flow 42 mL/min) was applied and the column flow was set to 1.4 mL/min. Low resolution mass analysis was performed on an Agilent 7890A connected to an Agilent 5975 MSD single quadrupole detector at the organic department of the university of Regensburg. The system was equipped with a capillary column (HP-5ms, length 30 m, diam. 0.25 mm, film 0.25 μ m) and worked with He as carrier gas. GC program: The initial temperature of the GC was set to 40 °C and kept for 3 minutes. Subsequently, the oven temperature was increased at a rate of 15 °C/min. until reaching 280 °C, which was maintained

for 5 min. Then, temperature was further increased (25 °C/min) until reaching 300 °C and final temperature was hold for 5 minutes. Injector temperature was set to 280 °C and temperature of the detecting unit to 310 °C. A split ratio of 40:1 (split flow 40 mL/min) was applied and the column flow was set to 1 mL/min. **Automated column chromatography** for purification of crude product mixtures was carried out on a Biotage® Isolera One flash purification system using flash silica gel. **Mass spectrometry (MS)** was performed in the Central Analytics Department of the University of Regensburg on a Finnigan MAT 95, an Agilent Q-TOF 6540 UHD, a Finnigan MAT SSQ 710 A and a ThermoQuest Finnigan TSQ 7000 for the determination of HRMS spectra. **Solvents and chemicals:** Solvents were employed either as p.a. grade or dried and distilled prior to use, according to literature known procedures.^[50] All commercial purchased chemicals (Sigma Aldrich, Alfa Aesar, Acros, Fluka, Maybridge, Merck, VWR, TCI) were used as received, without further purification. Air- and moisture-sensitive syntheses were performed under nitrogen atmosphere in flame dried glassware. Commercial purchased yellowish *N*-methylpyrrole **4a** was distilled prior to use and stored in the fridge under nitrogen atmosphere. **LEDs:** Reaction mixtures were irradiated with blue LEDs ($\lambda = 455 \pm 15$ nm, 700 mA, average radiant flux 232 ± 23 mW) and green LEDs ($\lambda = 535$ nm, 700 mA, average radiant flux 29 ± 5 mW). **Cyclic voltammetry** measurements were examined with a three-electrode system consisting a glassy carbon working electrode, a platinum wire counter electrode and a silver wire as a reference electrode. Data was processed on a potentiostat PGSTAT302N from Metrohm Autolab. Prior to the measurement the solvent DMSO (dry) was degassed with argon and TBATFB (0.1M) was added as supporting electrolyte. All experiments were performed under argon atmosphere. The ferrocen/ferrocenium couple was used as an internal reference. Measurements were performed at a scan rate of 0.05 V·s⁻¹. Potentials are reported against saturated calomel electrode (SCE) as reference. **UV-vis** measurements were performed on an Agilent Technologies Cary Series UV-Vis Spectrophotometer. Prior to measurements a solvent blank was recorded and subtracted. Precision cells (1 cm × 1 cm) made of quartz SUPRASIL® from Hellma® Analytics were used. **Luminescence** measurements were performed on a Horiba® Scientific FluoroMax-4 instrument using the above-mentioned quartz cells. **Luminescence lifetime** measurements were performed on a Horiba® Scientific DeltaPro™ fluorescence lifetime system using a 452 nm laser diode from Horibe Scientific DeltaDiode™ and above-mentioned quartz cells.

3.4.2 Synthesis of Catalysts and Reagents

3.4.2.1 Synthesis of Anthrone-catalysts 1

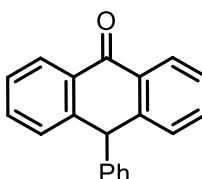
10-Bromoanthracen-9(10*H*)-one (**1b**)



Based on a literature known procedure^[51], crystalline 9-anthrone was grinded in a mortar to give a fine powder. A 100 mL round bottom flask equipped with stirring bar was charged with grinded 9-anthrone (5.0 g, 26 mmol, 1 equiv.) and chloroform (35 mL) was added. To the stirred suspension Br₂ (1.3 mL, 25 mmol, 1 equiv., dissolved in 7 mL CHCl₃) was added dropwise in the dark within 15 minutes. The resulting mixture was vigorously stirred for 2 hours. After that time HBr formation ceased which indicated completion of the reaction. The crude mixture was concentrated *in vacuo*, filtered off and washed with hexanes (100 mL). The crude material was further purified by stirring in boiling hexanes to give the title compound as pale-yellow powder (5.2 g, 74%).

¹H-NMR (400 MHz, CDCl₃) δ 8.28 (dd, *J* = 7.8, 1.4 Hz, 2H), 7.74 – 7.69 (m, 2H), 7.65 (td, *J* = 7.5, 1.5 Hz, 2H), 7.53 (td, *J* = 7.6, 1.3 Hz, 2H), 6.64 (s, 1H). **¹³C-NMR** (101 MHz, CDCl₃) δ 183.1, 141.1, 133.7, 131.3, 130.2, 129.4, 128.0, 43.9.

10-Phenylanthracen-9(10*H*)-one (**1c**)

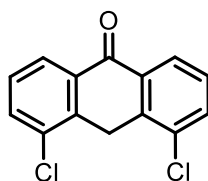


According to a literature known procedure^[52] a 25 mL two-neck flask equipped with stirring bar and reflux condenser was charged with **1b** (1.0 g, 3.7 mmol, 1 equiv.) and benzene (5 mL) was added. The resulting mixture was heated to reflux and AlCl₃ (1.3 g, 9.9 mmol, 2.7 equiv.) was added in small portions. Upon addition, the yellowish solution turned into dark. After the addition was finished, the reaction mixture was refluxed for 90 minutes. The solution was cooled down to room temperature and was poured into diluted aq. HCl (100 mL). The

resulting emulsion was extracted with benzene (3×25 mL) and the combined organic layers were washed with NaHCO₃, water and brine and dried over Na₂SO₄. The crude material was first recrystallized from ethanol and a second time from Et₂O. However, NMR spectra of the recrystallized compound indicated a mixture of compounds. To purify the compound, silica gel flash column chromatography was examined using a mixture of hexanes and DCM. The title compound was obtained as a reddish solid (173 mg, 18%).

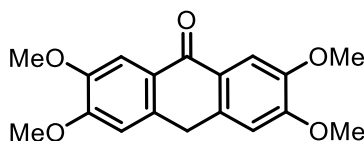
¹H-NMR (300 MHz, CDCl₃) δ 8.38 (dd, *J* = 7.8, 1.6 Hz, 2H), 7.55 – 7.39 (m, 4H), 7.32 – 7.16 (m, 5H), 7.15 – 7.08 (m, 2H), 5.43 (s, 1H). **¹³C-NMR** (75 MHz, CDCl₃) δ 184.5, 144.5, 144.3, 133.3, 131.2, 129.8, 129.2, 129.0, 127.4, 127.3, 127.0, 48.6.

4,5-Dichloroanthracen-9(10*H*)-one (1f)



Based on a literature known procedure^[53] a 250 mL three-necked flask equipped with condenser and dropping funnel was charged with 1,8-dichloroanthraquinone (2.8 g, 10 mmol, 1 equiv.) and glacial acetic acid (140 mL). The resulting solution was refluxed and over a period of 3 hours a mixture of SnCl₂·2H₂O (20.3 g, 90 mmol, 9 equiv.) in 37% HCl (38 mL) was added dropwise. The solution was cooled down to ambient temperature and for complete crystallization, the reaction was stored overnight in the fridge. The resulting crystals were filtered off and washed with glacial acetic acid. The crude mixture was purified by silica gel flash column chromatography (EtOAc/hexanes 8:2) to give the title compound as pale-yellow needles (530 mg, 20%).

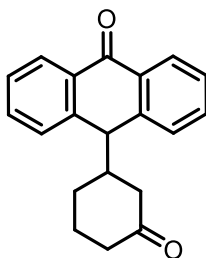
¹H-NMR (300 MHz, CDCl₃) δ 8.29 (dd, *J* = 7.9, 1.3 Hz, 2H), 7.71 (dd, *J* = 7.9, 1.3 Hz, 2H), 7.53 – 7.40 (m, 2H), 4.24 (s, 2H). **¹³C-NMR** (75 MHz, CDCl₃) δ 182.8 (C_q), 137.4 (C_q), 134.3 (C_q), 133.8 (CH_{ar}), 132.9 (C_q), 128.2 (CH_{ar}), 126.5 (CH_{ar}), 29.6 (CH₂).

2,3,6,7-tetramethoxyanthracen-9(10H)-one (1g)

(a) Synthesis of 9,10-diethyl-2,3,6,7-tetramethoxyanthracene: Based on a literature known procedure^[54] a 250 mL round bottom flask equipped with stirring bar was charged with conc. H₂SO₄ (50 mL) and cooled down to 0 °C. Over a period of 20 minutes, a solution of veratrole (26.6 mL, 0.2 mol, 1 equiv.), propanal (14.4 mL, 0.2 mol, 1 equiv.) and acetonitrile (10.5 mL, 0.2 mol, 1 equiv.) was added dropwise while stirring vigorously. Afterwards, the solution was stirred for 45 minutes at room temperature and poured carefully into 0.5 L of ice water. The reddish, sticky precipitate formed was filtered off, washed with water and was dried in air. For further purification, the crude material was recrystallized from MeOH to give the title compound as pale-yellow powder (1.97 g, 6%). (b) Synthesis of 2,3,6,7-tetramethoxy-9,10-anthraquinone: Based on a literature known procedure^[6] a 250 mL round bottom flask was charged with 9,10-diethyl-2,3,6,7-tetramethoxyanthracene (1.95 g, 5.5 mmol, 1 equiv.) and K₂Cr₂O₇ (8.1 g, 27.5 mmol, 5 equiv.). The compounds were suspended in acetic acid (65 mL) and stirred at 90 °C for 1 h. The mixture was cooled down to room temperature and the resulting yellow precipitate was filtered off, washed with water and Et₂O. The residue was dried in air and the title compound was obtained as yellow powder (0.77 g, 42%). (c) Synthesis of 2,3,6,7-tetramethoxyanthracen-9(10H)-one: Based on a literature known procedure^[55] an autoclave equipped with stirring bar was charged with 2,3,6,7-Tetramethoxyanthracene-9,10-dione (351 mg, 1.1 mmol, 1 equiv.) and 10% Pd/C (50 mg). The compounds were suspended in acetic acid (40 mL) and a hydrogen pressure of approx. 5 bar was applied to the autoclave. In an oil bath, the reaction mixture was heated to 90 °C and stirred for 1.5 h. After cooling down to room temperature, the hydrogen pressure was released, and the reaction mixture was extracted with CHCl₃ (3×25 mL). The combined organic layers were washed with 10% aqueous NaHCO₃ and brine, dried over Na₂SO₄ and concentrated *in vacuo*. The crude mixture was purified by silica flash column chromatography (DCM/Et₂O 97:3) to give the tetramethoxyanthrone **1g** as yellow solid (101 mg, 30%).

¹H-NMR (300 MHz, CDCl₃) δ 7.80 (s, 2H), 6.84 (s, 2H), 4.18 (s, 2H), 3.99 (d, *J* = 4.8 Hz, 12H). ¹³C-NMR (75 MHz, CDCl₃) δ 182.4 (C_q), 153.1 (C_q), 148.6 (C_q), 135.2 (C_q), 125.4 (C_q), 109.7 (CH_{ar}), 108.5 (CH_{ar}), 56.3 (CH_{ar}), 32.0 (CH₂).

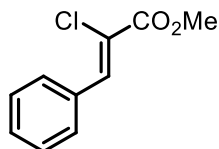
10-(3-Oxocyclohexyl)anthracen-9(10*H*)-one (1h)



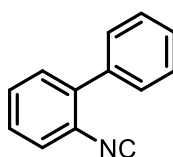
Based on a literature known procedure^[56] a 25 mL Schlenk flask equipped with stirring bar and reflux condenser was put under nitrogen atmosphere and charged with 9-anthrone (500 mg, 2.6 mmol, 1 equiv.), 2-cyclohexen-1-one (1.14g 11.9 mmol 4.6 equiv.), sodium methoxide (18.3 mg, 0.34 mmol, 0.13 equiv.) and methanol (5 mL). The resulting mixture was heated to reflux and stirred for 3 hours. After concentrating the crude mixture in vacuum, purification was accomplished by silica flash column chromatography (hexanes/EtOAc 90:10). Separation *via* chromatography was not complete, however recrystallization from EtOH using hot filtration technique afforded the title compound as white crystals (391 mg, 52%).

¹H-NMR (400 MHz, CDCl₃) δ 8.25 (ddd, *J* = 7.8, 3.9, 1.4 Hz, 2H), 7.59 (qd, *J* = 7.4, 1.5 Hz, 2H), 7.52 – 7.40 (m, 3H), 7.37 (d, *J* = 7.6 Hz, 1H), 4.19 (d, *J* = 3.4 Hz, 1H), 2.24 (dddd, *J* = 18.9, 12.3, 4.5, 2.6 Hz, 3H), 2.04 – 1.83 (m, 3H), 1.71 – 1.58 (m, 1H), 1.50 – 1.34 (m, 1H), 1.05 (qd, *J* = 12.9, 3.7 Hz, 1H). **¹³C-NMR** (101 MHz, CDCl₃) δ 210.6 (C_q), 185.2 (C_q), 142.4 (C_q), 141.9 (C_q), 133.6 (C_q), 132.7 (CH_{ar}), 132.6 (CH_{ar}), 128.8 (CH_{ar}), 128.7 (CH_{ar}), 127.7 (CH_{ar}), 127.7 (CH_{ar}), 127.5 (CH_{ar}), 127.3 (CH_{ar}), 48.8 (CH), 48.5 (CH), 45.4 (CH₂), 41.1 (CH₂), 27.7 (CH₂), 24.9 (CH₂).

3.4.2.2 Synthesis of Compounds used in Photoreactions

Methyl (Z)-2-chloro-3-phenylacrylate (3q)

According to a literature known procedure^[57] a flame dried 50 mL Schlenk flask equipped with stirring bar and septum stopper was charged with benzaldehyde (1.0 mL, 10 mmol, 1 equiv.), methyl chloroacetate (0.96 mL, 11 mmol, 1.1 equiv.) and dry DCM (15 mL). To the stirred mixture, a solution containing TiCl_4 (1.3 mL, 12 mmol, 1.2 equiv.) dissolved in DCM (12 mL, 1.0 M) was added dropwise over a period of 10 minutes and the resulting mixture was stirred for 30 minutes at room temperature. The flask was placed into a water cooling bath to maintain a temperature below 30 °C and Et_3N (2.8 mL, 20 mmol, 2 equiv.) was added dropwise over a period of 10 minutes. The reaction was stirred overnight and diluted with DCM (20 mL). The crude mixture was washed with 1.0 N aq. HCl (15 mL), water and brine. After drying over Na_2SO_4 , the solution was concentrated *in vacuo*. Purification was done by silica gel flash column chromatography (hexanes/ EtOAc 9:1) to obtain the title compound as white solid (0.57 g, 29%). **$^1\text{H-NMR}$** (400 MHz, CDCl_3) δ 7.92 (s, 1H), 7.87 – 7.82 (m, 2H), 7.48 – 7.40 (m, 3H), 3.91 (s, 3H). **$^{13}\text{C-NMR}$** (101 MHz, CDCl_3) δ 164.1 (C_q), 137.4 (CH), 133.0 (C_q), 130.8 (CH_{ar}), 130.4(CH_{ar}), 128.7(CH_{ar}), 121.9 (C_q), 53.5 (CH_3).

2-Isocyano-1,1'-biphenyl (4'i, 4'j, 4'm)

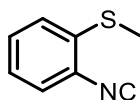
(a) Synthesis of *N*-([1,1'-biphenyl]-2-yl)formamide: According to a literature known procedure^[58] a 50 mL round bottom flask equipped with stirring bar was charged with 2-aminobiphenyl (1.1 g, 6.5 mmol, 1 equiv.) and THF (12 mL) and the resulting mixture was cooled down to 0 °C. Acetic formic anhydride (40 mmol, 6 equiv.) was freshly prepared from acetic anhydride (3.8 mL, 40 mmol) and formic acid (1.7 mL, 45 mmol) by stirring for 3 hours at 55 °C and added dropwise to the cooled reaction mixture. After stirring at room temperature

for 2 hours, the reaction was quenched with aqueous NaHCO_3 and extracted with EtOAc (3×10 mL). The combined organic layers were dried over Na_2SO_4 and concentrated under reduced pressure. The title compound was obtained as pale-yellow oil and was used without further purification for subsequent dehydration. (b) Synthesis of 2-isocyano-1,1'-biphenyl: Based on a literature known procedure^[9] a flame dried Schlenk flask equipped with stirring bar and septum stopper was charged under nitrogen with dry THF (12 mL), Et_3N (5.9 mL, 42 mmol, 7 equiv.) and *N*-([1,1'-biphenyl]-2-yl)formamide (1.18 g, 6.00 mmol, 1 equiv.) and the resulting mixture was cooled down to 0 °C. POCl_3 (0.95 mL, 10.2 mmol, 1.7 equiv.) was added dropwise over a period of 1 hour *via* syringe pump. Afterwards, the reaction mixture was stirred for 2 hours at 0 °C. The reaction was quenched by adding sat. aqueous solution of Na_2CO_3 and stirred for 1 hour at room temperature. The solution was extracted with CHCl_3 (3×10 mL) and the combined organic layers were dried over Na_2SO_4 . The compound was concentrated under reduced pressure and purified via silica gel flash column chromatography to obtain the title compound as dark green oil.

$^1\text{H-NMR}$ (400 MHz, CDCl_3) δ 7.55 – 7.40 (m, 8H), 7.38 (ddd, J = 7.8, 6.8, 2.2 Hz, 1H).

$^{13}\text{C-NMR}$ (101 MHz, CDCl_3) δ 139.0 (C_q), 137.1 (C_q), 130.7 (CH_{ar}), 129.7 (CH_{ar}), 129.1 (CH_{ar}), 128.7 (CH_{ar}), 128.5 (CH_{ar}), 128.3 (CH_{ar}), 128.0 (CH_{ar}).

(2-Isocyanophenyl)(methyl)sulfane (4'k, 4'l)



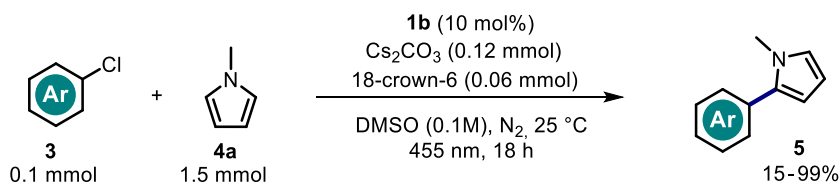
(a) Synthesis of *N*-(2-(methylthio)phenyl)formamide: According to a literature known procedure^[42] acetic formic anhydride was freshly prepared from acetic anhydride (3.8 mL, 40 mmol) and formic acid (1.7 mL, 45 mmol) by stirring at 55 °C for 3 hours. A 50 mL round bottom flask equipped with stirring bar and septum stopper was charged with thioaniline (1.5 g, 10.8 mmol, 1 equiv.) and DCM (20 mL) and the resulting mixture was cooled down to 0 °C. The freshly prepared acetic formic anhydride solution was added dropwise to the stirred reaction and the resulting mixture was stirred for 3 hours at room temperature. The reaction was quenched upon adding sat. aqueous Na_2CO_3 and was extracted with DCM (3×25 mL). The combined organic layers were dried over Na_2SO_4 , filtered and concentrated under reduced pressure to give the formamide as a slightly yellowish oil, which was used without further

purification in a subsequent dehydration reaction. (b) Synthesis of (2-Isocyanophenyl)(methyl)sulfane: Based on a literature known procedure^[42] a flame dried Schlenk flask equipped with stirring bar and septum stopper was charged with *N*-(2-(methylthio)phenyl)formamide (1.6 g, 9.5 mmol, 1 equiv.), NEt₃ (9.3 mL, 66.5 mmol, 7 equiv.) and dry THF (15 mL). The resulting mixture was cooled down to 0 °C and POCl₃ (1.5 mL, 16.2 mmol, 1.7 equiv.) was added dropwise over a period of 1 hour *via* syringe pump. Afterwards, the reaction was stirred for 2 hours at 0 °C. The mixture was diluted by adding EtOAc (15 mL) and slowly quenched with sat. aqueous Na₂CO₃ while stirring for 30 minutes. The crude mixture was extracted with EtOAc (3×10 mL) and the combined organic layers were dried over Na₂SO₄, filtered and concentrated under reduced pressure. Purification was done by silica flash column chromatography (hexanes/EtOAc) to obtain the title compound as yellow oil with unpleasant odour.

¹H-NMR (300 MHz, CDCl₃) δ 7.36 (dd, *J* = 8.2, 6.7 Hz, 2H), 7.28 – 7.21 (m, 1H), 7.15 (ddd, *J* = 8.0, 7.2, 1.4 Hz, 1H), 2.52 (s, 3H). **¹³C-NMR** (75 MHz, CDCl₃) δ 136.7 (C_q), 129.7 (CH_{ar}), 127.2 (CH_{ar}), 125.8 (CH_{ar}), 125.3 (CH_{ar}), 15.1 (CH₃).

3.4.3 General Procedures for the Photocatalyzed Reactions

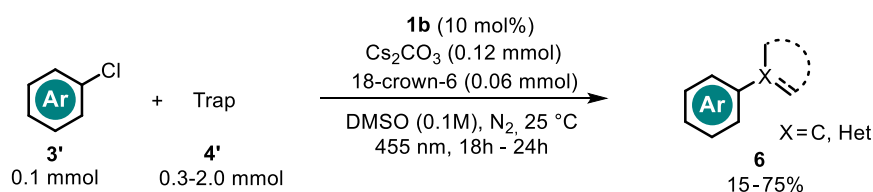
3.4.3.1 General Procedure A for the Photocatalyzed Arylation of *N*-methylpyrrole



A crimp vial (5 mL) equipped with stirring bar was charged with aryl chloride (0.1 mmol, 1 equiv.) and 10-bromo-9-anthrone (**1b**, 2.7 mg, 0.010 mmol, 10 mol%). Cesium carbonate (39.1 mg, 0.12 mmol, 1.2 equiv.) was added, the vial was sealed with a septum cap and deaerated *via* syringe needle. The reaction mixture was dissolved in a degassed solution of dry DMSO and crown ether (1.0 mL, 0.06 M). The reaction vessel was deaerated and flushed with nitrogen (3×) to exclude oxygen. Distilled pyrrole **4a** (133 μL, 1.5 mmol, 15 equiv.) was added *via* a gastight Hamilton® syringe and the vials were irradiated from the plane bottom side. Reaction temperature (25 °C) was maintained constant by employing a water cooling circuit connected to a thermostat. The reaction progress was monitored by GC-FID analysis. For

isolating compounds **5**, the reaction mixtures of three vessels run in parallel were combined. The crude mixture was washed with aqueous ammonium nitrate and extracted with ethyl acetate (3×20 mL). The combined organic layers were dried over Na₂SO₄, filtered and concentrated *in vacuo*. The crude material was purified by silica flash column chromatography using mixtures of hexanes and ethyl acetate as mobile phase.

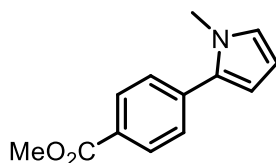
3.4.3.2 General Procedure B for the Photocatalyzed Arylation of (Hetero)arenes, Phosphite and Boronate esters



A crimp vial (5 mL) equipped with stirring bar was charged with aryl chloride (0.1 mmol, 1 equiv.) and 10-bromo-9-anthrone (**1b**, 2.7 mg, 0.010 mmol, 10 mol%). Cesium carbonate (39.1 mg, 0.12 mmol, 1.2 equiv.) was added, the vial was sealed with a septum cap and deaerated *via* syringe needle. The reaction mixture was dissolved in a degassed solution of dry DMSO and crown ether (1.0 mL, 0.06 M). The reaction vessel was deaerated and flushed with nitrogen (3×) to exclude oxygen. Trapping agent **4'** (0.3-2.0 mmol, 3-15 equiv.) was added either *via* a gastight Hamilton® syringe (liquids) or was added before sealing the vial (solids). The vials were irradiated from the plane bottom side. Reaction temperature (25 °C) was maintained constant by employing a water-cooling circuit connected to a thermostat. The reaction progress was monitored by GC-FID analysis. For isolating compounds **6**, the reaction mixtures of three vessels were combined. The crude mixture was washed with aqueous ammonium nitrate and extracted with ethyl acetate (3×20 mL). The combined organic layers were dried over Na₂SO₄, filtered and concentrated *in vacuo*. The crude material was purified by silica flash column chromatography using mixtures of hexanes and ethyl acetate as mobile phase.

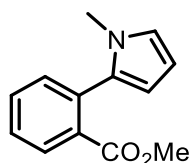
3.4.4 Characterization of the Products

Methyl 4-(1-methyl-1*H*-pyrrol-2-yl)benzoate (5a)



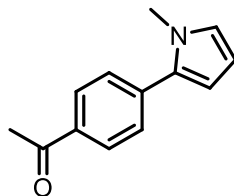
Compound was synthesized according to general procedure A using methyl 4-chlorobenzoate (17.1 mg, 0.1 mmol, 1 equiv.) and could be isolated as a white needles (95%). **¹H-NMR** (400 MHz, CDCl₃) δ 8.11 – 8.02 (m, 2H), 7.53 – 7.44 (m, 2H), 6.77 (t, *J* = 2.2 Hz, 1H), 6.34 (dd, *J* = 3.7, 1.8 Hz, 1H), 6.23 (dd, *J* = 3.7, 2.7 Hz, 1H), 3.94 (s, 3H), 3.72 (s, 3H). **¹³C-NMR** (101 MHz, CDCl₃) δ 167.1, 137.9, 133.6, 129.9, 128.0, 128.0, 125.2, 110.2, 108.4, 52.2, 35.5. **HRMS** (ESI⁺): calculated *m/z* for C₁₃H₁₄NO₂ [(M+H)⁺] 216.1019; found 216.1023. Spectral data is in accordance with literature.^[59]

Methyl 2-(1-methyl-1*H*-pyrrol-2-yl)benzoate (5b)



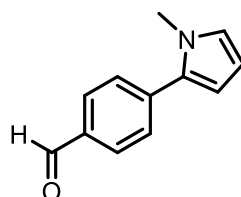
Compound was synthesized according to general procedure A using methyl 2-chlorobenzoate (17.1 mg, 0.1 mmol, 1 equiv.) and could be isolated as a colorless oil (51%). **¹H-NMR** (300 MHz, CDCl₃) δ 7.91 (dd, *J* = 7.7, 1.5 Hz, 1H), 7.54 (td, *J* = 7.5, 1.5 Hz, 1H), 7.48 – 7.36 (m, 2H), 6.81 – 6.64 (m, 1H), 6.20 (dd, *J* = 3.6, 2.0 Hz, 1H), 6.08 (d, *J* = 3.4 Hz, 1H), 3.74 (s, 3H), 3.41 (s, 3H). **¹³C-NMR** (75 MHz, CDCl₃) δ 168.2, 134.0, 132.7, 132.5, 132.0, 131.5, 129.9, 127.9, 122.4, 108.5, 107.6, 52.4, 34.3. **HRMS** (ESI⁺): calculated *m/z* for C₁₃H₁₄NO₂ [(M+H)⁺] 216.1019; found 216.1022 Spectral data is in accordance with literature.^[5]

1-(4-(1-Methyl-1*H*-pyrrol-2-yl)phenyl)ethan-1-one (5c)



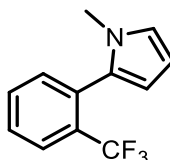
Compound was synthesized according to general procedure A using 4-chloroacetophenone (15.5 mg, 0.1 mmol, 1 equiv.) and could be isolated as a yellow solid (36%). **¹H-NMR** (400 MHz, DMSO-*d*₆) δ 8.01 – 7.93 (m, 2H), 7.62 – 7.57 (m, 2H), 6.93 (t, *J* = 2.2 Hz, 1H), 6.35 (dd, *J* = 3.7, 1.8 Hz, 1H), 6.11 (dd, *J* = 3.7, 2.7 Hz, 1H), 3.72 (s, 3H), 2.59 (s, 3H). **¹³C-NMR** (101 MHz, DMSO-*d*₆) δ 197.2, 137.4, 134.3, 132.3, 128.5, 127.3, 126.1, 110.1, 107.9, 35.3, 26.6. **HRMS** (ESI+): calculated *m/z* for C₁₃H₁₄NO [(M+H)⁺] 200.107; found 200.1075. Spectral data is in accordance with literature.^[6]

4-(1-Methyl-1*H*-pyrrol-2-yl)benzaldehyde (5d)



Compound was synthesized according to general procedure A using 4-chlorobenzaldehyde (14.1 mg, 0.1 mmol, 1 equiv.) and could be isolated as brownish solid (15%). **¹H-NMR** (400 MHz, DMSO-*d*₆) δ 10.00 (s, 1H), 7.94 – 7.90 (m, 2H), 7.71 – 7.66 (m, 2H), 6.95 (t, *J* = 2.2 Hz, 1H), 6.40 (dd, *J* = 3.7, 1.8 Hz, 1H), 6.13 (dd, *J* = 3.7, 2.6 Hz, 1H), 3.74 (s, 3H). **¹³C-NMR** (101 MHz, DMSO-*d*₆) δ 192.4, 138.6, 133.7, 130.9, 129.8, 127.6, 126.5, 110.6, 108.0, 35.4. **HRMS** (ESI+): calculated *m/z* for C₁₂H₁₂NO [(M+H)⁺] 186.0913; found 186.0912 Spectral data is in accordance with literature.^[12]

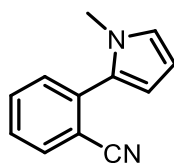
1-Methyl-2-(2-(trifluoromethyl)phenyl)-1*H*-pyrrole (5e)



Compound was synthesized according to general procedure A using 2-chlorobenzotrifluoride (18.1 mg, 0.1 mmol, 1 equiv.). Deviation of general procedure A: Et₂O was used to extract the crude reaction mixture as the compound is volatile. The title compound could be isolated as a

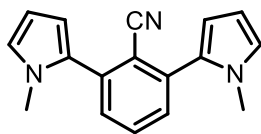
colorless oil (52%). **¹H-NMR** (300 MHz, CDCl₃) δ 7.80 – 7.73 (m, 1H), 7.62 – 7.45 (m, 2H), 7.39 (ddt, *J* = 7.5, 1.5, 0.7 Hz, 1H), 6.74 – 6.71 (m, 1H), 6.22 (dd, *J* = 3.6, 2.7 Hz, 1H), 6.16 (ddd, *J* = 3.7, 1.8, 0.7 Hz, 1H), 3.38 (s, 3H). **¹³C-NMR** (75 MHz, CDCl₃) δ 133.6, 132.6 (q, *J* = 2.1 Hz), 131.2, 130.9 (q, *J* = 29.2 Hz), 129.6, 128.3, 126.3 (q, *J* = 5.2 Hz), 124.0 (q, *J* = 27.4 Hz), 122.4, 110.3 (q, *J* = 1.7 Hz), 107.4, 34.4. **¹⁹F-NMR** (282 MHz, CDCl₃) δ -59.8. **HRMS** (EI): calculated *m/z* for C₁₂H₁₀F₃N [M⁺] 225.07599; found 225.07593. Spectral data is in accordance with literature.^[60]

2-(1-Methyl-1*H*-pyrrol-2-yl)benzonitrile (5f)



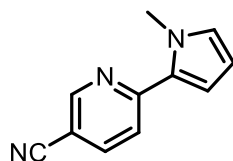
Compound was synthesized according to general procedure A using 2-chlorobenzonitrile (13.8 mg, 0.1 mmol, 1 equiv.) and could be isolated as a colorless oil (92%). **¹H-NMR** (400 MHz, CDCl₃) δ 7.78 – 7.70 (m, 1H), 7.61 (td, *J* = 7.7, 1.4 Hz, 1H), 7.47 – 7.36 (m, 2H), 6.83 – 6.76 (m, 1H), 6.41 (dd, *J* = 3.7, 1.7 Hz, 1H), 6.25 (dd, *J* = 3.7, 2.7 Hz, 1H), 3.61 (s, 3H). **¹³C-NMR** (101 MHz, CDCl₃) δ 137.1, 133.6, 132.5, 131.0, 130.1, 127.5, 124.9, 118.7, 113.0, 111.6, 108.4, 35.0. **HRMS** (EI): calculated *m/z* for C₁₂H₁₀N₂ [M⁺] 182.08385; found 182.08344. Spectral data is in accordance with literature.^[5]

2,6-Bis(1-methyl-1*H*-pyrrol-2-yl)benzonitrile (5g)



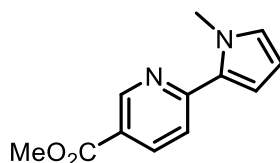
Compound was synthesized according to general procedure A using 2,6-dichlorobenzonitrile (17.2 mg, 0.1 mmol, 1 equiv.) and could be isolated as a colorless oil (84%). **¹H-NMR** (300 MHz, CDCl₃) δ 7.61 (dd, *J* = 8.2, 7.3 Hz, 1H), 7.43 – 7.34 (m, 2H), 6.81 (dd, *J* = 2.7, 1.8 Hz, 2H), 6.42 (dd, *J* = 3.7, 1.8 Hz, 2H), 6.26 (dd, *J* = 3.7, 2.7 Hz, 2H), 3.65 (s, 6H). **¹³C-NMR** (75 MHz, CDCl₃) δ 138.2, 131.8, 130.2, 129.7, 124.8, 117.9, 113.5, 111.6, 108.4, 35.0. **HRMS** (EI): calculated *m/z* for C₁₇H₁₅N₃ [M⁺] 261.12605; found 261.12538. Spectral data is in accordance with literature.^[4]

6-(1-Methyl-1*H*-pyrrol-2-yl)nicotinonitrile (**5h**)



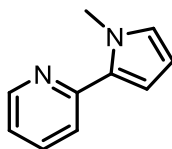
Compound was synthesized according to general procedure A using 2-chloro-5-cyanopyridine (13.9 mg, 0.1 mmol, 1 equiv.) and could be isolated as a pale-yellow solid (95%). **¹H-NMR** (400 MHz, CDCl₃) δ 8.76 (d, *J* = 1.6 Hz, 1H), 7.81 (dd, *J* = 8.5, 2.2 Hz, 1H), 7.60 (d, *J* = 8.4 Hz, 1H), 6.81 (t, *J* = 2.2 Hz, 1H), 6.77 (dd, *J* = 4.0, 1.8 Hz, 1H), 6.21 (dd, *J* = 4.0, 2.6 Hz, 1H), 4.04 (s, 3H). **¹³C-NMR** (101 MHz, CDCl₃) δ 155.3, 151.9, 138.8, 130.4, 129.4, 120.1, 117.7, 114.1, 108.8, 104.9, 38.2. **HRMS** (EI): calculated *m/z* for C₁₁H₉N₃ [M⁺] 183.07910; found 183.07852. Spectral data is in accordance with literature.^[4]

Methyl 6-(1-methyl-1*H*-pyrrol-2-yl)nicotinate (**5i**)



Compound was synthesized according to general procedure A using methyl 6-chloropyridine-3-carboxylate (13.9 mg, 0.1 mmol, 1 equiv.) and could be isolated as white needles (95%). **¹H-NMR** (400 MHz, CDCl₃) δ 9.13 (d, *J* = 1.6 Hz, 1H), 8.19 (dd, *J* = 8.5, 2.2 Hz, 1H), 7.63 – 7.53 (m, 1H), 6.79 (t, *J* = 2.2 Hz, 1H), 6.74 (dd, *J* = 3.9, 1.8 Hz, 1H), 6.20 (dd, *J* = 3.9, 2.6 Hz, 1H), 4.05 (s, 3H), 3.94 (s, 3H). **¹³C-NMR** (101 MHz, CDCl₃) δ 166.2, 156.0, 150.3, 137.2, 131.3, 128.4, 121.9, 120.1, 113.1, 108.4, 52.3, 37.8. **HRMS** (ESI⁺): calculated *m/z* for C₁₂H₁₃N₂O₂ [(M+H)⁺] 217.0972; found 217.0976.

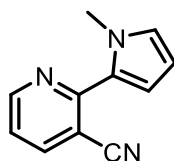
2-(1-methyl-1*H*-pyrrol-2-yl)pyridine (**5j**)



Compound was synthesized following the general procedure A using 2-chloropyridine (11.4 mg, 0.1 mmol, 1 equiv.). Deviation from the general procedure: 9(10*H*)-Acridanone **1e** (3.9 mg, 0.02 mmol, 20 mol%) was used instead of catalyst **1b**, **4a** (178 μL, 2.0 mmol, 20 equiv.), Cs₂CO₃ (65.2 mg, 0.2 mmol, 2 equiv) and 18-crown-6 (26.4 mg, 0.1 mmol, 1 equiv.)

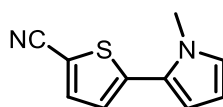
were used. The reaction was irradiated for 24 hours. The product was obtained as colorless oil (35%). **¹H-NMR** (300 MHz, CDCl₃) δ 8.57 (d, *J* = 4.2 Hz, 1H), 7.65 (td, *J* = 7.9, 1.7 Hz, 1H), 7.53 (d, *J* = 8.0 Hz, 1H), 7.08 (ddd, *J* = 7.3, 4.9, 1.1 Hz, 1H), 6.79 – 6.69 (m, 1H), 6.58 (dd, *J* = 3.7, 1.8 Hz, 1H), 6.19 (dd, *J* = 3.7, 2.6 Hz, 1H), 4.00 (s, 3H). **¹³C-NMR** (75 MHz, CDCl₃) δ 152.7, 148.6, 136.4, 132.3, 126.5, 121.6, 120.4, 110.9, 107.8, 37.0. Spectral data in accordance with literature.^[8]

2-(1-Methyl-1*H*-pyrrol-2-yl)nicotinonitrile (5k)



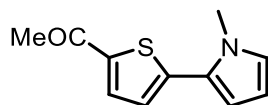
Compound was synthesized according to general procedure A using 2-chloro-3-cyanopyridine (13.9 mg, 0.1 mmol, 1 equiv.) and could be isolated as a white solid (99%). **¹H-NMR** (400 MHz, CDCl₃) δ 8.73 (dd, *J* = 4.8, 1.8 Hz, 1H), 7.98 (dd, *J* = 7.9, 1.9 Hz, 1H), 7.17 (dd, *J* = 7.9, 4.8 Hz, 1H), 7.08 (dd, *J* = 4.0, 1.7 Hz, 1H), 6.82 (dd, *J* = 2.6, 1.8 Hz, 1H), 6.24 (dd, *J* = 4.0, 2.6 Hz, 1H), 3.91 (s, 3H). **¹³C-NMR** (101 MHz, CDCl₃) δ 153.8(C_q), 151.8 (CH_{ar}), 142.1 (CH_{ar}), 128.5 (C_q), 128.2 (CH_{ar}), 119.6 (CH_{ar}), 118.4 (C_q), 115.3 (CH_{ar}), 108.4 (CH_{ar}), 106.2 (C_q), 36.9 (CH₃). **HRMS** (EI): calculated *m/z* for C₁₁H₉N₃ [M⁺] 183.07910; found 183.07862. Spectral data in accordance with literature.^[61]

5-(1-Methyl-1*H*-pyrrol-2-yl)thiophene-2-carbonitrile (5l)



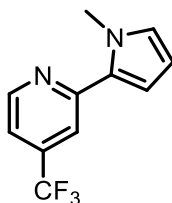
Compound was synthesized according to general procedure A using 2-acetyl-5-chlorothiopen (16.1 mg, 0.1 mmol, 1 equiv.) and could be isolated as a pale-yellow solid (65%). **¹H-NMR** (400 MHz, CDCl₃) δ 7.55 (d, *J* = 3.9 Hz, 1H), 6.99 (d, *J* = 3.9 Hz, 1H), 6.76 (t, *J* = 2.2 Hz, 1H), 6.46 (dd, *J* = 3.8, 1.8 Hz, 1H), 6.18 (dd, *J* = 3.8, 2.7 Hz, 1H), 3.77 (s, 3H). **¹³C-NMR** (101 MHz, CDCl₃) δ 142.8, 138.0, 126.3, 125.3, 123.8, 114.5, 112.2, 108.9, 107.1, 35.7. **HRMS** (EI): calculated *m/z* for C₁₀H₈N₂S [M⁺] 187.03245; found 187.03263.

1-(5-(1-Methyl-1*H*-pyrrol-2-yl)thiophen-2-yl)ethan-1-one (5m)

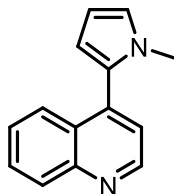


Compound was synthesized according to general procedure A using 5-chloro-2-thiophencarbonitrile (14.4 mg, 0.1 mmol, 1 equiv.) and could be isolated as an orange oil (67%). **¹H-NMR** (400 MHz, CDCl₃) δ 7.62 (d, *J* = 4.0 Hz, 1H), 7.05 (d, *J* = 4.0 Hz, 1H), 6.75 (t, *J* = 2.2 Hz, 1H), 6.50 (dd, *J* = 3.8, 1.7 Hz, 1H), 6.18 (dd, *J* = 3.8, 2.7 Hz, 1H), 3.80 (s, 3H), 2.55 (s, 3H). **¹³C-NMR** (101 MHz, CDCl₃) δ 190.6, 144.0, 141.8, 133.3, 126.9, 126.2, 124.4, 111.7, 108.7, 36.0, 26.6. **HRMS** (ESI⁺): calculated *m/z* for C₁₁H₁₂NOS [(M+H)⁺] 206.0634; found 206.0637. Spectral data is in accordance with literature.^[5]

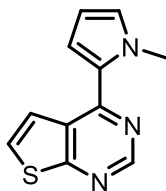
2-(1-Methyl-1*H*-pyrrol-2-yl)-4-(trifluoromethyl)pyridine (5n)



Compound was synthesized according to general procedure A using 2-chloro-4-(trifluoromethyl)pyridine (18.2 mg, 0.1 mmol, 1 equiv.). Deviation of general procedure A: Et₂O was used to extract the crude reaction mixture as the compound is volatile. The title compound could be isolated as colorless oil (61%). **¹H-NMR** (300 MHz, CDCl₃) δ 8.70 (d, *J* = 5.1 Hz, 1H), 7.75 – 7.70 (m, 1H), 7.26 – 7.22 (m, 1H), 6.78 (t, *J* = 2.2 Hz, 1H), 6.69 (dd, *J* = 3.9, 1.8 Hz, 1H), 6.21 (dd, *J* = 3.8, 2.6 Hz, 1H), 4.02 (s, 3H). **¹³C-NMR** (75 MHz, CDCl₃) δ 153.8, 149.6, 138.7 (q, *J* = 33.7 Hz), 131.1, 128.5, 123.1 (q, *J* = 273.1 Hz), 116.7 (q, *J* = 3.8 Hz), 115.3 (q, *J* = 3.4 Hz), 112.2, 108.2, 37.5. **¹⁹F-NMR** (282 MHz, CDCl₃) δ -65.5. **HRMS** (EI): calculated *m/z* for C₁₁H₉F₃N₂ [M⁺] 225.06341; found 225.06386. Spectral data is in accordance with literature.^[6]

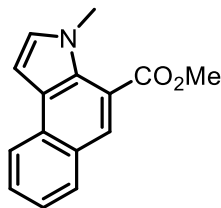
4-(1-Methyl-1*H*-pyrrol-2-yl)quinoline (5o)

Compound was synthesized according to general procedure A using 4-chloroquinoline (16.4 mg, 0.1 mmol, 1 equiv.) and could be isolated as a pale orange oil (91%). **¹H-NMR** (400 MHz, CDCl₃) δ 8.94 (d, *J* = 4.4 Hz, 1H), 8.16 (d, *J* = 8.4 Hz, 1H), 7.90 (d, *J* = 8.0 Hz, 1H), 7.73 (ddd, *J* = 8.4, 6.8, 1.5 Hz, 1H), 7.53 (ddd, *J* = 8.3, 6.8, 1.3 Hz, 1H), 7.33 (d, *J* = 4.4 Hz, 1H), 6.90 – 6.83 (m, 1H), 6.37 (dd, *J* = 3.6, 1.7 Hz, 1H), 6.35 – 6.30 (m, 1H), 3.50 (s, 3H). **¹³C-NMR** (101 MHz, CDCl₃) δ 149.9, 148.9, 139.8, 129.9, 129.6, 129.6, 128.0, 126.9, 126.5, 124.5, 122.5, 111.9, 108.4, 35.0. **HRMS** (EI): calculated *m/z* for C₁₄H₁₂N₂ [M⁺] 208.09927; found 208.09950. Spectral data is in accordance with literature.^[4]

4-(1-Methyl-1*H*-pyrrol-2-yl)thieno[2,3-*d*]pyrimidine (5p)

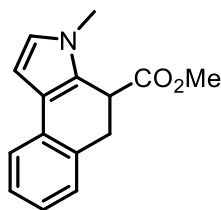
Compound was synthesized according to general procedure A using 4-chlorothieno[2,3-*d*]pyrimidine (17.1 mg, 0.1 mmol, 1 equiv.) and could be isolated as white needles (47%). **¹H-NMR** (400 MHz, CDCl₃) δ 9.01 (s, 1H), 7.66 (d, *J* = 6.1 Hz, 1H), 7.49 (d, *J* = 6.1 Hz, 1H), 6.93 – 6.84 (m, 2H), 6.29 (dd, *J* = 3.9, 2.6 Hz, 1H), 4.05 (s, 3H). **¹³C-NMR** (101 MHz, CDCl₃) δ 169.2 (C_q), 153.7 (C_q), 152.7 (CH_{ar}), 128.9 (C_q), 128.8 (CH_{ar}), 127.1 (C_q), 126.1 (CH_{ar}), 121.9 (CH_{ar}), 116.3 (CH_{ar}), 108.8 (CH_{ar}), 37.0 (CH₃). **HRMS** (EI): calculated *m/z* for C₁₁H₉N₃S [M⁺]; 215.05117 found 215.04981.

Methyl 3-methyl-3*H*-benzo[*e*]indole-4-carboxylate (5q-ox)

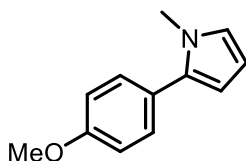


Compound was synthesized according to general procedure A using the vinyl chloride methyl (*Z*)-2-chloro-3-phenylacrylate (19.7 mg, 0.1 mmol, 1 equiv.) and could be isolated as a reddish solid (53%). **¹H-NMR** (400 MHz, CDCl₃) δ 8.23 (d, *J* = 8.3 Hz, 1H), 8.09 (s, 1H), 7.93 (d, *J* = 8.1 Hz, 1H), 7.61 (ddd, *J* = 8.3, 6.9, 1.3 Hz, 1H), 7.44 (ddd, *J* = 8.2, 6.9, 1.2 Hz, 1H), 7.14 (d, *J* = 3.1 Hz, 1H), 7.07 (d, *J* = 3.1 Hz, 1H), 4.03 (s, 3H), 3.97 (s, 3H). **¹³C-NMR** (101 MHz, CDCl₃) δ 168.2 (C_q, C=O), 130.1 (CH_{ar}), 130.0 (C_q), 129.4 (CH_{ar}), 129.3 (C_q), 127.8 (CH_{ar}), 127.5 (C_q), 126.6 (CH_{ar}), 126.2 (C_q), 124.0 (CH_{ar}), 122.9 (CH_{ar}), 118.1 (C_q), 100.6 (CH_{ar}), 52.5 (CH₃), 37.6 (CH₃). **HRMS** (ESI⁺): calculated *m/z* for C₁₅H₁₄NO₂ [(M+H)⁺]; 240.1019 found 240.102.

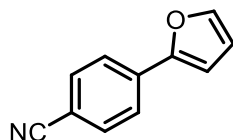
Methyl 3-methyl-4,5-dihydro-3*H*-benzo[*e*]indole-4-carboxylate (5q-red)



Compound was synthesized according to general procedure A using 4-chloroacetophenone (15.5 mg, 0.1 mmol, 1 equiv.) and could be isolated as a colorless oil (44%). **¹H-NMR** (300 MHz, CDCl₃) δ 7.40 – 7.33 (m, 1H), 7.22 – 7.15 (m, 2H), 7.08 – 6.99 (m, 1H), 6.62 (d, *J* = 2.8 Hz, 1H), 6.42 (d, *J* = 2.9 Hz, 1H), 3.84 (dd, *J* = 7.5, 2.3 Hz, 1H), 3.65 (s, 3H), 3.59 (s, 3H), 3.43 (dd, *J* = 15.7, 2.2 Hz, 1H), 3.27 (dd, *J* = 15.7, 7.5 Hz, 1H). **¹³C-NMR** (75 MHz, CDCl₃) δ 172.4 (C_q), 132.6 (C_q), 130.7 (C_q), 128.1 (CH_{ar}), 127.0 (CH_{ar}), 125.9 (C_q), 124.9 (CH_{ar}), 123.2 (CH_{ar}), 121.7 (CH_{ar}), 119.9 (C_q), 102.6 (CH_{ar}), 52.4 (CH), 37.2 (CH₃), 33.8 (CH₃), 32.7 (CH₂). **HRMS** (EI): calculated *m/z* for C₁₅H₁₅NO₂ [M⁺]; 241.10973 found 241.10957.

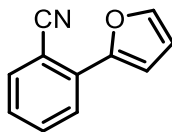
2-(4-methoxyphenyl)-1-methyl-1*H*-pyrrole (5r)

Compound was synthesized according to general procedure A using 4-chloroanisole (15.5 mg, 0.1 mmol, 1 equiv.) and catalyst **1g** (0.015 mmol, 15 mol%) in presence of Cs₂CO₃ (0.2 mmol, 2 equiv.) and could be isolated as a pale-yellow oil (9%). **¹H-NMR** (400 MHz, CDCl₃) δ 7.35 – 7.30 (m, 2H), 6.97 – 6.90 (m, 2H), 6.69 (dd, *J* = 2.7, 1.9 Hz, 1H), 6.19 (dd, *J* = 3.6, 2.7 Hz, 1H), 6.15 (dd, *J* = 3.5, 1.9 Hz, 1H), 3.84 (s, 3H), 3.63 (s, 3H). **¹³C-NMR** (101 MHz, CDCl₃) δ 158.8 (C_q), 134.5 (C_q), 130.2, 126.1 (C_q), 123.1, 113.9, 108.1, 107.7, 55.5, 35.0. Spectral data in accordance with literature.^[5]

4-(Furan-2-yl)benzonitrile (6a)

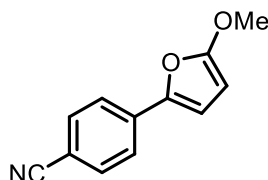
Compound was synthesized according to general procedure B using 4-chlorobenzonitrile (13.8 mg, 0.1 mmol, 1 equiv.) and furan (156 μL, 2.0 mmol, 20 equiv.). The title compound was obtained as white needles (49%). **¹H-NMR** (400 MHz, CDCl₃) δ 7.80 – 7.71 (m, 2H), 7.69 – 7.61 (m, 2H), 7.54 (d, *J* = 1.7 Hz, 1H), 6.81 (d, *J* = 3.4 Hz, 1H), 6.53 (dd, *J* = 3.5, 1.8 Hz, 1H). **¹³C-NMR** (101 MHz, CDCl₃) δ 152.1 (C_q), 143.8 (CH_{ar}), 134.8 (CH_{ar}), 132.7 (C_q), 124.1 (CH_{ar}), 119.1 (C_q), 112.4 (CH_{ar}), 110.4 (CH_{ar}), 108.3 (C_q). **HRMS** (EI): calculated *m/z* for C₁₁H₇NO [M⁺] 169.05222; found 169.05270. Spectral data in accordance with literature.^[62]

2-(Furan-2-yl)benzonitrile (6b)

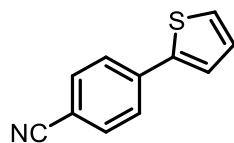


Compound was synthesized according to general procedure B using 2-chlorobenzonitrile (13.8 mg, 0.1 mmol, 1 equiv.) and furan (109 μ L, 1.5 mmol, 15 equiv.). Deviation from the general procedure: Perylene (2.5 mg, 0.01 mmol, 10 mol%) and DIPEA (8.7 μ L, 0.05 mmol, 0.5 equiv.) was added and 3 equiv. of Cs_2CO_3 were used. The title compound was obtained as slightly yellow solid (62%). **$^1\text{H-NMR}$** (400 MHz, CDCl_3) δ 7.89 (dt, J = 8.1, 0.8 Hz, 1H), 7.70 (dd, J = 7.8, 1.0 Hz, 1H), 7.65 – 7.58 (m, 1H), 7.56 (dd, J = 1.8, 0.7 Hz, 1H), 7.37 – 7.27 (m, 2H), 6.56 (dd, J = 3.5, 1.8 Hz, 1H). **$^{13}\text{C-NMR}$** (101 MHz, CDCl_3) δ 149.9 (C_q), 143.5 (CH_{ar}), 134.3 (CH_{ar}), 133.4 (CH_{ar}), 133.1 (CH_{ar}), 127.2 (CH_{ar}), 126.1 (CH_{ar}), 119.1 (C_q), 112.4 (CH_{ar}), 110.6 (CH_{ar}), 107.0 (C_q). **HRMS** (EI): calculated m/z for $\text{C}_{11}\text{H}_7\text{NO}$ [M^+] 169.05222; found 169.05266. Spectral data in accordance with literature.^[63]

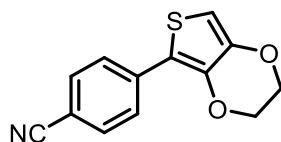
4-(5-Methoxyfuran-2-yl)benzonitrile (6c)



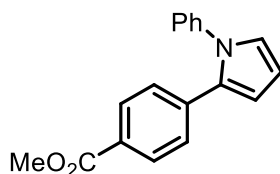
Compound was synthesized according to general procedure B using 4-chlorobenzonitrile (13.8 mg, 0.1 mmol, 1 equiv.) and 2-methoxyfuran (138 μ L, 1.5 mmol, 15 equiv.). The title compound was obtained as colorless needles (21%). **$^1\text{H-NMR}$** (300 MHz, CDCl_3) δ 7.58 (s, 4H), 6.72 (d, J = 3.5 Hz, 1H), 5.32 (d, J = 3.4 Hz, 1H), 3.93 (s, 3H). **$^{13}\text{C-NMR}$** (75 MHz, CDCl_3) δ 162.8 (C_q), 142.3 (C_q), 134.7 (C_q), 132.7 (CH_{ar}), 122.5 (CH_{ar}), 119.4 (C_q), 110.4 (CH_{ar}), 108.9 (C_q), 82.8 (CH_{ar}), 58.0 (CH_3). **LRMS** (EI): calculated m/z for $\text{C}_{12}\text{H}_9\text{NO}_2$ [M^+]; 199.0633 found 199.0625

4-(Thiophen-2-yl)benzonitrile (6d)

Compound was synthesized according to general procedure B using 4-chlorobenzonitrile (13.8 mg, 0.1 mmol, 1 equiv.) and thiophene (120 μ L, 1.5 mmol, 15 equiv.). The title compound was obtained as white solid (34%). **¹H-NMR** (300 MHz, CDCl₃) δ 7.72 – 7.63 (m, 4H), 7.44 – 7.39 (m, 2H), 7.13 (dd, J = 5.1, 3.7 Hz, 1H). **¹³C-NMR** (75 MHz, CDCl₃) δ 142.2 (C_q), 138.8 (C_q), 132.9 (CH_{ar}), 128.7 (CH_{ar}), 127.2 (CH_{ar}), 126.2 (CH_{ar}), 125.2 (CH_{ar}), 119.0 (C_q), 110.7 (C_q). **HRMS** (EI): calculated m/z for C₁₁H₇NS [M⁺] 185.02937; found 185.02911. Spectral data in accordance with literature.^[64]

4-(2,3-Dihydrothieno[3,4-*b*][1,4]dioxin-5-yl)benzonitrile (6e)

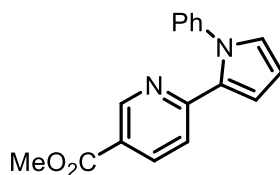
Compound was synthesized according to general procedure B using 4-chlorobenzonitrile (13.8 mg, 0.1 mmol, 1 equiv.) and 3,4-ethylenedioxythiophene (161 μ L, 1.5 mmol, 15 equiv.). The title compound was obtained as white needles (33%). **¹H-NMR** (300 MHz, CDCl₃) δ 7.84 – 7.76 (m, 2H), 7.64 – 7.56 (m, 2H), 6.42 (s, 1H), 4.37 – 4.33 (m, 2H), 4.30 – 4.23 (m, 2H). **¹³C-NMR** (75 MHz, CDCl₃) δ 142.5, 140.2, 137.8, 132.5, 126.0, 119.3, 115.6, 109.3, 100.3, 65.1, 64.4. **HRMS** (EI): calculated m/z for C₁₃H₉NO₂S [M⁺] 243.03485; found 243.03444. Spectral data is in accordance with literature.^[65]

Methyl 4-(1-phenyl-1*H*-pyrrol-2-yl)benzoate (6f)

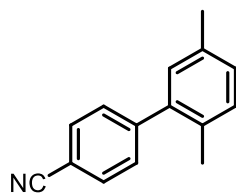
Compound was synthesized according to general procedure B using methyl 4-chlorobenzoate (17.1 mg, 0.1 mmol, 1 equiv.) and 1-phenylpyrrole (143 mg, 1.0 mmol, 10 equiv.). Deviation from general procedure: 3 equiv. of Cs₂CO₃ were used, DIPEA (4.4 μ L, 0.05 mmol, 25 mol%) was added and the reaction was irradiated for 22 h. The title compound was obtained as pale-

yellow solid (41%). **¹H-NMR** (400 MHz, CDCl₃) δ 7.89 – 7.84 (m, 2H), 7.38 – 7.27 (m, 3H), 7.20 – 7.15 (m, 4H), 6.98 (dd, *J* = 2.8, 1.8 Hz, 1H), 6.56 (dd, *J* = 3.6, 1.7 Hz, 1H), 6.39 (dd, *J* = 3.6, 2.8 Hz, 1H), 3.88 (s, 3H). **¹³C-NMR** (101 MHz, CDCl₃) δ 167.1, 140.4, 137.5, 132.8, 129.6, 129.3, 127.8, 127.6, 127.1, 125.9, 112.2, 109.8, 52.1. Spectral data in accordance with literature.^[66]

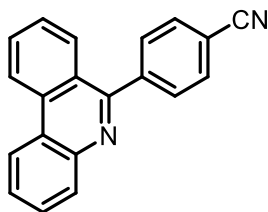
Methyl 6-(1-phenyl-1*H*-pyrrol-2-yl)nicotinate (6g)



Compound was synthesized according to general procedure B using methyl 6-chloropyridine-3-carboxylate (17.2 mg, 0.1 mmol, 1 equiv.) and 1-phenylpyrrole (143 mg, 1.0 mmol, 10 equiv.). Deviation from general procedure: 3 equiv. of Cs₂CO₃ were used, DIPEA (4.4 μL, 0.05 mmol, 25 mol%) was added and the reaction was irradiated for 22 h. The title compound was obtained as pale yellow solid (48%). **¹H-NMR** (400 MHz, CDCl₃) δ 9.02 (d, *J* = 1.6 Hz, 1H), 8.03 (dd, *J* = 8.4, 2.2 Hz, 1H), 7.41 – 7.32 (m, 3H), 7.24 – 7.19 (m, 2H), 7.05 – 6.93 (m, 3H), 6.41 (dd, *J* = 3.7, 2.8 Hz, 1H), 3.90 (s, 3H). **¹³C-NMR** (101 MHz, CDCl₃) δ 166.0 (C_q), 154.8 (C_q), 150.7 (CH_{ar}), 140.9 (C_q), 136.9 (CH_{ar}), 129.3 (CH_{ar}), 128.0 (CH_{ar}), 127.3 (CH_{ar}), 125.9 (CH_{ar}), 122.4 (C_q), 122.1 (C_q), 120.8 (CH_{ar}), 115.2 (CH_{ar}), 110.2 (CH_{ar}), 52.3 (CH₃). **HRMS** (ED): calculated *m/z* for C₁₇H₁₄N₂O₂ [M⁺] 278.10498; found 278.10402.

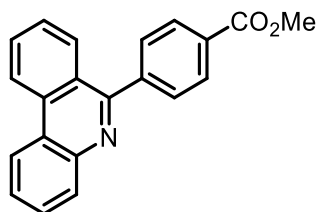
2',5'-Dimethyl-[1,1'-biphenyl]-4-carbonitrile (6h)

Compound was synthesized according to general procedure B using 4-chlorobenzonitrile (13.8 mg, 0.1 mmol, 1 equiv.) and *p*-xylene (185 μ L, 1.5 mmol, 15 equiv.). The title compound was obtained as colorless oil (15%). **¹H-NMR** (300 MHz, CDCl₃) δ 7.74 – 7.66 (m, 2H), 7.47 – 7.39 (m, 2H), 7.19 (d, *J* = 7.8 Hz, 1H), 7.12 (dd, *J* = 7.7, 1.8 Hz, 1H), 7.03 – 6.98 (m, 1H), 2.36 (s, 3H), 2.21 (s, 3H). **¹³C-NMR** (75 MHz, CDCl₃) δ 147.1 (C_q), 140.0 (C_q), 135.7 (C_q), 132.1 (CH_{ar}), 132.0 (C_q), 130.7 (CH_{ar}), 130.2 (CH_{ar}), 130.1 (CH_{ar}), 129.1 (CH_{ar}), 119.2 (C_q), 110.7 (C_q), 21.0 (CH₃), 20.0 (CH₃). **HRMS** (EI): calculated *m/z* for C₁₅H₁₃N [M⁺] 207.10425; found 207.10412. Spectral data is in accordance with literature.^[67]

4-(phenanthridin-6-yl)benzonitrile (6i)

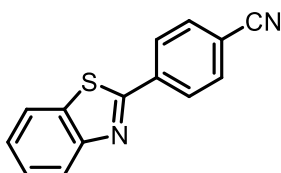
Compound was synthesized according to general procedure B using 4-chlorobenzonitrile (13.8 mg, 0.1 mmol, 1 equiv.) and 2-isocyano-1,1'-biphenyl (89.6 mg, 0.5 mmol, 5 equiv.). The title compound was obtained as brown solid (47%). **¹H-NMR** (300 MHz, CDCl₃) δ 8.74 (d, *J* = 8.4 Hz, 1H), 8.68 – 8.60 (m, 1H), 8.27 – 8.19 (m, 1H), 8.02 – 7.95 (m, 1H), 7.95 – 7.83 (m, 5H), 7.83 – 7.70 (m, 2H), 7.65 (ddd, *J* = 8.2, 7.0, 1.2 Hz, 1H). **¹³C-NMR** (75 MHz, CDCl₃) δ 159.2 (C_q), 144.4 (C_q), 143.7 (C_q), 133.7 (C_q), 132.4 (CH_{ar}), 131.1 (CH_{ar}), 130.7 (CH_{ar}), 130.5 (CH_{ar}), 129.3 (CH_{ar}), 128.1 (CH_{ar}), 127.7 (CH_{ar}), 127.6 (CH_{ar}), 124.7 (C_q), 124.0 (C_q), 122.7 (CH_{ar}), 122.2 (CH_{ar}), 118.8 (C_q), 112.7 (C_q). **HRMS** (ESI⁺): calculated *m/z* for C₂₀H₁₃N₂ [(M+H)⁺] 281.1073; found 281.1074. Spectral data in accordance with literature.^[68]

Methyl 4-(phenanthridin-6-yl)benzoate (6j)

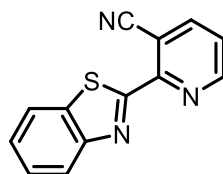


Compound was synthesized according to general procedure B using methyl 4-chlorobenzoate (17.1 mg, 0.1 mmol, 1 equiv.) and 2-isocyano-1,1'-biphenyl (89.6 mg, 0.5 mmol, 5 equiv.). The title compound was obtained as pale yellow solid (37%) **¹H-NMR** (400 MHz, CDCl₃) δ 8.71 (d, *J* = 8.3 Hz, 1H), 8.62 (dd, *J* = 8.2, 1.2 Hz, 1H), 8.30 – 8.21 (m, 3H), 8.06 – 8.00 (m, 1H), 7.87 (ddd, *J* = 8.3, 7.0, 1.3 Hz, 1H), 7.85 – 7.81 (m, 2H), 7.78 (ddd, *J* = 8.3, 7.0, 1.5 Hz, 1H), 7.71 (ddd, *J* = 8.3, 7.0, 1.4 Hz, 1H), 7.62 (ddd, *J* = 8.2, 7.0, 1.2 Hz, 1H), 3.99 (s, 3H). **¹³C-NMR** (101 MHz, CDCl₃) δ 167.0, 160.2, 144.2, 143.7, 133.6, 130.9, 130.5, 130.4, 130.0, 129.8, 129.1, 128.6, 127.5, 127.4, 125.0, 124.0, 122.5, 122.1, 52.4. **HRMS** (EI): calculated *m/z* for C₂₁H₁₅NO₂ [*M*⁺] 313.10973; found 313.10799. Spectral data in accordance with literature.^[69]

4-(benzo[*d*]thiazol-2-yl)benzonitrile (6k)



Compound was synthesized according to general procedure B using 4-chlorobenzonitrile (13.8 mg, 0.1 mmol, 1 equiv.) and 2-isocyanophenyl(methyl)sulfane (74.6 mg, 0.5 mmol, 5 equiv.). The title compound was obtained as white needles (38%) **¹H-NMR** (400 MHz, CDCl₃) δ 8.23 – 8.16 (m, 2H), 8.11 (d, *J* = 8.1 Hz, 1H), 7.94 (d, *J* = 8.0 Hz, 1H), 7.82 – 7.74 (m, 2H), 7.54 (ddd, *J* = 8.3, 7.2, 1.3 Hz, 1H), 7.45 (ddd, *J* = 8.3, 7.2, 1.2 Hz, 1H). **¹³C-NMR** (101 MHz, CDCl₃) δ 165.5, 154.1, 137.6, 135.4, 132.9, 128.1, 127.0, 126.2, 123.9, 121.9, 118.4, 114.3. **HRMS** (EI): calculated *m/z* for C₁₄H₈N₂S [*M*⁺] 236.04027; found 236.04036. Spectral data in accordance with literature.^[70]

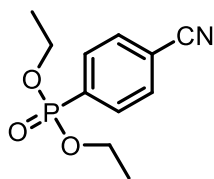
2-(Benzo[d]thiazol-2-yl)nicotinonitrile (6l)

Compound was synthesized according to general procedure B using 2-chloro-3-cyanopyridine (13.9 mg, 0.1 mmol, 1 equiv.) and 2-isocyanophenyl(methyl)sulfane (44.8 mg, 0.3 mmol, 3 equiv.). The title compound was obtained as pale-yellow needles (50%). **¹H-NMR** (400 MHz, CDCl₃) δ 8.86 (dd, *J* = 4.8, 1.7 Hz, 1H), 8.24 (d, *J* = 8.2 Hz, 1H), 8.18 (dd, *J* = 7.9, 1.7 Hz, 1H), 7.98 (d, *J* = 7.8 Hz, 1H), 7.55 (ddd, *J* = 8.3, 7.2, 1.3 Hz, 1H), 7.53 – 7.46 (m, 2H). **¹³C-NMR** (101 MHz, CDCl₃) δ 165.6 (C_q), 154.3 (C_q), 152.4 (CH_{ar}), 152.0 (C_q), 143.0 (CH_{ar}), 136.6 (C_q), 126.8 (CH_{ar}), 126.8 (CH_{ar}), 125.1 (CH_{ar}), 124.2 (CH_{ar}), 121.9 (CH_{ar}), 116.6 (C_q), 106.7 (C_q). **HRMS** (EI): calculated *m/z* for C₁₃H₇N₃S [M⁺] 237.03552; found 237.03548.

2-(Phenanthridin-6-yl)nicotinonitrile (6m)

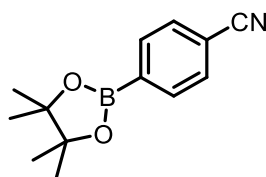
Compound was synthesized according to general procedure B using 2-chloro-3-cyanopyridine (13.9 mg, 0.1 mmol, 1 equiv.) and 2-isocyanato-1,1'-biphenyl (53.8 mg, 0.3 mmol, 3 equiv.). The title compound was obtained as brown solid (31%). **¹H-NMR** (400 MHz, CDCl₃) δ 8.97 (d, *J* = 4.9 Hz, 1H), 8.74 (d, *J* = 8.3 Hz, 1H), 8.66 (d, *J* = 8.0 Hz, 1H), 8.28 (dd, *J* = 20.3, 7.9 Hz, 2H), 8.16 (d, *J* = 8.3 Hz, 1H), 7.90 (t, *J* = 7.7 Hz, 1H), 7.78 (dt, *J* = 16.2, 7.2 Hz, 2H), 7.67 (t, *J* = 7.6 Hz, 1H), 7.57 (dd, *J* = 8.0, 4.9 Hz, 1H). **¹³C-NMR** (101 MHz, CDCl₃) δ 160.5 (C_q), 155.2 (C_q), 151.6 (CH_{ar}), 143.3 (C_q), 142.0 (CH_{ar}), 133.9 (C_q), 131.2 (CH_{ar}), 130.8 (CH_{ar}), 129.3 (CH_{ar}), 128.3 (CH_{ar}), 127.9 (CH_{ar}), 127.7 (CH_{ar}), 124.6 (C_q), 124.4 (C_q), 123.1 (CH_{ar}), 122.6 (CH_{ar}), 122.2 (CH_{ar}), 116.5 (C_q), 111.2 (C_q). **HRMS** (ESI⁺): calculated *m/z* for C₁₉H₁₂N₃ [(M+H)⁺] 282.1026; found 282.1027.

Diethyl (4-cyanophenyl)phosphonate (**6n**)



Compound was synthesized according to general procedure B using 4-chlorobenzonitrile (13.8 mg, 0.1 mmol, 1 equiv.) and triethyl phosphite (257 μ L, 1.5 mmol, 15 equiv.). The title compound was obtained as colorless oil (75%). **¹H-NMR** (400 MHz, CDCl₃) δ 7.95 – 7.87 (m, 2H), 7.77 – 7.71 (m, 2H), 4.25 – 4.02 (m, 4H), 1.32 (t, J = 7.0 Hz, 6H). **¹³C-NMR** (101 MHz, CDCl₃) δ 134.1 (d, J = 187.8 Hz), 132.4 (d, J = 9.8 Hz), 132.1 (d, J = 15.0 Hz), 117.9 (d, J = 1.4 Hz), 116.4 (d, J = 3.6 Hz), 62.8 (d, J = 5.7 Hz), 16.4 (d, J = 6.3 Hz). **³¹P-NMR** (162 MHz, CDCl₃) δ 16.0. **HRMS** (ESI⁺): calculated m/z for C₁₁H₁₅NO₃P [(M+H)⁺] 240.0784; found 240.0790. Spectral data is in accordance with literature.^[5]

4-(4,4,5,5-tetramethyl-1,3,2-dioxaborolan-2-yl)benzonitrile (**6o**)



Compound was synthesized according to general procedure B using 4-chlorobenzonitrile (13.8 mg, 0.1 mmol, 1 equiv.) and bis(pinacolato)diboron (127 mg, 0.5 mmol, 5 equiv.). Deviation from the general procedure B: The yield of **6o** was determined by crude proton NMR after reaction work up with internal standard method, as aryl boronic ester cannot be purified by silica gel chromatography. Mesitylene (1.7 mg, 14.14 μ mol) was added as internal standard to the crude **6o** (46.2 mg). A ratio of 1:1.22 in favor of **6o** was obtained after evaluating proton signal integration. Total mass of crude material (307.9 mg). Total amount of employed starting material (297.7 μ mol). Hence, a NMR yield of 39% was obtained. **¹H-NMR** (400 MHz, CDCl₃) δ 7.91 – 7.85 (m, 2H), 7.65 – 7.60 (m, 2H), 1.35 (s, 12H). **¹³C-NMR** (101 MHz, CDCl₃) δ 135.2, 131.2, 118.9, 114.6, 84.6, 25.0. Aromatic carbon atom adjacent to boronate ester could not be detected. **¹¹B-NMR** (128 MHz, CDCl₃) δ 30.4. Spectral data is in accordance with literature.^[5]

3.4.5 NMR Spectra

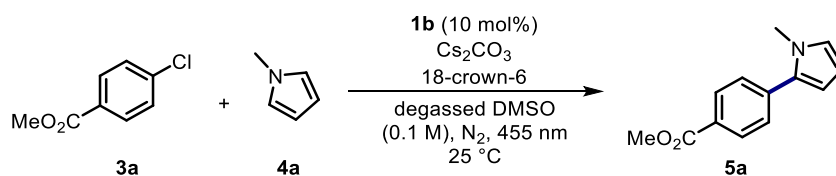
The corresponding NMR spectra of the compounds **5a-q** and **6a-o** are included in the Appendix (see section 7.3.1).

3.4.6 Reaction Monitoring and Optimization

3.4.6.1 Monitoring the progress of the catalyzed and the background reaction

Reactions were stopped after a certain time and results were analyzed by GC-FID to compare the progress of the anthrolate catalyzed reaction and the reaction in absence of catalyst **1b** (Table S3-1). For a graphical representation of the reaction progress see Figure S3-1.

Table S3-1. Reaction progress was monitored in presence and absence of catalyst **1b**.



Entry	1b [mol%]	Time [h]	Conversion ^a [%]	Yield ^a [%]
1	-	0.5	2	0
2	-	1	7	0
3	-	2	7	0
4	10	2	48	18
5	-	4	32	2
6	10	4	74	38
7	-	6	48	10
8	10	6	80	44
9	-	8	50	16
10	10	8	85	58
11	-	10	43	28
12	10	10	88	79
13 ^b	-	10	7	6

^a Results were determined by calibrated GC-FID analysis with internal standard method. ^b K₂CO₃ (1.2 equiv.) was used.

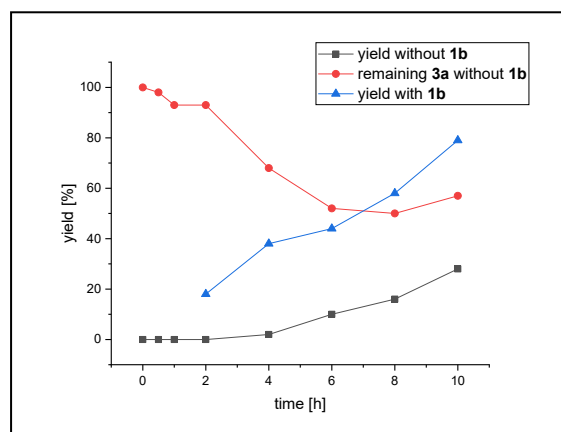
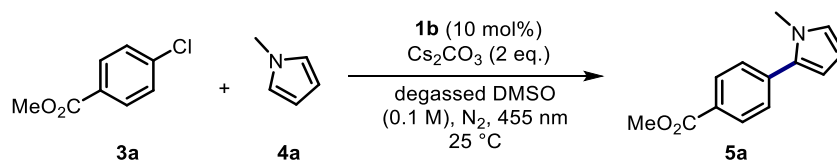


Figure S3-1. Monitored reaction progress represented graphically. The grey curve indicates product formation in absence of catalyst **1b**, the blue curve in presence of **1b**. Remaining starting material **3a** in absence of catalyst is given as red curve. Data taken from Table S3-1.

3.4.6.2 Optimizing the Reaction Conditions: Changing the amount of added **4a**

The ratio and amount of substrate **3a** and trapping reagent **4a** was changed, and obtained results are summarized in Table S3-2.

Table S3-2. Varying amount and ratio of substrate and trapping agent.



Entry	3a [mmol]	4a [mmol]	Time [h]	Conversion ^a [%]	Yield ^a [%]
1	0.1	0.1	18	36	11 (5)
2	0.1	0.05	18	32	10 (6)
3	0.1	0.033	18	29	7 (6)
4	0.1	-	18	32	0 (6)
5	0.1	0.5	4.5	55	25 (4)
6	0.1	1.0	4.5	78	38 (3)
7	0.2	1.0	4.5	42	18 (1)
8	0.2	3.0	4.5	59	35 (1)
9	0.2	0.1	4.5	28	6 (2)
10	0.4	0.2	4.5	18	3 (1)

^a Results were determined by calibrated GC-FID analysis with internal standard method. Numbers in parenthesis correspond to dechlorinated starting material **3a**.

Efforts to obtain double functionalized pyrroles by employing the substrate in excess were unsuccessful. Furthermore, reducing the excess amount of **4a** led to significantly reduced product yield and conversion. We therefore conclude, that a fast and efficient conversion of the aryl radical intermediate is necessary to turn over the reaction and to avoid adverse side reactions of the reactive aryl radical.

3.4.6.3 Optimizing C–H arylation of furan: Comparison with other Catalysts

Table S3-3. Optimizing arylation of furan with **3f** catalyzed by anthrone derivatives and frequently used reducing photocatalysts.

Entry	Catalyst (mol%)	Solvent	Cs ₂ CO ₃ [mmol]	DIPEA [mmol]	Yield ^a [%]
1	1a (10)	DMSO	0.3	0.05	49
2	1b (10)	DMSO	0.3	0.05	61
3	1d (10)	DMSO	0.3	0.05	62
4	1g (10)	DMSO	0.3	0.05	53
5	1a (10) + Perylene (10)	DMSO	0.2	0.05	44
6	1b (10) + Perylene (10)	DMSO	0.3	0.05	88
7	1d (10) + Perylene (10)	DMSO	0.3	0.05	61
8	1g (10) + Perylene (10)	DMSO	0.3	0.05	75
9	Perylene (20)	DMSO	0.2	0.05	10
10	4CzIPN ^{b[71]} (10)	DMF	-	0.25	trace
11	Phenoxazine ^{b[72]} (10)	DMF	-	0.25	12
12	<i>fac</i> -Ir(ppy) ₃ (1)	MeCN	-	0.25	6
13	[Ir{dF(CF ₃) ₂ (ppy) ₂ }(dtbbpy)]PF ₆ (1)	MeCN	-	0.25	5
14	Rhodamine 6G ^b (10)	DMSO	-	0.25	3

4CzIPN

Phenoxazine catalyst

Rhodamine 6G

^a Results were determined by calibrated GC-FID analysis with internal standard method; ^b Structures for organic photocatalysts used are given above.

To optimize the reaction of 2-chlorobenzonitrile (**3f**) and furan (**4'a**), several conditions were screened and the most meaningful are summarized in Table S3-3. Employing solely catalyst **1** (Table S3-3, Entry 1-4) led to a very similar reaction outcome. However, adding catalytic amount of the polyaromatic hydrocarbon perylene (0.01 mmol, 10 mol%) caused a significant increase in product yield when either anthrone catalyst **1b** or **1g** were present (Entry 6 and 8). No change in yield was observed when perylene was combined with anthrone **1a** or bianthrone **1d** and a control reaction with solely perylene resulted in poor product yield (Entry 5,7 and 9). In preliminary experiments, we found that adding DIPEA in sub-stoichiometric amount supports the product formation as it might prevent the catalyst from bleaching. However, these results could not be confirmed during the preparation of the substrate scope and hence, DIPEA was omitted in most of the reactions. With other frequently used photoredox catalysts such as 4CzIPN, 3,7-di(4-biphenyl) 1-naphthalene-10-phenoxazine, rhodamine 6G or iridium-based polypyridyl complexes, the arylation product of furan (**6b**) was obtained only in poor yield.

3.4.7 Supporting Spectroscopic Investigations

3.4.7.1 UV-vis Absorption Spectra

Absorption spectra of derivatives **1** in the absence and the presence of base 1,1,3,3-tetramethylguanidine (TMG) were measured. Dry degassed DMSO was used as solvent. UV-vis spectra were recorded in a gas-tight quartz cuvette under nitrogen atmosphere. The concentration of **1** (0.42 mM) was similar for all anthrone derivatives. Tetramethylguanidine (20 equiv.) was added *via* syringe. A red-shift of the absorption was found for all the investigated anthrone derivatives **1** upon addition of the base. The corresponding UV-vis spectra (Figure S3-2) can be found in the Appendix (see section 7.3.2).

3.4.7.2 Emission Spectra

Samples of catalyst derivatives **1** in presence of TMG to record the emission spectra were prepared as reported in 3.3.6.1 with a lowered concentration (25 μ M). The excitation wavelength was set to 420 or 430 nm. The corresponding combined absorption and emission spectra (Figure S3-3) can be found in the Appendix (see section 7.3.3).

3.4.7.3 Luminescence Lifetime and Quenching Studies

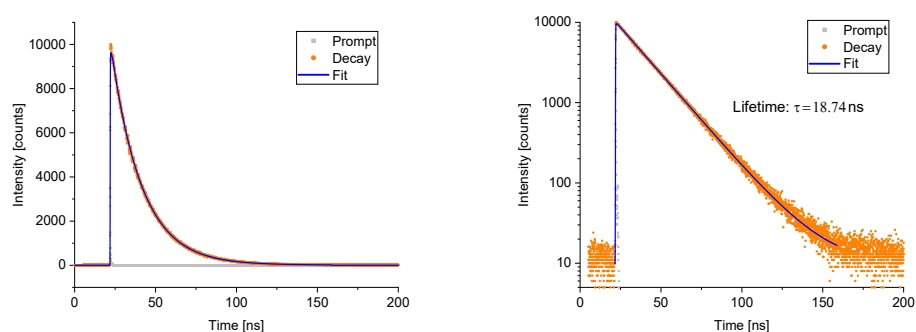


Figure S3-4. Luminescence decay of 9-anthrolate **2a** generated from **1a** in presence of Cs_2CO_3 . The lifetime was determined by a mono-exponential fit function.

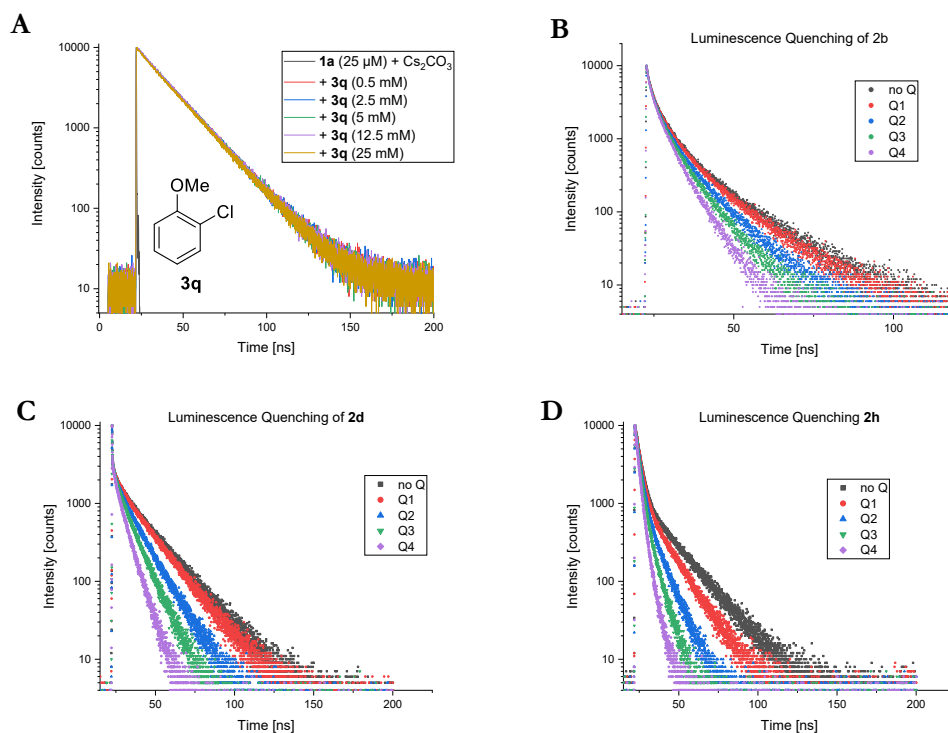


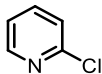
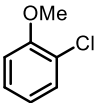
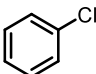
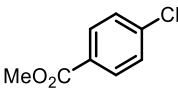
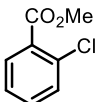
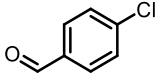
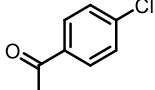
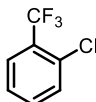
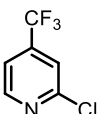
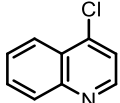
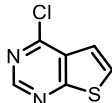
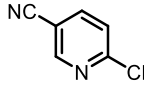
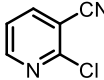
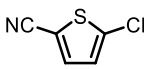
Figure S3-5. **A:** Luminescence lifetime of **2a** is not affected upon addition of aryl chloride **3q**. The luminescence decays of catalysts **2b** (**B**), **2d** (**C**) and **2h** (**D**) are of higher order. Addition of 2-chlorobenzonitrile (**3f**) affects the measured decays and suggest a luminescence quenching.

The time-resolved luminescence quenching experiments of catalysts **2c**, **e**, **f**, **g** with **3f** (2-chlorobenzonitrile) as quencher and the derived Stern-Volmer plot (Figure S3-6) can be found in the Appendix (section 7.3.4).

3.4.7.4 Cyclic Voltammetry of Aryl Chlorides

Reduction potentials of employed aryl chlorides **3** were determined by cyclic voltammetry or are reported in literature.^[12] Irreversible peaks are obtained as the corresponding radical anion fragments into the aryl radical and the halide anion. Ferrocene was added as internal reference. Obtained potentials *vs.* Fc^+/Fc were converted to yield approximated potentials against saturated calomel electrode (Table S3-4a).^[73] The recorded cyclic voltammograms are depicted in Table S3-4b in the Appendix (Section 7.3.5).

Table S3-4a. Obtained reduction potentials for aryl chlorides.

			
-2.40 V <i>vs.</i> SCE	-2.83 V <i>vs.</i> SCE	-2.81 V <i>vs.</i> SCE	-1.95 V <i>vs.</i> SCE
			
-1.96 V <i>vs.</i> SCE	-1.72 V <i>vs.</i> SCE	-1.82 V <i>vs.</i> SCE	-2.27 V <i>vs.</i> SCE
			
-1.82 V <i>vs.</i> SCE	-1.80 V <i>vs.</i> SCE	-1.77 V <i>vs.</i> SCE	-1.75 V <i>vs.</i> SCE
			
-1.65 V <i>vs.</i> SCE	-1.65 V <i>vs.</i> SCE		

3.4.7.5 Cyclic Voltammetry of Catalysts

The electrochemical ground-state potentials of catalysts **1** in absence and presence of base (Cs_2CO_3 or TMG) were determined by cyclic voltammetry. Potentials were recorded against the ferrocene/ferrocenium redox-couple and converted, as reported in literature^[73], to approximated potentials *vs.* saturated calomel electrode (SCE). The obtained data is summarized in Table S3-5. The recorded cyclic voltammograms (Figure S3-7) can be found in the Appendix (Section 7.3.6).

3.4.7.6 Spectroelectrochemistry of Catalyst **2a**

A 5 mL crimp vial was charged with 9-anthrone (10.2 mg, 50 μmol) and Cs_2CO_3 (407 mg, 1.25 mmol). The vessel was sealed, deaerated and flushed with nitrogen (3 \times). Dry, degassed DMSO (5 mL) was added *via* syringe and nitrogen was passed through the solution for 15 minutes. A nitrogen flushed OTTE cell was charged with the prepared solution, placed into the light beam of a UV-vis spectrophotometer and connected to a potentiostat. A linearly ramped potential was applied starting from -1.7 V (potential against pseudo reference Ag wire) with a scan rate of 0.002 $\text{V}\cdot\text{s}^{-1}$. The turning point was set to +0.7 V. UV-vis spectra were recorded every 10 seconds. The changes in analyte absorption at various potentials are depicted in Figure S3-8 B-D. The cyclic voltammogram shown in Figure S3-8 A, was recorded independently.

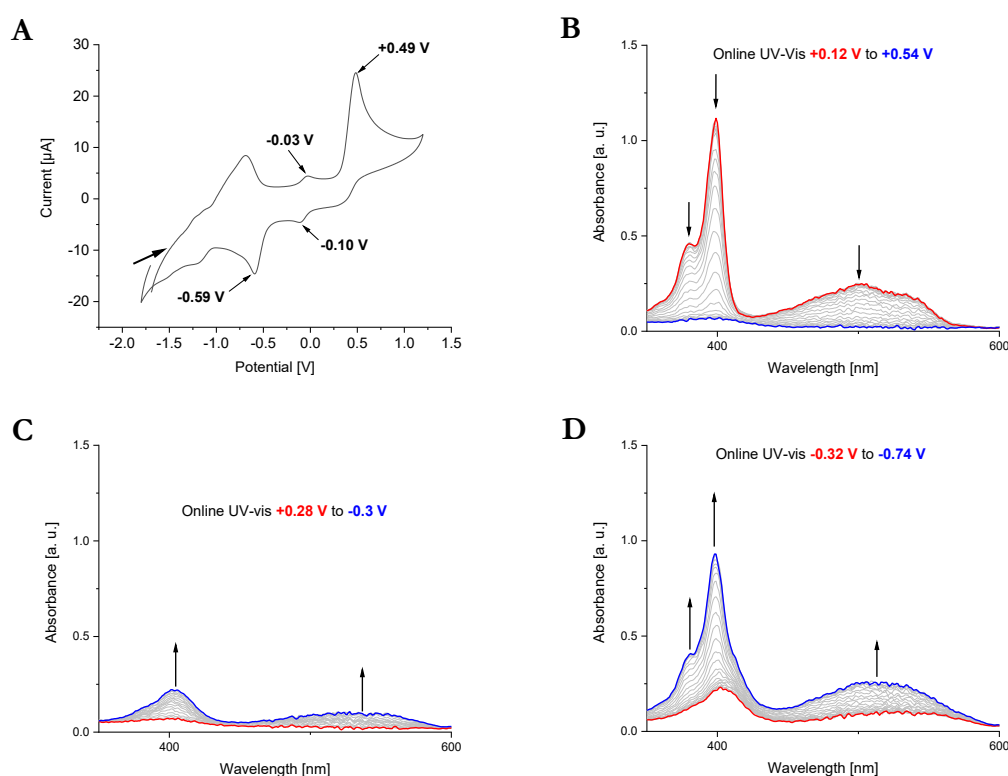


Figure S3-8. (A) Cyclic voltammogram of **2a** starting off at -1.7 V. Superimposed UV-vis absorption spectra recorded at various applied potentials. Sweeping towards positive potentials (B) caused a constant decrease in absorption intensity (*cf.*, cathodic peak current at +0.49 V, A) indicative for the oxidation of **2a**. After reaching the turning point at +0.7 V, the applied potential was decreased towards -0.3 V (C) and the absorption intensity increased slightly. A significant increase in absorption intensity was obtained when the potential was driven towards -0.7 V (*cf.*, anodic peak current at -0.59 V, A) suggesting the reduction to regenerate the oxidized **2a**.

3.4.7.7 Summarized Properties of examined Catalysts

Table S3-5. Measured photophysical and electrochemical properties of catalysts **1** and **2**.

Catalyst	$E_{1/2}^{\text{a}}$ [V vs. SCE]		$E_{ox}^{*\text{ b}}$ [V vs. SCE]		τ [ns]	$E_{0,0}^{\text{c}}$ [kJ·mol ⁻¹]	K_{SV}^{d} [M ⁻¹]	$k_q \times 10^9^{\text{d}}$ [M ⁻¹ ·s ⁻¹]
	1a-h		2a-h					
	E_{ox}	E_{red}	E_{ox}	E_{ox}^*				
a	0.27	−1.64	−0.34	−2.54	18.74	212	90.3	4.82
b	0.77	−1.39	−0.83	−3.00	− ^c	209	− ^c	− ^c
c	0.52	−1.64	−0.24	−2.40	4.39	208	16.6	3.78
d	−	−1.41	−0.47	−2.53	− ^c	199	− ^c	− ^c
e	1.21	−1.93	0.27	−2.40	18.47	242	59.6	3.23
f	0.43	−1.43	−0.16	−2.35	18.36	211	38.5	2.10
g	0.17	−1.58	−0.51	−2.78	22.08	219	90.4	4.28
h	−	−1.73	−0.33	−2.41	− ^c	201	− ^c	− ^c

^a Ground-state redox potentials were obtained by measuring cyclic voltammetry in DMSO with ferrocene as internal standard. Obtained potentials vs. Fc/Fc⁺ were converted to yield approximated potentials against saturated calomel electrode^[71]; ^b Excited-state oxidation potentials are estimated based on the obtained data for ground state potentials and excited state energy $E_{0,0}$ ^[17]; ^c Excited state energy refers to wavelength of the maxima of the emission spectra; ^d Stern-Volmer constant K_{SV} and bimolecular quenching constant k_q was obtained by measuring time-resolved luminescence quenching studies with 2-chlorobenzonitrile as quencher; ^e Data could not be obtained as luminescence decay varied from first order kinetics (see Figure S3-5 B-D).

3.5 References

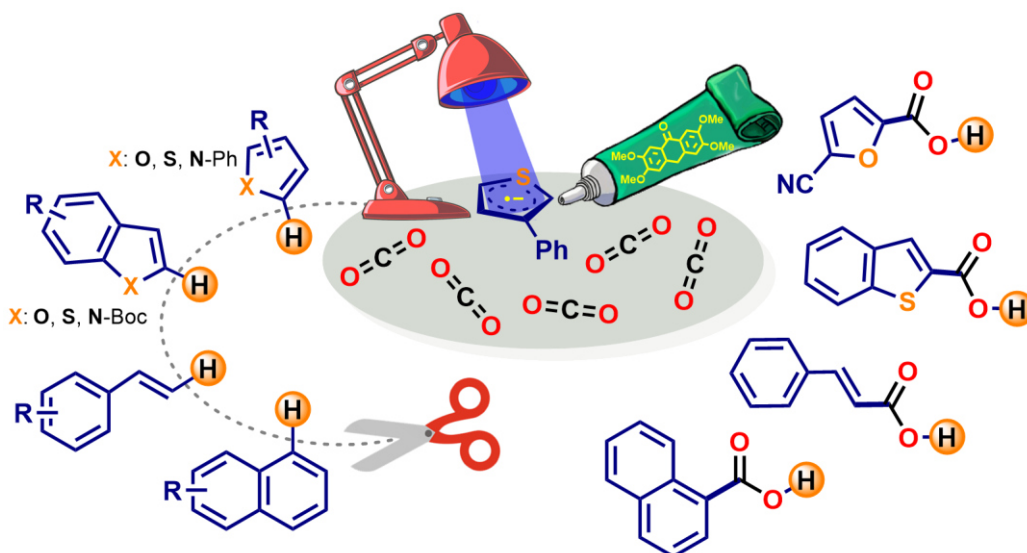
- [1] I. Ghosh, L. Marzo, A. Das, R. Shaikh, B. König, *Acc. Chem. Res.* **2016**, *49*, 1566–1577.
- [2] R. Matsubara, T. Yabuta, U. Md Idros, M. Hayashi, F. Ema, Y. Kobori, K. Sakata, *J. Org. Chem.* **2018**, *83*, 9381–9390.
- [3] D. Liu, M.-J. Jiao, Z.-T. Feng, X.-Z. Wang, G.-Q. Xu, P.-F. Xu, *Org. Lett.* **2018**, *20*, 5700–5704.
- [4] I. Ghosh, R. S. Shaikh, B. König, *Angew. Chem. Int. Ed.* **2017**, *56*, 8544–8549.
- [5] M. Neumeier, D. Sampedro, M. Májek, V. A. de la Peña O'Shea, A. Jacobi von Wangelin, R. Pérez-Ruiz, *Chem. Eur. J.* **2018**, *24*, 105–108.
- [6] J. I. Bardagi, I. Ghosh, M. Schmalzbauer, T. Ghosh, B. König, *Eur. J. Org. Chem.* **2018**, *2018*, 34–40.
- [7] T. Fukuyama, Y. Fujita, H. Miyoshi, I. Ryu, S.-C. Kao, Y.-K. Wu, *Chem. Commun.* **2018**, *54*, 5582–5585.
- [8] E. T. Nadres, A. Lazareva, O. Daugulis, *J. Org. Chem.* **2011**, *76*, 471–483.
- [9] C. Costentin, M. Robert, J.-M. Savéant, *J. Am. Chem. Soc.* **2004**, *126*, 16051–16057.
- [10] M. Montalti, A. Credi, L. Prodi, M. T. Gandolfi, *Handbook of Photochemistry*, CRC Press, Boca Raton, 3rd edn, **2006**.
- [11] E. H. Discekici, N. J. Treat, S. O. Poelma, K. M. Mattson, Z. M. Hudson, Y. Luo, C. J. Hawker, J. R. de Alaniz, *Chem. Commun.* **2015**, *51*, 11705–11708.
- [12] I. Ghosh, T. Ghosh, J. I. Bardagi, B. König, *Science* **2014**, *346*, 725–728.
- [13] I. Ghosh, B. König, *Angew. Chem. Int. Ed.* **2016**, *55*, 7676–7679.
- [14] X. Li, D. Liang, W. Huang, H. Sun, L. Wang, M. Ren, B. Wang, Y. Ma, *Tetrahedron* **2017**, *73*, 7094–7099.
- [15] S. Fukuzumi, K. Ohkubo, *Org. Biomol. Chem.* **2014**, *12*, 6059–6071.
- [16] A. Joshi-Pangu, F. Lévesque, H. G. Roth, S. F. Oliver, L.-C. Campeau, D. Nicewicz, D. A. DiRocco, *J. Org. Chem.* **2016**, *81*, 7244–7249.
- [17] N. A. Romero, D. A. Nicewicz, *Chem. Rev.* **2016**, *116*, 10075–10166.
- [18] W. P. Todd, J. P. Dinnocenzo, S. Farid, J. L. Goodman, I. R. Gould, *J. Am. Chem. Soc.* **1991**, *113*, 3601–3602.
- [19] B. Legros, P. Vandereecken, J. P. Soumillion, *J. Phys. Chem.* **1991**, *95*, 4752–4761.
- [20] E. Hasegawa, K. Mori, S. Tsuji, K. Nemoto, T. Ohta, H. Iwamoto, *Aust. J. Chem.* **2015**, *68*, 1648–1652.
- [21] E. Hasegawa, Y. Nagakura, N. Izumiya, K. Matsumoto, T. Tanaka, T. Miura, T. Ikoma, H. Iwamoto, K. Wakamatsu, *J. Org. Chem.* **2018**, *83*, 10813–10825.
- [22] C. Kerzig, M. Goetz, *Phys. Chem. Chem. Phys.* **2015**, *17*, 13829–13836.
- [23] S. G. Mills, P. Beak, *J. Org. Chem.* **1985**, *50*, 1216–1224.
- [24] G. M. McCann, C. M. McDonnell, L. Magris, R. A. More O'Ferrall, *J. Chem. Soc. Perkin Trans. 2* **2002**, 784–795.
- [25] B. Freiermuth, B. Hellrung, S. Peterli, M.-F. Schultz, D. Wintgens, J. Wirz, *Helv. Chim. Acta* **2001**, *84*, 3796–3809.
- [26] F. G. Bordwell, R. J. McCallum, W. N. Olmstead, *J. Org. Chem.* **1984**, *49*, 1424–1427.
- [27] T. Fujii, S. Mishima, N. Tanaka, O. Kawauchi, K. Kodaira, H. Nishikiori, Y. Kawai, *Res. Chem. Intermed.* **1997**, *23*, 829–839.
- [28] Y. Ogata, Y. Kosugi, K. Nate, *Tetrahedron* **1971**, *27*, 2705–2711.
- [29] M. E. Budén, J. I. Bardagi, M. Puiatti, R. A. Rossi, *J. Org. Chem.* **2017**, *82*, 8325–8333.
- [30] The species responsible for the background reaction is not well understood at present and requires further investigations.

- [31] During the photoreaction the photocatalyst may bleach and the degraded or photodimerised products (wherever applicable) may also participate in the chemical transformations affording the desired coupling products.
- [32] Efforts to generate twofold substituted pyrroles by using an excess amount of **3a** (Table S2, Experimental Part) remained unsuccessful with low conversion of the starting material. We speculate that under our reaction conditions a fast and efficient conversion of the aryl radical intermediate is important for an effective catalytic transformations.
- [33] The monosubstituted product was obtained only in traces.
- [34] Determined reduction potentials using CV measurements: 4-chloroacetophenone ($E_{\text{red}} = -1.82 \text{ V vs. SCE}$), 4-chlorobenzaldehyde ($E_{\text{red}} = -1.72 \text{ V vs. SCE}$) and methyl 4-chlorobenzoate ($E_{\text{red}} = -1.95 \text{ V vs. SCE}$). For further information see the Experimental Part.
- [35] Although the reduction potential values suggest a very similar thermodynamically favourable electron transfer from the excited catalyst to these compounds compared to **3a**, a competing side reaction might be the reduction of the carbonyl group ($E_{\text{red}} = -1.93 \text{ V vs. SCE}$ for 4-chlorobenzaldehyde) giving the ketyl radical anion.
- [36] C. Wang, H. Dong, W. Hu, Y. Liu, D. Zhu, *Chem. Rev.* **2012**, *112*, 2208–2267.
- [37] S. Suzuki, J. Yamaguchi, *Chem. Commun.* **2017**, *53*, 1568–1582.
- [38] S. I. Panchamukhi, A. K. Mohammed Iqbal, A. Y. Khan, M. B. Kalashetti, I. M. Khazi, *Pharm. Chem. J.* **2011**, *44*, 694–696.
- [39] S. Paria, O. Reiser, *Adv. Synth. Catal.* **2014**, *356*, 557–562.
- [40] T. Föll, J. Rehbein, O. Reiser, *Org. Lett.* **2018**, *20*, 5794–5798.
- [41] I. Ghosh, B. König, *Angew. Chem. Int. Ed.* **2016**, *55*, 7676–7679.
- [42] W. C. Yang, K. Wei, X. Sun, J. Zhu, L. Wu, *Org. Lett.* **2018**, *20*, 3144–3147.
- [43] P. Natarajan, A. Bala, S. K. Mehta, K. K. Bhasin, *Tetrahedron* **2016**, *72*, 2521–2526.
- [44] D. P. Hari, P. Schroll, B. König, *J. Am. Chem. Soc.* **2012**, *134*, 2958–2961.
- [45] A. Arora, J. D. Weaver, *Org. Lett.* **2016**, *18*, 3996–3999.
- [46] We found that adding perylene (10 mol%) to the reaction mixture led to a further increase in the product yield. Using **3f** as the starting material, the product was obtained in 88% GC-yield (Table S3, Experimental Part).
- [47] These trapping reagents are deeply coloured dyes. To allow efficient light penetration through the reaction solution, the addition of isocyanide was kept between 0.3 and 0.5 mmol.
- [48] J. C. Walton, *J. Phys. Chem. A* **2018**, *122*, 1422–1431.
- [49] A. Studer, D. P. Curran, *Nat. Chem.* **2014**, *6*, 765–773.
- [50] D. B. G. Williams, M. Lawton, *J. Org. Chem.* **2010**, *75*, 8351–8354.
- [51] H. Prinz, P. Schmidt, K. J. Böhm, S. Baasner, K. Müller, M. Gerlach, E. G. Günther, E. Unger, *Bioorg. Med. Chem.* **2011**, *19*, 4183–4191.
- [52] S. E. Branz, J. A. Carr, *Synth. Commun.* **1986**, *16*, 441–451.
- [53] C. C. J. Loh, X. Fang, B. Peters, M. Lautens, *Chem. Eur. J.* **2015**, *21*, 13883–13887.
- [54] Y. V Shklyayev, Y. V Nifontov, *Russ. Chem. Bull.* **2002**, *51*, 844–849.
- [55] Q. Miao, T.-Q. Nguyen, T. Someya, G. B. Blanchet, C. Nuckolls, *J. Am. Chem. Soc.* **2003**, *125*, 10284–10287.
- [56] W.-P. Baik, C.-H. Yoon, S.-H. Koo, H.-K. Kim, J.-H. Kim, J.-R. Kim, S.-D. Hong, *Bull. Korean Chem. Soc.* **2004**, *25*, 491–500.
- [57] J. K. Augustine, A. Bombrun, S. Venkatachaliah, A. Jothi, *Org. Biomol. Chem.* **2013**, *11*, 8065.
- [58] M. Tobisu, K. Koh, T. Furukawa, N. Chatani, *Angew. Chem. Int. Ed.* **2012**, *51*, 11363–11366.

-
- [59] M. Obst, R. S. Shaikh, B. König, *React. Chem. Eng.* **2017**, *2*, 472–478.
- [60] F. Bilodeau, M.-C. Brochu, N. Guimond, K. H. Thesen, P. Forgione, *J. Org. Chem.* **2010**, *75*, 1550–1560.
- [61] H. Al-Matar, K. Khalil, M. Elnagdi, *Curr. Org. Synth.* **2014**, *11*, 922–928.
- [62] Y.-F. Liang, R. Steinbock, L. Yang, L. Ackermann, *Angew. Chem. Int. Ed.* **2018**, *57*, 10625–10629.
- [63] D. Wu, Z.-X. Wang, *Org. Biomol. Chem.* **2014**, *12*, 6414.
- [64] Q. Cao, J. L. Howard, E. Wheatley, D. L. Browne, *Angew. Chem. Int. Ed.* **2018**, *57*, 11339–11343.
- [65] I. Stolić, H. Čipčić Paljetak, M. Perić, M. Matijašić, V. Stepanić, D. Verbanac, M. Bajić, *Eur. J. Med. Chem.* **2015**, *90*, 68–81.
- [66] Y.-X. Liu, D. Xue, J.-D. Wang, C.-J. Zhao, Q.-Z. Zou, C. Wang, J. Xiao, *Synlett* **2013**, *24*, 507–513.
- [67] K. L. Billingsley, T. E. Barder, S. L. Buchwald, *Angew. Chem. Int. Ed.* **2007**, *46*, 5359–5363.
- [68] C. J. Evoniuk, G. dos P. Gomes, S. P. Hill, S. Fujita, K. Hanson, I. V. Alabugin, *J. Am. Chem. Soc.* **2017**, *139*, 16210–16221.
- [69] A. Korotvička, D. Frejka, Z. Hampejsová, I. Císařová, M. Katora, *Synthesis* **2016**, *48*, 987–996.
- [70] Y. Huang, P. Zhou, W. Wu, H. Jiang, *J. Org. Chem.* **2018**, *83*, 2460–2466.
- [71] H. Uoyama, K. Goushi, K. Shizu, H. Nomura, C. Adachi, *Nature* **2012**, *492*, 234–238.
- [72] R. M. Pearson, C.-H. Lim, B. G. McCarthy, C. B. Musgrave, G. M. Miyake, *J. Am. Chem. Soc.* **2016**, *138*, 11399–11407.
- [73] V. V. Pavlishchuk, A. W. Addison, *Inorganica Chim. Acta* **2000**, *298*, 97–102.

CHAPTER 4

4 Redox-neutral Photocatalytic C–H Carboxylation of Arenes and Styrenes with CO₂



This chapter has been published in: M. Schmalzbauer, T. D. Svejstrup, F. Fricke, P. Brandt, M. J. Johansson, G. Bergonzini, B. König, **2020**, DOI: 10.26434/chemrxiv.12485786.v1.

M.S. developed the catalytic system, optimized the reaction, isolated the compounds **2a-d**, **4a-f**, **4i-t**, **4v-w**, **8a-m**, **9pa-pc**, designed and carried out the gram-scale reaction and conducted all experiments to investigate the reaction mechanism. T.D.S. designed and performed the high-throughput-screening and isolated compounds **2f-g**, **4g-h**, **4u**, **4x**, **6a-e**. F.F. prepared compounds and isolated compound **2e**. M.S. wrote the manuscript and Supplemental Information with help from T.D.S and input from all of the authors. P.B. conducted the computational studies. M.J.J., G.B. and B.K. supervised the project.

Abstract

Carbon dioxide (CO₂) is an attractive one-carbon (C1) building block in terms of sustainability and abundance. However, its low reactivity limits applications in organic synthesis as typically high-energy reagents are required to drive transformations. Here, we present a redox-neutral C–H carboxylation of arenes and styrenes using a photocatalytic approach. Upon blue-light excitation, the anthrolate anion photocatalyst is able to reduce many aromatic compounds to their corresponding radical anions, which react with CO₂ to afford carboxylic acids. High-throughput screening and computational analysis suggest that a correct balance between electron affinity and nucleophilicity of substrates is essential. This novel methodology enables the carboxylation of numerous aromatic compounds, including many that are not tolerated in classical carboxylation chemistry. Over 50 examples of C–H functionalizations using CO₂ or ketones illustrate a broad applicability. The method opens new opportunities for late-stage C–H carboxylation and valorization of common arenes.

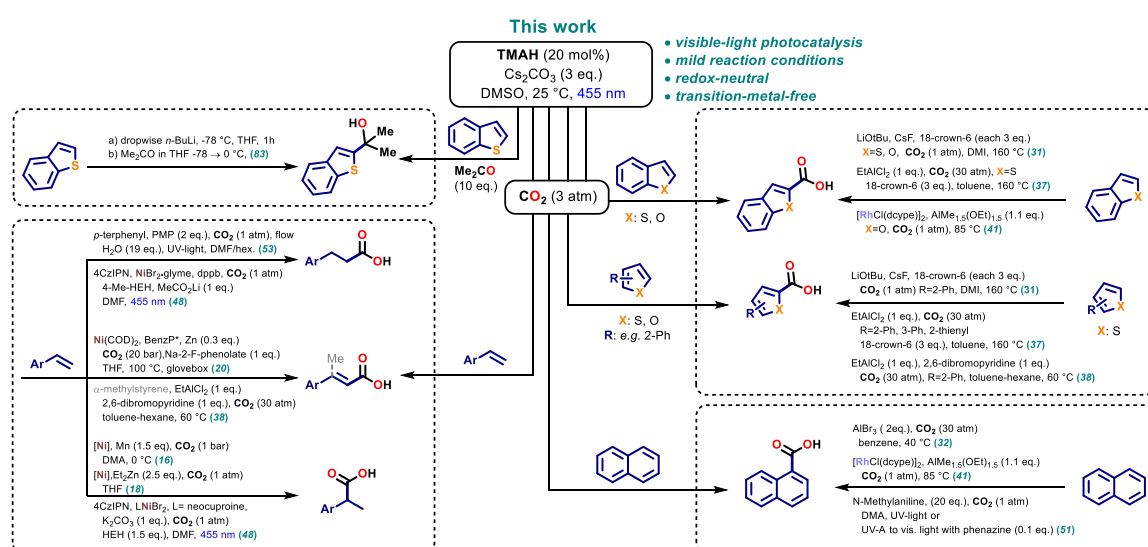
4.1 Introduction

Photosynthesis, the most important photobiological process on our planet, allows photoautotrophs to store energy in form of chemical bonds by absorbing sunlight. Driven by that energy, CO₂ is captured from the atmosphere and serves as carbon feedstock for the organisms to build up sugars and biomass in the Calvin cycle.^[1]

Electrochemical and catalytic dihydrogen reductions of carbon dioxide have been developed in the field of renewable energy storage.^[2–4] However, the use of CO₂ as a C1 building block in organic synthesis has received far less attention despite resembling the principle of the biological carbon fixation process the most.^[5] The high thermodynamic stability and kinetic inertness of CO₂ require the use of stoichiometric amounts of reactive reaction partners such as Grignard reagents or organolithium compounds for chemical conversion.^[6] Aiming for a better efficiency and an increased atom economy, a variety of catalytic carboxylation methods have been developed. These processes make use of readily available aryl bromides which undergo carboxylation with CO₂ in the presence of catalytic Pd(OAc)₂, as reported by Martín and Correa.^[7] Daugulis showed that Cu(I) catalyzes the carboxylation of aryl iodides.^[8] Tsuji and co-workers applied NiCl₂(PPh₃)₂ to carboxylate more inert aryl and vinyl chlorides under 1 atm CO₂ at room temperature.^[9] The reaction scope was extended to sulfonates,^[10] ester derivatives,^[11,12] allylic alcohols,^[13] benzylic ammonium salts,^[14] arylsulfonium salts^[15] and unsaturated hydrocarbons.^[16–20] However, all these systems require stoichiometric reducing reagents based on Et₂Zn, AlMe₃, Mn and Zn powder or prefunctionalized starting materials.^[21] Electrical current may also be used to drive reductive carboxylation chemistry. Buckley and co-workers reported the regioselective hydrocarboxylation of styrenes using a non-sacrificial electrode system.^[22] Ackermann *et al.* showed that allyl chlorides derived from cinnamyl chloride are carboxylated in presence of a cobalt catalyst.^[23] Concomitantly, difunctionalizations of alkenes *via* radical addition and subsequent reduction were reported affording thio-,^[24] carbo-^[25–27] phosphono-^[28] or silylcarboxylation^[27] products.

Non-catalytic C(sp²)-H carboxylations typically require stoichiometric amounts of either strong bases, such as NaH^[29] or LiO^tBu,^[30,31] or Lewis acids, like AlX₃ (X = Br, Cl),^[32–35] Me₂AlCl^[36] and EtAlCl₂^[37,38] to activate CO₂. Transition metal-catalyzed directed C(sp²)-H carboxylation reactions have been reported with Au,^[39] Cu^[39,40] and Rh^[41] complexes.^[42] Moreover, direct carboxylation of non-activated C(sp²)-H was reported in molten alkali carbonate salts under elevated temperatures (>200 °C) and high CO₂ pressure.^[43,44]

More recently, photoredox catalysis has been applied in the field of carboxylation chemistry. Photocatalytic carboxylation of aryl-^[45,46] and alkyl-halides^[46] were the first transformations to be reported, followed by direct C–H carboxylation of alkynes^[47] and styrenes.^[48,49] These methods utilize a dual catalytic approach consisting of a photocatalyst and an *in situ* generated low-valent transition metal complex enabled by an excess amount of a sacrificial electron donor. Visible-light mediated benzylic C–H carboxylation was recently reported by our group using 4CzIPN and an organo-silanethiol HAT reagent, which allowed to generate carbanions.^[50]



Scheme 4-1. Overview of representative literature procedures for the direct C–H carboxylation with CO₂ or hydroxyalkylation with acetone considering the herein discussed substrate classes. References are given in parenthesis.

Direct UV-light excitation of polyaromatic hydrocarbons in presence of sacrificial amines and CO₂ was reported to yield the corresponding carboxylic acids.^[51,52] Jamison employed *p*-terphenyl, which forms a radical anion upon UV-light excitation in the presence of amines.^[53] The *p*-terphenyl radical anion is capable of the kinetically slow one-electron reduction of CO₂ to its radical anion, which is used in the hydrocarboxylation of styrenes (see Scheme 4-1). Murakami and co-workers employed UV-excited xanthone as hydrogen-atom-transfer (HAT) reagent in combination with a Cu complex or a Ni catalyst to carboxylate allylic^[54] and benzylic^[55] C(sp³)–H, respectively. Remarkably, the latter report also demonstrates the carboxylation of aliphatic C–H bonds albeit in low yield, using a combination of benzophenone sensitizer and nickel catalyst.

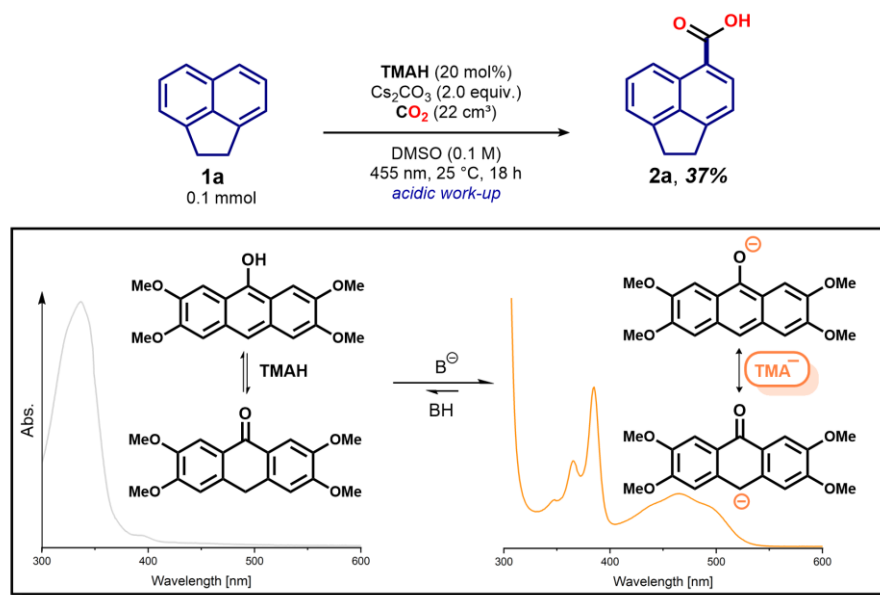
However, despite the great progress achieved in thermal and photochemical carboxylation methods, the efficient redox-neutral carboxylation of $C(sp^2)-H$ in arenes, heteroarenes and alkenes remains challenging. Here, we report a mechanistically different catalytic approach in which aromatic compounds are converted into their radical anions by photoinduced single-electron transfer (SET) from a visible-light excited anthrolate anion. The generated nucleophilic arene radical anions react with CO_2 to provide (hetero)aromatic carboxylic- and cinnamic acids.

4.2 Results and Discussion

Recently, we showed that commercially available 9-anthrone and derivatives are deprotonated in presence of base (Scheme 4-2 and Figure S6, Experimental Part) and readily generate strong reductants upon photoexcitation, capable of activating aryl chlorides (*cf.*, Chapter 3).^[56] While comparing reported reduction potentials of various aromatic compounds, we noticed that many arenes lay within the range of the approximated excited state oxidation potential of the strongest photo-reductant 2,3,6,7-tetramethoxyanthracen-9(10*H*)-one (**TMAH**) shown in that series [E_{ox}^* (**TMA**[•] / **TMA**^{-•}) = -2.92 V *vs.* SCE]. We thus envisioned a direct activation of arenes *via* radical anion formation, which may subsequently react with CO_2 to form aromatic carboxylic acids. Strong carbon nucleophiles (*e.g.* organolithium and -magnesium reagents)^[57-60] or carbanions are well known to react with CO_2 . By contrast, aromatic radical anions formed in the presence of alkali metal have always been considered as poor nucleophiles,^[61] yet still showed reactivity towards CO_2 .^[62,63] With a strongly reducing photoredox catalyst in hand and inspired by early literature reports, we questioned if a similar reactivity of aromatic radical anions towards carbon dioxide can be obtained under much milder photocatalytic conditions.

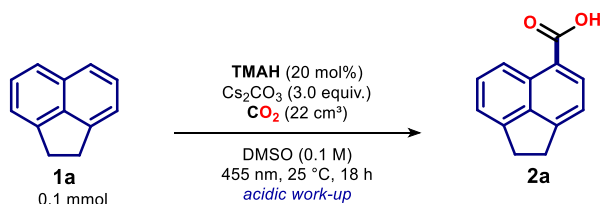
4.2.1 Initial Experiments and Optimization

We chose acenaphthene (**1a**, Scheme 4-2) as a model substrate and applied the established combination of **TMAH** as the photocatalyst and cesium carbonate as the base. To our delight, after 18 hours of irradiation with blue LED light and acidic work-up, the desired carboxylic acid **2a** could be isolated in 37% yield as a single regioisomer. Encouraged by this first result we run an intensive screening of the reaction conditions to improve the yield (Table 4-1).



Scheme 4-2. (top) Photocatalytic C–H carboxylation of acenaphthene **1a**; (bottom) Base-promoted formation of TMA[−] and the influence on the absorption spectrum.

During the optimization studies, we observed that the reaction outcome was dependent on the amount of Cs₂CO₃. The use of less than 3 equivalents of base led to significantly lower product yield (Entry 2) while more equivalents of Cs₂CO₃ reduced the yield (Entry 3). A lower catalyst loading reduced the overall amount of base required, while the carboxylated product **2a** was still obtained in good yield (Entry 4-5). We assume that an incomplete deprotonation of the added catalyst has a detrimental effect on the reaction. K₂CO₃, although being scarcely soluble in DMSO, was also able to promote the carboxylation reaction and useful product yields were obtained in combination with crown-ether (Entry 6). Monitoring the reaction progress over time (Figure S4-8, Experimental Part) showed that the reaction was not complete after 6 hours (Entry 7). An overpressure of CO₂ was found to be beneficial for the reaction outcome (Entry 8 and 9). The solubility of CO₂ is reported to be higher in DMF compared to DMSO, yet better yield was obtained in the latter (Entry 10).^[64] Using green light (535 nm) resulted in lower product yield (Entry 11), which can be explained by both weaker catalyst absorption and LED radiant flux. Control experiments revealed that all reagents and light are crucial, as no product was detected in the absence of either photocatalyst, cesium carbonate, carbon dioxide or light (Entry 12-15).

Table 4-1. Optimized reaction conditions and effects upon deviation.

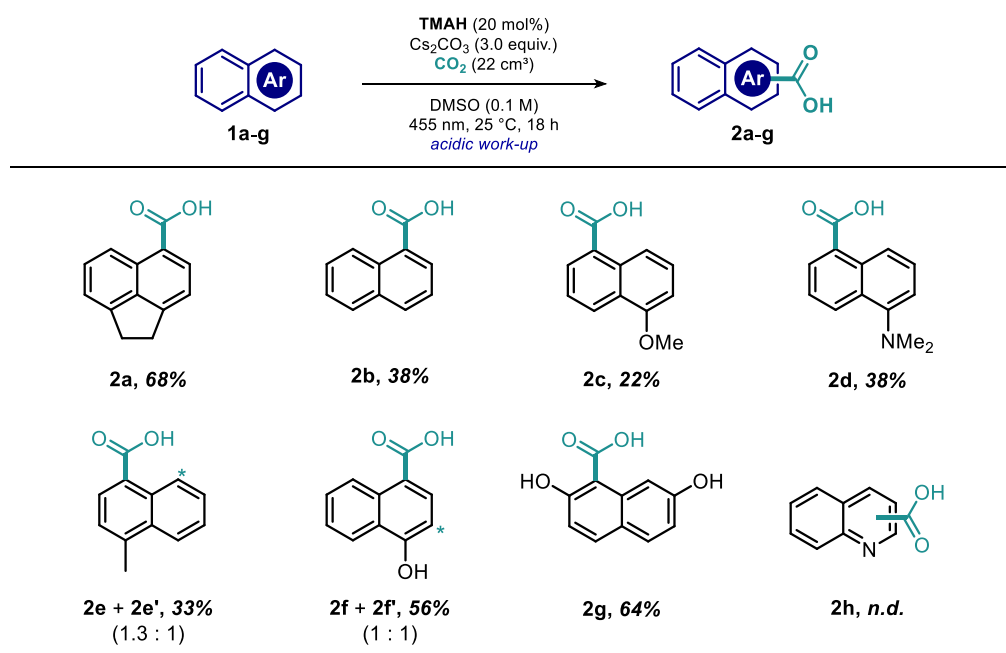
Entry	Deviations from optimized conditions	Yield 2a [%] ^a
1	none	68 ^b
2	Cs ₂ CO ₃ (2 equiv.)	37 ^b
3	Cs ₂ CO ₃ (4 equiv.)	59
4	TMAH (5 mol%), Cs ₂ CO ₃ (2 equiv.)	54
5	TMAH (10 mol%), Cs ₂ CO ₃ (2 equiv.)	60
6 ^c	TMAH (10 mol%), K ₂ CO ₃ instead of Cs ₂ CO ₃ , 18-crown-6	47
7	6 hours instead of 18 hours	44
8	no CO ₂ pressure (1 atm)	37
9	11 cm ³ CO ₂ instead of 22 cm ³	48
10	DMF instead of DMSO	35
11 ^d	535 nm instead of 455 nm	29
12	no TMAH	n.d.
13	no Cs ₂ CO ₃	n.d.
14	N ₂ (1 atm) instead of CO ₂	n.d.
15 ^e	no light	n.d.

Optimized reaction conditions: **1a** (0.1 mmol), **TMAH** (20 mol%) and Cs₂CO₃ (0.3 mmol) were added to a 5 mL crimp top vial equipped with a stirring bar. The vial was sealed, evacuated and backfilled with CO₂ (5×). Degassed, anhydrous DMSO (1 mL) was added *via* syringe. The septum was further sealed with Parafilm® and gaseous CO₂ (22 cm³) was added to the headspace *via* syringe. While stirring, the reaction was irradiated from the bottom side (blue LED, 455 ± 15 nm) and constant temperature was maintained by an aluminum cooling block and a water-cooling circuit. For complete optimization table, please see Table S4-1, Experimental Part. n.d. = not detected. ^a Product yield was determined after acidic work-up by crude ¹H-NMR with an internal standard. ^b Combined isolated yield of four reactions. ^c Crown ether 18-crown-6 (1 equiv.) was added to the reaction. ^d Radiant flux is lowered by a factor of 8 compared to 455 nm LED (see Experimental Part). ^e Reaction mixture was stirred in the dark.

4.2.2 Substrate Scope of the Carboxylation Reaction

With the optimized reaction conditions in hand (*cf.*, Table 4-1), we explored the scope of this novel transformation. Naphthalene derivatives were investigated, as their reported potentials are in a feasible range (−2.49 up to −2.65 V *vs.* SCE)^[65] for reduction by the photocatalyst

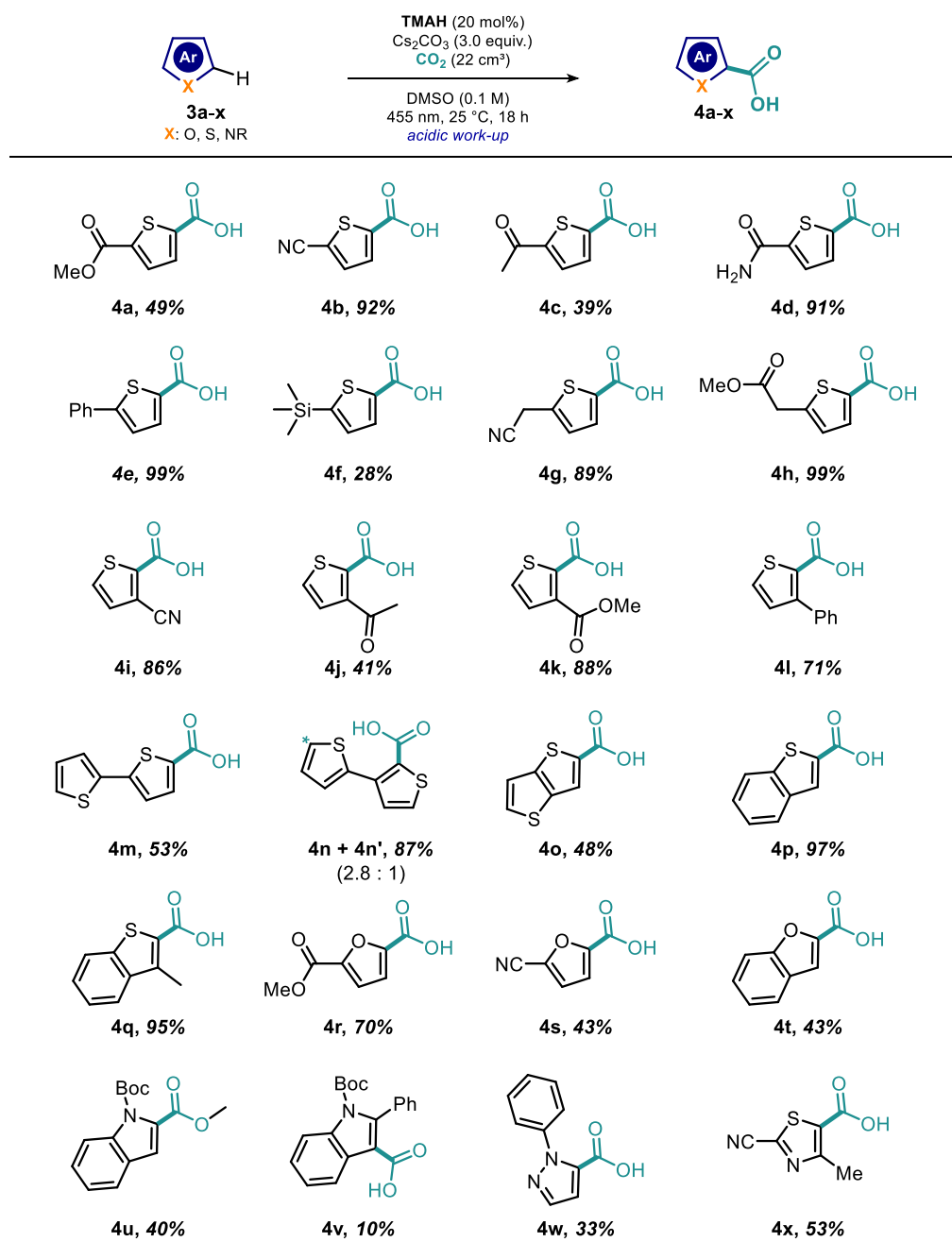
(Scheme 4-3). We were pleased to see that unsubstituted as well as substituted naphthalene derivatives were converted to the corresponding aromatic carboxylic acids (**2b–g**) and could be isolated in useful yields. The regioselectivity of the reaction was found to be affected by strong electron-donating groups (–OMe **2c**, –NMe₂ **2d**) in the C1-position giving selectively 5-naphtoic acids as single regioisomers. In contrast, the directing effect of electronically neutral substituents (–Me, **2e**) was minor and led to a mixture of 4- and 5-naphtoic acid. Remarkably, carboxylation in the C8-position was not observed. Notably, unprotected hydroxyl groups (**2f**, **2g**) were tolerated. Utilizing 1-naphthol (**1f**) led to the formation of two regioisomers of the corresponding acid in 2- and 4-position. 2,7-Dihydroxynaphthalene (**1g**) reacted smoothly under our reaction conditions to yield the corresponding 1-naphtoic acid (**2g**) as a single regioisomer. Quinoline (**1h**), isoquinoline or quinazoline, although quenching the photoexcited state of the catalyst, failed to yield any product.



Scheme 4-3. Substrate scope for the carboxylation of naphthalene derivatives.

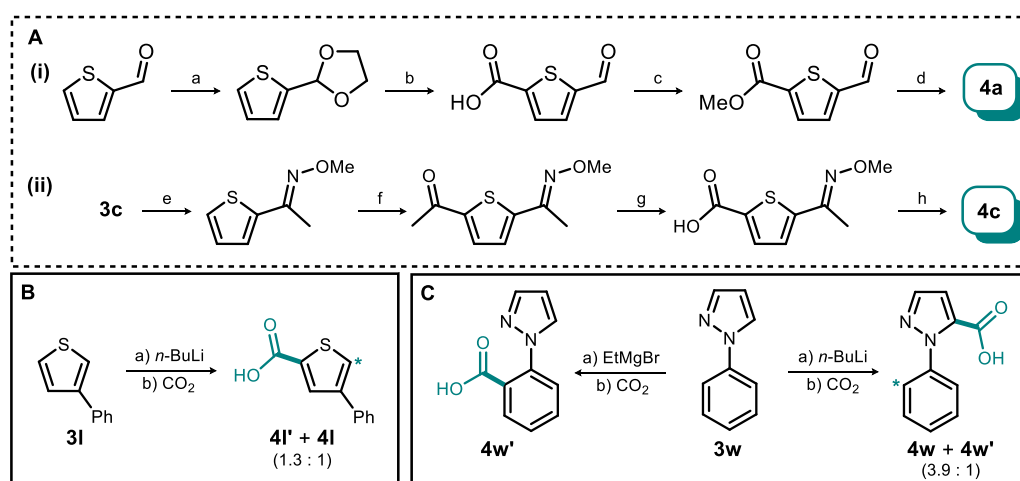
Pleasingly, many other heteroaromatic compounds were suitable substrates for our carboxylation method (Scheme 4-4). Thiophenes, bearing electron-deficient (**3a–d**, **3f**, **3i–k**) and -neutral (**3e**, **3g–h**, **3l–n**) substituents smoothly converted into the corresponding thiophenecarboxylic acids **4a–n** in good to excellent yield. Remarkably, a broad range of functional groups including ketones, esters, amides, –CH₂CO₂Me, –CH₂CN, phenyl-, trimethylsilyl-, nitrile were tolerated. However, unfunctionalized thiophene could not be

activated by the photocatalyst (see Figure S4-11b, Experimental Part). Due to the mild nature of this reaction, we were pleased to see that regioselectivity was maintained even with substrates containing acidic C–H (**4c**, **4i**) or active methylene groups (**4g–h**). This is in contrast to reported base promoted methods that are usually selective for the most acidic position of the substrates and that fail in the presence of sensitive functionalities



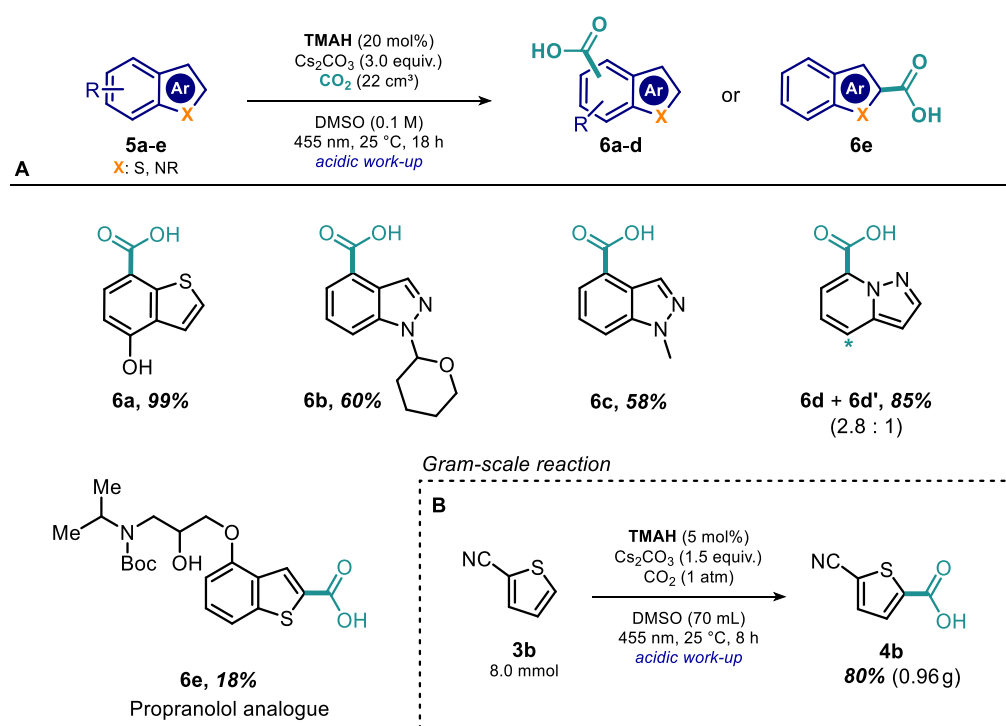
Scheme 4-4. Substrate scope for the carboxylation of 5-membered (hetero)arenes.

Our procedure allowed for the conversion of methyl thiophene-2-carboxylate to 5-(methoxycarbonyl)thiophene-2-carboxylic acid (**4a**) in one step, providing a much shorter route than by using other reported methods [Scheme 4-5, A(i)].^[66] Moreover, it allowed the formation of 5-carboxy-2-acetylthiophene (**4c**), an important building block for the synthesis of the alpha/beta blocker arotinolol,^[67] in one step from 1-(thiophen-2-yl)ethan-1-one (**3c**). This is significantly shorter than well-established synthetic routes [Scheme 4-5, A(ii)].^[68] Remarkably, we also found that 3-substituted thiophenes were exclusively carboxylated in the 2-position (**4i-1**) which highlights the excellent regioselectivity of this reaction. In comparison, a previous literature report on the lithiation of 3-phenylthiophene (**3l**) and subsequent carboxylation led to a mixture of **4l** and **4l'** (Scheme 4-5, B).^[69] Perfect regioselectivity was also observed for the photocatalyzed carboxylation of 1-phenylpyrazole where only **4w** was obtained. In this case, due to the chelating effect of nitrogen, the use of organometallic reagents resulted in product mixtures (*n*-BuLi)⁷⁰ or an inverse regioselectivity (EtMgBr)⁷¹ (Scheme 4-5, C).



Scheme 4-5. Commonly applied synthetic routes to obtain products **4a** and **4c** (A). Regioselectivity of organometallic carboxylation (B+C). (A) Reported four-step synthesis for compound **4a** (i)⁶⁶ and **4c** (ii)⁶⁸; conditions: (a) ethane-1,2-diol, Al₂O₃, CCl₄, Δ, 48 h; (b) *n*-BuLi, THF, −78 °C, then CO₂ followed by H₂SO₄ (10%); (c) MeI, Na₂CO₃, DMF, 20 °C, 48 h; (d) Jones reagent; (e) MeONH₂·HCl, Na₂CO₃, H₂O, MeOH, AcOH (pH 5), Δ, 3 h; (f) ZnCl₂, CHCl₃, Ac₂O, 100 °C, 12 h, r.t., aq. HCl (20%) (g) MeOH, aq. NaOCl (5.5%), 70 °C, 4 h, r.t., HCl conc.; (h) aq. HCl, 65 °C, 12 h. (B) *n*-BuLi promoted carboxylation of **3l** leads to a mixture of regioisomers. (C) Organometallic methods for carboxylation of 1-phenylpyrazole. Due to the chelating effect of nitrogen, the use of organometallic reagents causes a mixture of regioisomers (*n*-BuLi) or leads to an inversion of regioselectivity (EtMgBr) yielding benzoic acid **4w'** as single product.

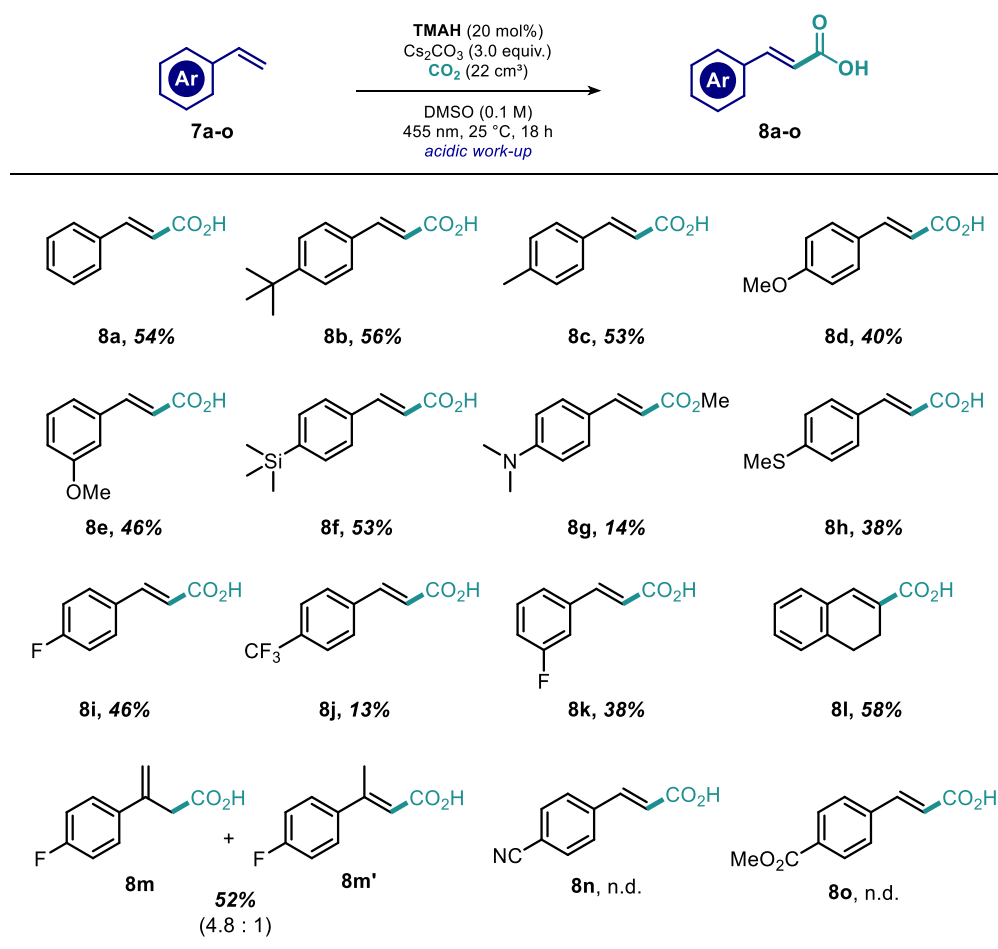
This photocatalyzed carboxylation method could also be extended to benzothiophenes (**4p-q**), furans (**4r-s**), benzofuran **4t**, Boc-protected indoles (**4u-v**) and thiocarbazole **4x**. Non-protected 1*H*-indoles however, were found to get carboxylated at the nitrogen atom, as reported in literature.^[30] Noteworthy, modifying the conditions during the reaction work-up of **4r** allows the formation of either 2,5-furandicarboxylic acid (FDCA) or dimethyl 2,5-furandicarboxylate (DMFDC, see Scheme S4-4, Experimental Part). Both are important monomers for the manufacture of polyesters derived from biomass, including polyethylene furandicarboxylate (PEF), a potential large-scale substitute for fossil-based polyethylene terephthalate (PET).^[72,73] Lignocellulose is converted into furfural on an industrial scale^[74] and catalytic follow-up procedures have been reported to yield methyl furoate quantitatively.^[75,76] Starting from methyl furan-2-carboxylate **3r**, our procedure offers a new one-step synthetic route to form lignocellulose-derived monomers.



Scheme 4-6. (A) Substrate scope for the carboxylation of (hetero)arenes on the six-membered ring and example of late-stage functionalization. (B) Reaction conditions for the gram-scale carboxylation of **3b**.

Remarkably, all examined heterocycles were carboxylated at the five-membered ring in α -position (except **4v**, where the α -position is blocked) to the heteroatom. Contrarily, hydroxybenzothiophene **6a** or condensed heterocycles such as indazoles (**6b-c**) and pyrazolo[1,5-*a*]pyridine (**6d**) showed exclusive selectivity for the six-membered ring

(Scheme 4-6 A). With mild carboxylation conditions in hand, we postulated that this methodology could be applied for the late-stage functionalization of biologically active molecules. To this end, a Boc-protected thiophene analogue of propranolol, a well-established beta blocker bearing a free hydroxyl group in the side chain, was subjected to our reaction conditions. Pleasantly, regioselective carboxylation was successfully achieved to provide **6e**, albeit in modest yield. To demonstrate the scalability of our reaction, we repeated the synthesis of **4b** on a gram-scale. 2-Cyanothiophene **3b** was reacted in a custom-built glass reactor (see Figure S4-2, Experimental Part) with a reduced amount of both **TMAH** (5 mol%) and cesium carbonate (1.5 equiv.) in DMSO (Scheme 4-6 B). Remarkably, as working with CO₂ overpressure was not possible with this reaction vessel, a gentle stream of CO₂ was sufficient to obtain the product after 8 hours of reaction time in good yield.



Scheme 4-7. Substrate scope for the carboxylation of styrene derivatives.

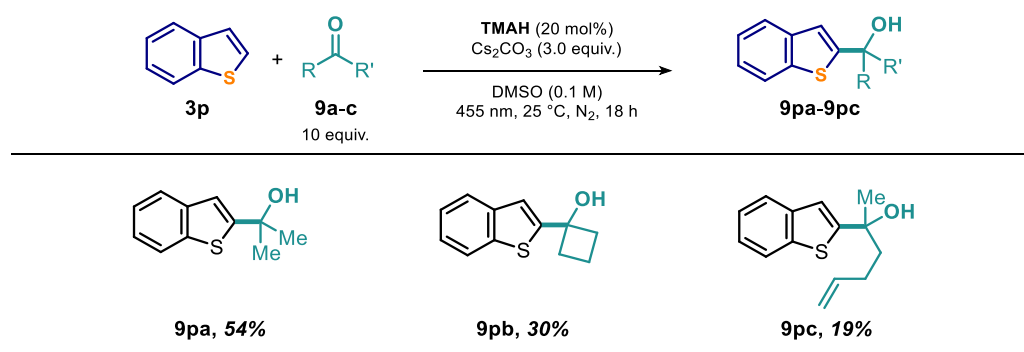
We then questioned whether our photocatalytic system could be further utilized for the direct carboxylation of other stabilized sp²-hybridized carbon atoms. To this end, we examined

styrene derivatives (Scheme 4-7) and we were delighted to see that under the presented redox-neutral conditions only the corresponding *trans*-cinnamic acids were obtained. Our protocol thus provides a complementary method to previous net-reductive approaches where excess of sacrificial reductant or electrical current yielded hydrocarboxylated products (*cf.*, Scheme 4-1).^[22,48,53] Despite the limitation posed by competing polymerization reactions, a variety of vinyl benzenes could be converted into *trans*-cinnamic acid derivatives **8b-1** (Scheme 4-7), which find applications in the food industry, material science^[77] and cosmetics.^[78] While styrene derivatives bearing electron-donating substituents (**7d-f**, **7h**) reacted smoothly, the reaction with the electron-poor 4-(trifluoromethyl)styrene resulted in low product yield. 4-Cyanostyrene (**7n**) or methyl-4-vinylbenzoate (**7o**) were not suitable substrates under these conditions. As the electron transfer from the excited photocatalyst to an electron-poor styrene is thermodynamically favored, we postulated that electron-withdrawing groups stabilize the negative charge and reduce the nucleophilicity of the corresponding radical anion. When using α -methylstyrene, we observed the formation of 3-aryl-3-butenic acid **8m** in favor of the thermodynamically more stable α,β -unsaturated acid **8m'**.^[38]

4.2.3 Mechanistic Insights

We propose a photoinduced single-electron transfer (SET) from the excited **TMA**^{-*} to the substrate as the first step. The excited photocatalyst **TMA**^{-*} is strongly emissive and its luminescence decay follows first-order kinetics (see Figure S4-4 a-b and Figure S4-5, Experimental Part). In presence of chosen (hetero)arenes (*cf.*, Scheme 4-4) as well as styrenes (*cf.*, Scheme 4-7) we observed a decrease in the luminescence lifetime of **TMA**^{-*}. Based on the obtained data, a Stern-Volmer plot was derived (see Figure S4-11 a-b, Experimental Part). The luminescence lifetime of **TMA**^{-*} in a CO₂-saturated solution of DMSO remains almost unchanged, indicating that CO₂ is not reduced by the photocatalyst. Reduction of CO₂ by SET to achieve carbon-bond formation has been reported, but it requires reagents such as *p*-terphenyl radical anion^[53,79]. Although a direct reduction of CO₂ (-2.21 V *vs.* SCE in DMF)^[80] by **TMA**^{-*} is thermodynamically feasible, we assume a kinetic barrier preventing the formation of the bent CO₂ radical anion within the excited state lifetime of **TMA**^{-*}. Thus, we ascertained that the productive pathway is dominated by the formation of an aromatic radical anion, which subsequently reacts with CO₂ *via* nucleophilic addition. In order to get further insight into the reaction mechanism, we tested other electrophiles than CO₂. We decided to use ketones for

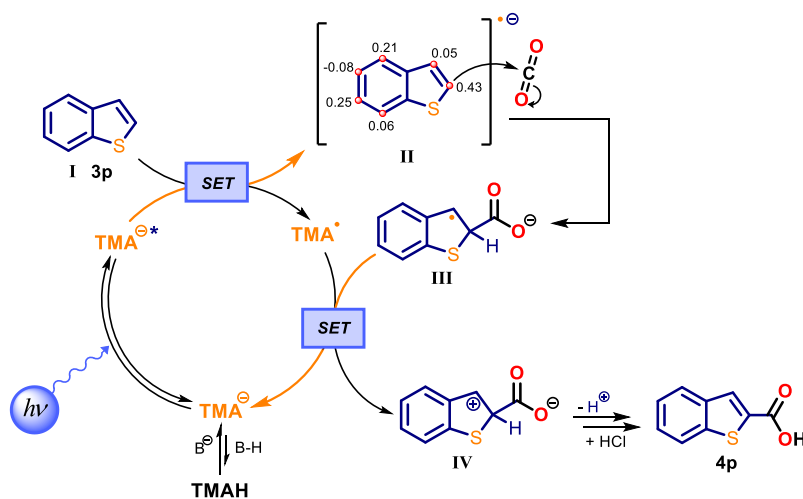
this study, as single-electron reduction from the excited photocatalyst to the ketone would give a ketyl radical anion. In sharp contrast to the radical anion of CO₂, ketyl radical anions are considered as electron-rich species acting as single-electron reductants rather than forming C–C bonds *via* radical reactions.^[81] When benzo[*b*]thiophene (**3p**, Scheme 4-8) was reacted with acetone (**9a**), the corresponding tertiary alcohol adduct **9pa** was formed in good yield. The luminescence lifetime of **TMA**^{−*} remains unchanged upon titration with acetone (−2.84 V *vs.* SCE in DMF)^[82] and thus, the formation of a ketyl radical anion is unlikely (Figure S4-11d, Experimental Part). Remarkably, similar transformations require very harsh reaction conditions (−78 °C, excess of *n*-BuLi) and are not viable in a one-pot procedure.^[83] Moderate yield of the resulting tertiary alcohol were also obtained using cyclic ketone **9b** and non-conjugated enone **9c** as electrophiles.



Scheme 4-8. Mechanistic investigations: Probing the possibility of other electrophiles as viable candidates for reactivity with aromatic radical anions.

In addition, we performed deuterium-labeling experiments using D₂O and ³BuOD respectively. Upon formation of the nucleophilic arene radical anion, we envisioned a fast acid-base reaction followed by reoxidation and deprotonation to yield a mixture of H and D in the substrate (see Scheme S4-3, Experimental Part). However, as water in the reaction mixture was found to be detrimental and protic solvents were shown to inhibit the reaction (*cf.*, Table S4-1, Experimental Part), only small amounts of incorporated deuterium were detected using benzothiophene **3q** (Table S4-3, Experimental Part). Based on the aforementioned results we propose the following reaction mechanism for the photocatalytic C–H carboxylation of (hetero)arenes (Scheme 4-9). In the presence of a base, the pre-catalyst **TMAH** is chemically activated by deprotonation to form an anionic species **TMA**[−], indicated by the solution colour change. Upon irradiation with visible light (455 nm) a strongly-reducing excited anion **TMA**^{−*} is formed. The excited state is then quenched by the arene **I** *via* SET to afford the radical of

the photocatalyst **TMA**[•] and the electron rich radical anion of the arene (**II**). The Mulliken spin population for each aromatic sp²-hybridized carbon atom, indicative of reactivity towards CO₂, is shown for the benzothiophene radical anion (**II**). In the bond-forming step CO₂ is attacked by **II** to generate a radical carboxylate **III** as an intermediate. The catalytic cycle is closed *via* SET to recapture the active catalyst **TMA**[•] followed by re-aromatization of the cationic arene **IV** upon deprotonation. Despite the weakly oxidizing nature of the photocatalyst, the electron transfer from **III** to **TMA**[•] may be driven by the stabilization energy gained upon re-aromatization of **IV**. It remains to be shown if this re-aromatization occurs *via* electron transfer and subsequent deprotonation as proposed, or *via* a direct H-atom abstraction by the oxidized photocatalyst



Scheme 9. Proposed mechanism for the C–H carboxylation of (hetero)arenes exemplified by the carboxylation of benzothiophene.

During the exploration of the substrate scope, we found that several aromatic compounds that quench the excited state of the photocatalyst did not undergo carboxylation (see Figure S4-11c, Experimental Part). While some functional groups are understandably not tolerated under our reaction conditions, such as aromatic halides (these may undergo fast mesolytic bond-cleavage to form aryl radicals) or highly electrophilic moieties, we were surprised that only certain radical anions showed reactivity towards CO₂. In order to determine the required electronic characteristics for reactivity and to improve our insight regarding functional group tolerance, high-throughput screening (HTS) of various arenes containing a large array of functionalities and differing in complexity was carried out (see Figure S4-9, Experimental Part). The analysis of the HTS outcome indicates that aldehydes, halides (with the exception of

fluorine), aliphatic amines, 6-membered N-heterocycles and nitro groups are not compatible with the reaction conditions. Beyond functional group interference, the applicability of our methodology is related to the arene electron affinity and the nucleophilicity of the resulting radical anion. Arenes may be able to accept an electron with ease, but the radical anion formed may not be nucleophilic enough to add to CO₂. Conversely, some aromatic radical anions may be highly nucleophilic, but their formation may be beyond the reductive capabilities of the photocatalyst or a functional group present may be reduced instead. The estimated electron affinities of the arenes, and the Mulliken spin population and charges for the arene radical anions were derived from DFT calculations. The importance of a correct balance of electron affinity of the arene and the nucleophilicity of the aromatic radical anion for a successful reaction is illustrated in Schemes S4-12a-d (Experimental Part). The regioselectivity is generally well predicted by comparing the Mulliken spin population for the aromatic carbons in each substrate.

4.3 Conclusion

We have developed a mild, direct, redox-neutral and transition-metal-free insertion of CO₂ into non-prefunctionalized C(sp²)–H bonds, leading to an efficient method for producing valuable aromatic carboxylic acids and *trans*-cinnamic acids in a single operation. A reaction performed on gram-scale demonstrated the scalability of this carboxylation method, while ketones could be used as alternative electrophiles to CO₂ yielding tertiary alcohols. The scope of the reaction can be predicted by DFT-estimated reduction potential of the substrates and nucleophilicity of the intermediate arene radical anions. These findings may open new opportunities for atom-economic and energy efficient use of CO₂ as a C1 building block in the chemical processing of aromatic hydrocarbons, as well as for developing new photocatalytic late-stage functionalizations of drug-like compounds.

4.4 Experimental Part

4.4.1 General Information

All required fine chemicals were purchased from commercial suppliers (abcr, Acros, Alfa Aesar, Fluka, Fluorochem, Merck, Sigma Aldrich, TCI) and were used directly without purification unless stated otherwise. All air and moisture sensitive reactions were carried out under nitrogen atmosphere using standard Schlenk manifold technique. Anhydrous DMSO was used directly from the bottle or dried using activated 4Å molecular sieves. ^1H and ^{13}C Nuclear Magnetic Resonance (NMR) spectra were acquired at room temperature with field strengths as indicated and were referenced to CDCl_3 (7.26 and 77.16 ppm for ^1H and ^{13}C respectively), DMSO-d_6 (2.50 and 39.52 for ^1H and ^{13}C respectively) or CD_3OD (3.31 and 49.0 ppm for ^1H and ^{13}C respectively). ^1H -NMR coupling constants are reported in Hertz and refer to apparent multiplicities and not true coupling constants. Data are reported as follows: chemical shift, multiplicity (s = singlet, bs = broad singlet, d = doublet, t = triplet, q = quartet, qi = quintet, sx = sextet, sp = septet, m = multiplet, dd = doublet of doublets, etc.), coupling constants, integration, proton assignment (determined by 2D NMR experiments: COSY, HSQC and HMBC) where possible. ^{13}C -NMR assignment was aided using DEPT 135 techniques (DEPT = distortion less enhancement by polarization transfer) to distinguish CH_2 groups from CH and CH_3 groups and to assign quaternary carbon atoms (C_q). ^{19}F -NMR spectra were recorded for compounds containing fluorine atoms.

Analytical TLC was performed on silica gel coated aluminium sheets (Merck, TLC Silica gel 60 F_{254}) Compounds were visualized by exposure to UV-light (254 or 366 nm) or by dipping the plates in staining solutions (permanganate stain, bromocresol green stain, ceric ammonium molybdate stain) followed by heating. Flash column chromatography was performed using Merck Silica Gel 60 (40–63 μm) & Medium pressure liquid chromatography (MPLC) was performed on a Grace Reveleris® X2 from Büchi with built-in UV-detector and fraction collector using Biotage® sfär silica HC D 20 μm column cartridges or on a Biotage® Isolera One flash purification system using flash silica gel. All mixed solvent eluents are reported as v/v solutions. High resolution mass spectrometry (HRMS) were performed at the Central Analytical Laboratory of the University of Regensburg. Mass spectra were recorded on a Finnigan MAT 95, ThermoQuest Finnigan TSQ 7000, Finnigan MAT SSQ 710 A or Agilent Q-TOF 6540 UHD instrument and a Waters Acquity UPLC system equipped with Waters

PDA, sample manager, sample organizer, column oven and Waters Xevo QTOF mass spectrometer. Photoreactions in regular scale were irradiated with blue LEDs (OSRAM Oslon SSL 80 royal-blue, $\lambda = 455 \text{ nm}$ (± 15), average radiant flux $232 \pm 23 \text{ mW}$, 2.9 V, 350 mA) or green LEDs ($\lambda = 535 \text{ nm}$, average radiant flux, $29 \pm 5 \text{ mW}$) and were exposed to light from the flat bottom side of the vial. The temperature of the reaction mixtures was controlled by a water-cooling circuit consisting of an aluminium cooling block connected to a thermostat (Figure S4-1). An exemplary reaction in larger scale was carried out in a custom-built glass reactor which upon vigorous stirring generates a thin film of the reaction mixture between the reaction vessel and an attached cold finger. A hose which was dipped in the solution provided CO₂ gas from the cylinder. The reaction vessel was surrounded by blue LED arrays (OSRAM Oslon SSL 80 LT-2010, $\lambda = 451 \text{ nm}$, 700 mA) generating a total radiant flux of 12 W (Figure S4-2). For the high-throughput screening experiments, Kessil PR160L 456 nm LEDs were used. Cyclic voltammetry measurements were performed with a three-electrode system consisting of a glassy carbon working electrode, a platinum wire counter electrode and a silver wire as a reference electrode. Data was processed on a potentiostat PGSTAT302N from Metrohm Autolab. Prior to the measurement the solvent DMSO (dry) was degassed with argon and TBATFB (0.1M) was added as supporting electrolyte. All experiments were performed under argon atmosphere. Ferrocene was used as an internal reference. Measurements were performed at a scan rate of 0.05 Vs^{-1} . Potentials are reported against saturated calomel electrode (SCE) as reference.

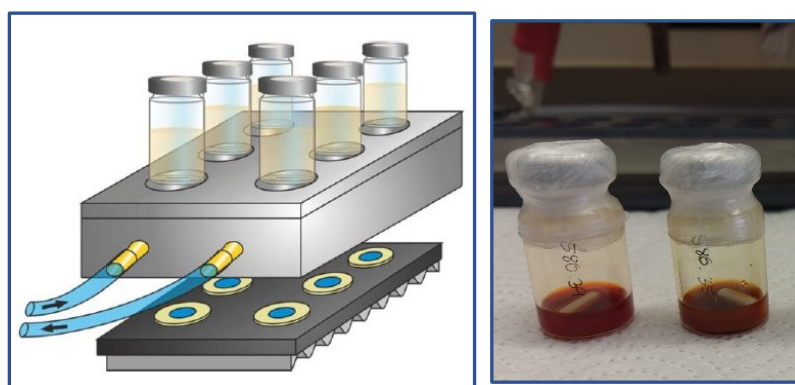


Figure S4-1. Schematic picture of the setup for photoreactions (left); crimp vials charged with stirring bar and reaction mixture and sealed with aluminium crimp seal with septum and Parafilm® (right).

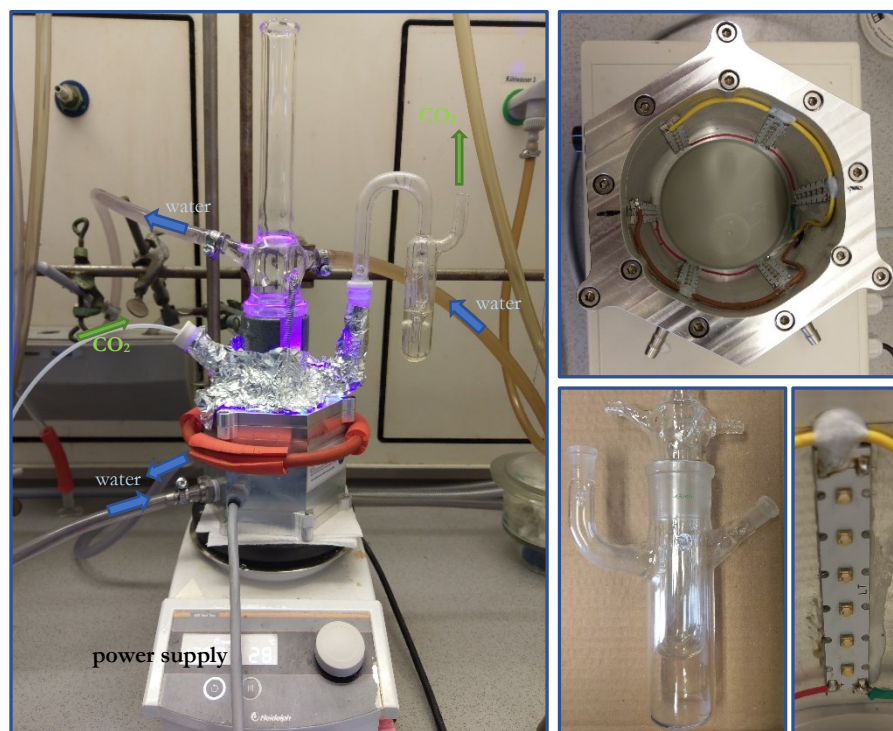


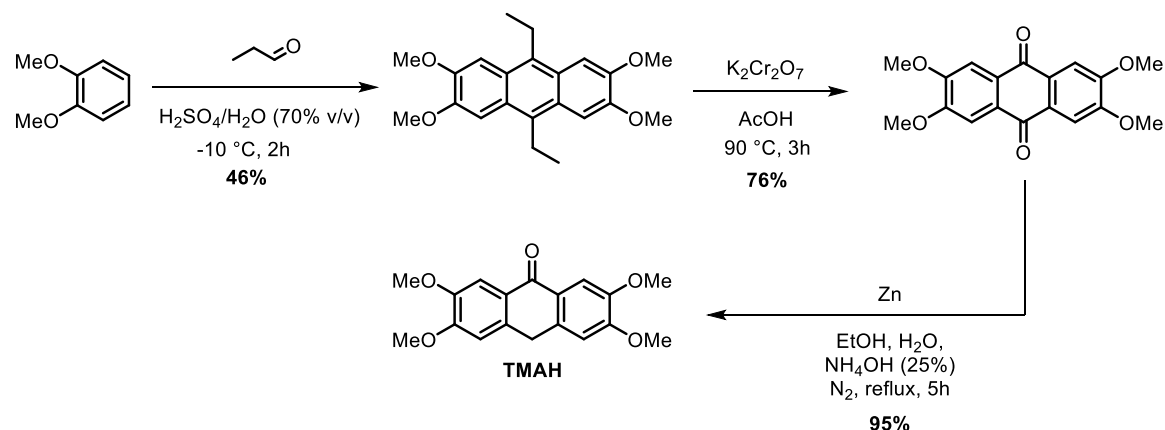
Figure S4-2. Custom-built glass reactor for upscaling of the photocatalytic carboxylation reaction.

UV-vis measurements were performed on an Agilent Cary 4000 UV-Vis Spectrophotometer. Prior to measurements a solvent blank was recorded and subtracted. Precision cells (1×1 cm) made of quartz SUPRASIL® from Hellma® Analytics were used. Luminescence measurements were performed on a Horiba® Scientific FluoroMax-4 instrument using the above-mentioned quartz cells. Luminescence lifetime measurements were performed on a Horiba® Scientific DeltraPro™ fluorescence lifetime system using a 452 nm laser diode from Horiba® Scientific DeltaDiode™ as excitation source and above-mentioned quartz cells. The instrument response function (IRF) was determined prior to measurements by using colloidal silica (LUDOX®) in water.

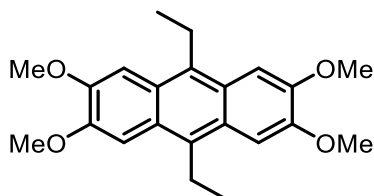
4.4.2 Catalyst Synthesis and Physicochemical Properties

4.4.2.1 Synthesis of the Photocatalyst

2,3,6,7-tetramethoxyanthracen-9(10*H*)-one **TMAH** was synthesized in three steps with an overall yield of 33%. The catalyst in its neutral form is a bench stable compound and can be stored easily.

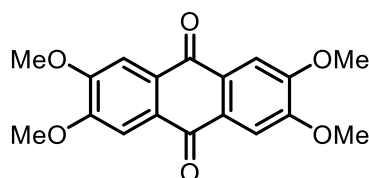


Scheme S4-1. Overview of the synthetic steps in the synthesis of the used photocatalyst **TMAH**; overall yield 33% (3 steps).

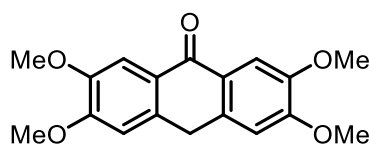


Synthesis of 9,10-diethyl-2,3,6,7-tetramethoxyanthracene: Referring to literature known procedures,^[84,85] a 250 mL round bottom flask equipped with stirring bar was charged with H₂SO₄ (70 mL, 70% v/v in H₂O) and veratrole (12.8 mL, 0.1 mol, 1 equiv.) and the resulting mixture was cooled to -10 °C. Under vigorous stirring, propanal (14.3 mL, 0.2 mol, 2 equiv.) was added dropwise *via* a syringe pump within 2 hrs. Care was taken, that the reaction temperature during addition of aldehyde was kept below 0 °C. The reaction mixture was poured into ice water (ca. 500 mL) and the resulting precipitate was filtered off and washed with water. The filter cake was dried over night by lyophilization and was washed in boiling

EtOH. The precipitate was filtered off, washed with EtOH and dried under vacuo to give the title compound (8.06 g, 23 mmol, 46%) as pale-yellow powder. **¹H-NMR** (400 MHz, Chloroform-*d*) δ 7.41 (s, 4H), 4.07 (s, 12H), 3.47 (q, J = 7.6 Hz, 4H), 1.44 (t, J = 7.6 Hz, 6H). **¹³C-NMR** (101 MHz, CDCl₃) δ 149.0 (*C_q*), 130.7 (*C_q*), 125.1 (*C_q*), 102.4, 55.8, 22.0 (CH₂), 14.6.



Synthesis of 2,3,6,7-tetraethoxy-9,10-anthraquinone: According to a literature known procedure^[86] a 500 mL round bottom flask was charged with 9,10-diethyl-2,3,6,7-tetraethoxyanthracene (8.0 g, 22.6 mmol, 1 equiv.) and K₂Cr₂O₇ (33.2 g, 113 mmol, 5 equiv.) and the solids were suspended in glacial acetic acid (270 mL). The resulting mixture was heated to 90 °C for 3 hrs. After the mixture was cooled to ambient temperature the yellow precipitate was filtered off and washed several times with water to remove excess of K₂Cr₂O₇. The filter cake was freeze-dried and finally washed with Et₂O and dried in vacuo to afford the title compound as yellow powder (5.67 g, 17.3 mmol, 76%), which was used without further purification for the next step. **¹H-NMR** (300 MHz, Chloroform-*d*) δ 7.68 (s, 4H), 4.07 (s, 12H). **¹³C-NMR** (101 MHz, CDCl₃) δ 182.1(*C_q*), 153.6 (*C_q*), 128.6 (*C_q*), 108.5, 56.7.



Synthesis of 2,3,6,7-tetraethoxyanthracen-9(10*H*)-one (TMAH): Referring to a literature known procedure^[87] a 500 mL Schlenk flask equipped with stirring bar and condenser was charged with 2,3,6,7-tetraethoxy-9,10-anthraquinone (5.60 g, 17.1 mmol, 1 equiv) and zinc dust (3.40 g, 52.0 mmol, 3.1 equiv.). The flask was set under N₂ atmosphere and equipped with a bubble counter and a mixture of aq. ammonia solution (135 mL, 25%), EtOH (135 mL) and water (135 mL) was added. The resulting mixture was refluxed for 5 hrs under N₂ atmosphere and vigorous stirring. The mixture was allowed to cool to ambient temperature and was poured in ice water (ca. 1 L). Conc. HCl (150 mL) was added to dissolve excess zinc

and the mixture was stirred overnight. The turbid solution was filtered and the residue was washed several times with water and was freeze-dried to yield **TMAH** as pale-yellow powder (5.10 g, 16.2 mmol, 95%). ¹H-NMR (400 MHz, Chloroform-*d*) δ 7.79 (s, 2H), 6.82 (s, 2H), 4.15 (s, 2H), 3.98 (d, *J* = 7.3 Hz, 12H). ¹³C-NMR (101 MHz, CDCl₃) δ 182.4 (C_q), 153.1 (C_q), 148.6 (C_q), 135.1 (C_q), 125.4 (C_q), 109.7, 108.5, 56.2, 32.0 (CH₂). Data in accordance with the literature.^[86]

4.4.2.2 Spectroscopic and Photochemical Characteristics

The properties of the used photocatalyst (PC) were investigated in various spectroscopic experiments.

UV-vis Absorption

The absorption of the photocatalyst was recorded in dry, degassed DMSO (50 μM) by using a quartz cuvette (1×1 cm) with septum screw cap. The cuvette was degassed *in vacuo* and backfilled with N₂ (5×) before the solvent and the catalyst solution were added *via* syringe. In presence of cesium carbonate, a distinct absorption band arises in the visible range of the spectrum (Figure S4-3). This process can also be followed by naked eye, as the solution turns from colorless to yellow.

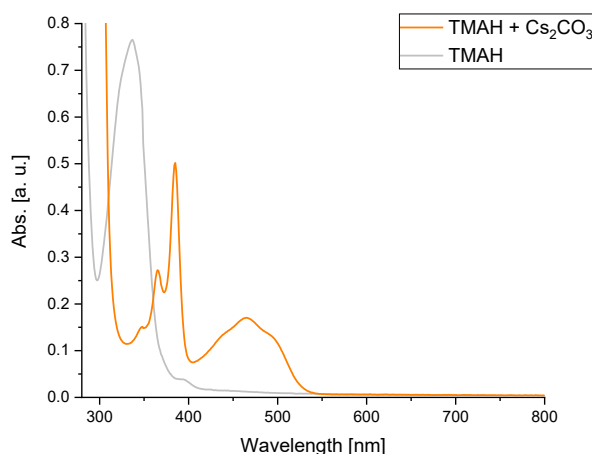


Figure S4-3. UV-vis spectra of (PC) in DMSO and in presence (orange) and absence (gray) of cesium carbonate.

Emission Spectra

The emission spectrum of the photocatalyst was recorded in dry, degassed DMSO (25 μ M) in presence of cesium carbonate by using a quartz cuvette (1 \times 1 cm) with septum screw cap. The cuvette was degassed *in vacuo* and backfilled with N₂ (5 \times) before the solvent and the catalyst solution were added *via* syringe. The excitation wavelength was set to 420 nm (entrance-/exit slit 1 nm) and the emission was measured starting from 450 nm to 800 nm (Increment 1 nm, entrance-/exit slit 2 nm). Relative intensities are plotted for absorption and emission (Figure S4-4a).

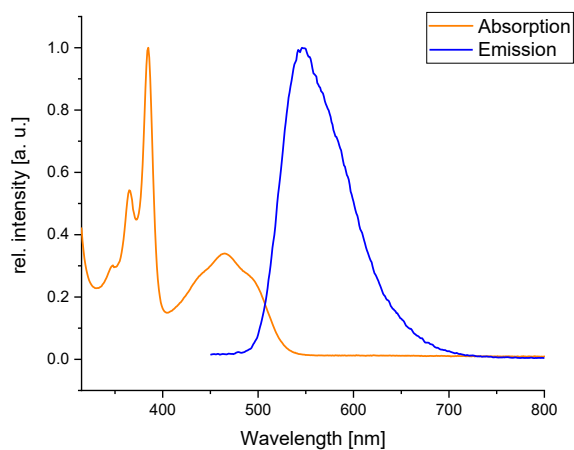


Figure S4-4a. Superimposed absorption and emission spectra of the photocatalyst in DMSO.

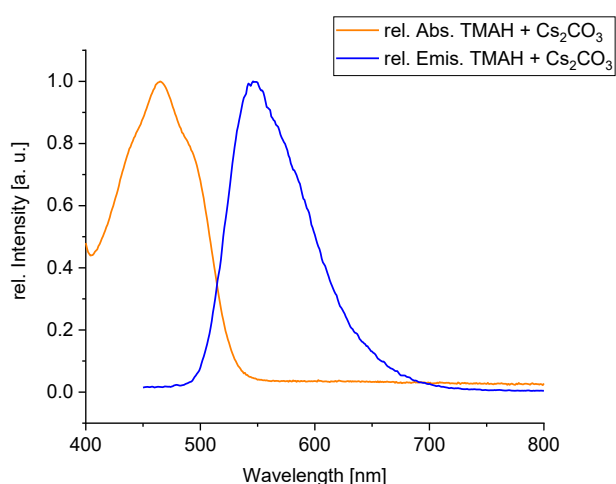


Figure S4-4b. Superimposed normalized absorption- and emission spectra of the photocatalyst in DMSO and in presence of cesium carbonate with an intersection at $\lambda_{\text{isec}} = 514$ nm.

To determine the intersection between normalized symmetrical absorption- and emission spectra, relative intensities for the lowest energy absorption band ($\lambda > 400$ nm) were calculated and plotted (Figure S4-4b).

Excited State Lifetime

The luminescence lifetime of the PC was recorded in dry, degassed DMSO (40 μ M) in presence of cesium carbonate by using a quartz cuvette (1×1 cm) with septum screw cap (Figure S4-5).

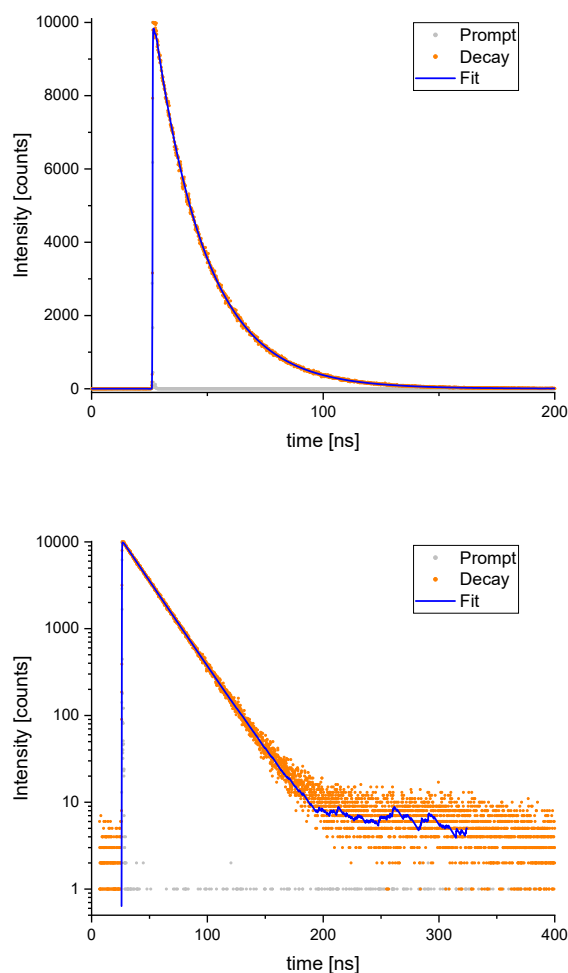


Figure S4-5. Luminescence decay of the excited photocatalyst with fit function in a linear plot (top) and logarithmic plot (bottom).

The cuvette was degassed *in vacuo* and backfilled with N₂ (5×) before the solvent and the catalyst solution were added *via* syringe. For excitation of the sample, a 452 nm laser diode was

used and an optical longpass filter (cut-on wavelength 500 nm) was installed before the detection unit. The time range for the measurement was set to 400 ns. The experimental data were fitted and according to the parameters of the single-exponential fit function, a luminescence lifetime of 22.08 ns (CHISQ = 1.416859) was found.

¹H-NMR Spectroscopy of TMAH

Proton NMR spectra of **TMAH** were recorded in absence and presence of Cs₂CO₃ (Figure S4-6a and S4-6b) in dried, degassed DMSO-d₆. For the measurement in presence of base, a NMR tube with septum and screw-cap was used and the spectra was recorded under N₂ atmosphere. Integration over the NMR signals in presence of Cs₂CO₃ confirms the quantitative formation of the anionic species **TMA⁻**.

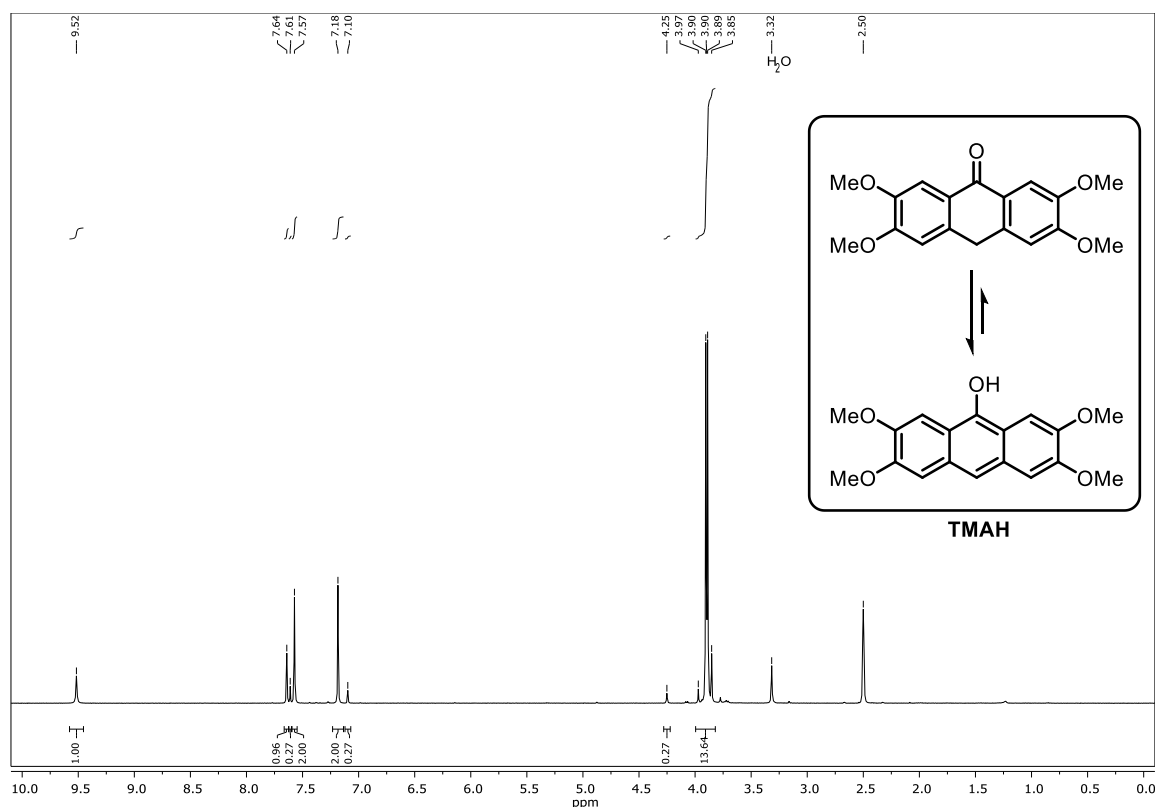


Figure S4-6a. ¹H-NMR of **TMAH** in DMSO-d₆. The keto-enol tautomerism causes two sets of signals; The peak at 3.32 ppm is caused by residual water in the sample.

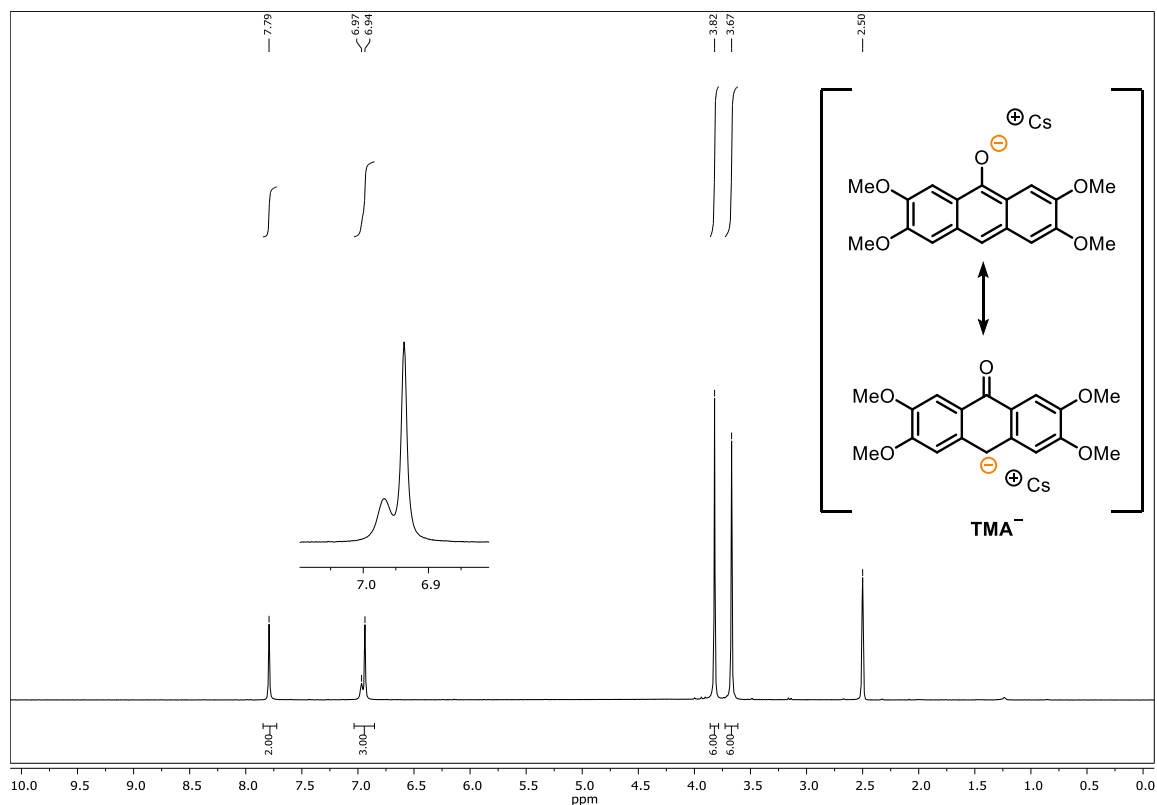


Figure S4-6b. ¹H-NMR of TMA⁻ in presence of Cs₂CO₃ (6 equiv.) in DMSO-d₆.

Ground-State and Excited-State Potentials

The ground state potential of the photocatalyst was investigated by cyclic voltammetry. In presence of 1,1,3,3-tetramethylguanidine the anionic photocatalyst was oxidized (Figure S4-7) upon sweeping to positive potentials. Obtained potentials *vs.* Fc⁺/Fc were converted to potentials against SCE.^[88] The estimated excited state oxidation potential ($E_{ox}^* = -2.92$ V *vs.* SCE) of the photocatalyst was determined according to the free enthalpy change of PET (neglecting the solvent-dependent electrostatic work term) as described in literature^[89,90] by taking the excited state energy ($E_{0,0} = 2.41$ eV, $\lambda_{isec} = 514$ nm) and the converted ground state potential ($E_{p,ox} = -0.51$ V *vs.* SCE) into account.

$$E_{ox}^* = E_{p,ox} - E_{0,0} + \omega$$

The obtained value for E_{ox}^* is based on following approximations: (a) As reported in literature,^[91,92] the single electron oxidation of an organic anion usually causes an irreversible peak in the cyclic voltammogram and an accurate value for the ground state oxidation potential is not accessible. Thus, for the anionic photocatalyst the peak potential $E_{p,ox}$ obtained for this

irreversible process (Figure S4-7) was used to determine the excited-state potential. (b) The excited-state energy $E_{0,0}$ can be estimated in a number of ways. When using the wavelength at the luminescence maximum $\lambda_{\text{emis,max}}$ (546 nm) an underestimation of $E_{0,0}$ is likely.^[89] Furthermore, it is possible to use the midpoint between the absorption maximum of the most red shifted absorption band and the emission maximum (506 nm). The most common way to determine $E_{0,0}$ is by taking the intersection between symmetric normalized absorption- and emission spectra (Figure S4-4b, $\lambda_{\text{isec}} = 514$ nm) which was used for the calculation herein. (c) The solvent-dependent electrostatic work term ω contributes little to the free enthalpy change of PET when working in polar solvents like DMSO and hence was omitted in the calculation.

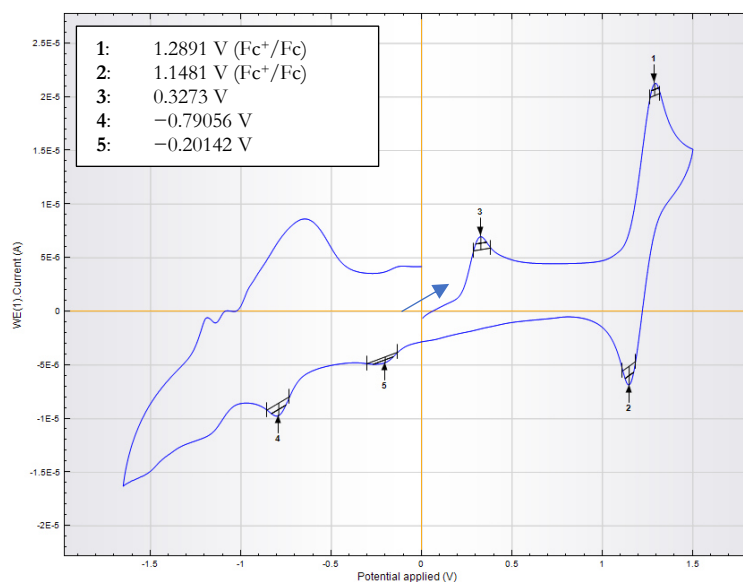
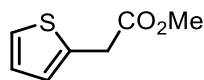


Figure S4-7. Cyclic voltammetry of the photocatalyst was recorded in anhydrous, degassed DMSO, in presence of 1,1,3,3-tetramethylguanidine as base and ferrocene (peaks 1, 2) as internal reference.

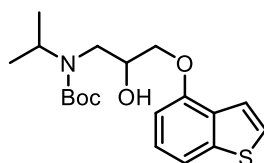
4.4.3 Substrate Synthesis

Methyl 2-(thiophen-2-yl)acetate (3h)

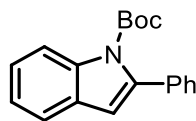


To a solution of 2-thiopheneacetic acid (123 mg, 0.2 mmol) in methanol (2 mL) was added conc. H₂SO₄ (2 drops) and the reaction was heated at reflux for 4 h. The solution was cooled, diluted with water (20 mL) and extracted with diethyl ether (3×20 mL). The combined organics were washed with brine (2×50 mL), dried via a phase separator and concentrated *in vacuo*. Purification by column chromatography on silica gel eluting with heptane : EtOAc (9:1) gave the title compound as a colorless oil (125 mg, 92%). **¹H-NMR** (400 MHz, CDCl₃) δ 7.22 (dd, *J* = 4.9, 1.4 Hz, 1H), 6.98–6.95 (m, 2H), 3.85 (s, 2H), 3.73 (s, 3H); **¹³C-NMR** (100 MHz, CDCl₃) δ 171.2, 135.3, 127.2, 127.1, 125.4, 52.6, 35.5. Data in accordance with the literature.^[93]

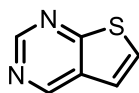
tert-Butyl (3-(benzo[*b*]thiophen-4-yloxy)-2-hydroxypropyl)(isopropyl)carbamate (5e)



1-(Benzo[*b*]thiophen-4-yloxy)-3-(isopropylamino)propan-2-ol (239 mg, 0.9 mmol), triethylamine (0.377 mL, 2.70 mmol), and di-*tert*-butyl dicarbonate (0.236 g, 1.08 mmol) were added to a 50 mL round bottom flask. DCM (25 mL) was added and the mixture stirred at room temperature for 2 h. Water (25 mL) was subsequently added and the layers were separated. The organic layer was washed brine (2 x 25 mL) with then dried *via* a phase separator and concentrated *in vacuo*. Purification by column chromatography on silica gel eluting with heptane : EtOAc (9:1) gave the title compound as a yellow/orange oil (151 mg, 45%). *R*_f 0.56 [petrol : EtOAc (9:1)]; **¹H-NMR** (400 MHz, DMSO) δ 7.66 (d, *J* = 5.4 Hz, 1H), 7.53 (dd, *J* = 10.5, 2.3 Hz, 2H), 7.30 (t, *J* = 8.0 Hz, 1H), 6.84 (d, *J* = 7.9 Hz, 1H), 5.76 (s, 1H), 5.17 (d, *J* = 5.2 Hz, 1H), 4.23 – 3.89 (m, 4H), 3.54 – 3.22 (m, 1H), 1.38 (s, 9H), 1.24 – 1.01 (m, 6H). **¹³C-NMR** (125 MHz, DMSO) δ 156.4, 155.2, 141.5, 131.1, 130.0, 128.9, 123.2, 121.1, 109.1, 80.3, 71.5, 68.2, 49.0, 45.5, 28.3, 19.5.

***tert*-Butyl 2-phenyl-1*H*-indole-1-carboxylate (3v)**

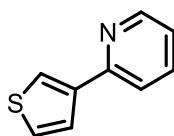
The compound was synthesized according to a literature known procedure.^[94] In a flame dried 100 mL Schlenk flask under N₂ atmosphere equipped with stirring bar, (Boc)₂O (1.20 g, 5.50 mmol, 1.1 equiv.) was added to a solution of 2-phenylindole (0.966 g, 5.0 mmol, 1 equiv.) and 4-(*N,N*-dimethylamino)pyridine in dry MeCN (30 mL). The resulting mixture was stirred at room temperature for 24 h and was then concentrated *in vacuo*. After the addition of water, the mixture was extracted with EtOAc (3×). The combined organic layers were washed with brine, dried over Na₂SO₄, filtered and concentrated under reduced pressure. The crude material was purified by flash silica gel column chromatography using a mixture of hexanes/EtOAc to provide the title compound as white solid (1.40 g, 4.8 mmol, 96%). **¹H-NMR** (400 MHz, Chloroform-*d*) δ 8.27 – 8.20 (m, 1H), 7.59 – 7.54 (m, 1H), 7.46 – 7.31 (m, 6H), 7.27 (td, *J* = 7.6, 0.9 Hz, 1H), 6.57 (s, 1H), 1.32 (s, 9H). **¹³C-NMR** (101 MHz, CDCl₃) δ 150.3 (C_q), 140.6 (C_q), 137.6 (C_q), 135.1 (C_q), 129.3 (C_q), 128.9, 127.9, 127.7, 124.4, 123.0, 120.6, 115.3, 110.0, 83.5 (C_q), 27.7.

Thieno[2,3-*d*]pyrimidine (3y)

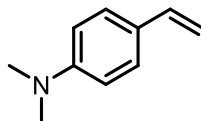
Based on a literature reported procedure for dehalogenation of aromatic compounds^[95], a 5 mL crimp vial equipped with stirring bar was charged with 4-chlorothieno[2,3-*d*]pyrimidine (17.1 mg, 0.1 mmol, 1 equiv.) and 10-phenylphenothiazine (2.8 mg, 0.01 mmol, 10 mol%) and sealed with an aluminium crimp seal with septum. The vial was degassed and flushed with N₂ and tributylamine (119 μL, 0.5 mmol, 5 equiv.), formic acid (18.9 μL, 0.5 mmol, 5 equiv.) and dry MeCN (1 mL) were added. The reaction mixture was degassed by freeze-pump-thaw cycles (3×) and backfilled with N₂. The crimp vial was irradiated from the bottom side with 365 nm LED light for 22 hrs and a constant reaction temperature (25°C) was maintained by employing a water-cooling circuit connected to a thermostat. For isolation of the compound, 10 reactions were combined. The reactions were quenched by adding water and brine and the resulting

mixture was extracted with EtOAc (3×). The combined organic layers were dried over Na₂SO₄, filtered and concentrated *in vacuo*. Purification was accomplished by flash silica gel chromatography using a mixture of hexanes/EtOAc as eluents and subsequent recrystallization from hexanes to afford the title compound as pale-yellow needles (31.8 mg, 0.23 mmol, 23%). **¹H-NMR** (400 MHz, Chloroform-*d*) δ 9.16 (s, 1H), 9.10 (s, 1H), 7.57 (d, *J* = 6.0 Hz, 1H), 7.36 (d, *J* = 6.0 Hz, 1H). Data in accordance with the literature.^[93]

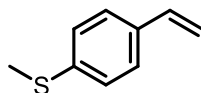
2-(Thiophen-3-yl)pyridine (3z)



Following a literature known procedure^[97] a 10 mL crimp vial was charged with 3-thienylboronic acid (130 mg, 1.01 mmol, 1.2 equiv.), K₂CO₃ (326 mg, 2.36 mmol, 2.8 equiv.), [Pd(PPh₃)₂Cl₂] (29.6 mg, 0.042 mmol, 0.05 equiv.), DME (2.5 mL) and water (1.17 mL). The vial was sealed with an aluminium crimp seal with septum and argon was bubbled through the solution for 10 minutes. Bromopyridine (81 μL, 0.842 mmol, 1 equiv.) was added *via* syringe and the reaction was stirred in a pre-heated heating block for 18 hrs at 80 °C. The reaction was allowed to cool to ambient temperature, was quenched by adding water and was extracted with EtOAc (3×). The combined organic layers were washed with brine, dried over Na₂SO₄, filtered and concentrated *in vacuo*. The crude product was purified by flash silica gel column chromatography using a mixture of hexanes/EtOAc and was obtained as colorless oil (127 mg, 0.79 mmol, 94%). **¹H-NMR** (400 MHz, Chloroform-*d*) δ 8.62 (ddd, *J* = 4.9, 1.8, 0.9 Hz, 1H), 7.90 (dd, *J* = 3.0, 1.3 Hz, 1H), 7.70 (td, *J* = 7.7, 1.8 Hz, 1H), 7.66 (dd, *J* = 5.0, 1.3 Hz, 1H), 7.62 (dt, *J* = 8.0, 1.1 Hz, 1H), 7.40 (dd, *J* = 5.0, 3.0 Hz, 1H), 7.17 (ddd, *J* = 7.4, 4.9, 1.2 Hz, 1H). **¹³C-NMR** (101 MHz, CDCl₃) δ 153.7 (C_q), 149.8, 142.3 (C_q), 136.8, 126.4, 126.3, 123.6, 121.9, 120.4.

***N,N*-Dimethyl-4-vinylaniline (7g)**

According to a literature known procedure^[98] a flame-dried 250 mL Schlenk flask was charged under N₂ atmosphere with methyltriphenylphosphonium bromide (14.4 g, 40.3 mmol, 1 equiv.) and dry THF (60 mL). The suspension was cooled to 0 °C and *n*-BuLi (1.6M in hexane, 25.2 mL, 40.3 mmol, 1 equiv.) was slowly added *via* syringe and the resulting mixture was stirred for 1 h. A solution of 4-(*N,N*-dimethylamino)benzaldehyde (6.02 g, 40.3 mmol, 1 equiv.) in dry THF (20 mL) was added dropwise and the reaction was further stirred at 0 °C for 1 h and at ambient temperature for 18 hrs. The reaction was quenched by adding sat. aq. NH₄Cl (30 mL) and the resulting mixture was extracted with DCM (3×20 mL) and the combined organic layers were dried over Na₂SO₄, filtered and concentrated *in vacuo*. Purification by vacuum distillation (0.8 mbar, 75 °C) afforded the title compound as yellowish oil (4.70 g, 31.9 mmol, 79%). **¹H-NMR** (300 MHz, Chloroform-*d*) δ 7.37 – 7.27 (m, 2H), 6.75 – 6.58 (m, 3H), 5.55 (dd, *J* = 17.6, 1.1 Hz, 1H), 5.03 (dd, *J* = 10.9, 1.1 Hz, 1H), 2.97 (s, 6H). **¹³C-NMR** (75 MHz, CDCl₃) δ 150.4 (C_q), 136.7, 127.3, 126.3 (C_q), 112.5, 109.5 (CH₂), 40.7.

Methyl(4-vinylphenyl)sulfane (7h)

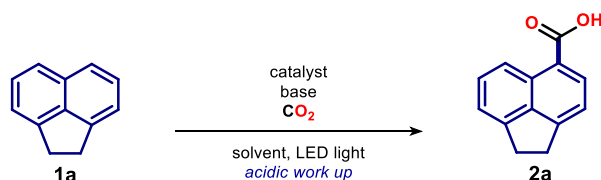
According to a literature known procedure^[98] a flame-dried 250 mL Schlenk flask was charged under N₂ atmosphere with methyltriphenylphosphonium bromide (14.1 g, 39.5 mmol, 1 equiv.) and dry THF (60 mL). The suspension was cooled to 0 °C and *n*-BuLi (1.6M in hexane, 30 mL, 48 mmol, 1.2 equiv.) was slowly added *via* syringe and the resulting mixture was stirred for 1 h. 4-(Methylthio)benzaldehyde (5.24 mL, 38.4 mmol, 1 equiv.) was added dropwise *via* syringe and the reaction mixture was stirred for further 2.5 h at 0 °C. After dilution with THF (20 mL) the reaction was stirred at ambient temperature overnight and was quenched by adding sat. aq. NH₄Cl (20 mL). The crude mixture was extracted with DCM (3×20 mL) and the combined organic layers were dried over Na₂SO₄, filtered and concentrated *in vacuo*. Purification by flash silica gel chromatography (hexanes/MTBE) afforded the title

compound as colorless liquid (4.04 g, 26.9 mmol, 68%). **¹H-NMR** (400 MHz, Chloroform-*d*) δ 7.37 – 7.32 (m, 2H), 7.25 – 7.20 (m, 2H), 6.69 (dd, *J* = 17.6, 10.9 Hz, 1H), 5.73 (dt, *J* = 17.6, 0.9 Hz, 1H), 5.23 (dt, *J* = 10.8, 0.9 Hz, 1H), 2.50 (s, 3H). **¹³C-NMR** (101 MHz, CDCl₃) δ 138.1 (C_q), 136.3, 134.6 (C_q), 126.7, 126.7, 113.3 (CH₂), 15.9.

4.4.4 Carboxylation Reactions

4.4.4.1 Reaction Optimization

General Procedure for the Reaction Optimization – GP1

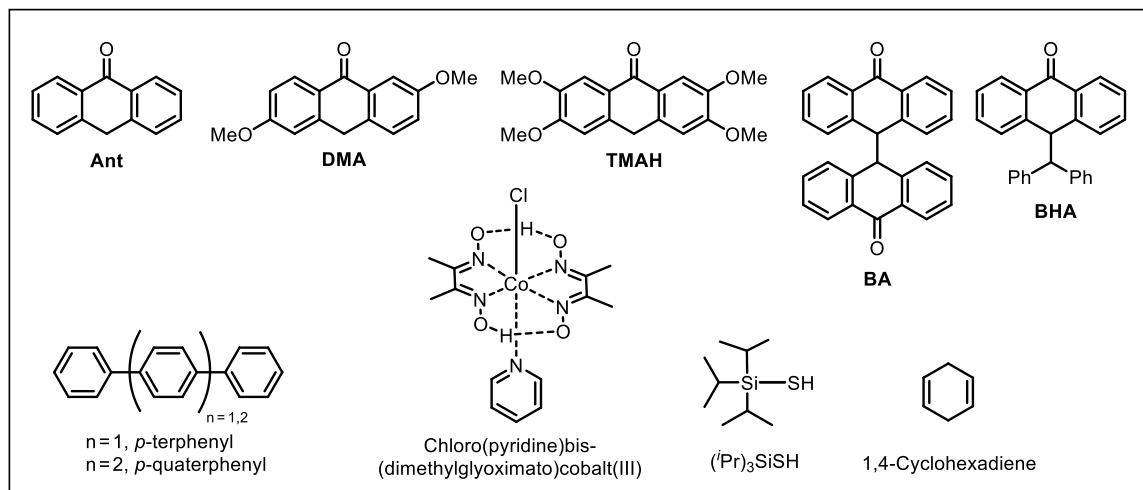


To a dry flat-bottomed crimp vial (5 mL) equipped with stirring bar, was added acenaphthene (**1a**, 0.1-0.2 mmol, 1 equiv.) and photocatalyst (5-20 mol%, Scheme S2). Base (if solid) was quickly added and the vial was sealed with a Supelco aluminium crimp seal with septum (PTFE/butyl). The vial was then evacuated and refilled with CO₂ (5×) *via* syringe needle. The reaction mixture was dissolved in the solvent (dry and degassed by bubbling with N₂) and base (if liquid) was added *via* syringe. The vial was sealed with two layers of Parafilm® and then had gaseous CO₂ added *via* a Luer Lock Monoject™ (20 ccm) syringe, into the head space. The vial was then stirred and irradiated from the bottom side and a constant reaction temperature (0 °C or 25 °C) was maintained by employing a cooling circuit connected to a thermostat. After 18 hrs the reaction was transferred with aq. NaOH (0.1M) into a centrifuge tube and was washed with Et₂O (2×) to remove left over starting material or non-polar side products. The aqueous layer was acidified by adding aq. HCl (2M) and was extracted with EtOAc (3×). The combined organic layers were dried over Na₂SO₄, filtered and concentrated *in vacuo*. As internal standard a stock solution of 1,3,5-trimethoxybenzene in DMSO-*d*₆ (0.7 mL, 42.9 mM) was added and the mixture was analyzed by ¹H-NMR spectroscopy. The ¹H-NMR yield was determined by integration over product signals and internal standard signals.

Table S4-1. Optimization of the photocatalyzed aromatic C–H carboxylation.

entry	PC (mol%)	base (eq.)	solvent	λ [nm]	V(CO ₂) added [ccm]	NMR yield [%]
1	Ant (20)	Cs ₂ CO ₃ (2)	DMSO	455	22	n.d. ^a
2	DMA (20)	Cs ₂ CO ₃ (2)	DMSO	455	22	n.d.
3	TMA (20)	Cs ₂ CO ₃ (2)	DMSO	455	22	37 ^b
4	BA (20)	Cs ₂ CO ₃ (2)	DMSO	455	22	trace
5	BHA (20)	Cs ₂ CO ₃ (2)	DMSO	455	22	n.d.
6	TMAH (20)	Cs ₂ CO ₃ (1)	DMSO	455	22	1
7	TMAH (20)	Cs ₂ CO ₃ (3)	DMSO	455	22	68 ^b
8	TMAH (20)	Cs ₂ CO ₃ (4)	DMSO	455	22	59
9	TMAH (5)	Cs ₂ CO ₃ (2)	DMSO	455	22	54
10	TMAH (10)	Cs ₂ CO ₃ (2)	DMSO	455	22	60
11	TMAH (10)	Cs ₂ CO ₃ (3)	DMSO	455	22	56
12 ^c	TMAH (20)	Cs ₂ CO ₃ (3)	DMSO	455	22	52
13	TMAH (20)	Na ₂ CO ₃ (2)	DMSO	455	22	1
14	TMAH (20)	K ₂ CO ₃ (2)	DMSO	455	22	17
15	TMAH (10)	K ₂ CO ₃ (3)	DMSO	455	22	25
16 ^c	TMAH (10)	K ₂ CO ₃ (3)	DMSO	455	22	47
17 ^c	TMAH (20)	K ₂ CO ₃ (3)	DMSO	455	22	38
18	TMAH (20)	(NH ₄) ₂ CO ₃ (3)	DMSO	455	22	2
19	TMAH (20)	Cs pivalate (3)	DMSO	455	22	6
20	TMAH (20)	K ₃ PO ₄ (3)	DMSO	455	22	trace
21	TMAH (20)	(NBu ₄)H ₂ PO ₄ (3)	DMSO	455	22	7
22	TMAH (20)	DBU (3)	DMSO	455	22	28
23	TMAH (20)	TMG (3)	DMSO	455	22	22
24	TMAH (20)	BTMG (3)	DMSO	455	22	25
25	TMAH (20)	Cs ₂ CO ₃ (3)	DMF	455	22	35
26	TMAH (20)	Cs ₂ CO ₃ (3)	DMA	455	22	12
27	TMAH (20)	Cs ₂ CO ₃ (3)	NMP	455	22	14
28	TMAH (20)	Cs ₂ CO ₃ (3)	^t PrOH	455	22	n.d.
29	TMAH (20)	Cs ₂ CO ₃ (3)	DCM	455	22	n.d.
30	TMAH (20)	Cs ₂ CO ₃ (3)	acetone	455	22	trace
31	TMAH (20)	Cs ₂ CO ₃ (3)	DMSO	400	22	14
32	TMAH (20)	Cs ₂ CO ₃ (3)	DMSO	535	22	29
33	TMAH (20)	Cs ₂ CO ₃ (3)	DMSO	white ^d	22	27
34	TMAH (20)	Cs ₂ CO ₃ (3)	DMSO	455 ^e	22	23
35	TMAH (20)	Cs ₂ CO ₃ (3)	DMSO	455 ^f	22	56
36 ^g	TMAH (20)	Cs ₂ CO ₃ (3)	DMSO/DMF (1:1)	455	22	17
37	TMAH (20)	Cs ₂ CO ₃ (3)	DMSO	455	– ^h	37
38	TMAH (20)	Cs ₂ CO ₃ (3)	DMSO	455	11	48
39 ⁱ	TMAH (20)	Cs ₂ CO ₃ (3)	DMSO	455	22	39
40 ^j	TMAH (20)	Cs ₂ CO ₃ (3)	DMSO	455	22	51
41 ^k	TMAH (20)	Cs ₂ CO ₃ (3)	DMSO	455	22	13
42 ^l	TMAH (20)	Cs ₂ CO ₃ (3)	DMSO	455	22	34
43 ^m	TMAH (20)	Cs ₂ CO ₃ (3)	DMSO	455	22	49
44 ⁿ	TMAH (20)	Cs ₂ CO ₃ (3)	DMSO	455	22	57
45 ^o	TMAH (20)	Cs ₂ CO ₃ (3)	DMSO	455	22	52

All reactions, if not otherwise stated, were run following GP1. Chemical Structures of catalysts and additives are given in Scheme S4-2: ^a product was not detected; ^b isolated yield following GP2a; ^c reaction was run with 18-crown-6 (1 equiv.); ^d cold white LED; ^e fan-cooled high-power LED setup (7 W) was used. Due to inefficient cooling, the reaction temperature was significantly elevated; ^f water-cooled high-power LED setup (1.4 W) was used. DMSO was saturated with CO₂ by bubbling gas through the solvent; ^g reaction was run at 0 °C; ^h reaction was run without pressure (1 atm) of CO₂; ⁱ reaction was run with 0.2 mmol of substrate; ^j concentration was changed to 0.05 M (0.1 mmol substrate in 2 mL DMSO); ^k reaction with chloro(pyridine)bis(dimethylglyoximate)cobalt(III) (5 mol%); ^l reaction with *p*-terphenyl (5 mol%); ^m reaction with *p*-quaterphenyl (5 mol%); ⁿ reaction with (^tPr)₃SiSH (10 mol%); ^o reaction with 1,4-cyclohexadiene (20 mol%).



Scheme S4-2. Tested 9-anthrone based derivatives and additives used for the optimization of the carboxylation reaction; 9-anthrone (**Ant**), 2,6-dimethoxyanthracen-9(10H)-one (**DMA**), 2,3,6,7-tetramethoxyanthracen-9(10H)-one (**TMAH**), bianthrone (**BA**), 10-benzhydryl-anthrone (**BHA**).

Kinetic Profile of the Aromatic Carboxylation Reaction

Under the optimized conditions the kinetic profile of the reaction was monitored within the first six hours of the reaction (Figure S4-8). Reactions were run following GP1 and the product yield was determined by crude ¹H-NMR with internal standard method.

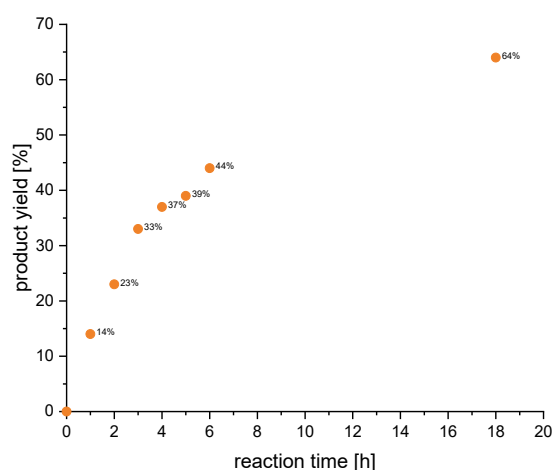


Figure S4-8. The progress of the carboxylation reaction was monitored within the first six hours.

Control Reactions

Conducted control experiments revealed that all compounds and light are crucial for product formation (Table S4-2). To exclude a base promoted carboxylation reaction, substrates **3c** & **3j** possessing acidic C-H bonds were tested in absence of catalyst and light and upon work-up, the respective products **4c** & **4j** could not be detected. Substrates **3b** and **3p** gave excellent yields of the respective carboxylation products following GP2a. No product was formed in absence of light and catalyst, demonstrating the photocatalytic nature of this reaction.

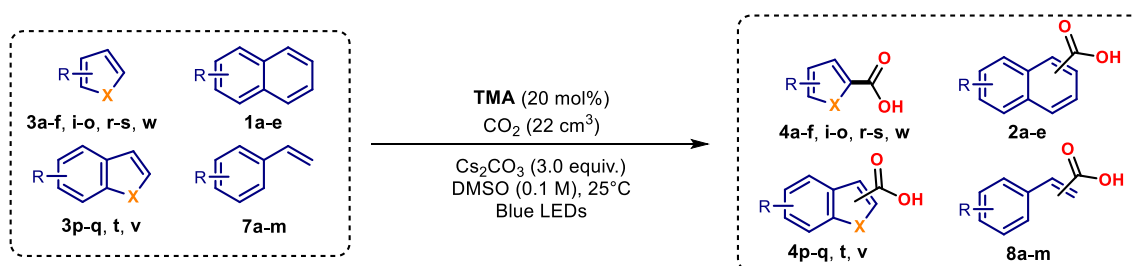
Table S4-2. Control reactions of the TMAH catalyzed C-H carboxylation.

entry	PC (mol%)	Substrate	base (eq.)	λ [nm]	V(CO ₂) added [ccm]	Product	NMR yield [%]
1	-	1a	Cs ₂ CO ₃ (3)	455	22	2a	n.d. ^a
2	TMAH (20)	1a	-	455	22	2a	n.d.
3	TMAH (20)	1a	Cs ₂ CO ₃ (3)	455	no CO ₂ ^b	2a	n.d.
4	TMAH (20)	1a	Cs ₂ CO ₃ (3)	dark ^c	22	2a	n.d.
5	-	3b ^d	Cs ₂ CO ₃ (3)	dark	22	4b	n.d.
6	-	3c ^e	Cs ₂ CO ₃ (3)	dark	22	4c	n.d.
7	-	3j ^f	Cs ₂ CO ₃ (3)	dark	22	4j	n.d.
8	-	3p ^g	Cs ₂ CO ₃ (3)	dark	22	4p	n.d.

All reactions, if not otherwise stated, were run following GP1: ^aproduct was not detected; ^breaction was run under N₂ atmosphere; ^creaction was stirred in the dark; ^dreaction was run following GP1 using **3b** (0.1 mmol) as substrate; ^ereaction was run following GP1 using **3c** (0.1 mmol) as substrate; ^freaction was run following GP1 using **3j** (0.1 mmol) as substrate; ^greaction was run following GP1 using **3p** (0.1 mmol) as substrate.

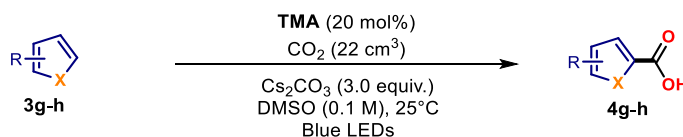
4.4.4.2 Substrate Scope

General Procedure for Carboxylation of Hetero(arenes) and Styrenes – GP2a



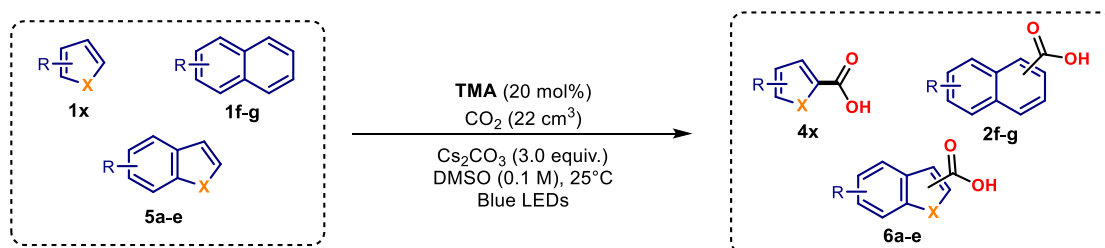
To a dry flat-bottomed crimp vial (5 mL) equipped with stirring bar, was added the arene (if solid) (0.1 mmol) and 2,3,6,7-tetramethoxyanthracen-9(10*H*)-one (6.3 mg, 0.02 mmol, 20 mol%). Cs₂CO₃ (98 mg, 3 equiv.) was quickly added and the vial was sealed with a Supelco aluminium crimp seal with septum (PTFE/butyl). The vial was then evacuated and refilled with CO₂ (5×) *via* syringe needle. The reaction mixture was dissolved in DMSO (1 mL, dry and degassed by bubbling with N₂) and the arene (0.1 mmol) (if liquid) was added *via* syringe. The vial was sealed with two layers of Parafilm® and then had gaseous CO₂ added *via* a Luer Lock Monoject™ (20 ccm) syringe, into the head space. The vial was then irradiated from the bottom side with blue LED light and a constant reaction temperature (25°C) was maintained by employing a water-cooling circuit connected to a thermostat. After 18 hrs of reaction time the pressure was released. For product isolation, the reaction mixtures of 4 reactions run in parallel were combined and transferred with water and Et₂O into a separating funnel. The ether layer was extracted with water (3×) and the combined aqueous layers were acidified with aq. HCl (2M) to adjust to an acidic pH. The aqueous layer was extracted with EtOAc (3×) and the combined EtOAc layers were dried over Na₂SO₄, filtered and concentrated *in vacuo*. The crude material was purified by silica flash column chromatography using mixtures of hexanes and ethyl acetate with 0.5% HOAc (v/v) as eluents.

General Procedure for Carboxylation of Arenes – GP2b (no glovebox)



To a dry flat-bottomed crimp vial (5 mL) equipped with stirring bar, was added the arene (if solid) (0.1 mmol) and 2,3,6,7-tetramethoxyanthracen-9(10H)-one (6.3 mg, 0.02 mmol, 20 mol%). Cs₂CO₃ (98 mg, 3 equiv.) was quickly added and the vial was sealed with a Supelco aluminium crimp seal with septum (PTFE/butyl). The vial was then evacuated and refilled with N₂ (3×) *via* syringe needle. The reaction mixture was dissolved in DMSO (1 mL, dry and degassed by bubbling with N₂) and the arene (0.1 mmol) (if liquid) was added *via* syringe. The reaction mixture then had gaseous CO₂ (22 cm³) added *via* a gastight Hamilton® syringe, into the head space of the vial. The vial was then irradiated from the bottom side with blue light and a constant reaction temperature (25°C) was maintained by employing a water-cooling circuit connected to a thermostat. After the designated time the reactions were extracted *via* an acid base wash. The combined organic layers were dried over Na₂SO₄, filtered and concentrated *in vacuo*.

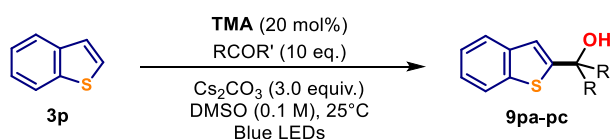
General Procedure for Carboxylation of Arenes – GP2c (glovebox)



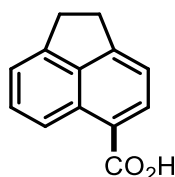
To a dry microwave vial (5 mL) equipped with stirring bar, was added the arene (if solid) (0.1 mmol) and 2,3,6,7-tetramethoxyanthracen-9(10H)-one (6.3 mg, 0.02 mmol, 20 mol%). The vials were sealed and transferred to a glovebox after the vial had evacuated and refilled with N₂ (×3) within the antechamber *via* syringe. Cs₂CO₃ (98 mg, 3 equiv.) and DMSO (1 mL) was added and the vial was sealed with a Supelco aluminium crimp seal with septum (PTFE/butyl). The vials were removed from the glovebox and the arene (0.1 mmol) (if liquid) was added *via* syringe. The reaction mixture then had gaseous CO₂ (22 cm³) added *via* a gastight Hamilton® syringe, into the head space of the vial. The vial was then irradiated from two sides

by two kessil lamps (vials approximately 6 cm away from the light source) with fans placed in front of the vials for cooling (temperatures measured via IR ranged between 25–30 °C). After 18 hrs. the irradiation was stopped and the vials were decapped quenched with aq. HCl (1 mL, 0.3M) and monitored by LCMS and ¹H NMR. Reactions were filtered of any solids and purified directly *via* prep-HPLC.

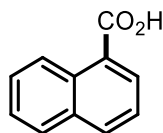
General Procedure for the Hydroxyalkylation of benzo[*b*]thiophene with ketones – GP3



To a dry flat-bottomed crimp vial (5 mL) equipped with stirring bar, was added the benzo[*b*]thiophene (13.4 mg, 0.1 mmol, 1 equiv.) and 2,3,6,7-tetramethoxyanthracen-9(10*H*)-one (6.3 mg, 0.02 mmol, 20 mol%). Cs₂CO₃ (98 mg, 0.3 mmol, 3 equiv.) was quickly added and the vial was sealed with a Supelco aluminium crimp seal with septum (PTFE/butyl). The vial was then evacuated and refilled with N₂ (5×) *via* syringe needle. The reaction mixture was dissolved in DMSO (1mL, dry and degassed by bubbling with N₂) and the ketone (1.0 mmol, 10 equiv.) was added *via* syringe. The vial was then irradiated from the bottom side with blue LED light and a constant reaction temperature (25°C) was maintained by employing a water-cooling circuit connected to a thermostat. After 18 hrs the reaction was quenched by adding water. For product isolation, the reaction mixtures of 4 reactions run in parallel were combined and transferred with water and EtOAc into a separating funnel. The reaction mixture was extracted with EtOAc (3×) and the combined organic layers were dried over Na₂SO₄, filtered and concentrated *in vacuo*. The crude material was purified by silica flash column chromatography using mixtures of hexanes and ethyl acetate as eluents.

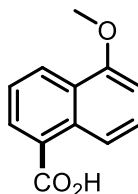
1,2-Dihydroacenaphthylene-5-carboxylic acid (2a)

Following GP2a, acenaphthene (0.4 mmol) gave **2a** (68%) as a pale orange solid; **¹H-NMR** (400 MHz, Chloroform-*d*) δ 8.74 (d, J = 8.5 Hz, 1H), 8.45 (d, J = 7.3 Hz, 1H), 7.63 (dd, J = 8.6, 6.9 Hz, 1H), 7.37 (dd, J = 12.2, 7.1 Hz, 2H), 3.45 (s, 4H). **¹H-NMR** (400 MHz, DMSO-*d*₆) δ 12.85 (bs, 1H), 8.60 (d, J = 8.5 Hz, 1H), 8.22 (d, J = 7.3 Hz, 1H), 7.57 (dd, J = 8.6, 6.9 Hz, 1H), 7.36 (t, J = 6.6 Hz, 2H), 3.35 (s, 4H). **¹³C-NMR** (101 MHz, DMSO) δ 168.3 (*C*_q), 152.5 (*C*_q), 146.2 (*C*_q), 139.1 (*C*_q), 132.9, 129.8 (*C*_q), 129.6, 122.3 (*C*_q), 121.6, 119.9, 118.6, 29.9. **HRMS** (EI+): calculated m/z for C₁₃H₁₀O₂ [*M*⁺] 198.06753; found 198.06722. Data in accordance with the literature.^[99]

1-Naphthoic acid (2b)

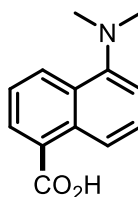
Following GP2a, naphthalene (0.3 mmol) gave **2b** (38%) as a white solid; **¹H-NMR** (400 MHz, DMSO-*d*₆) δ 13.13 (bs, 1H), 8.86 (d, J = 8.5 Hz, 1H), 8.20 – 8.10 (m, 2H), 8.02 (d, J = 7.7 Hz, 1H), 7.70 – 7.52 (m, 3H). **¹³C-NMR** (101 MHz, DMSO) δ 168.6 (*C*_q), 133.5 (*C*_q), 132.9, 130.7 (*C*_q), 129.8, 128.6, 127.7 (*C*_q), 127.5, 126.2, 125.5, 124.9. **HRMS** (EI+): calculated m/z for C₁₁H₈O₂ [*M*⁺] 172.05188; found 172.05143. Data in accordance with the literature.^[100]

5-Methoxy-1-naphthoic acid (**2c**)



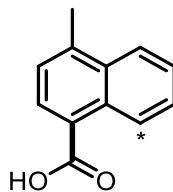
Following GP2a, 1-methoxynaphthalene (0.4 mmol) gave **2c** (22%) as a pale-yellow solid; **¹H-NMR** (400 MHz, DMSO-*d*₆) δ 12.95 (bs, 1H), 8.45 – 8.35 (m, 2H), 8.13 (dd, *J* = 7.2, 1.3 Hz, 1H), 7.60 – 7.51 (m, 2H), 7.05 (d, *J* = 7.8 Hz, 1H), 3.99 (s, 3H). **¹³C-NMR** (101 MHz, DMSO) δ 168.8 (*C_q*), 154.9 (*C_q*), 131.6 (*C_q*), 130.0, 127.8, 127.7 (*C_q*), 126.1, 125.3 (*C_q*), 124.2, 117.5, 104.7, 55.7. **HRMS** (EI+): calculated *m/z* for C₁₂H₁₀O₃ [*M*⁺] 202.06245; found 202.06283. Data in accordance with the literature.^[101]

5-(Dimethylamino)-1-naphthoic acid (**2d**)



Following GP2a, 1-dimethylaminonaphthalen (0.4 mmol) gave **2d** (38%) as a yellow solid; **¹H-NMR** (400 MHz, DMSO-*d*₆) δ 13.04 (bs, 1H), 8.43 (dd, *J* = 15.9, 8.6 Hz, 2H), 8.08 (dd, *J* = 7.1, 1.0 Hz, 1H), 7.54 (ddd, *J* = 18.0, 8.6, 7.3 Hz, 2H), 7.19 (d, *J* = 7.3 Hz, 1H), 2.82 (s, 6H). **¹³C-NMR** (101 MHz, DMSO) δ 168.9 (*C_q*), 151.0 (*C_q*), 132.0 (*C_q*), 129.3, 128.6 (*C_q*), 128.5 (*C_q*), 128.4, 127.4, 124.0, 120.0, 114.4, 45.0. **HRMS** (ESI+): calculated *m/z* for C₁₃H₁₄NO₂ [(*M*+*H*)⁺] 216.1019; found 216.1022.

4-Methyl-1-naphthoic acid (**2e**) & 5-Methyl-1-naphthoic acid (**2e'**)

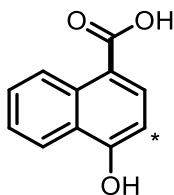


Following GP2a, 1-methylnaphthalene (0.1 mmol) gave **2e** (19%) and **2e'** (14%) as a beige solid. **2e:2e'** = 1.3:1. The ratio of products was determined by $^1\text{H-NMR}$ analysis. **HRMS** (EI+): calculated m/z for $\text{C}_{12}\text{H}_{10}\text{O}_2$ [M^+] 186.06753; found 186.06731.

Data for **2e**: **$^1\text{H-NMR}$** (300 MHz, Chloroform- d) δ 9.22 – 9.13 (m, 1H), 8.34 (d, J = 7.5 Hz, 1H), 8.13 – 8.05 (m, 1H), 7.73 – 7.50 (m, 2H), 7.41 (d, J = 7.5 Hz, 1H), 2.78 (s, 3H). **$^1\text{H-NMR}$** (400 MHz, DMSO- d_6) δ 13.06 (bs, 1H), 9.00 – 8.88 (m, 1H), 8.11 (m, 1H), 8.06 (d, J = 7.4 Hz, 1H), 7.68 – 7.58 (m, 2H), 7.44 (d, J = 7.0 Hz, 1H), 2.70 (s, 3H). **$^{13}\text{C-NMR}$** (101 MHz, DMSO) δ 168.7, 139.7, 132.4, 130.9, 129.8, 127.2, 126.1, 126.0, 125.9, 125.7, 124.7, 19.6. Data in accordance with literature.^[102,103]

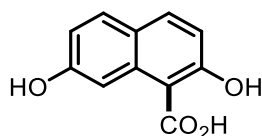
Data for **2e'**: **$^1\text{H-NMR}$** (300 MHz, CD_3OD) δ 8.95 (d, J = 8.8 Hz, 1H), 8.40 (dd, J = 7.3, 1.3 Hz, 1H), 8.30 (dt, J = 8.5, 1.1 Hz, 1H), 7.71 – 7.51 (m, 2H), 7.41 (d, J = 7.5 Hz, 1H), 2.75 (s, 3H). **$^1\text{H-NMR}$** (400 MHz, DMSO- d_6) δ 13.06 (bs, 1H), 8.67 (d, J = 8.6 Hz, 1H), 8.25 (d, J = 8.5 Hz, 1H), 8.14 – 8.08 (m, 1H), 7.68 – 7.58 (m, 1H), 7.54 – 7.48 (m, 1H), 7.39 – 7.47 (m, 1H), 2.68 (s, 3H). **$^{13}\text{C-NMR}$** (101 MHz, DMSO) δ 169.0, 134.5, 132.5, 130.8, 129.1, 128.7, 128.6, 127.1, 126.9, 124.8, 123.7, 19.5. Data in accordance with the literature.^[104]

1-Hydroxy-4-naphthoic acid (**2f**) & 1-hydroxy-2-naphthoic acid (**2f'**)

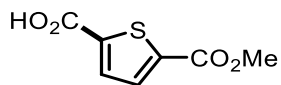


Following GP2c, 1-naphthol (0.1 mmol) gave **2f** & **2f'** (56%) as an inseparable mixture (1:1), as a waxy solid. **¹H-NMR** (500 MHz, DMSO) δ 12.58 (s, 2H), 11.02 (s, 2H), 9.03 (d, J = 8.7 Hz, 1H), 8.23 (d, J = 7.7 Hz, 1H), 8.13 (d, J = 8.1 Hz, 1H), 7.87 (dd, J = 8.3, 1.0 Hz, 1H), 7.61 (ddd, J = 8.5, 6.8, 1.4 Hz, 1H), 7.50 (ddd, J = 8.2, 6.8, 1.2 Hz, 1H), 7.48 – 7.42 (m, 1H), 7.41 – 7.32 (m, 3H), 6.91 (d, J = 8.2 Hz, 1H), 6.87 (dd, J = 7.2, 1.3 Hz, 1H). **¹³C-NMR** (126 MHz, DMSO) δ 171.88, 168.30, 157.80, 134.78, 133.04, 132.85, 128.74, 127.86, 126.98, 125.54, 125.08, 124.75, 124.56, 123.59, 122.43, 118.63, 116.69, 109.60, 106.95, 104.40. Data in accordance with the literature.^[101,105]

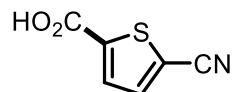
2,7-dihydroxy-1-naphthoic acid (**2g**)



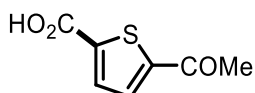
Following GP2c, naphthalene-2,7-diol (0.1 mmol) gave **2g** (64%) as a yellow solid. **¹H-NMR** (500 MHz, DMSO-*d*₆) δ 12.43 (bs, 1H), 9.82 (s, 2H), 7.95 (s, 1H), 7.84 (d, J = 8.8 Hz, 1H), 7.68 (d, J = 8.8 Hz, 1H), 6.95–6.77 (m, 2H); **¹³C-NMR** (126 MHz, DMSO-*d*₆) δ 173.0, 161.8, 157.5, 135.1, 133.6, 130.5, 122.5, 115.1, 115.1, 107.5, 105.8; **HRMS** (ESI⁺): calculated m/z for C₁₁H₉O₄ [(M+H)⁺] 205.0495; found 205.0497.

5-(methoxycarbonyl)thiophene-2-carboxylic acid (4a)

Following GP2a, methyl thiophene-2-carboxylate (0.4 mmol) gave **4a** (49%) as a white solid; **¹H-NMR** (400 MHz, DMSO-*d*₆) δ 13.65 (bs, 1H), 7.78 (d, *J* = 3.9 Hz, 1H), 7.72 (d, *J* = 3.9 Hz, 1H), 3.85 (s, 3H). **¹³C-NMR** (101 MHz, DMSO) δ 162.3 (*C_q*), 161.4 (*C_q*), 140.4 (*C_q*), 137.5 (*C_q*), 133.7, 133.2, 52.7. **HRMS** (EI⁺): calculated *m/z* for C₇H₆O₄S [M⁺] 185.99813; found 185.99833. Data in accordance with the literature.^[106]

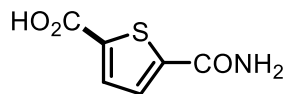
5-Cyanothiophene-2-carboxylic acid (4b)

Following GP2a, thiophene-2-carbonitrile (0.4 mmol) gave **4b** (92%) as a pale-yellow solid; **¹H-NMR** (400 MHz, DMSO-*d*₆) δ 13.98 (bs, 1H), 8.00 (d, *J* = 4.0 Hz, 1H), 7.79 (d, *J* = 4.0 Hz, 1H). **¹³C-NMR** (101 MHz, DMSO) δ 161.5 (*C_q*), 141.7 (*C_q*), 139.5 (*C_q*), 132.9 (*C_q*), 113.6, 113.3. **HRMS** (EI⁺): calculated *m/z* for C₆H₃NO₂S [M⁺] 152.98790; found 152.98804. Data in accordance with the literature.^[107]

5-Acetylthiophene-2-carboxylic acid (4c)

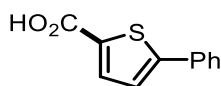
Following GP2a, 2-acetylthiophene (0.4 mmol) gave **4c** (39%) as a pale-yellow solid; **¹H-NMR** (300 MHz, DMSO-*d*₆) δ 13.55 (bs, 1H), 7.92 (d, *J* = 4.0 Hz, 1H), 7.76 (d, *J* = 3.9 Hz, 1H), 2.58 (s, 3H). **¹³C-NMR** (75 MHz, DMSO) δ 191.5 (*C_q*), 162.5 (*C_q*), 148.2 (*C_q*), 141.0 (*C_q*), 133.7, 133.6, 26.8. **HRMS** (EI⁺): calculated *m/z* for C₇H₆O₃S [M⁺] 170.00322; found 170.00333. Data in accordance with literature.^[107]

5-Carbamoylthiophene-2-carboxylic acid (**4d**)



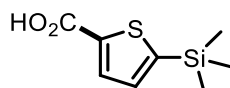
The title compound was prepared according to GP2a. Isolation of the compound was accomplished by employing C18 reversed-phase silica gel column chromatography using a mixture of water and acetonitrile as eluents. Thiophene-2-carboxamide (0.4 mmol) gave **4d** (91%) as a white solid; **¹H-NMR** (400 MHz, DMSO-*d*₆) δ 13.40 (bs, 1H), 8.17 (bs, 1H), 7.73 (d, *J* = 3.9 Hz, 1H), 7.69 (d, *J* = 3.9 Hz, 1H), 7.64 (bs, 1H). **¹³C-NMR** (101 MHz, DMSO) δ 162.7 (*C_q*), 162.2 (*C_q*), 145.7 (*C_q*), 137.9 (*C_q*), 133.3, 128.9. **HRMS** (ESI⁺): calculated *m/z* for C₆H₆O₃S [(M+H)⁺] 172.0063; found 172.0065.

5-Phenylthiophene-2-carboxylic acid (**4e**)

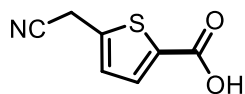


Following GP2a, 3-phenylthiophene (0.4 mmol) gave **4e** (99%) as a white solid; **¹H-NMR** (300 MHz, DMSO-*d*₆) δ 13.18 (bs, 1H), 7.77 – 7.68 (m, 3H), 7.55 (d, *J* = 4.0 Hz, 1H), 7.49 – 7.33 (m, 3H). **¹³C-NMR** (75 MHz, DMSO) δ 162.9 (*C_q*), 149.8 (*C_q*), 134.4, 133.4 (*C_q*), 132.9 (*C_q*), 129.3, 128.9, 125.9, 124.6. **HRMS** (ESI⁺): calculated *m/z* for C₁₁H₉O₂S [(M+H)⁺] 205.0318; found 205.0321. Data in accordance with the literature.^[108]

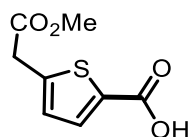
5-(Trimethylsilyl)thiophene-2-carboxylic acid (**4f**)



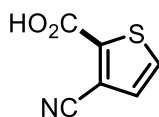
Following GP2a, trimethyl(thiophen-2-yl)silane (0.4 mmol) gave **4f** (28%) as a white solid; **¹H-NMR** (400 MHz, DMSO-*d*₆) δ 13.02 (bs, 1H), 7.75 (d, *J* = 3.5 Hz, 1H), 7.34 (d, *J* = 3.5 Hz, 1H), 0.31 (s, 9H). **¹³C-NMR** (101 MHz, DMSO) δ 162.6 (*C_q*), 148.1 (*C_q*), 139.5 (*C_q*), 135.0, 133.9, −0.4. **HRMS** (EI⁺): calculated *m/z* for C₈H₁₂O₂SiS [M⁺] 200.03218; found 200.03162.

5-(cyanomethyl)thiophene-2-carboxylic acid (4g)

Following GP2b, 2-(thiophen-2-yl)acetonitrile (0.1 mmol) gave **4g** (89%) as a white solid. **¹H-NMR** (500 MHz, CDCl₃) δ 7.78 (d, *J* = 3.8 Hz, 1H), 7.13 (d, *J* = 3.8 Hz, 1H), 3.96 (s, 2H); **¹³C-NMR** (126 MHz, CDCl₃) δ 165.6 (C_q), 139.8 (C_q), 135.3, 133.2 (C_q), 128.3, 115.9 (C_q), 19.3 (CH₂); **HRMS** (ESI): calculated *m/z* for C₇H₄NO₂S [(M-H)⁺] 165.9968; found 165.9967.

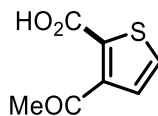
5-(2-methoxy-2-oxoethyl)thiophene-2-carboxylic acid (4h)

Following GP2b, methyl 2-(thiophen-2-yl)acetate (0.1 mmol) gave **4h** (99%) as a waxy solid. **¹H-NMR** (500 MHz, CDCl₃) δ 7.76 (d, *J* = 3.8 Hz, 1H), 6.99 (d, *J* = 3.8 Hz, 1H), 3.8 (s, 2H), 3.76 (s, 3H); **¹³C-NMR** (126 MHz, CDCl₃) δ 170.0, 167.4, 144.5, 135.2, 132.2, 128.2, 52.7, 35.9; **HRMS** (ESI): calculated *m/z* for C₈H₇O₄S [(M-H)⁺] 199.0065; found 199.0065.

3-Cyanothiophene-2-carboxylic acid (4i)

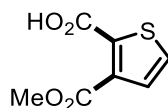
Following GP2a, thiophene-3-carbonitrile (0.4 mmol) gave **4i** (86%) as a pale-yellow solid; **¹H-NMR** (300 MHz, DMSO-*d*₆) δ 14.12 (bs, 1H), 8.06 (d, *J* = 5.2 Hz, 1H), 7.62 (d, *J* = 5.1 Hz, 1H). **¹³C-NMR** (75 MHz, DMSO) δ 160.7 (C_q), 141.9 (C_q), 133.9, 131.6, 114.1 (C_q), 113.0 (C_q). **HRMS** (ESI⁺): calculated *m/z* for C₆H₄NO₂S [(M+H)⁺] 153.9957; found 153.9957. Data in accordance with the literature.^[109]

3-Acetylthiophene-2-carboxylic acid (**4j**)



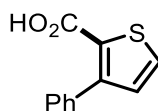
Following GP2a, 3-acetylthiophene (0.4 mmol) gave **4j** (41%) as a pale-yellow solid; ¹H-NMR (300 MHz, Acetonitrile-*d*₃) δ 7.78 (d, *J* = 5.4 Hz, 1H), 7.71 (d, *J* = 5.4 Hz, 1H), 2.73 (s, 3H). ¹H-NMR (400 MHz, DMSO-*d*₆) δ 13.59 (bs, 1H), 7.85 (d, *J* = 5.0 Hz, 1H), 7.24 (d, *J* = 5.0 Hz, 1H), 2.50 (s, 3H). ¹³C-NMR (101 MHz, DMSO) δ 199.3 (*C*_q), 162.3 (*C*_q), 146.9 (*C*_q), 132.2 (*C*_q), 132.1, 128.1, 30.9. HRMS (EI+): calculated *m/z* for C₇H₆O₃S [M⁺] 170.00322; found 170.00304.

3-(Methoxycarbonyl)thiophene-2-carboxylic acid (**4k**)

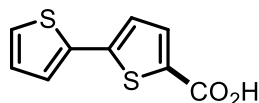


Following GP2a, methyl thiophene-2-carboxylate (0.4 mmol) gave **4k** (88%) as a white solid; ¹H-NMR (400 MHz, DMSO-*d*₆) δ 13.53 (bs, 1H), 7.86 (d, *J* = 5.1 Hz, 1H), 7.31 (d, *J* = 5.1 Hz, 1H), 3.80 (s, 3H). ¹³C-NMR (101 MHz, DMSO) δ 164.8 (*C*_q), 161.9 (*C*_q), 136.8 (*C*_q), 134.5 (*C*_q), 131.8, 128.3, 52.5. HRMS (ESI+): calculated *m/z* for C₇H₇O₄S [(M+H)⁺] 187.0060; found 187.0059.

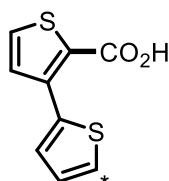
3-Phenylthiophene-2-carboxylic acid (**4l**)



Following GP2a, 3-phenylthiophene (0.4 mmol) gave **4l** (71%) as a pale-yellow solid; ¹H-NMR (400 MHz, DMSO-*d*₆) δ 12.86 (bs, 1H), 7.85 (d, *J* = 5.0 Hz, 1H), 7.49 – 7.42 (m, 2H), 7.42 – 7.32 (m, 3H), 7.17 (d, *J* = 5.1 Hz, 1H). ¹³C-NMR (101 MHz, DMSO) δ 162.8 (*C*_q), 147.1 (*C*_q), 135.5 (*C*_q), 131.7, 131.0, 129.3, 128.1 (*C*_q), 127.7, 127.6. HRMS (ESI+): calculated *m/z* for C₁₁H₉O₂S [(M+H)⁺] 205.0318; found 205.0319. Data in accordance with the literature.^[110]

[2,2'-Bithiophene]-5-carboxylic acid (4m)

Following GP2a, 2,2'-bithiophene (0.4 mmol) gave **4m** (53%) as a pale-yellow solid; **¹H-NMR** (400 MHz, DMSO-*d*₆) δ 13.15 (bs, 1H), 7.66 (d, *J* = 3.9 Hz, 1H), 7.62 (dd, *J* = 5.1, 1.1 Hz, 1H), 7.48 (dd, *J* = 3.7, 1.1 Hz, 1H), 7.34 (d, *J* = 3.9 Hz, 1H), 7.13 (dd, *J* = 5.1, 3.6 Hz, 1H). **¹³C-NMR** (101 MHz, DMSO) δ 162.6 (*C*_q), 142.9 (*C*_q), 135.4 (*C*_q), 134.2, 132.5 (*C*_q), 128.6, 127.2, 125.9, 124.5. **HRMS** (ESI+): calculated *m/z* for C₉H₇O₂S₂ [(M+H)⁺] 210.9882; found 210.9884. Data in accordance with the literature.^[111]

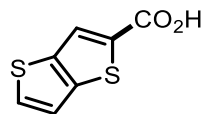
[2,3'-Bithiophene]-2'-carboxylic acid (4n) & [2,3'-bithiophene]-5-carboxylic acid (4n')

Following GP2a, 2,3'-bithiophene (0.4 mmol) gave **4n** (64%) as a white solid and **4n'** (23%) as a pale-yellow solid. **4n:4n'** = 2.8:1.

Data for **4n**: **¹H-NMR** (400 MHz, Chloroform-*d*) δ 7.60 (dd, *J* = 3.7, 1.2 Hz, 1H), 7.56 (d, *J* = 5.2 Hz, 1H), 7.40 (dd, *J* = 5.1, 1.2 Hz, 1H), 7.27 (d, *J* = 5.2 Hz, 1H), 7.10 (dd, *J* = 5.1, 3.7 Hz, 1H). **¹H-NMR** (400 MHz, DMSO-*d*₆) δ 13.07 (bs, 1H), 7.84 (d, *J* = 5.2 Hz, 1H), 7.65 – 7.59 (m, 2H), 7.36 (d, *J* = 5.2 Hz, 1H), 7.11 (dd, *J* = 5.1, 3.7 Hz, 1H). **¹³C-NMR** (101 MHz, DMSO) δ 162.8 (*C*_q), 138.7 (*C*_q), 135.9 (*C*_q), 131.3, 131.2, 129.0, 127.3, 127.2, 126.7 (*C*_q). **HRMS** (ESI+): calculated *m/z* for C₉H₇O₂S₂ [(M+H)⁺] 210.9882; found 210.9883. Data in accordance with the literature.^[112]

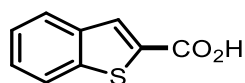
Data for **4n'**: **¹H-NMR** (400 MHz, DMSO-*d*₆) δ 7.93 (dd, *J* = 2.9, 1.4 Hz, 1H), 7.69 – 7.64 (m, 2H), 7.49 (dd, *J* = 5.0, 1.4 Hz, 1H), 7.44 (d, *J* = 3.8 Hz, 1H). **¹³C-NMR** (101 MHz, DMSO) δ 162.9 (*C*_q), 144.7 (*C*_q), 134.3 (*C*_q), 134.0, 132.6 (*C*_q), 128.0, 126.0, 124.5, 122.4. Data in accordance with the literature.^[113]

Thieno[3,2-*b*]thiophene-2-carboxylic acid (**4o**)



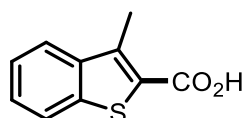
Following GP2a, thieno[3,2-*b*]thiophene (0.4 mmol) gave **4o** (48%) as a pale green solid; **¹H-NMR** (400 MHz, DMSO-*d*₆) δ 13.20 (bs, 1H), 8.11 (s, 1H), 7.92 (d, *J* = 5.3 Hz, 1H), 7.51 (d, *J* = 5.3 Hz, 1H). **¹³C-NMR** (101 MHz, DMSO) δ 163.4 (*C*_q), 143.2 (*C*_q), 138.6 (*C*_q), 135.7 (*C*_q), 133.0, 126.1, 120.3. **HRMS** (ESI⁺): calculated *m/z* for C₇H₅O₂S₂ [(M+H)⁺] 184.9725; found 184.9728. Data in accordance with the literature.^[114]

Benzo[*b*]thiophene-2-carboxylic acid (**4p**)

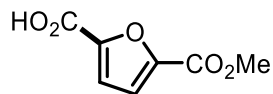


Following GP2a, benzo[*b*]thiophene (0.4 mmol) gave **4p** (97%) as a white solid; **¹H-NMR** (400 MHz, DMSO-*d*₆) δ 13.45 (bs, 1H), 8.11 (s, 1H), 8.06 – 7.96 (m, 2H), 7.54 – 7.41 (m, 2H). **¹³C-NMR** (101 MHz, DMSO) δ 163.5 (*C*_q), 141.3 (*C*_q), 138.7 (*C*_q), 134.8 (*C*_q), 130.2, 127.0, 125.7, 125.1, 123.0. **HRMS** (ESI⁺): calculated *m/z* for C₉H₇O₂S [(M+H)⁺] 179.0161; found 179.0163. Data in accordance with the literature.^[115]

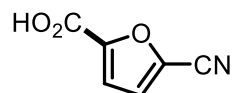
3-Methylbenzo[*b*]thiophene-2-carboxylic acid (**4q**)



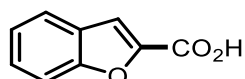
Following GP2a, 3-methylbenzo[*b*]thiophene (0.4 mmol) gave **4q** (95%) as a white solid; **¹H-NMR** (300 MHz, DMSO-*d*₆) δ 13.37 (bs, 1H), 8.01 – 7.88 (m, 2H), 7.55 – 7.41 (m, 2H), 2.70 (s, 3H). **¹³C-NMR** (75 MHz, DMSO) δ 164.4 (*C*_q), 140.0 (*C*_q), 139.8 (*C*_q), 139.4 (*C*_q), 127.9 (*C*_q), 127.3, 124.7, 123.9, 122.8, 12.8. **HRMS** (ESI⁺): calculated *m/z* for C₁₀H₉O₂S [(M+H)⁺] 193.0318; found 193.0319. Data in accordance with the literature.^[116]

5-(Methoxycarbonyl)furan-2-carboxylic acid (4r)

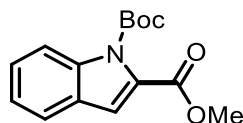
Following GP2a, methyl furan-2-carboxylate (0.4 mmol) gave **4r** (70%) as a pale-yellow solid. **¹H-NMR** (400 MHz, DMSO-*d*₆) δ 13.72 (bs, 1H), 7.39 (d, *J* = 3.6 Hz, 1H), 7.32 (d, *J* = 3.6 Hz, 1H), 3.85 (s, 3H). **¹³C-NMR** (101 MHz, DMSO) δ 158.8 (*C*_q), 157.9 (*C*_q), 147.4 (*C*_q), 145.6 (*C*_q), 119.0, 118.4, 52.3. **HRMS** (ESI+): calculated *m/z* for C₇H₇O₅ [(M+H)⁺] 171.0288; found 171.0289. Data in accordance with the literature.^[117]

5-Cyanofuran-2-carboxylic acid (4s)

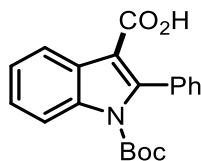
Following GP2a, furan-2-carbonitrile (0.4 mmol) gave **4s** (43%) as a pale-yellow solid; **¹H-NMR** (400 MHz, DMSO-*d*₆) δ 13.98 (bs, 1H), 7.72 (d, *J* = 3.8 Hz, 1H), 7.40 (d, *J* = 3.8 Hz, 1H). **¹³C-NMR** (101 MHz, DMSO) δ 158.0 (*C*_q), 149.0 (*C*_q), 126.9 (*C*_q), 124.6, 117.8, 111.0 (*C*_q). **HRMS** (EI+): calculated *m/z* for C₆H₃NO₃ [M⁺] 137.01074; found 137.01037.

Benzofuran-2-carboxylic acid (4t)

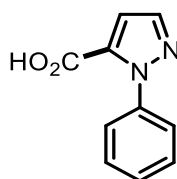
Following GP2a, benzofuran (0.4 mmol) gave **4t** (47%) as a pale-yellow solid; **¹H-NMR** (400 MHz, DMSO-*d*₆) δ 13.55 (bs, 1H), 7.78 (d, *J* = 7.8 Hz, 1H), 7.69 (d, *J* = 8.4 Hz, 1H), 7.67 – 7.63 (m, 1H), 7.49 (ddd, *J* = 8.4, 7.1, 1.3 Hz, 1H), 7.38 – 7.32 (m, 1H). **¹³C-NMR** (101 MHz, DMSO) δ 160.1 (*C*_q), 155.0 (*C*_q), 146.3 (*C*_q), 127.5, 126.9 (*C*_q), 123.8, 123.1, 113.4, 112.1. **HRMS** (EI+): calculated *m/z* for C₉H₆O₃ [M⁺] 162.03115; found 162.03138. Data in accordance with the literature.^[100]

1-(*tert*-butyl) 2-methyl 1*H*-indole-1,2-dicarboxylate (4u)


A dry microwave vial (5 mL) equipped with stirring bar, was charged with *tert*-butyl 1*H*-indole-1-carboxylate (0.1 mmol) and 2,3,6,7-tetramethoxyanthracen-9(10*H*)-one (20 mol%). The vial was sealed and transferred to a glovebox after the vial had evacuated and refilled with N₂ (3×) within the antechamber *via* syringe. Cs₂CO₃ (3.0 equiv.) and dry DMSO (1 mL) was added and the vial was sealed with a Supelco aluminium crimp seal with septum (PTFE/butyl). The vial was removed from the glovebox. The reaction mixture then had gaseous CO₂ (22 cm³) added *via* a gastight Hamilton® syringe, into the head space of the vial. The vial was then irradiated from two sides by two kessil lamps (vials approximately 6 cm away from the light source) with fans placed in front of the vials for cooling (temperatures measured *via* IR ranged between 25–30 °C). After 18 hrs the irradiation was stopped, the pressure was vented *via* syringe and MeI (31 µL, 0.5 mmol) was added. The reaction mixture was left to stir for 4 hrs. The vial was decapped and quenched with aq. HCl (1 mL, 0.3M). The reaction was diluted with brine (10 mL) extracted with EtOAc (3×5 mL). The organic layers were combined and washed with brine (3×10 mL) and then dried *via* phase separator and concentrated *in vacuo*. Purification by column chromatography on silica gel eluting with heptane : EtOAc (9:1) gave the title compound **4u** (40%) as a white waxy solid. R_f 0.51 [Heptane–EtOAc (9:1)]; 8.10 (dq, *J* = 8.5, 0.9 Hz, 1H), 7.60 (ddd, *J* = 7.8, 1.2, 0.8 Hz, 1H), 7.42 (ddd, *J* = 8.5, 7.2, 1.3 Hz, 1H), 7.27 (ddd, *J* = 8.1, 7.2, 1.0 Hz, 1H), 7.11 (d, *J* = 0.8 Hz, 1H), 3.93 (s, 3H), 1.63 (s, 9H). ¹³C-NMR (101 MHz, CDCl₃) δ 162.5, 149.4, 137.9, 130.5, 127.6, 126.9, 123.4, 122.3, 115.0, 115.0, 84.7, 52.5, 27.9. Data in accordance with the literature.^[118]

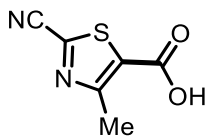
1-(*tert*-Butoxycarbonyl)-2-phenyl-1*H*-indole-3-carboxylic acid (4v)

Following GP2a, *tert*-butyl 2-phenyl-1*H*-indole-1-carboxylate (0.4 mmol) gave **4v** (10%) as a white solid; **¹H-NMR** (400 MHz, DMSO-*d*₆) δ 12.40 (bs, 1H), 8.17 – 8.12 (m, 1H), 8.12 – 8.07 (m, 1H), 7.48 – 7.32 (m, 7H), 1.16 (s, 9H). **¹³C-NMR** (101 MHz, DMSO) δ 164.9 (C_q), 148.9 (C_q), 143.8 (C_q), 135.3 (C_q), 133.1 (C_q), 129.7, 128.1, 127.4, 126.9 (C_q), 124.9, 123.7, 121.6, 114.2, 111.4 (C_q), 84.3 (C_q), 26.8. **HRMS** (ESI⁺): calculated *m/z* for C₂₀H₂₀NO₄ [(M+H)⁺] 338.1387; found 338.1391.

1-Phenyl-1*H*-pyrazole-5-carboxylic acid (4w)

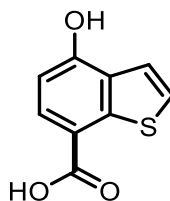
Following GP2a, 1-phenylpyrazole (0.4 mmol) gave **4w** (33%) as a white solid; **¹H-NMR** (300 MHz, Methanol-*d*₄) δ 7.72 (d, *J* = 2.0 Hz, 1H), 7.52 – 7.39 (m, 5H), 7.05 (d, *J* = 2.0 Hz, 1H). **¹H-NMR** (400 MHz, DMSO-*d*₆) δ 13.29 (bs, 1H), 7.77 (d, *J* = 1.9 Hz, 1H), 7.52 – 7.41 (m, 5H), 7.03 (d, *J* = 1.9 Hz, 1H). **¹³C-NMR** (101 MHz, DMSO) δ 160.0 (C_q), 140.2 (C_q), 139.7, 134.1 (C_q), 128.5, 128.2, 125.7, 112.5. **HRMS** (ESI⁺): calculated *m/z* for C₁₀H₉N₂O₂ [(M+H)⁺] 189.0659; found 189.0661. Data in accordance with the literature.^[119]

2-cyano-4-methylthiazole-5-carboxylic acid (**4x**)

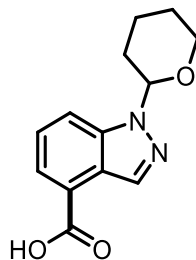


Following GP2c, 4-methylthiazole-2-carbonitrile (0.1 mmol) gave **4x** (53%) as a white solid. **¹H-NMR** (500 MHz, CDCl₃) δ 2.83 (3H, s); **¹³C-NMR** (126 MHz, CDCl₃) δ 165.4 (C_q), 163.3 (C_q), 139.3 (C_q), 126.6 (C_q), 112.1 (C_q), 17.7; **HRMS** (EI): calculated m/z for C₆H₄N₂O₂S [M⁺] 167.9992; found 168.0003.

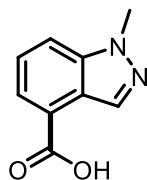
4-hydroxybenzo[*b*]thiophene-7-carboxylic acid (**6a**)



Following GP2c, 4-hydroxybenzo[*b*]thiophene (0.1 mmol) gave **6a** (99%) as a white solid. **¹H-NMR** (500 MHz, DMSO-*d*₆) δ 7.91 (d, *J* = 8.2 Hz, 1H), 7.66 (d, *J* = 5.6 Hz, 1H), 7.51 (d, *J* = 5.6 Hz, 1H), 6.85 (d, *J* = 8.2 Hz, 1H); **¹³C-NMR** (126 MHz, DMSO-*d*₆) δ 166.9 (C_q), 157.0 (C_q), 141.8 (C_q), 129.8 (C_q), 129.3, 127.7, 119.8, 115.6 (C_q), 108.9; **HRMS** (ESI): calculated m/z for C₉H₅O₃S [(M-H)⁺] 192.9965; found 192.9965.

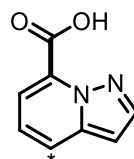
1-(Tetrahydro-2*H*-pyran-2-yl)-1*H*-indazole-4-carboxylic acid (6b)


Following GP2c, 1-(tetrahydro-2*H*-pyran-2-yl)-1*H*-indazole (0.1 mmol) gave **6b** (60%) as a white solid. **¹H-NMR** (500 MHz, DMSO-*d*₆): δ 12.88 (bs, 1H), 8.42 (s, 1H), 8.03 (d, *J* = 8.4 Hz, 1H), 7.83 (d, *J* = 7.1 Hz, 1H), 7.63-7.43 (m, 1H), 5.92 (dd, *J* = 9.6, 2.1 Hz, 1H), 3.88 (d, *J* = 11.2 Hz, 1H), 3.80-3.71 (m, 1H), 2.42 (qd, *J* = 3.7, 13.0 Hz, 1H), 2.15-1.94 (m, 2H), 1.88-1.67 (m, 1H), 1.65-1.52 (m, 2H); **¹³C-NMR** (126 MHz, DMSO-*d*₆): δ 167.0, 139.8, 133.6, 125.9, 124.4, 123.3, 122.5, 115.3, 84.0, 66.5, 28.9, 24.7, 22.1; **HRMS** (ESI): calculated *m/z* for C₁₃H₁₅N₂O₃ [(M+H)⁺] 247.1077; found 247.1066.

1-Methyl-1*H*-indazole-4-carboxylic acid (6c)


Following GP2c, 1-methyl-1*H*-indazole (0.1 mmol) gave **6c** (58%) as a white solid. **¹H-NMR** (500 MHz, CDCl₃): δ 8.58 (s, 1H), 8.05 (d, *J* = 6.9 Hz, 1H), 7.69 (d, *J* = 8.8 Hz, 1H), 7.44-7.56 (m, 1H), 4.16 (s, 3H); **¹³C-NMR** (126 MHz, CDCl₃): 171.3, 140.5, 133.9, 125.7, 125.3, 122.8, 122.3, 114.9, 35.9; **HRMS** (ESI): calculated *m/z* for C₉H₉N₂O₂ [(M+H)⁺] 177.0664; found 177.0669.

Pyrazolo[1,5-*a*]pyridine-7-carboxylic acid (6d) & pyrazolo[1,5-*a*]pyridine-4-carboxylic acid (6d')

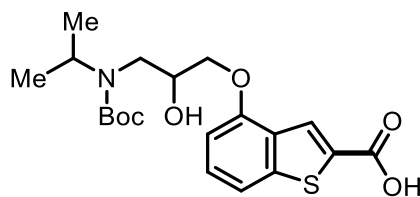


Following GP2c, pyrazolo[1,5-*a*]pyridine (0.1 mmol) gave **6d** (63%) as a white solid & **6d'** (22%) as a white solid. **6d:6d'** = 2.8:1.

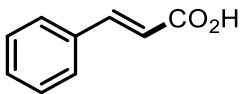
Data for 6d: ¹H-NMR (500 MHz, DMSO-*d*₆) δ 8.20 (d, *J* = 2.3 Hz, 1H), 8.14–7.88 (m, 1H), 7.73–7.58 (m, 1H), 7.38 (dd, *J* = 7.1, 8.8 Hz, 1H), 6.87 (d, *J* = 2.3 Hz, 1H); ¹³C-NMR (126 MHz, DMSO-*d*₆) δ 161.8, 140.8, 140.6, 129.3, 123.6, 122.3, 116.9, 98.5. Data in accordance with the literature.^[120]

Data for 6d': ¹H-NMR (500 MHz, DMSO-*d*₆) δ 13.34 (bs, 1H), 8.94 (d, *J* = 6.8 Hz, 1H), 8.12 (d, *J* = 2.1 Hz, 1H), 7.95 (d, *J* = 6.4 Hz, 1H), 7.03–6.98 (m, 2H); ¹³C-NMR (126 MHz, DMSO-*d*₆) δ 165.5, 142.9, 137.9, 133.0, 128.6, 120.7, 110.9, 98.6. Data in accordance with the literature.^[120]

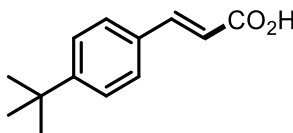
4-(3-((*tert*-butoxycarbonyl)(isopropyl)amino)-2-hydroxypropoxy)benzo[*b*]thiophene-2-carboxylic acid (6e)



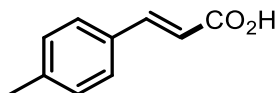
Following GP2c, *tert*-butyl (3-(benzo[*b*]thiophen-4-yloxy)-2-hydroxypropyl)(isopropyl)-carbamate (0.1 mmol) gave **6e** (18%) as a yellow oil. ¹H-NMR (500 MHz, CDCl₃): δ 8.26 (s, 1H), 7.32–7.49 (m, 2H), 6.77 (d, *J* = 7.5 Hz, 1H), 4.28–4.11 (m, 3H), 4.10–3.99 (m, 1H), 3.47 (s, 2H), 2.05 (s, 1H), 1.50 (s, 9H), 1.18 (dd, *J* = 6.5, 31.4 Hz, 6H); ¹³C-NMR (126 MHz, CDCl₃) δ ¹³C NMR (126 MHz, CDCl₃) δ 165.6, 154.3, 143.4, 131.0, 129.1, 127.7, 127.3, 114.4, 104.2, 80.0, 71.0, 69.1, 48.0, 46.1, 27.6, 19.7 **HRMS** (ESI): calculated *m/z* for C₂₀H₂₈NO₆S [(M+H)⁺] 410.1637; found 410.1655.

Cinnamic acid (8a)

Following GP2a, styrene (0.4 mmol) gave **8a** (54%) as a white solid; **¹H-NMR** (400 MHz, DMSO-*d*₆) δ 12.40 (bs, 1H), 7.72 – 7.64 (m, 2H), 7.59 (d, *J* = 16.0 Hz, 1H), 7.45 – 7.37 (m, 3H), 6.53 (d, *J* = 16.0 Hz, 1H). **¹³C-NMR** (101 MHz, DMSO) δ 167.6 (*C*_q), 143.9, 134.2 (*C*_q), 130.2, 128.9, 128.2, 119.3. **HRMS** (EI+): calculated *m/z* for C₉H₈O₂ [*M*⁺] 148.05188; found 148.05161. Data in accordance with the literature.^[121]

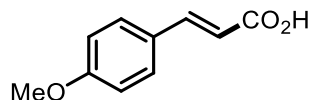
(*E*)-3-(4-(*tert*-Butyl)phenyl)acrylic acid (8b)

Following GP2a, 1-(*tert*-butyl)-4-vinylbenzene (0.4 mmol) gave **8b** (56%) as a white solid; **¹H-NMR** (400 MHz, DMSO-*d*₆) δ 12.33 (bs, 1H), 7.62 – 7.53 (m, 3H), 7.46 – 7.38 (m, 2H), 6.47 (d, *J* = 16.0 Hz, 1H), 1.27 (s, 9H). **¹³C-NMR** (101 MHz, DMSO) δ 167.7 (*C*_q), 153.1 (*C*_q), 143.8, 131.5 (*C*_q), 128.0, 125.7, 118.3, 34.6 (*C*_q), 30.9. **HRMS** (EI+): calculated *m/z* for C₁₃H₁₆O₂ [*M*⁺] 204.11448; found 204.11415.

(*E*)-3-(*p*-Tolyl)acrylic acid (8c)

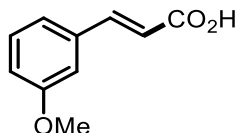
Following GP2a, 4-methylstyrene (0.4 mmol) gave **8c** (53%) as a white solid; **¹H-NMR** (400 MHz, DMSO-*d*₆) δ 12.31 (bs, 1H), 7.60 – 7.51 (m, 3H), 7.22 (d, *J* = 7.9 Hz, 2H), 6.46 (d, *J* = 16.0 Hz, 1H), 2.32 (s, 3H). **¹³C-NMR** (101 MHz, DMSO) δ 167.7 (*C*_q), 143.9, 140.1 (*C*_q), 131.5 (*C*_q), 129.5, 128.2, 118.1, 21.0. **HRMS** (EI+): calculated *m/z* for C₁₀H₁₀O₂ [*M*⁺] 162.06753; found 162.06783.

(*E*)-3-(4-Methoxyphenyl)acrylic acid (8d)



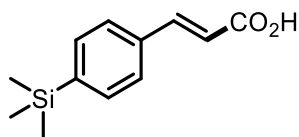
Following GP2a, 4-methoxystyrene (0.4 mmol) gave **8d** (40%) as a pale-yellow solid; **¹H-NMR** (400 MHz, DMSO-*d*₆) δ 12.21 (bs, 1H), 7.66 – 7.60 (m, 2H), 7.54 (d, *J* = 16.0 Hz, 1H), 7.00 – 6.93 (m, 2H), 6.37 (d, *J* = 15.9 Hz, 1H), 3.79 (s, 3H). **¹³C-NMR** (101 MHz, DMSO) δ 167.8 (*C*_q), 160.9 (*C*_q), 143.7, 129.9, 126.8 (*C*_q), 116.5, 114.3, 55.3. **HRMS** (EI+): calculated *m/z* for C₁₀H₁₀O₃ [*M*⁺] 178.06245; found 178.06194.

(*E*)-3-(3-Methoxyphenyl)acrylic acid (8e)

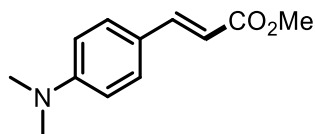


Following GP2a, 3-methoxystyrene (0.4 mmol) gave **8e** (46%) as a white solid; **¹H-NMR** (400 MHz, DMSO-*d*₆) δ 12.40 (bs, 1H), 7.56 (d, *J* = 16.0 Hz, 1H), 7.36 – 7.20 (m, 3H), 7.03 – 6.92 (m, 1H), 6.55 (d, *J* = 16.0 Hz, 1H), 3.79 (s, 3H). **¹³C-NMR** (101 MHz, DMSO) δ 167.6 (*C*_q), 159.6 (*C*_q), 143.9, 135.7 (*C*_q), 129.9, 120.8, 119.6, 116.2, 112.9, 55.2. **HRMS** (EI+): calculated *m/z* for C₁₀H₁₀O₃ [*M*⁺] 178.06245; found 178.06210.

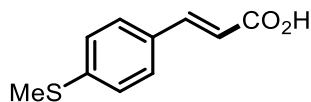
(*E*)-3-(4-(Trimethylsilyl)phenyl)acrylic acid (8f)



Following GP2a, trimethyl(4-vinylphenyl)silane (0.4 mmol) gave **8f** (53%) as a pale-yellow solid; **¹H-NMR** (400 MHz, DMSO-*d*₆) δ 12.38 (bs, 1H), 7.67 – 7.62 (m, 2H), 7.61 – 7.52 (m, 3H), 6.54 (d, *J* = 16.0 Hz, 1H), 0.24 (s, 9H). **¹³C-NMR** (101 MHz, DMSO) δ 167.5 (*C*_q), 143.9, 142.6 (*C*_q), 134.6 (*C*_q), 133.7, 127.3, 119.4, –1.3. **HRMS** (EI+): calculated *m/z* for C₁₂H₁₆O₂Si [*M*⁺] 220.09141; found 220.09148.

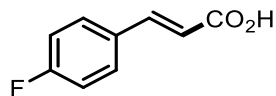
Methyl (*E*)-3-(4-(dimethylamino)phenyl)acrylate (8g**)**

The title compound was prepared according to GP2a with *N,N*-dimethyl-4-vinylaniline (0.4 mmol). After irradiating the mixture for 18 hrs the reaction vial was vented and MeI (18.7 μ L, 0.3 mmol, 3 equiv.) was added *via* syringe. The resulting mixture was stirred for 2 hrs at 35 °C and was quenched by adding water. The crude mixture was extracted with DCM (3 \times) and the combined organic layers were dried over Na₂SO₄, filtered and concentrated *in vacuo*. Flash silica gel column chromatography with a mixture of hexanes+NEt₃ (1% v/v) and EtOAc provided the title compound **8g** (14%) as a pale brown solid; **¹H-NMR** (400 MHz, Chloroform-*d*) δ 7.63 (d, *J* = 15.9 Hz, 1H), 7.45 – 7.38 (m, 2H), 6.70 – 6.62 (m, 2H), 6.22 (d, *J* = 15.8 Hz, 1H), 3.78 (s, 3H), 3.01 (s, 6H). **¹³C-NMR** (101 MHz, CDCl₃) δ 168.5 (C_q), 151.9 (C_q), 145.5, 129.9, 122.3 (C_q), 112.2, 112.0, 51.5, 40.3. **HRMS** (EI+): calculated *m/z* for C₁₂H₁₅NO₂ [M⁺] 205.10973; found 205.10937.

(*E*)-3-(4-(Methylthio)phenyl)acrylic acid (8h**)**

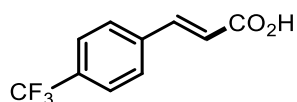
Following GP2a, methyl(4-vinylphenyl)sulfane (0.4 mmol) gave **8h** (38%) as a white solid; **¹H-NMR** (400 MHz, DMSO-*d*₆) δ 12.32 (bs, 1H), 7.65 – 7.60 (m, 2H), 7.55 (d, *J* = 16.0 Hz, 1H), 7.31 – 7.24 (m, 2H), 6.48 (d, *J* = 16.0 Hz, 1H), 2.51 (s, 3H). **¹³C-NMR** (101 MHz, DMSO) δ 167.7 (C_q), 143.4, 141.3 (C_q), 130.6 (C_q), 128.7, 125.6, 118.0, 14.2. **HRMS** (EI+): calculated *m/z* for C₁₀H₁₀O₂S [M⁺] 194.03960; found 194.03936.

(*E*)-3-(4-Fluorophenyl)acrylic acid (8i**)**

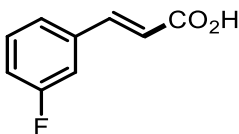


Following GP2a, 4-fluorostyrene (0.4 mmol) gave **8i** (46%) as a white solid; **¹H-NMR** (400 MHz, DMSO-*d*₆) δ 12.39 (bs, 1H), 7.80 – 7.71 (m, 2H), 7.59 (d, *J* = 16.0 Hz, 1H), 7.29 – 7.19 (m, 2H), 6.49 (d, *J* = 16.0 Hz, 1H). **¹³C-NMR** (101 MHz, DMSO-*d*₆) δ 167.5 (*C*_q), 163.1 (d, *J* = 248.3 Hz, *C*_q), 142.7, 130.9 (d, *J* = 3.2 Hz, *C*_q), 130.5 (d, *J* = 8.6 Hz), 119.1 (d, *J* = 2.2 Hz), 115.9 (d, *J* = 21.7 Hz). **¹⁹F-NMR** (376 MHz, DMSO) δ -110.0. **HRMS** (EI+): calculated *m/z* for C₉H₇FO₂ [*M*⁺] 166.04246; found 166.04203.

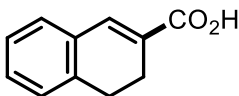
(*E*)-3-(4-(Trifluoromethyl)phenyl)acrylic acid (8j**)**



Following GP2a, 1-(trifluoromethyl)-4-vinylbenzene (0.4 mmol) gave **8j** (13%) as a white solid; **¹H-NMR** (400 MHz, DMSO-*d*₆) δ 12.58 (bs, 1H), 7.92 (d, *J* = 8.1 Hz, 2H), 7.76 (d, *J* = 8.1 Hz, 2H), 7.66 (d, *J* = 16.1 Hz, 1H), 6.68 (d, *J* = 16.1 Hz, 1H). **¹³C-NMR** (101 MHz, DMSO) δ 167.2 (*C*_q), 142.0, 138.3 (d, *J* = 1.3 Hz, *C*_q), 129.8 (q, *J* = 31.8 Hz, *C*_q), 128.8, 125.7 (q, *J* = 3.7 Hz), 124.0 (q, *J* = 272.1 Hz, *C*_q), 122.3. **¹⁹F-NMR** (376 MHz, DMSO) δ -60.8. **HRMS** (ESI+): calculated *m/z* for C₁₀H₈F₃O₂ [(*M*+*H*)⁺] 217.0471; found 217.0472. Data in accordance with the literature.^[121]

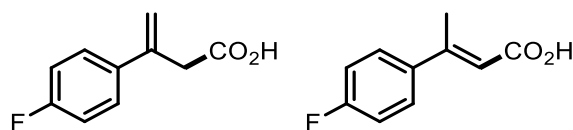
(*E*)-3-(3-Fluorophenyl)acrylic acid (8k)

Following GP2a, 3-fluorostyrene (0.4 mmol) gave **8k** (38%) as a white solid; **¹H-NMR** (400 MHz, DMSO-*d*₆) δ 12.49 (bs, 1H), 7.64 – 7.49 (m, 3H), 7.49 – 7.41 (m, 1H), 7.29 – 7.19 (m, 1H), 6.61 (d, *J* = 16.0 Hz, 1H). **¹³C-NMR** (101 MHz, DMSO-*d*₆) δ 167.4 (*C*_q), 162.42 (d, *J* = 243.7 Hz, *C*_q), 142.51 (d, *J* = 2.6 Hz), 136.82 (d, *J* = 8.1 Hz, *C*_q), 130.81 (d, *J* = 8.4 Hz), 124.63 (d, *J* = 2.6 Hz), 120.9, 116.86 (d, *J* = 21.3 Hz), 114.38 (d, *J* = 22.0 Hz). **¹⁹F-NMR** (377 MHz, DMSO) δ -112.4. **HRMS** (ESI+): calculated *m/z* for C₉H₈FO₂ [(M+H)⁺] 167.0503; found 167.0502.

3,4-Dihydronaphthalene-2-carboxylic acid (8l)

Following GP2a, 1,2-dihydronaphthalene (0.4 mmol) gave **8l** (58%) as a white solid; **¹H-NMR** (400 MHz, DMSO-*d*₆) δ 12.43 (bs, 1H), 7.47 (s, 1H), 7.34 – 7.18 (m, 4H), 2.81 (t, *J* = 8.3 Hz, 2H), 2.49 – 2.43 (m, 2H). **¹³C-NMR** (101 MHz, DMSO) δ 168.1 (*C*_q), 136.5 (*C*_q), 135.3, 132.3 (*C*_q), 130.0 (*C*_q), 129.3, 128.3, 127.5, 126.7, 26.9 (CH₂), 21.9 (CH₂). **HRMS** (EI+): calculated *m/z* for C₁₁H₁₀O₂ [M⁺] 174.06753; found 174.06707. Data in accordance with the literature.^[122]

3-(4-Fluorophenyl)but-3-enoic acid (**8m**) & (*E*)-3-(4-fluorophenyl)but-2-enoic acid (**8m'**)

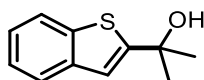


Following GP2a, 4-fluoro- α -methylstyrene (0.4 mmol) gave **8m** (43%) as a white solid and **8m'** (9%) as a pale yellow solid. **8m**:**8m'** = 4.8:1. **HRMS** (EI+): calculated m/z for C₁₀H₉FO₂ [M^{+}] 180.05811; found 180.05831.

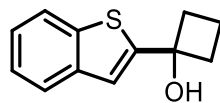
Data for 8m: **¹H-NMR** (400 MHz, Chloroform-*d*) δ 9.83 (bs, 1H), 7.45 – 7.35 (m, 2H), 7.06 – 6.97 (m, 2H), 5.52 (s, 1H), 5.24 (s, 1H), 3.52 (s, 2H). **¹³C-NMR** (101 MHz, Chloroform-*d*) δ 177.5 (C_q), 162.7 (d, J = 247.3 Hz, C_q), 139.3 (C_q), 135.7 (d, J = 3.3 Hz, C_q), 127.61 (d, J = 8.1 Hz), 116.98 (d, J = 1.3 Hz, CH₂), 115.49 (d, J = 21.5 Hz), 41.1 (CH₂). **¹⁹F-NMR** (376 MHz, CDCl₃) δ –114.8.

Data for 8m': **¹H-NMR** (400 MHz, Chloroform-*d*) δ 7.51 – 7.45 (m, 2H), 7.11 – 7.04 (m, 2H), 6.13 (s, 1H), 2.58 (d, J = 0.7 Hz, 3H). **¹⁹F-NMR** (376 MHz, CDCl₃) δ –112.4. Data in accordance with the literature.^[123]

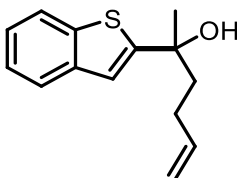
2-(Benzo[*b*]thiophen-2-yl)propan-2-ol (**9pa**)



According to GP3 benzo[*b*]thiophene and acetone gave **9pa** (54%) as a white solid; **¹H-NMR** (400 MHz, Chloroform-*d*) δ 7.80 (d, J = 7.8 Hz, 1H), 7.71 (d, J = 7.7 Hz, 1H), 7.31 (dt, J = 15.1, 7.4 Hz, 2H), 7.16 (s, 1H), 2.26 (s, 1H), 1.73 (s, 6H). **¹³C-NMR** (101 MHz, CDCl₃) δ 155.1 (C_q), 139.9 (C_q), 139.3 (C_q), 124.3, 124.1, 123.5, 122.4, 118.5, 71.8 (C_q), 32.1. **HRMS** (ESI+): calculated m/z for C₁₁H₁₃O₂S [$(M+H)^{+}$] 175.0576; found 175.0577.

1-(Benzo[*b*]thiophen-2-yl)cyclobutan-1-ol (9pb)

According to GP3 benzo[*b*]thiophene and cyclobutanone gave **9pb** (30%) as a pale-yellow oil; **¹H-NMR** (300 MHz, Methanol-*d*₄) δ 7.84 – 7.73 (m, 1H), 7.76 – 7.70 (m, 1H), 7.35 – 7.22 (m, 3H), 2.65 – 2.52 (m, 2H), 2.52 – 2.38 (m, 2H), 2.06 – 1.77 (m, 2H). **¹³C-NMR** (75 MHz, MeOD) δ 154.1 (C_q), 141.3 (C_q), 141.0 (C_q), 125.1, 125.0, 124.4, 123.2, 119.8, 75.7 (C_q), 39.0 (CH₂), 13.7 (CH₂). **HRMS** (ESI⁺): calculated *m/z* for C₁₂H₁₃OS [(M+H)⁺] 187.0576; found 187.0577.

2-(Benzo[*b*]thiophen-2-yl)hex-5-en-2-ol (9pc)

According to GP3 benzo[*b*]thiophene and hex-5-en-2-one gave **9pc** (19%) as a colorless oil; **¹H-NMR** (400 MHz, Chloroform-*d*) δ 7.83 – 7.77 (m, 1H), 7.74 – 7.68 (m, 1H), 7.37 – 7.26 (m, 2H), 7.14 (s, 1H), 5.84 (ddt, *J* = 16.8, 10.2, 6.4 Hz, 1H), 5.02 (dq, *J* = 17.1, 1.7 Hz, 1H), 4.96 (dq, *J* = 9.9, 1.3 Hz, 1H), 2.24 – 2.07 (m, 3H), 2.06 – 1.99 (m, 2H), 1.70 (s, 3H). **¹³C-NMR** (101 MHz, CDCl₃) δ 153.9 (C_q), 140.0 (C_q), 139.4 (C_q), 138.4, 124.4, 124.1, 123.4, 122.4, 119.1, 115.1 (CH₂), 74.4 (C_q), 43.5 (CH₂), 30.7, 28.8 (CH₂). **HRMS** (EI⁺): calculated *m/z* for C₁₄H₁₆OS [M⁺] 232.09164; found 232.09159.

4.4.5 NMR Spectra

The corresponding NMR spectra of the compounds **2a-g**, **4a-x**, **6a-e** and **9pa-9pc** are included in the Appendix (see section 7.4).

4.4.6 Mechanistic Studies

4.4.6.1 General Procedure for High-throughput Screening of Arenes

To a paradox 96-well plate fitted with 0.5 mL glass vials containing magnetic stirrer bars was added the arene (0.03 mmol) and 2,3,6,7-tetramethoxyanthracen-9(10*H*)-one (2.0 mg, 20 mol%). The vials were partially-sealed and transferred to a glovebox antechamber after the vial had evacuated and refilled with N₂ (3×) within the antechamber. DMSO (0.3 mL) was dispensed to each of the vials followed by 1,1,3,3-tetramethylguanidine (11 µL, 0.09 mmol) and the plate was sealed with the plate lid, two rubber mats and a Teflon TFA film. The plate was then removed and transferred to a glove-bag filled with an over-pressure of CO₂. The plate was then unsealed and placed on a stirrer plate with 3×456 nm Kessil lamps clamped overhead. The vial was then irradiated from above by two Kessil lamps (vials approximately 10 cm away from the light source). After 18 hrs the irradiation was stopped and the plate was removed from the glove bag and quenched with aq. HCl (0.2 mL, 0.5M) and samples were taken and filtered before being placed on a plastic 96 well plate for HPLC analysis.

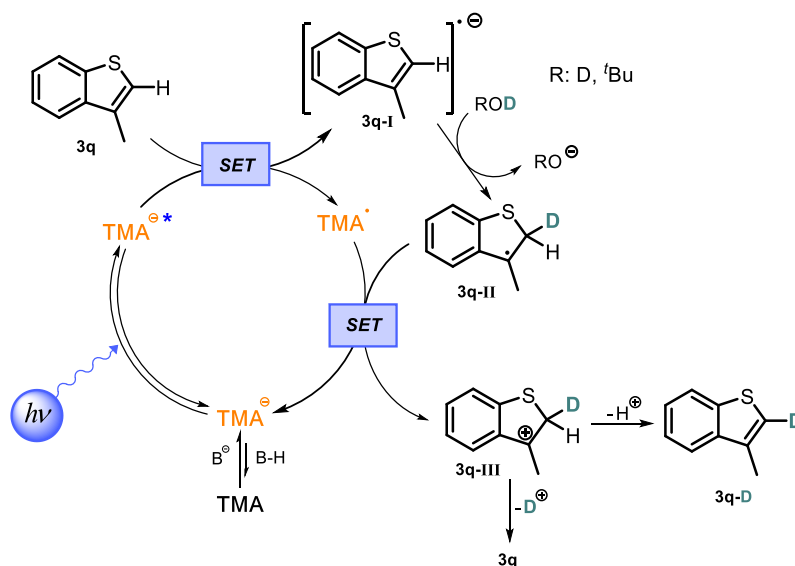


Figure S4-9. HTS 96 well plate reactions running in the CO₂ glove-bag set up.

4.4.6.2 Deuterium Labeling Experiments

Upon formation of an arene radical anion **3q-I** we envisioned a H/**D** exchange reaction giving rise to **3q-II** in presence of a deuterium source. After reoxidation and deprotonation **3q-D** would be formed (Scheme S4-3).

To a dry flat-bottomed crimp vial (5 mL) equipped with stirring bar, was added **3q** (0.1 mmol) and 2,3,6,7-tetramethoxyanthracen-9(10*H*)-one (6.3 mg, 0.02 mmol, 20 mol%, only for Entry 1-3, Table S4-3). Cs₂CO₃ (98 mg, 3 equiv.) was quickly added and the vial was sealed with a Supelco aluminium crimp seal with septum (PTFE/butyl). The vial was then evacuated and refilled with N₂ (5×) *via* syringe needle. The reaction mixture was dissolved in DMSO-*d*₆ (1 mL, dry and degassed by bubbling with N₂) and the deuterium source was added *via* syringe. The vial was then irradiated from the bottom side with blue LED light and a constant reaction temperature (25 °C) was maintained by employing a water-cooling circuit connected to a thermostat. After 18 hrs of reaction time the reaction was quenched by the addition of water and the crude mixture was extracted with Et₂O (3×). The combined organic layers were dried over Na₂SO₄, concentrated and purified *via* flash silica column chromatography using a mixture of hexanes and DCM (95:5) as eluent. The obtained product was dried in vacuo and analyzed by ¹H-NMR (Table S4-3 and Figures S4-10a-b) and GC-MS (Figure S4-10c).



Scheme S4-3. Proposed mechanism for the deuterium labeling experiments using **3q** as substrate.

Table S4-3. Deuterium labeling experiments.

<chem>Cc1ccc2sc(C)cc2c1</chem> $\xrightarrow[\text{DMSO-d}_6 \text{ (0.1 M), 25}^\circ\text{C, 455 nm, N}_2, 18\text{h}]{\text{TMAH (20 mol\%), ROD (3-15 eq.), Cs}_2\text{CO}_3 \text{ (3.0 equiv.)}}$ <chem>Cc1ccc2sc(C)c(C)cc2c1</chem> + <chem>Cc1ccc2sc(C)c(C)cc2c1</chem>				
Entry	Catalyst	λ [nm]	D-source (eq.)	D-incorporation [%] ^a
1	TMAH	455	D ₂ O (3)	10
2	TMAH	455	D ₂ O (15)	14
3	TMAH	455	^t BuOD (10)	15
4 ^b	-	dark	D ₂ O (15)	<1

^a Determined by ¹H-NMR integration upon isolation and purification of the reaction mixture; ^b Reaction was stirred in the dark.

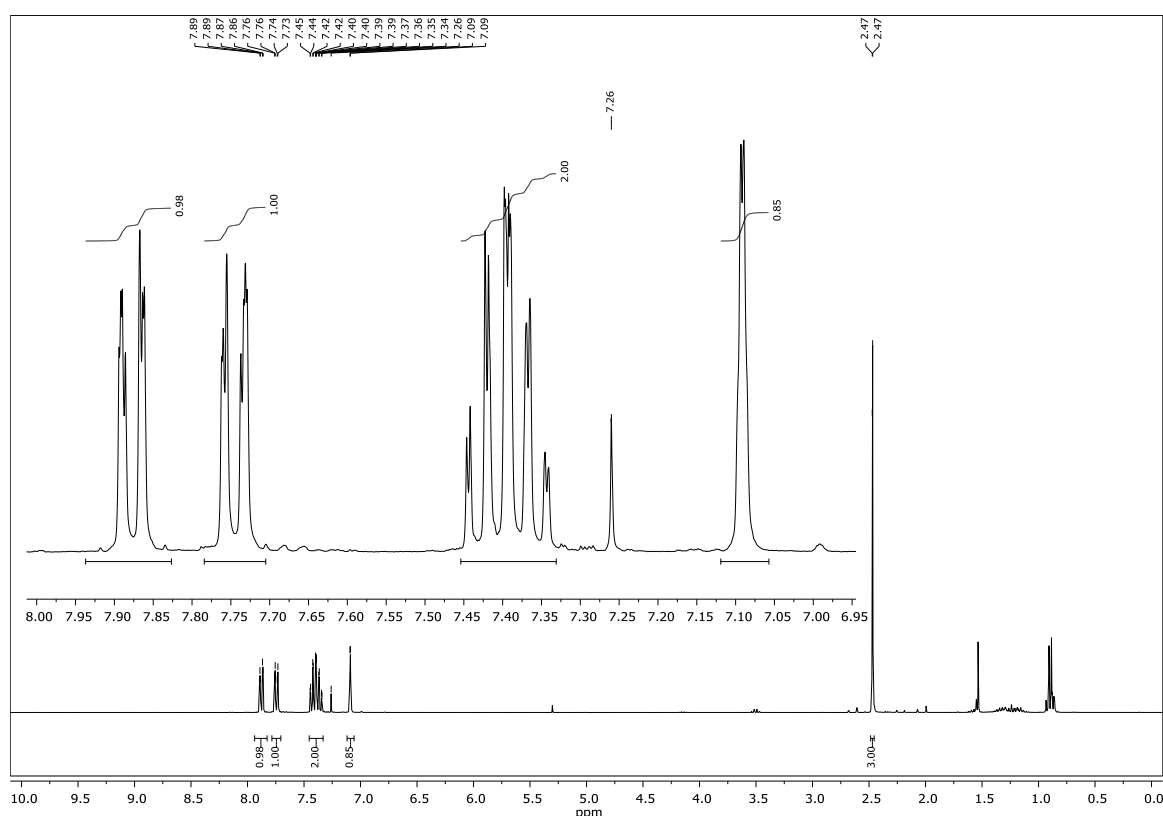


Figure S4-10a. ¹H-NMR recorded after reaction work-up and column chromatography according to Entry 3, Table S4-3. The signal at 7.1 ppm corresponds to the proton in position 2 of **3q**. Peak integration revealed a slightly reduced value of 0.85. The signal at 7.75 ppm served as reference and was set to integral 1.00.

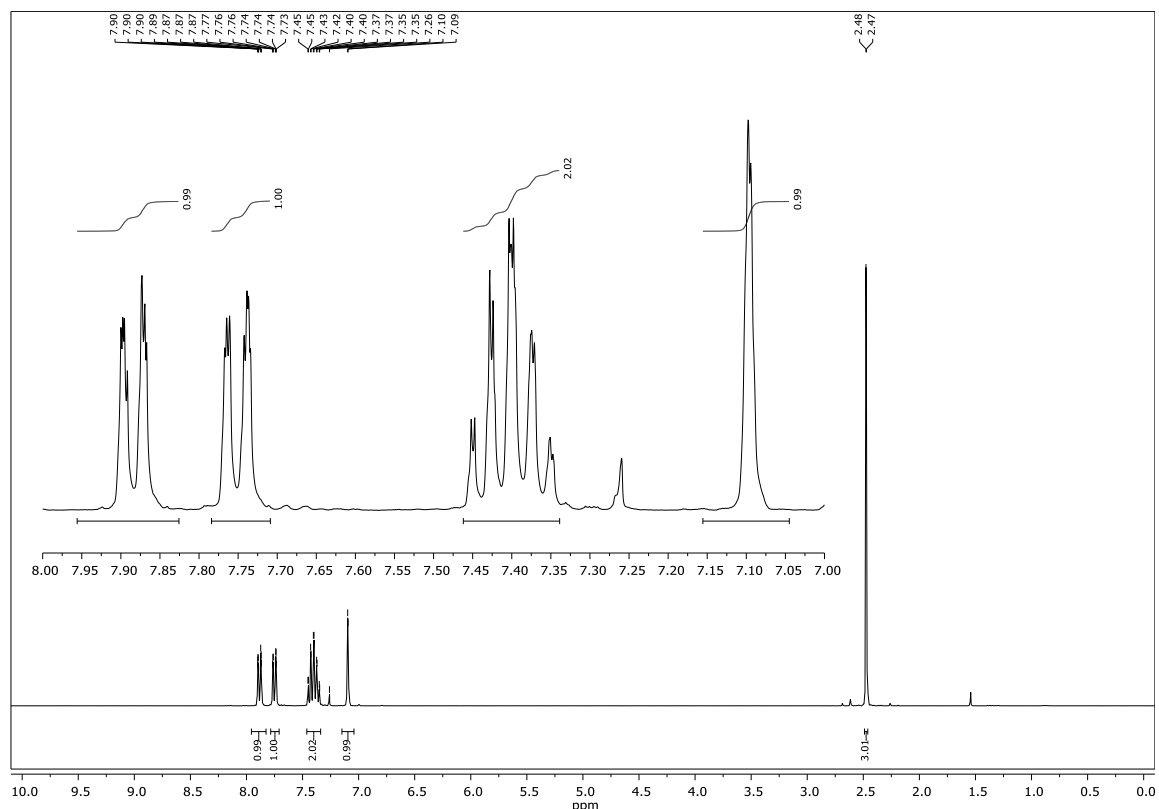


Figure S4-10b. ^1H -NMR recorded after reaction work up and column chromatography according to Entry 4, Table S4-3. The signal at 7.1 ppm corresponds to the proton in position 2 of **3q**. Peak integration revealed a value of 0.99. The signal at 7.75 ppm served as reference and was set to integral 1.00.

Figure S4-10a shows the ^1H -NMR spectrum from the isolated product of the deuterium labeling experiment in presence of $t\text{BuOD}$ (Entry 3, Table S4-3). Integration over the signal at 7.1 ppm, which corresponds to the proton in position 2 of benzothiophene **3q**, revealed a slightly decreased value (0.85 instead of 1.00). This deviance can be explained by the partial exchange of hydrogen by deuterium.

Figure S10b shows the ^1H -NMR spectrum from the isolated product of the control reaction (Entry 4, Table S4-3). Integration over the signal at 7.1 ppm gave a value close to unity and suggests no or only traces of incorporated deuterium.

In addition to ^1H -NMR analysis, the incorporation of deuterium was verified by GC mass. Compared to the set of peaks caused by the purchased starting material **3q** (Figure S4-10c, grey), the different ratios in the isotope pattern suggest the partial incorporation of deuterium into the product isolated upon deuterium labeling reaction (Entry 3, Table S4-3).

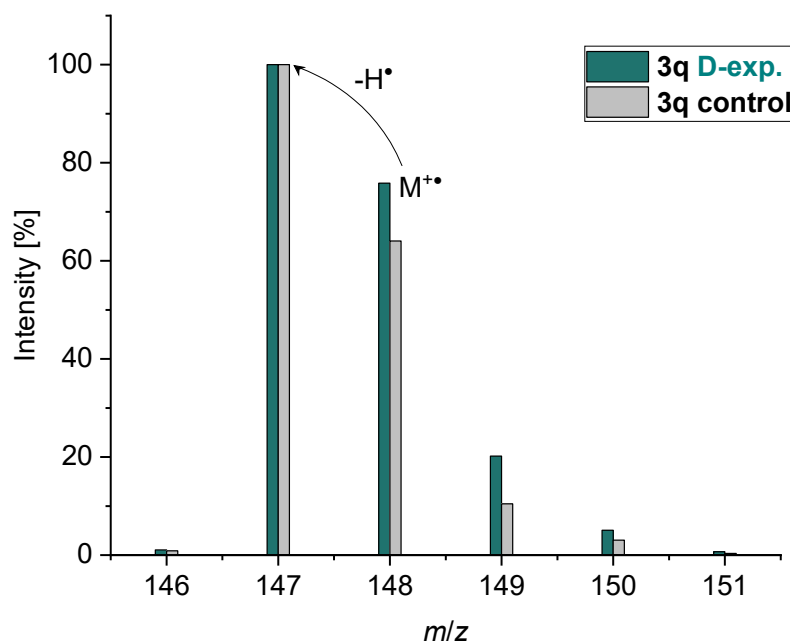


Figure S4-10c. GC-MS analysis after reaction work up and column chromatography according to Entry 3 from Table S4-3 (green) and purchased **3q** (grey). Mass spectra was recorded upon electron impact ionization (70 eV). The ionized **3q** is prone to lose a hydrogen atom causing the most intense peak at $m/z \approx 147$.

4.4.6.3 Time-resolved Luminescence Quenching Studies

A first prediction regarding possibly working substrates was made by time-resolved luminescence quenching of the photoexcited catalyst. If there is an interaction between the excited PC and the substrate (electron transfer is proposed), the luminescence lifetime is shortened. Such processes can be easily followed by luminescence lifetime analysis and from the data obtained a Stern-Volmer plot of the time-resolved experiment was developed (Figures S4-11a-d and S4-13). A linear correlation between concentration of quencher [Q] and $\tau_0 \times \tau^{-1}$ indicates a dynamic luminescence quenching. The luminescence lifetime was recorded in dry, degassed DMSO in presence of cesium carbonate by using a quartz cuvette (1×1 cm) with septum screw cap. The cuvette was degassed *in vacuo* and backfilled with N₂ (5×) before the stock solution of quencher and the catalyst solution were added *via* syringe. A **TMAH** concentration of $c(\text{TMAH}) = 40 \mu\text{M}$ in the cuvette was used for all experiments. For excitation of the sample, a 452 nm laser diode was used and an optical longpass filter (cut-on wavelength

500 nm) was installed before the detection unit. The time range for the measurement was set to 400 ns. The experimental data were fitted with a mono-exponential function. The quenching experiment using CO₂ as quencher was recorded as described above using a CO₂-saturated DMSO solution. The approximated concentration of dissolved CO₂ was calculated from literature data.^[124]

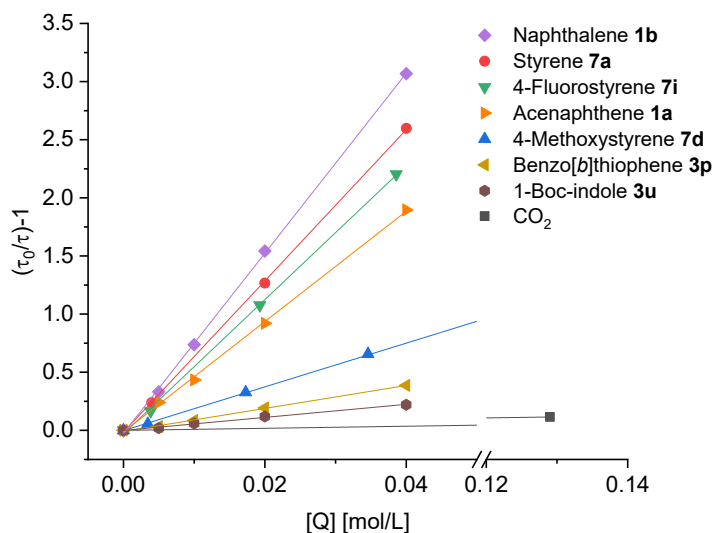


Figure S4-1a. Stern-Volmer plot developed with data obtained from time-resolved quenching experiments of **TMAH** in presence of Cs₂CO₃ with tolerated substrates and a CO₂-saturated solution of DMSO.

Thiophene derivatives **3c**, **e**, **j** are excellent quenchers and are tolerated in the carboxylation reaction whereas benzo[*b*]thiophene (**3p**) was found to quench the excited state of **TMA**^{•−}, however less efficiently. No quenching was observed in presence of thiophene and no carboxylation occurred when thiophene was used as substrate under the optimized reaction conditions (Figure S4-11b). The tested N-heteroarenes containing at least one nitrogen are quenching the excited photocatalyst. However, carboxylation products were only obtained using **3u** (Figure S4-11a) or **3w** (Figure S4-11c). Using acetone **9a** as electrophile instead of CO₂ gave rise to the respective tertiary alcohol **9pa**. Quenching studies revealed that adding acetone (up to 2000 eq. regarding to catalyst concentration) does not quench the photoexcited **TMA**^{•−} (Figure S4-11d), supporting the hypothesis of a nucleophilic arene radical anion which attacks the electrophile.

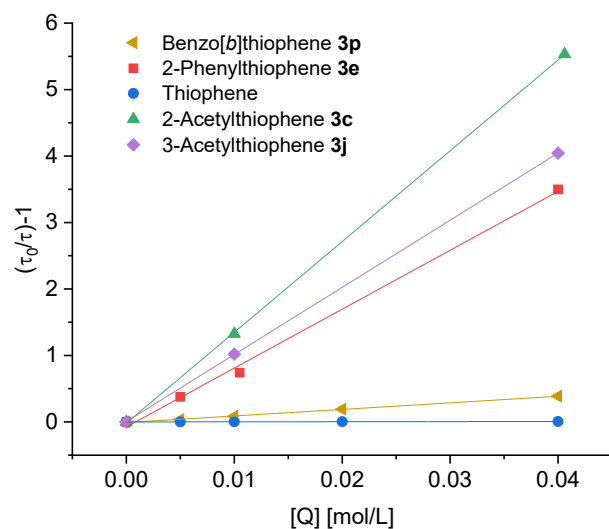


Figure S4-2b. Stern-Volmer plot developed with data obtained from time-resolved quenching experiments of **TMAH** in presence of Cs₂CO₃ with thiophene derivatives. In case of thiophene, no quenching was observed. No carboxylation occurred using thiophene as substrate under the optimized reaction conditions.

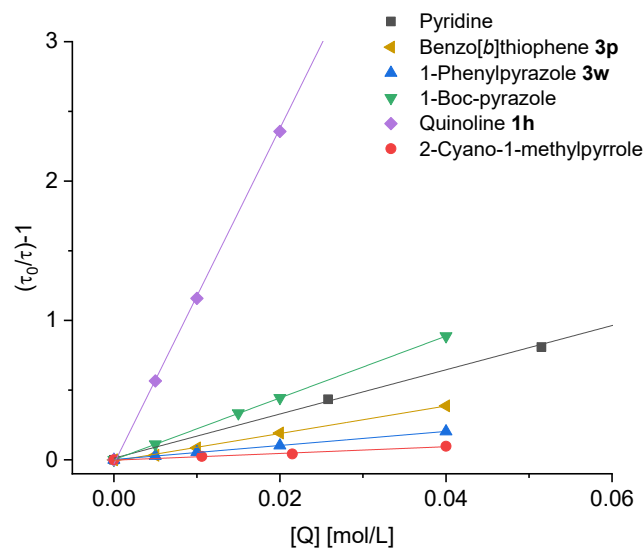


Figure S4-3c. Stern-Volmer plot developed with data obtained from time-resolved quenching experiments of **TMAH** in presence of Cs₂CO₃ with *N*-heteroarenes and benzo[*b*]thiophene as reference.

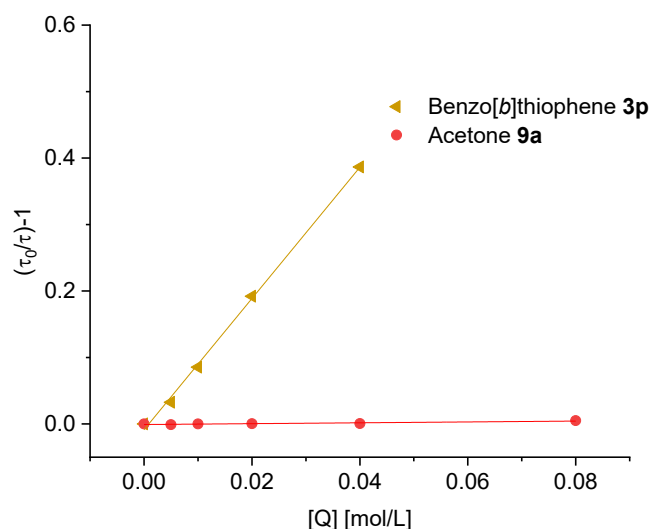


Figure S4-4d. Stern-Volmer plot developed with data obtained from time-resolved quenching experiments of **TMAH** in presence of Cs_2CO_3 with acetone and benzo[*b*]thiophene as reference.

4.4.6.4 Computational Analysis

Screening density functional theory (DFT) calculations were performed on substrates and radical anions to derive molecular and atomic properties that could rationalize the reaction outcomes. Geometries were optimized using the B3LYP-D3^[125] *a posteriori*-corrected hybrid functional^[126] with the LACVP**+ basis set, and final energies and atomic properties were calculated using B3LYP-D3/LACV3P**+ together with the PBF solvation model^[127] for DMSO. The calculations were performed within the Schrödinger Small-Molecule Drug Discovery Suite 2019-2 using Jaguar version 10.4.^[128] To facilitate convergence to a minimum, any apparent symmetry in the starting geometry was ignored in the optimizations (isymm=0). To facilitate SCF convergence for some radical anions the use of the pseudospectral method was turned off during all calculations (nops=1; *J* and *K* operators constructed from analytic two-electron integrals; no grid used). For each substrate and radical anion, Atomic Fukui indices, Mulliken charges and the spin population were calculated. The electron affinity for each substrate was roughly estimated by the direct DFT energy difference between the radical anion and the substrate and are given in kcal·mol⁻¹.

As seen in Figures S4-10-13, there is a strong correlation with reactivity and a positive outcome and calculated atomic descriptors and estimated electron affinities. However, there are also substrates that seem to fall within the acceptable range of estimated electron affinity, atomic charge, spin distribution and nucleophilicity that does not yield the desired products. This could be due to subsequent spontaneous decarboxylation as for **3u** (requiring trapping the carboxyl acid as an ester) or the presence of non-tolerated functional groups. According to the calculations, the regioselectivity is most strongly correlated to the Mulliken spin population.

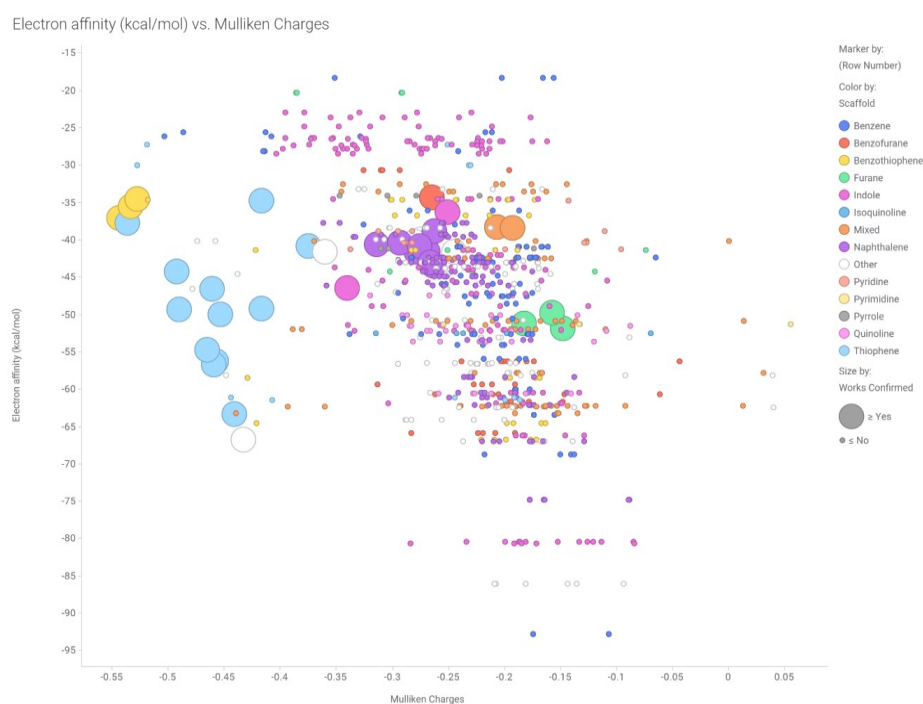


Figure S4-12a. A plot of the DFT estimated electron affinities (kcal mol⁻¹) *vs.* Mulliken charges of the radical anions for the carbons reacting with CO₂ and for all CH carbons in the aromatic rings of non-reacting substrates, highlighting that most of the reactive substrates are located within a triangle. Three reacting furans colored in green are outliers.

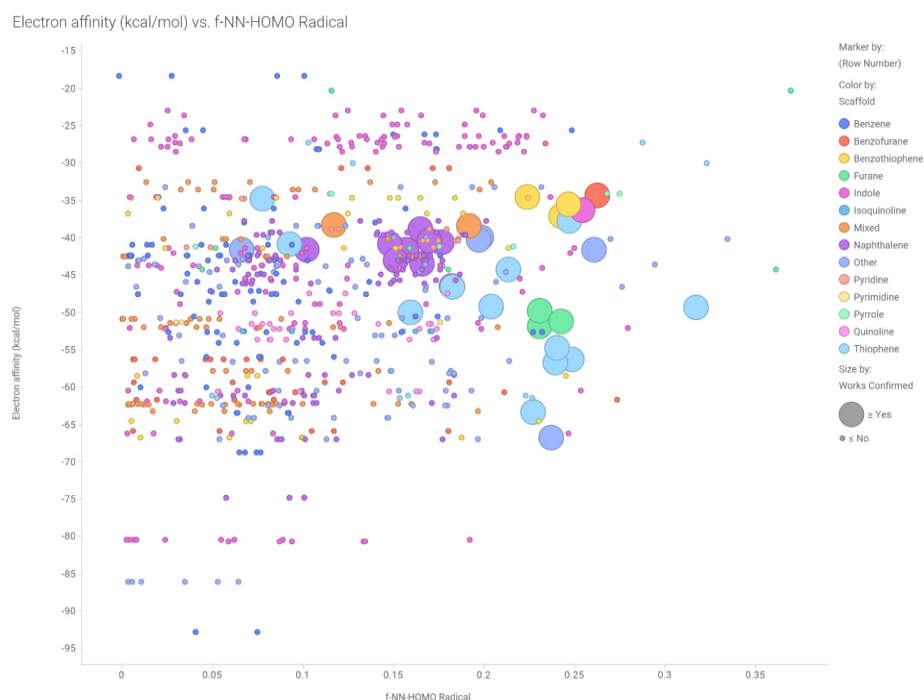


Figure S4-12b. A plot of the DFT estimated electron affinities (kcal mol^{-1}) *vs.* the Fukui f-NN-index (describing nucleophilicity) of the radical anions for the carbons reacting with CO_2 and all CH carbons in the aromatic rings of non-reacting substrates illustrating that most of the reactive substrates have more nucleophilic radical anions.

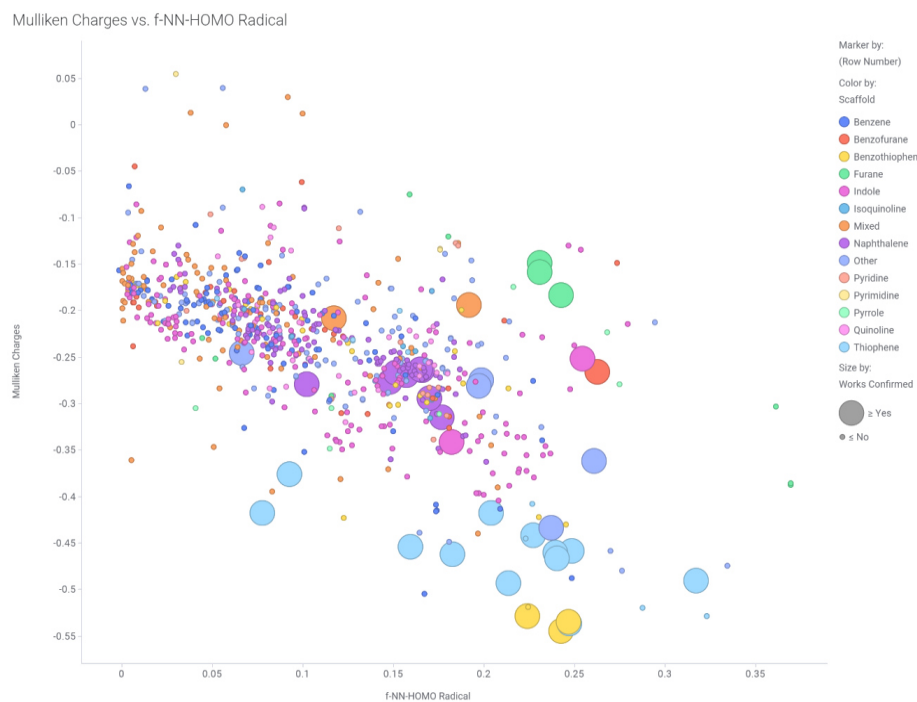


Figure S4-12c. A plot of the DFT Mulliken charges of the radical anions *vs.* Fukui f-NN-index of the radical anions for the carbons reacting with CO_2 and all CH carbons in the aromatic rings of non-reacting substrates illustrating that most of the non-reactive carbons are less negatively charged and have lower predicted nucleophilicity.

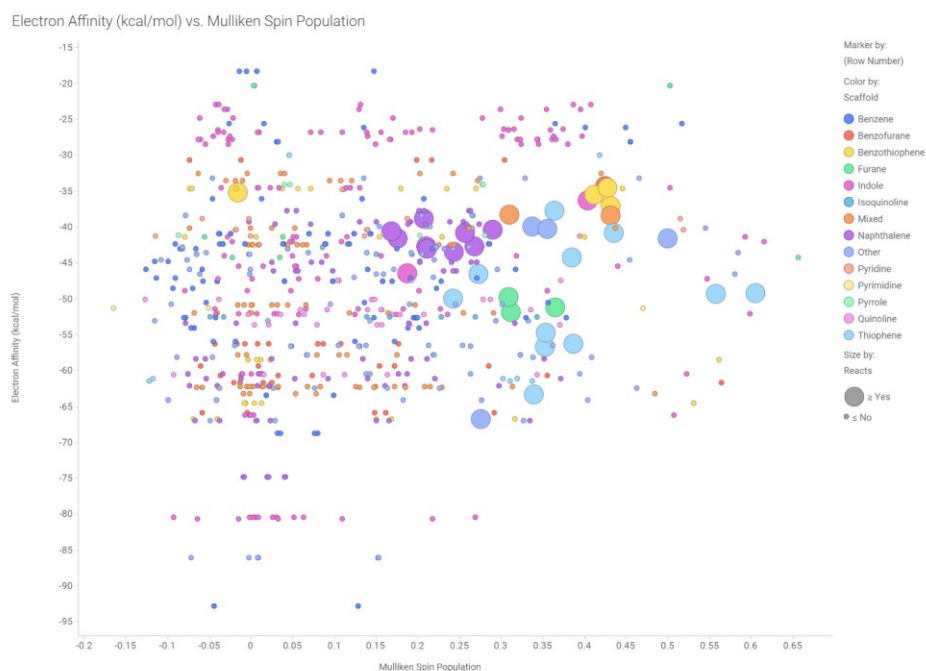
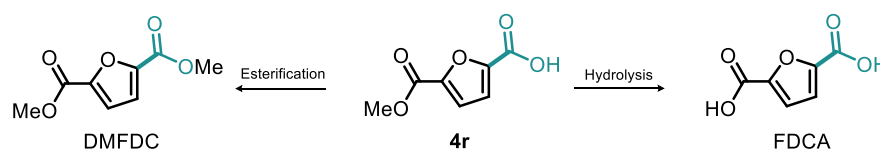


Figure S4-12d. A zoom in plot of the DFT Mulliken charges of the radical anions *vs.* Fukui *f*-NN-index of the radical anions for the carbons reacting with CO₂ and all CH carbons in the aromatic rings of non-reacting substrates including only compounds with DFT estimated electron affinities within the values among the substrates that react. Highlighted are substrates with required electron affinities and nucleophilicity but not reacting due to non-compatible functional groups.

4.4.7 Miscellaneous

4.4.7.1 Synthetic route towards FDCA and DMFDC

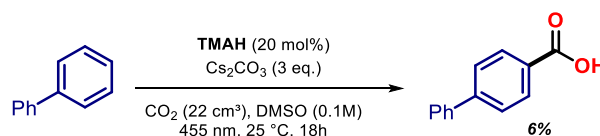
Modifying the conditions during reaction work-up allows for the direct transformation of the crude reaction mixture of **4r** to either 2,5-furandicarboxylic acid (FDCA) or dimethyl 2,5-furandicarboxylate (DMFDC). Both are important monomers for the manufacture of polyesters derived from biomass (Scheme S4). The reaction work-up with conc. HCl would cause the hydrolysis of the ester giving rise to the dicarboxylic acid FDCA. In contrast, the addition of MeI after releasing the CO₂ overpressure allows for the formation of dimethyl dicarboxylate DMFDC.



Scheme S4-4. Synthetic route towards FDCA and DMFDC starting from crude reaction mixture of **4r**.

4.4.7.2 Carboxylation of Biphenyl

Biphenyl acts as a good quencher (see Figure S4-13) but the resulting carboxylation product [1,1'-biphenyl]-4-carboxylic acid was only obtained in low yield (6%). Nevertheless, this result shows that also benzene derivatives can be activated towards a C–H carboxylation with our method. The thermodynamic driving force for this transformation with CO₂ however seems to be low.



Scheme S4-5. TMAH-catalyzed carboxylation reaction of biphenyl.

¹H-NMR (400 MHz, DMSO-*d*₆) δ 12.93 (s, 1H), 8.02 (d, *J* = 8.4 Hz, 2H), 7.80 (d, *J* = 8.4 Hz, 2H), 7.76 – 7.70 (m, 2H), 7.54 – 7.47 (m, 2H), 7.45 – 7.40 (m, 1H). **HRMS** (ESI⁺): calculated *m/z* for C₁₃H₁₁O₂ [(M+H)⁺] 199.0754; found 199.0751.

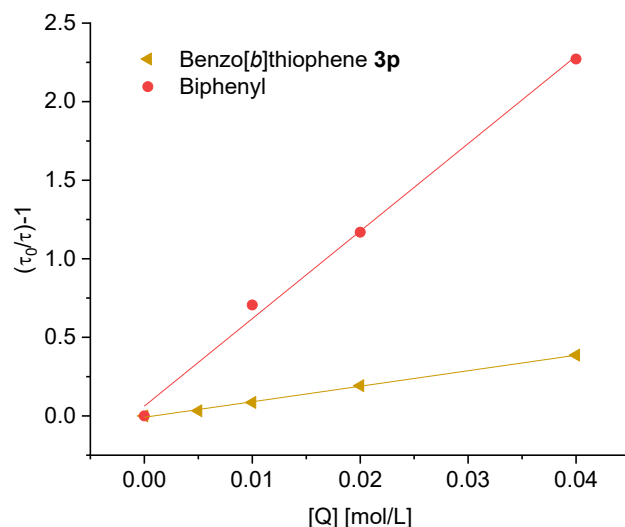


Figure S4-13. Stern-Volmer plot developed with data obtained from time-resolved quenching experiments of **TMAH** in presence of Cs₂CO₃ with biphenyl and benzo[*b*]thiophene **3p** as reference.

4.4.7.3 Unsuccessful Substrates

The following substrates (excerpt of examined scope) were found to be not successful under the reported reaction conditions (Figure S4-14a-c). Structures marked in red do not quench the excited photocatalyst, structures marked in blue were found to quench the excited photocatalyst and structures in black were not tested regarding luminescence quenching.

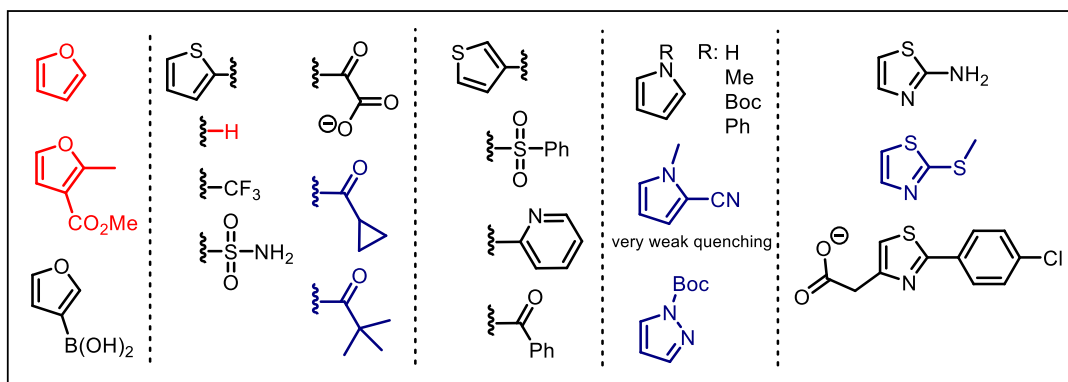


Figure S4-14a. Non-tolerated examined furans, thiophenes, pyrroles and thiazoles.

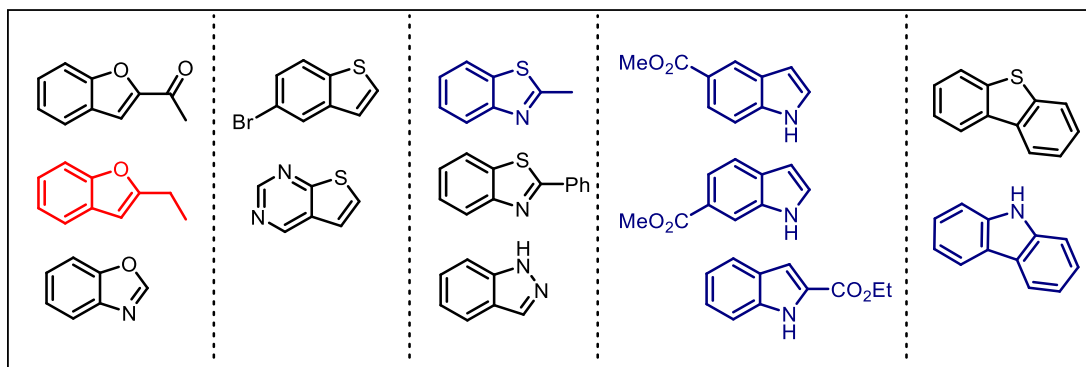


Figure S4-14b. Non-tolerated examined benzofurans, benzothiophenes, indoles, carbazoles and related heterocycles.

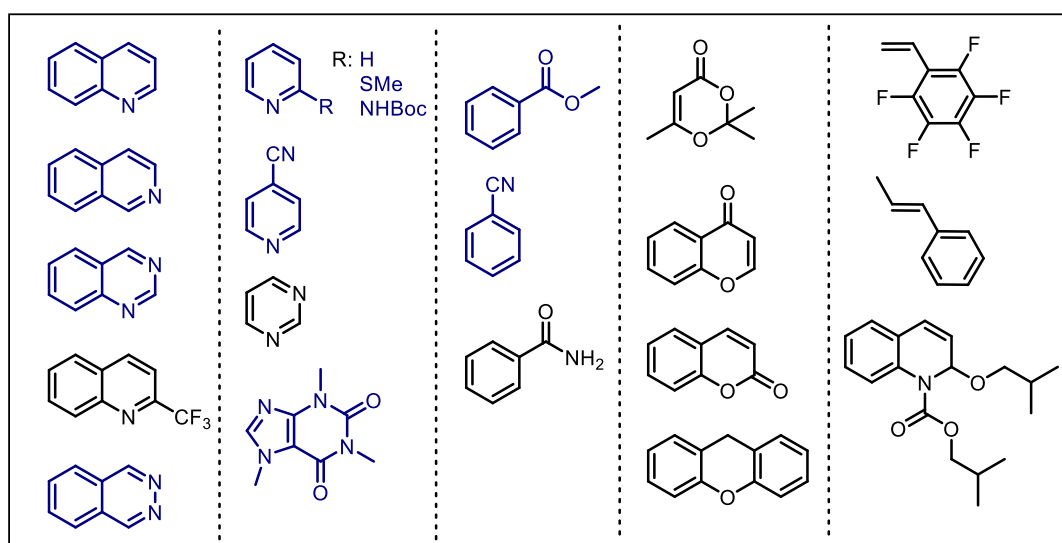


Figure S4-14c. Non-tolerated quinolines, pyridines, benzenes, benzopyrans, styrenes and related compounds.

4.5 References

- [1] H. J. M. Hou, M. M. Najafpour, G. F. Moore, S. I. Allakhverdiev, *Photosynthesis: Structures, Mechanisms, and Applications*, Springer International Publishing, **2017**.
- [2] S. Nitopi, E. Bertheussen, S. B. Scott, X. Liu, A. K. Engstfeld, S. Horch, B. Seger, I. E. L. Stephens, K. Chan, C. Hahn, et al., *Chem. Rev.* **2019**, *119*, 7610–7672.
- [3] R. Küngas, *J. Electrochem. Soc.* **2020**, *167*, 044508.
- [4] D. U. Nielsen, X. M. Hu, K. Daasbjerg, T. Skrydstrup, *Nat. Catal.* **2018**, *1*, 244–254.
- [5] Q. Liu, L. Wu, R. Jackstell, M. Beller, *Nat. Commun.* **2015**, *6*, 5933.
- [6] A. Correa, R. Martín, *Angew. Chem. Int. Ed.* **2009**, *48*, 6201–6204.
- [7] A. Correa, R. Martín, *J. Am. Chem. Soc.* **2009**, *131*, 15974–15975.
- [8] H. Tran-Vu, O. Daugulis, *ACS Catal.* **2013**, *3*, 2417–2420.
- [9] K. Nogi, Y. Tsuji, J. Terao, T. Xu, T. Fujihara, *J. Am. Chem. Soc.* **2012**, *134*, 9106–9109.
- [10] Y. Liu, J. Cornella, R. Martin, *J. Am. Chem. Soc.* **2014**, *136*, 11212–11215.
- [11] A. Correa, T. León, R. Martin, *J. Am. Chem. Soc.* **2014**, *136*, 1062–1069.
- [12] T. Moragas, J. Cornella, R. Martin, *J. Am. Chem. Soc.* **2014**, *136*, 17702–17705.
- [13] T. Mita, Y. Higuchi, Y. Sato, *Chem. Eur. J.* **2015**, *21*, 16391–16394.
- [14] T. Moragas, M. Gaydou, R. Martin, *Angew. Chem. Int. Ed.* **2016**, *55*, 5053–5057.
- [15] T. Yanagi, R. J. Somerville, K. Nogi, R. Martin, H. Yorimitsu, *ACS Catal.* **2020**, *10*, 2117–2123.
- [16] M. Gaydou, T. Moragas, F. Juliá-Hernández, R. Martin, *J. Am. Chem. Soc.* **2017**, *139*, 12161–12164.
- [17] K. Michigami, T. Mita, Y. Sato, *J. Am. Chem. Soc.* **2017**, *139*, 6094–6097.
- [18] C. M. Williams, J. B. Johnson, T. Rovis, *J. Am. Chem. Soc.* **2008**, *130*, 14936–14937.
- [19] A. Tortajada, R. Ninokata, R. Martin, *J. Am. Chem. Soc.* **2018**, *140*, 2050–2053.
- [20] N. Huguet, I. Jevtovikj, A. Gordillo, M. L. Lejkowski, R. Lindner, M. Bru, A. Y. Khalimon, F. Rominger, S. A. Schunk, P. Hofmann, et al., *Chem. Eur. J.* **2014**, *20*, 16858–16862.
- [21] Y. Yang, J. W. Lee, *Chem. Sci.* **2019**, *10*, 3905–3926.
- [22] A. Alkayal, V. Tabas, S. Montanaro, I. A. Wright, A. V. Malkov, B. R. Buckley, *J. Am. Chem. Soc.* **2020**, *142*, 1780–1785.
- [23] N. W. J. Ang, J. C. A. de Oliveira, L. Ackermann, *Angew. Chem. Int. Ed.* **2020**, doi.org/10.1002/anie.202003218.
- [24] J.-H. Ye, M. Miao, H. Huang, S.-S. Yan, Z.-B. Yin, W.-J. Zhou, D.-G. Yu, *Angew. Chem. Int. Ed.* **2017**, *56*, 15416–15420.
- [25] H. Wang, C. Zhou, G. Li, H. Wang, Y. Gao, C. Zhou, G. Li, *J. Am. Chem. Soc.* **2020**, *142*, 8122–8129.
- [26] V. R. Yatham, Y. Shen, R. Martin, *Angew. Chem. Int. Ed.* **2017**, *56*, 10915–10919.
- [27] J. Hou, A. Ee, H. Cao, H.-W. Ong, J.-H. Xu, J. Wu, *Angew. Chem. Int. Ed.* **2018**, *57*, 17220–17224.
- [28] Q. Fu, Z. Y. Bo, J. H. Ye, T. Ju, H. Huang, L. L. Liao, D. G. Yu, *Nat. Commun.* **2019**, *10*, 1–9.
- [29] J. Luo, S. Preciado, P. Xie, I. Larrosa, *Chem. Eur. J.* **2016**, *22*, 6798–6802.
- [30] W. J. Yoo, M. G. Capdevila, X. Du, S. Kobayashi, *Org. Lett.* **2012**, *14*, 5326–5329.
- [31] M. Shigeno, K. Hanasaka, K. Sasaki, K. Nozawa-Kumada, Y. Kondo, *Chem. Eur. J.* **2019**, *25*, 3235–3239.
- [32] Y. Suzuki, T. Hattori, T. Okuzawa, S. Miyano, *Chem. Lett.* **2002**, 102–103.
- [33] K. Nemoto, H. Yoshida, Y. Suzuki, N. Morohashi, T. Hattori, *Chem. Lett.* **2006**, *35*, 820–821.

- [34] K. Nemoto, H. Yoshida, N. Egusa, N. Morohashi, T. Hattori, *J. Org. Chem.* **2010**, *75*, 7855–7862.
- [35] G. A. Olah, B. Török, J. P. Joschek, I. Bucsí, P. M. Esteves, G. Rasul, G. K. S. Prakash, *J. Am. Chem. Soc.* **2002**, *124*, 11379–11391.
- [36] K. Nemoto, S. Onozawa, N. Egusa, N. Morohashi, T. Hattori, *Tetrahedron Lett.* **2009**, *50*, 4512–4514.
- [37] K. Nemoto, S. Onozawa, M. Konno, N. Morohashi, T. Hattori, *Bull. Chem. Soc. Jpn.* **2012**, *85*, 369–371.
- [38] S. Tanaka, K. Watanabe, Y. Tanaka, T. Hattori, *Org. Lett.* **2016**, *18*, 2576–2579.
- [39] I. I. F. Boogaerts, G. C. Fortman, M. R. L. Furst, C. S. J. Cazin, S. P. Nolan, *Angew. Chem. Int. Ed.* **2010**, *49*, 8674–8677.
- [40] L. Zhang, J. Cheng, T. Ohishi, Z. Hou, *Angew. Chem. Int. Ed.* **2010**, *49*, 8670–8673.
- [41] T. Suga, H. Mizuno, J. Takaya, N. Iwasawa, *Chem. Commun.* **2014**, *50*, 14360–14363.
- [42] J. Hong, M. Li, J. Zhang, B. Sun, F. Mo, *ChemSusChem* **2019**, *12*, 6–39.
- [43] A. Banerjee, G. R. Dick, T. Yoshino, M. W. Kanan, *Nature* **2016**, *531*, 215–219.
- [44] K. Kudo, M. Shima, Y. Kume, F. Ikoma, S. Mori, N. Sugita, *J. Jpn. Petrol. Inst.* **1995**, *38*, 40–47.
- [45] K. Shimomaki, K. Murata, R. Martin, N. Iwasawa, *J. Am. Chem. Soc.* **2017**, *139*, 9467–9470.
- [46] Q.-Y. Meng, S. Wang, B. König, *Angew. Chem. Int. Ed.* **2017**, *56*, 13426–13430.
- [47] J. Hou, A. Ee, W. Feng, J. H. Xu, Y. Zhao, J. Wu, *J. Am. Chem. Soc.* **2018**, *140*, 5257–5263.
- [48] Q. Y. Meng, S. Wang, G. S. Huff, B. König, *J. Am. Chem. Soc.* **2018**, *140*, 3198–3201.
- [49] K. Murata, N. Numasawa, K. Shimomaki, J. Takaya, N. Iwasawa, *Chem. Commun.* **2017**, *53*, 3098–3101.
- [50] Q.-Y. Meng, T. E. Schirmer, A. L. Berger, K. Donabauer, B. König, *J. Am. Chem. Soc.* **2019**, *141*, 11393–11397.
- [51] H. Tagaya, M. Onuki, Y. Tomioka, Y. Wada, M. Karasu, K. Chiba, *Bull. Chem. Soc. Jpn.* **1990**, *63*, 3233–3237.
- [52] M. Minabe, K. Isozumi, K. Kawai, M. Yoshida, *Bull. Chem. Soc. Jpn.* **1988**, *61*, 2063–2066.
- [53] H. Seo, A. Liu, T. F. Jamison, *J. Am. Chem. Soc.* **2017**, *139*, 13969–13972.
- [54] N. Ishida, Y. Masuda, S. Uemoto, M. Murakami, *Chem. Eur. J.* **2016**, *22*, 6524–6527.
- [55] N. Ishida, Y. Masuda, Y. Imamura, K. Yamazaki, M. Murakami, *J. Am. Chem. Soc.* **2020**, *141*, 19611–19615.
- [56] M. Schmalzbauer, I. Ghosh, B. König, *Faraday Discuss.* **2019**, *215*, 364–378.
- [57] I. Mutule, E. Suna, *Tetrahedron* **2005**, *61*, 11168–11176.
- [58] A. S. Hussey, *J. Am. Chem. Soc.* **1951**, *73*, 1364–1365.
- [59] A. Nagaki, Y. Takahashi, J. Yoshida, *Chem. Eur. J.* **2014**, *20*, 7931–7934.
- [60] A. Polyzos, M. O’Brien, T. P. Petersen, I. R. Baxendale, S. V. Ley, *Angew. Chem. Int. Ed.* **2011**, *50*, 1190–1193.
- [61] N. L. Holy, *Chem. Rev.* **1974**, *74*, 243–277.
- [62] W. Schlenk, E. Bergmann, *Justus Liebigs Ann. Chem.* **1928**, *463*, 1–97.
- [63] J. F. Walker, N. D. Scott, *J. Am. Chem. Soc.* **1938**, *60*, 951–955.
- [64] A. Gennaro, A. A. Isse, E. Vianello, *J. Electroanal. Chem.* **1990**, *289*, 203–215.
- [65] M. Montalti, A. Credi, L. Prodi, M. T. Gandolfi, *Handbook of Photochemistry 3rd ed.*, CRC Press, Boca Raton, **2006**.
- [66] S. Mahboobi, S. Dove, A. Sellmer, M. Winkler, E. Eichhorn, H. Pongratz, T. Ciossek, T. Baer, T. Maier, T. Beckers, *J. Med. Chem.* **2009**, *52*, 2265–2279.

- [67] Y. Hara, E. Sato, A. Miyagishi, A. Aisaka, T. Hibino, *J. Pharm. Sci.* **1978**, *67*, 1334–1335.
- [68] H. Liu, H. Tang, D. Yang, Q. Ji, *Chinese J. Pharm.* **2011**, *42*, 641–644.
- [69] H. W. Gschwend, H. R. Rodriguez, „Heteroatom-Facilitated Lithiations“, *Org. React.*, **1979**, *26*, 1–360.
- [70] P. W. Alley, D. A. Shirley, *J. Am. Chem. Soc.* **1958**, *80*, 6271–6274.
- [71] A. Marxer, M. Siegrist, *Helv. Chim. Acta* **1974**, *57*, 1988–2000.
- [72] M. B. Banella, J. Bonucci, M. Vannini, P. Marchese, C. Lorenzetti, A. Celli, *Ind. Eng. Chem. Res.* **2019**, *58*, 8955–8962.
- [73] A. F. Sousa, C. Vilela, A. C. Fonseca, M. Matos, C. S. R. Freire, G. J. M. Gruter, J. F. J. Coelho, A. J. D. Silvestre, *Polym. Chem.* **2015**, *6*, 5961–5983.
- [74] J.-P. Lange, E. van der Heide, J. van Buijtenen, R. Price, *ChemSusChem* **2012**, *5*, 150–166.
- [75] A. Cho, S. Byun, J. H. Cho, B. M. Kim, *ChemSusChem* **2019**, *12*, 2310–2317.
- [76] H. Zhou, S. Hong, H. Zhang, Y. Chen, H. Xu, X. Wang, Z. Jiang, S. Chen, Y. Liu, *Appl. Catal. B-Environ.* **2019**, *256*, 117767.
- [77] A. C. Fonseca, M. S. Lima, A. F. Sousa, A. J. Silvestre, J. F. J. Coelho, A. C. Serra, *Polym. Chem.* **2019**, *10*, 1696–1723.
- [78] A. Gunia-Krzyżak, K. Słoczyńska, J. Popiół, P. Koczurkiewicz, H. Marona, E. Pękala, *Int. J. Cosmet. Sci.* **2018**, *40*, 356–366.
- [79] H. Seo, M. H. Katcher, T. F. Jamison, *Nat. Chem.* **2017**, *9*, 453–456.
- [80] E. Lamy, L. Nadjo, J. M. Saveant, *J. Electroanal. Chem.* **1977**, *78*, 403–407.
- [81] Q. Xia, J. Dong, H. Song, Q. Wang, *Chem. Eur. J.* **2018**, *25*, 2949–2961.
- [82] T. Fuchigami, S. Inagi, M. Atobe, „Appendix B“ in *Fundamentals and Applications of Organic Electrochemistry*, John Wiley & Sons Ltd, Chichester, **2014**, pp. 217–222.
- [83] M. Raghu, J. Grover, S. S. V. Ramasastry, *Chem. Eur. J.* **2016**, *22*, 18316–18321.
- [84] A. Müller, M. Raltschewa, M. Papp, *Ber. Dtsch. Chem. Ges. A* **1942**, *75*, 692–703.
- [85] P. Stewart, C. M. Renney, T. J. Mooibroek, S. Ferheen, A. P. Davis, *Chem. Commun.* **2018**, *54*, 8649–8652.
- [86] Q. Miao, T.-Q. Nguyen, T. Someya, G. B. Blanchet, C. Nuckolls, *J. Am. Chem. Soc.* **2003**, *125*, 10284–10287.
- [87] F. Keller, C. Rüchardt, *J. prakt. Chem.* **1998**, *340*, 642–648.
- [88] V. V. Pavlishchuk, A. W. Addison, *Inorganica Chim. Acta* **2000**, *298*, 97–102.
- [89] N. A. Romero, D. A. Nicewicz, *Chem. Rev.* **2016**, *116*, 10075–10166.
- [90] D. Rehm, A. Weller, *Isr. J. Chem.* **1970**, *8*, 259–271.
- [91] L. M. Tolbert, S. M. Nesselroth, T. L. Netzel, N. Raya, M. Stapleton, *J. Phys. Chem.* **1992**, *96*, 4492–4496.
- [92] B. Legros, P. Vandereecken, J. P. Soumillion, *J. Phys. Chem.* **1991**, *95*, 4752–4761.
- [93] S. Vásquez-Céspedes, K. M. Chepiga, N. Möller, A. H. Schäfer, F. Glorius, *ACS Catal.* **2016**, *6*, 5954–5961.
- [94] X. Yu, E.-J. Park, T. P. Kondratyuk, J. M. Pezzuto, D. Sun, *Org. Biomol. Chem.* **2012**, *10*, 8835.
- [95] E. H. Discekici, N. J. Treat, S. O. Poelma, K. M. Mattson, Z. M. Hudson, Y. Luo, C. J. Hawker, J. R. de Alaniz, *Chem. Commun.* **2015**, *51*, 11705–11708.
- [96] S. Yamada, K. N. Flesch, K. Murakami, K. Itami, *Org. Lett.* **2020**, *22*, 1547–1551.
- [97] J. Pospech, A. Tlili, A. Spannenberg, H. Neumann, M. Beller, *Chem. Eur. J.* **2014**, *20*, 3135–3141.
- [98] F. Mäsing, A. Mardyukov, C. Doerenkamp, H. Eckert, U. Malkus, H. Nüsse, J. Klingauf, A. Studer, *Angew. Chem. Int. Ed.* **2015**, *54*, 12612–12617.

- [99] X. Chen, Y. Yin, K. Tanaka, H. Kita, K.-I. Okamoto, *High Perform. Polym.* **2006**, *18*, 637–654.
- [100] X. Zhang, W. Z. Zhang, L. L. Shi, C. X. Guo, L. L. Zhang, X. B. Lu, *Chem. Commun.* **2012**, *48*, 6292–6294.
- [101] A. I. Meyers, K. Higashiyama, *J. Org. Chem.* **1987**, *52*, 4592–4597.
- [102] P. Berger, A. Bessmertnykh, J. C. Caille, S. Mignonac, *Synthesis* **2006**, *2006*, 3106–3110.
- [103] K. Nemoto, H. Yoshida, N. Egusa, N. Morohashi, T. Hattori, *J. Org. Chem.* **2010**, *75*, 7855–7862.
- [104] S. Mori, D. Simkhada, H. Zhang, M. S. Erb, Y. Zhang, H. Williams, D. Fedoseyenko, W. K. Russell, D. Kim, N. Fleer, et al., *Biochemistry* **2016**, *55*, 704–714.
- [105] K. A. Suerbaev, M. K. Aldabergenov, N. Z. Kudaibergenov, *Green Process. Synth.* **2015**, *4*, 91–96.
- [106] S. Wang, L. Dupin, M. Noël, C. J. Carroux, L. Renaud, T. Géhin, A. Meyer, E. Souteyrand, J.-J. Vasseur, G. Vergoten, et al., *Chem. Eur. J.* **2016**, *22*, 11785–11794.
- [107] M. Abarbri, J. Thibonnet, L. Bérillon, F. Dehmel, M. Rottländer, P. Knochel, *J. Org. Chem.* **2000**, *65*, 4618–4634.
- [108] J. M. Chalker, C. S. C. Wood, B. G. Davis, *J. Am. Chem. Soc.* **2009**, *131*, 16346–16347.
- [109] J. A. Kaizerman, M. I. Gross, Y. Ge, S. White, W. Hu, J. X. Duan, E. E. Baird, K. W. Johnson, R. D. Tanaka, H. E. Moser, et al., *J. Med. Chem.* **2003**, *46*, 3914–3929.
- [110] J. J. Dai, W. T. Xu, Y. D. Wu, W. M. Zhang, Y. Gong, X. P. He, X. Q. Zhang, H. J. Xu, *J. Org. Chem.* **2015**, *80*, 911–919.
- [111] A. F. M. Kilbinger, A. P. H. J. Schenning, F. Goldoni, W. J. Feast, E. W. Meijer, *J. Am. Chem. Soc.* **2000**, *122*, 1820–1821.
- [112] S. Hagishita, M. Yamada, K. Shirahase, T. Okada, Y. Murakami, Y. Ito, T. Matsuura, M. Wada, T. Kato, M. Ueno, et al., *J. Med. Chem.* **1996**, *39*, 3636–3658.
- [113] M. Frizler, J. Schmitz, A. C. Schulz-Fincke, M. Gütschow, *J. Med. Chem.* **2012**, *55*, 5982–5986.
- [114] J. Podlesný, O. Pytela, M. Klikar, V. Jelínková, I. V. Kityk, K. Ozga, J. Jedryka, M. Rudysh, F. Bureš, *Org. Biomol. Chem.* **2019**, *17*, 3623–3634.
- [115] S. E. Baillie, T. D. Bluemke, W. Clegg, A. R. Kennedy, J. Klett, L. Russo, M. De Tullio, E. Hevia, *Chem. Commun.* **2014**, *50*, 12859–12862.
- [116] R. Shang, L. Ilies, E. Nakamura, *J. Am. Chem. Soc.* **2016**, *138*, 10132–10135.
- [117] K. Paridala, S. M. Lu, M. M. Wang, C. Li, *Chem. Commun.* **2018**, *54*, 11574–11577.
- [118] K. Kubota, K. Hayama, H. Iwamoto, H. Ito, *Angew. Chem. Int. Ed.* **2015**, *54*, 8809–8813.
- [119] J. Magalhães, N. Franko, G. Annunziato, M. Welch, S. K. Dolan, A. Bruno, A. Mozzarelli, S. Armao, A. Jirgensons, M. Pieroni, et al., *J. Enzym. Inhib. Med. Chem.* **2018**, *33*, 1444–1452.
- [120] L. Bettinetti, K. Schlotter, H. Hübner, P. Gmeiner, *J. Med. Chem.* **2002**, *45*, 4594–4597.
- [121] J. Takaya, S. Tadami, K. Ukai, N. Iwasawa, *Org. Lett.* **2008**, *10*, 2697–2700.
- [122] K. Nogi, T. Fujihara, J. Terao, Y. Tsuji, *J. Org. Chem.* **2015**, *80*, 11618–11623.
- [123] R. Liu, Z. Yang, Y. Ni, K. Song, K. Shen, S. Lin, Q. Pan, *J. Org. Chem.* **2017**, *82*, 8023–8030.
- [124] P. Fogg, G.T., in *IUPAC Solubility Data Ser. 50* (Eds.: J.W. Lorimer, H.L. Clever, C.L. Young), Pergamon, Oxford, **1992**, p. 362.
- [125] S. Grimme, J. Antony, S. Ehrlich, H. Krieg, *J. Chem. Phys.* **2010**, *132*, 154104.
- [126] A. D. Becke, *J. Chem. Phys.* **1993**, *98*, 5648–5652.
- [127] B. Marten, K. Kim, C. Cortis, R. A. Friesner, R. B. Murphy, M. N. Ringnalda, D. Sitkoff, B. Honig, *J. Phys. Chem.* **1996**, *100*, 11775–11788.

- [128] A. D. Bochevarov, E. Harder, T. F. Hughes, J. R. Greenwood, D. A. Braden, D. M. Philipp, D. Rinaldo, M. D. Halls, J. Zhang, R. A. Friesner, *Int. J. Quantum Chem.* **2013**, *113*, 2110–2142.

SUMMARY

5 Summary

Current efforts to slow down the ongoing climate change and the looming end of fossil fuels inevitably confronts our society with major challenges and requires to rethink the way of dealing with our limited resources towards a more responsible and sustainable usage. In this regard, it is highly desirable from a chemical point of view to develop new methods which allow to increase the reaction efficiency and atom economy while lowering the activation energy for a chemical transformation. Engineering a versatile catalytic system allows to address all aspects at once. Thus, the ever-growing field of organic photoredox catalysis harbors great potential to meet the demands for a more sustainable and resource-saving chemical processing.

This thesis presents various novel catalytic approaches to functionalize sp^2 -carbon centers *via* photoinduced single electron transfer events under mild and transition-metal-free conditions. Readily available organic anthracene derivatives were developed as a new class of cheap, sustainable and versatile photocatalysts and non-toxic DMSO was used as reaction media. Upon irradiation with visible-light, the *in-situ* formed open- or closed-shell excited anions of the examined catalysts reach remarkably negative electrochemical potentials which enabled the conversion of challenging substrates. Spectroscopic and electrochemical studies were examined to fully characterize the features of the herein discussed anthraquinone and anthrone derivatives and to get insights into the underlying reaction mechanisms.

Chapter 1 summarizes the main spectroscopic and electrochemical properties of anionic compounds and their influence on photoinduced electron transfer reactions. Further, it provides an overview of selected organic transformations utilizing the versatile chemistry of excited state anions. Based on the corresponding literature reports, the proposed mechanisms are discussed. The use of organic anions as cheap and sustainable photocatalysts holds enormous potential for applications in synthetic organic chemistry and an increasing interest applying photoexcited anions in synthesis can be pursued.

The photochemistry of natural occurring anthraquinone derivatives is presented in **Chapter 2**. Visible-light excitation of 1,8-dihydroxyanthraquinone in presence of a sacrificial amine generates the colored radical anion and semiquinone anion *via* photoinduced electron transfer processes. A subsequent excitation of such species accumulates sufficient redox-energy to activate the carbon-halogen bond of (hetero)aryl halides. The concept was demonstrated in various aromatic dehalogenation and C–C bond-forming reactions with

(hetero)arenes as coupling partners. Based on spectroscopic investigations a conceivable mechanism is proposed.

Chapter 3 deals with the photochemistry of 9-anthrone and closely related derivatives in alkaline media. Upon deprotonation in presence of carbonates, the formed anionic tricyclic aromatic ketones exhibit a significant bathochromic shift in their absorption spectra enabling photoexcitation with visible light. Exceptionally strong reducing abilities from the excited states of these species were found, which allowed for their application in demanding reductive transformations of (hetero)aryl chlorides *via* photoinduced electron transfer. The corresponding C–H arylation or coupling products were obtained in moderate to excellent yield while the reaction operates under very mild conditions and without the addition of any sacrificial electron donor. A rational design of the catalyst scaffold allowed to fine-tune the redox-properties.

A mild, direct and transition-metal-free insertion of carbon dioxide into non-prefunctionalized C–H bonds under redox-neutral, catalytic conditions is a highly desirable process and is discussed in **Chapter 4**. The high thermodynamic stability and kinetic inertness of CO₂ hamper its use as C1 building block in organic synthesis and previously reported methods often rely on the use of stoichiometric reducing agents or highly activated reaction partners. Bearing four methoxy groups, an electron rich 9-anthrolate derived photocatalyst was used to generate radical anions of (hetero)arenes and styrenes upon visible-light excitation. The formed nucleophilic radical anions react in presence of CO₂ to provide (hetero)aromatic carboxylic- and cinnamic acids. A reaction performed on gram-scale demonstrated the scalability of this carboxylation method, while ketones are tolerated as alternative electrophiles to CO₂ yielding tertiary alcohols. Using a new mechanistic manifold, the methodology presents a straightforward, sustainable and atom-efficient alternative to current approaches and paves the way to develop novel applications of CO₂ in chemical synthesis.

ZUSAMMENFASSUNG

6 Zusammenfassung

Die aktuellen Bestrebungen den voranschreitenden globalen Klimawandel zu verlangsamen sowie die zur Neige gehenden Vorräte an fossilen Brennstoffen stellen unsere Gesellschaft zwangsläufig vor große Herausforderungen und ein Umdenken im Umgang mit unseren beschränkten Ressourcen zugunsten eines verantwortungsbewussteren und nachhaltigeren Gebrauchs ist erforderlich. In diesem Zusammenhang ist die Entwicklung neuer, noch effizienterer Methoden, mit verbesserter Atomökonomie bei gleichzeitiger Verringerung der Aktivierungsenergie für Reaktionen, aus chemischer Sicht äußerst wünschenswert. All die genannten Aspekte können durch die Entwicklung eines ausgeklügelten, katalytischen Systems simultan adressiert werden. Auf dem Weg hin zu nachhaltigeren und ressourcenschonenderen chemischen Prozessen wird dem ständig wachsenden Gebiet der Photo-Redox-Katalyse dabei ein großes Potential zugesprochen.

Im Zuge dieser Arbeit werden verschiedene neue, katalytische Herangehensweisen vorgestellt, die eine Funktionalisierung von sp^2 -Kohlenstoff Zentren durch photoinduzierte Elektronentransferreaktionen unter milden und metallfreien Reaktionsbedingungen ermöglichen. Dabei wurde eine neue Klasse von organischen Photokatalysatoren basierend auf den Derivaten des Anthracens entwickelt, die sich aufgrund geringer Kosten und ihrer Vielseitigkeit auszeichnen. Als Reaktionsmedium wurde das vergleichsweise unbedenkliche DMSO verwendet. Nach Anregung mit sichtbarem Licht weisen die *in-situ* gebildeten Radikalanionen und Anionen der untersuchten Katalysatoren ein bemerkenswert starkes negatives elektrochemisches Potential auf, das die Umsetzung von schwierigen Substraten ermöglichte. Spektroskopische sowie elektrochemische Untersuchungen wurden durchgeführt um die Eigenschaften der in dieser Arbeit diskutierten Anthrachinon- und Anthron-Derivate zu bestimmen und somit Einblicke in die zugrundeliegenden Reaktionsmechanismen zu erhalten.

In **Kapitel 1** sind die grundlegenden spektroskopischen und elektrochemischen Eigenschaften von anionischen Verbindungen und deren Einflüsse auf photoinduzierte Elektronentransferreaktionen zusammengefasst. Darüber hinaus werden ausgewählte organische Umsetzungen, basierend auf der facettenreichen Chemie von angeregten Anionen, überblicksweise dargestellt. Die Diskussion der aufgeführten Reaktionsmechanismen wurde an Hand der angegebenen Literatur geführt. Der Einsatz von organischen Anionen als

günstige und nachhaltige Photokatalysatoren birgt großes Potential für Anwendungen in der organischen Synthese und stößt auf zunehmendes Interesse.

Kapitel 2 präsentiert die Photochemie von natürlich vorkommenden Anthrachinon-Derivaten. Die Anregung von 1,8-Dihydroxyanthrachinon mit sichtbarem Licht in Gegenwart von Aminen als Elektronendonatoren führt zur photochemischen Umsetzung in das farbige Radikalanion und Semichinon-Anion. Eine erneute Anregung dieser Spezies reichert genügend Redox-Energie an um aromatische Kohlenstoff-Halogen Bindungen zu aktivieren. Dieses Konzept wurde an Hand von aromatischen Dehalogenierungsreaktionen und in Gegenwart von (Hetero)aromaten unter Ausbildung einer neuen Kohlenstoff-Kohlenstoff Bindung demonstriert. Basierend auf den durchgeführten spektroskopischen Untersuchungen wurde ein denkbarer Reaktionsmechanismus vorgeschlagen.

Kapitel 3 befasst sich mit der Photochemie von 9-Anthron und verwandten Derivaten im alkalischen Medium. Die Deprotonierung der dreigliedrigen Ketone in Gegenwart von Carbonaten verursacht eine bathochrome Verschiebung der Absorptionsspektren die eine Anregung mit sichtbarem Licht ermöglicht. Ausgehend von ihren angeregten Zuständen weisen diese Spezies eine außergewöhnlich starke Reduktionskraft auf, welche die schwierige Umsetzung von chlorierten (Hetero)aromaten durch photoinduzierten Elektronentransfer erlaubt. Die resultierenden C-H Arylierungs- sowie Kupplungsprodukte konnten in angemessen bis hin zu ausgezeichneten Ausbeuten isoliert werden. Darüber hinaus verläuft die Reaktion unter besonders milden Bedingungen wobei der sonst übliche Zusatz eines Elektronendonators nicht nötig war. Zudem war eine Feinabstimmung der Redox-Eigenschaften durch Modifikationen am Gerüst des Katalysators möglich.

Die schonende, direkte Insertion von Kohlendioxid in eine, zu diesem Zweck nicht vorab funktionalisierte, C-H Bindung unter redox-neutralen, katalytischen Bedingungen und ohne den Einsatz von Übergangsmetallen, beschreibt einen äußerst attraktiven Prozess der in **Kapitel 4** diskutiert wird. CO₂ besitzt eine hohe thermodynamische Stabilität und reagiert daher sehr träge, was den Einsatz als C1 Baustein in der organischen Synthese erschwert. Daher nutzen viele Methoden stöchiometrische Mengen an Reduktionsmittel oder hochreaktiven Verbindungen als Reaktionspartner. Das mit vier Methoxygruppen ausgestattete, elektronenreiche Derivat des 9-Anthrolats wurde als Photokatalysator, zur Bildung der Radikalanionen von (Hetero)aromaten und Styrol Derivate unter Einsatz von sichtbarem Licht, genutzt. In Gegenwart von CO₂ reagieren die gebildeten nukleophilen

Radikalanionen und die entsprechenden (Hetero)aromatischen Carbonsäuren und Zimtsäure Derivate konnten isoliert werden. Die erfolgreiche Durchführung eines Gramm-Ansatzes weist auf eine unkomplizierte Vergrößerung des Reaktionsmaßstabs hin. Des Weiteren konnte gezeigt werden, dass neben CO_2 auch Ketone als Elektrophile toleriert werden und die entsprechenden tertiären Alkohole liefern. Basierend auf einem neuen mechanistischen Ansatz, stellt die präsentierte Methode eine unkomplizierte, nachhaltige und atomökonomische Alternative zu aktuellen Herangehensweisen dar und ebnet den Weg für zukünftige Anwendungen von CO_2 in der chemischen Synthese.

APPENDIX

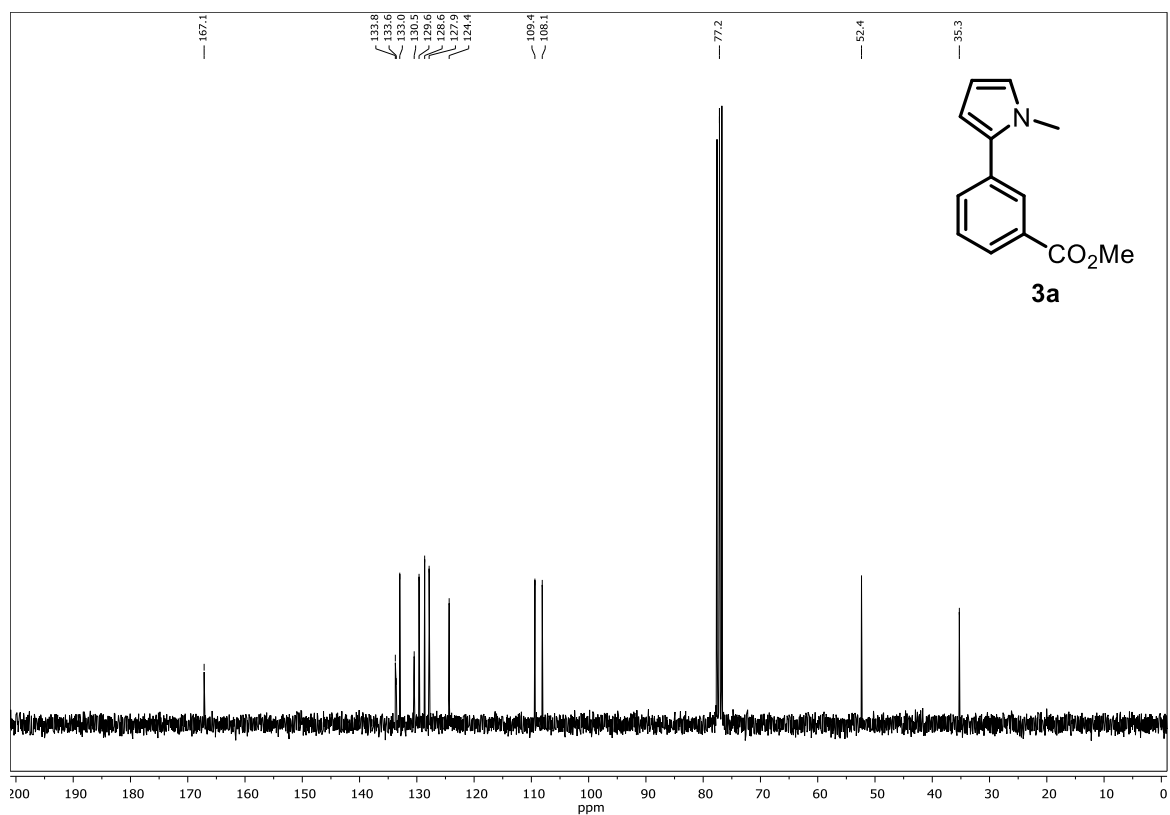
7 Appendix

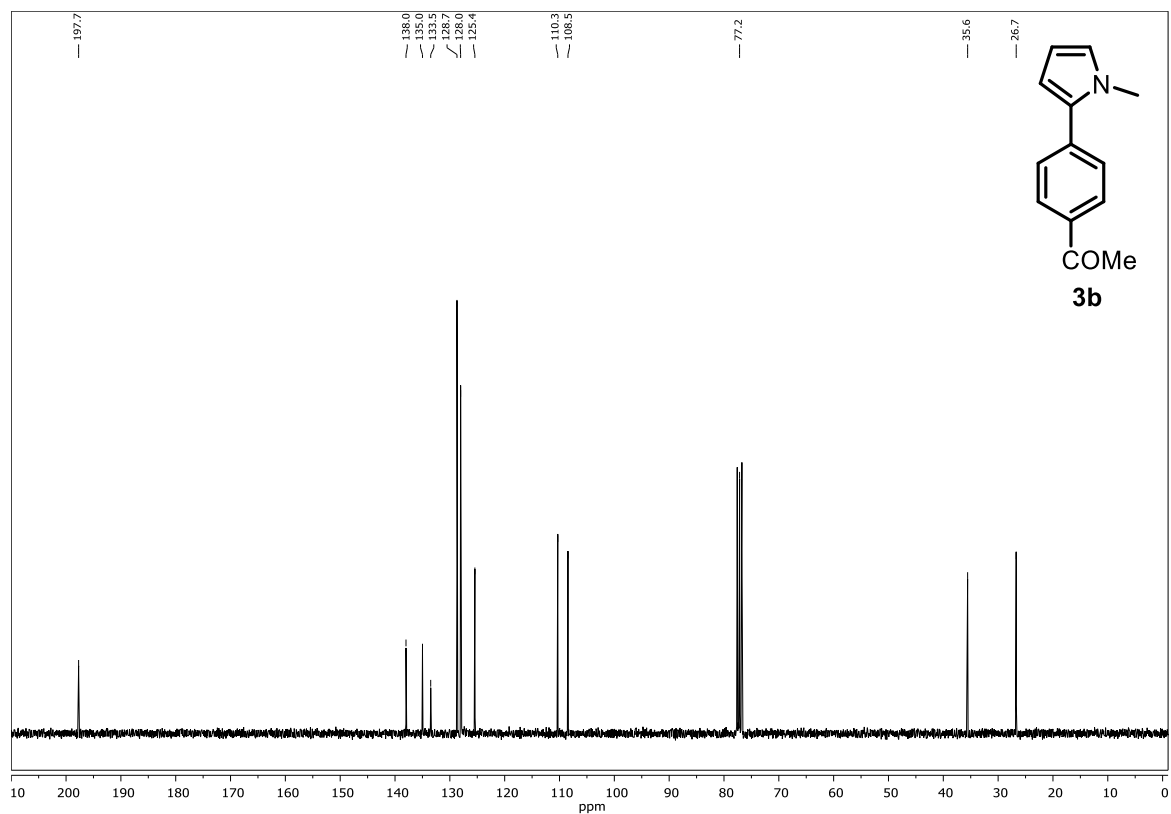
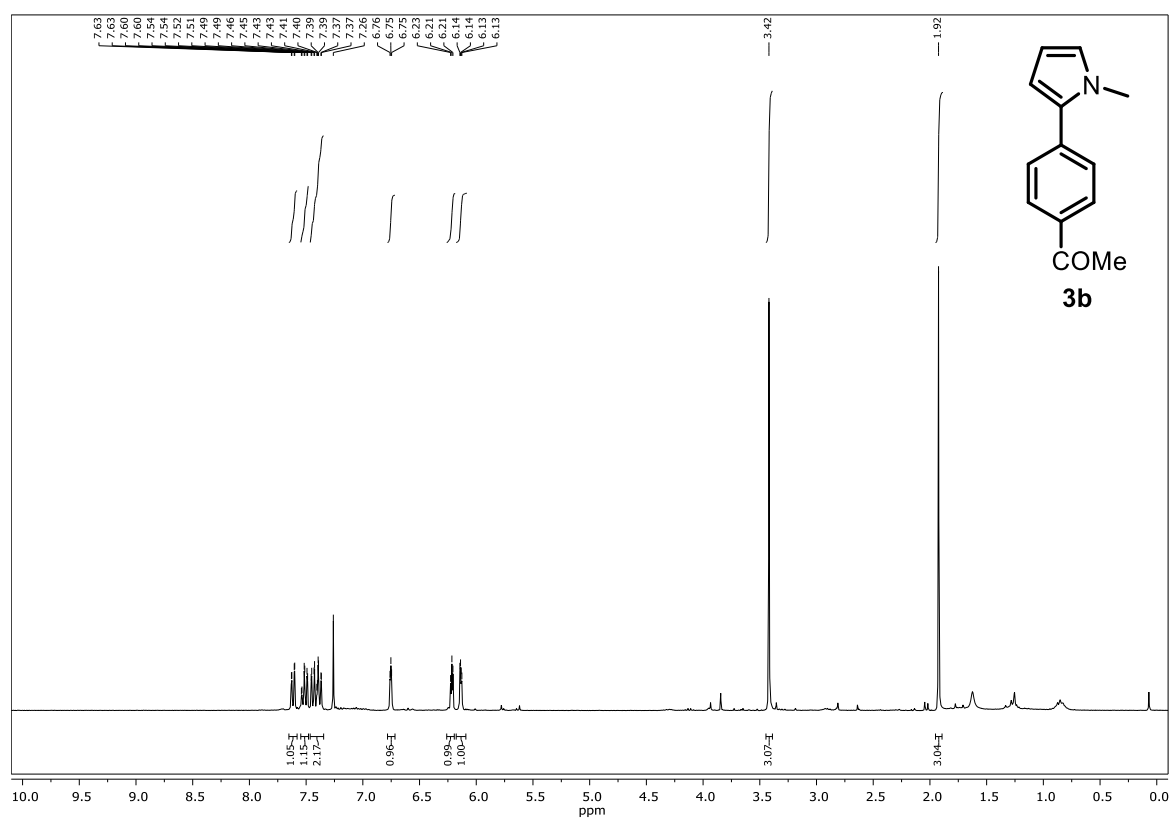
7.1 Abbreviations

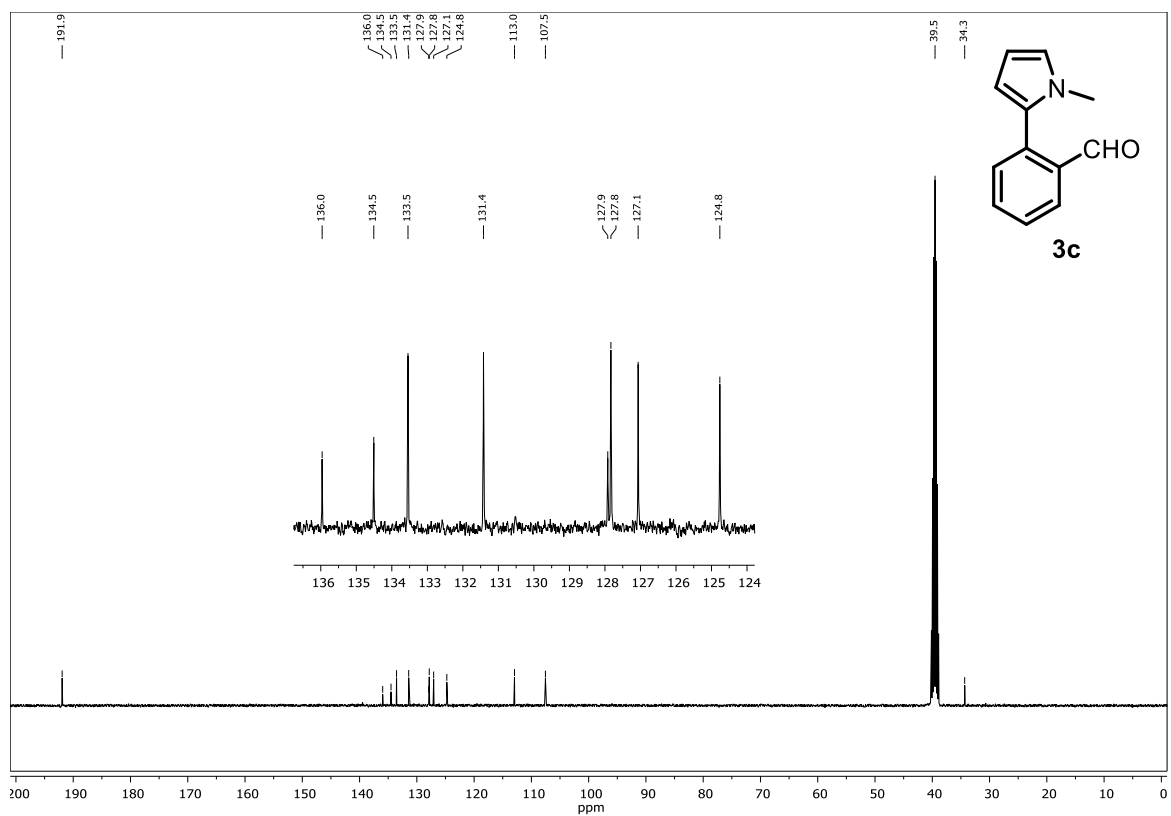
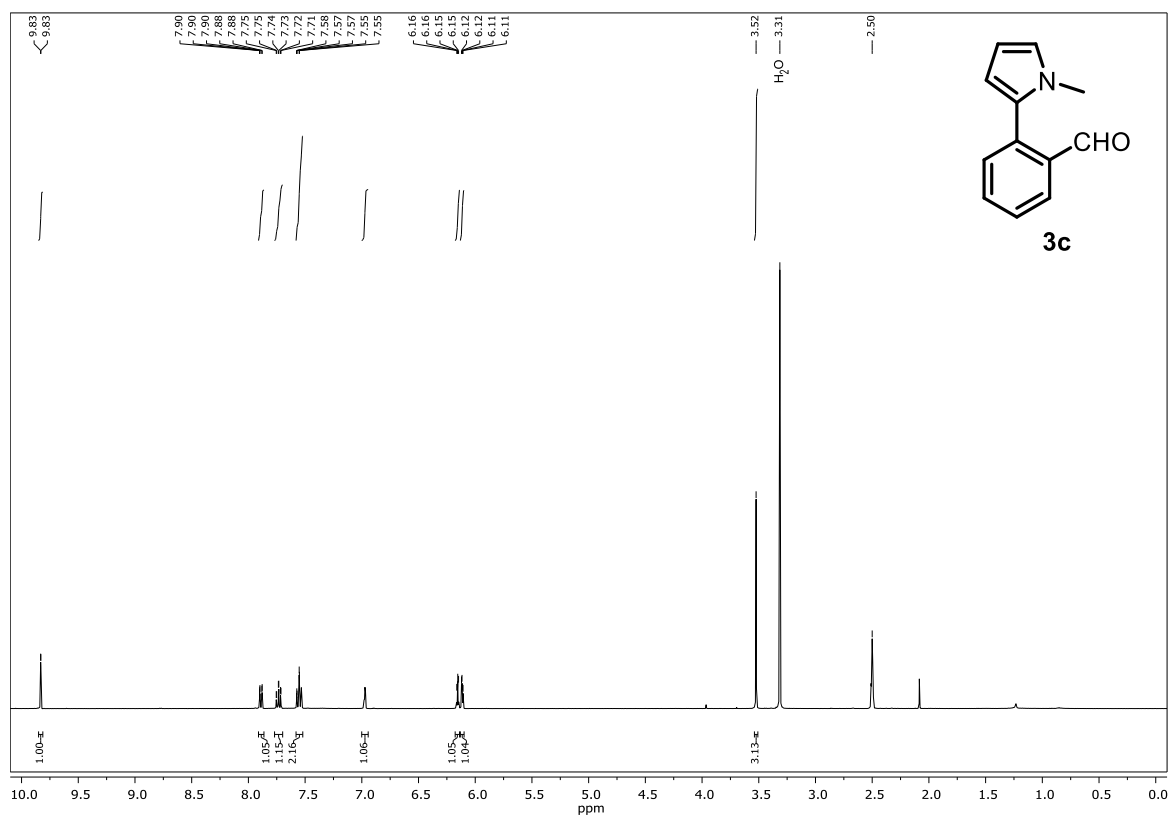
°C	degrees Celsius
Å	Ångström (10^{-10} m)
λ	wavelength
Ar	arene
BDE	bond dissociation energy
boc	<i>tert</i> -butyloxycarbonyl
bpy	2,2'-bipyridine
ccm or cm ³	cubic centimeters
<i>cf.</i>	compare (lat. confer)
cm	centimeter
CV	cyclic voltammetry
D ₂ O	deuterated water
DCM	dichloromethane
DFT	density functional theory
DIPEA	<i>N,N</i> -diisopropylethylamine
DMA	dimethylacetamide
DMF	dimethylformamide
DMSO	dimethyl sulfoxide
dtbpy/dtbbpy	di- <i>tert</i> -butyl-2,2'-bipyridine
<i>e.g.</i>	for example (<i>lat.</i> <i>exempli gratia</i>)
eq. or equiv.	equivalent
EI	electron ionization
ESI	electrospray ionization
<i>et al.</i>	and others (<i>lat.</i> <i>et alii</i>)
EtOAc	ethyl acetate
EtOH	ethanol
eV	electron volt
Fc	ferrocene
FID	flame ionization detector
g	gram

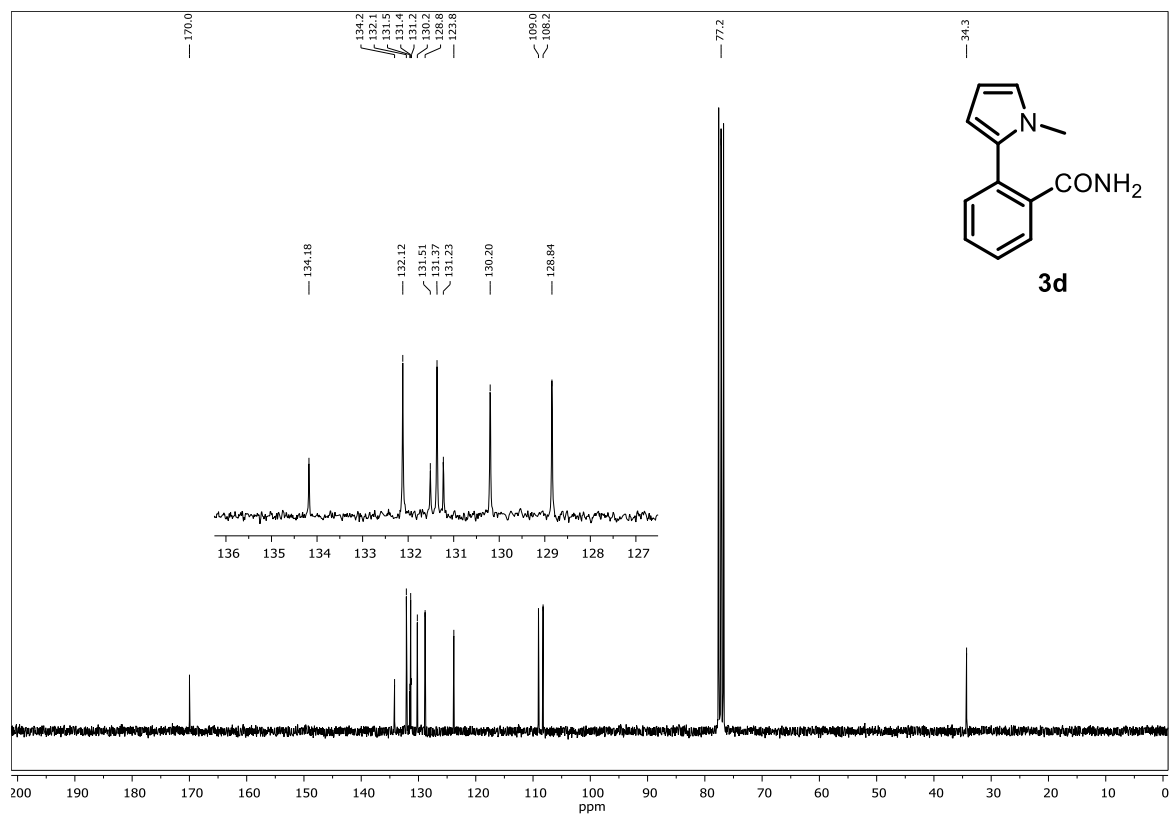
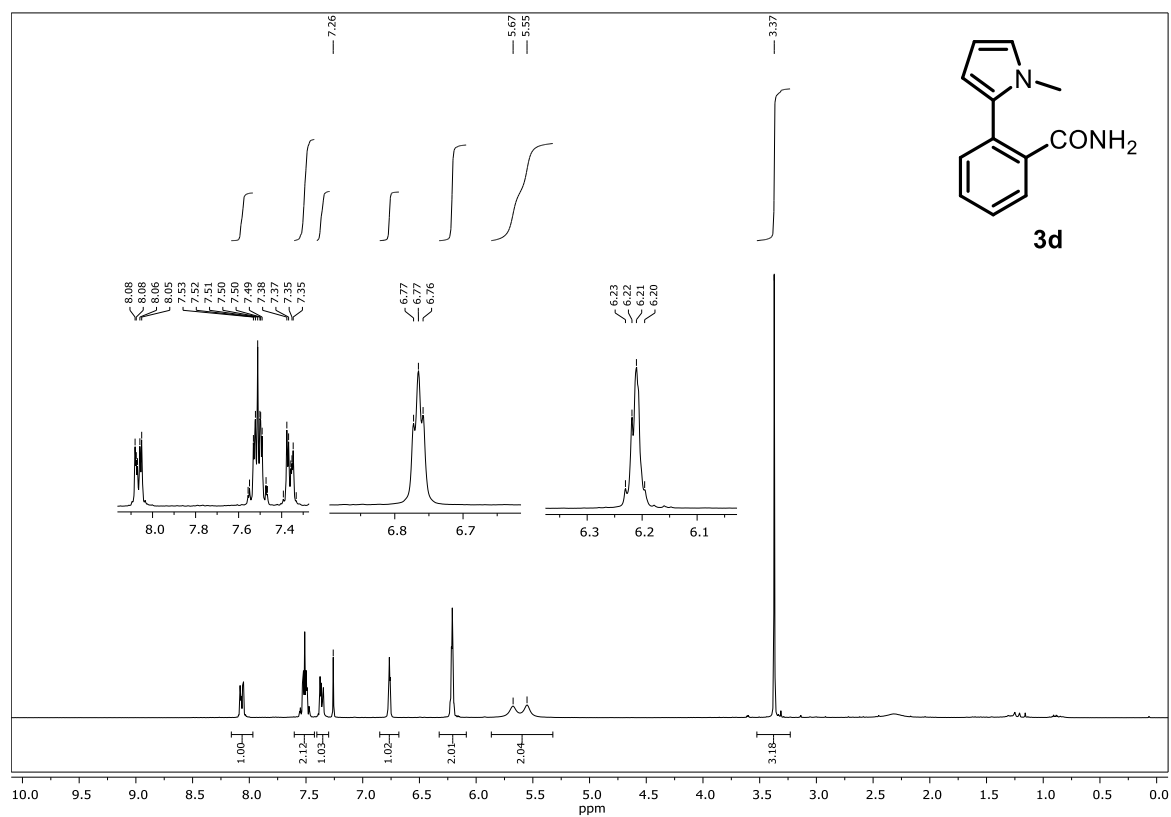
GC	gas chromatography
h or hrs	hour(s)
HAT	hydrogen atom transfer
HRMS	high resolution mass spectrometry
$h\nu$	incident photon energy
<i>i.e.</i>	that is (<i>lat. id est</i>)
^t Pr	isopropyl
K	Kelvin
L	liter
LED	light emitting diode
LCMS	liquid chromatography mass spectrometry
LRMS	low resolution mass spectrometry
M	molar (mol/L)
Me	methyl
MeCN	acetonitrile
MeOH	methanol
mg	milligram
Ms	methanesulfonyl group
min	minute
mL	milliliter
mM	millimolar (mmol/L)
mmol	millimole
MS	mass spectrometry
<i>n</i> -Bu	<i>n</i> -butyl
nm	nanometer
NMR	nuclear magnetic resonance
OAc	acetoxy group
p.a.	per analysis
PC	photocatalyst
PE	petroleum ether
PET	photoinduced electron transfer
Ph	phenyl group
p <i>K</i> _a	acid dissociation constant at logarithmic scale

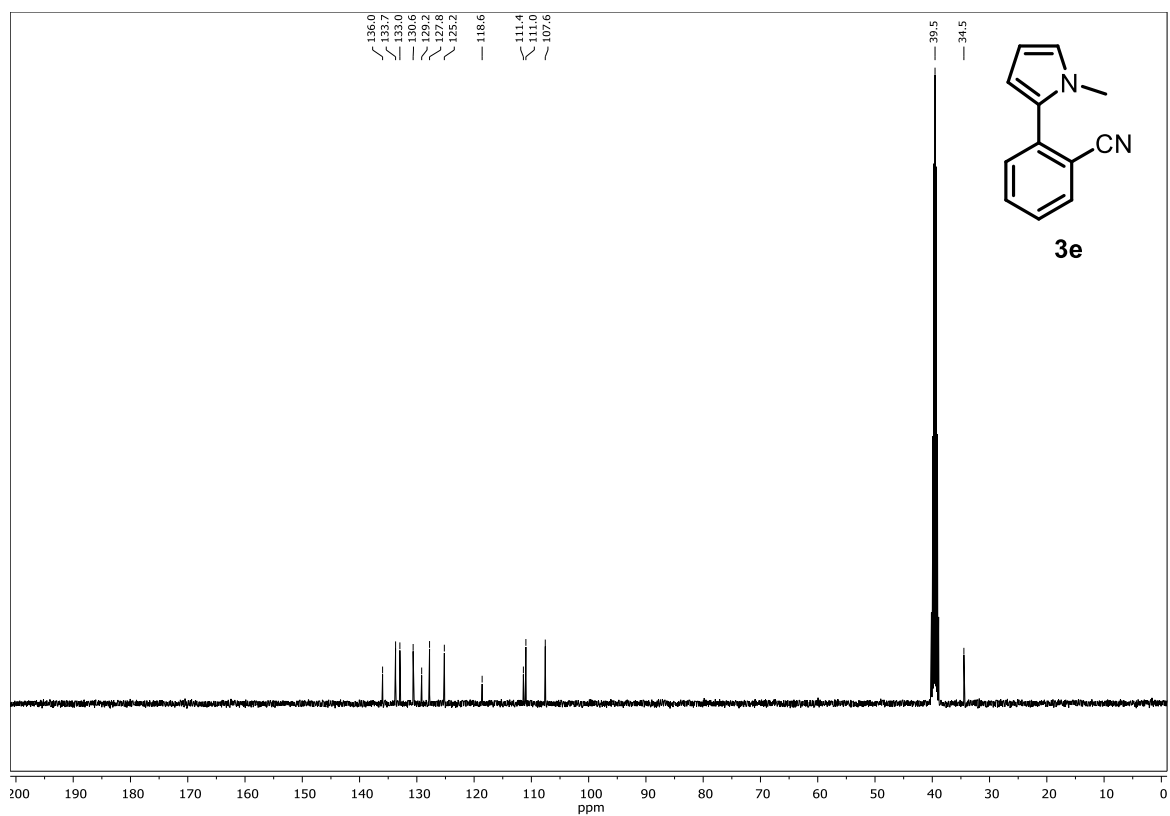
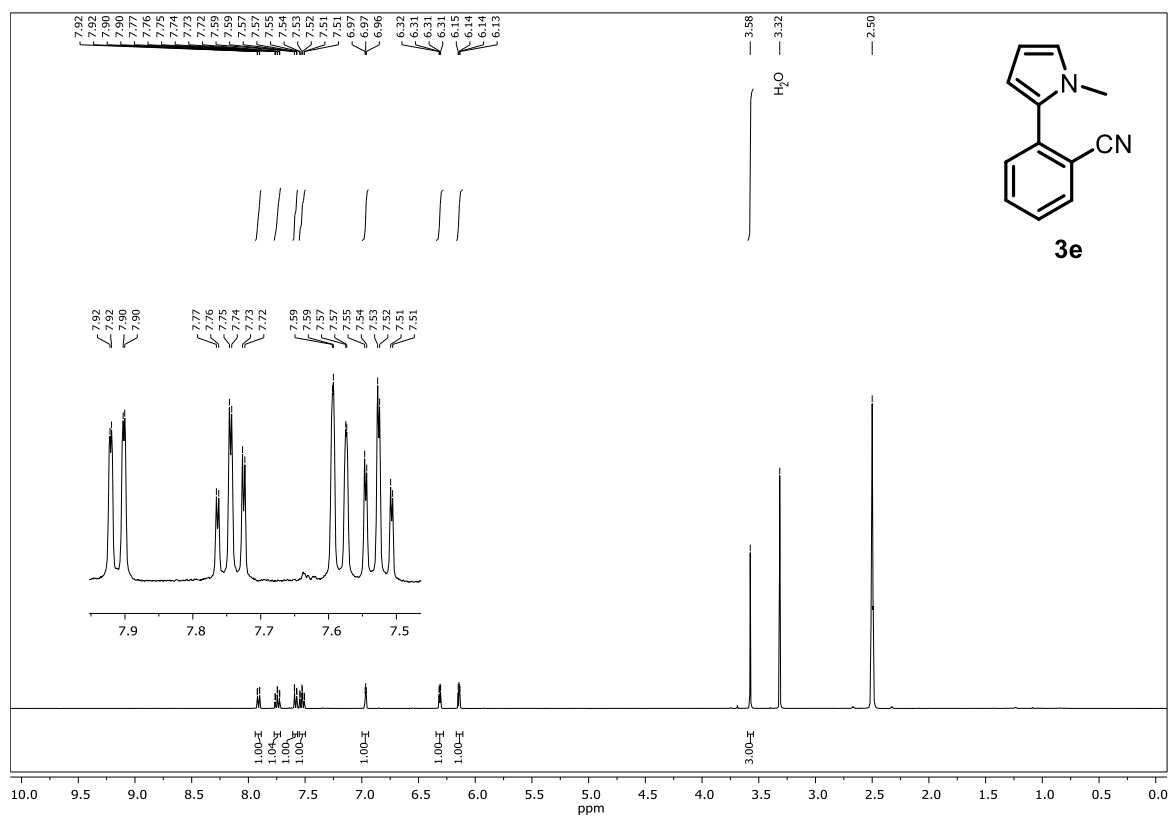
ppy	2-phenylpyridinato
PTFE	polytetrafluoroethylene
R	alkyl-, aryl- or functional groups
r.t.	room temperature
s	second
SCE	saturated calomel electrode
SET	single electron transfer
^t Bu	<i>tert</i> -butyl
^t BuOD	deuterated <i>tert</i> -butanol
TBATFB	tetrabutylammonium tetrafluoroborate
TEMPO	(2,2,6,6-tetramethylpiperidin-1-yl)oxyl
THF	tetrahydrofuran
TLC	thin layer chromatography
TMS	trimethylsilyl group
Ts	toluene sulfonyl group
UV	ultra violet
Vis	visible light
<i>vs.</i>	against (<i>lat.</i> versus)
w. r. t.	with reference to

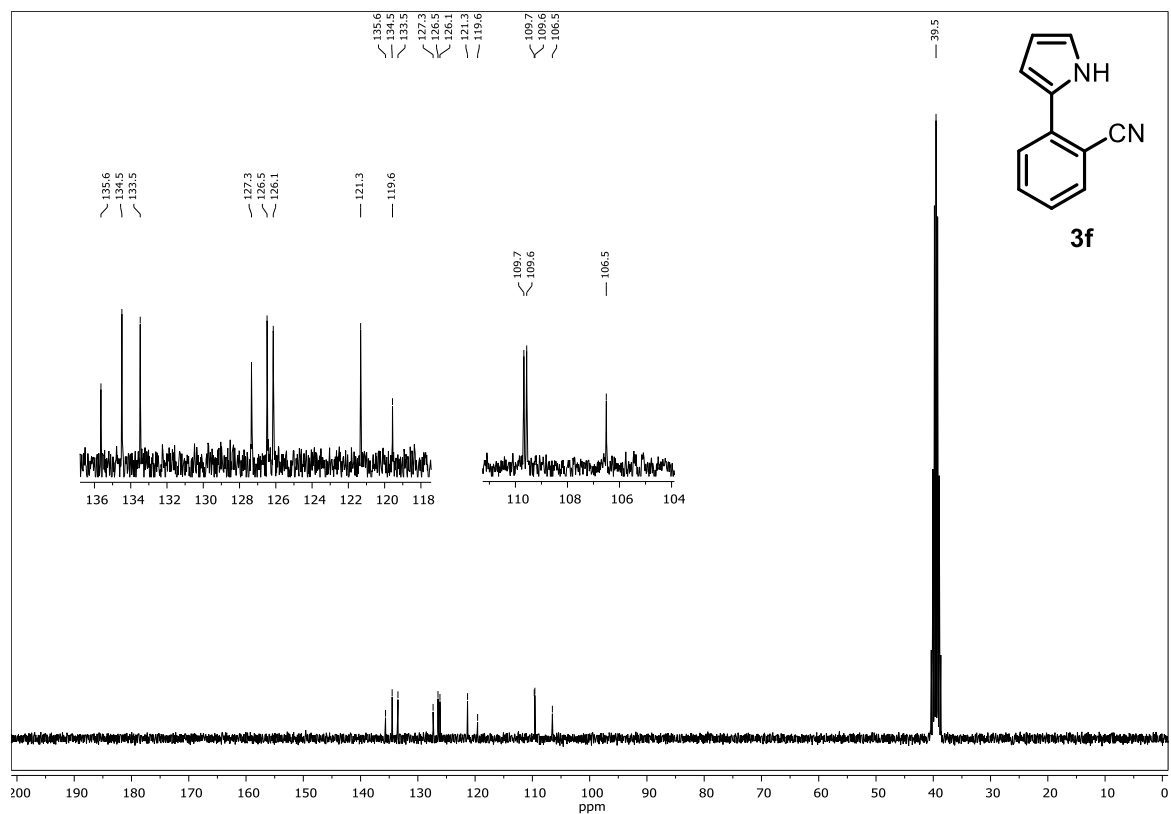
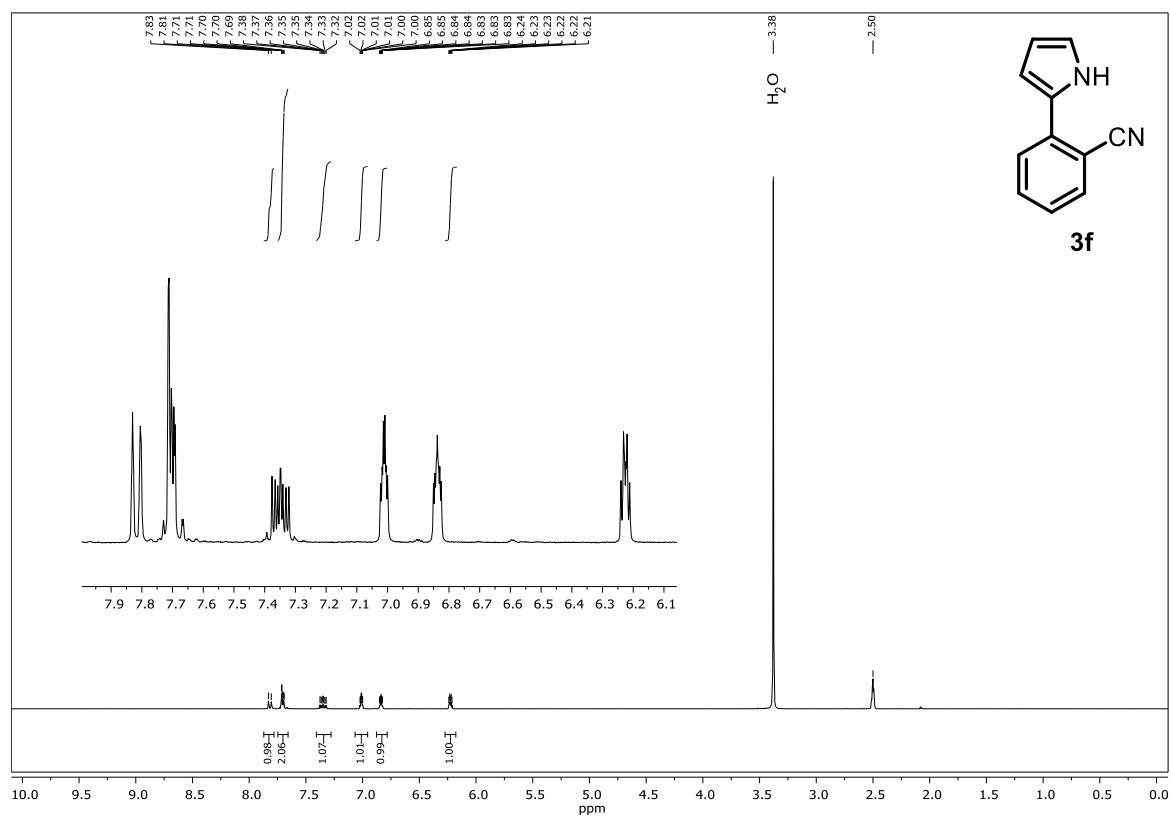


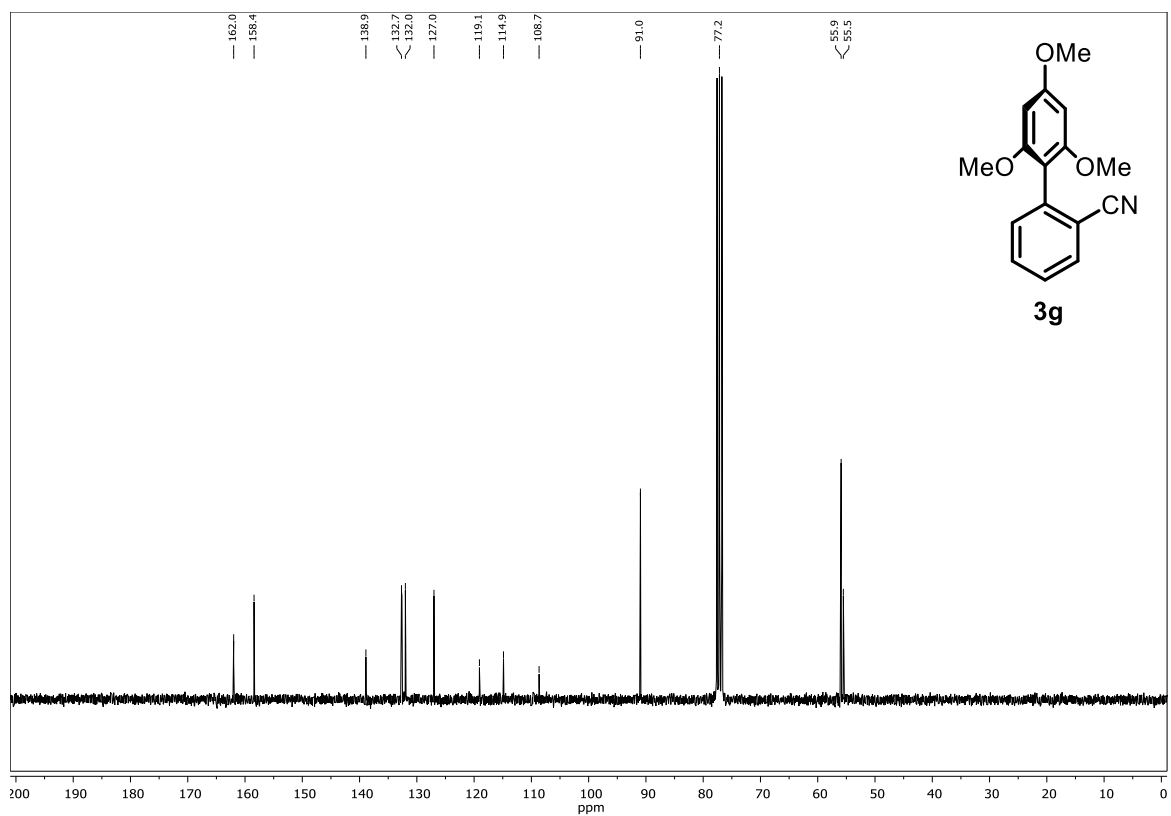
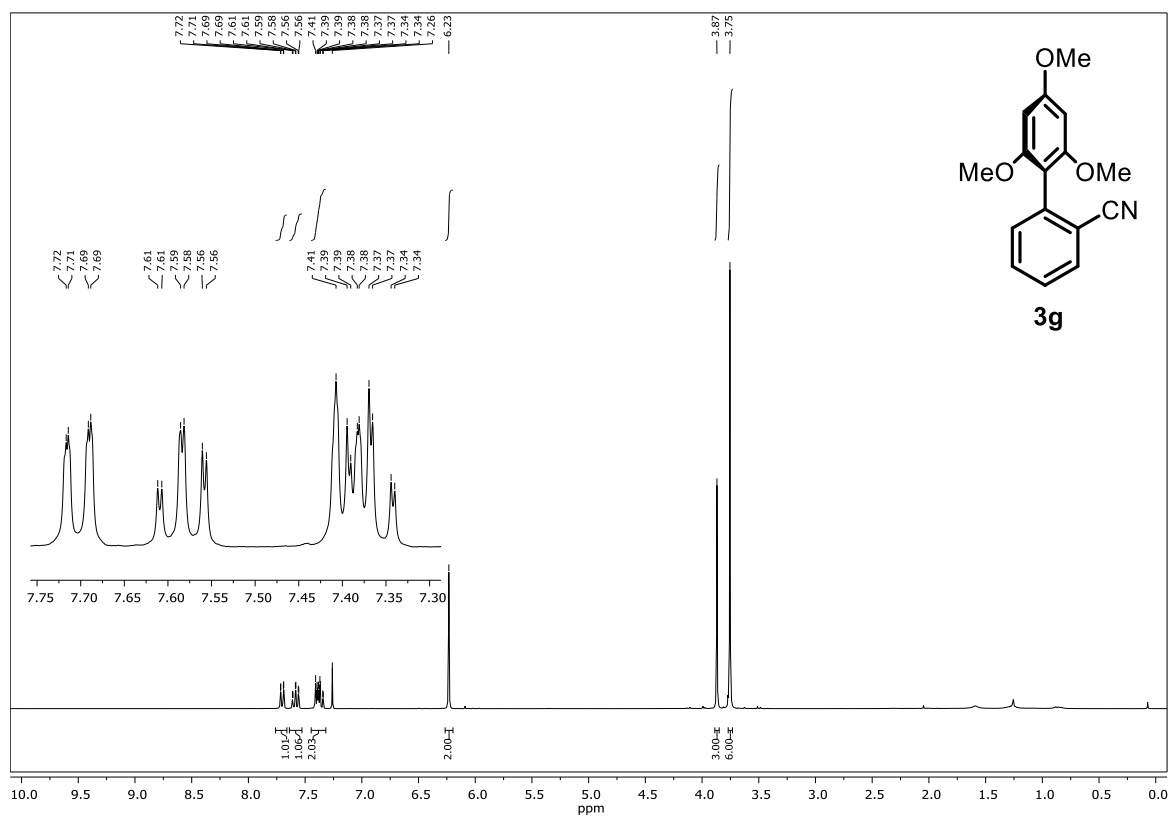


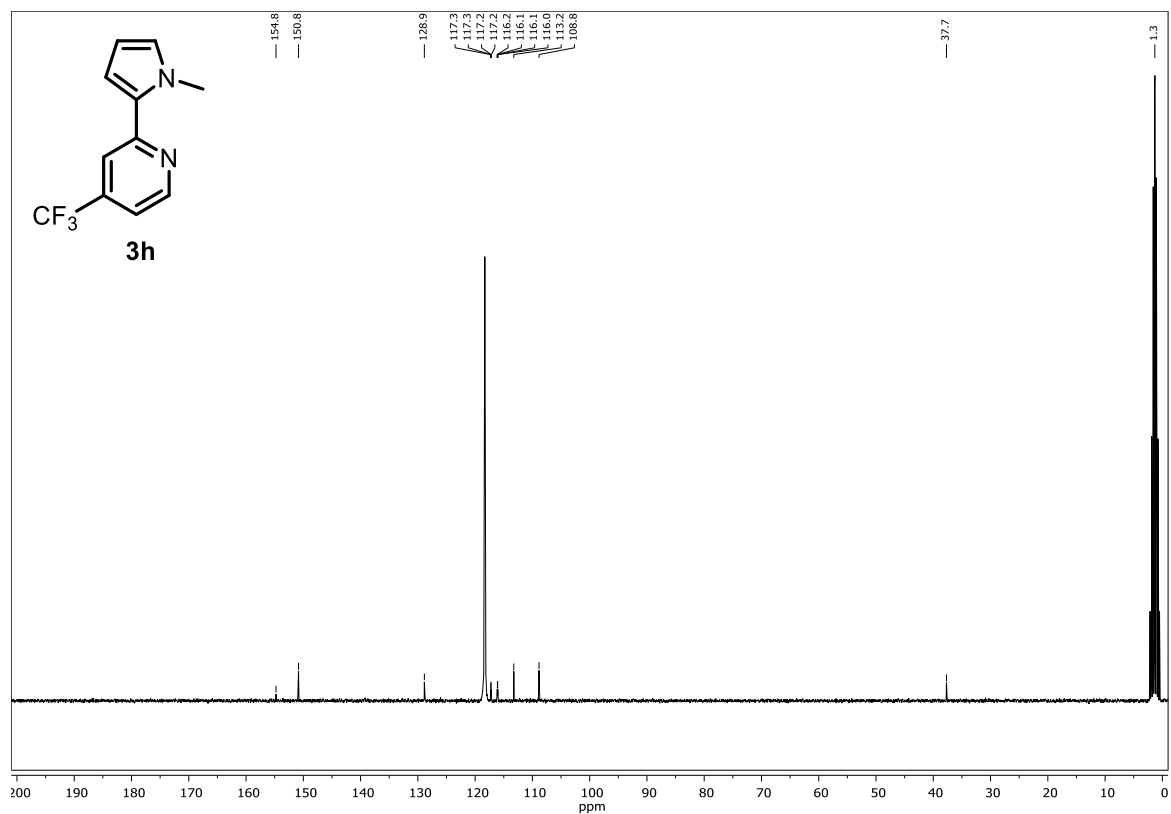
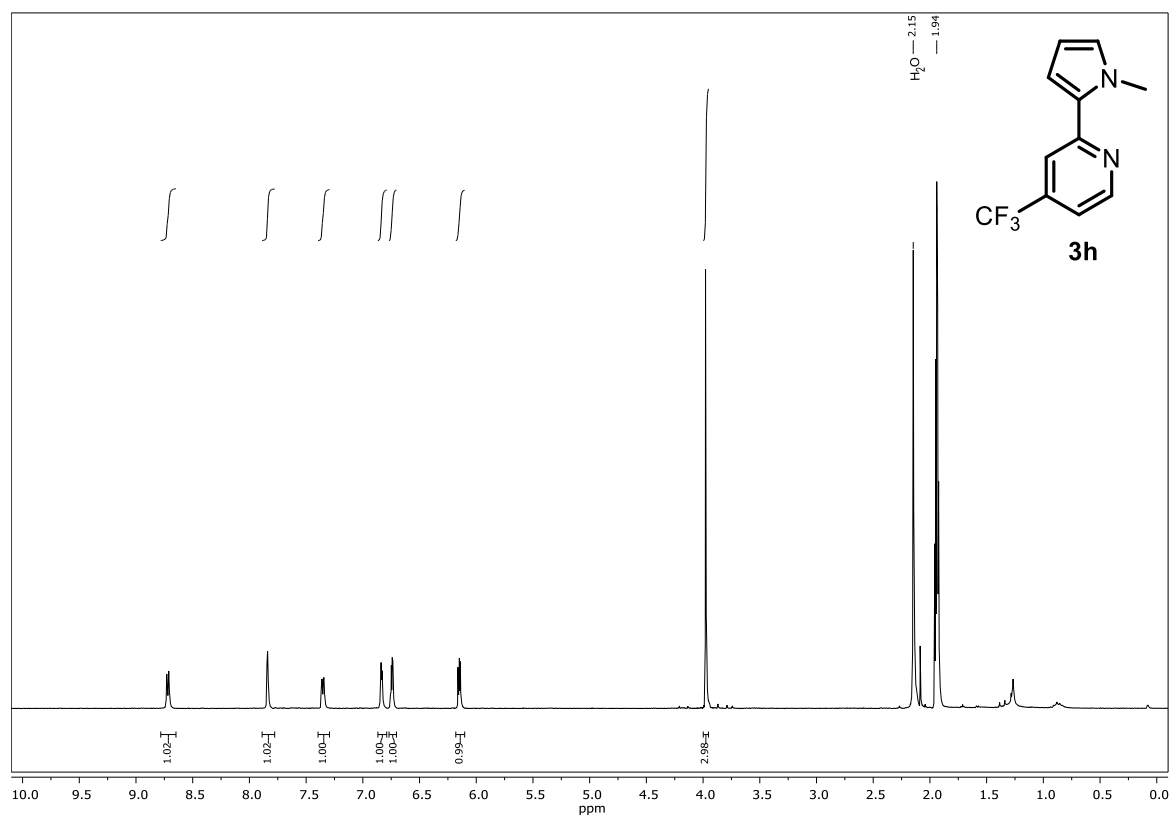


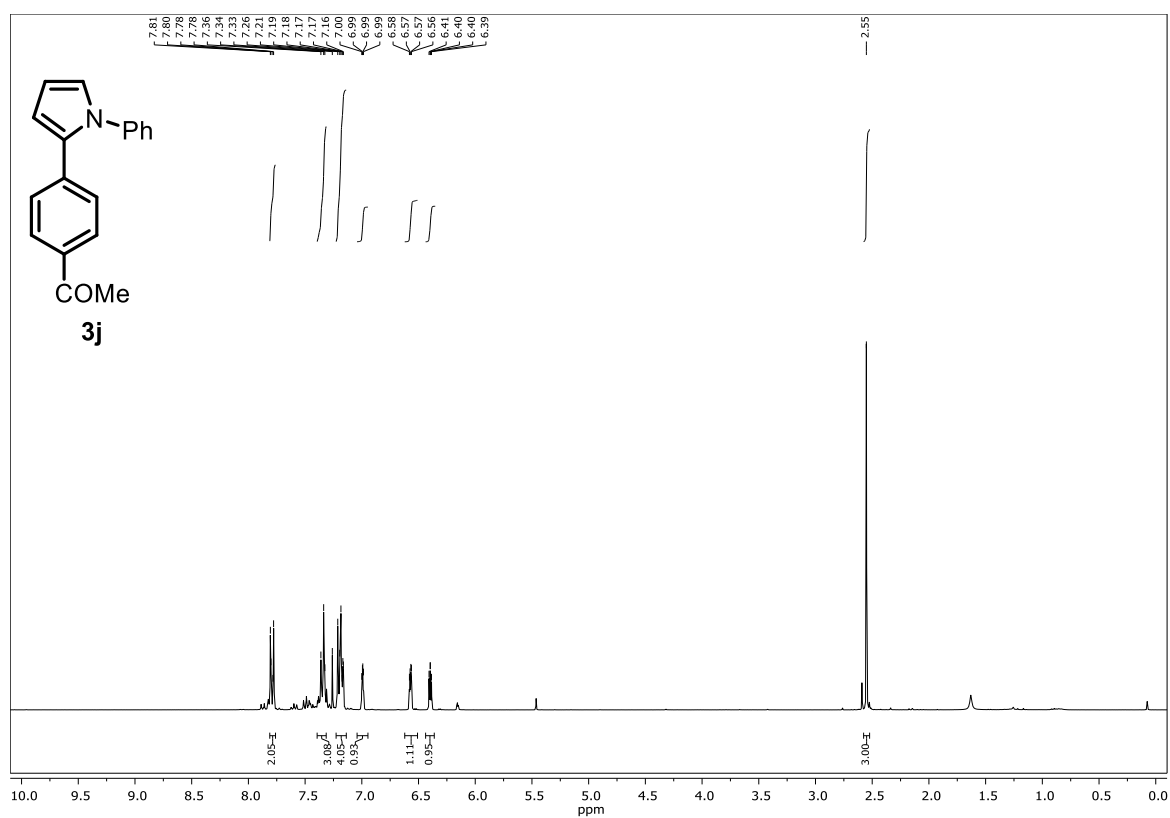
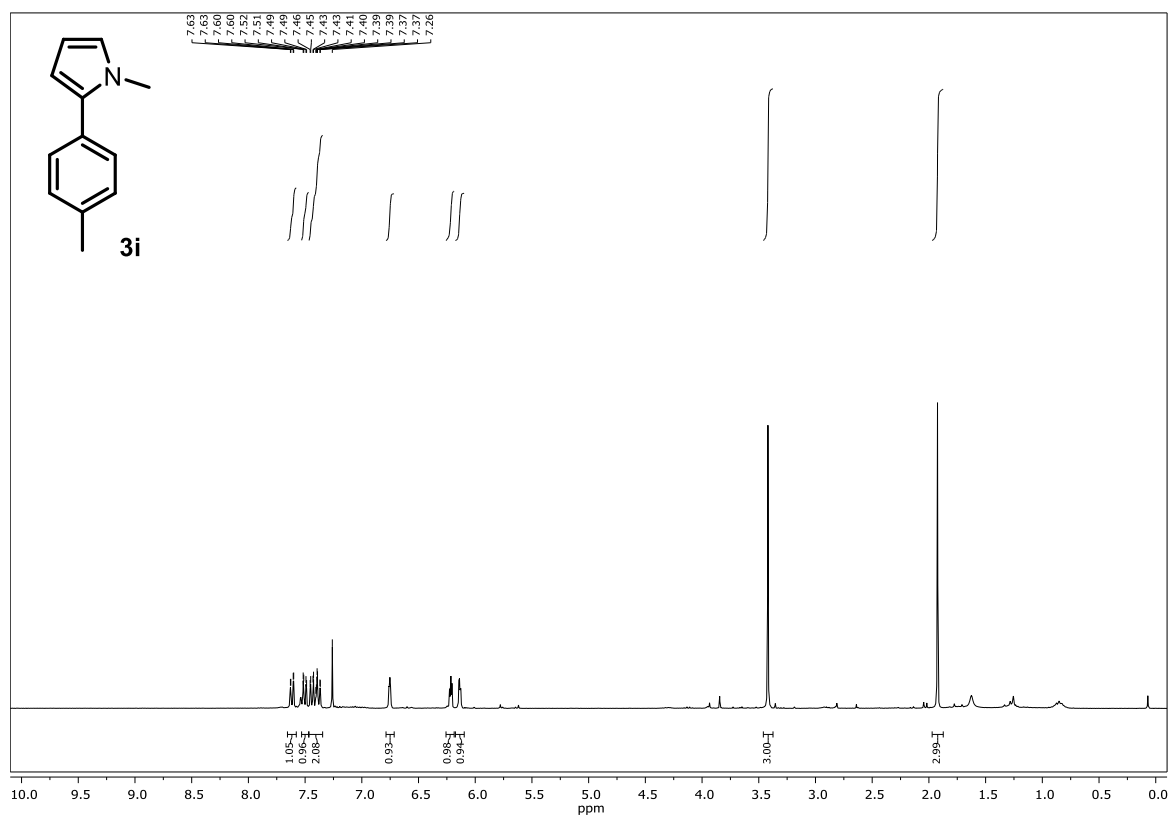


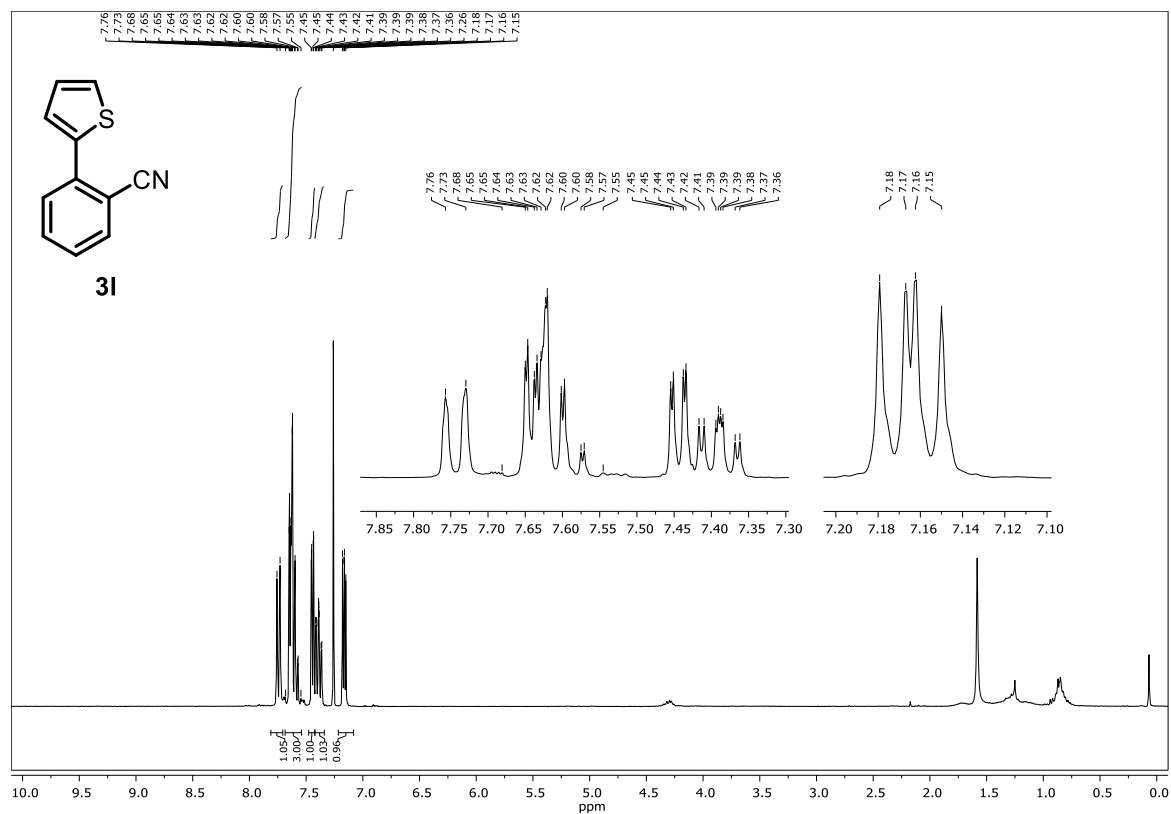
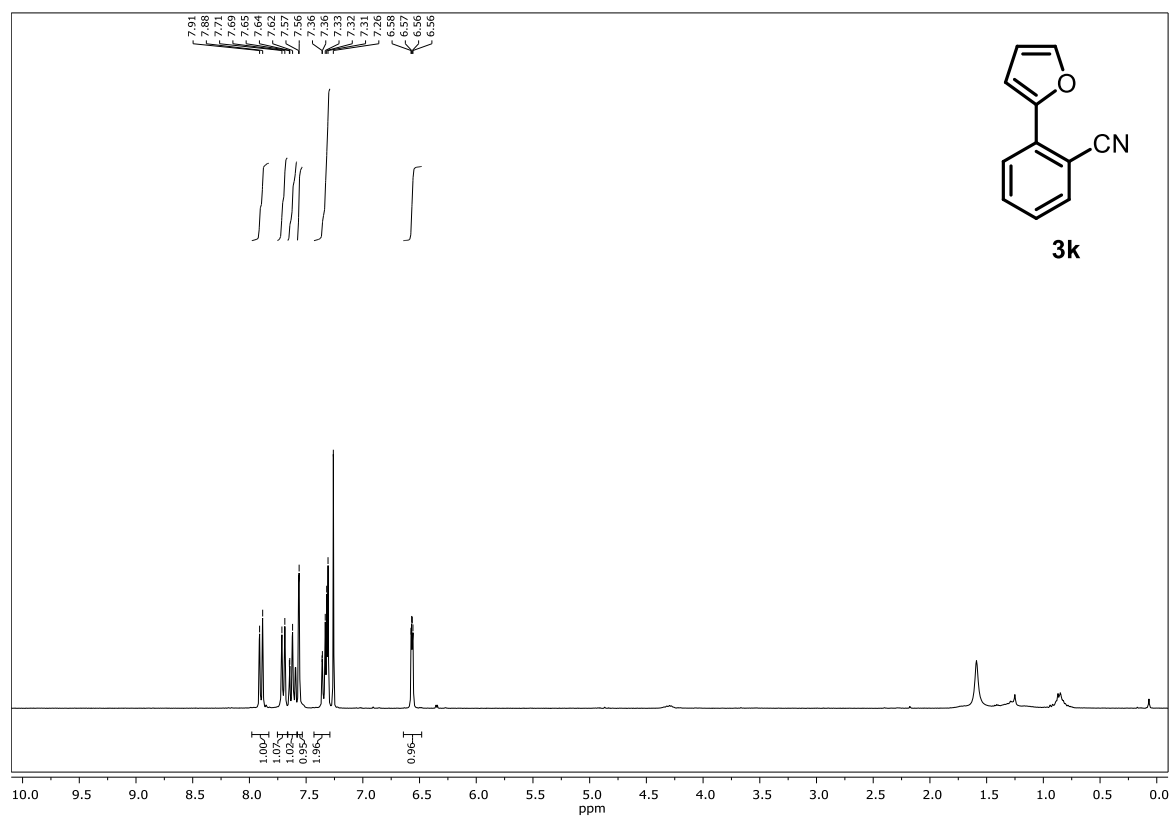


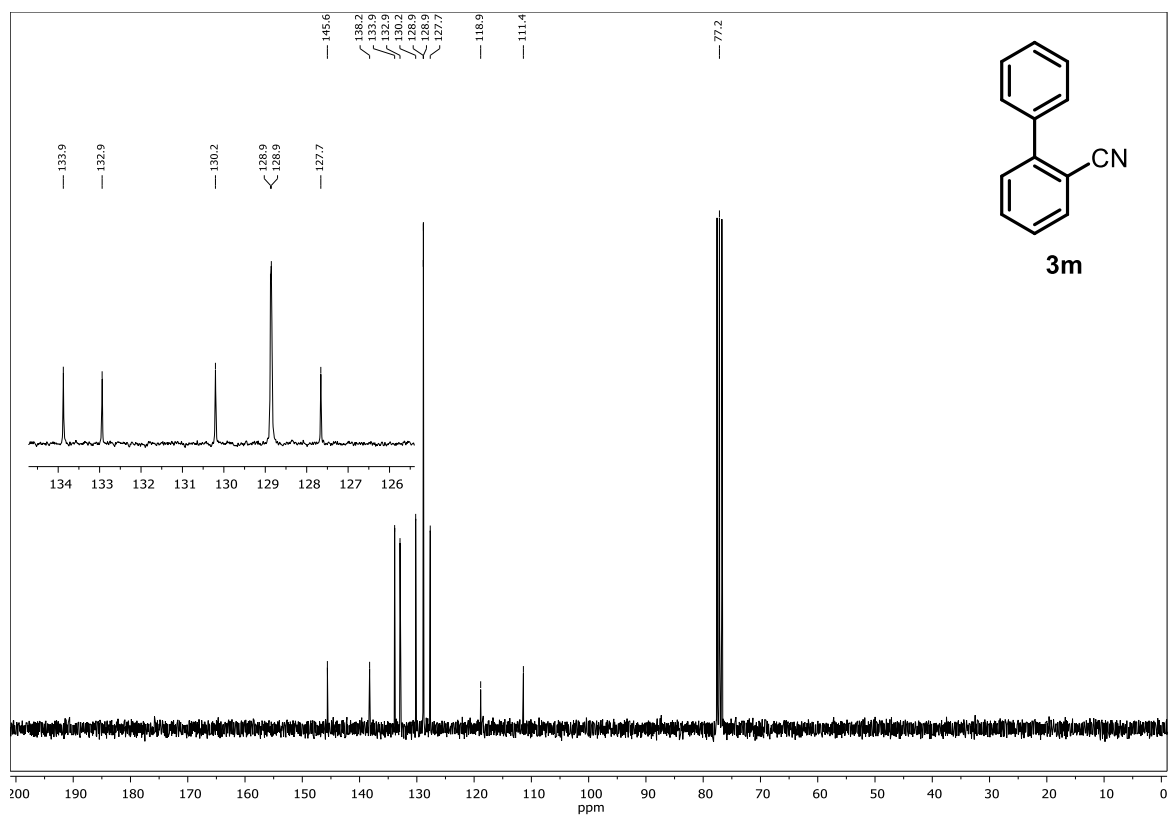
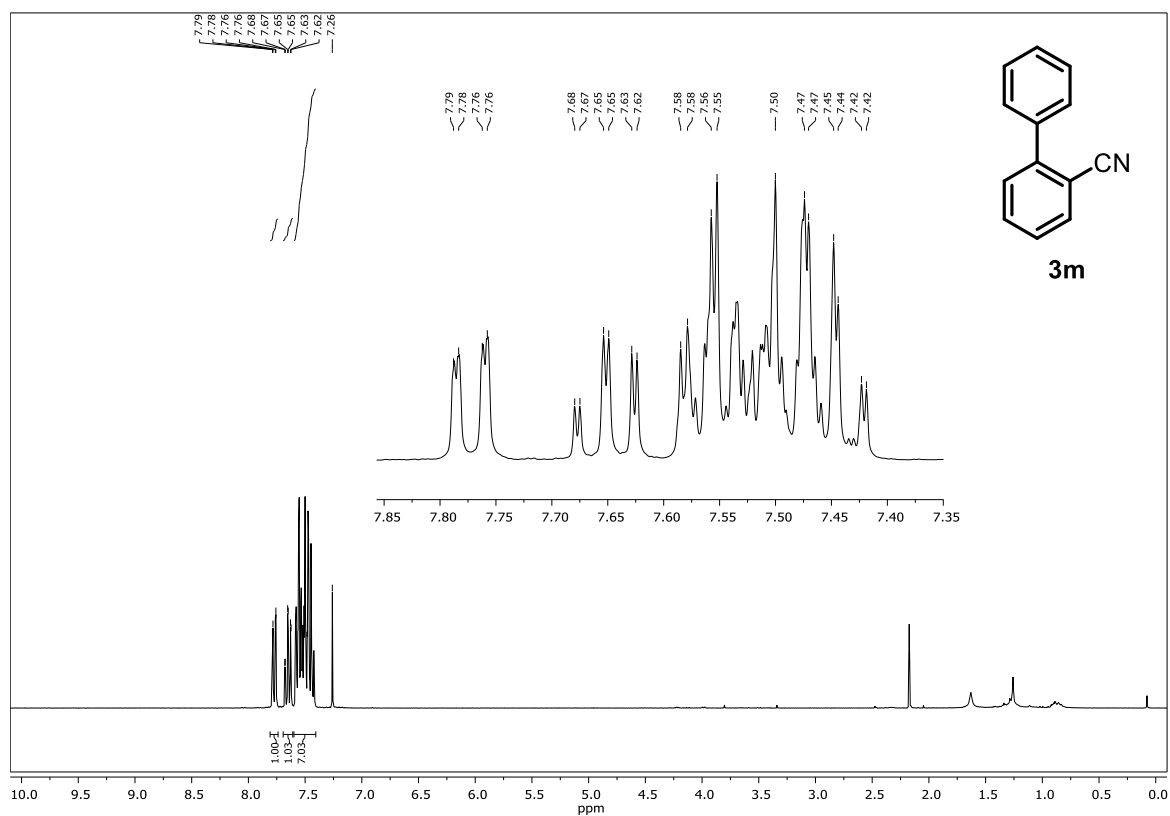


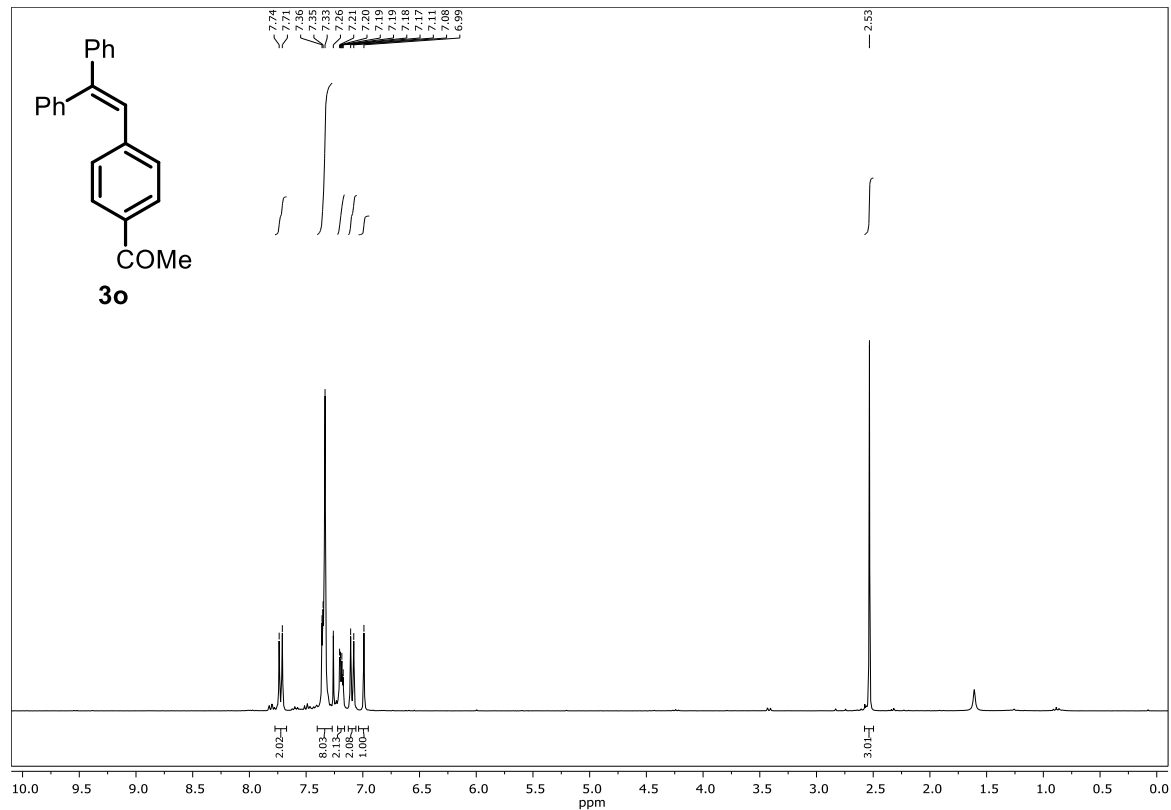






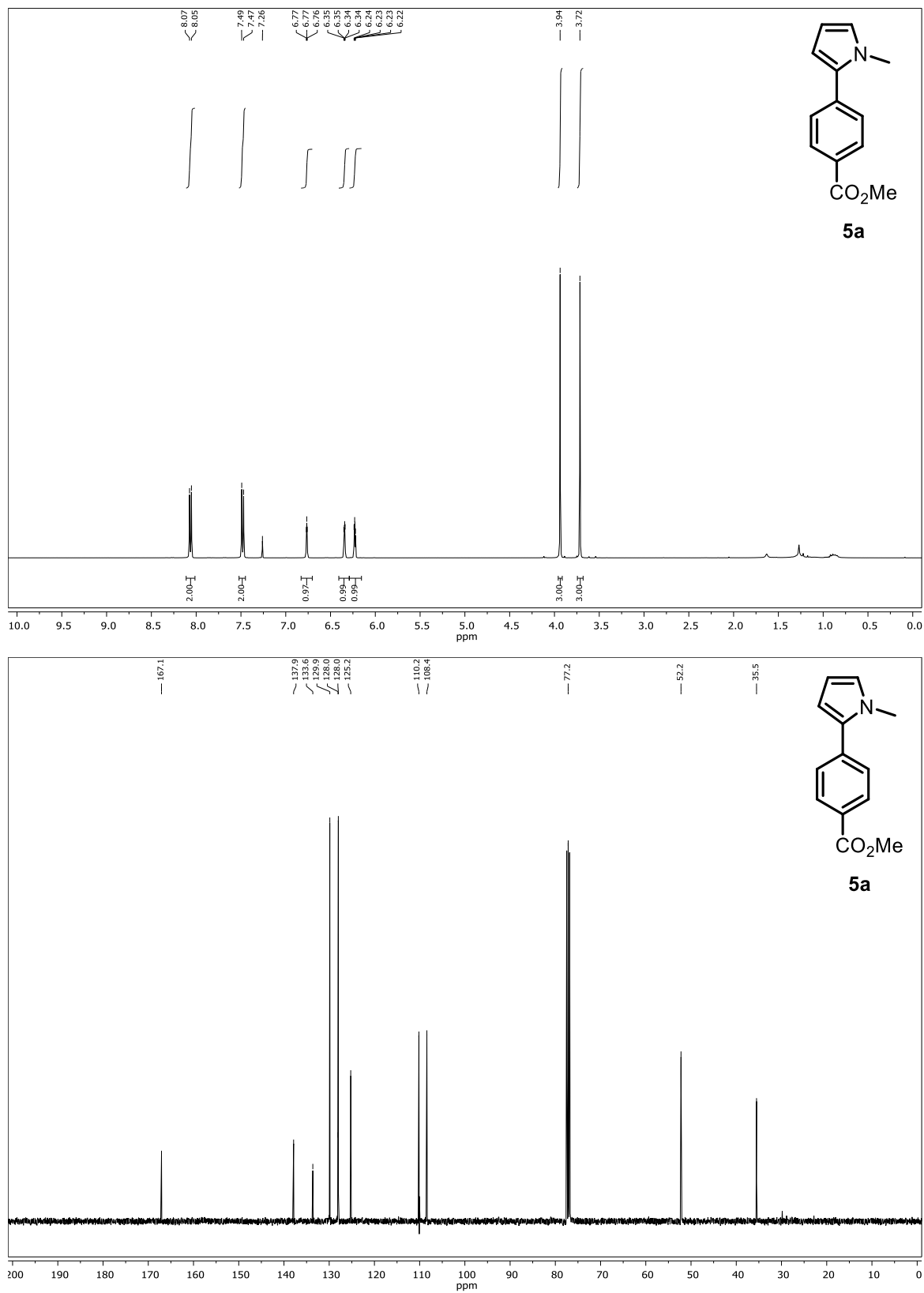


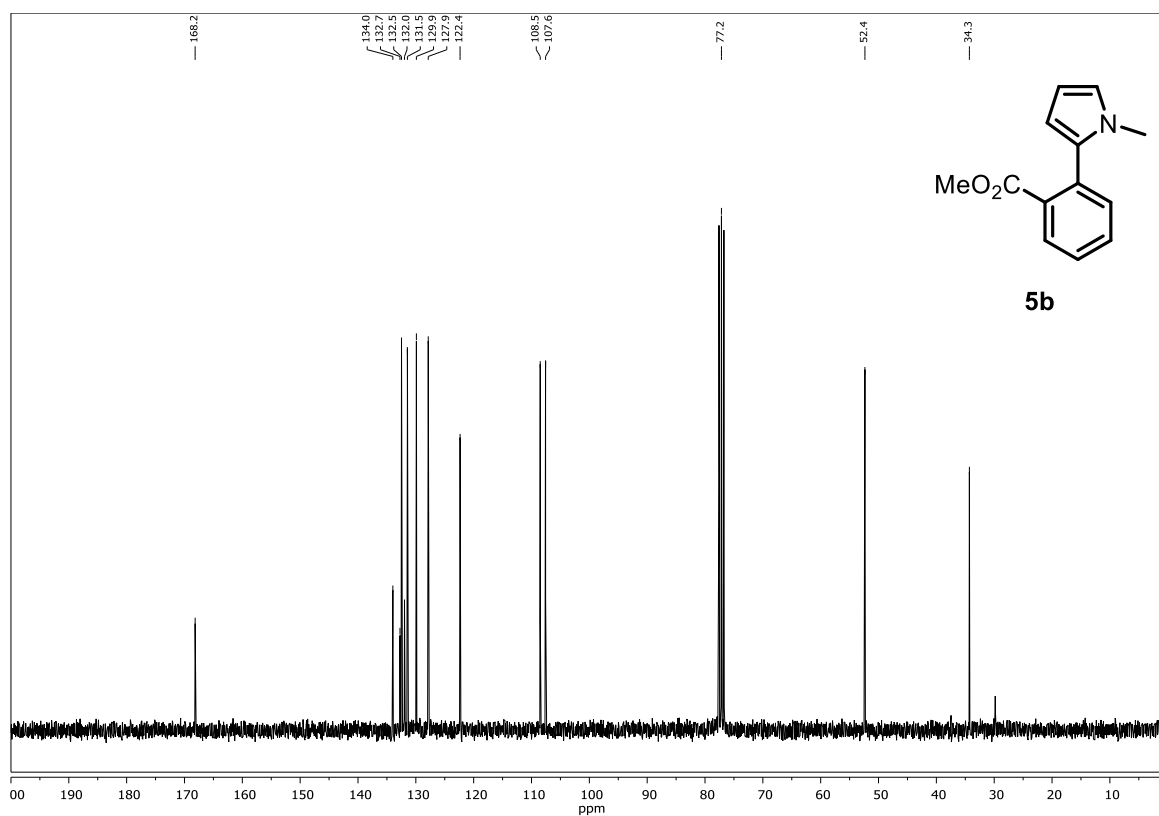
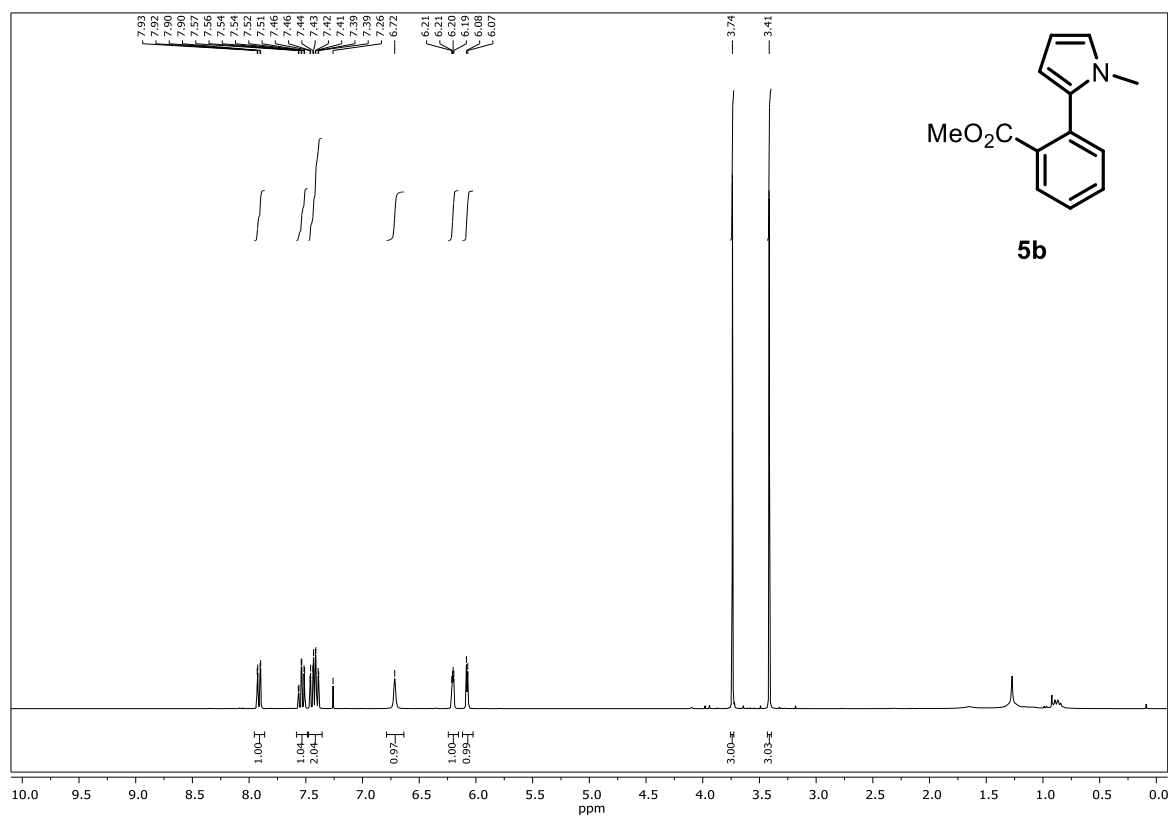


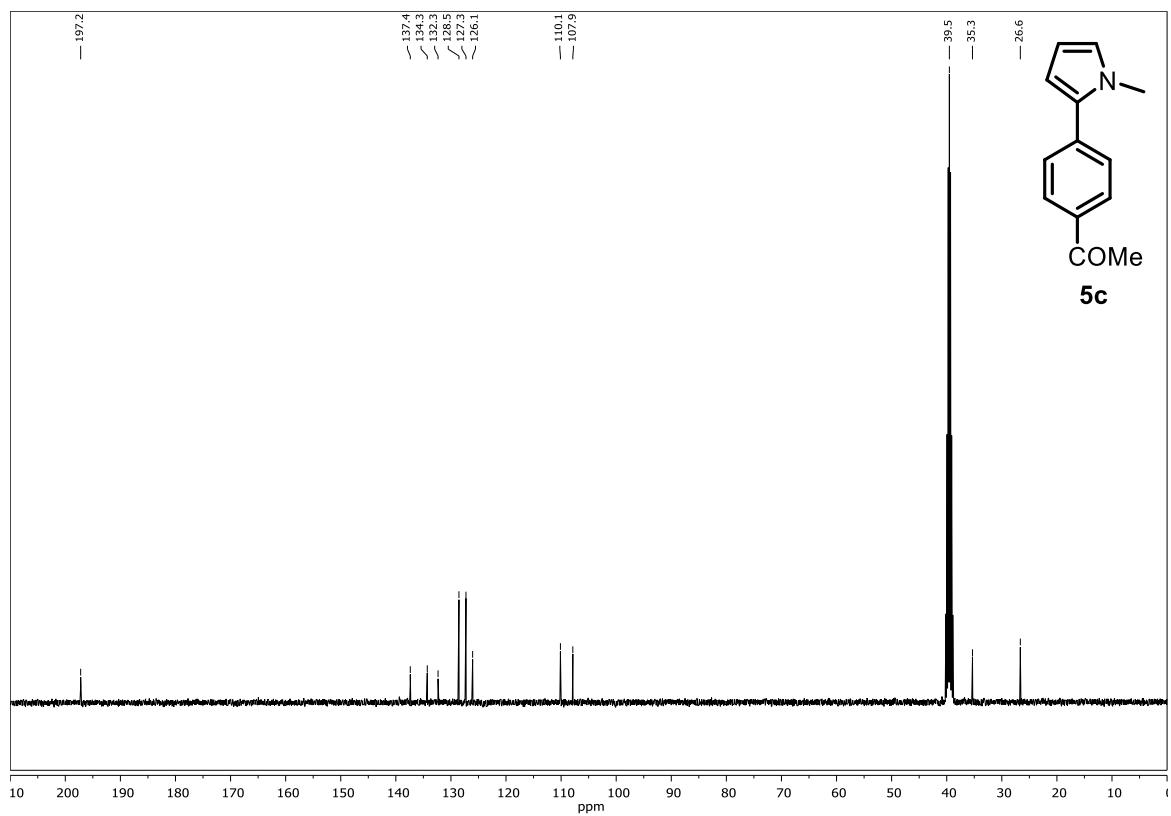
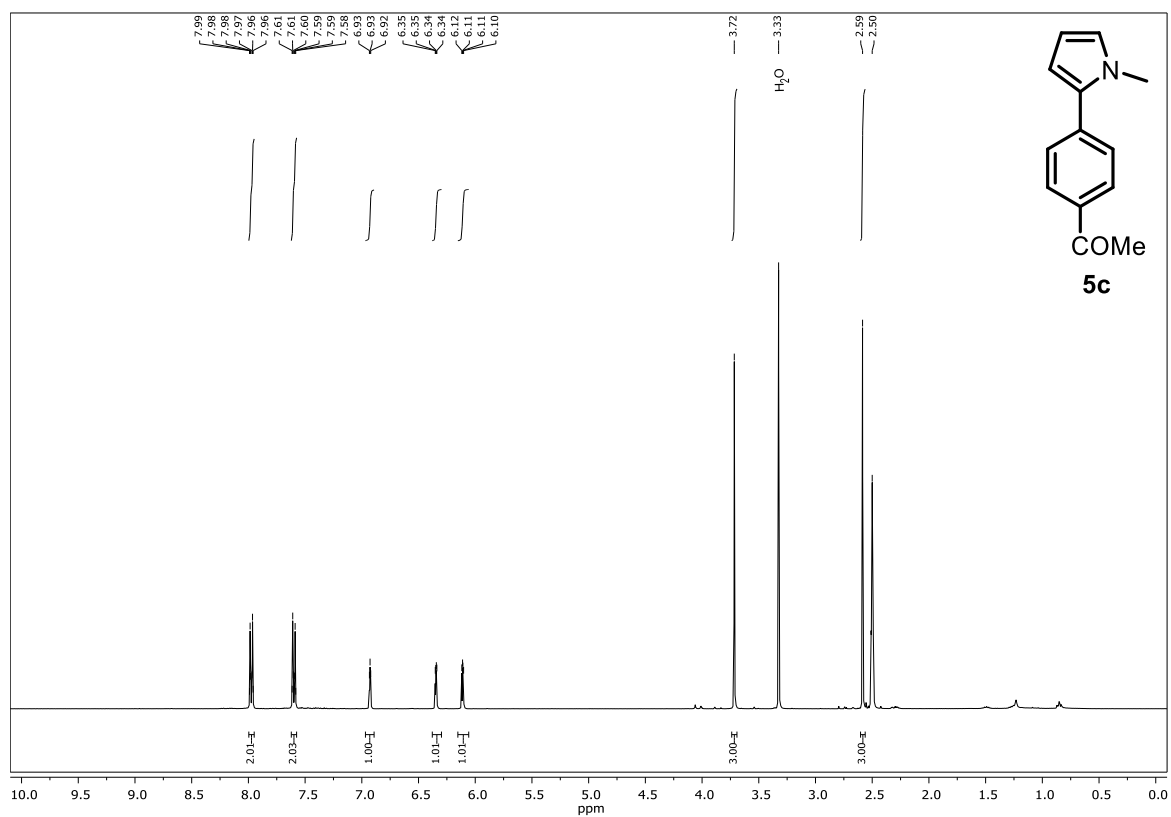


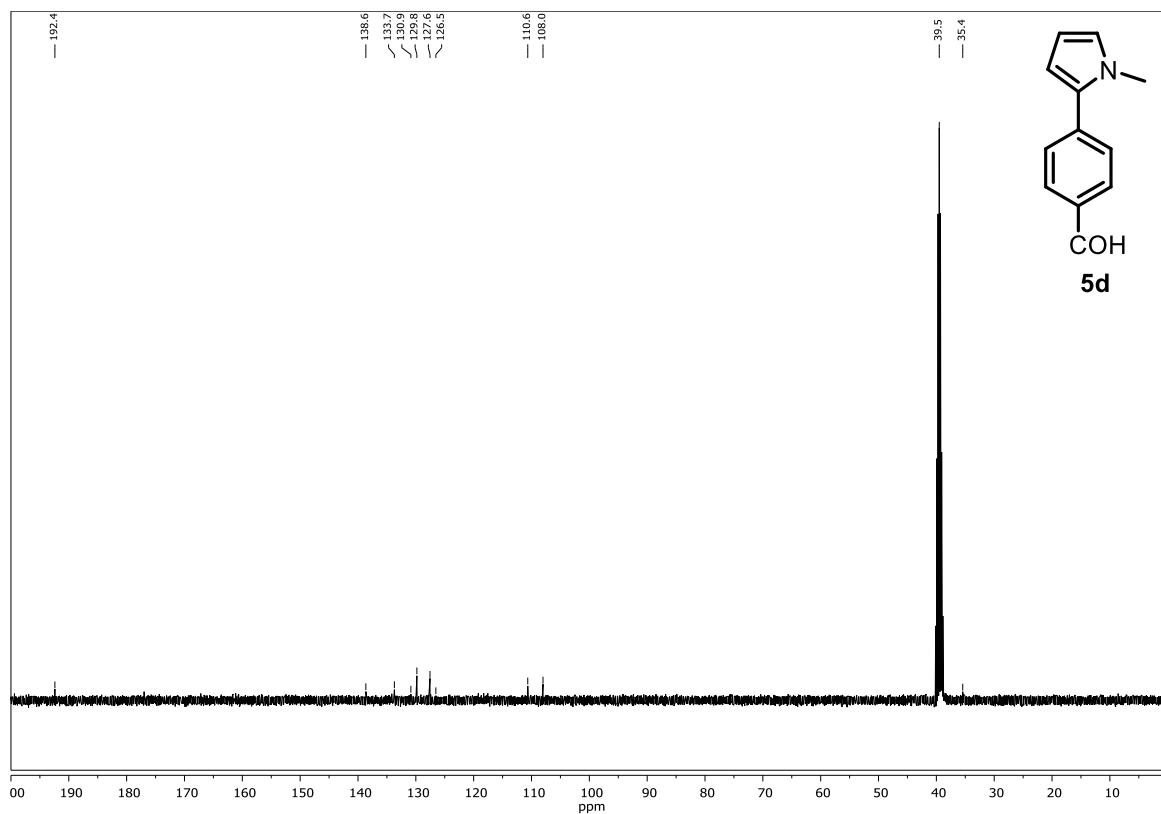
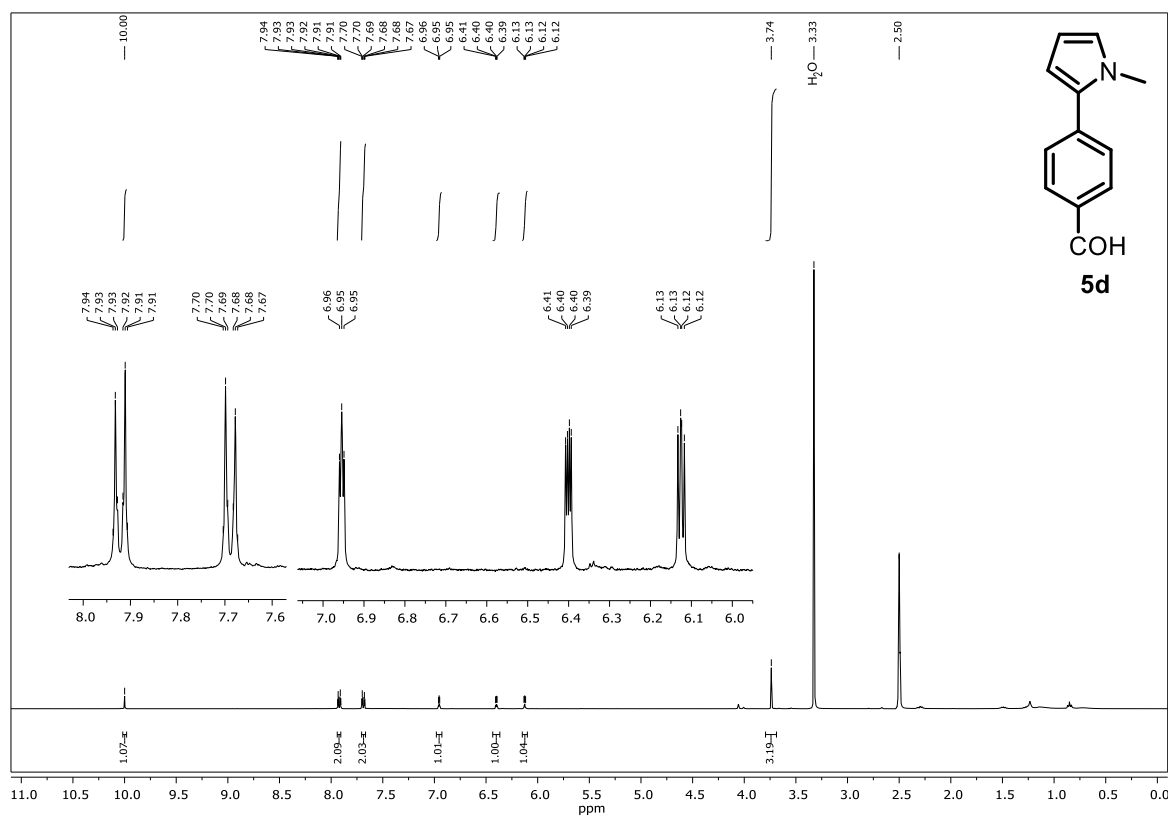
7.3 Appendix Chapter 3

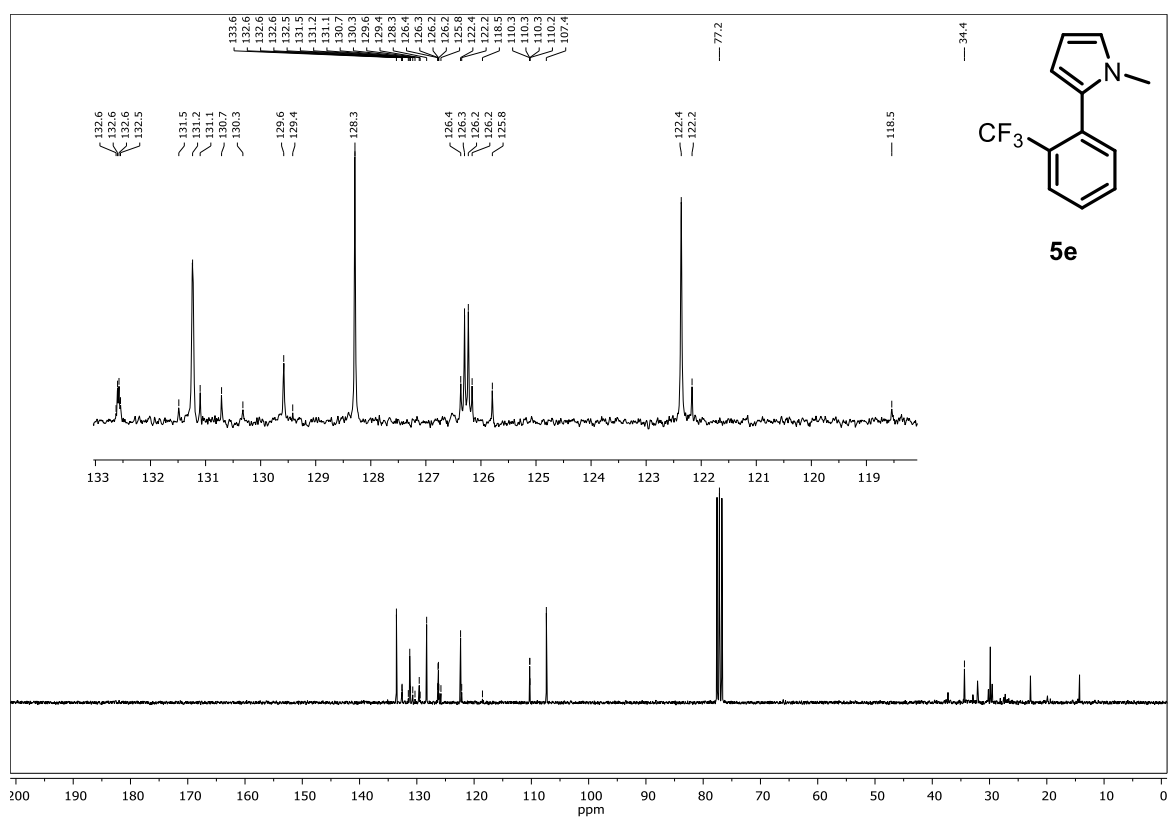
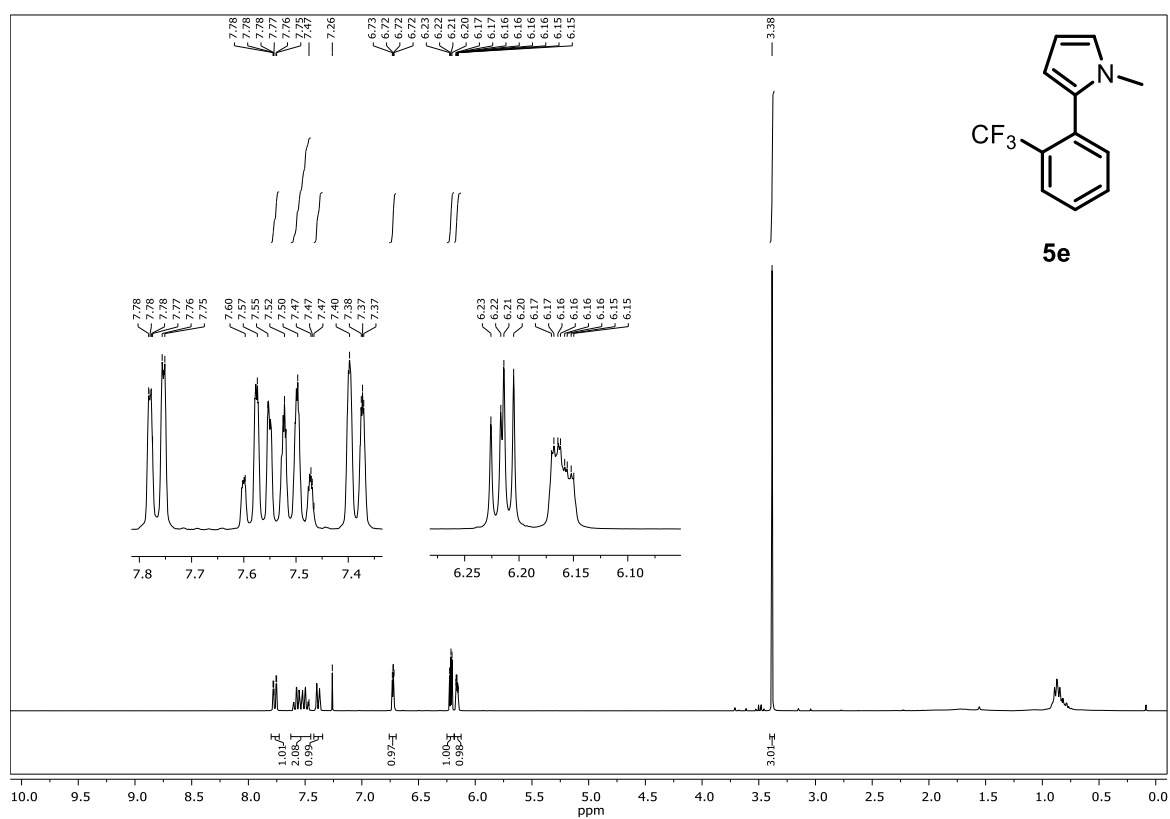
7.3.1 NMR Spectra

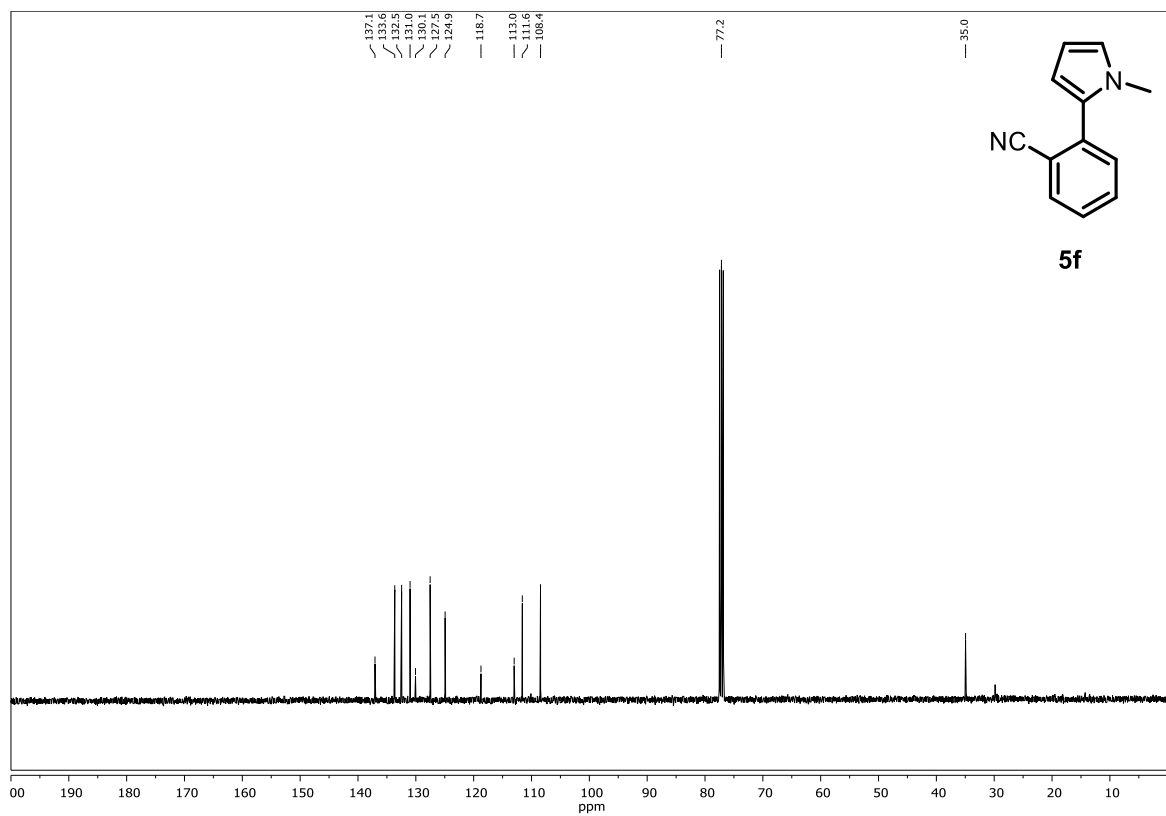
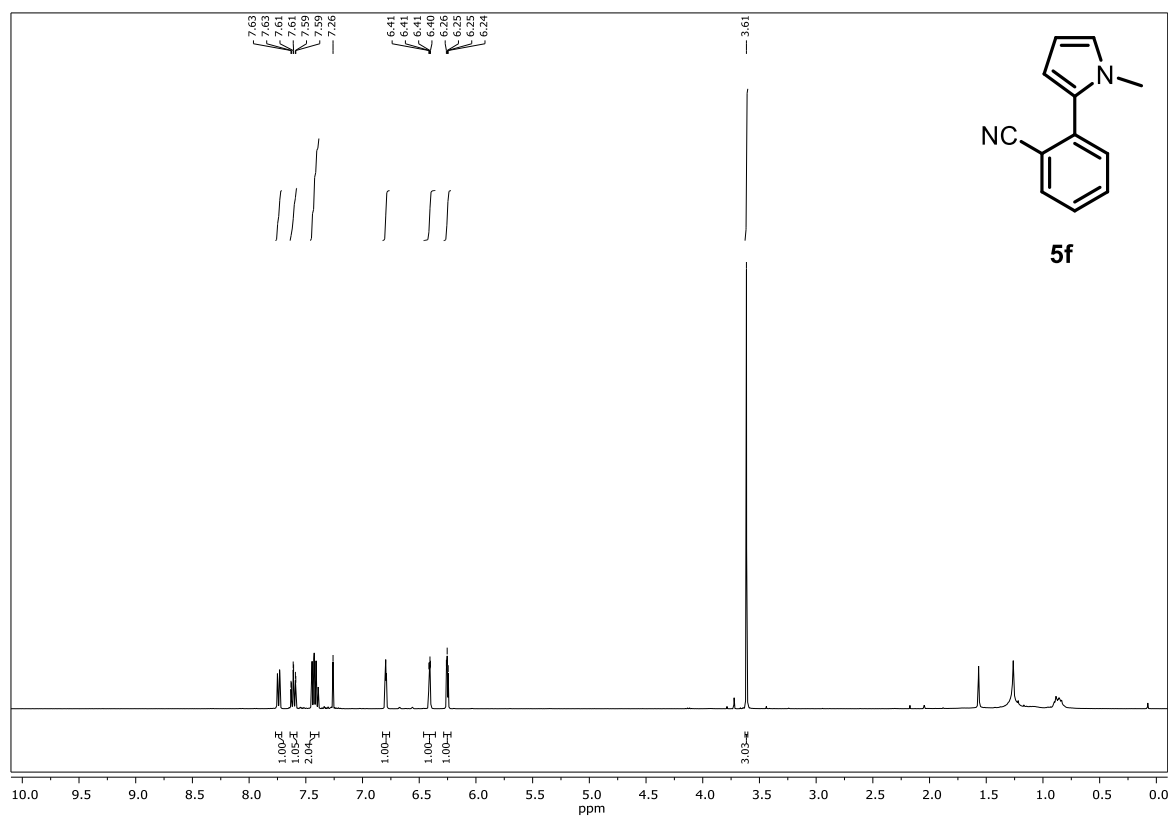


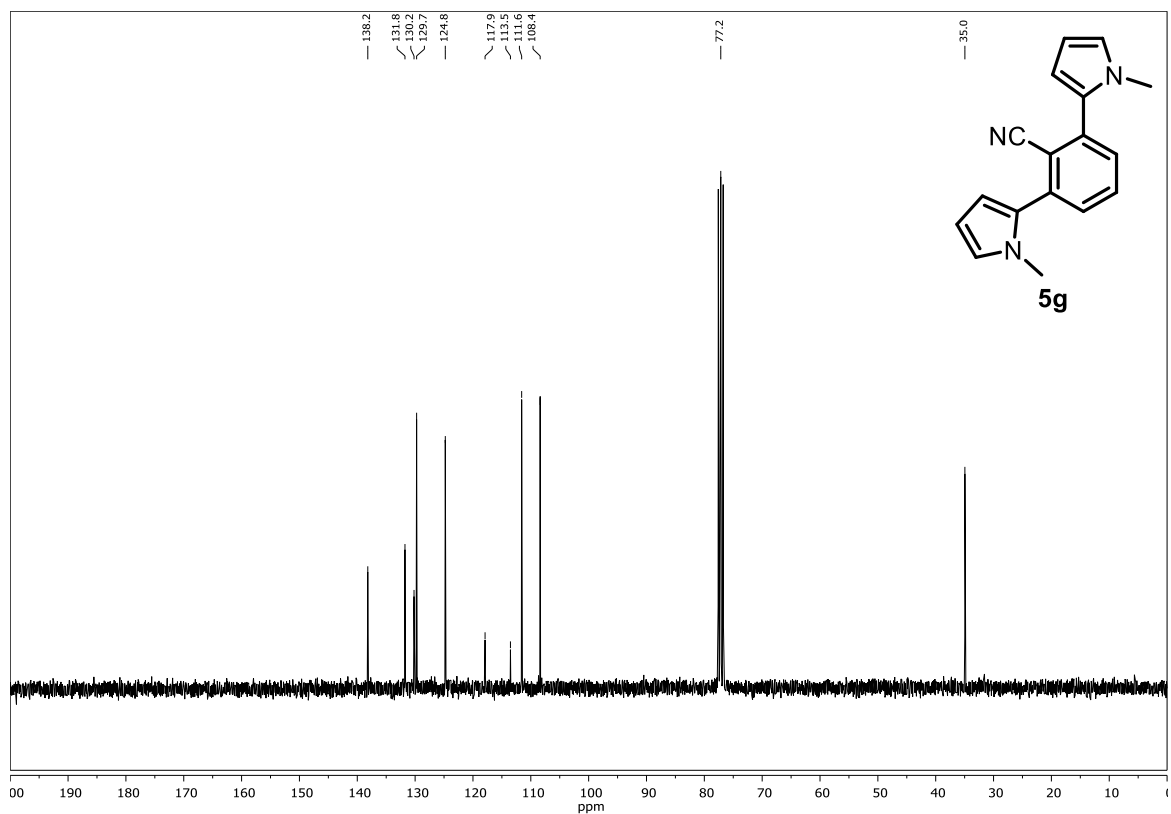
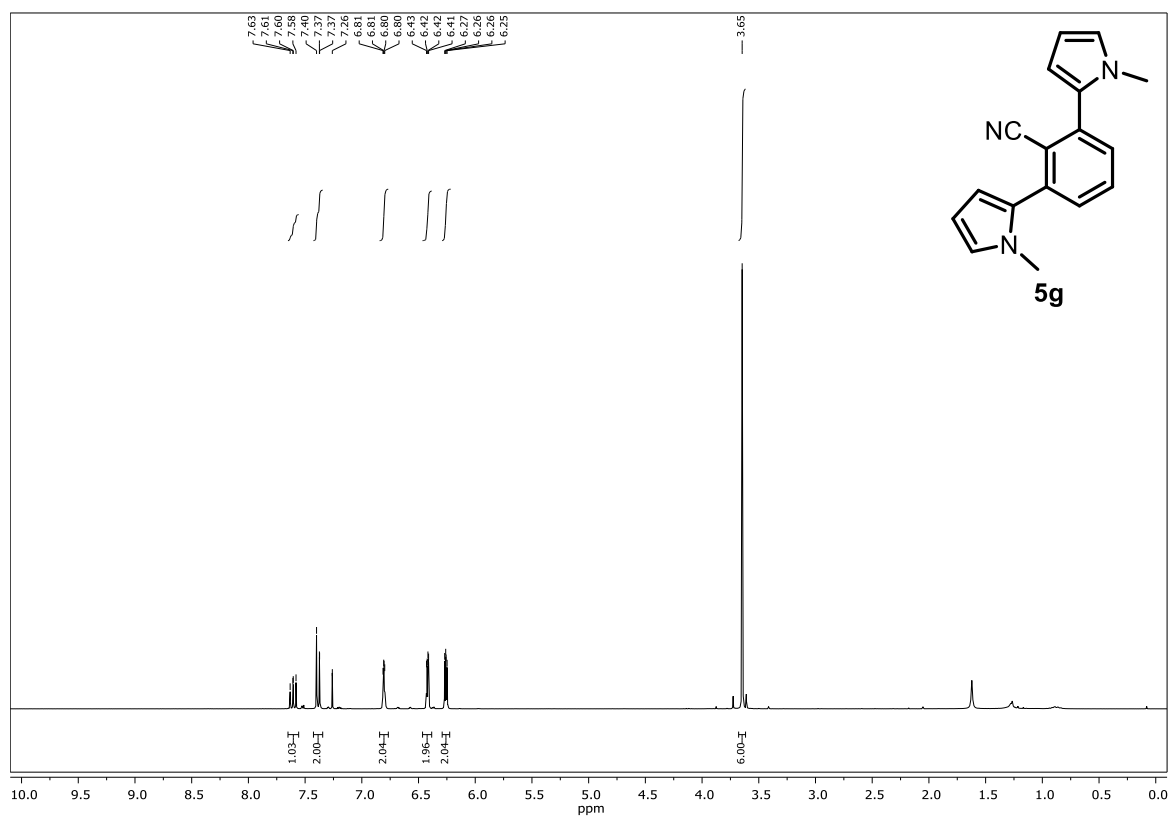


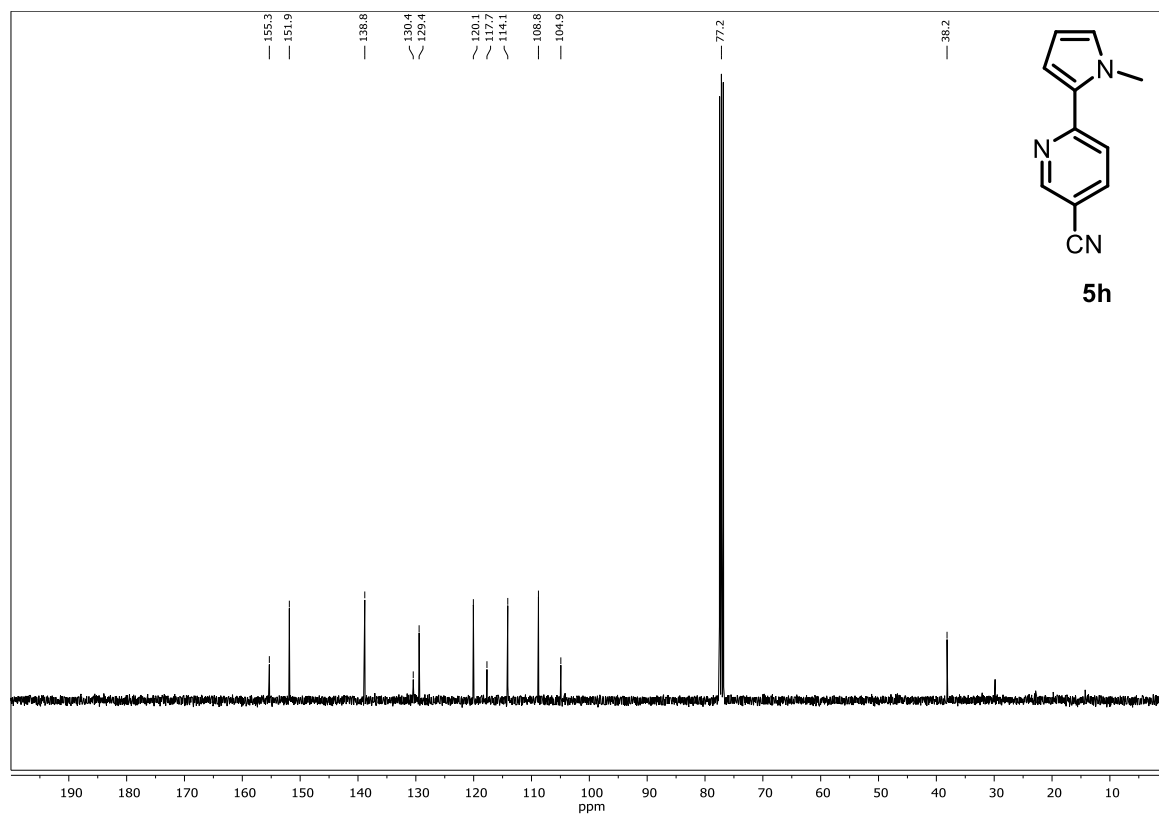
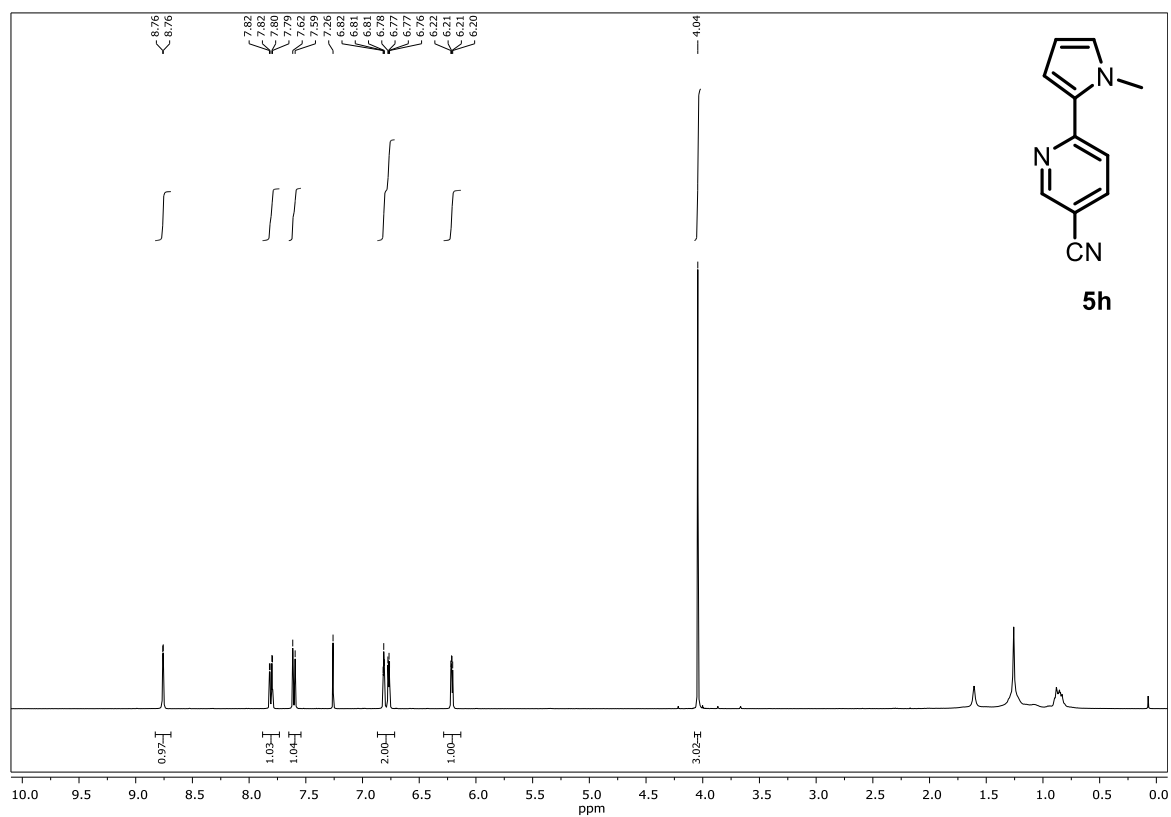


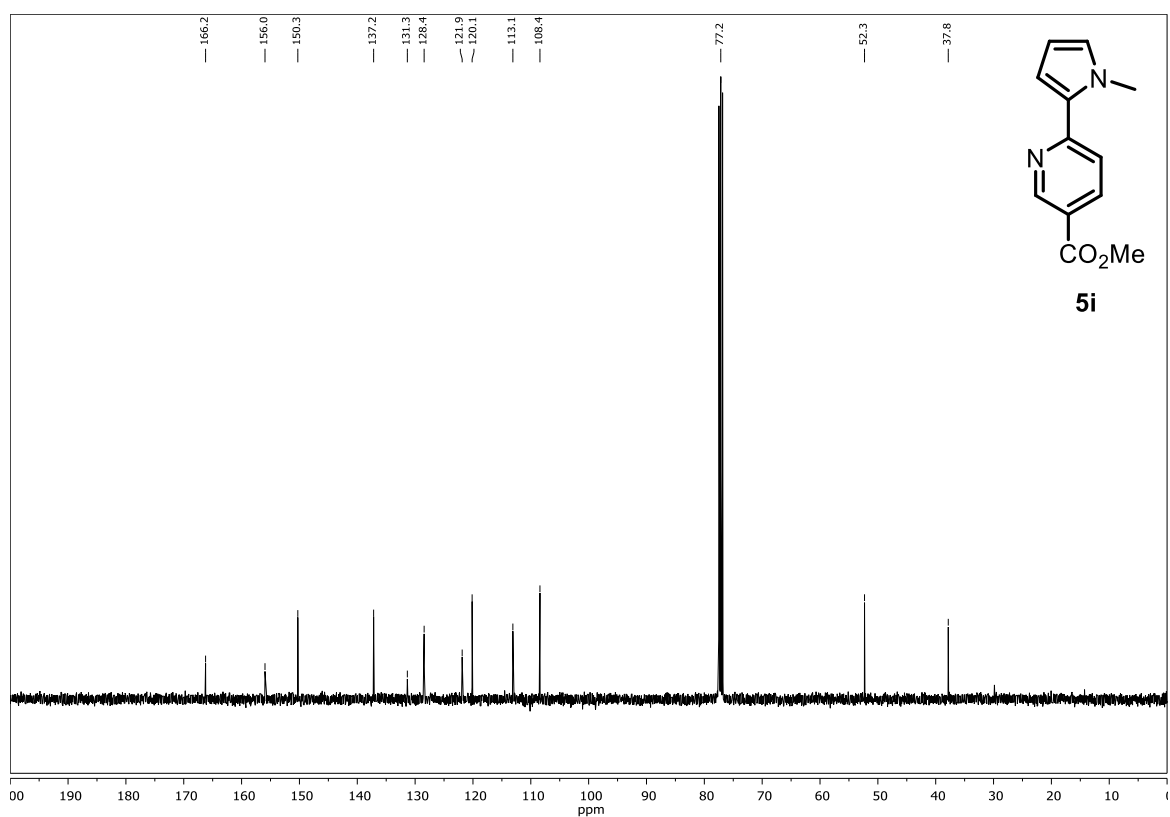
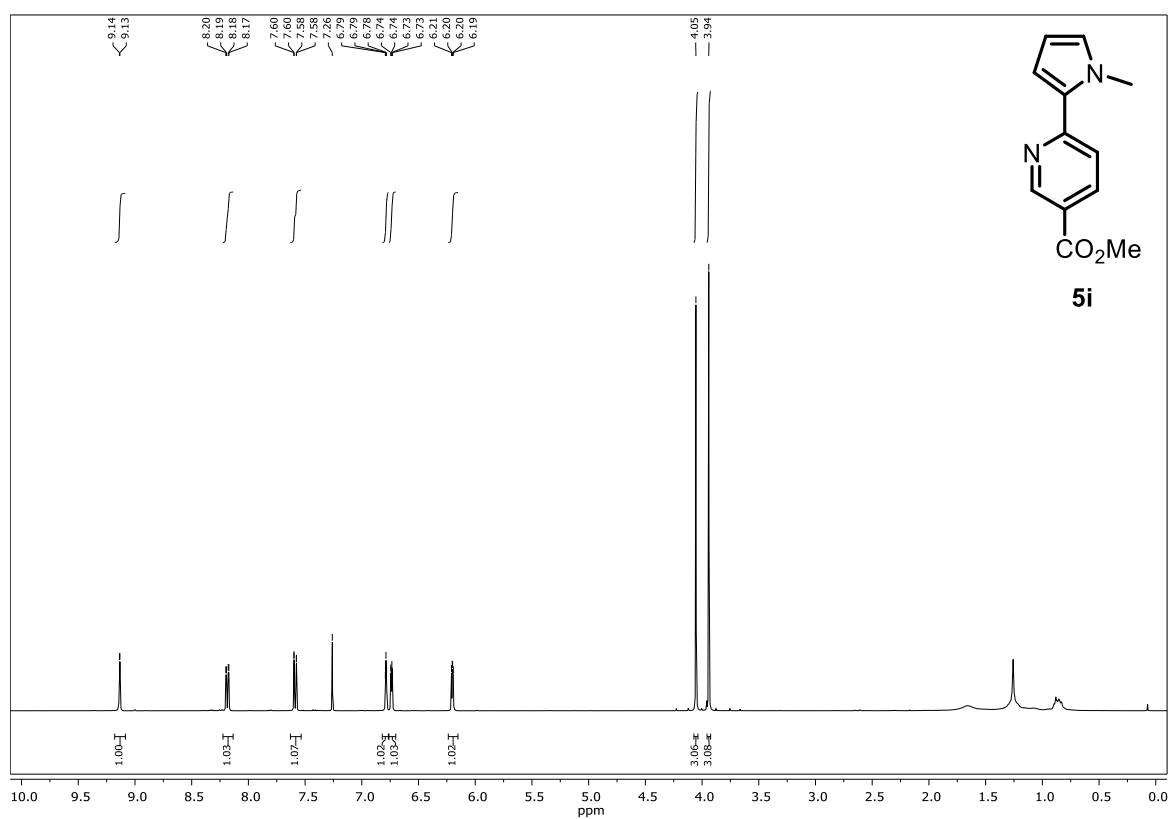


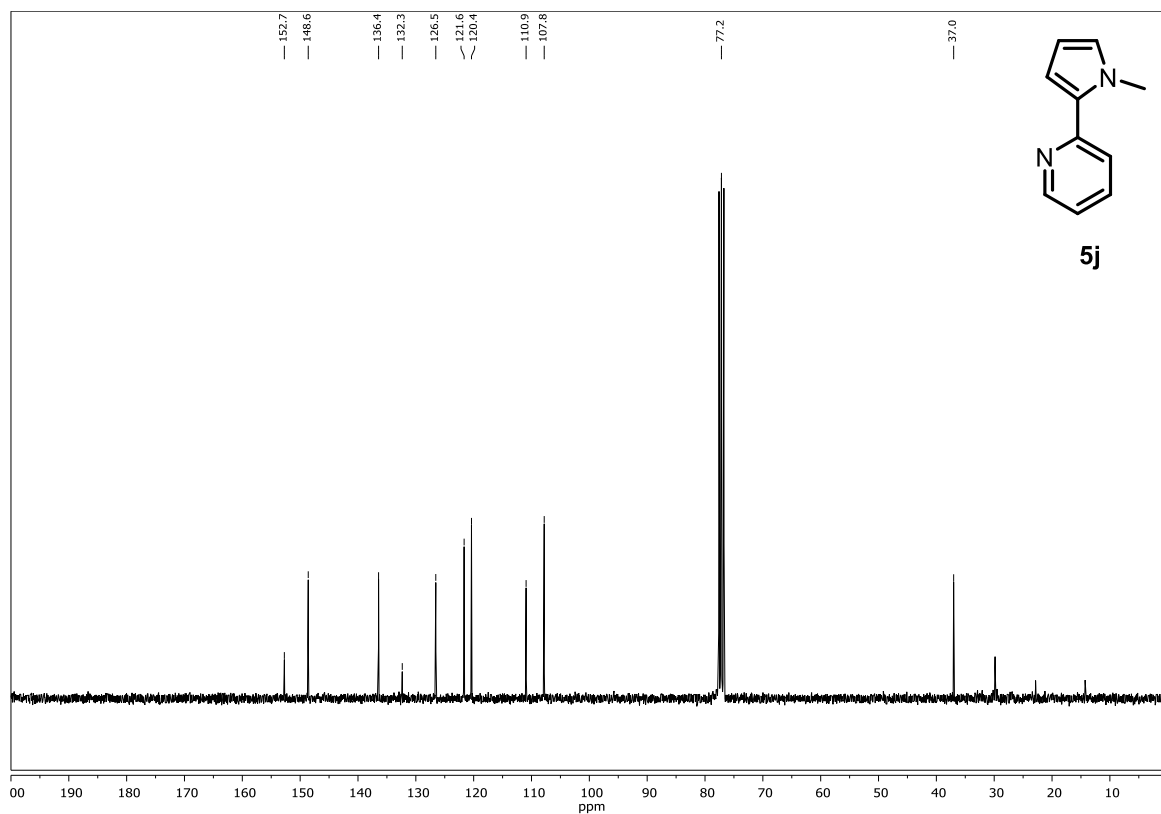
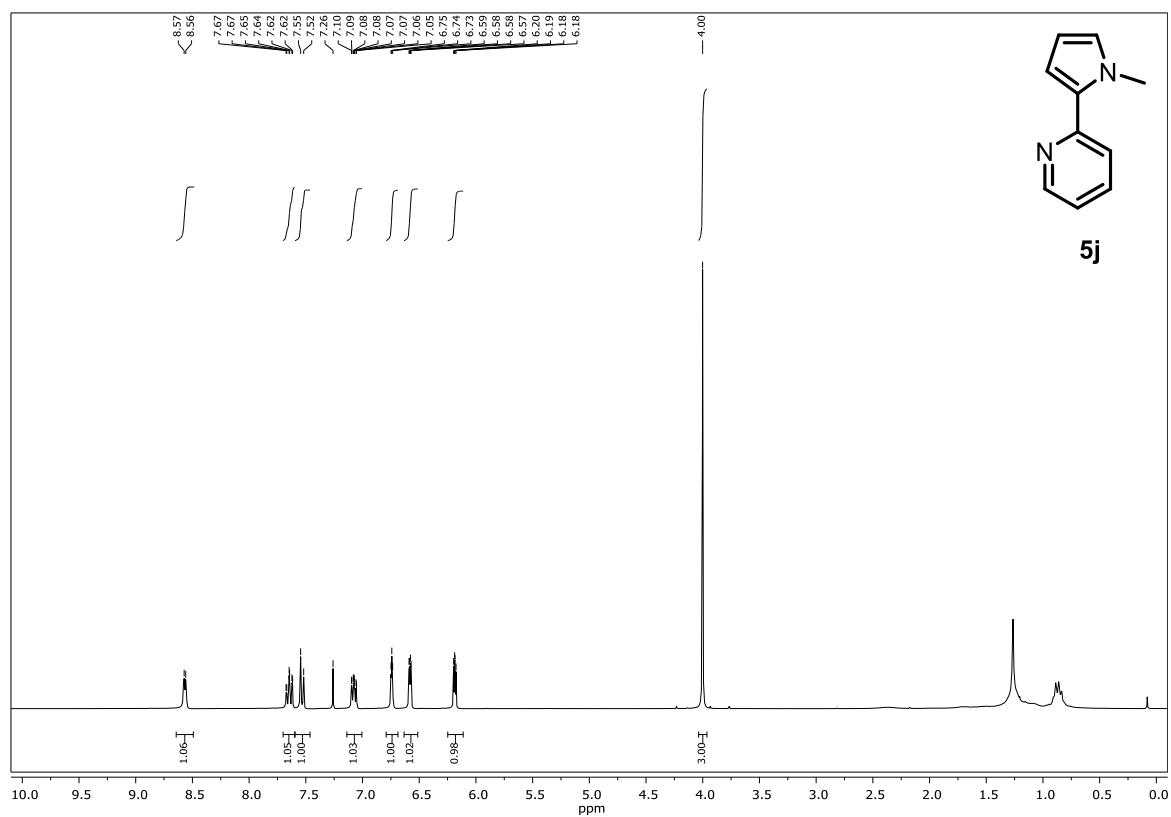


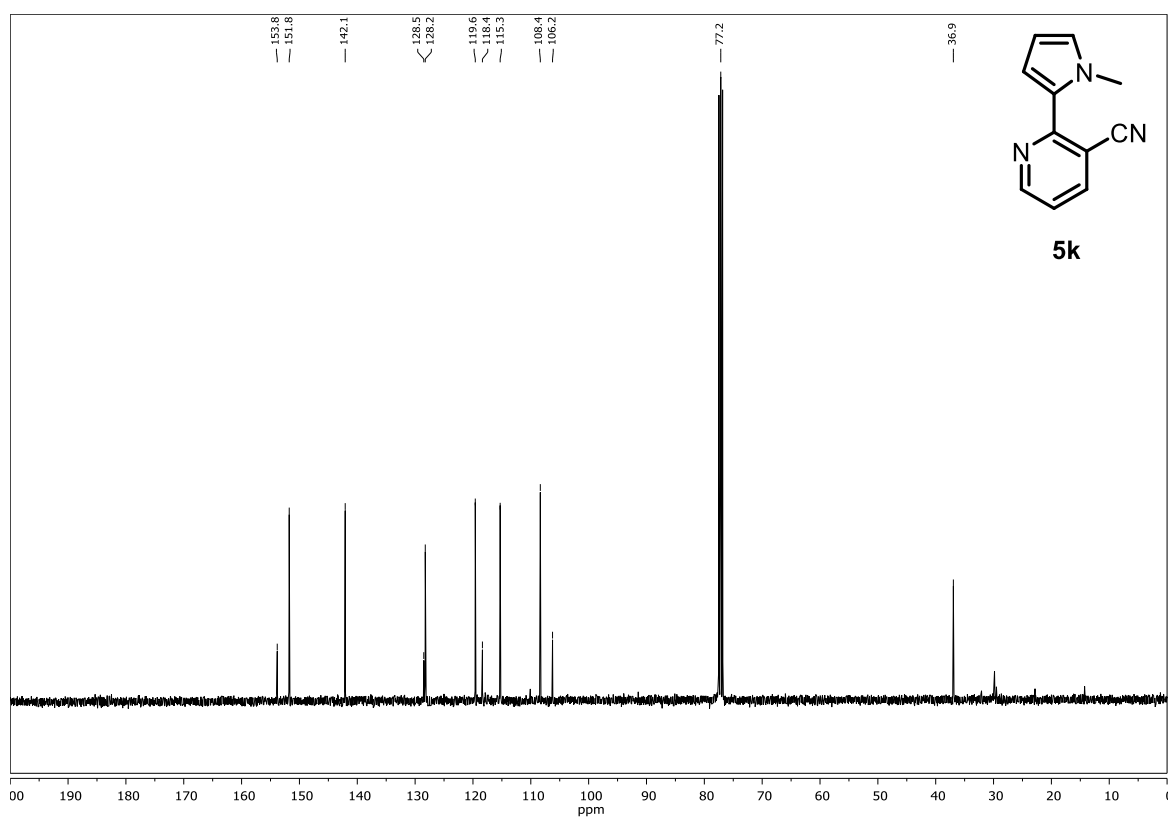
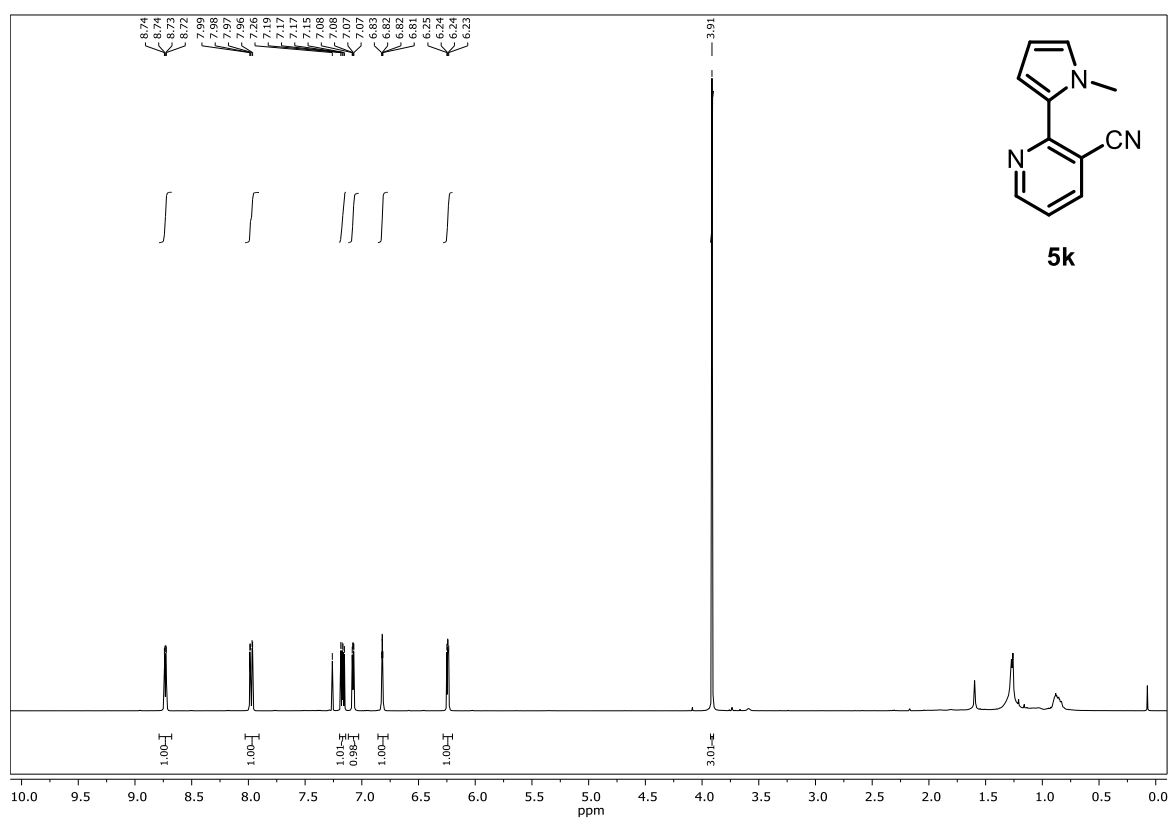


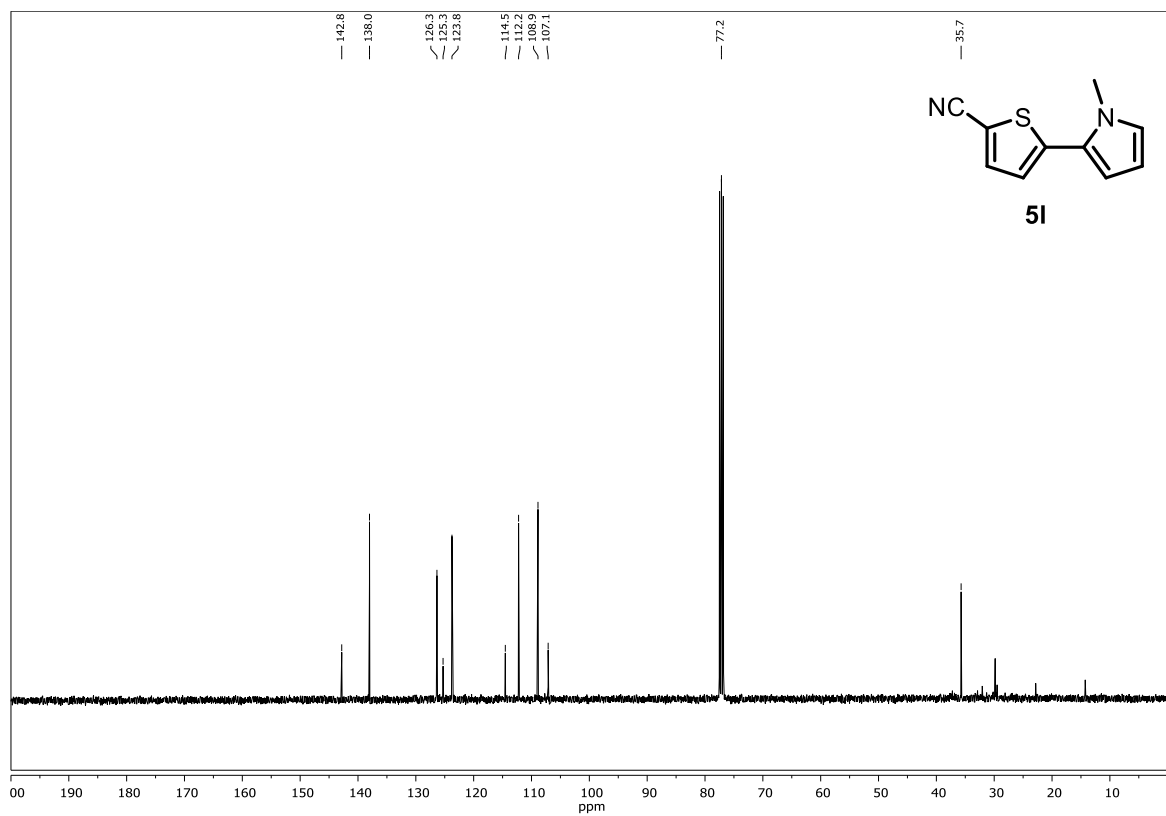
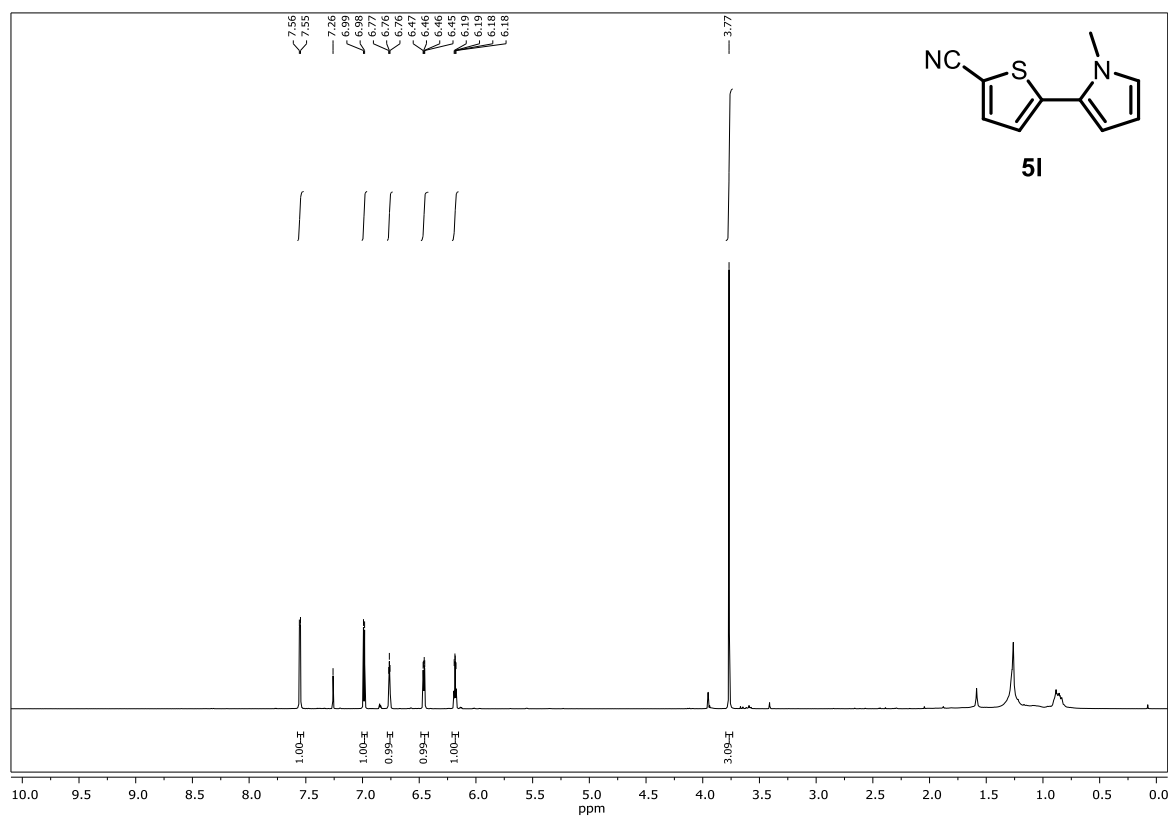


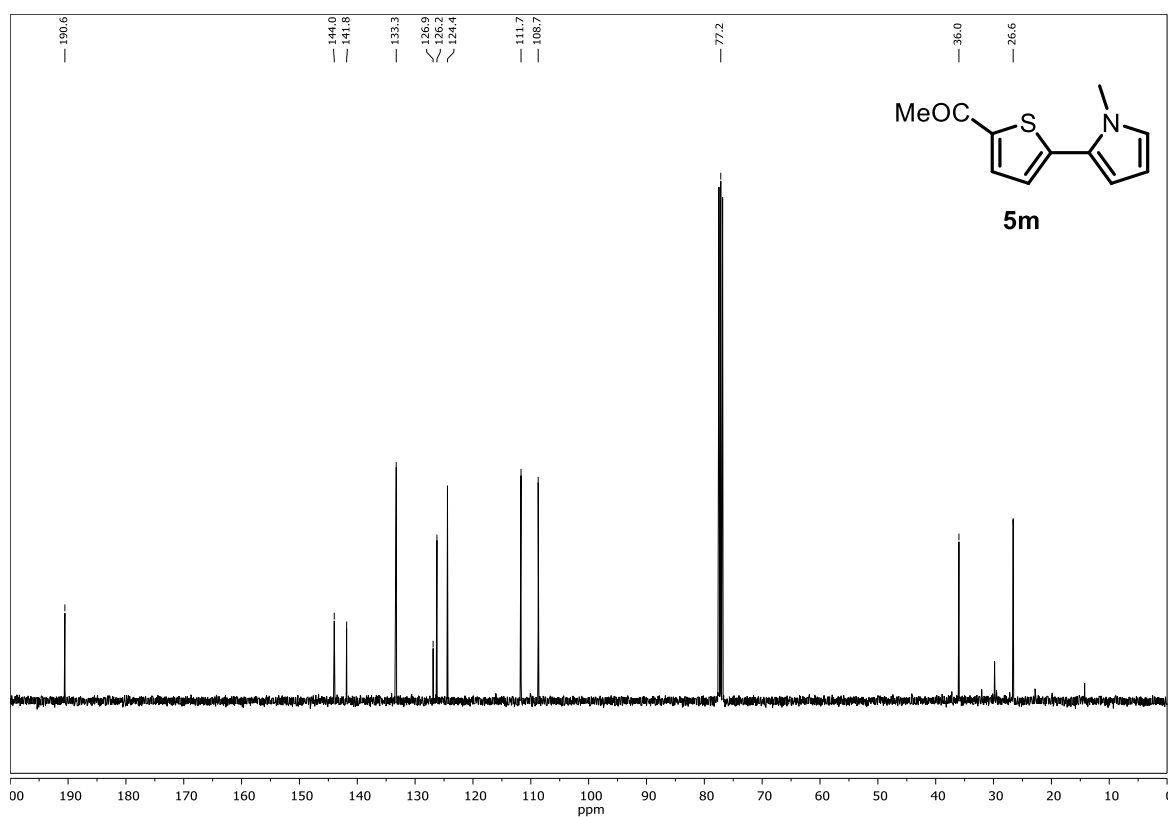
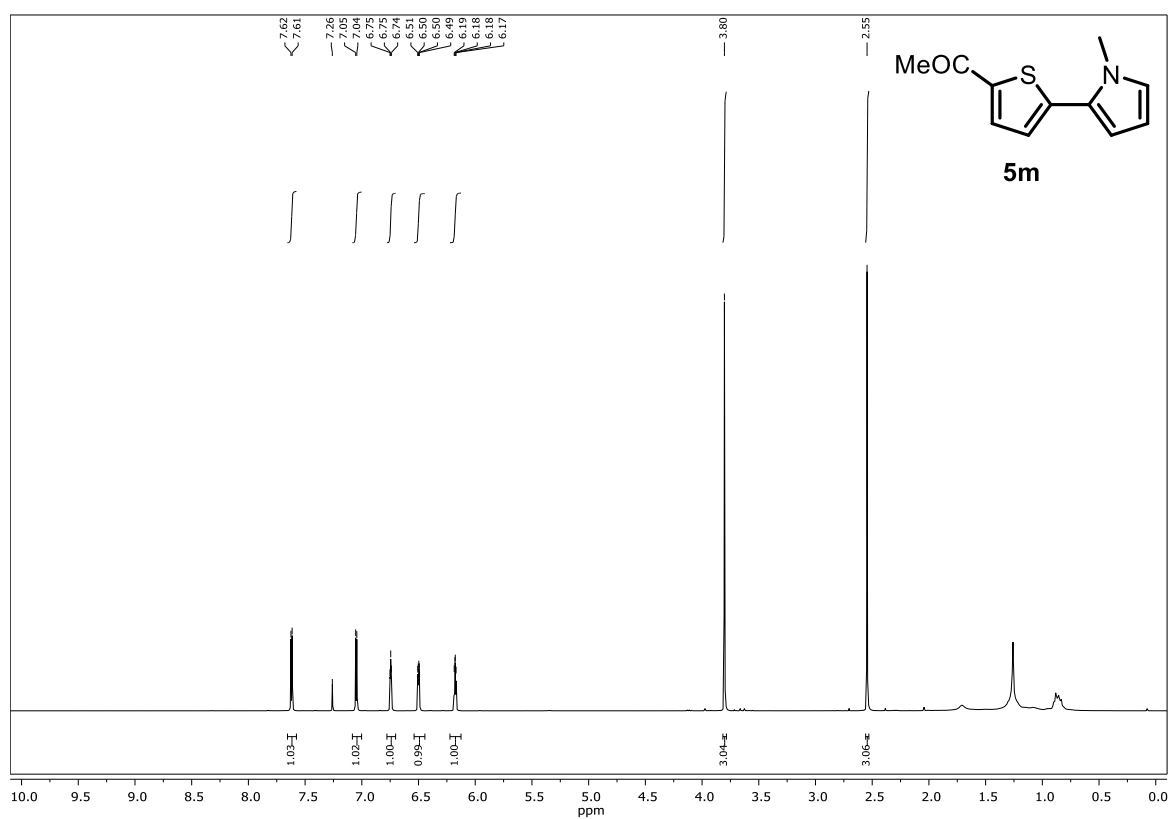


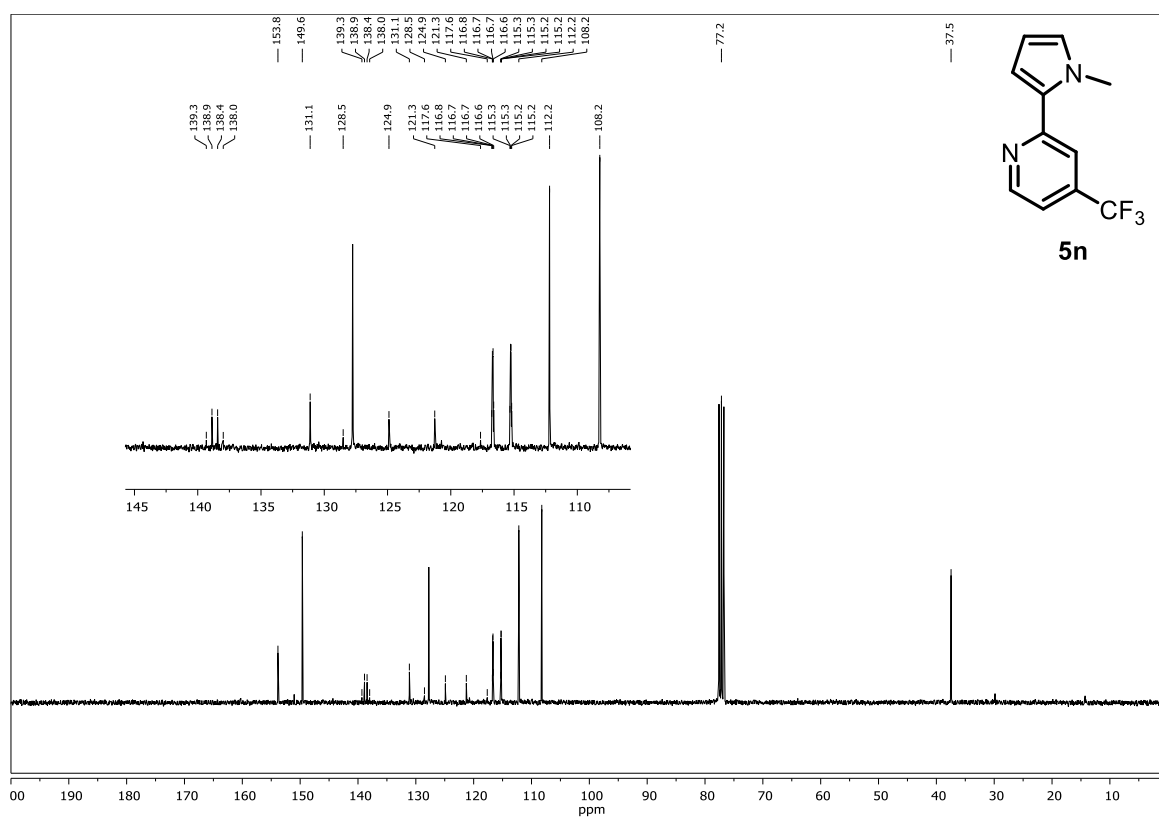
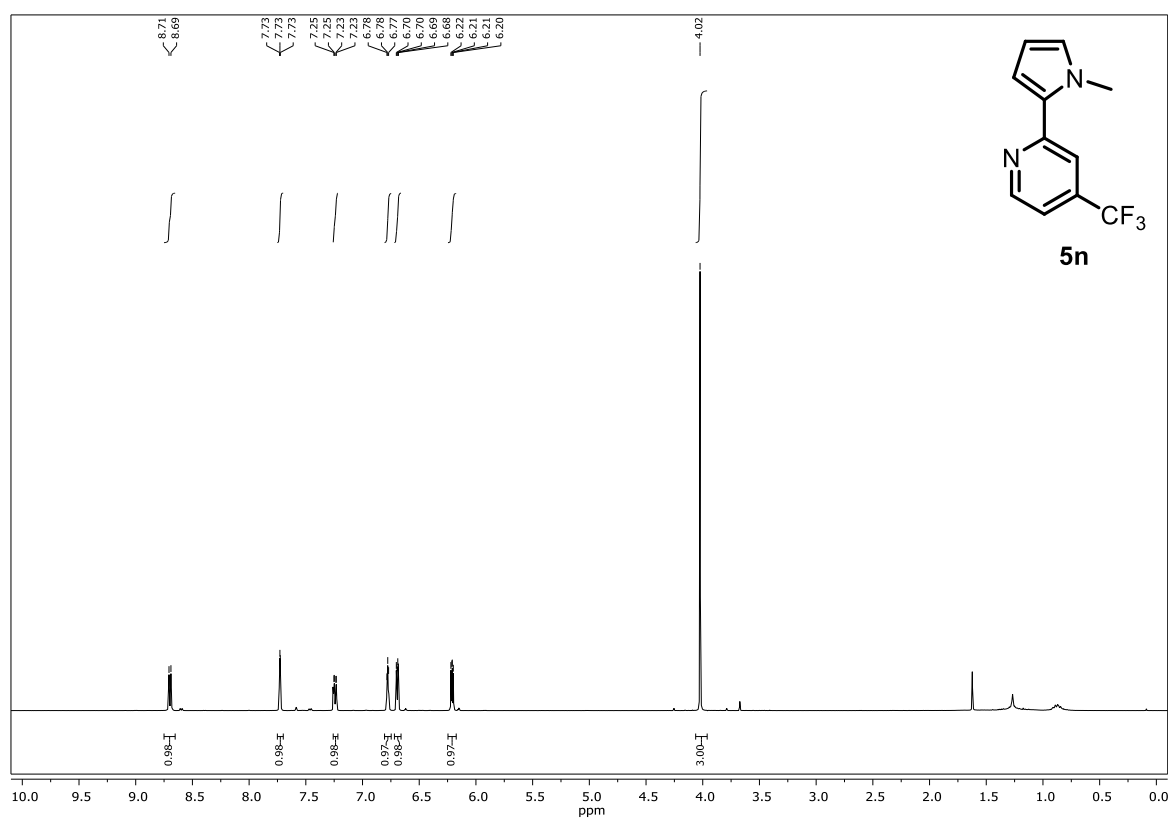


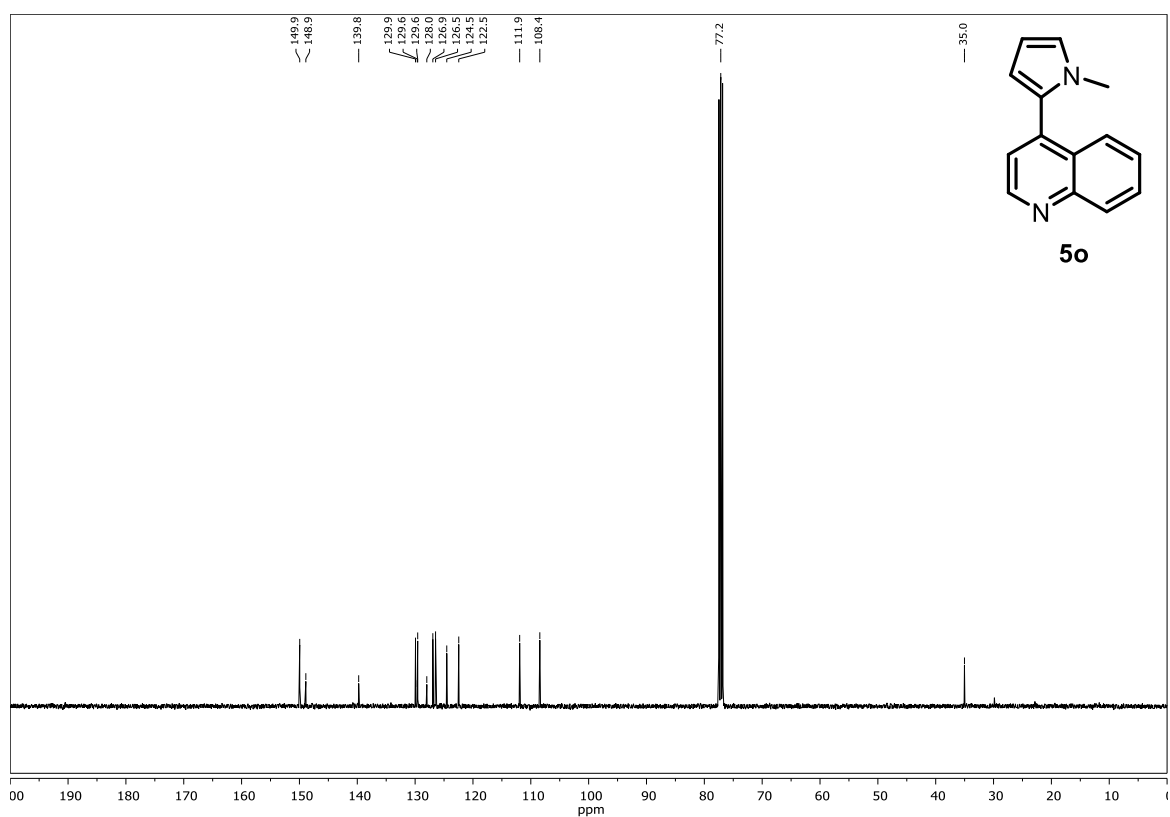
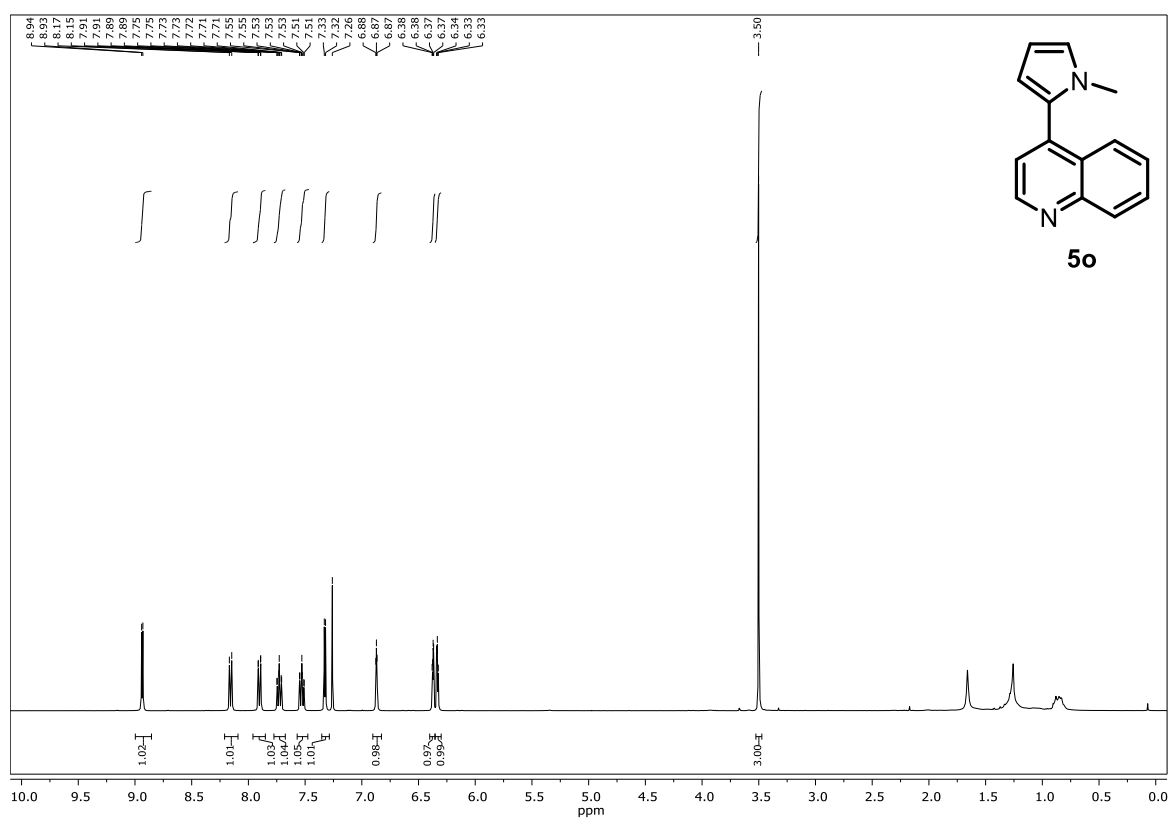


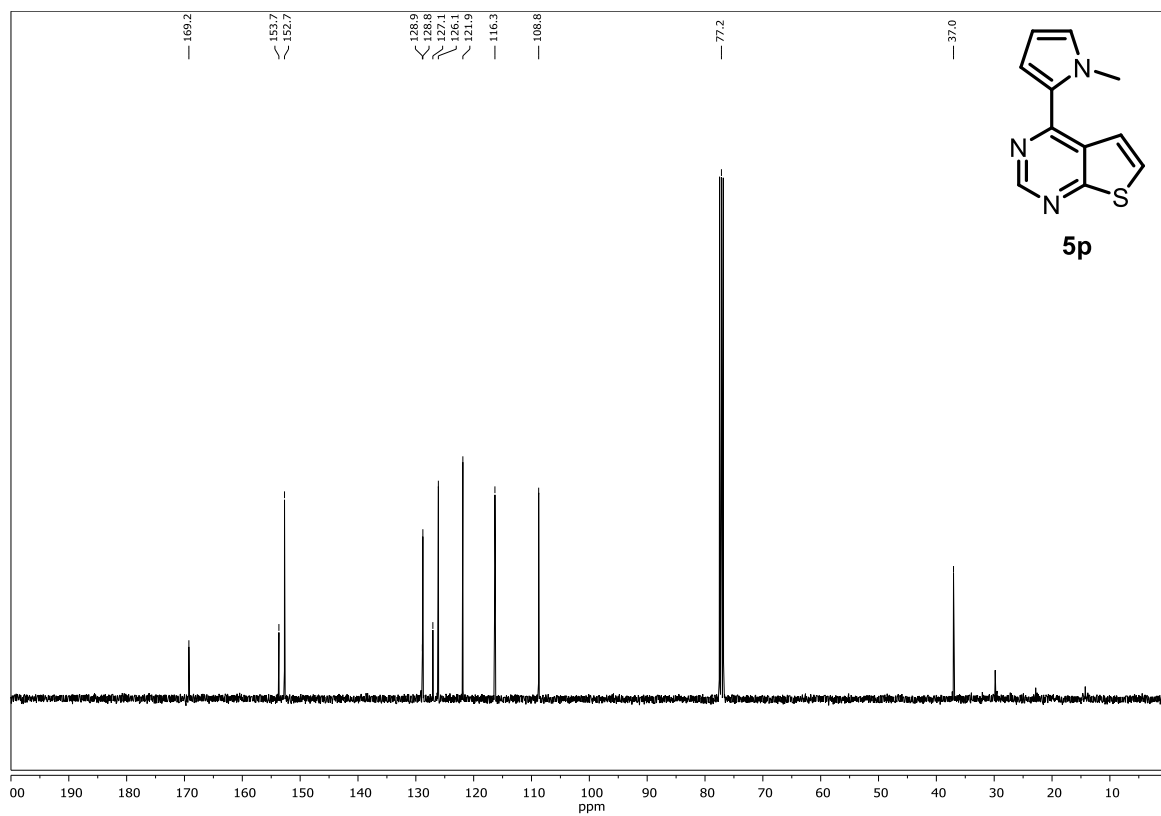
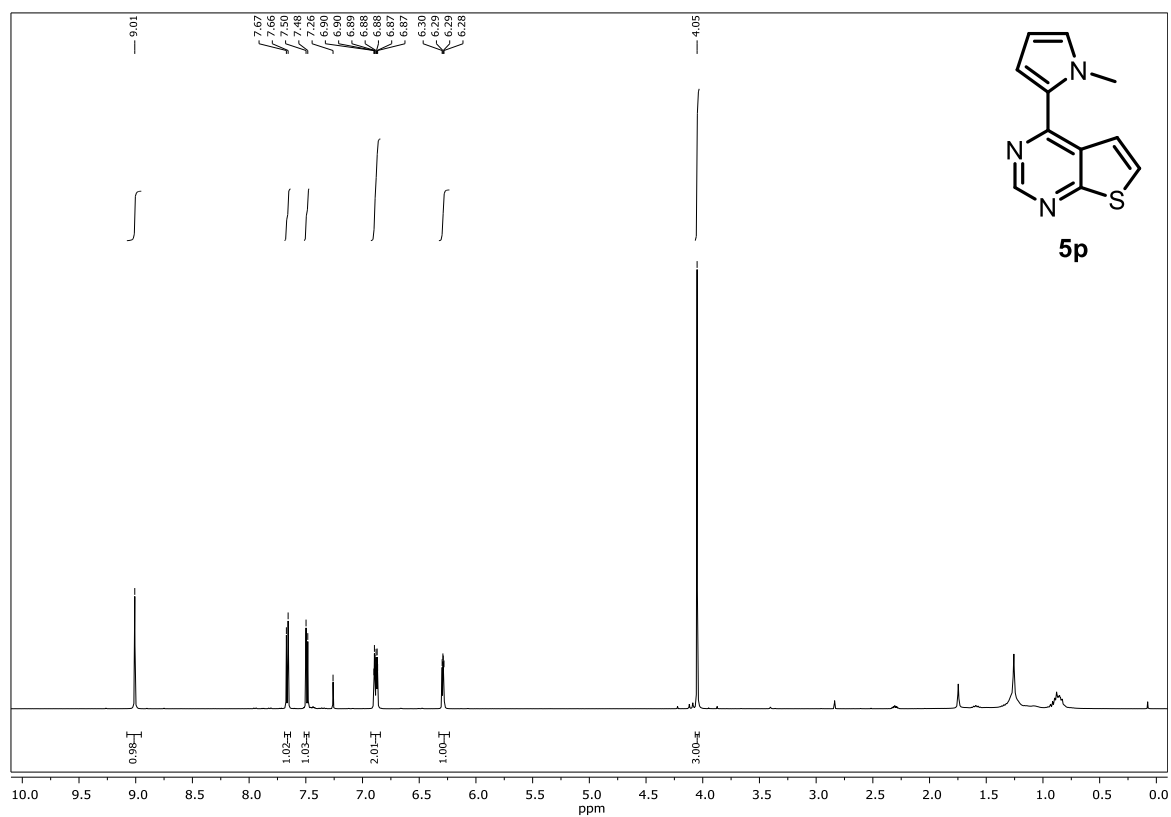


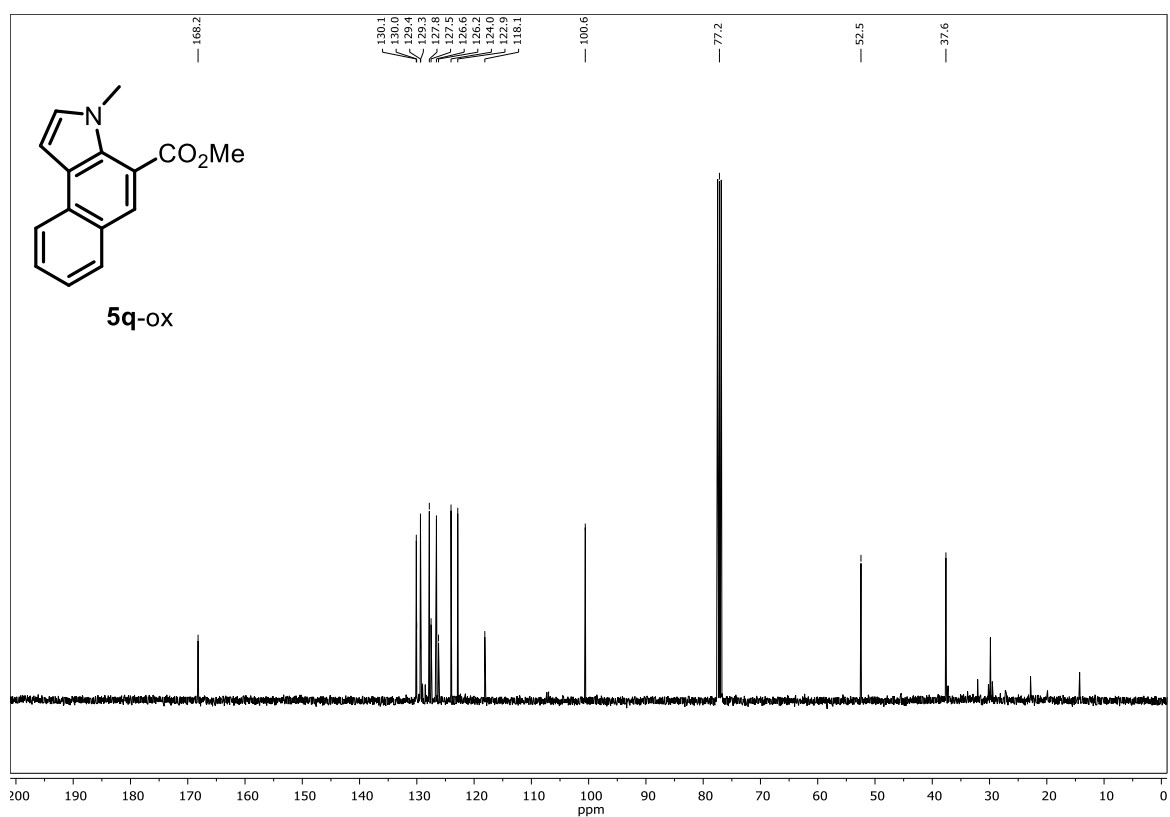
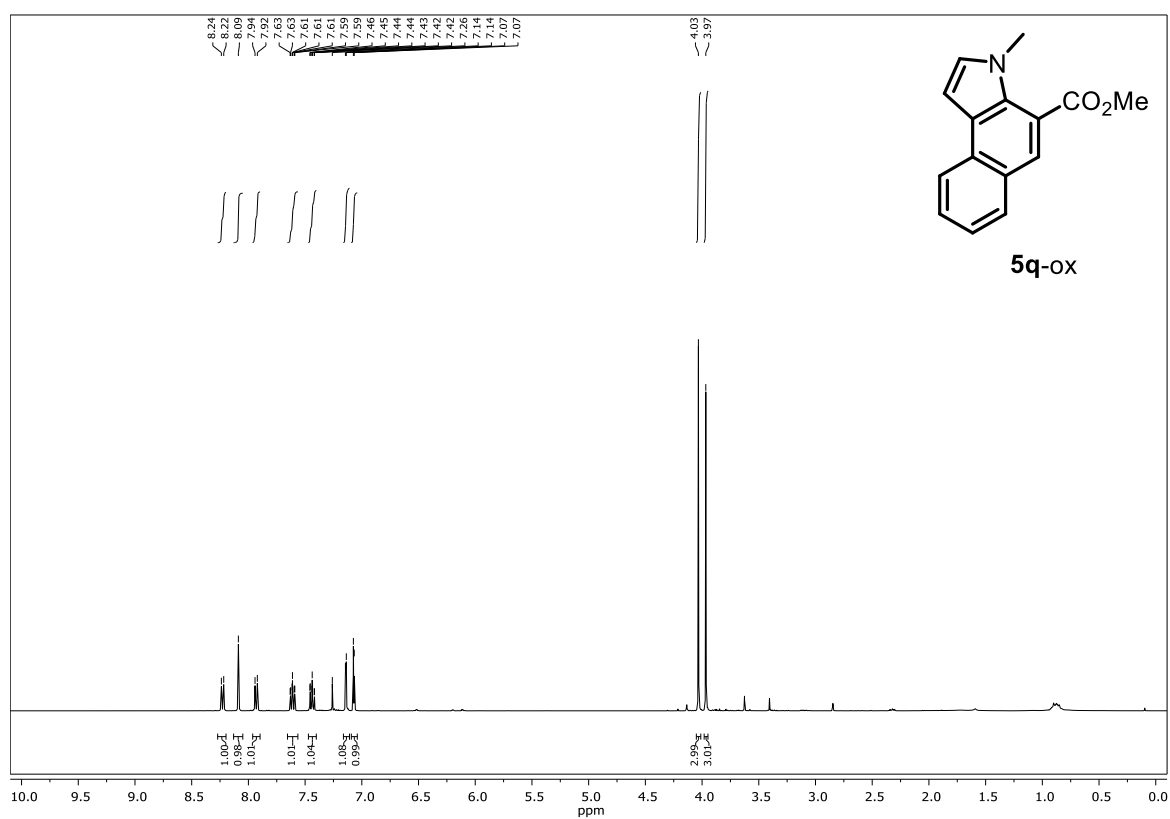


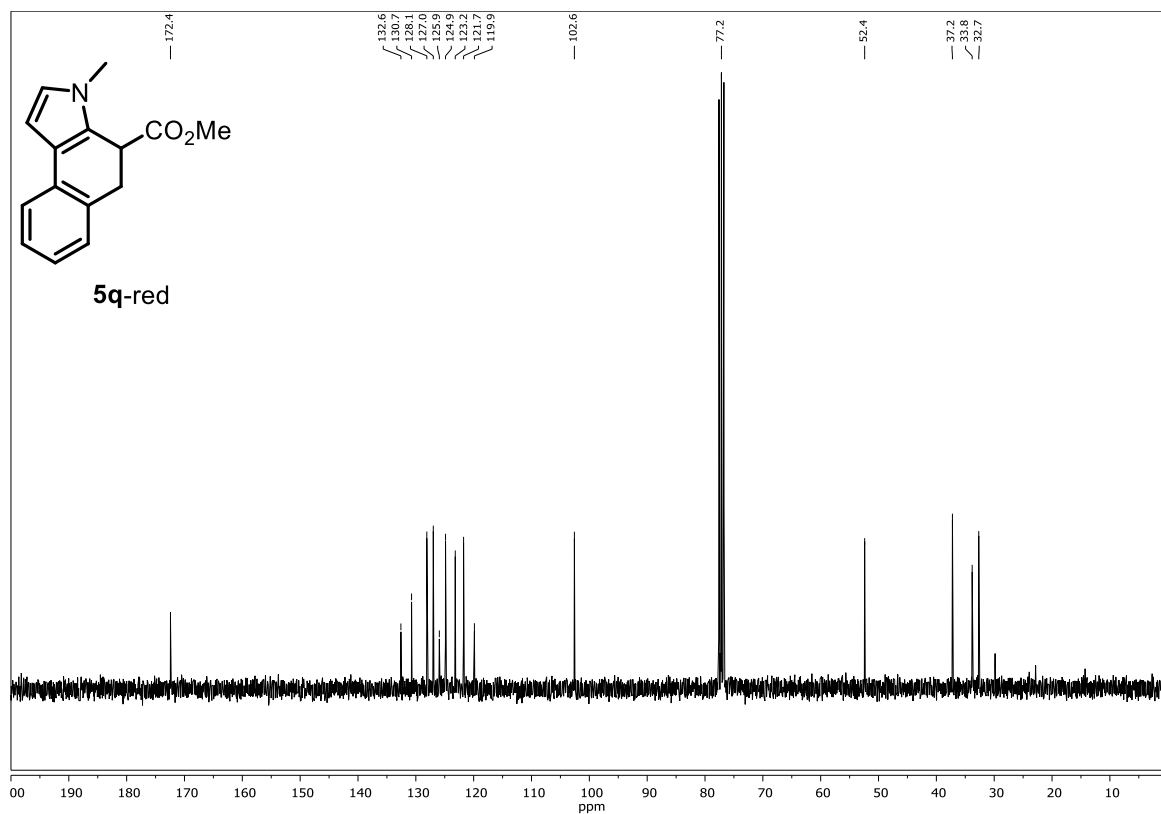
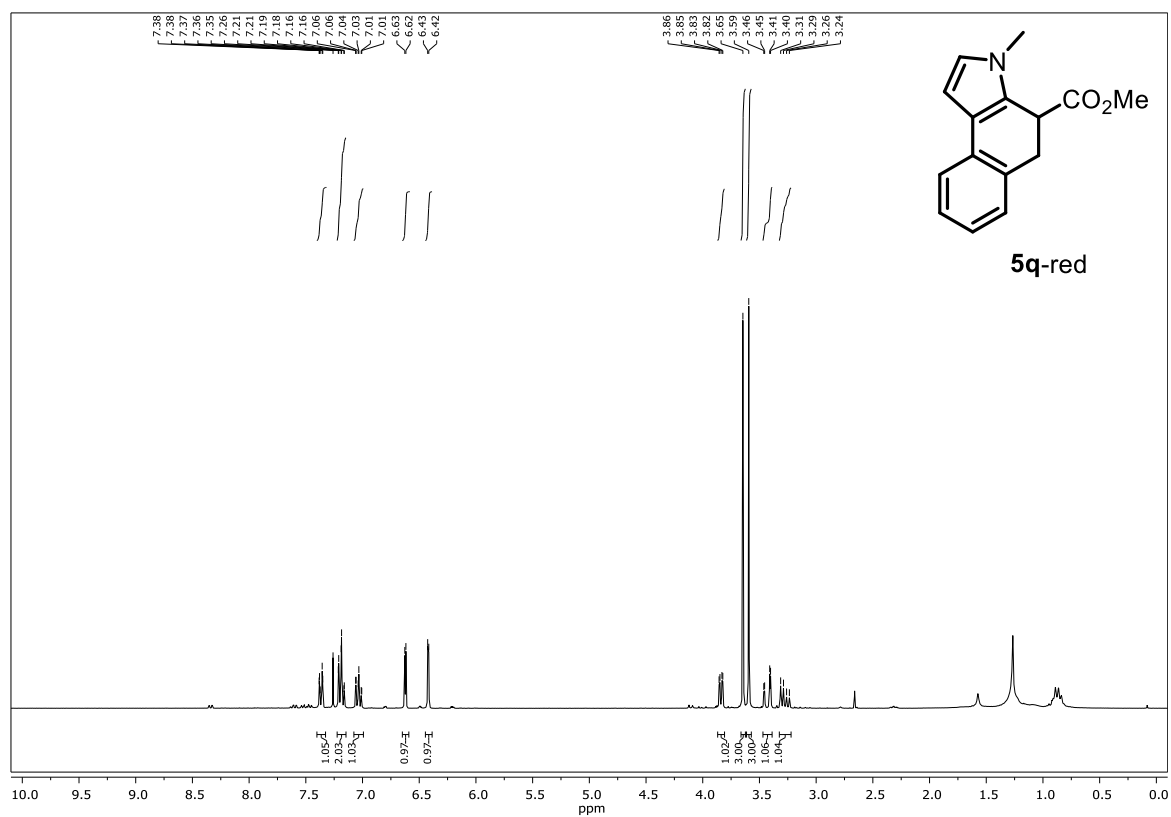


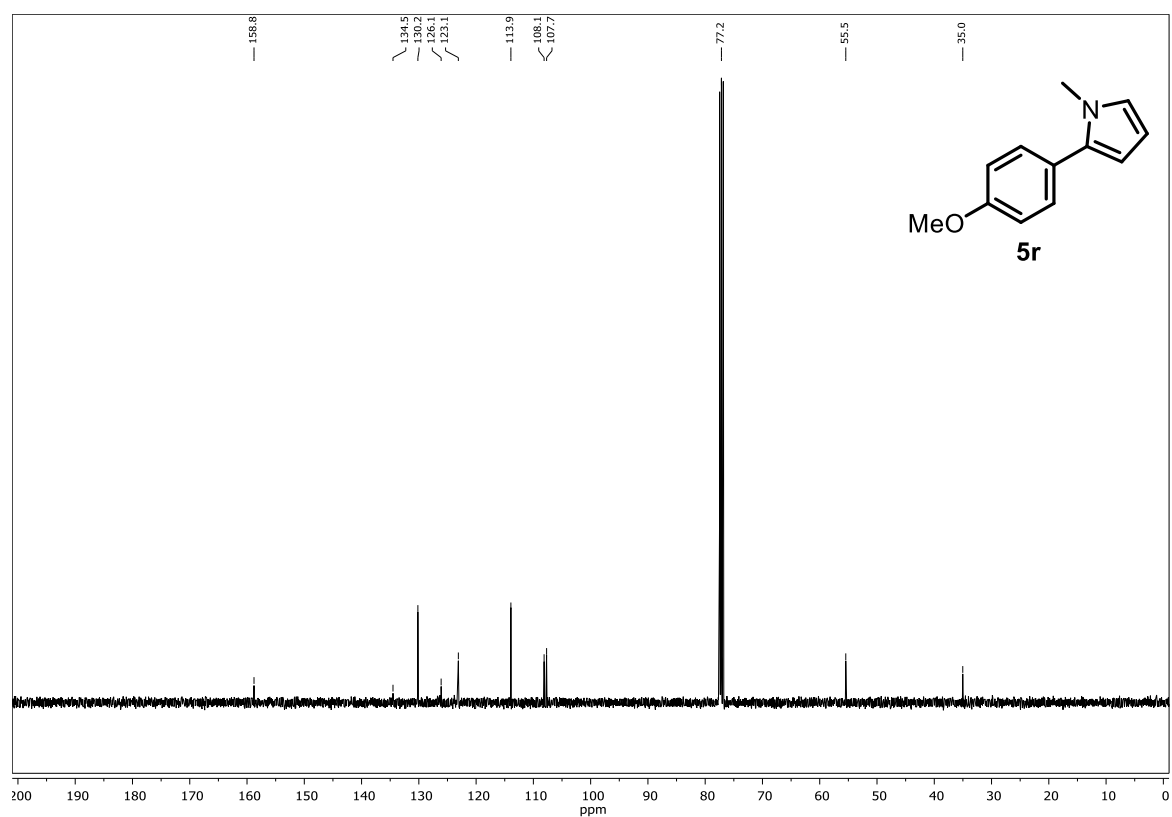
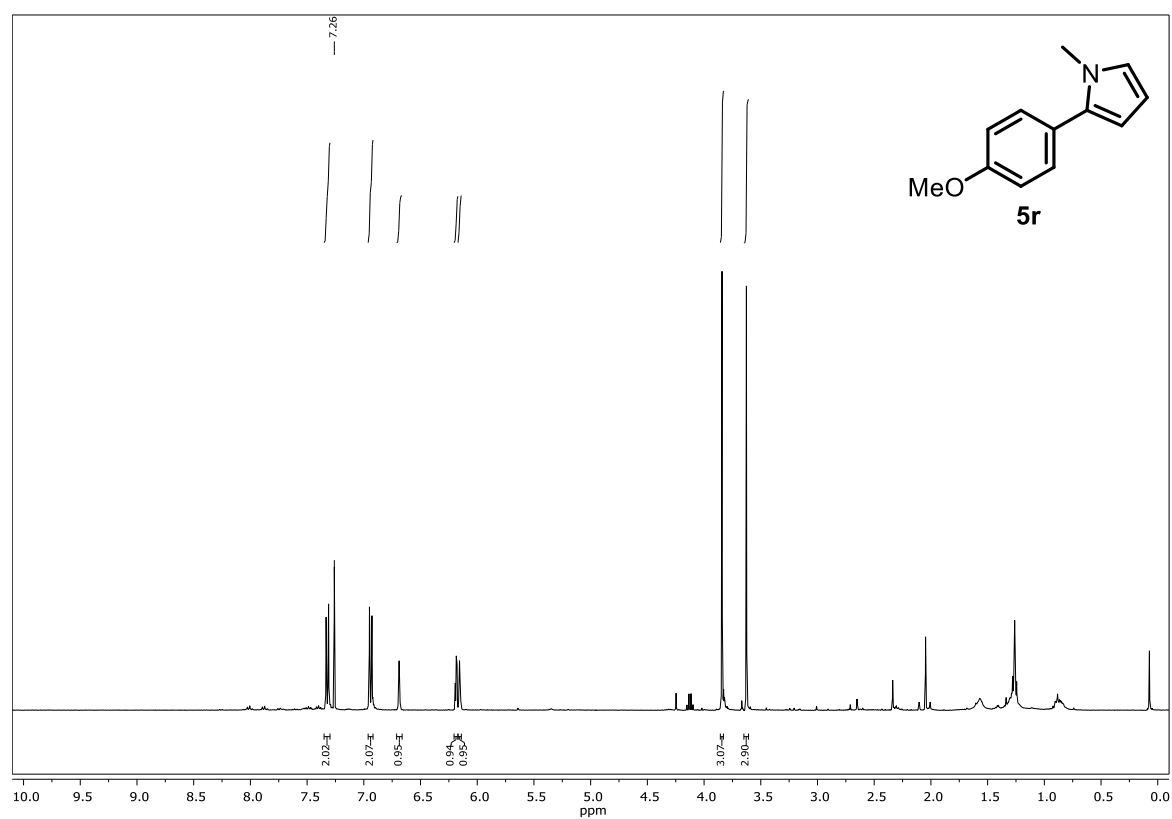


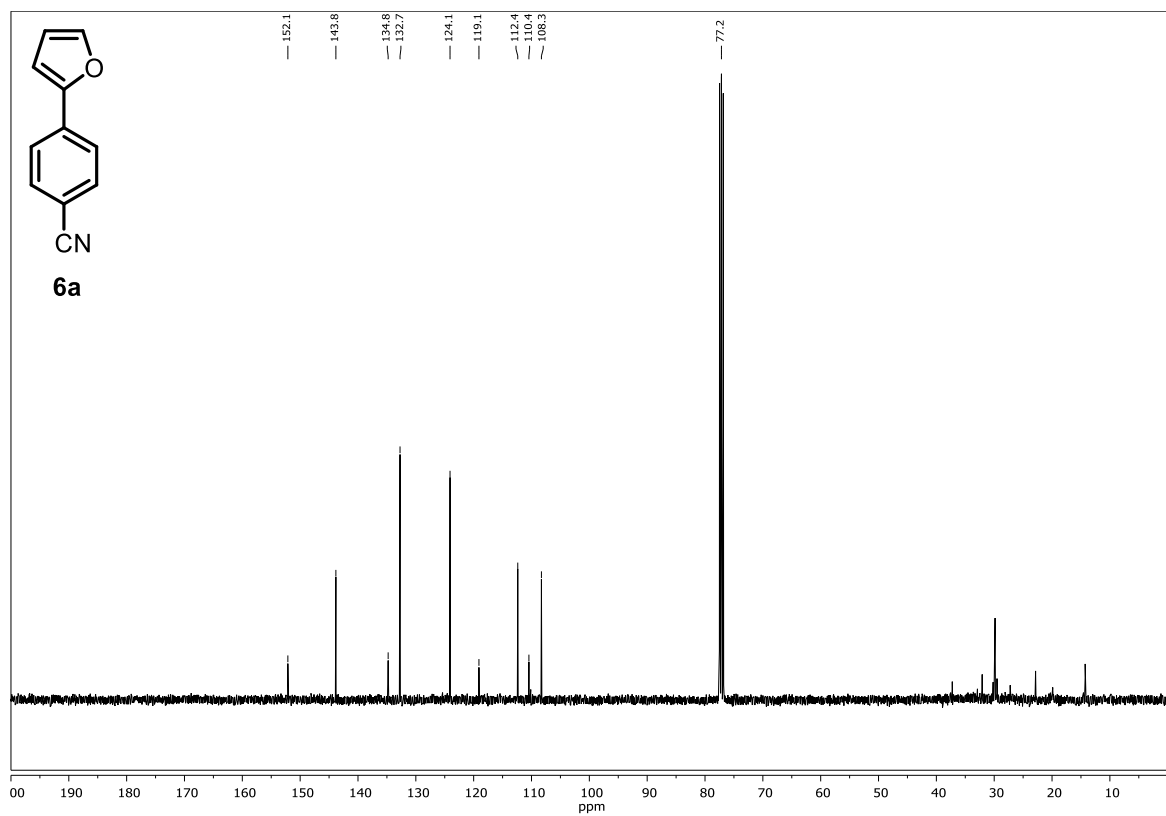
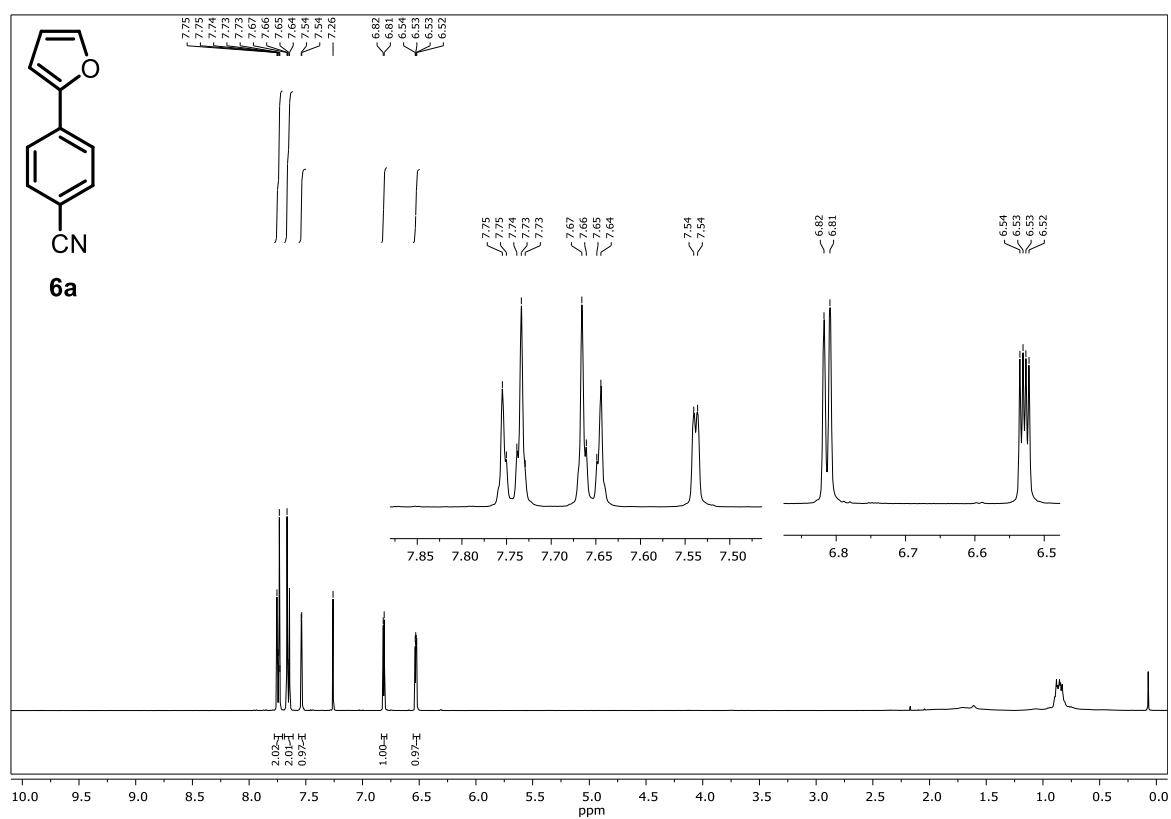


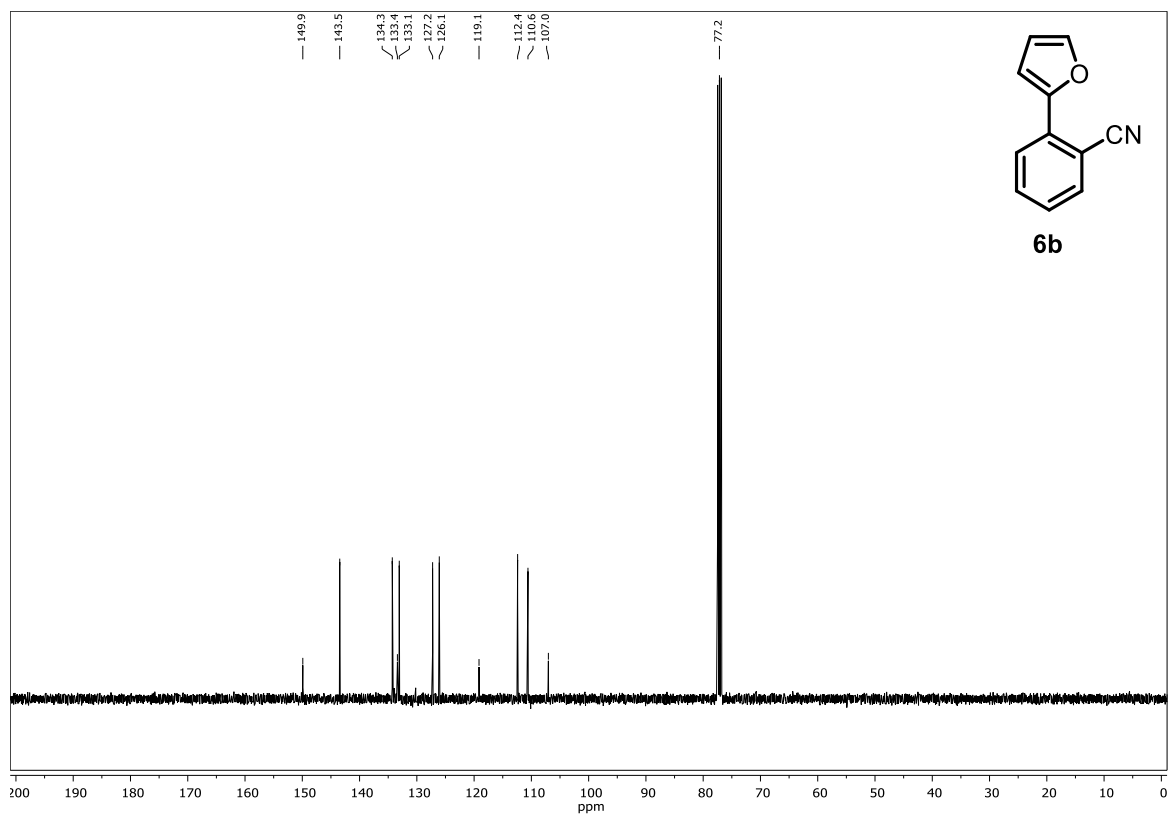
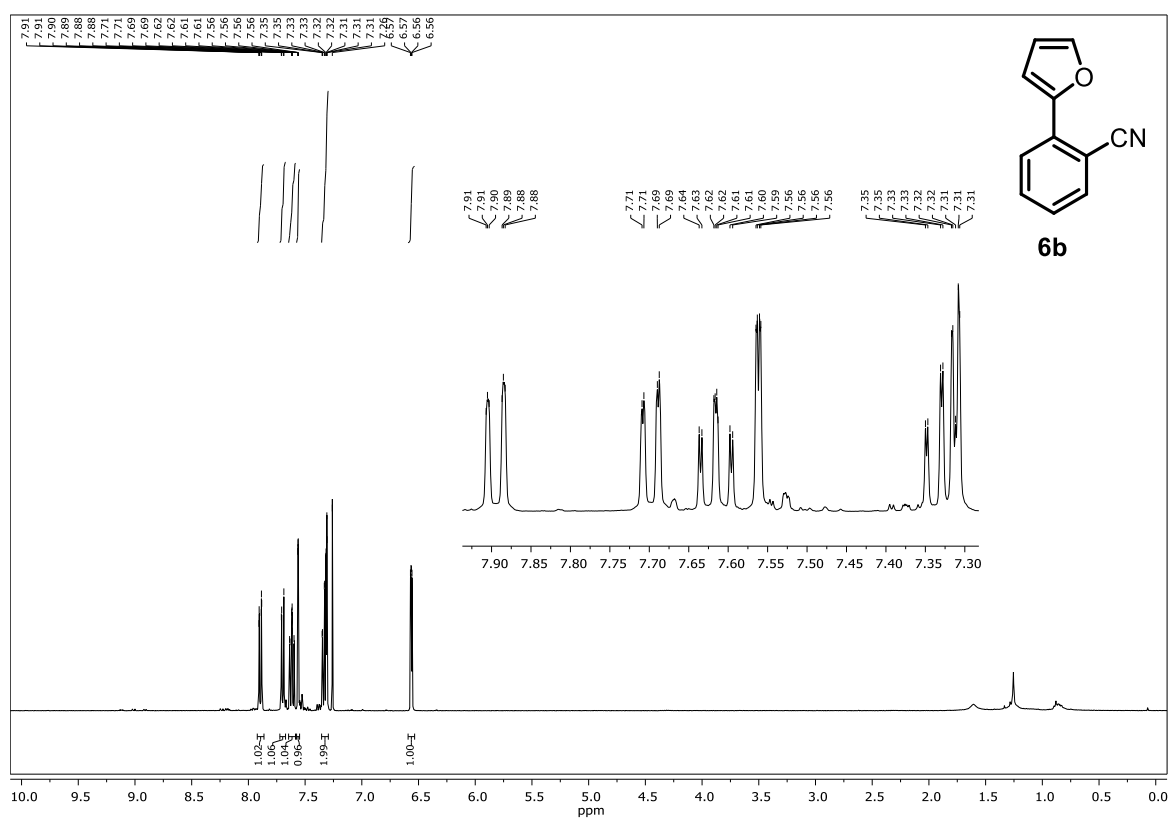


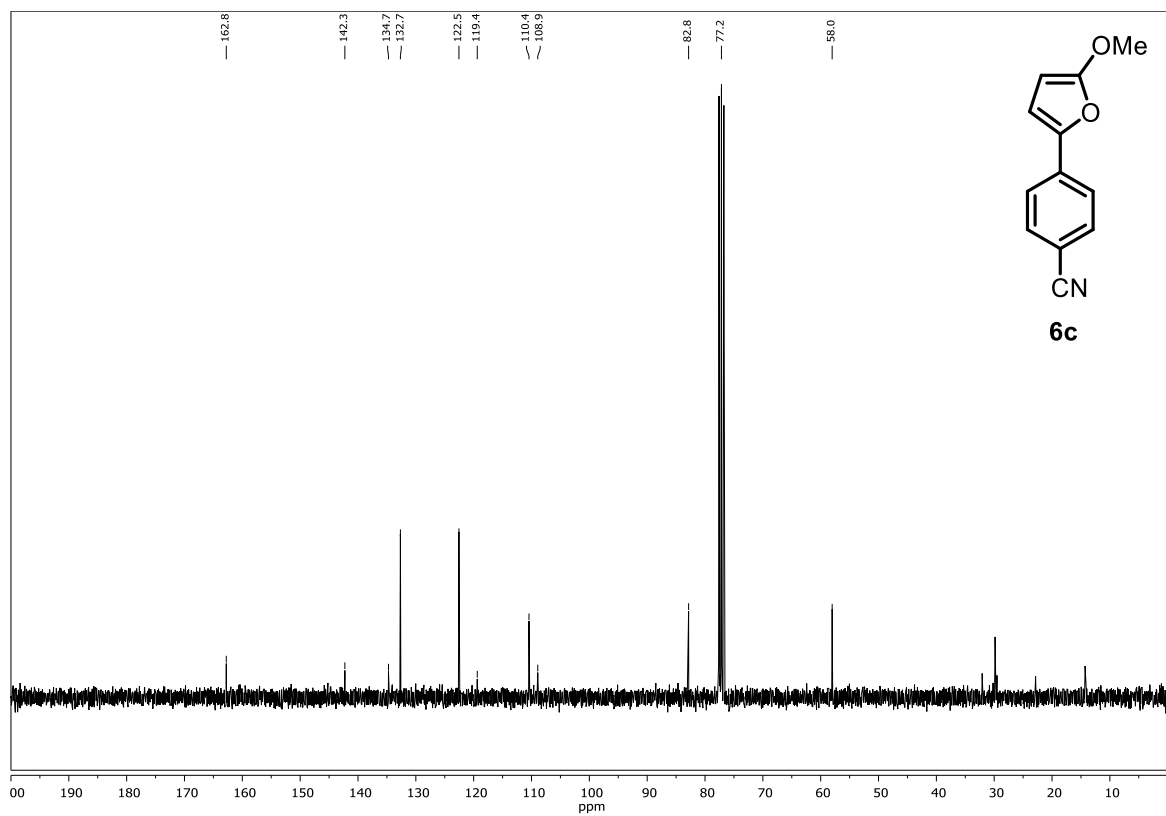
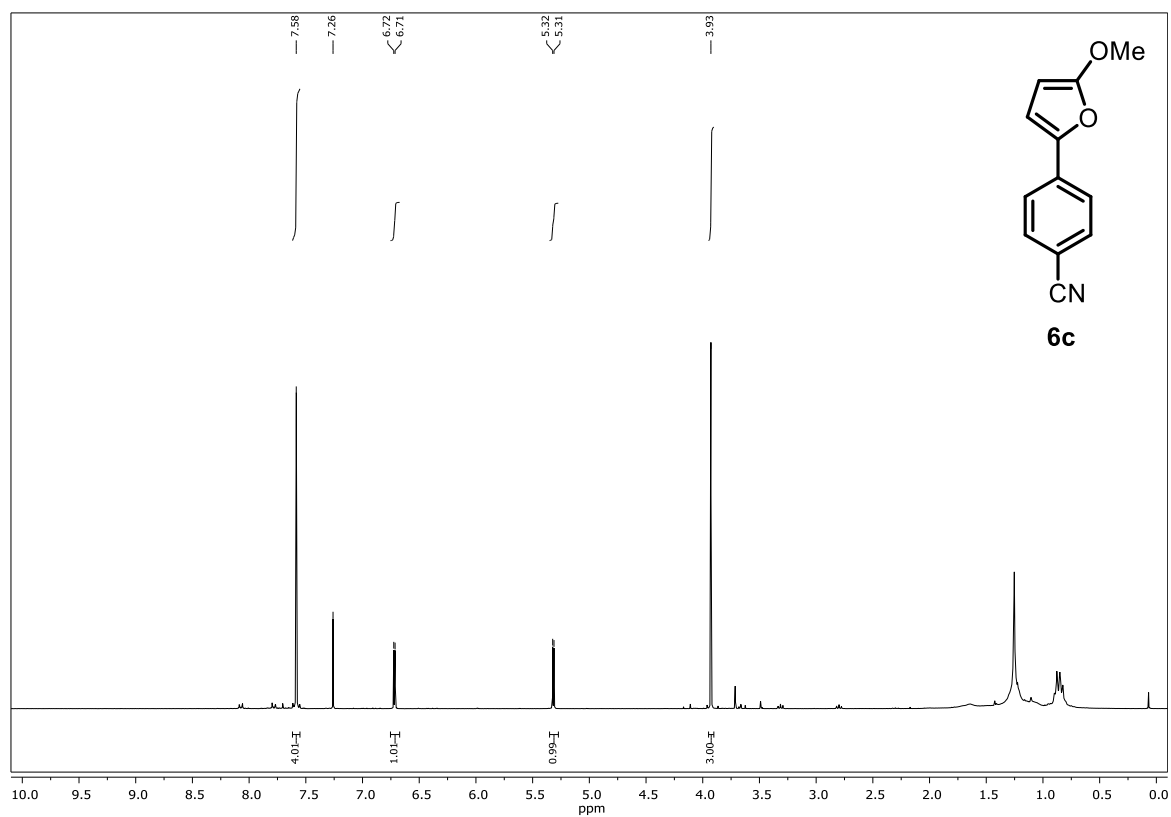


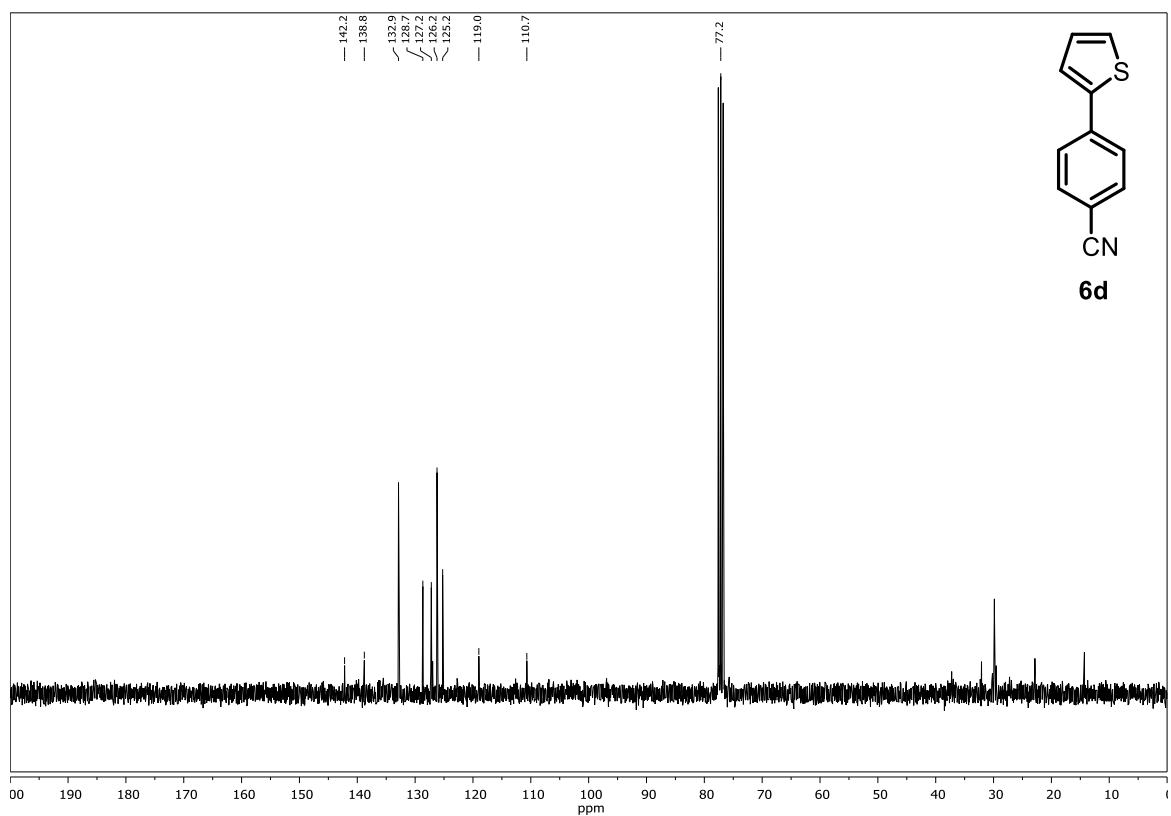
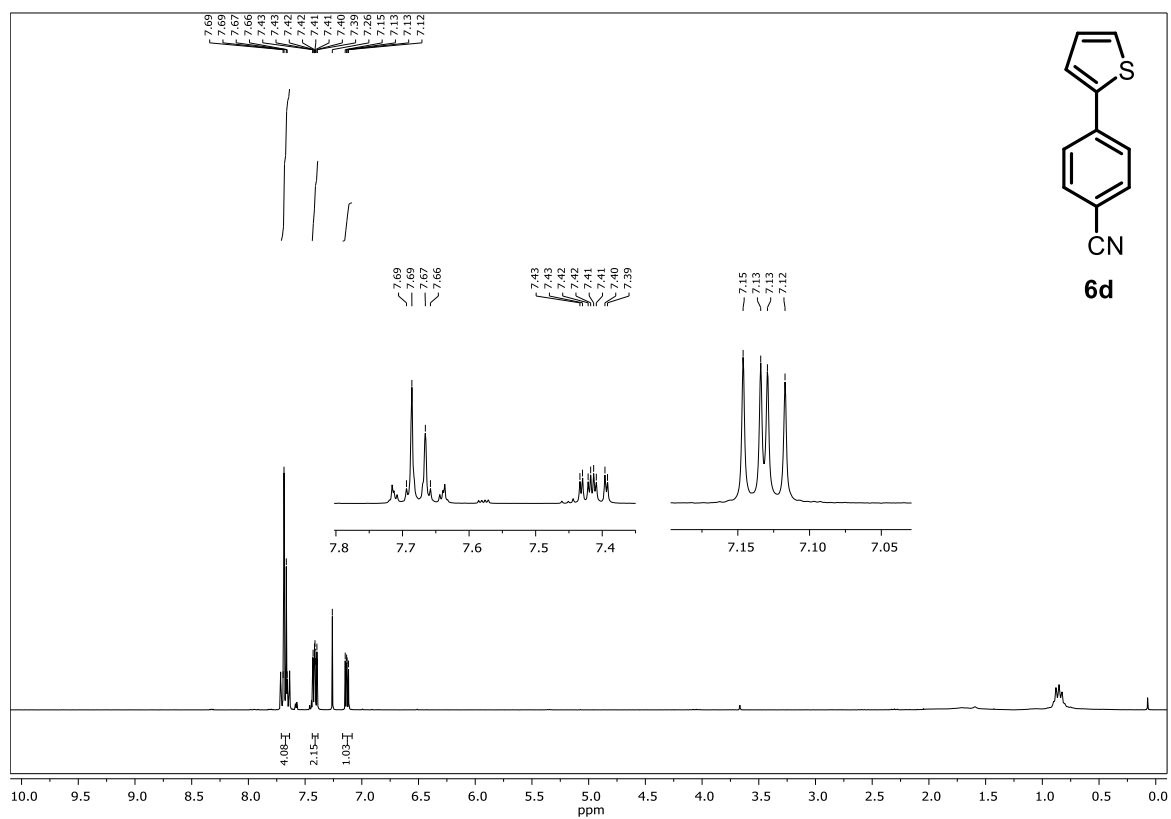


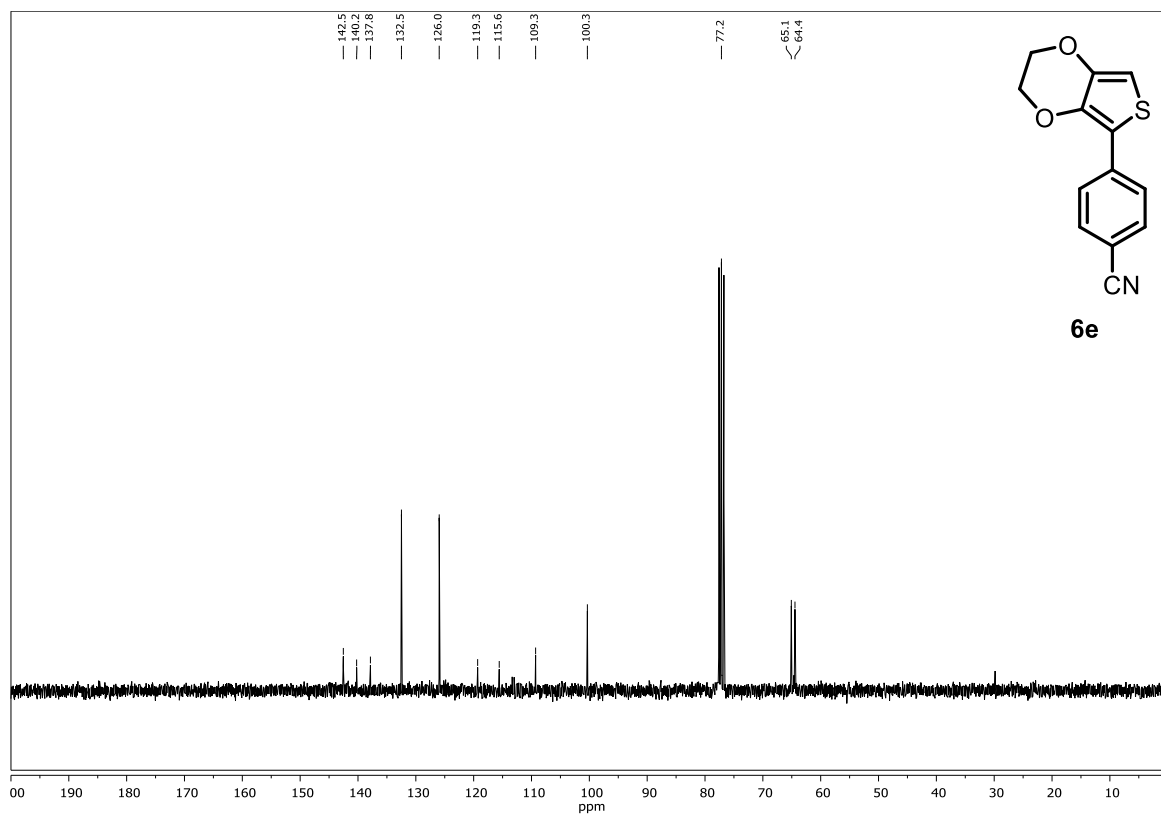
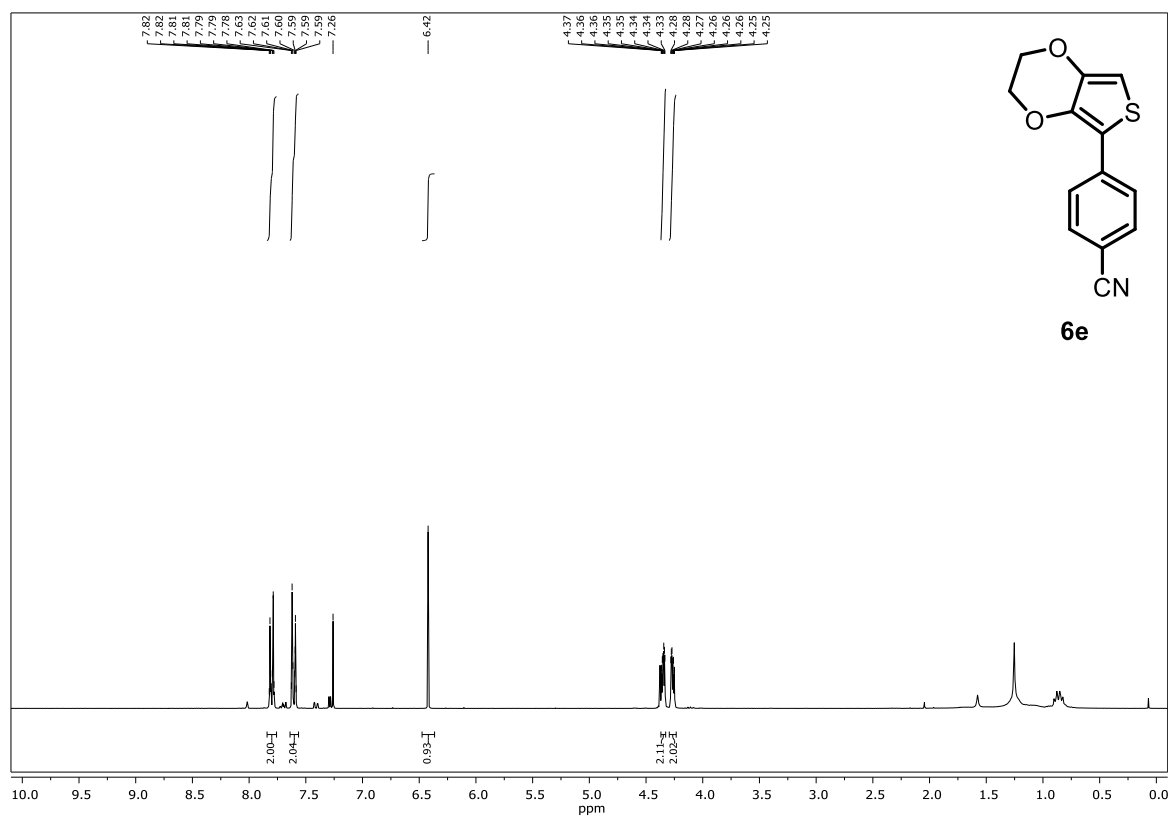


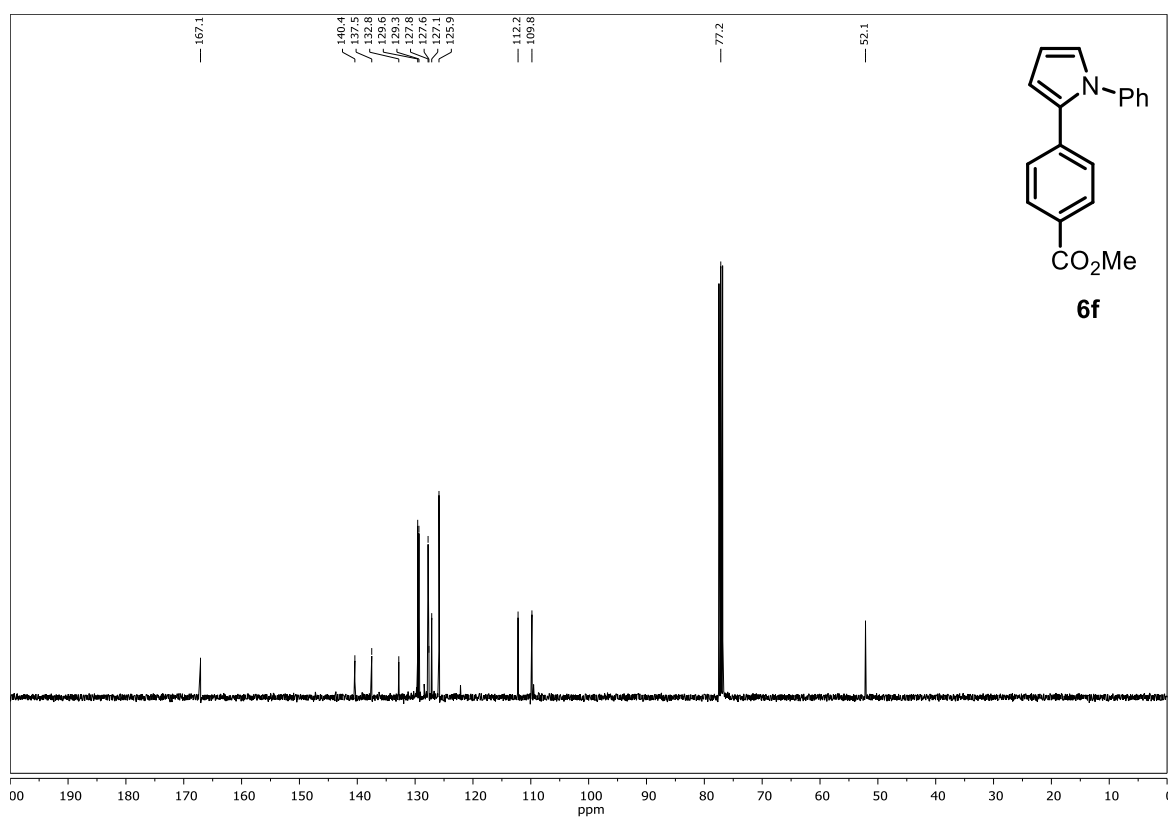
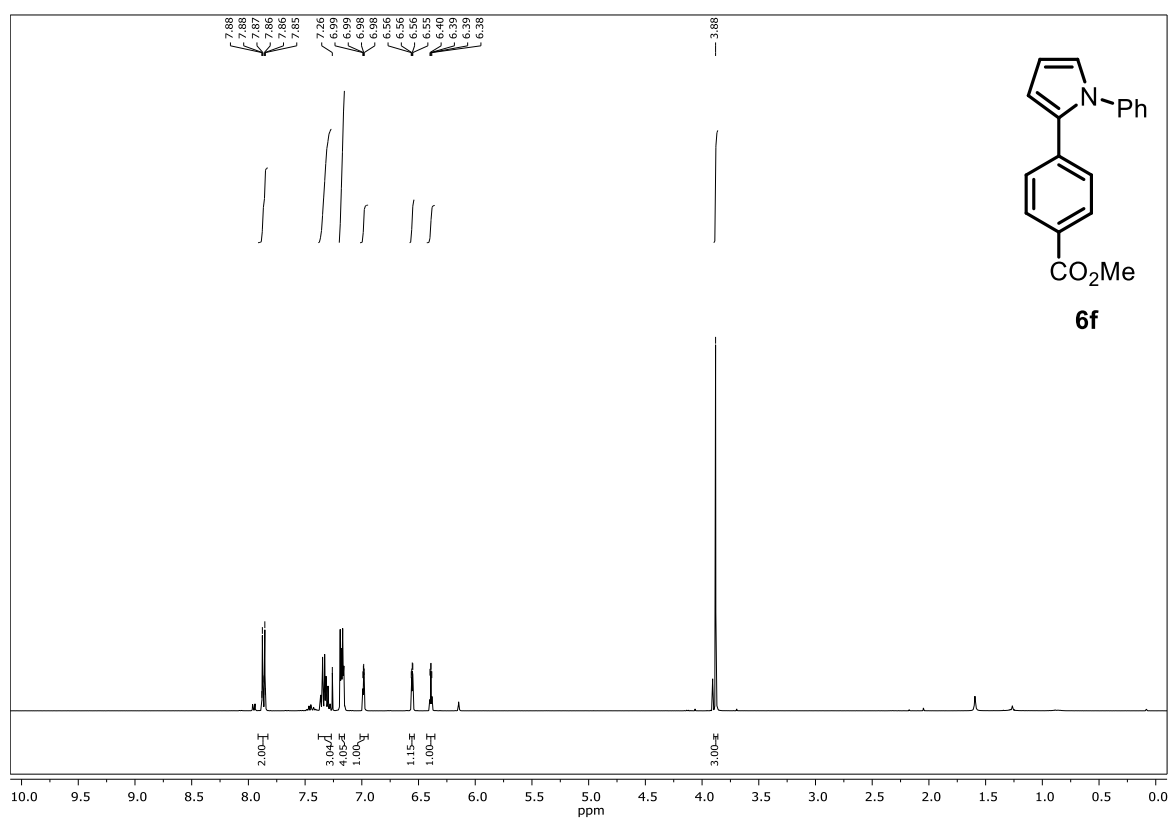


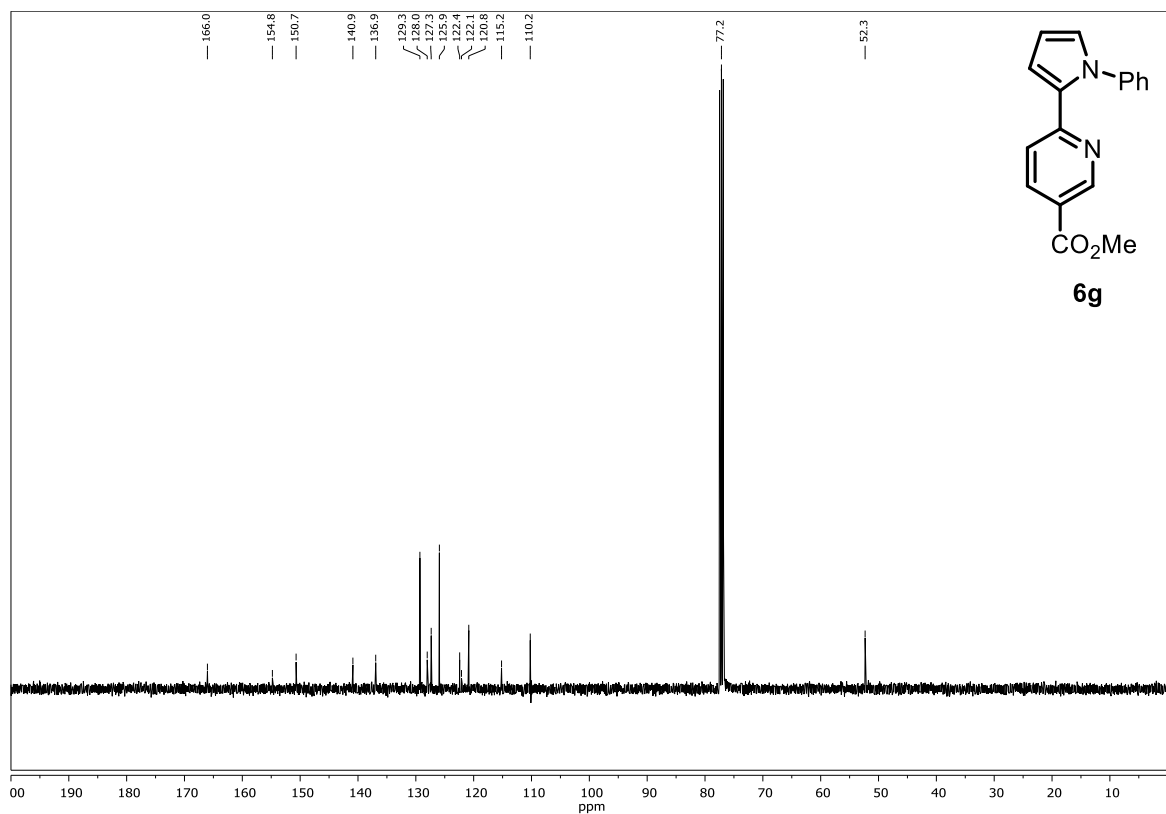
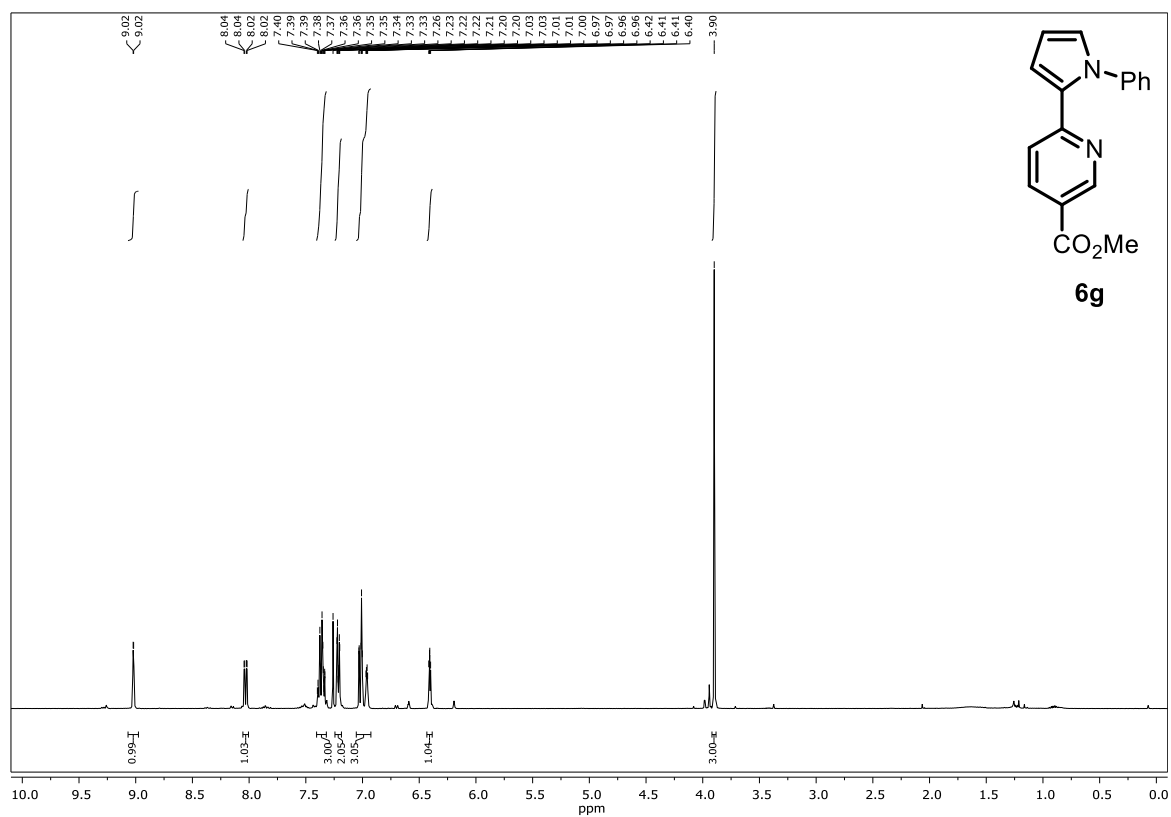


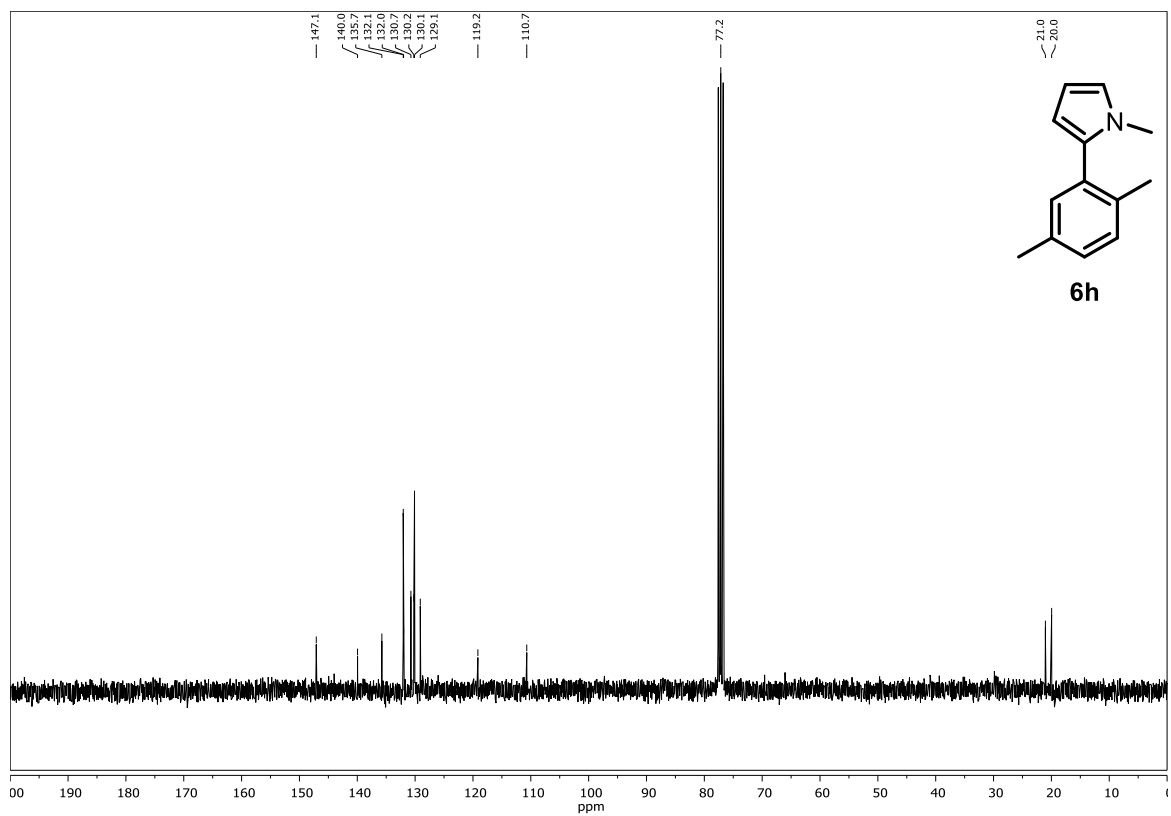
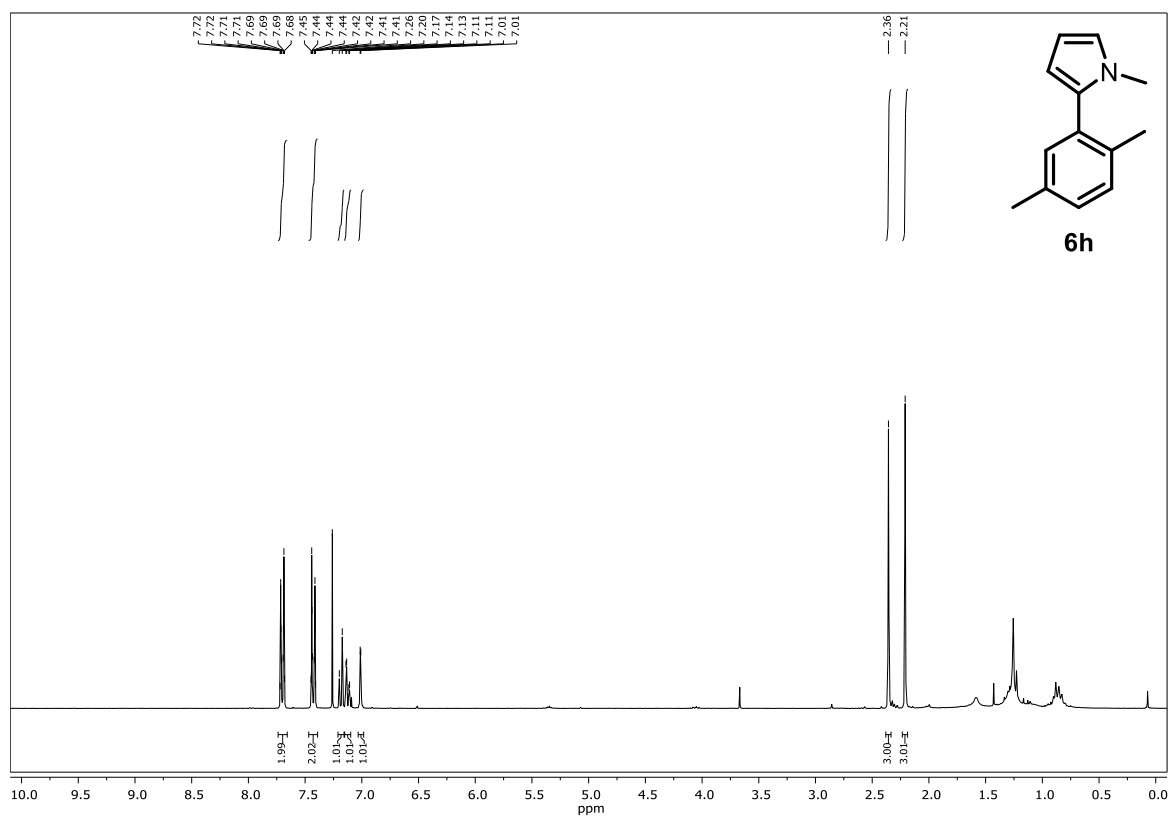


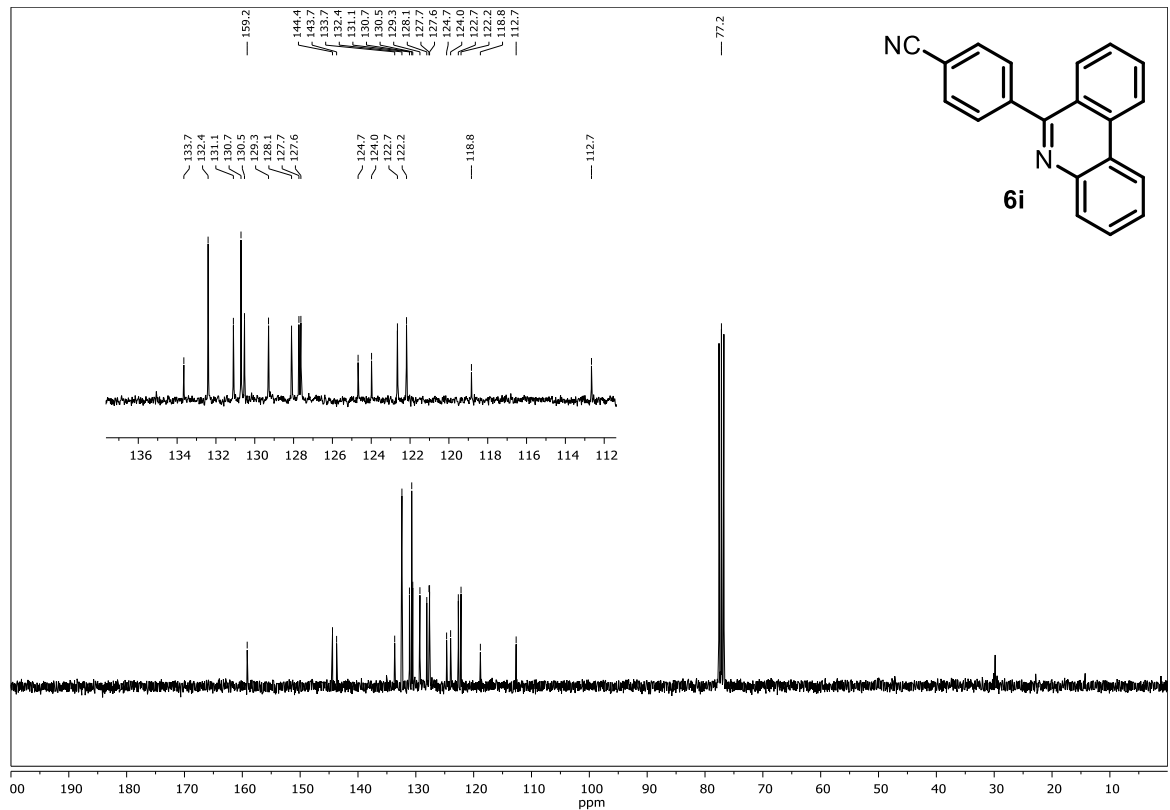


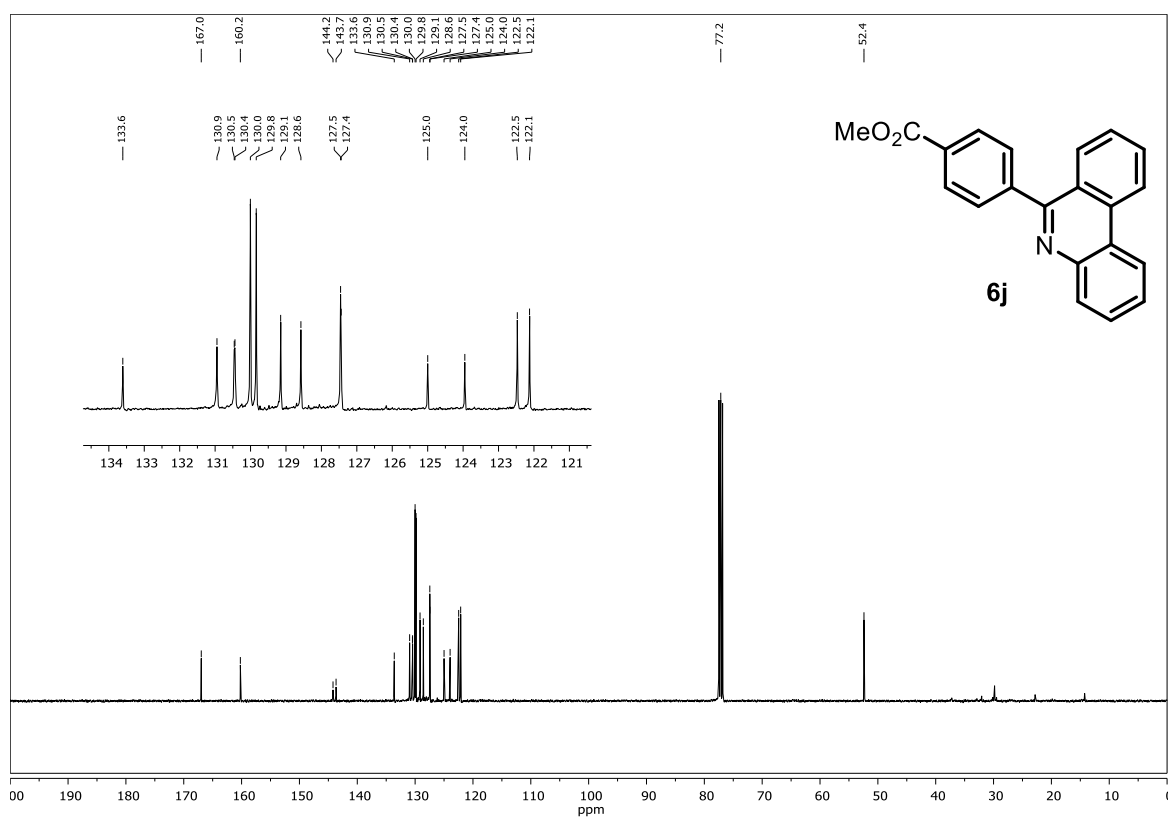
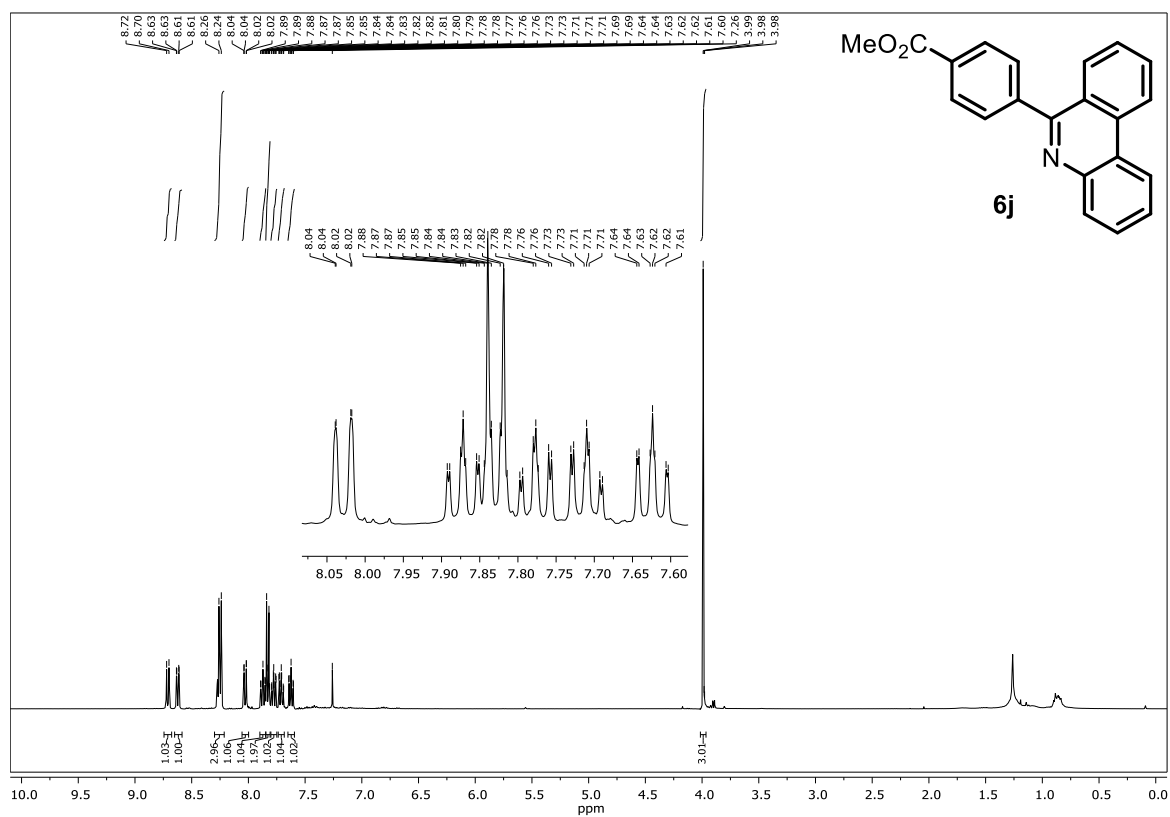


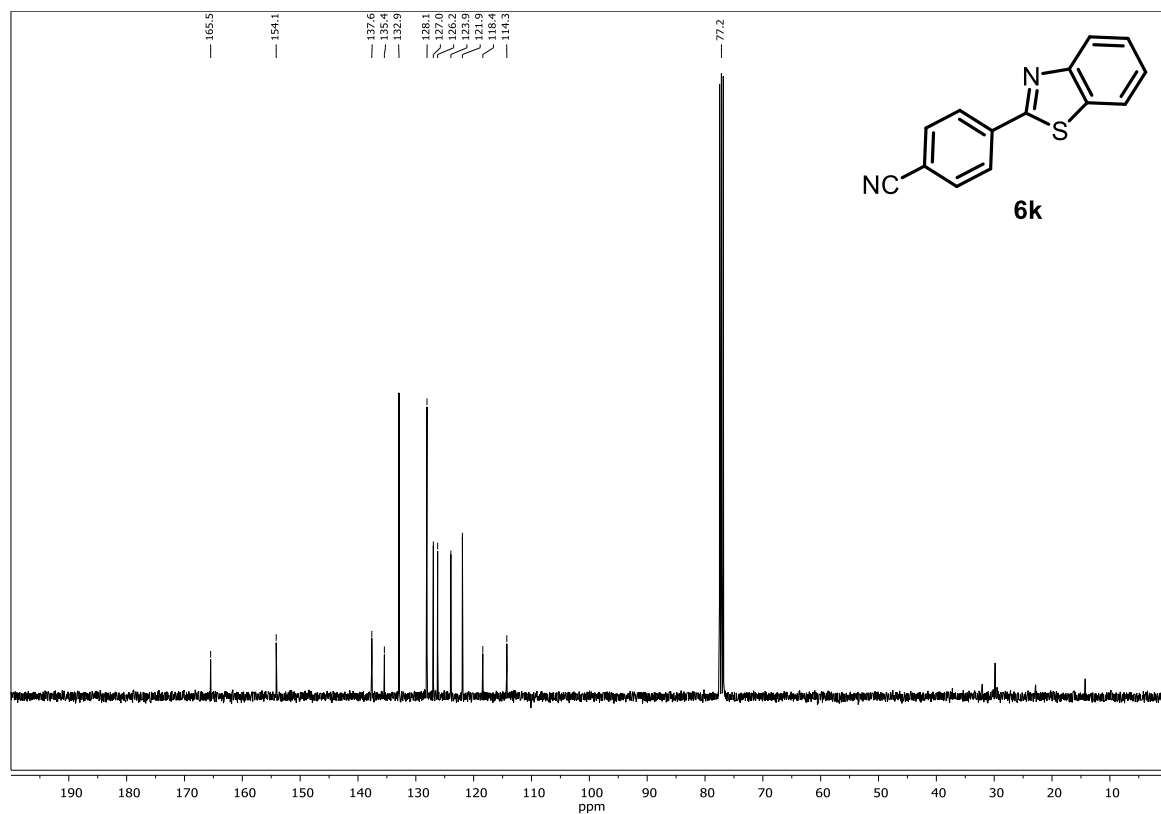
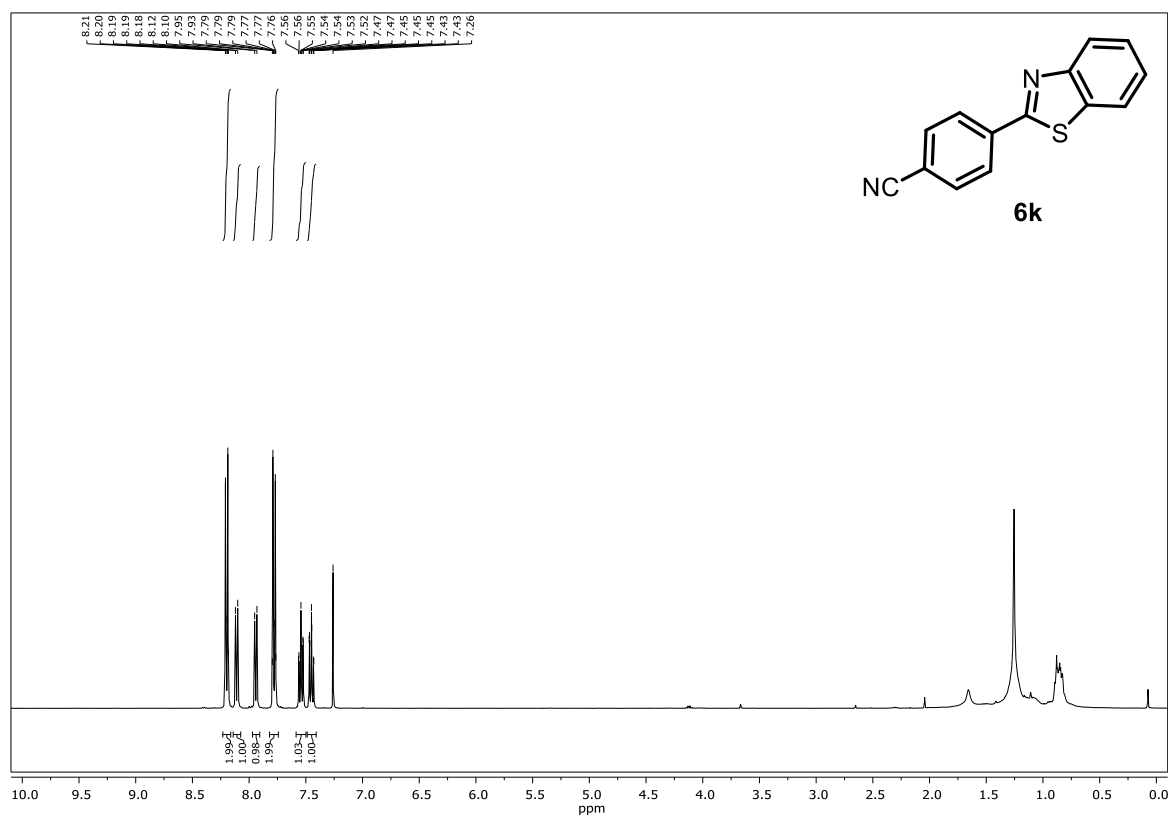


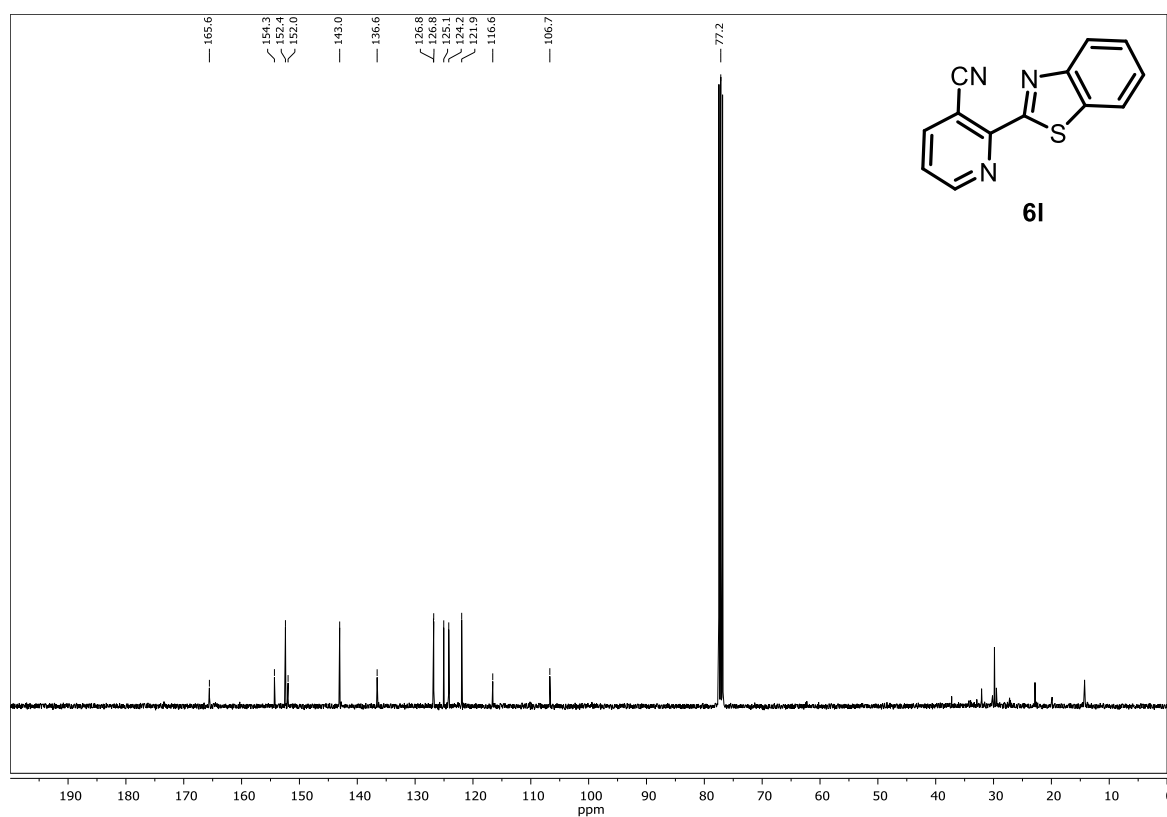
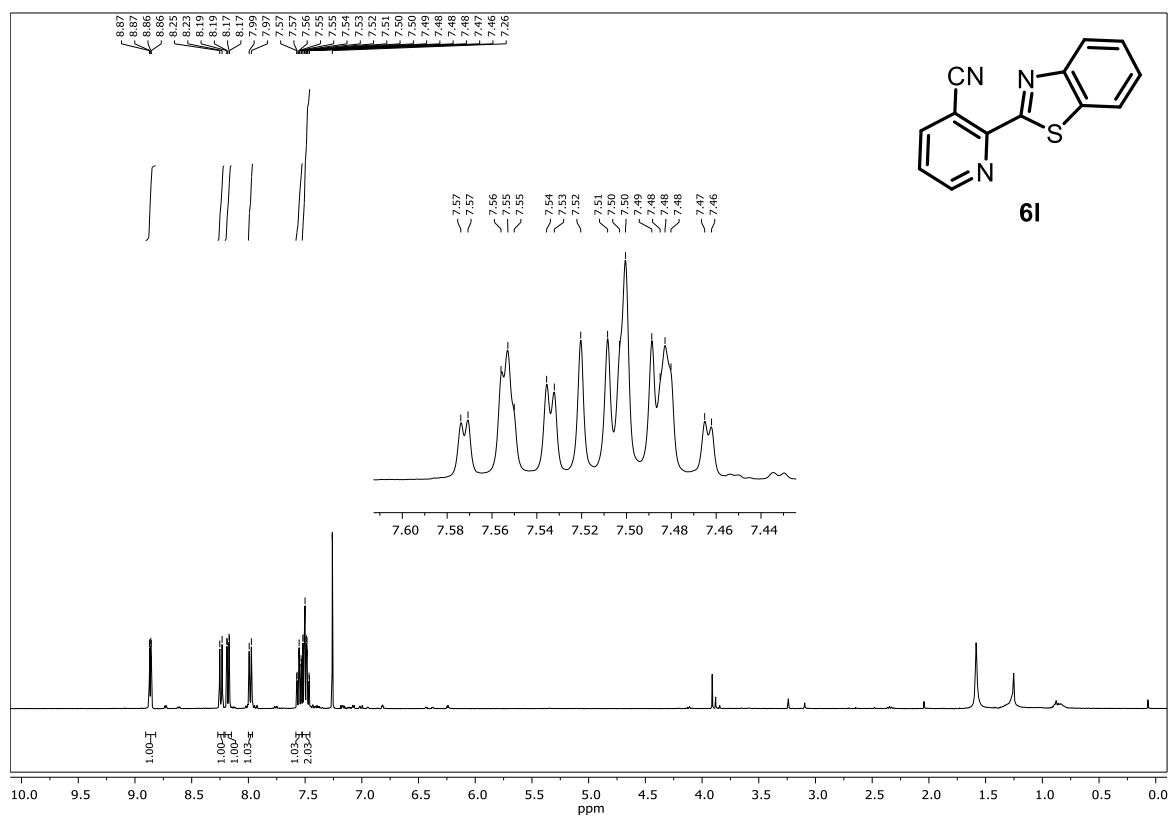


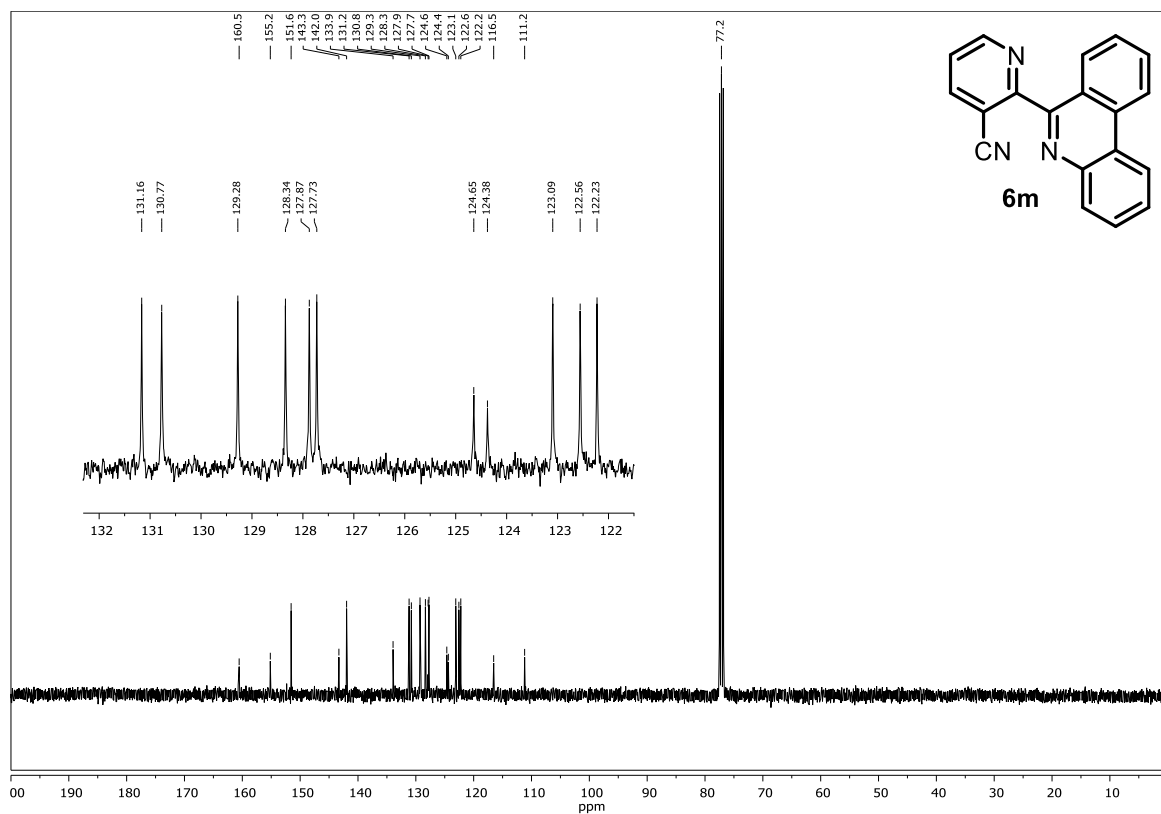
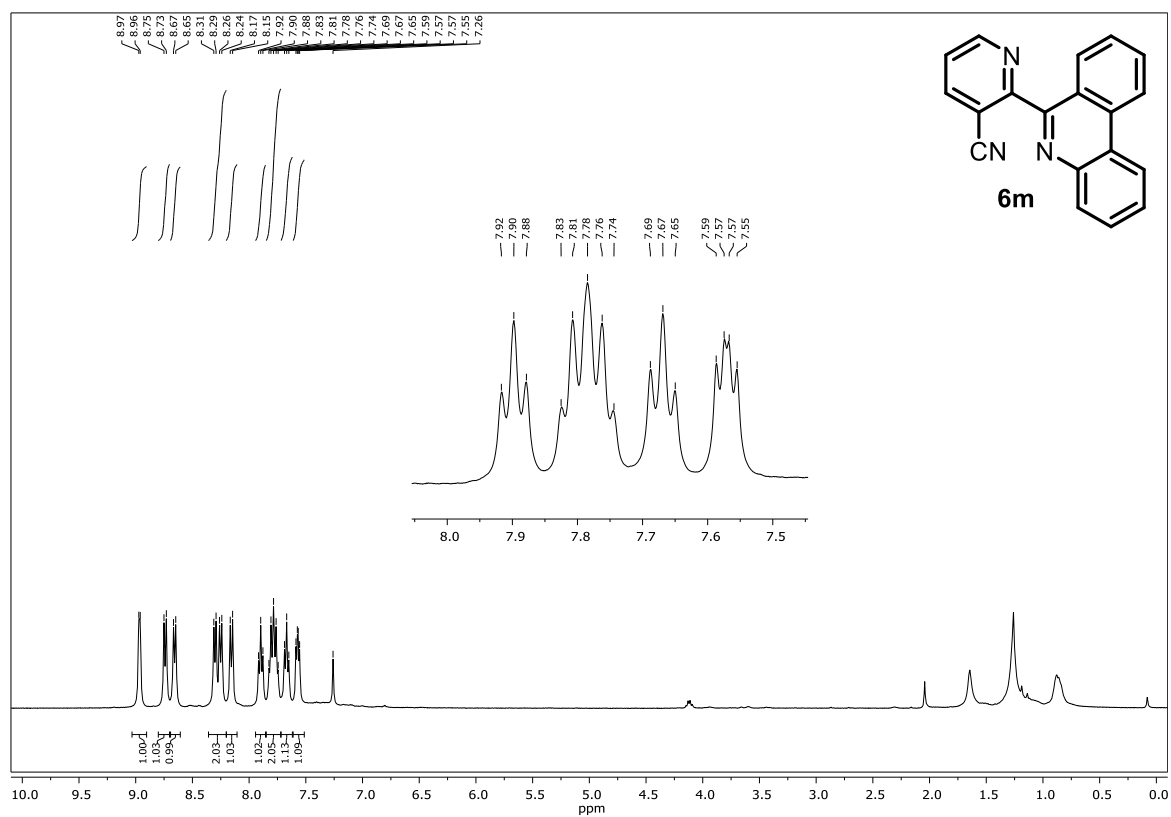


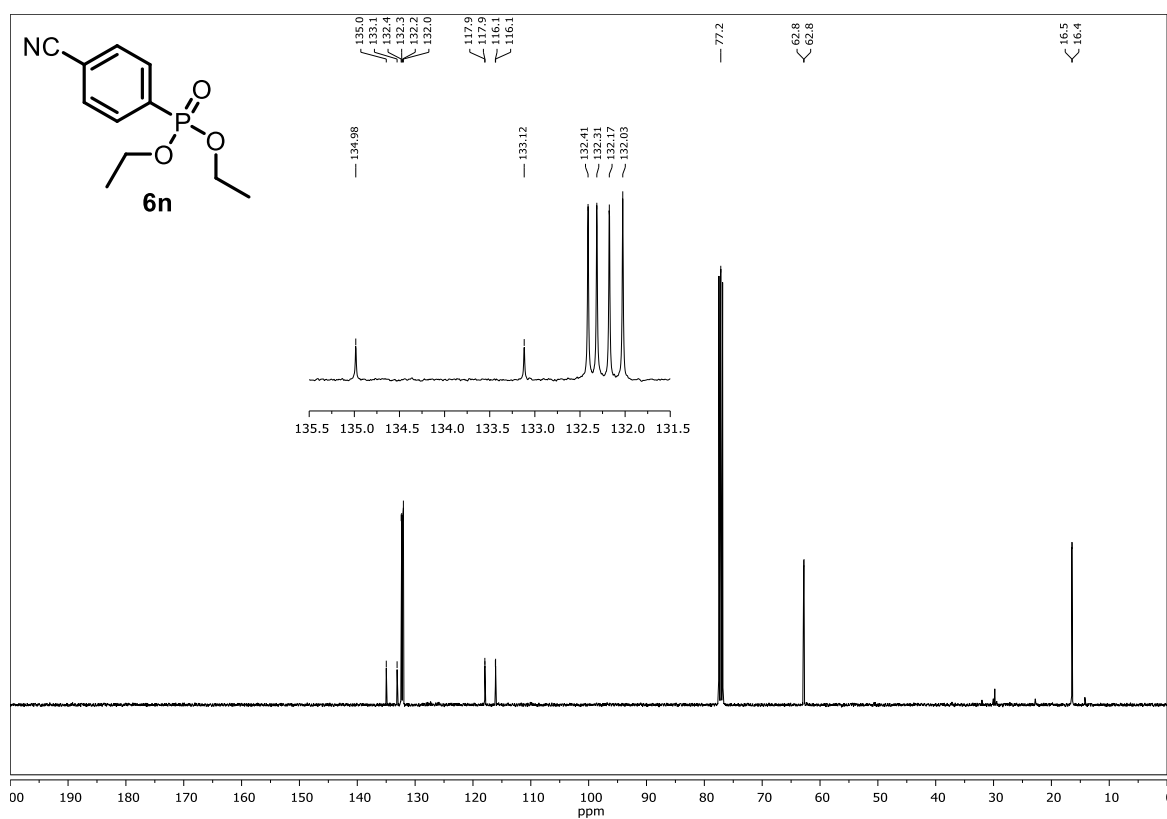
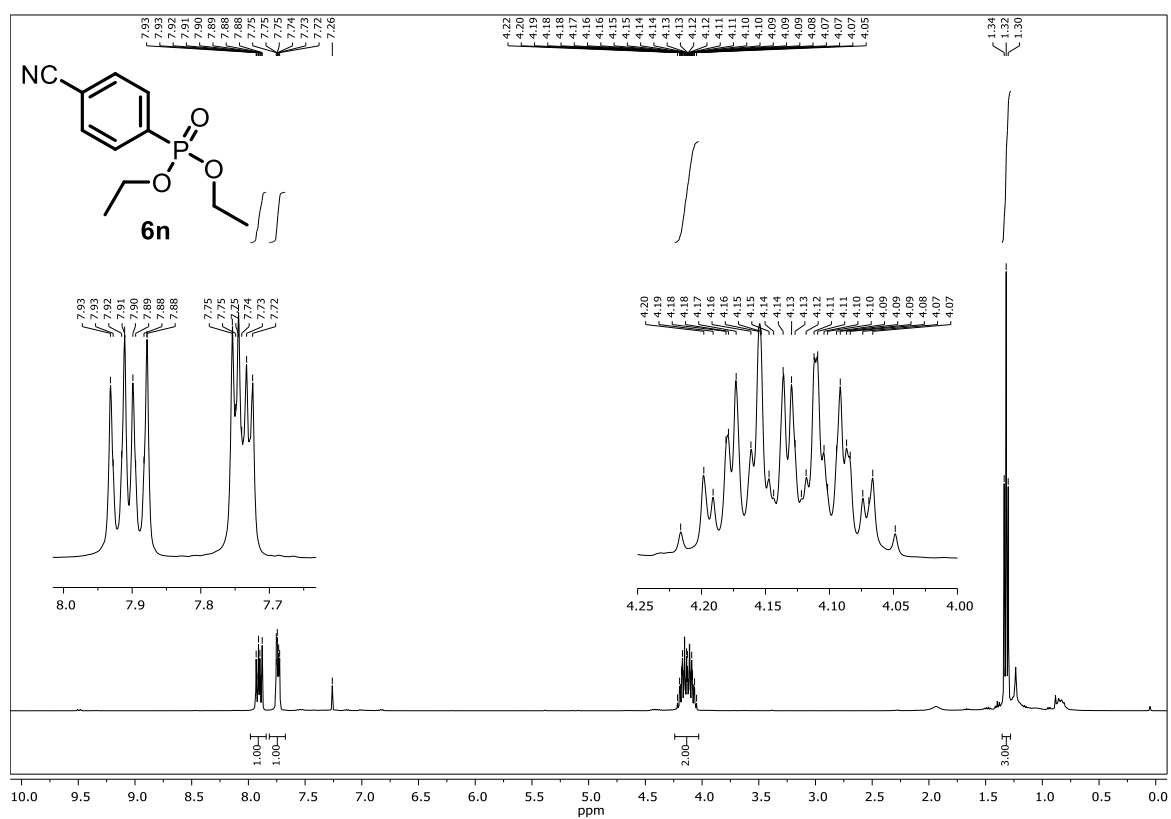


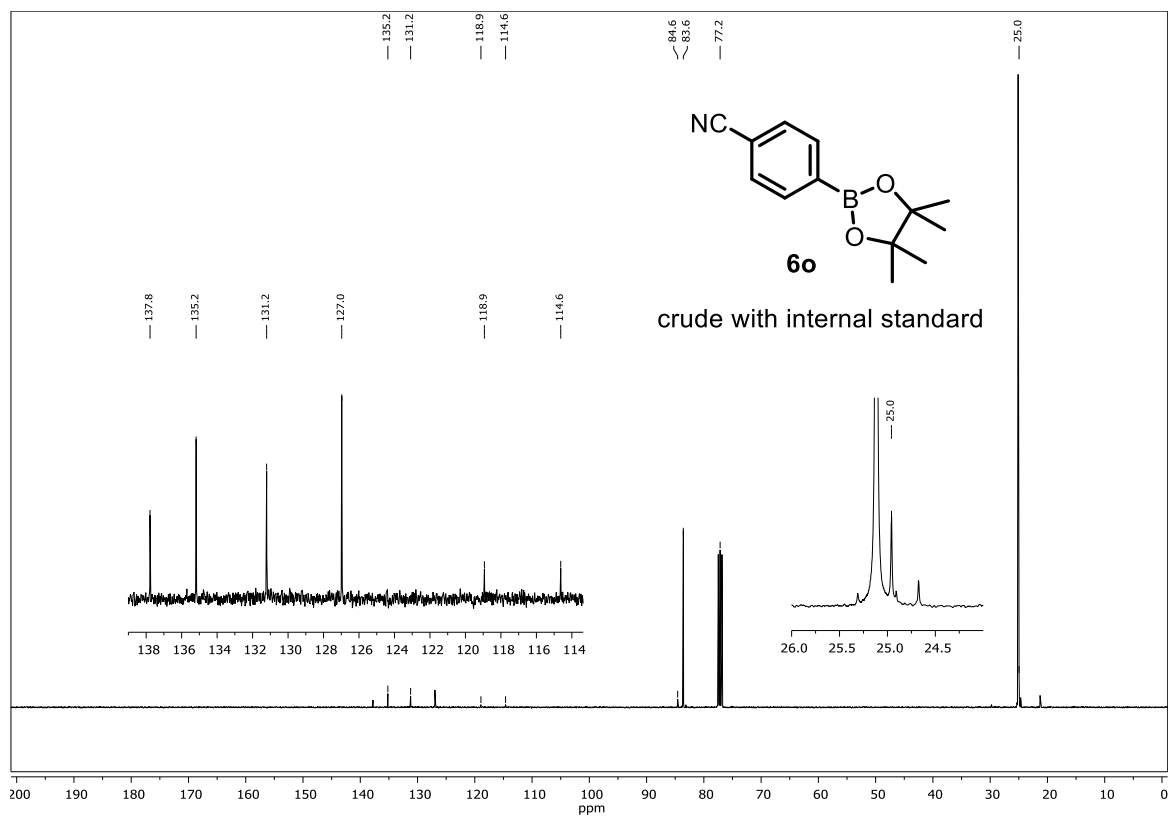
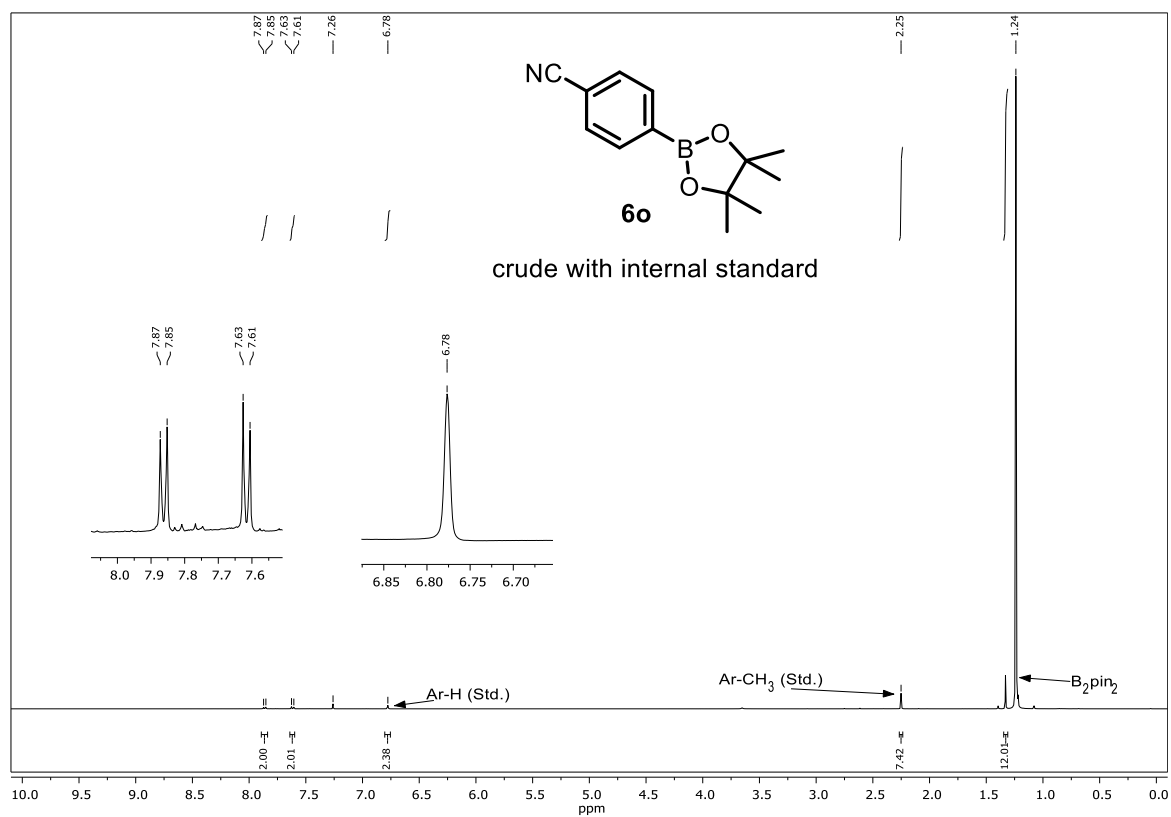












7.3.2 UV-vis Absorption Spectra

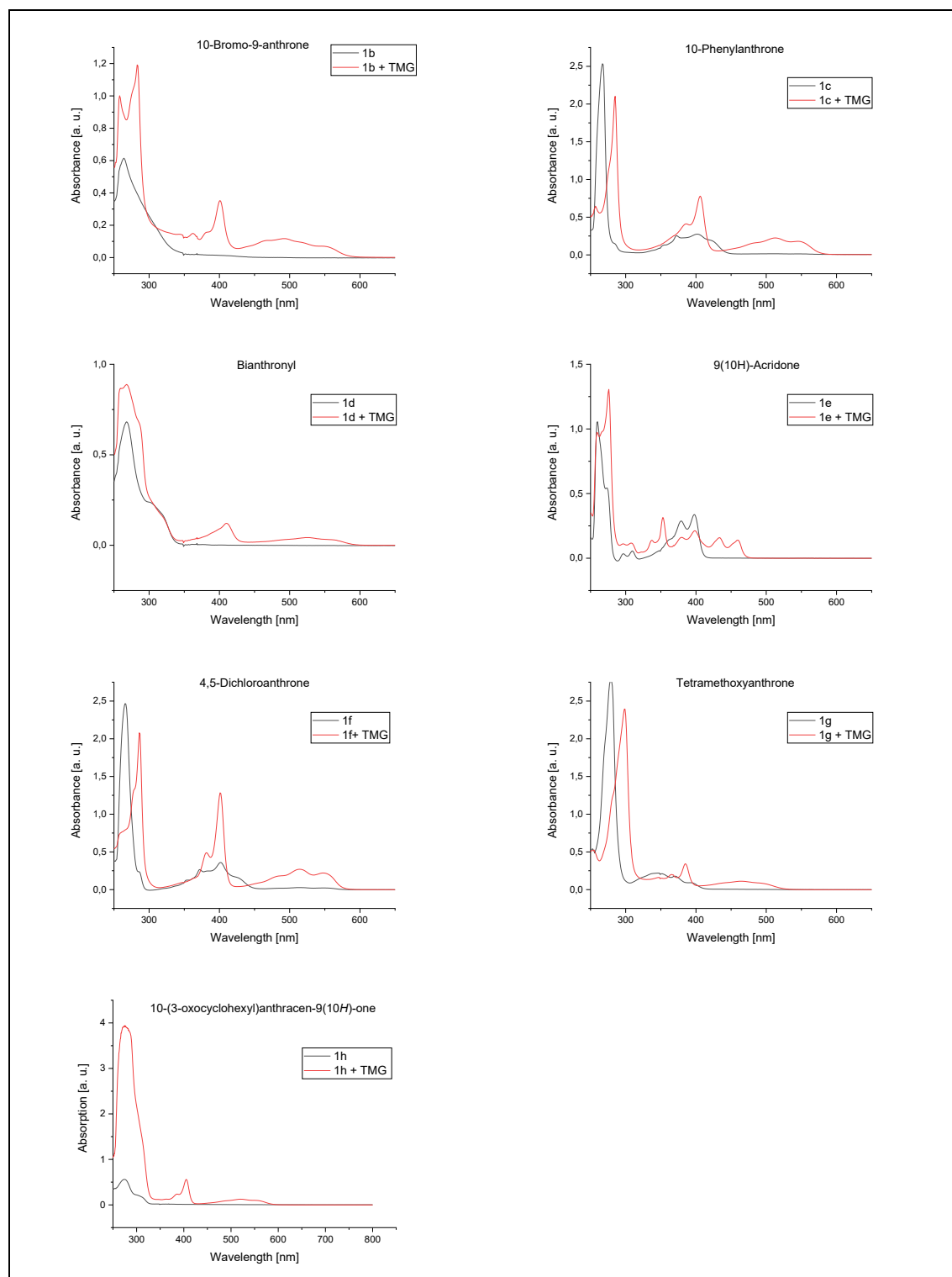


Figure S3-2. UV-vis absorption spectra of discussed compounds **1** in presence (red) and absence (black) of base 1,1,3,3-tetramethylguanidine (TMG).

7.3.3 Emission Spectra

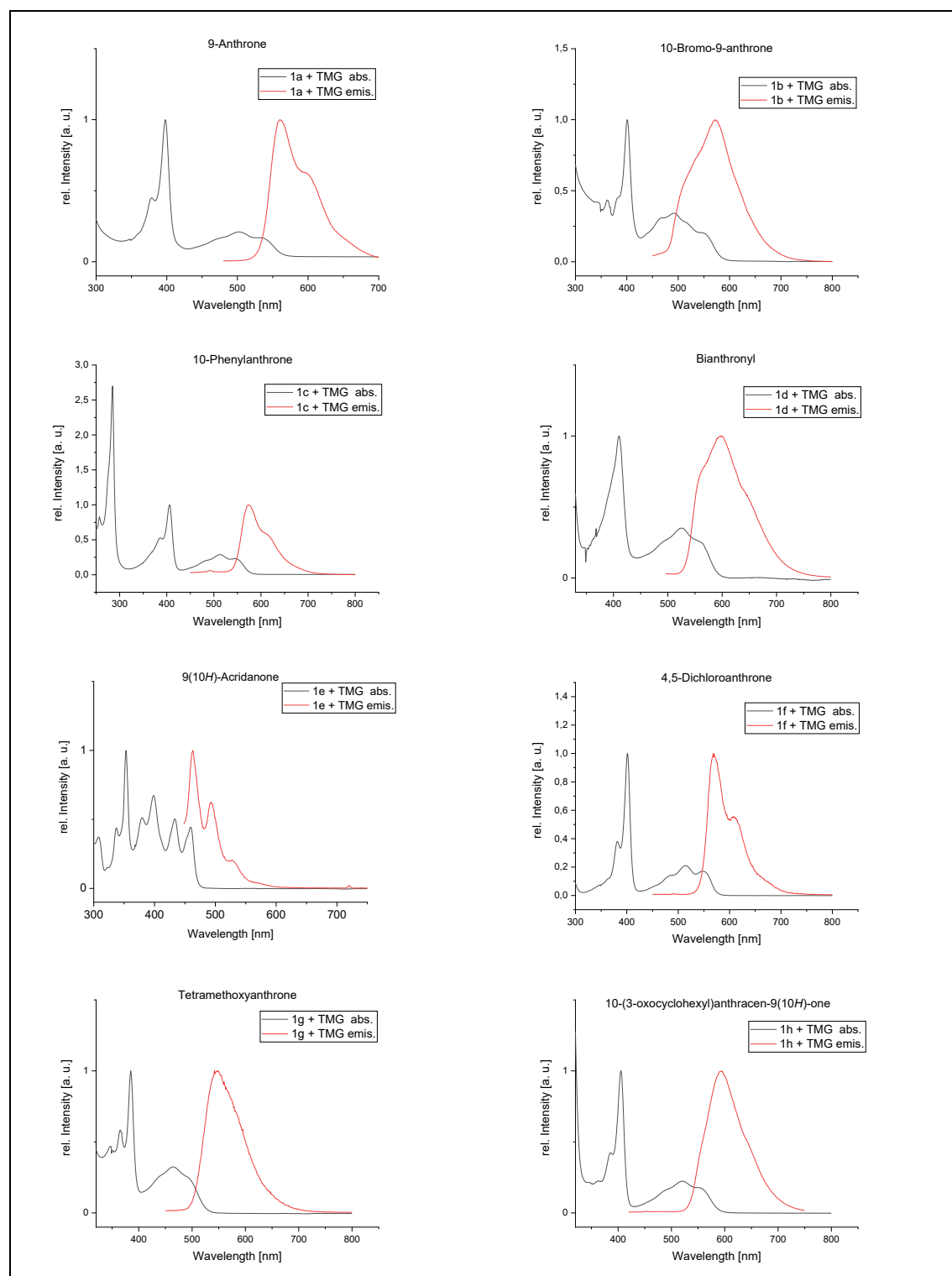


Figure S3-3. Normalized absorption (black) and emission (red) spectra of catalyst **1a-h** in presence of base 1,1,3,3-tetramethylguanidine (TMG).

7.3.4 Time-Resolved Luminescence Quenching

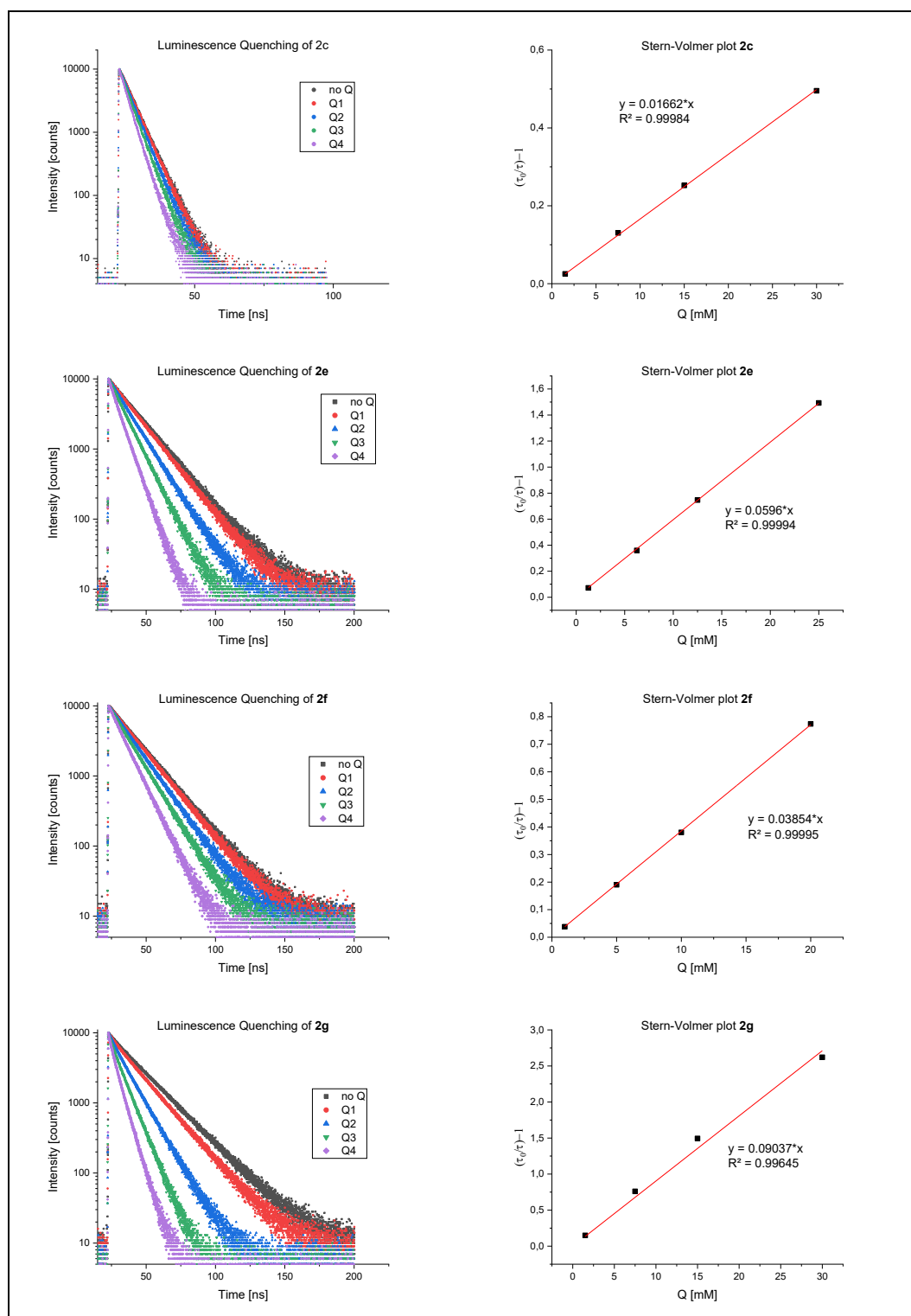
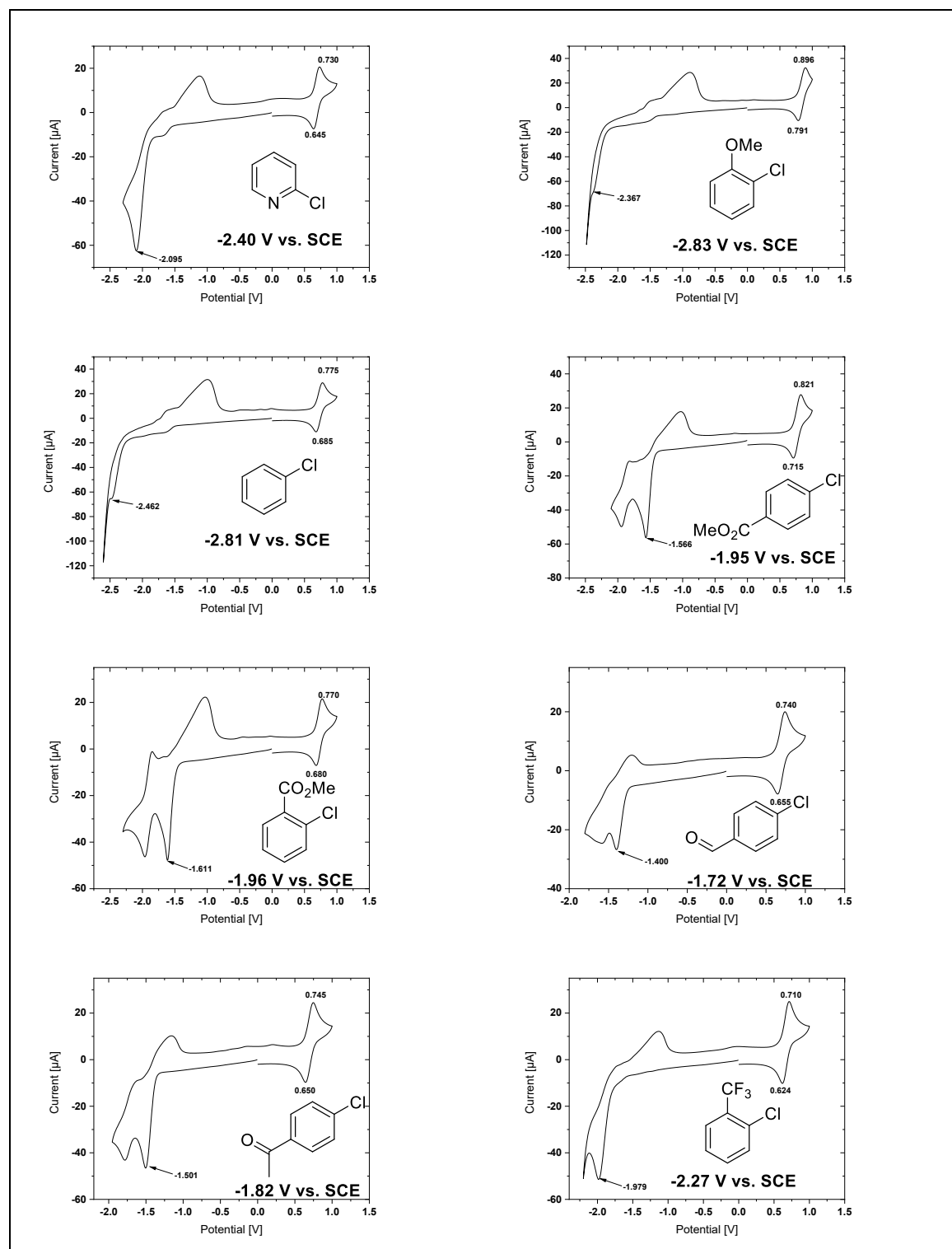
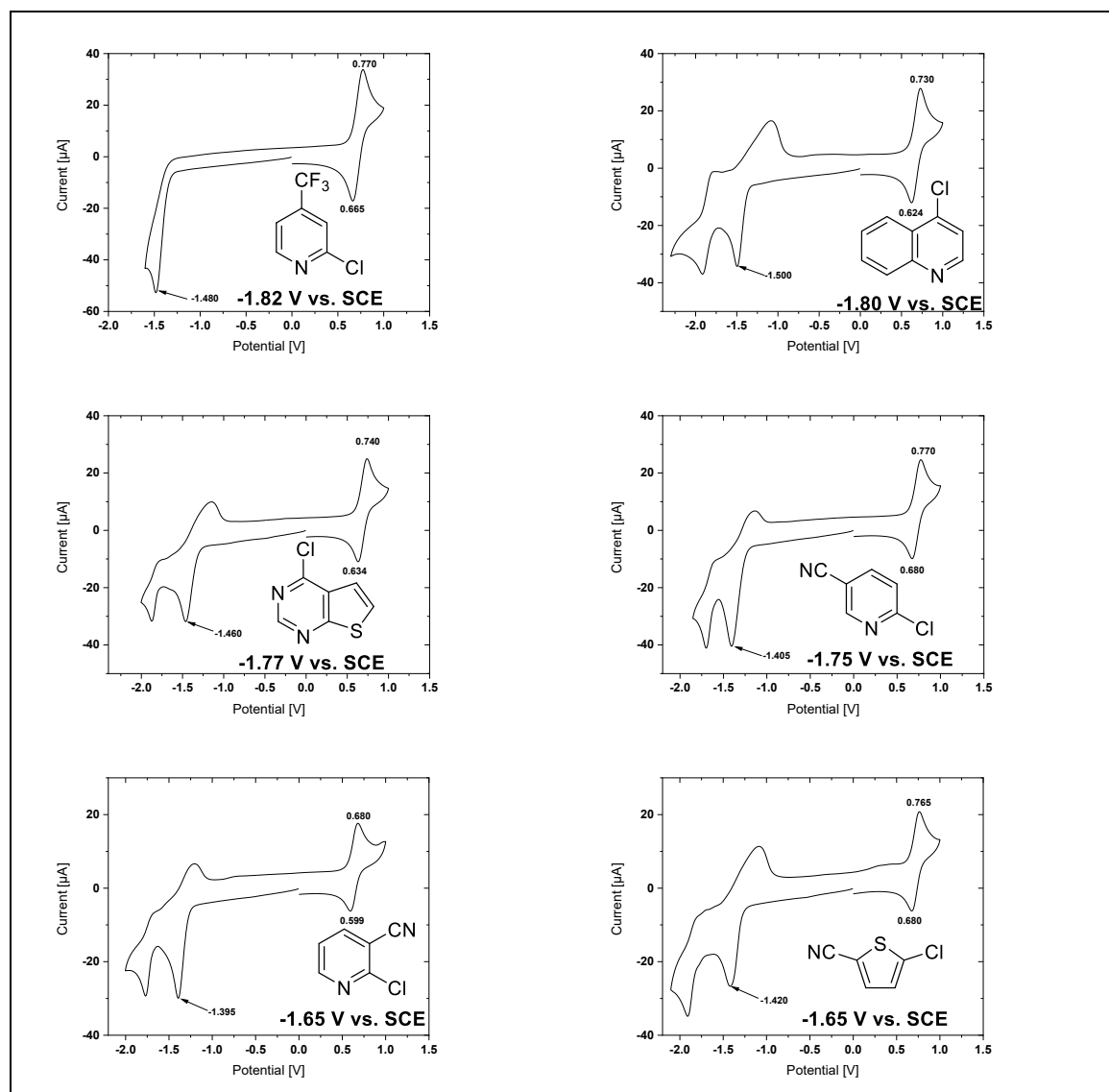


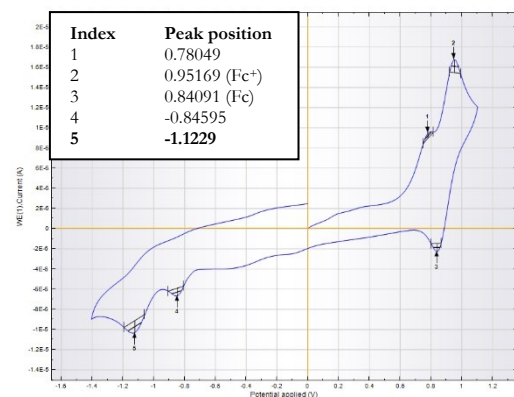
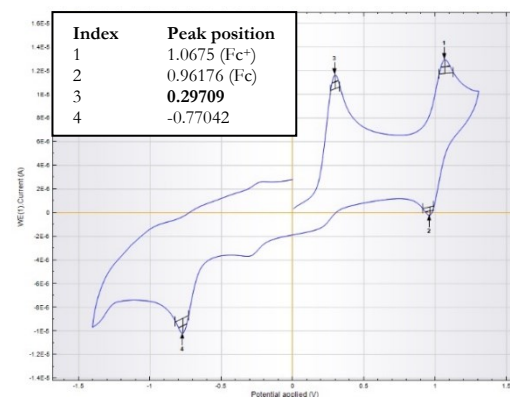
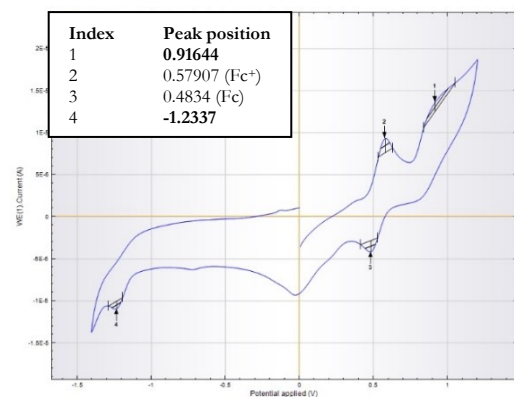
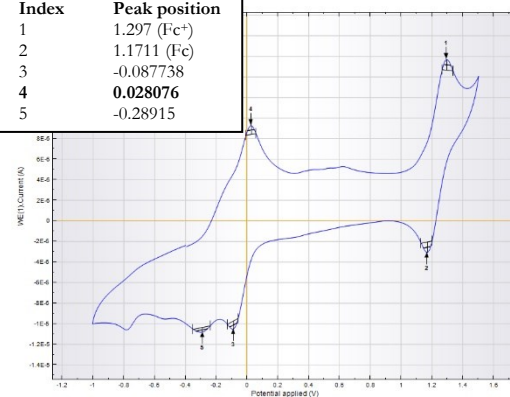
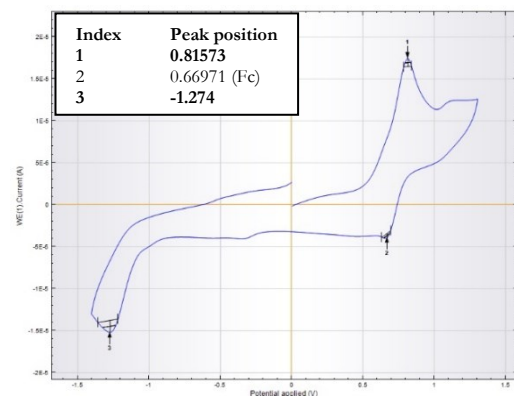
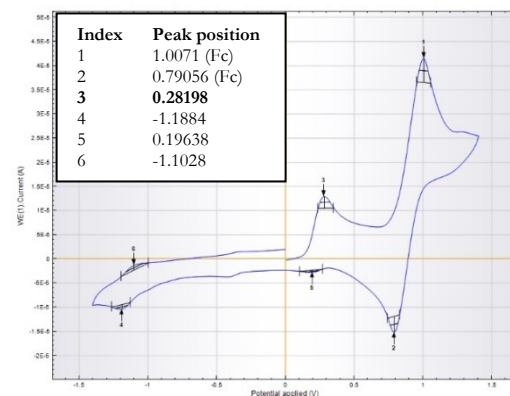
Figure S3-6. Time-resolved luminescence quenching experiments of catalysts **2** with **3f** (2-chlorobenzonitrile) as quencher. A Stern-Volmer plot was developed from the obtained data.

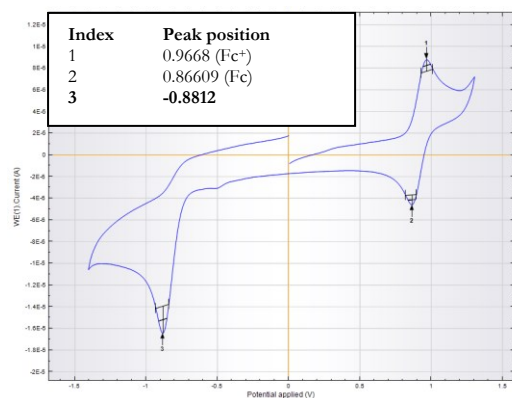
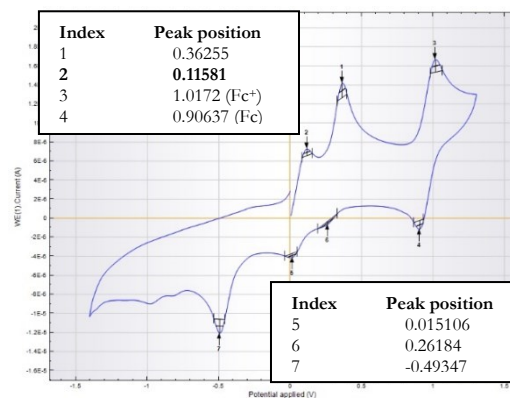
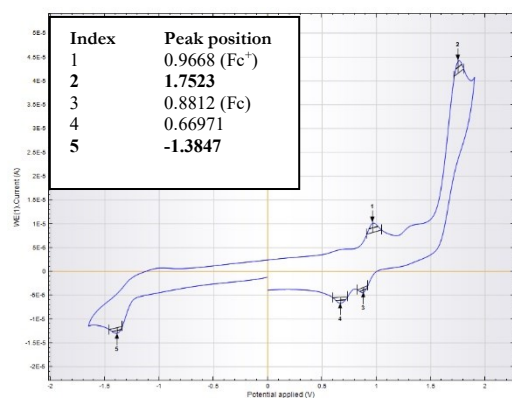
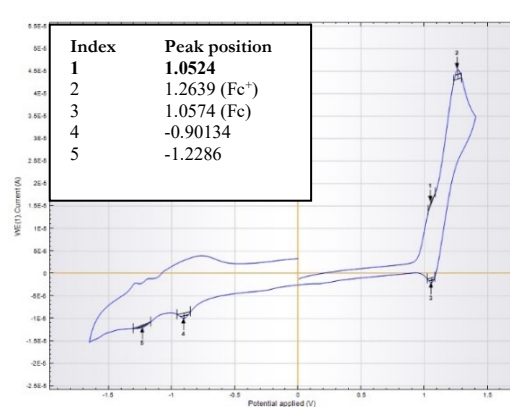
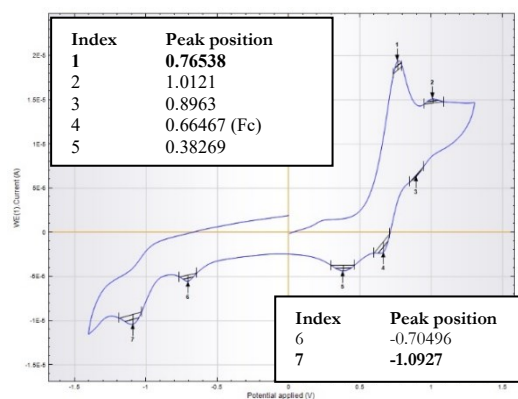
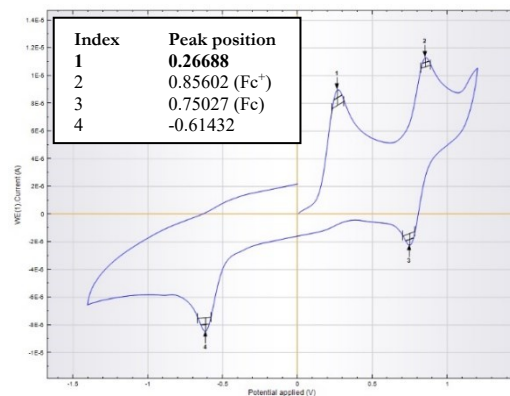
7.3.5 Cyclic Voltammetry of Aryl Chlorides

Table S3-4b. Overview of measured reduction potentials of the employed aryl chlorides. Potentials are reported against saturated calomel electrode SCE.



7.3.6 Cyclic Voltammetry of Catalysts

1a *vs.* ferrocene:2a with Cs₂CO₃ *vs.* ferrocene:1b *vs.* ferrocene:2b with TMG *vs.* ferrocene:1c *vs.* ferrocene:[†]2c with Cs₂CO₃ *vs.* ferrocene:

1d *vs.* ferrocene:**2d** with Cs₂CO₃ *vs.* ferrocene:**1e** *vs.* ferrocene:**2e** with TMG *vs.* ferrocene[†]**1f** *vs.* ferrocene:[†]**2f** with Cs₂CO₃ *vs.* ferrocene:

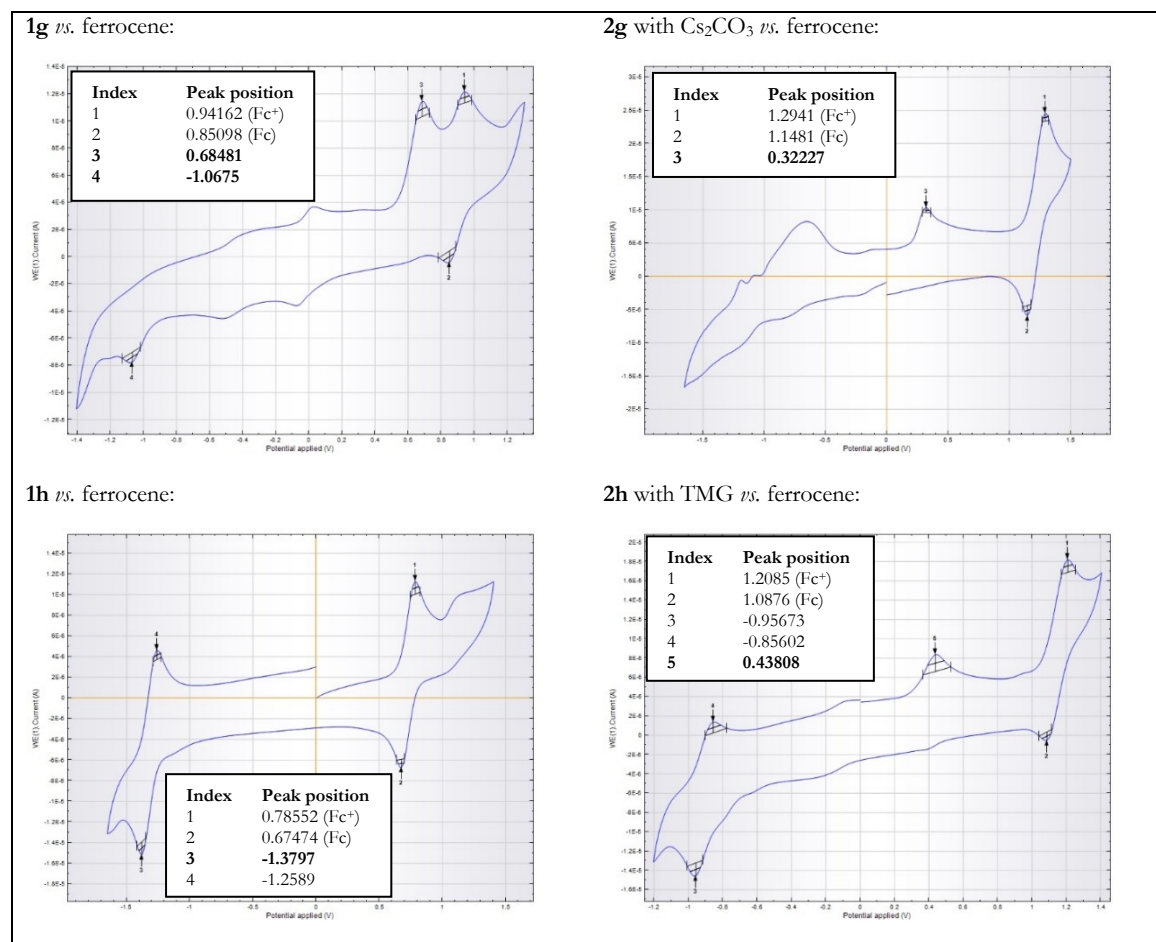
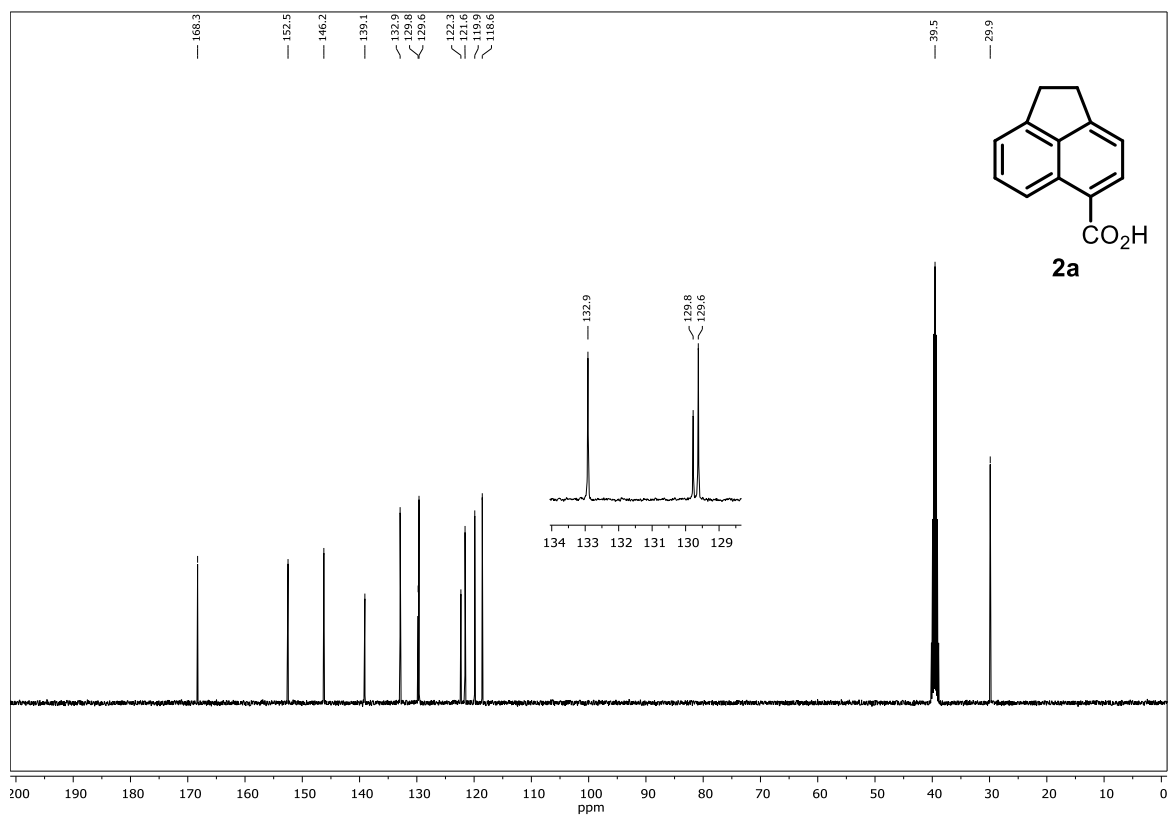
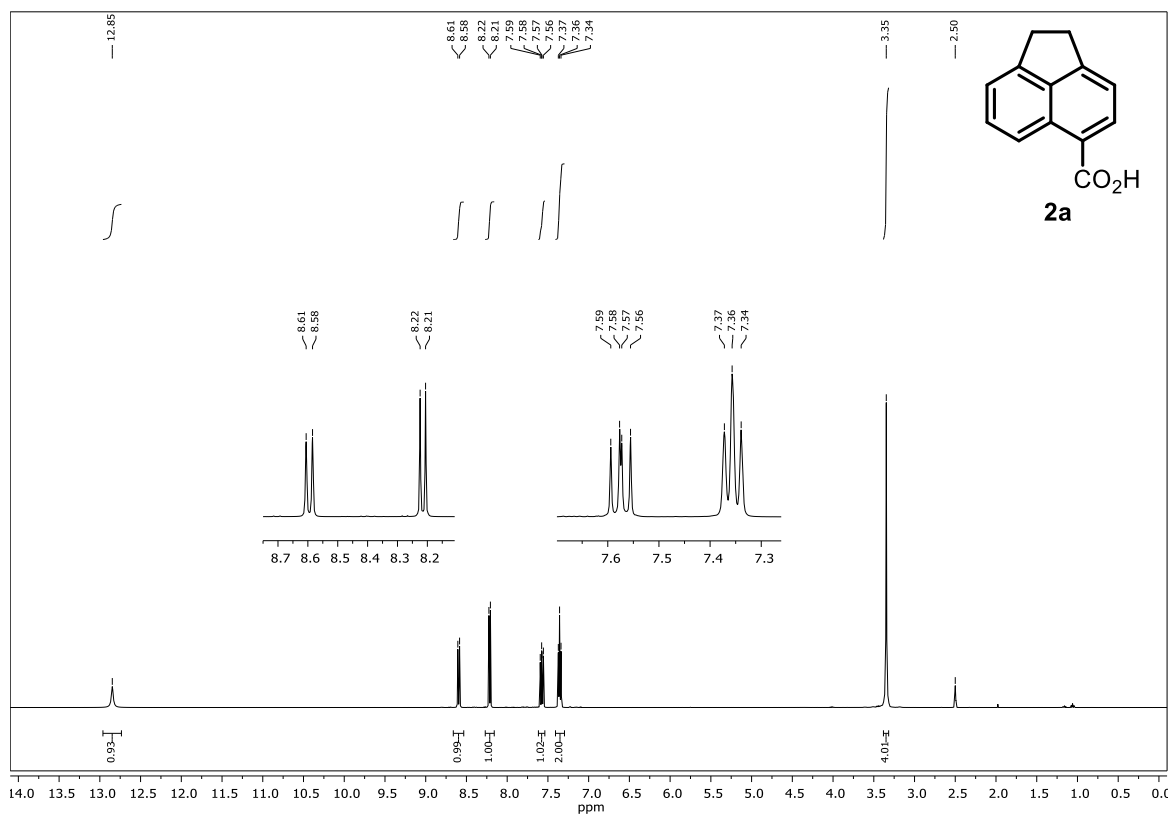
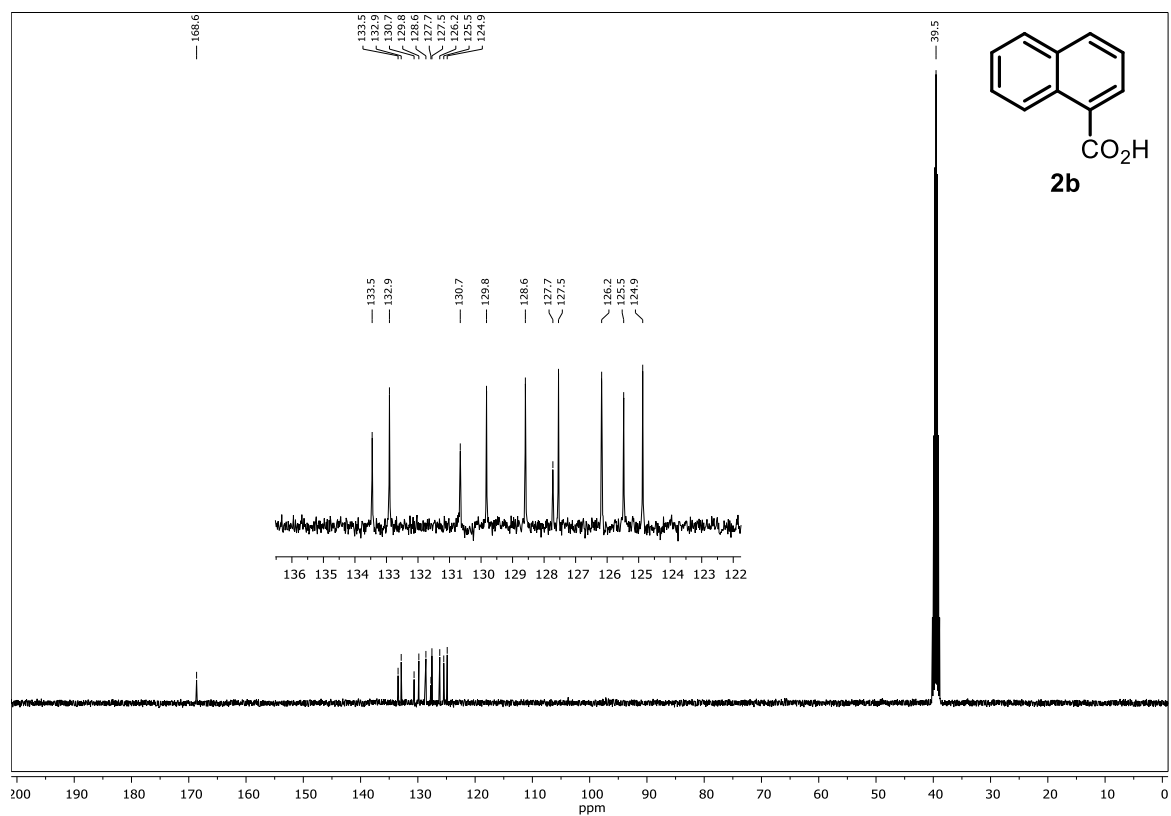
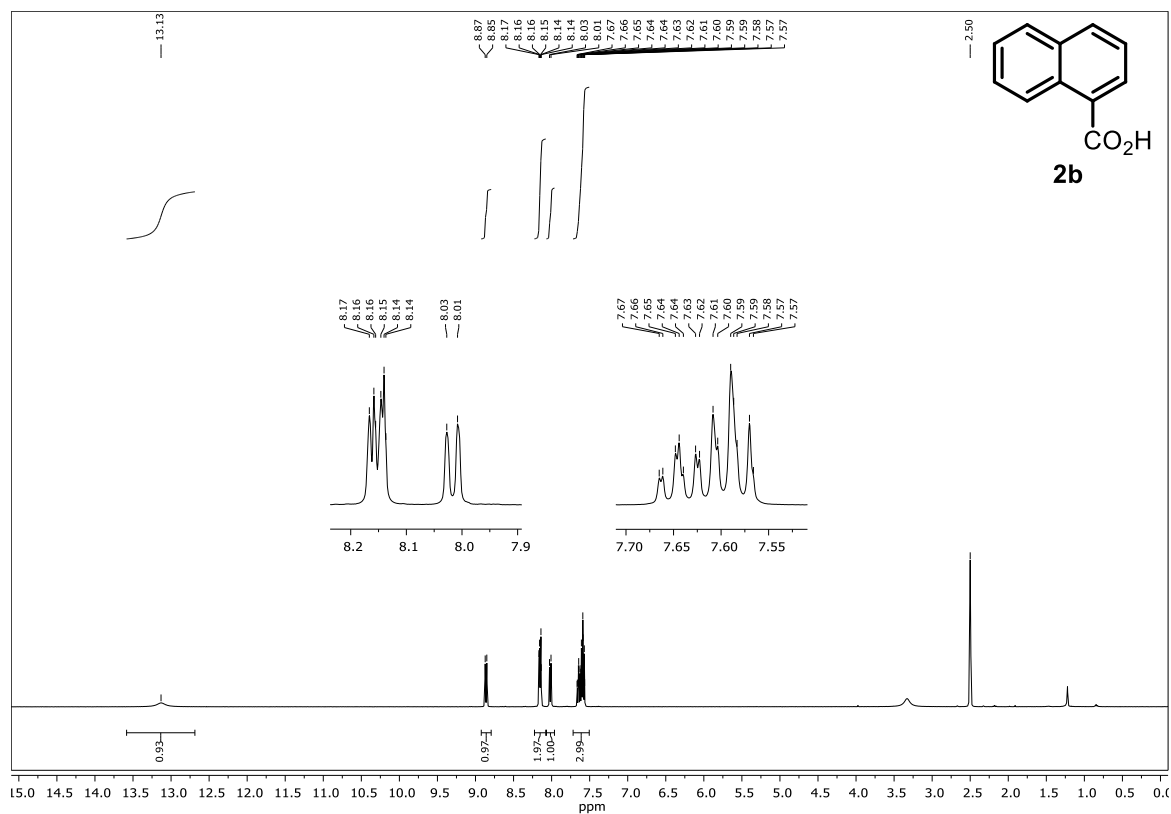
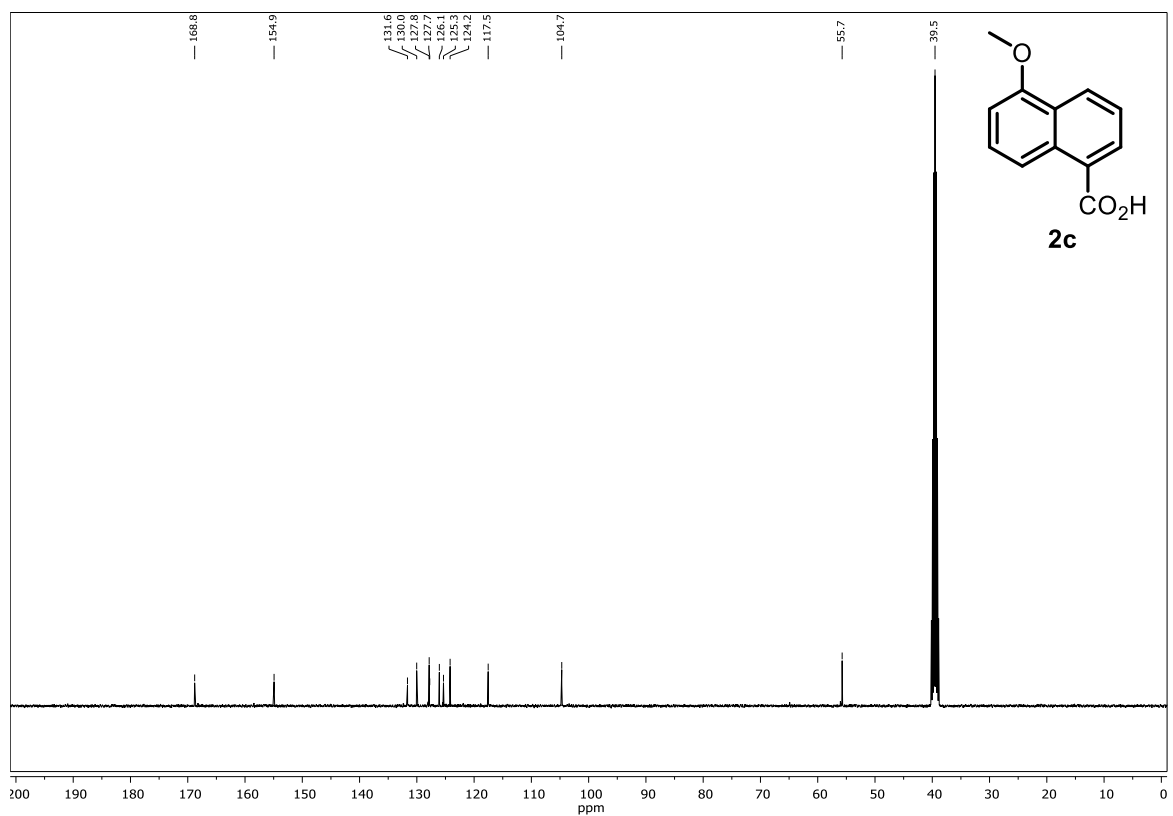
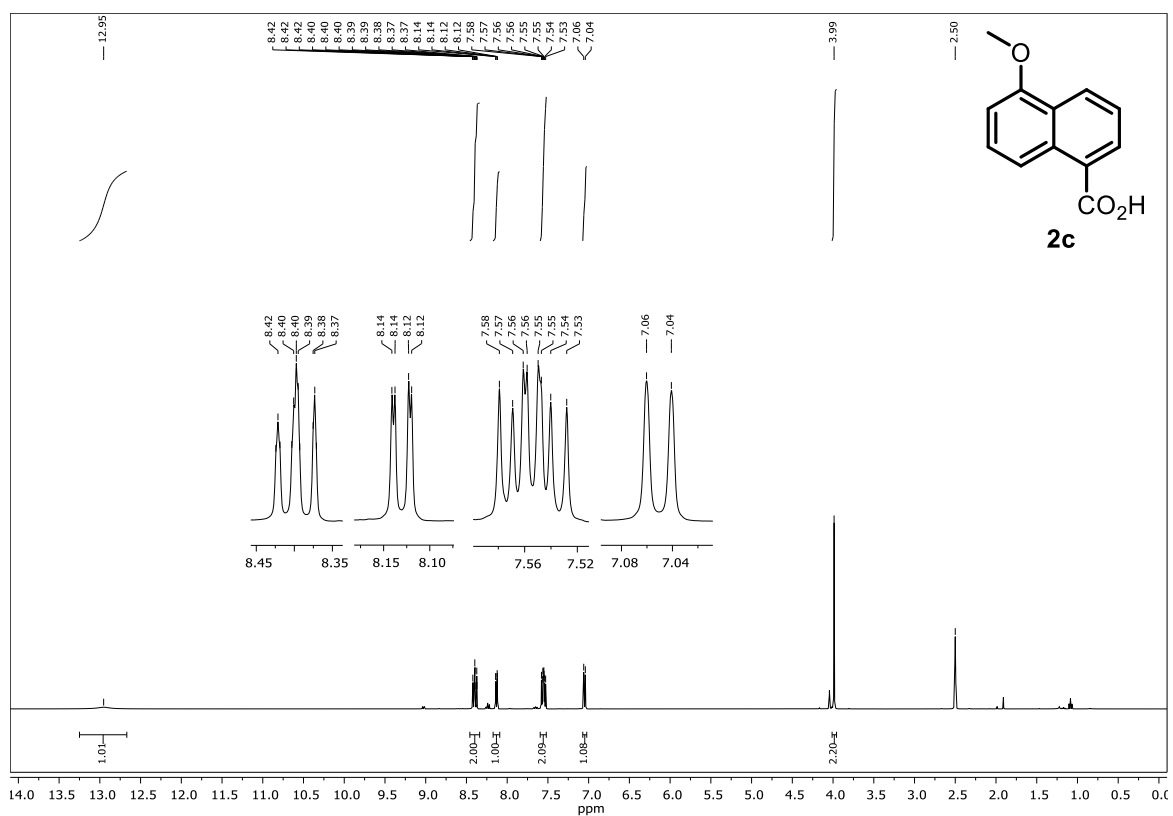


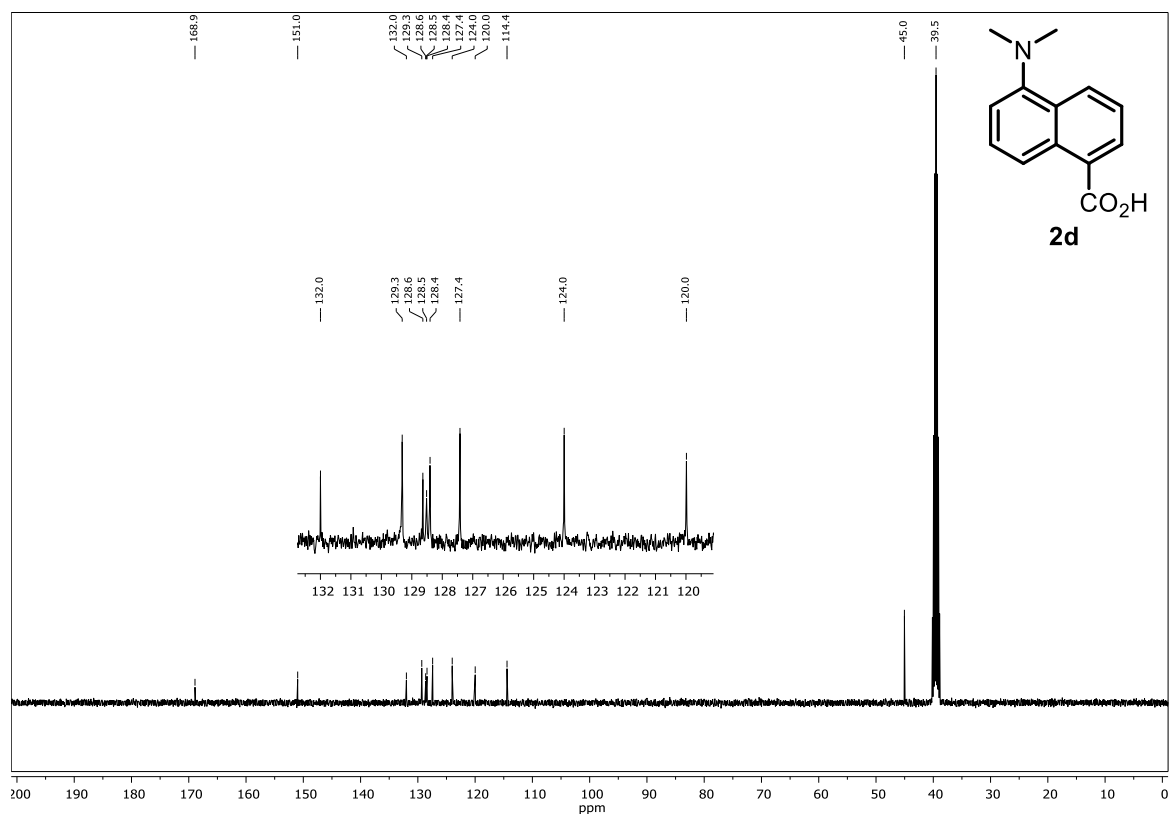
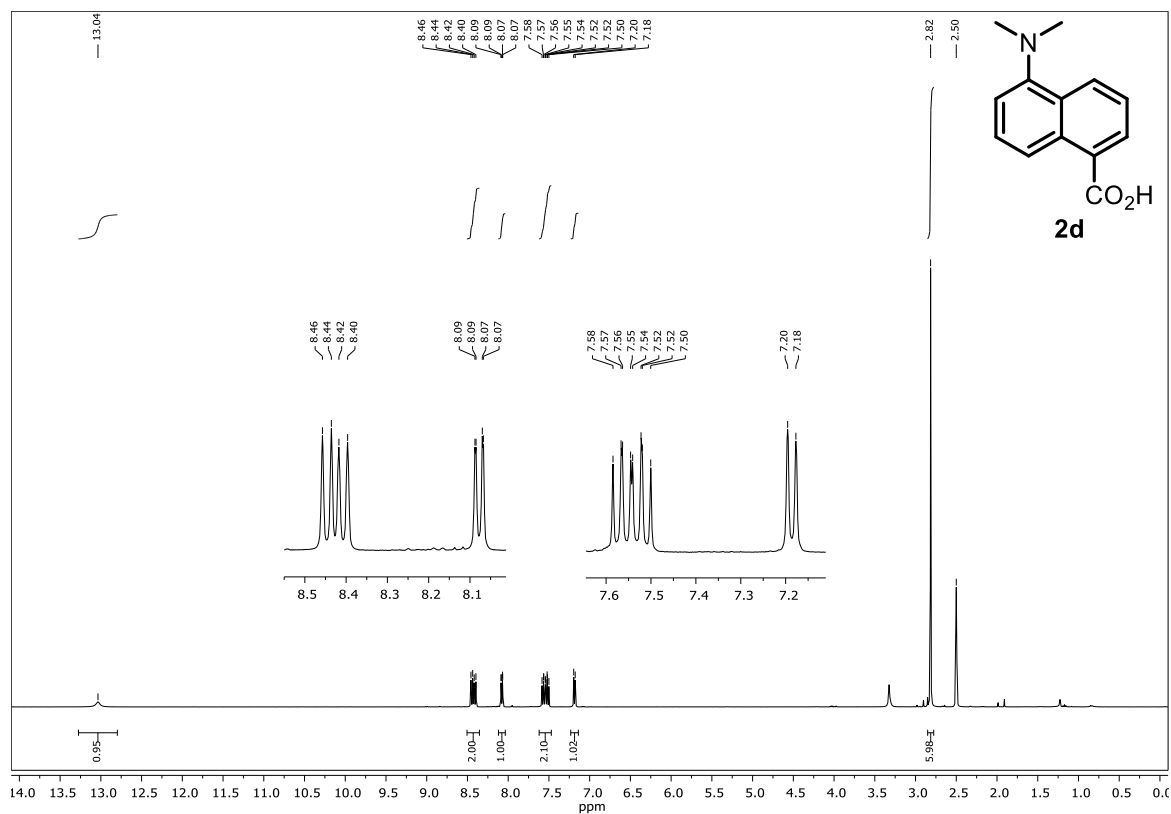
Figure S3-7. Cyclic voltammetry was recorded for catalysts **1a-h** in absence and presence of base (affording **2a-h** with either Cs₂CO₃ or TMG). Peaks marked in bold were used to calculate electrochemical potentials against the internal reference ferrocene. †Peak of the redox couple Fc⁺/Fc overlaps with a signal peak of the analyte; an estimated half-wave potential of 0.11 V between Fc⁺/Fc was assumed for calculation.

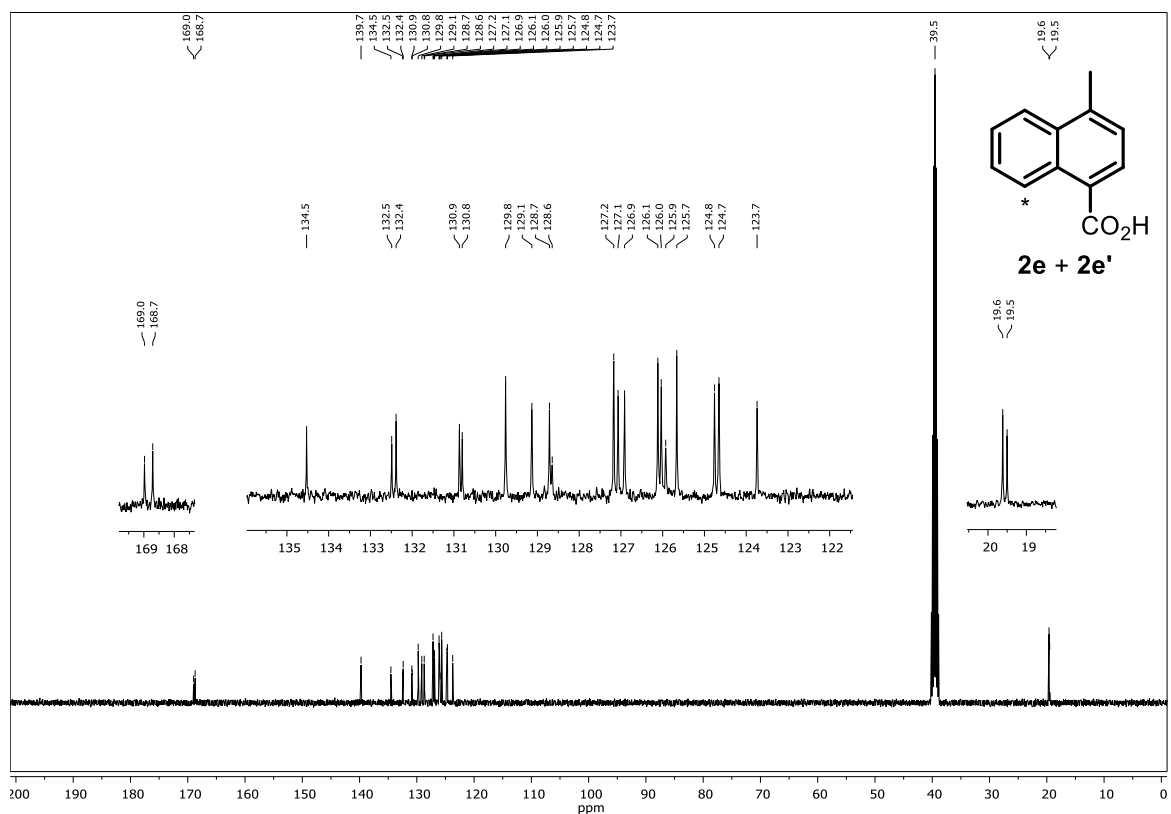
7.4 NMR Spectra Chapter 4

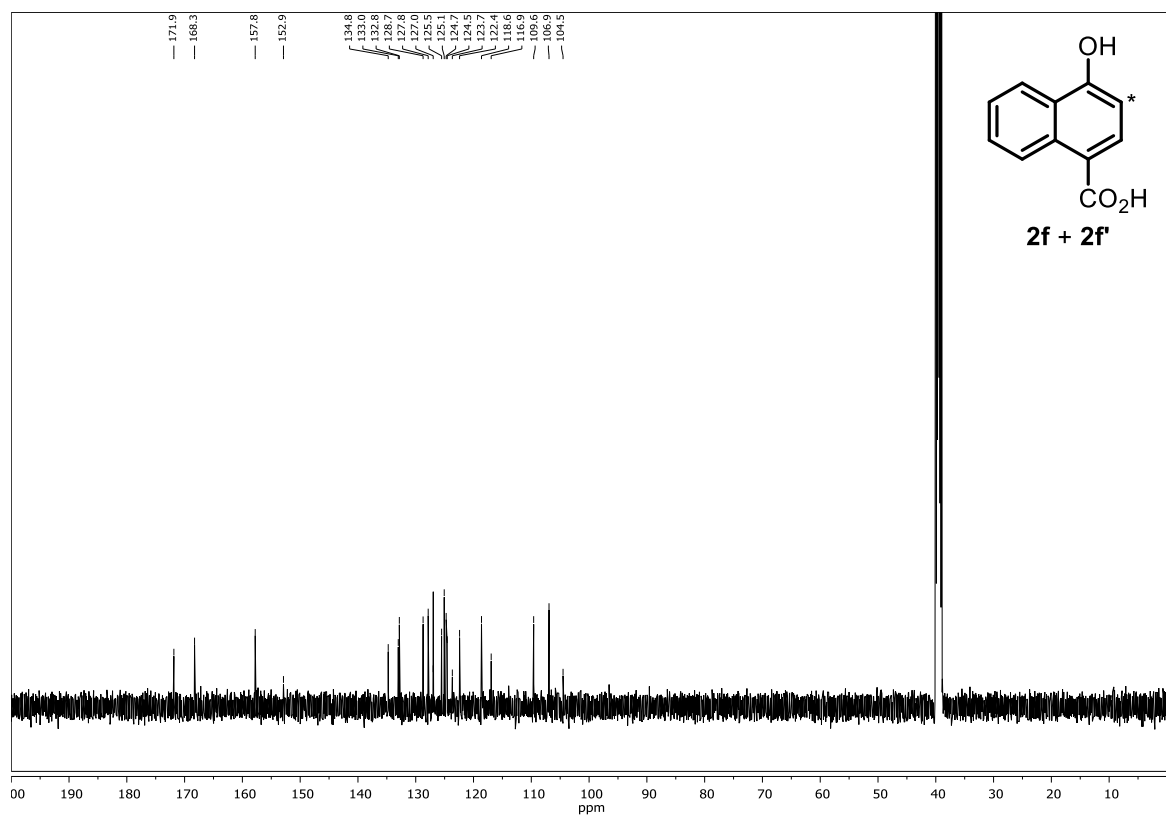
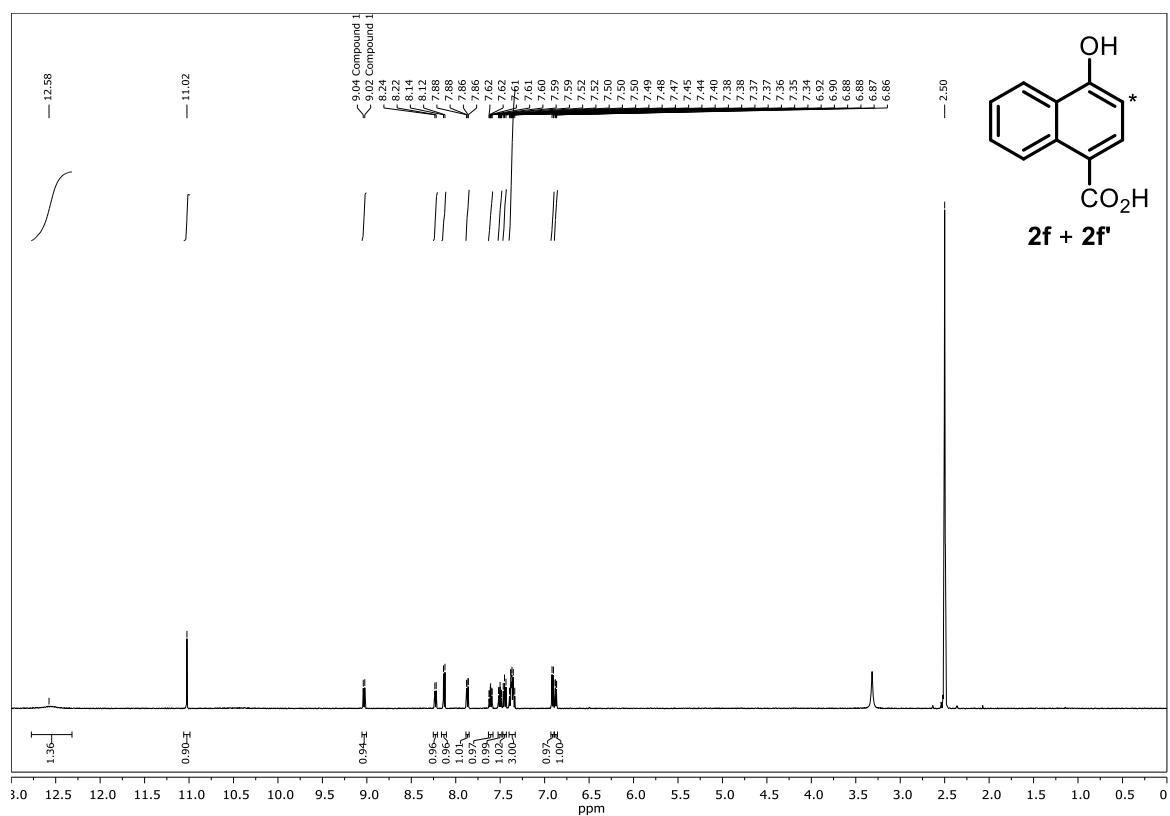


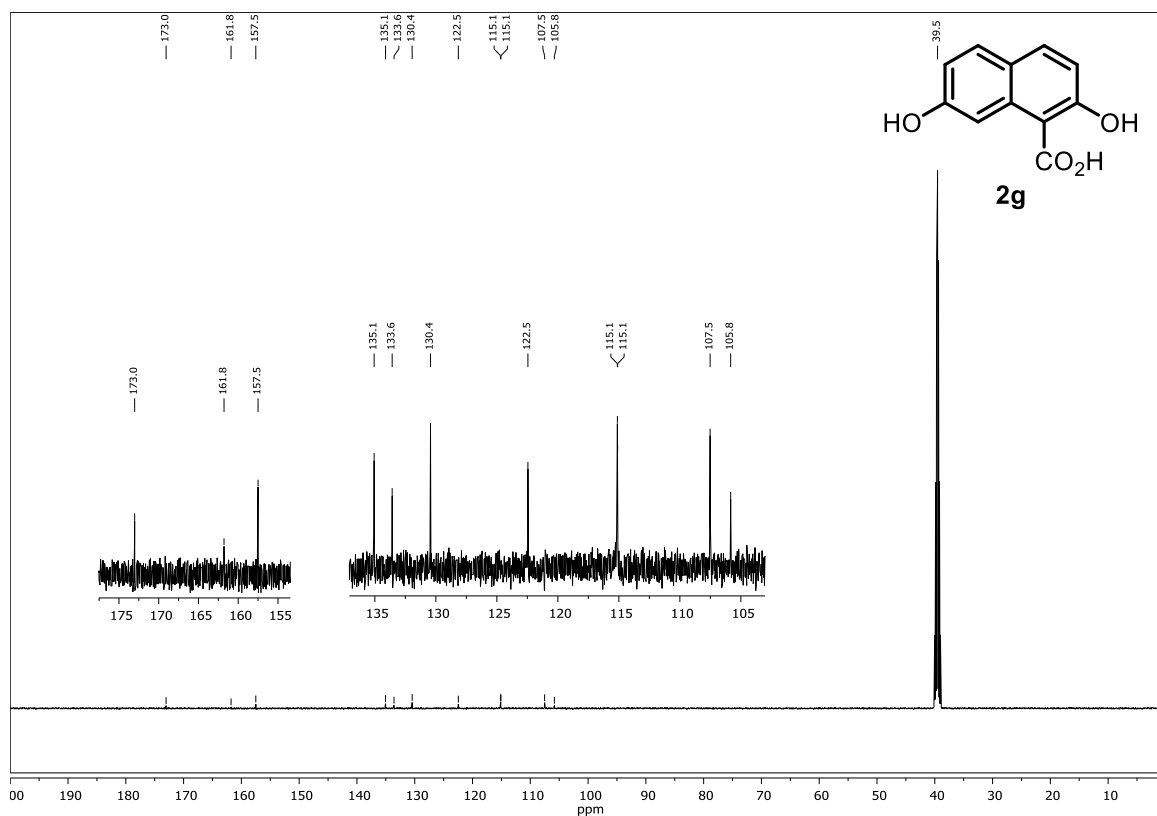
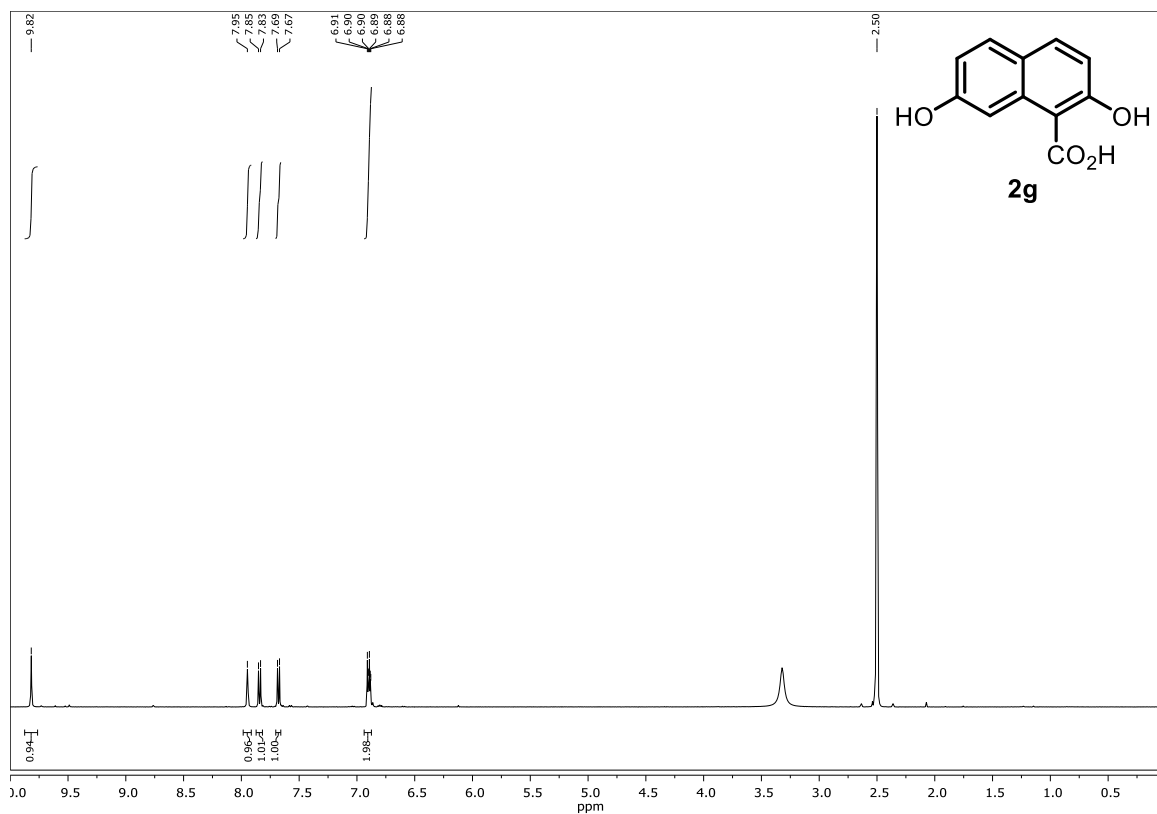


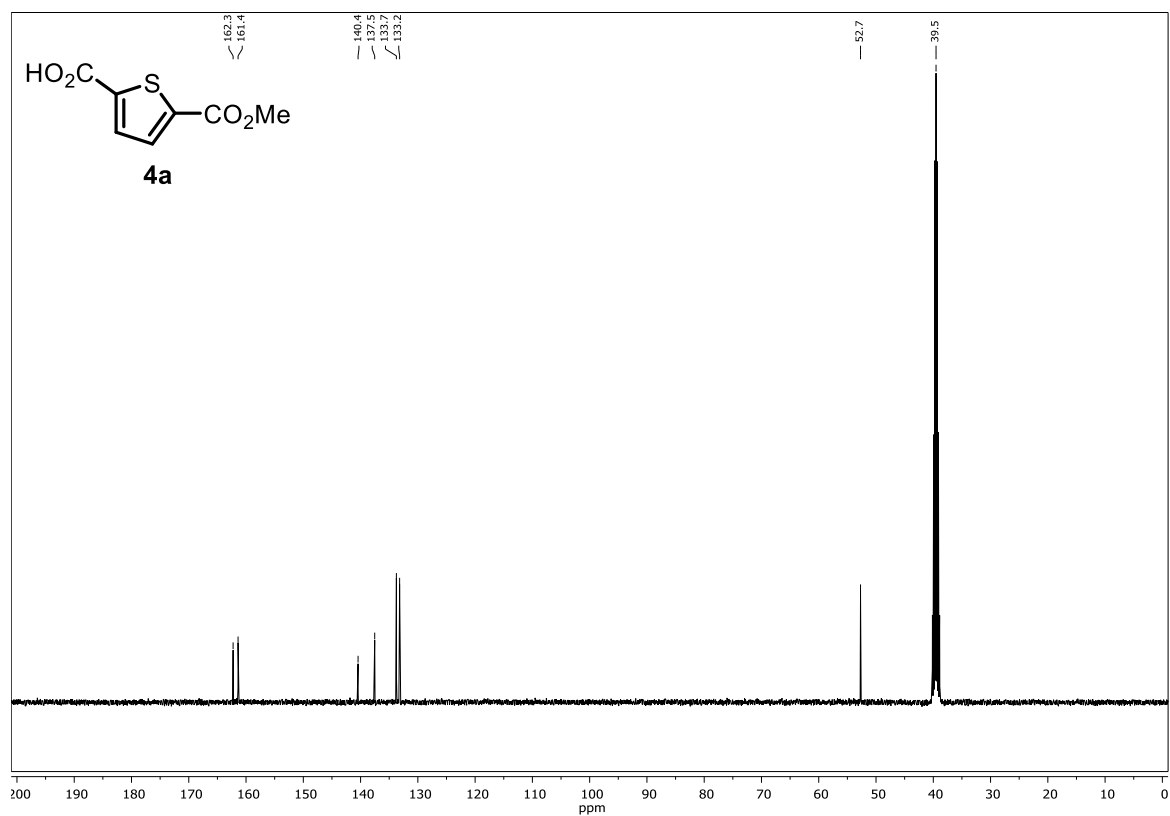
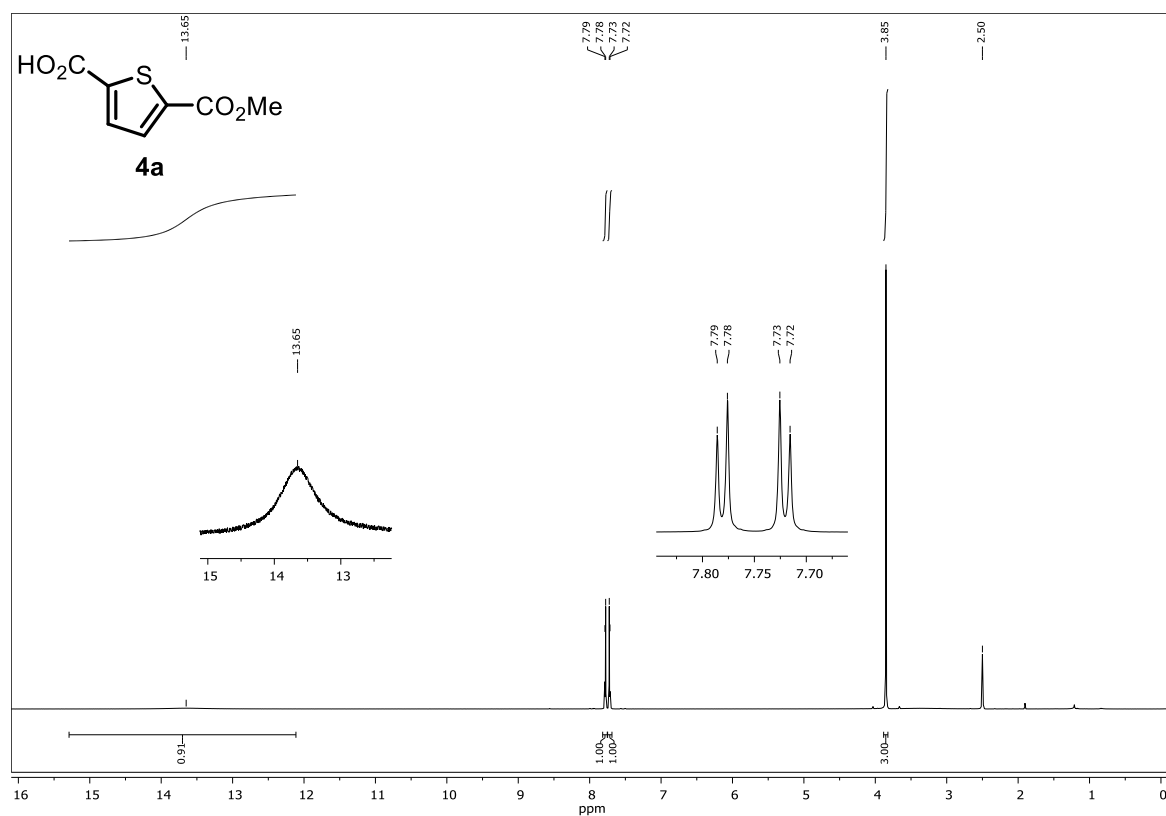


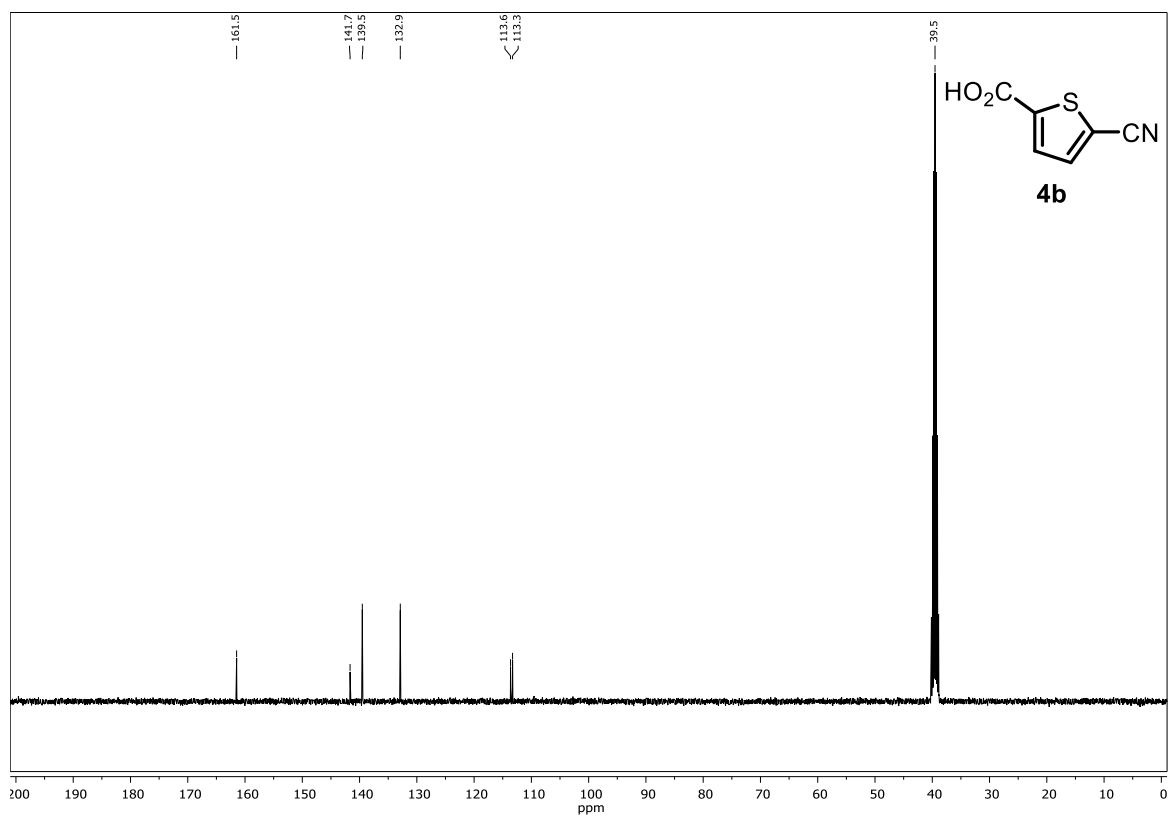
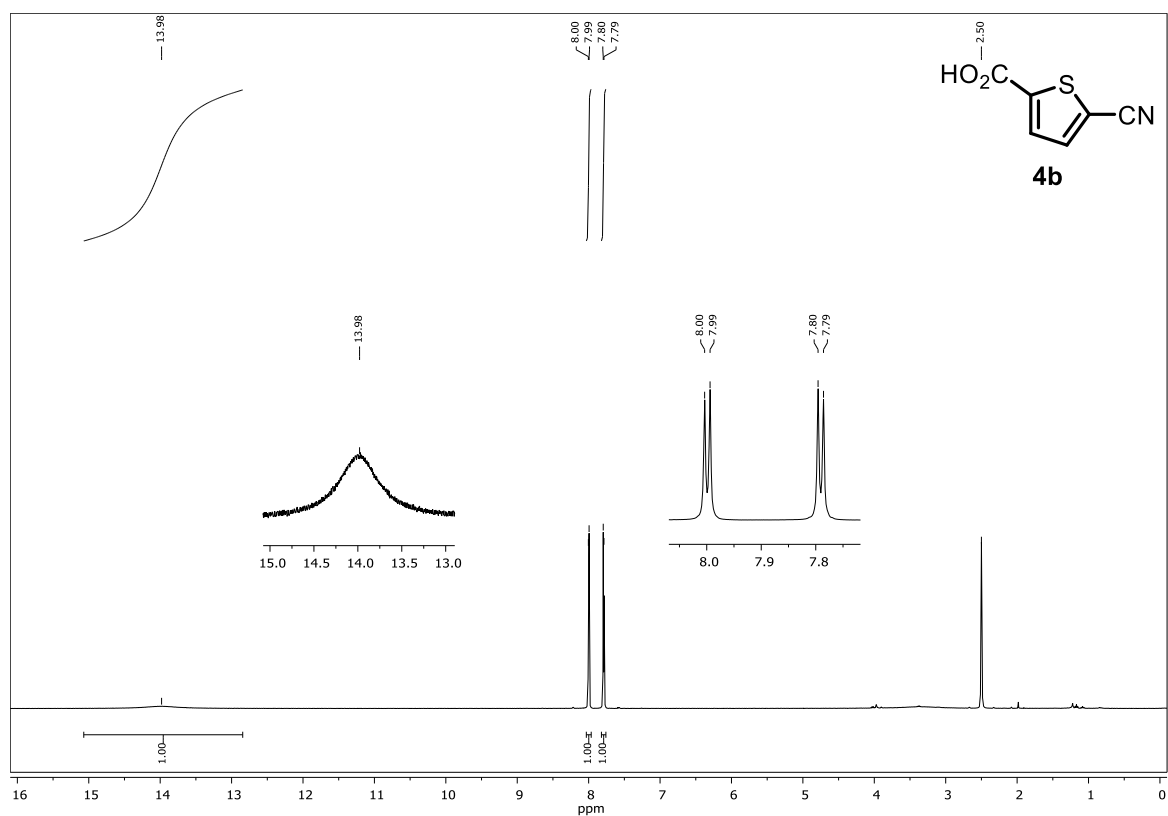


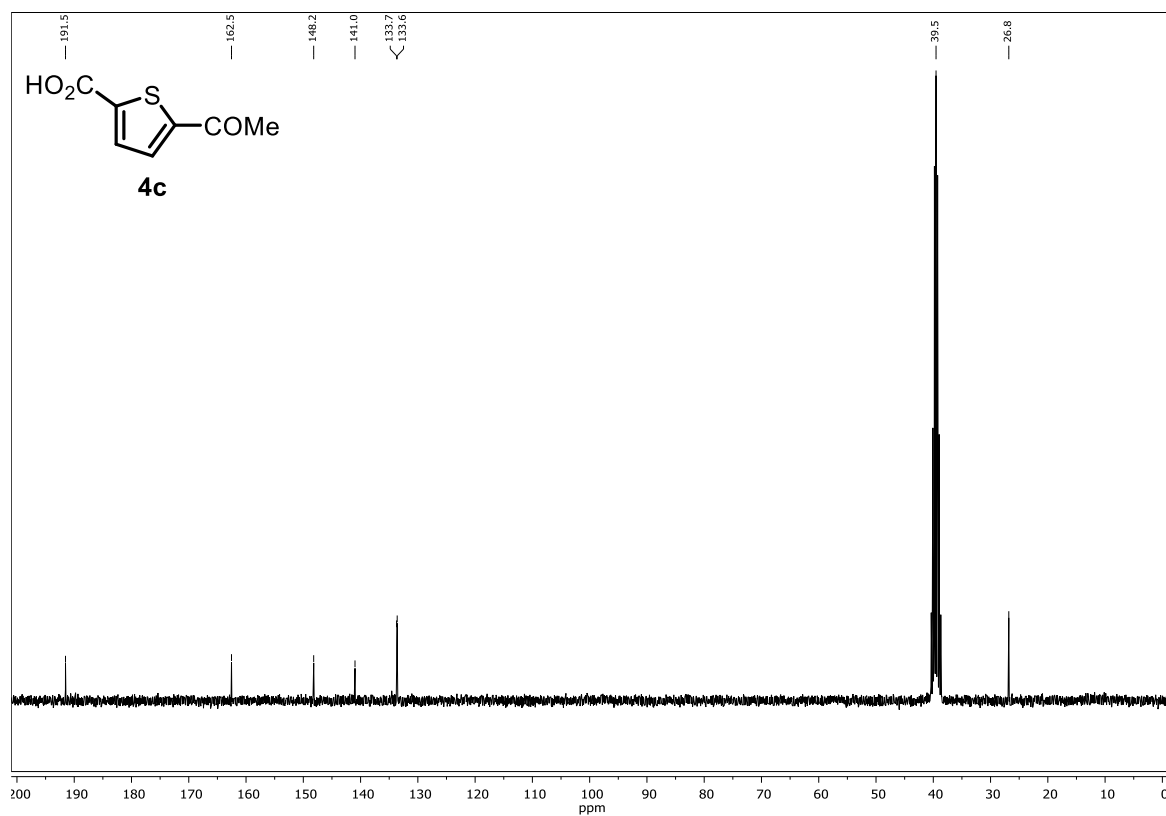
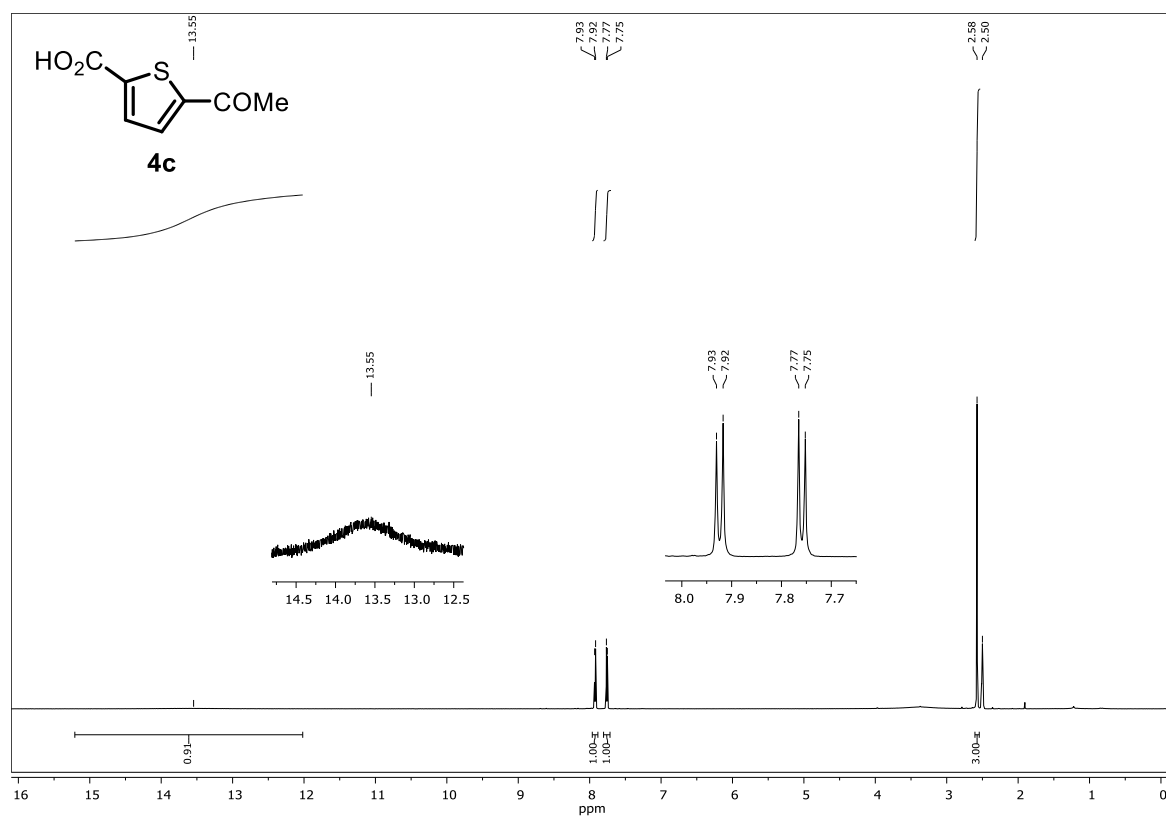


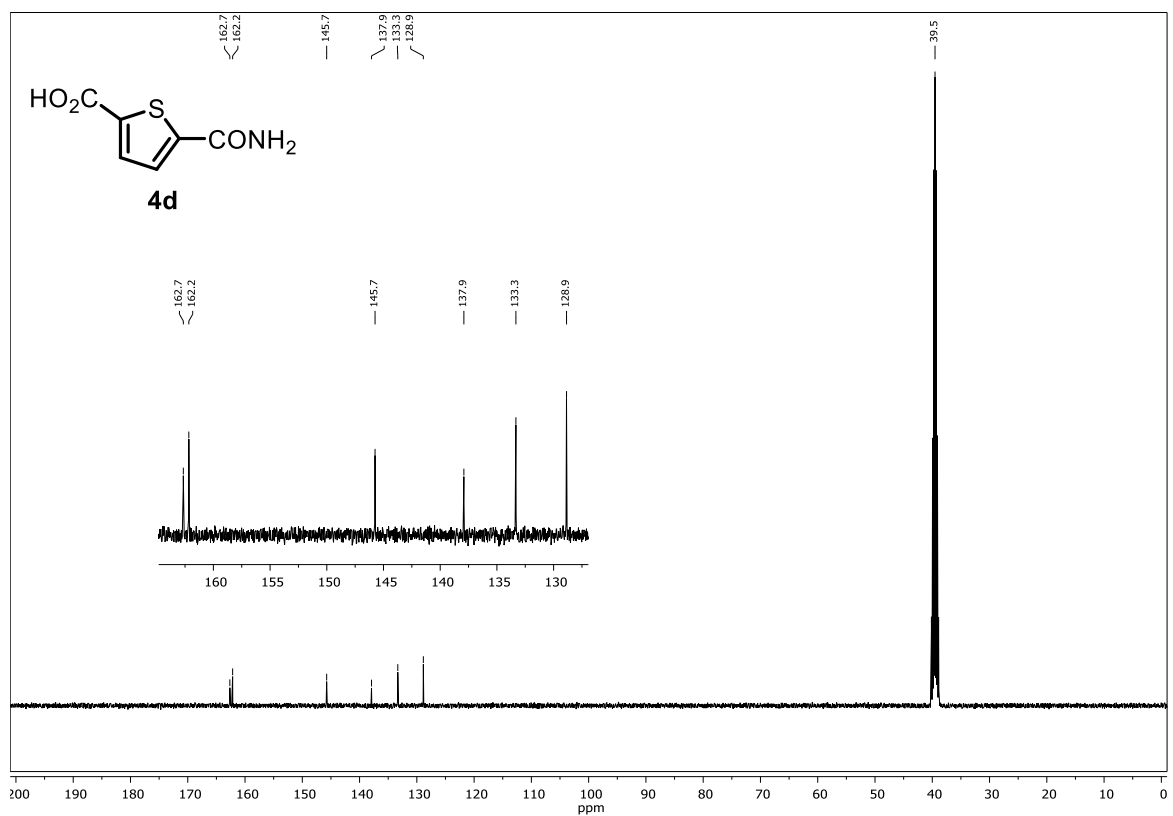
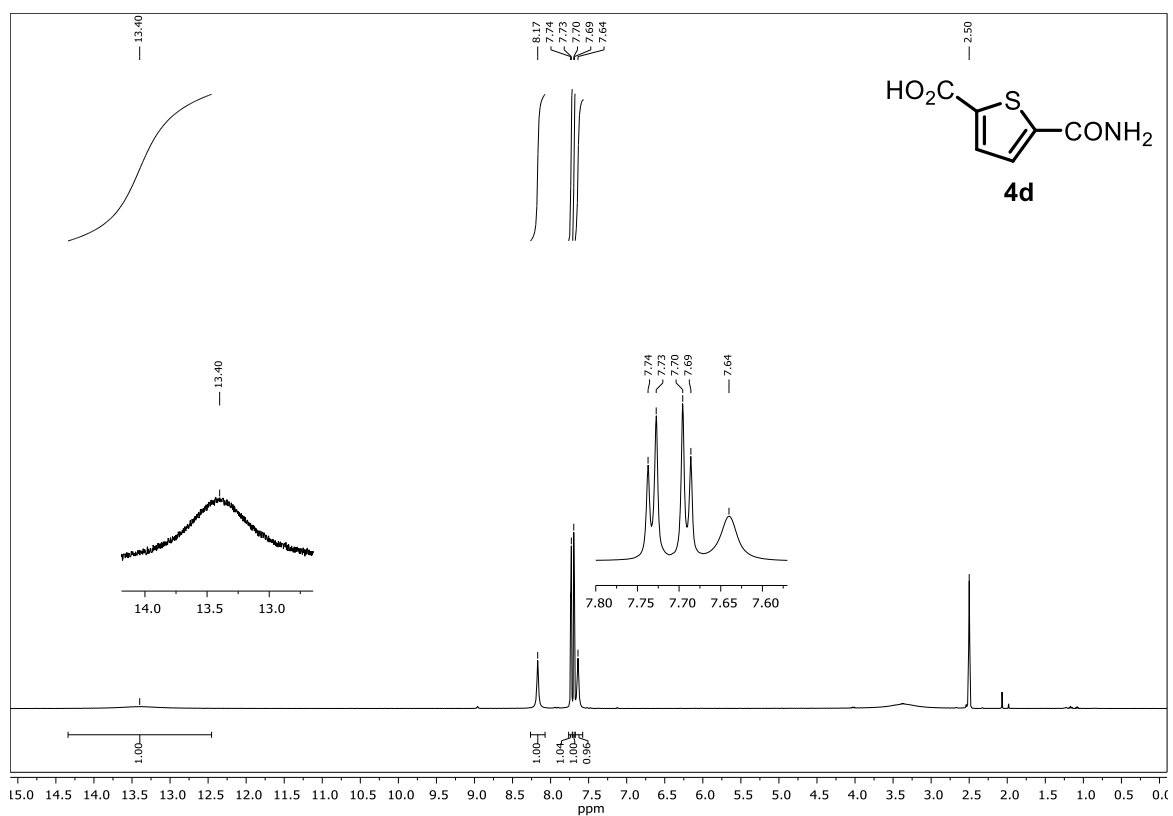


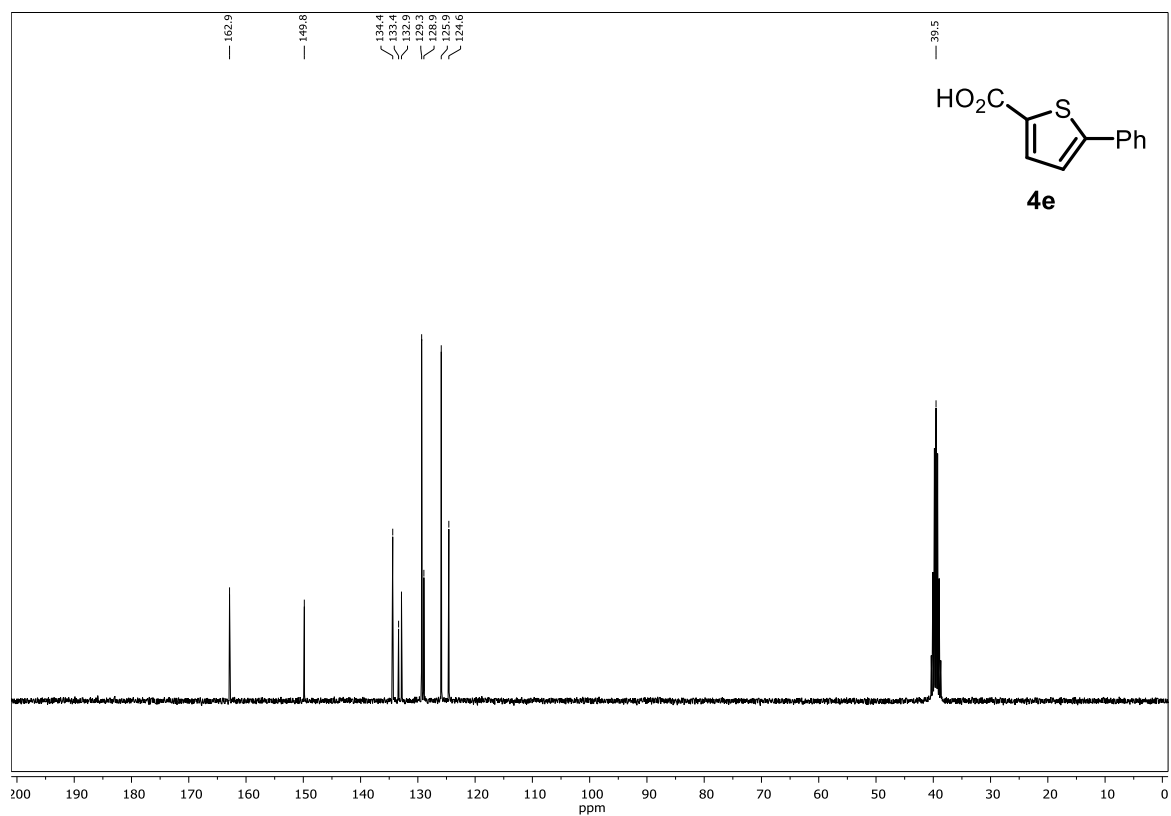
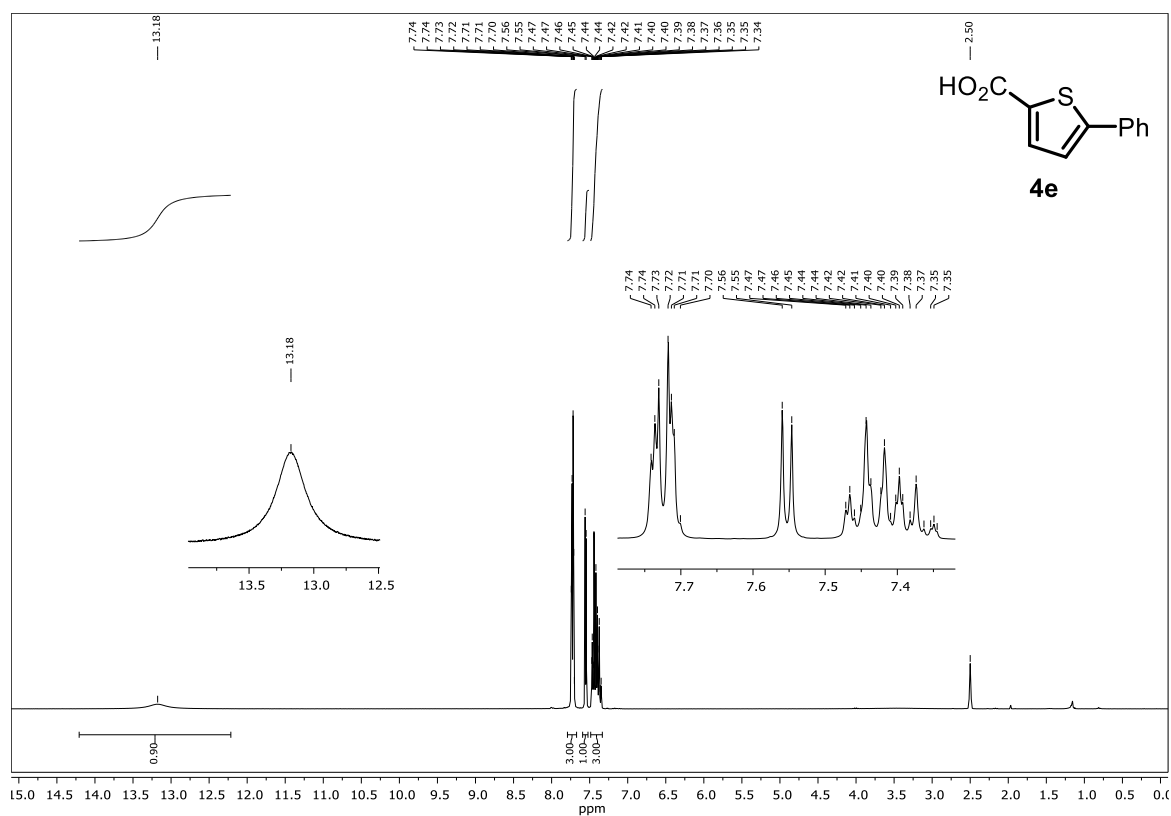


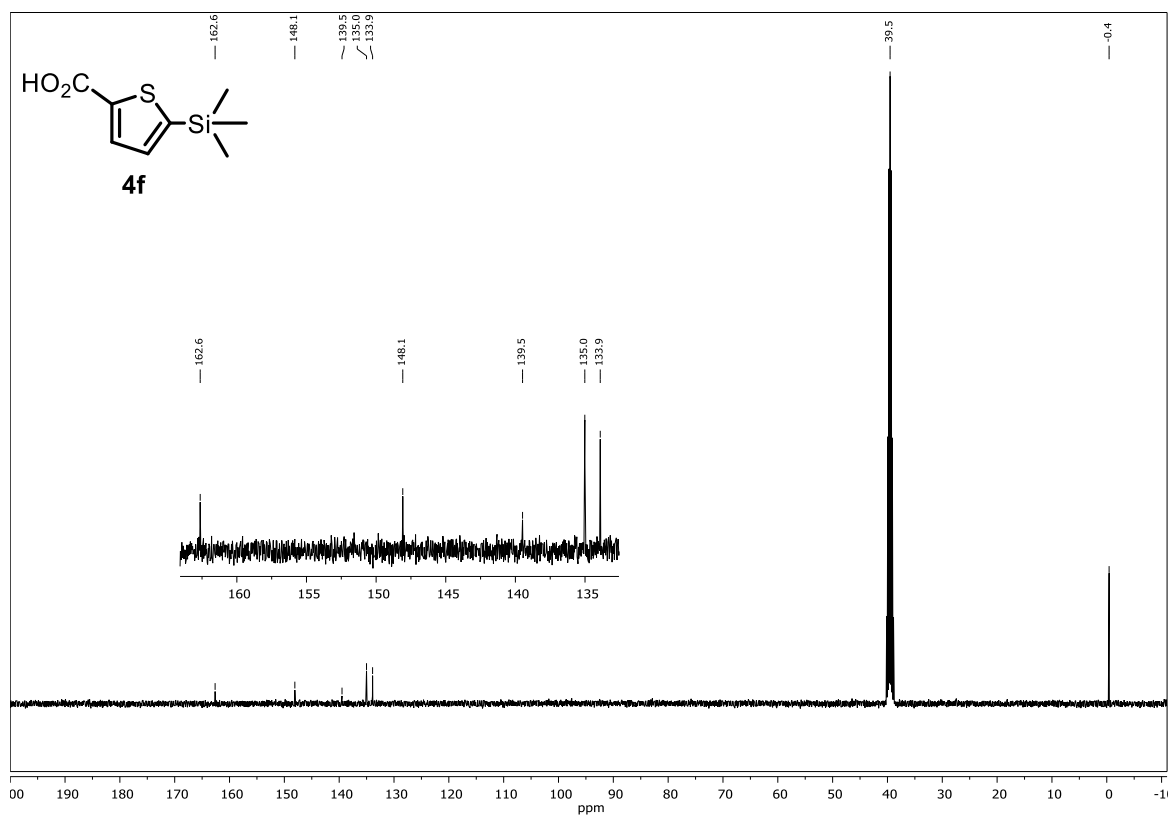
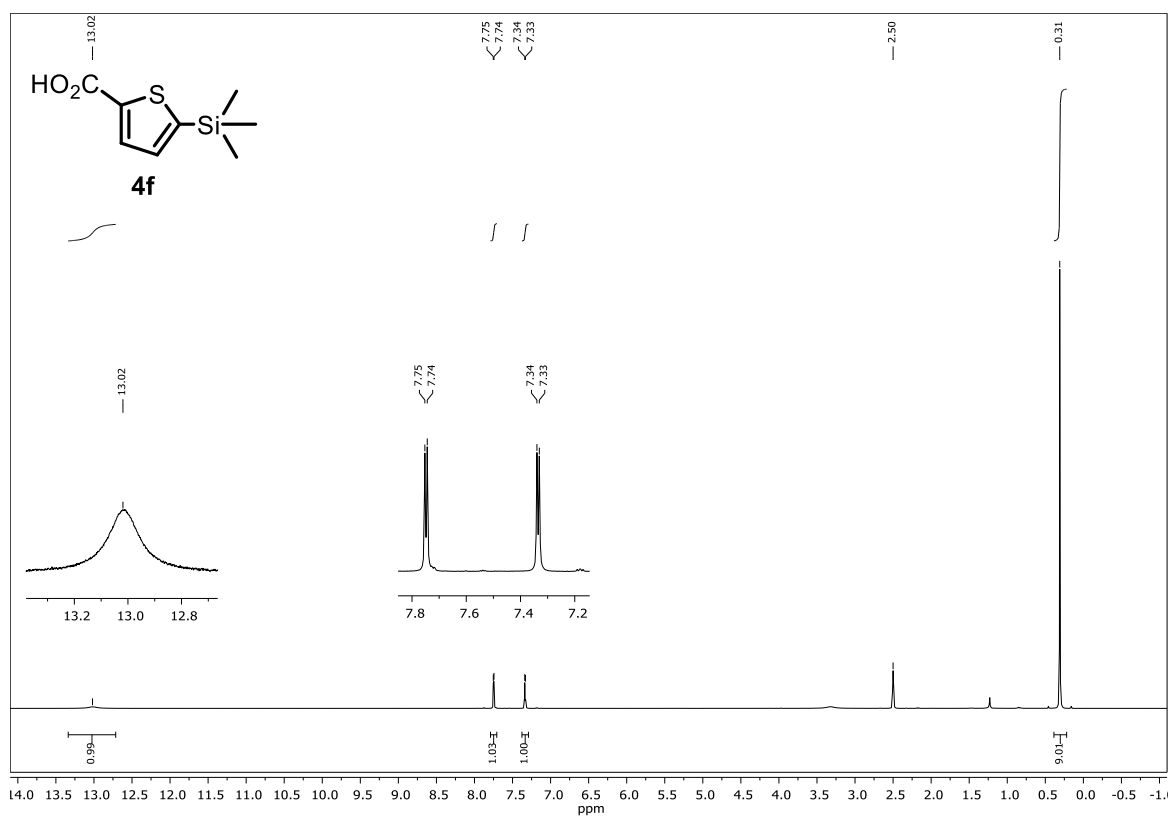


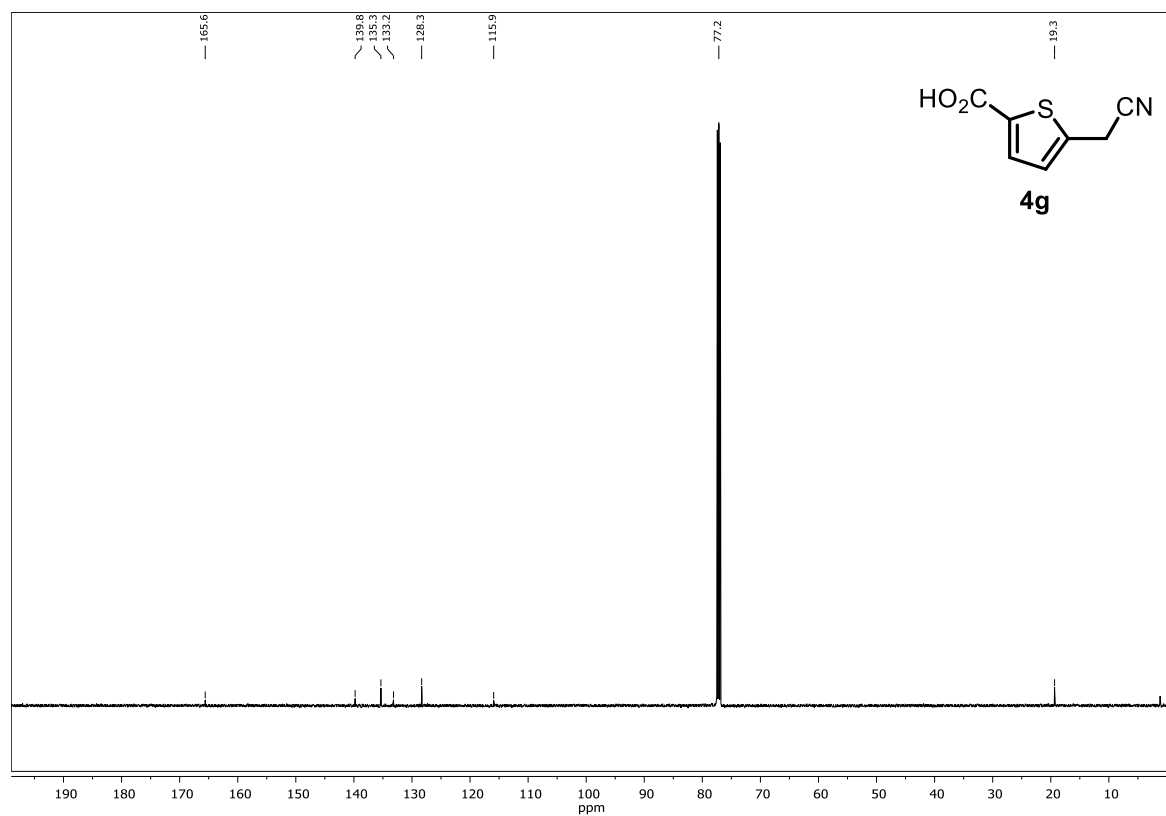
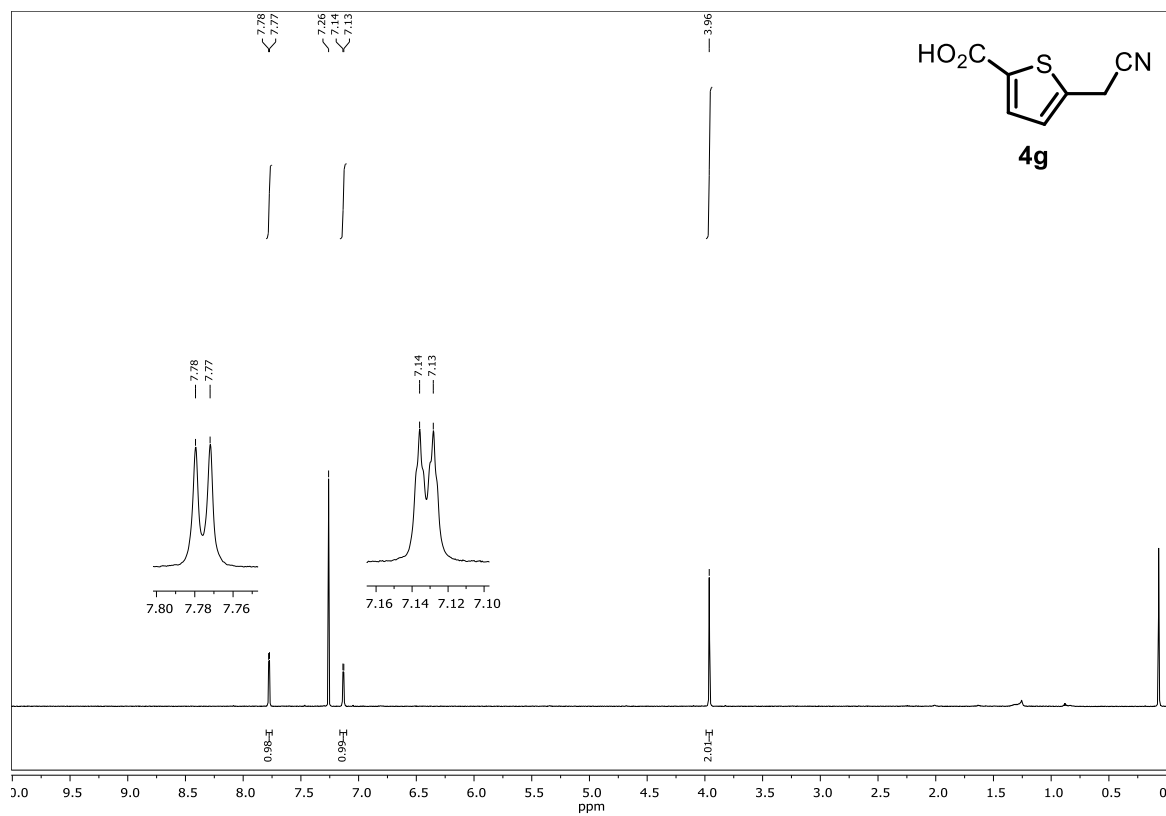


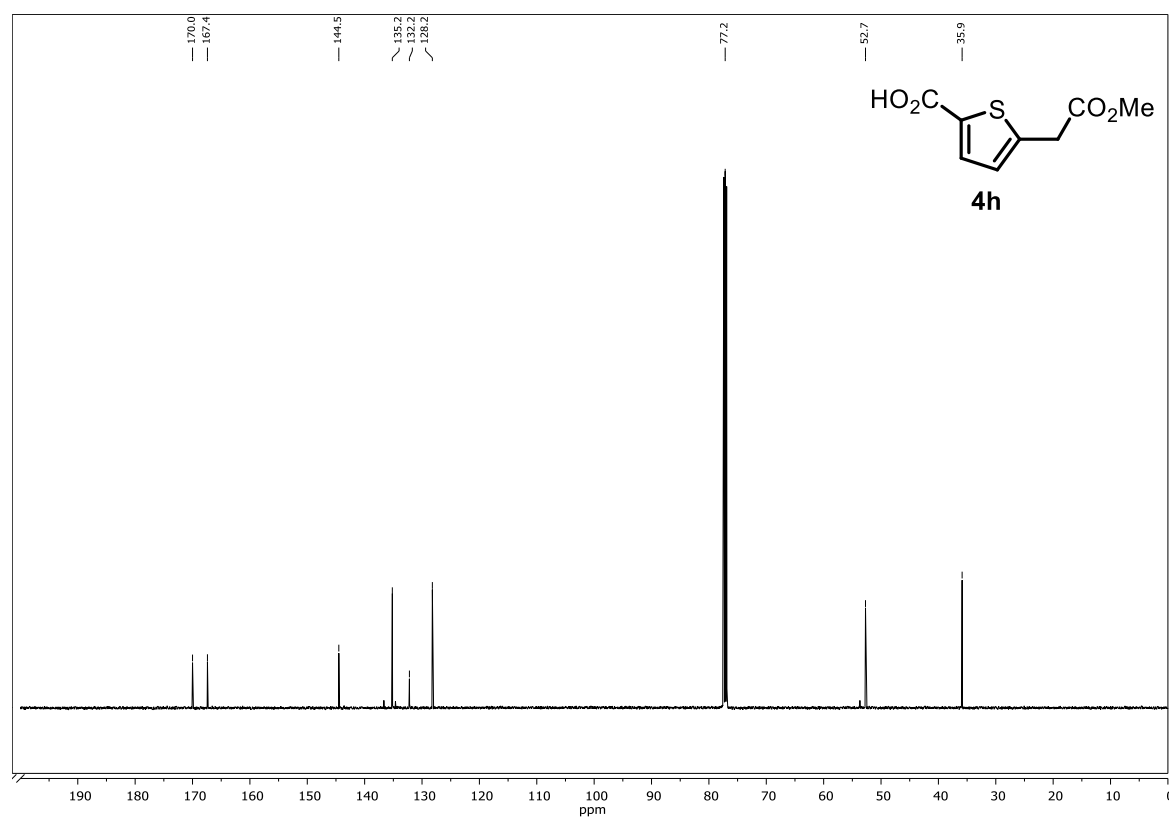
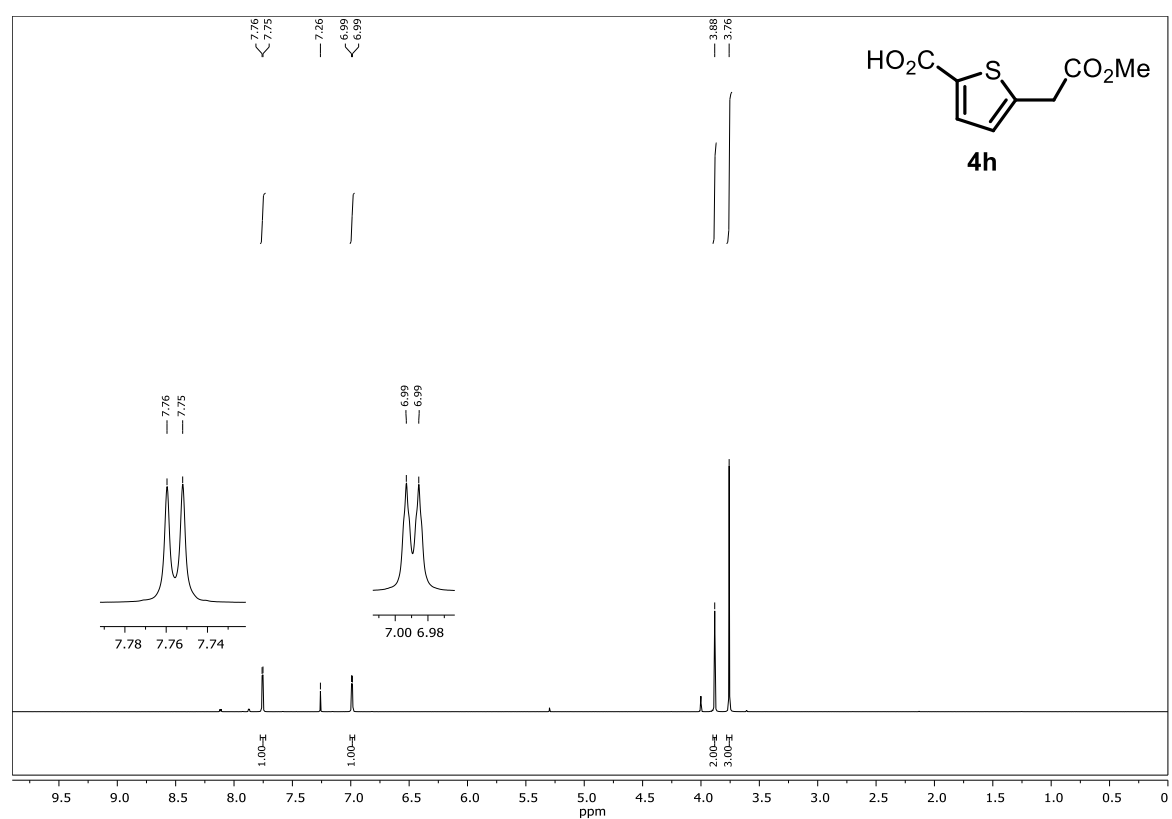


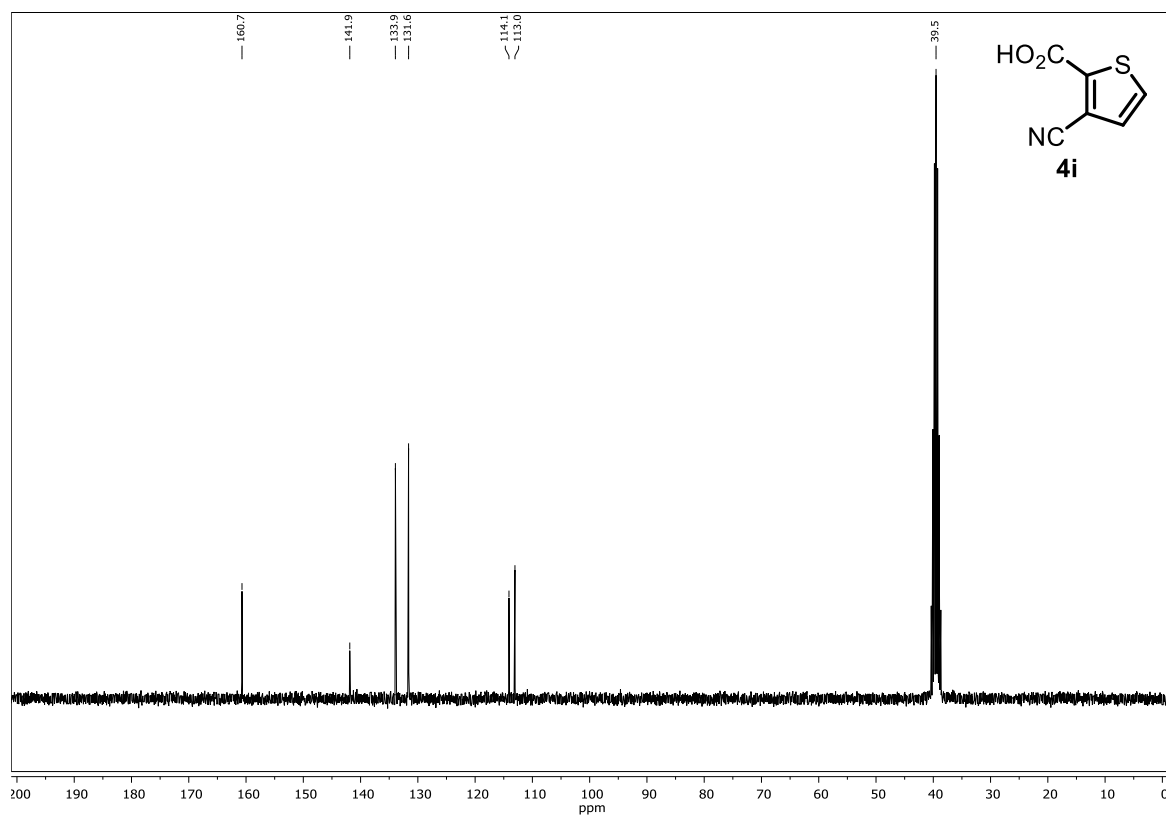
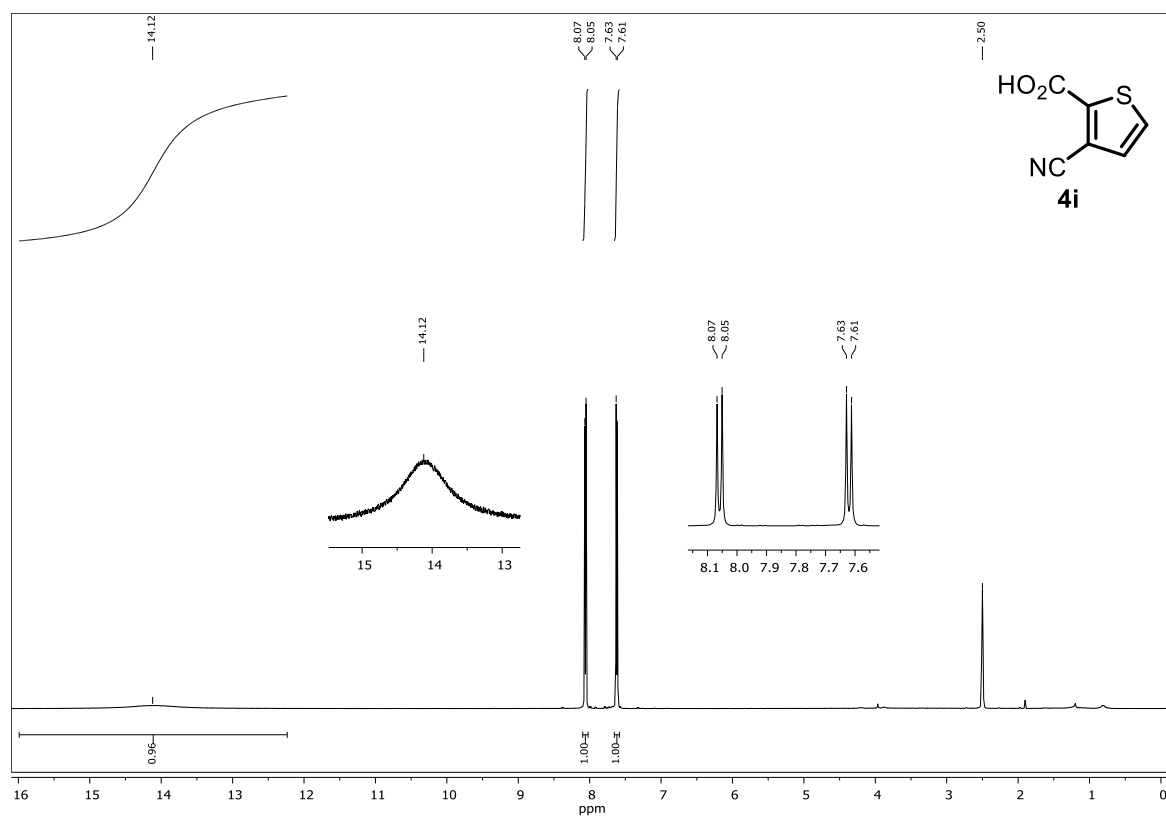


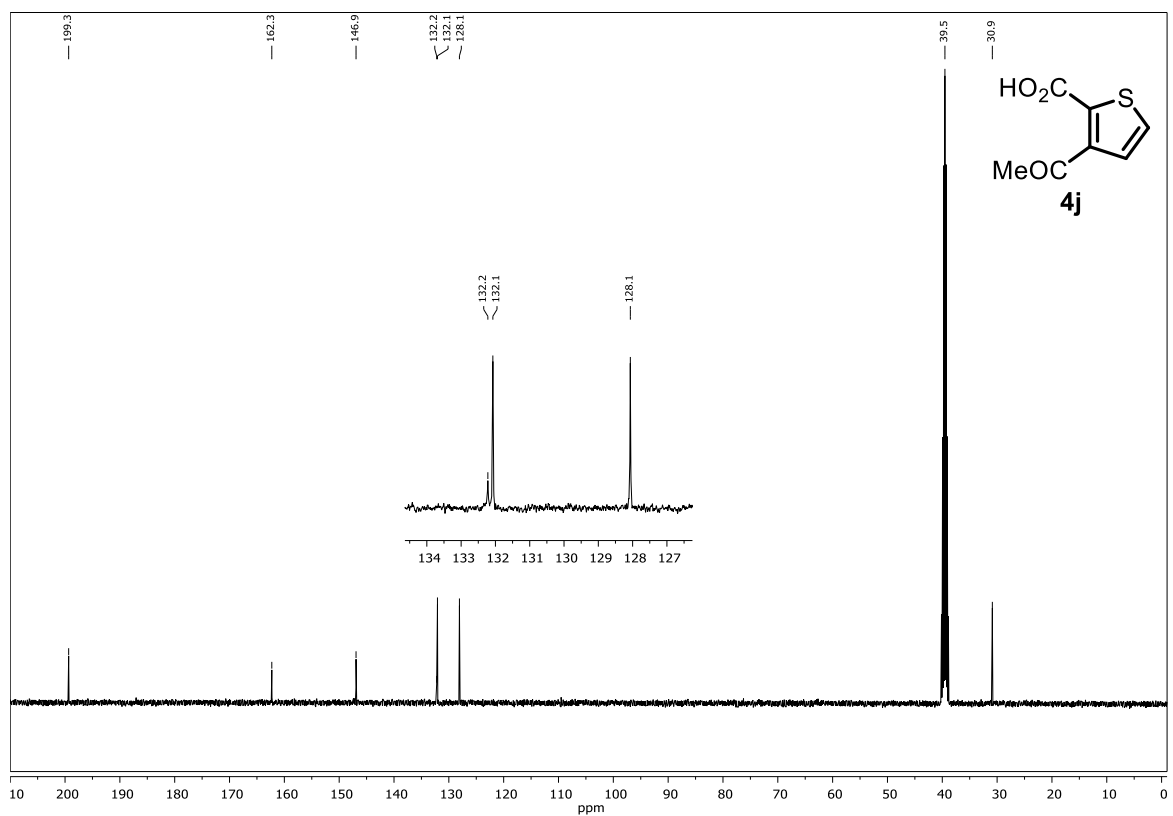
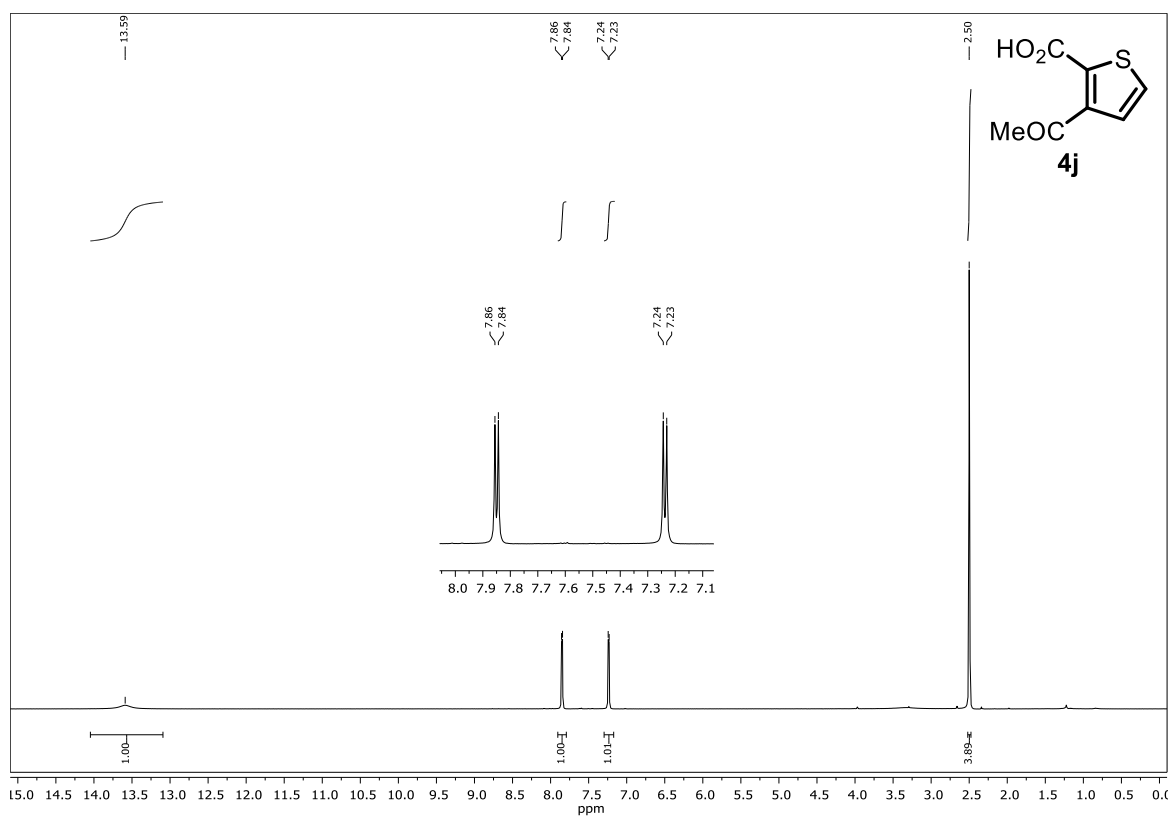


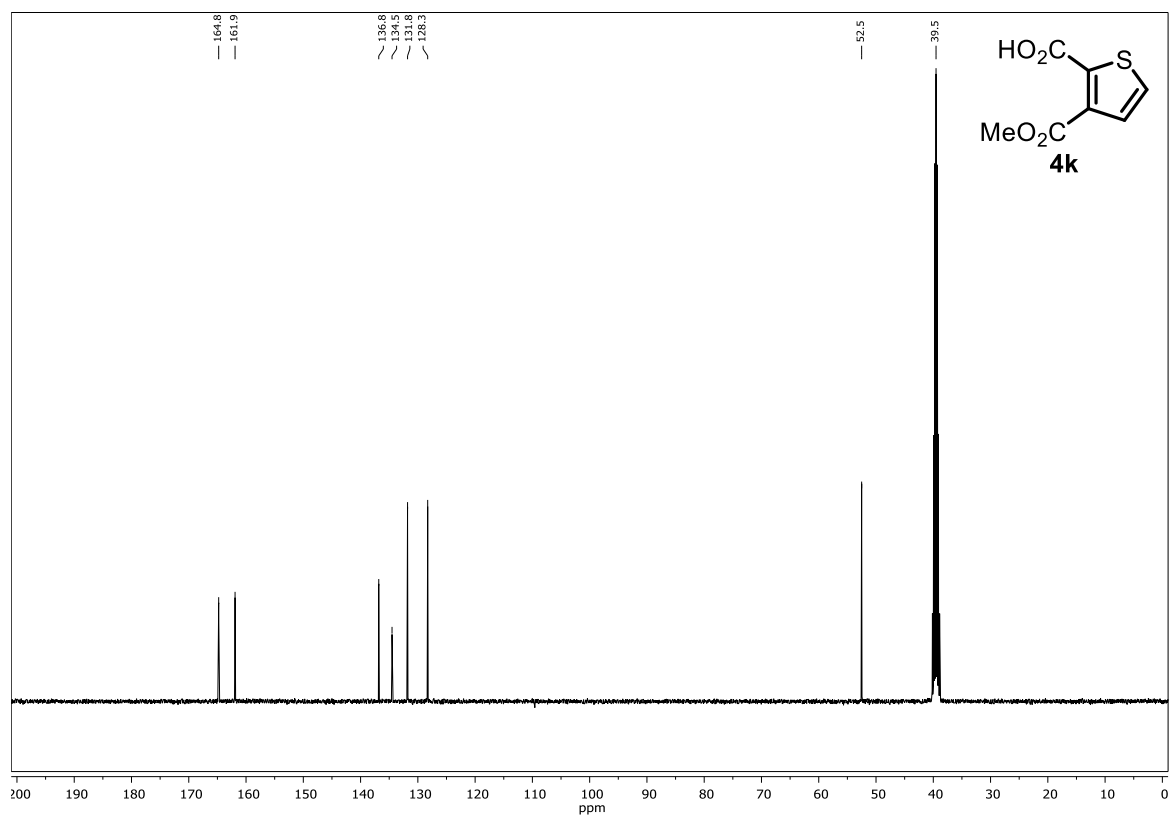
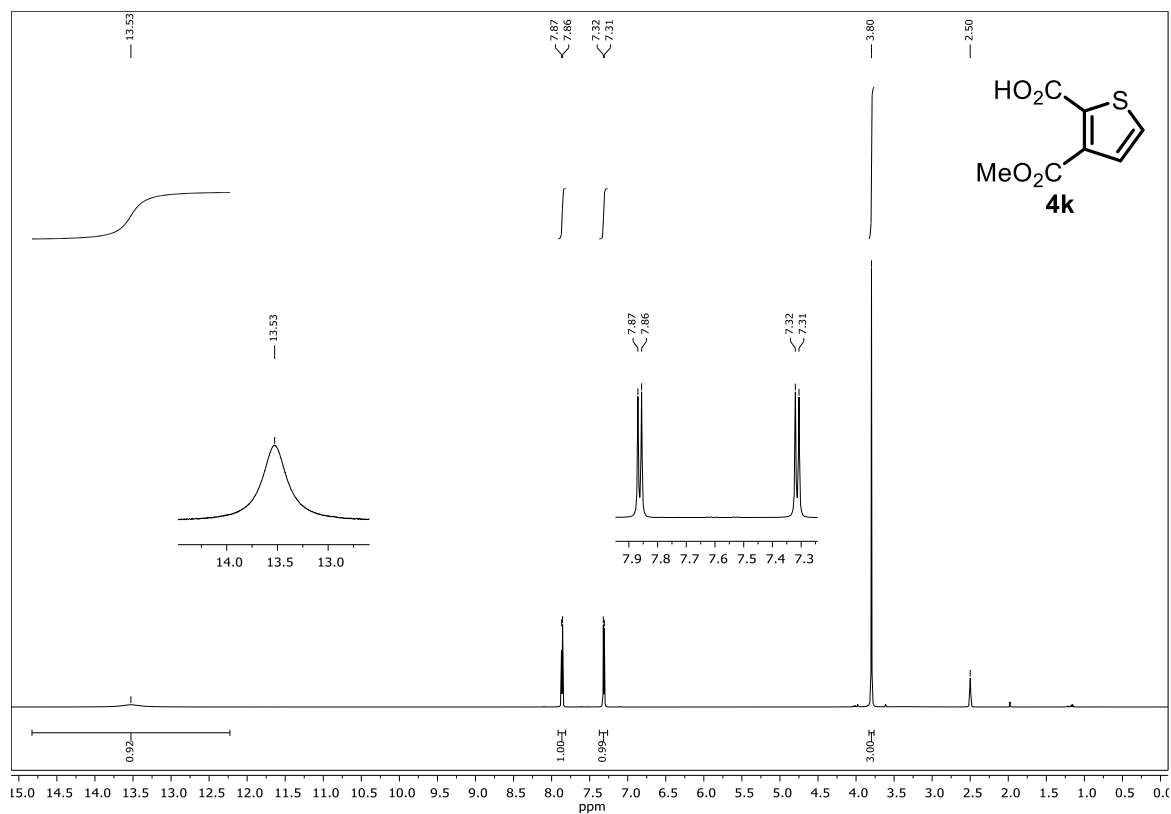


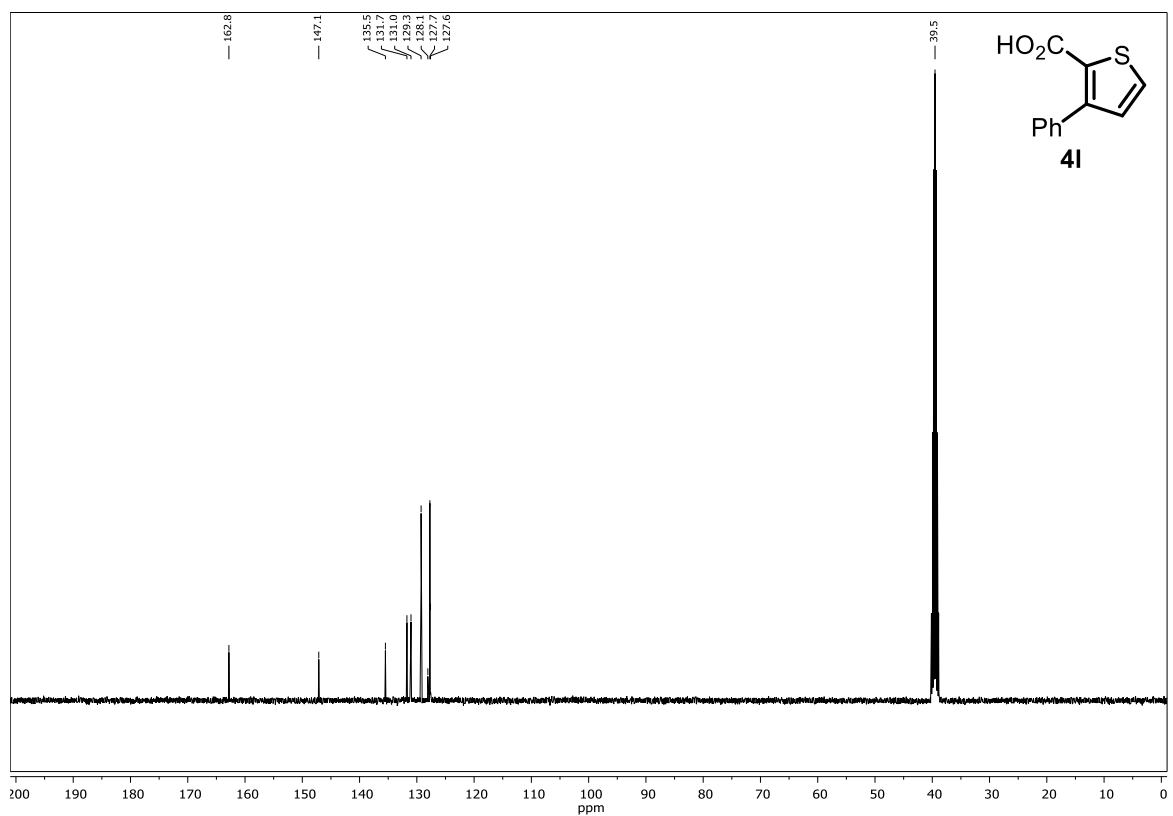
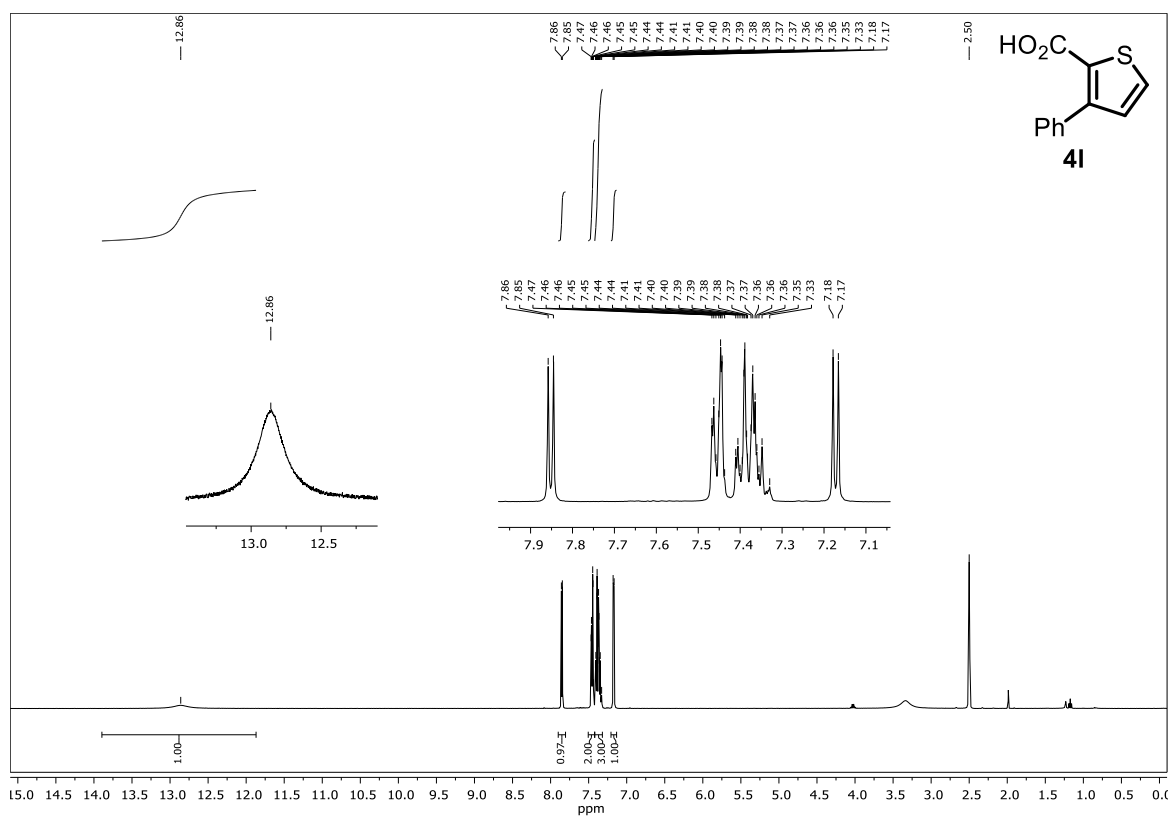




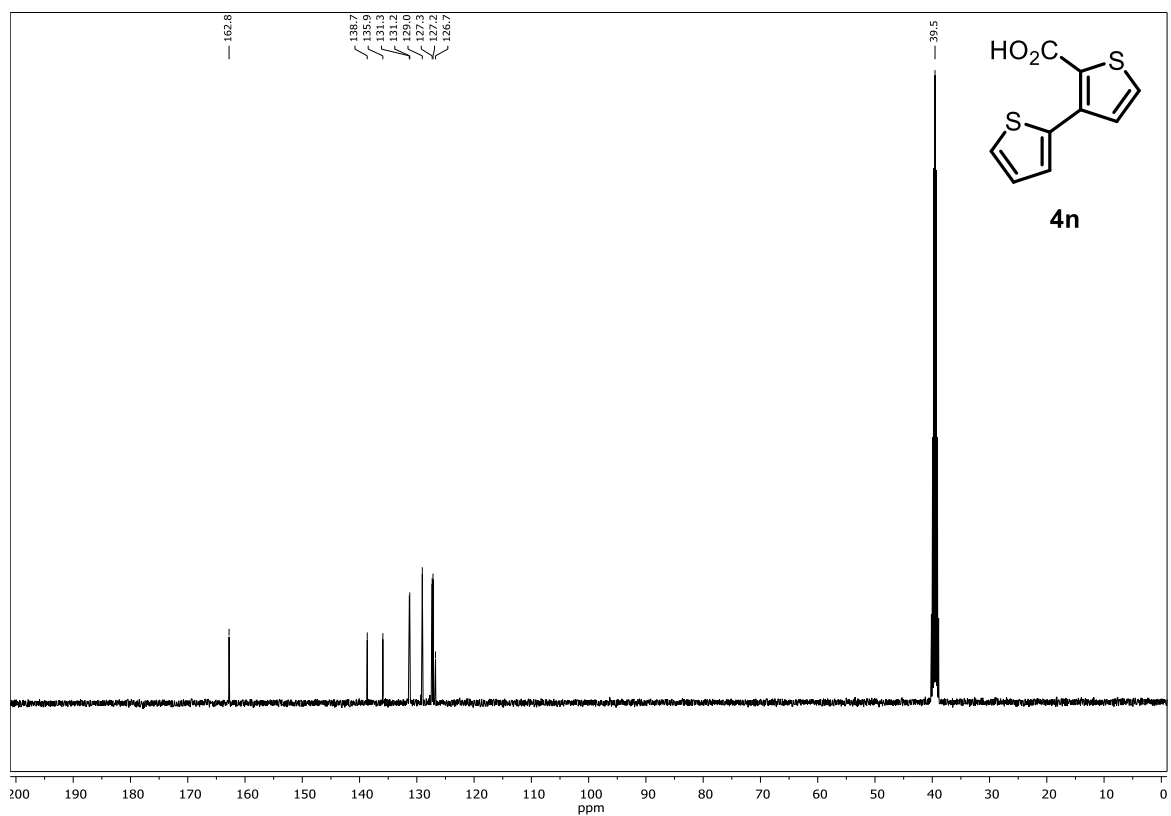
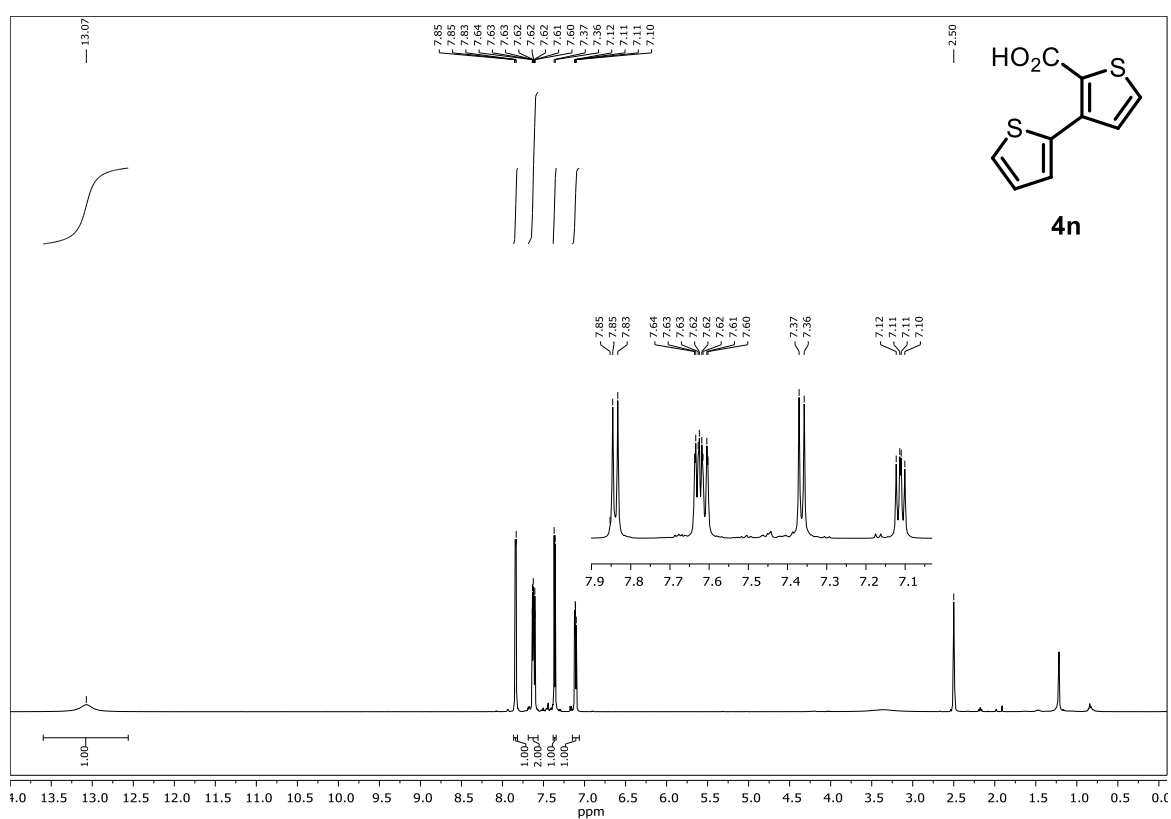


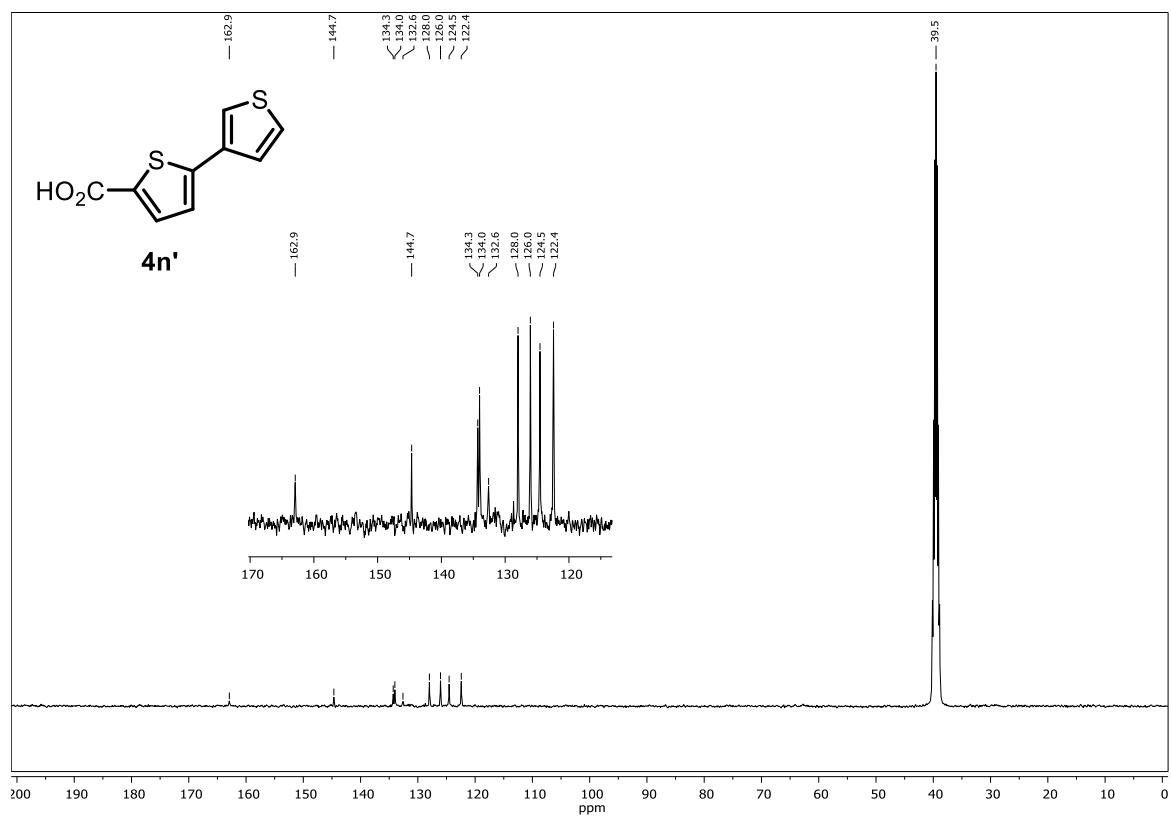
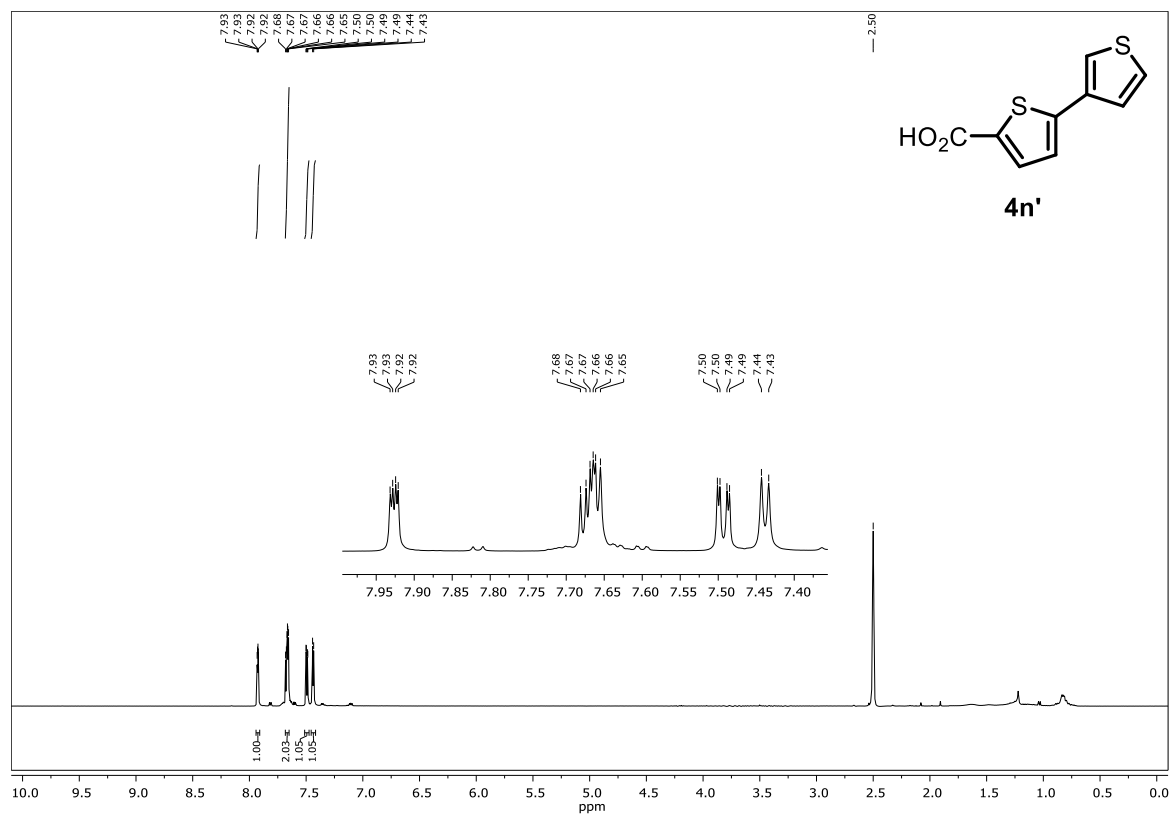


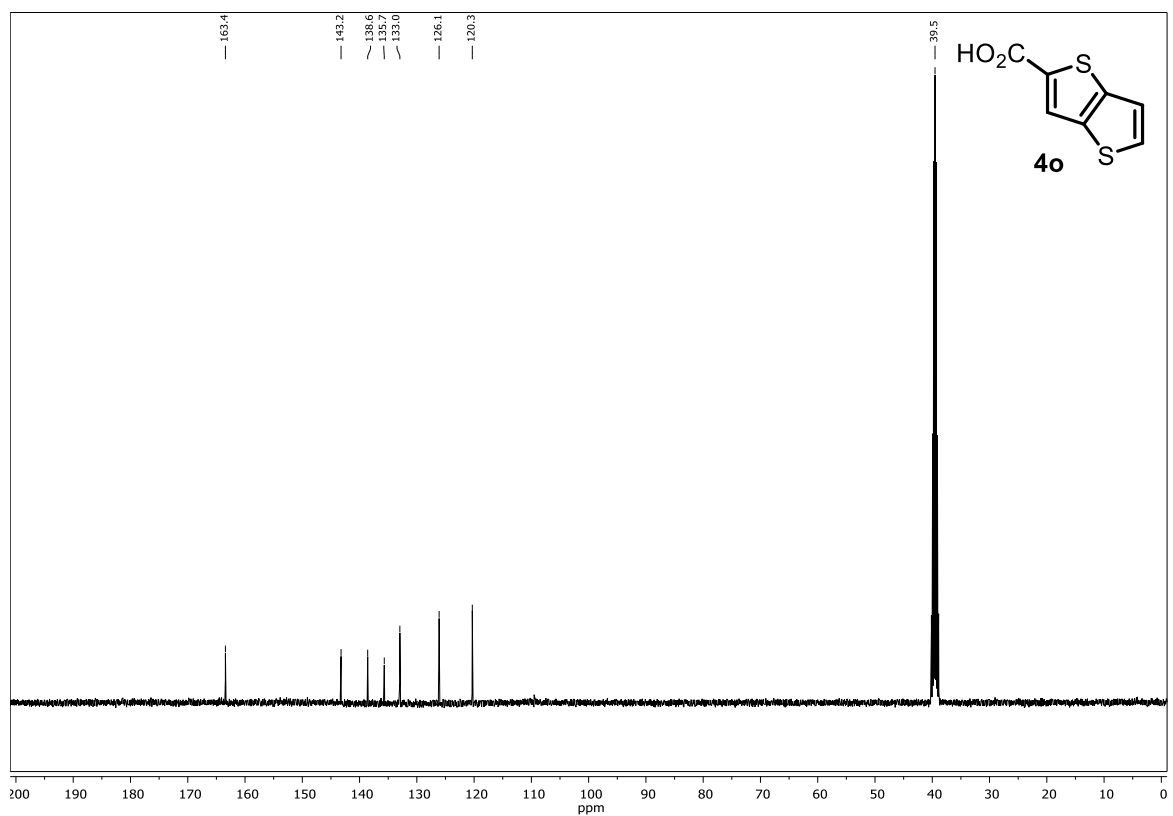
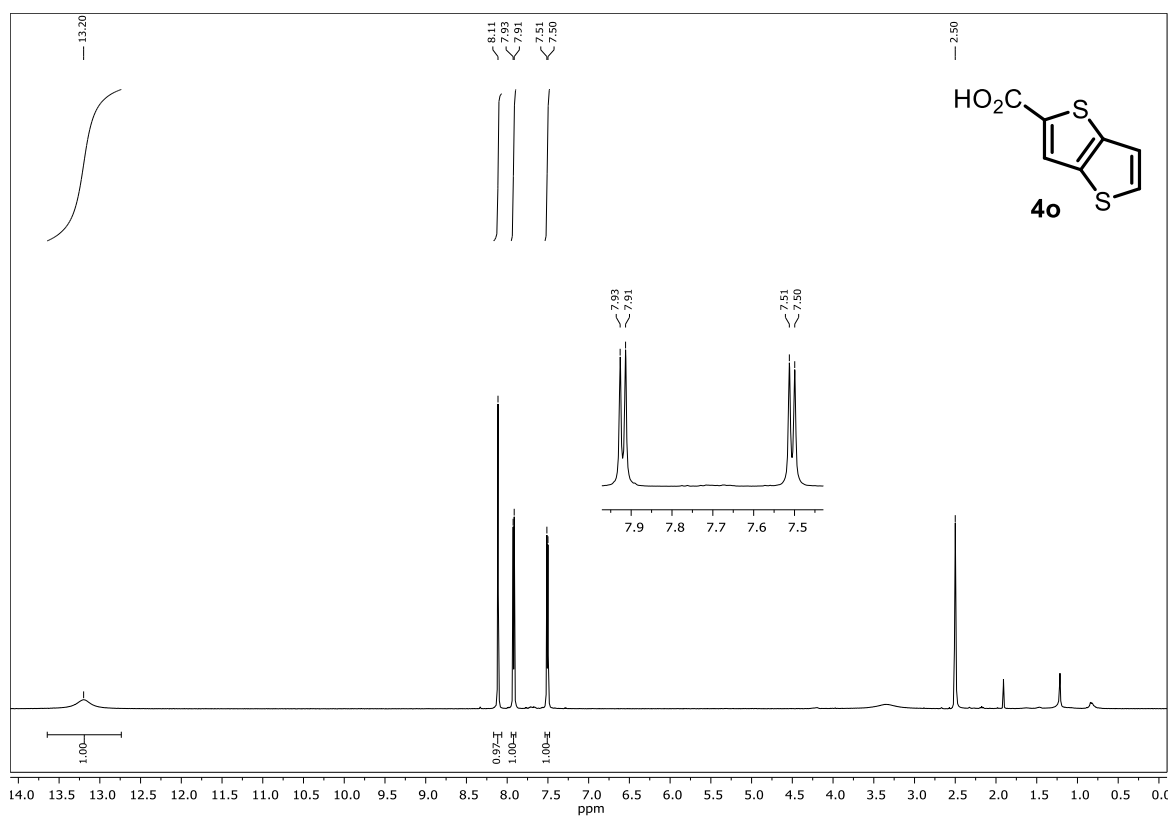


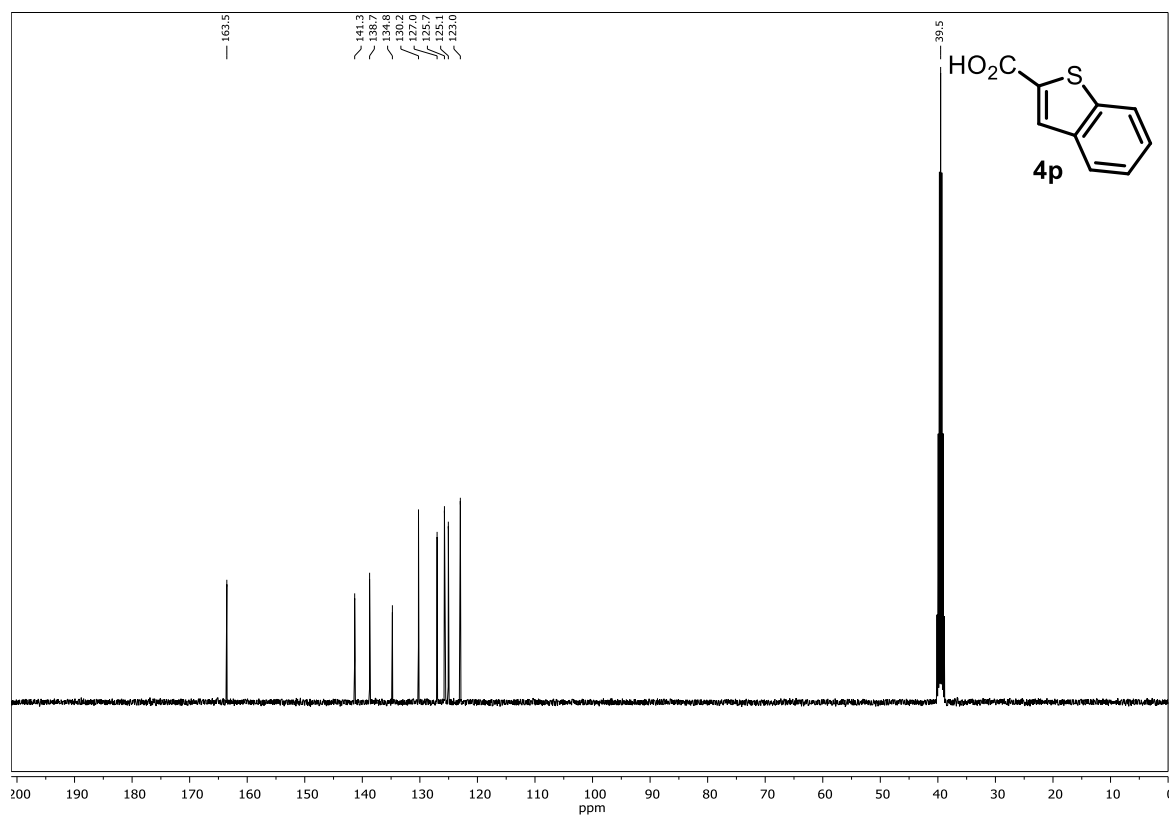
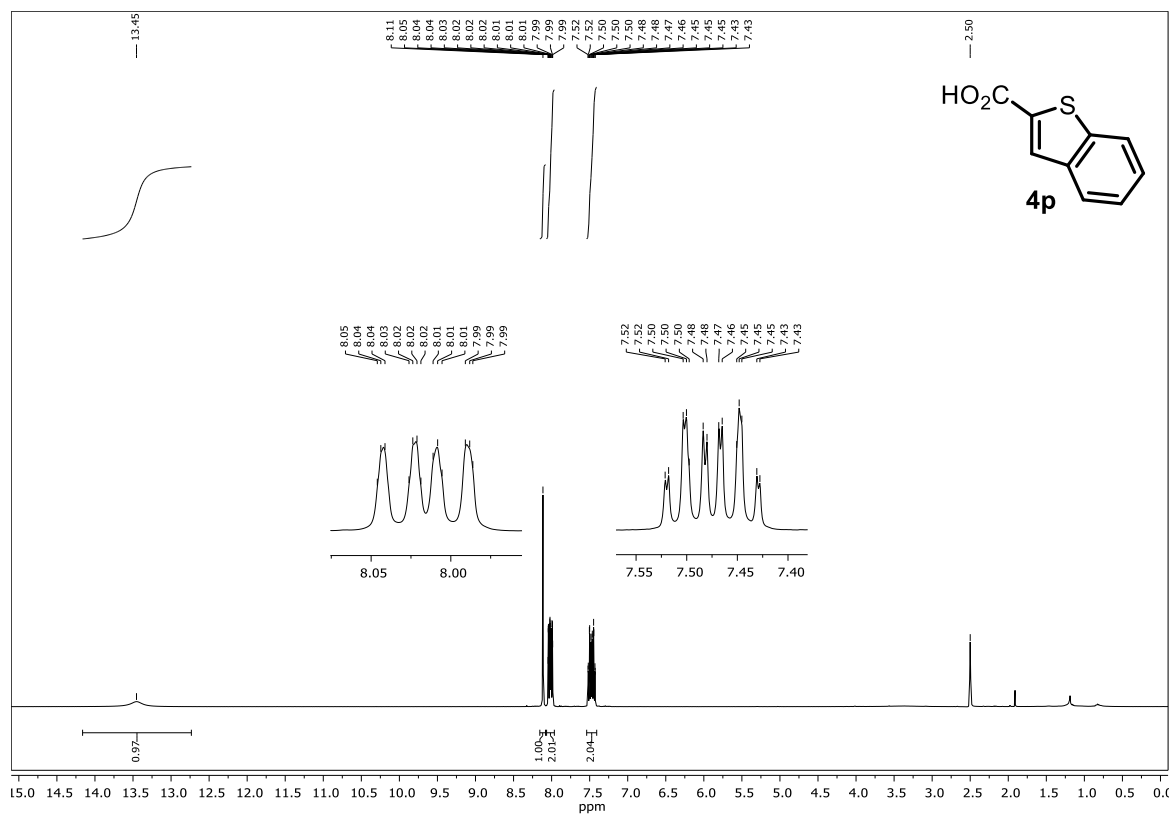


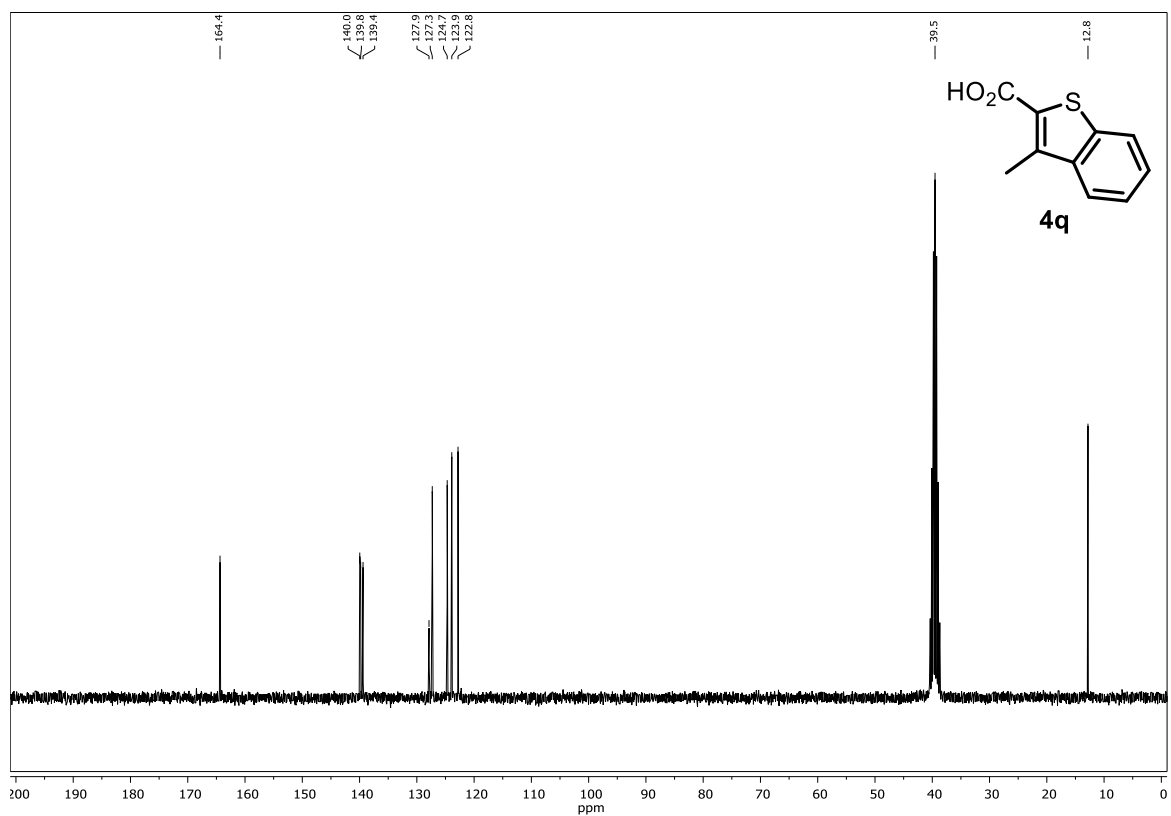
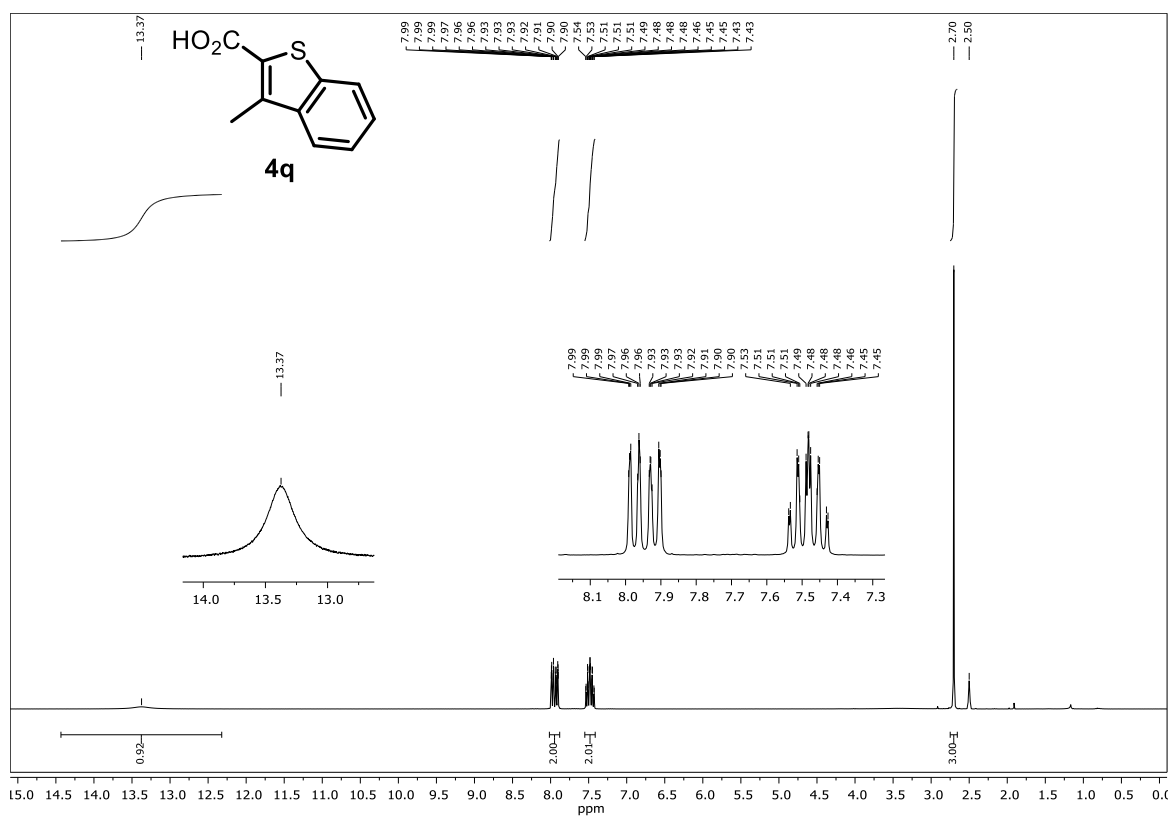


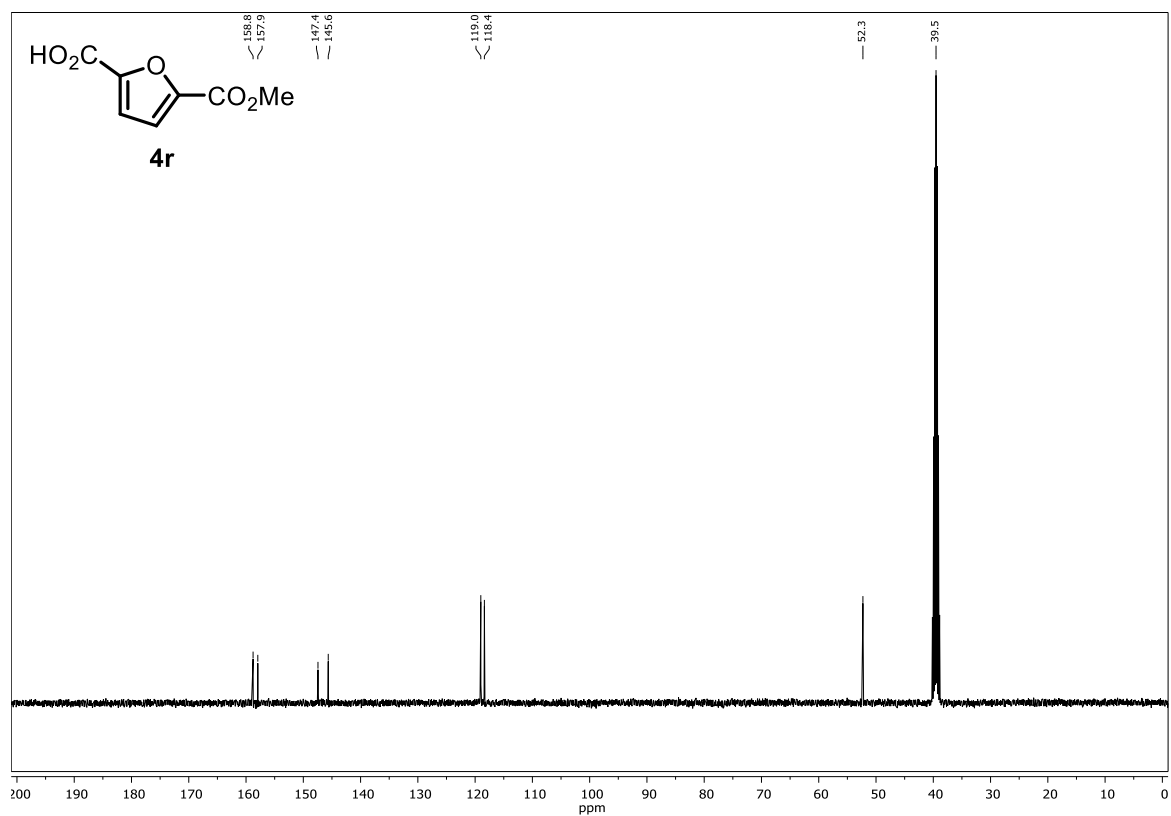
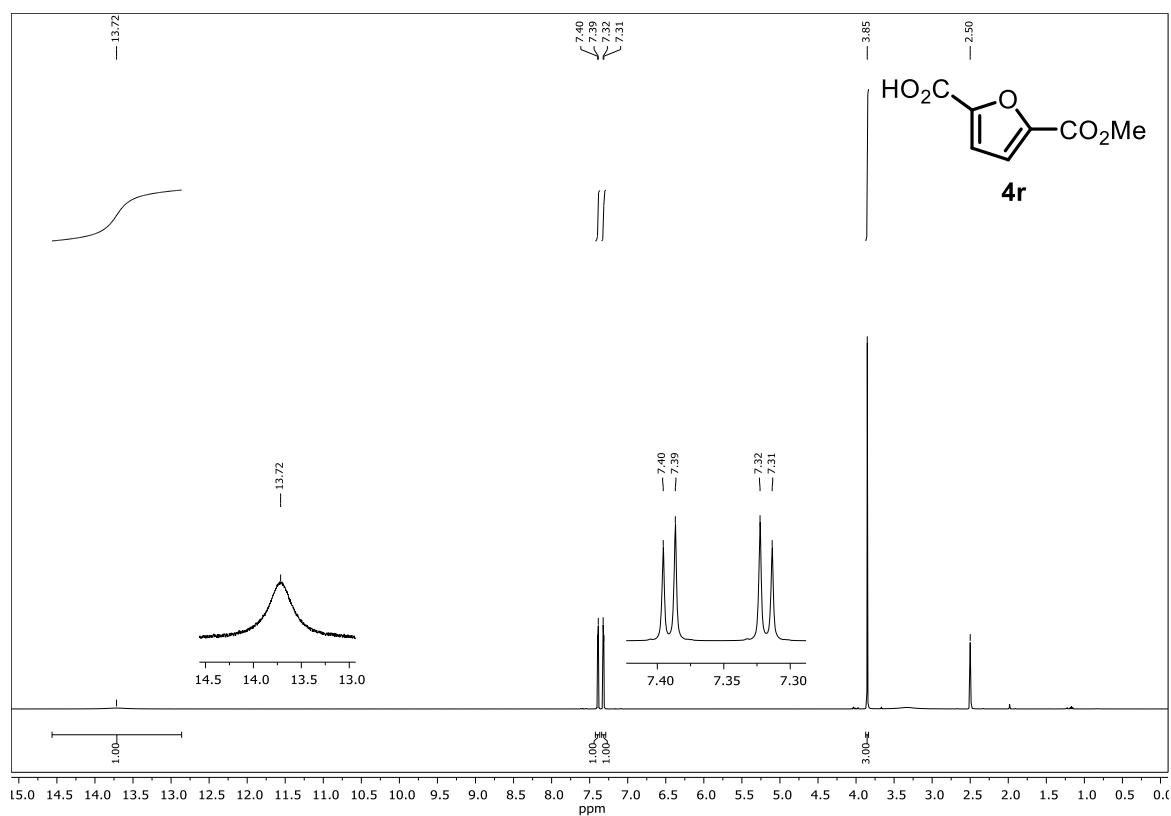


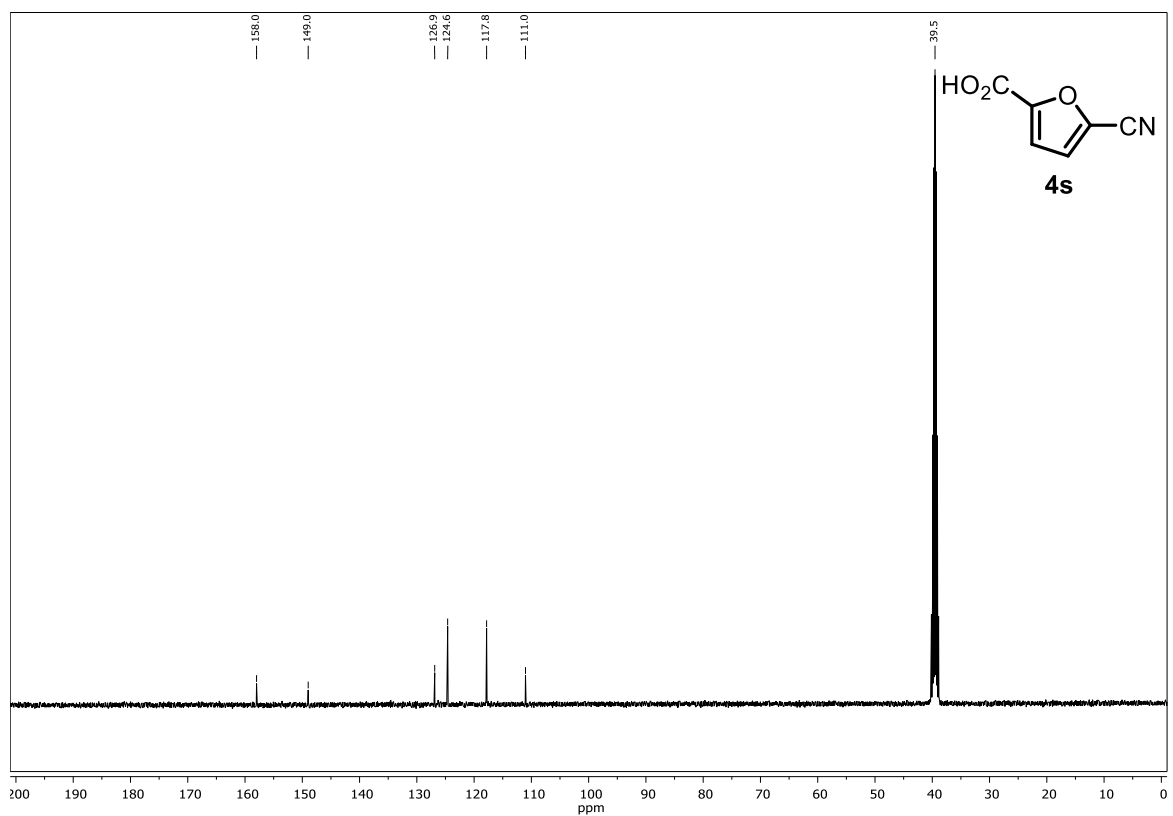
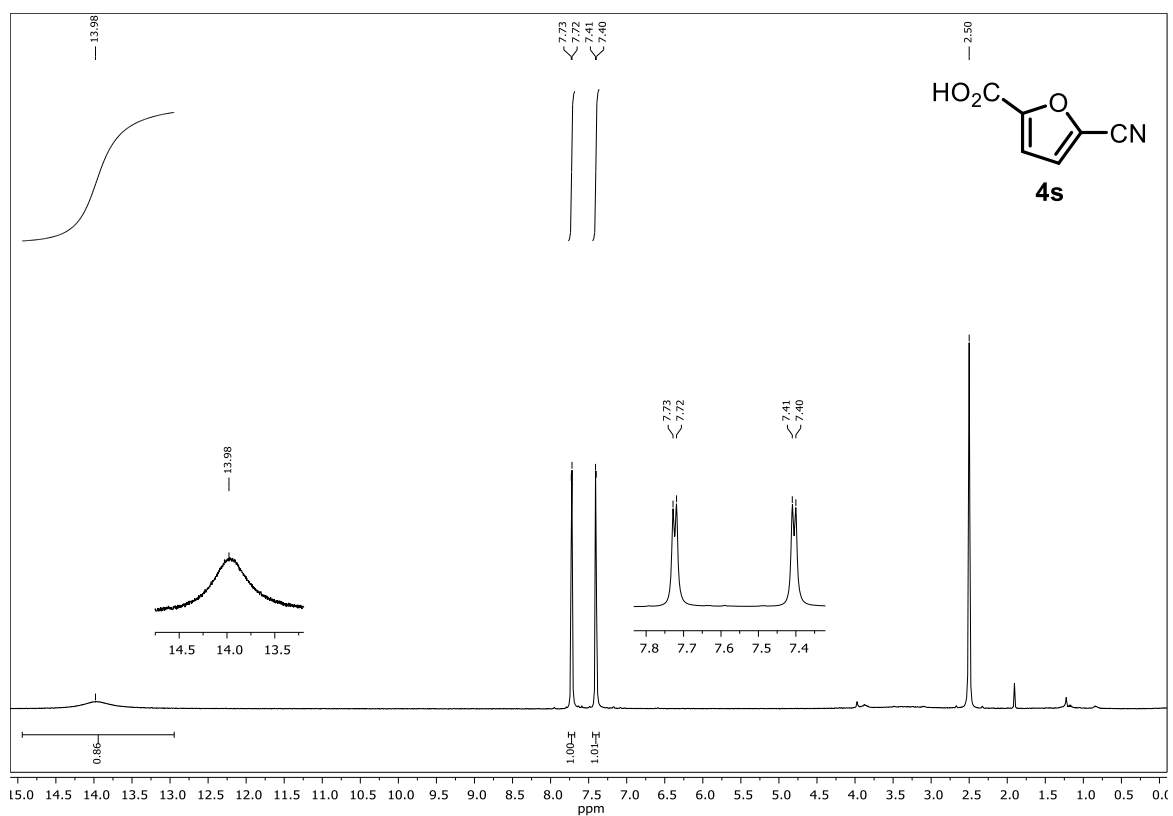


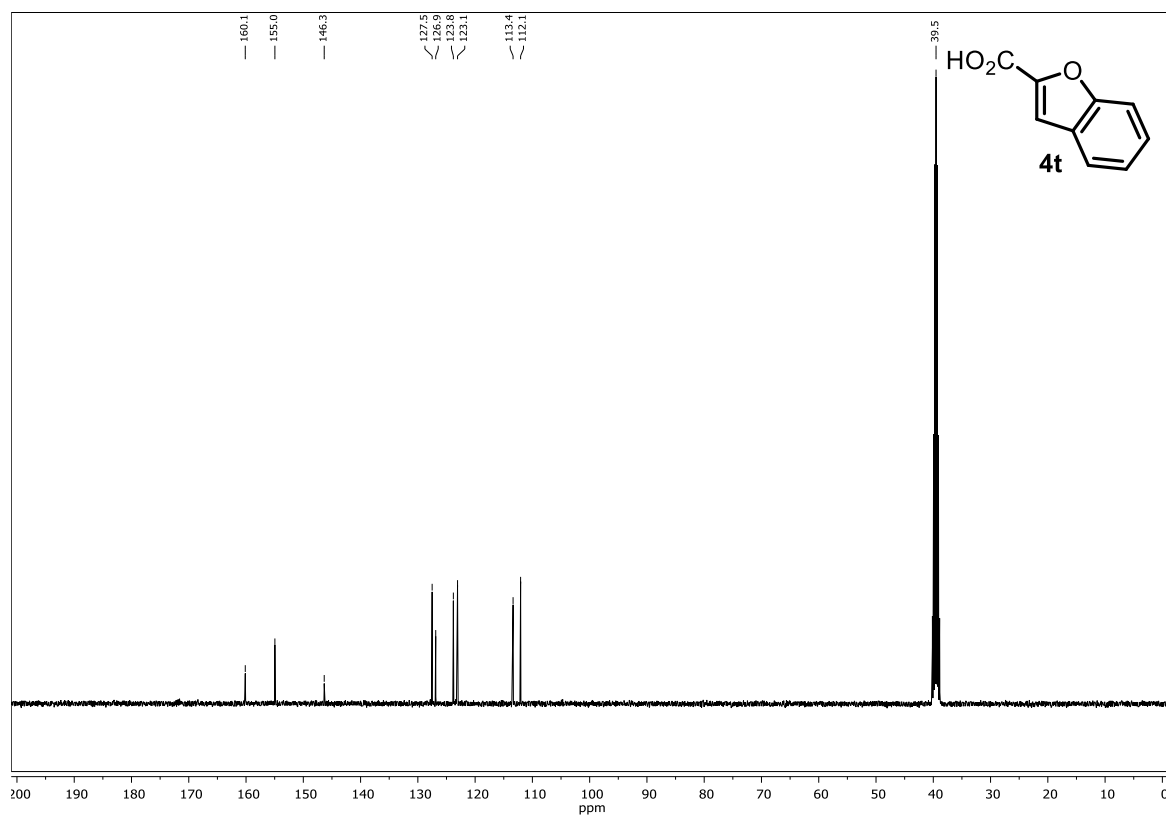
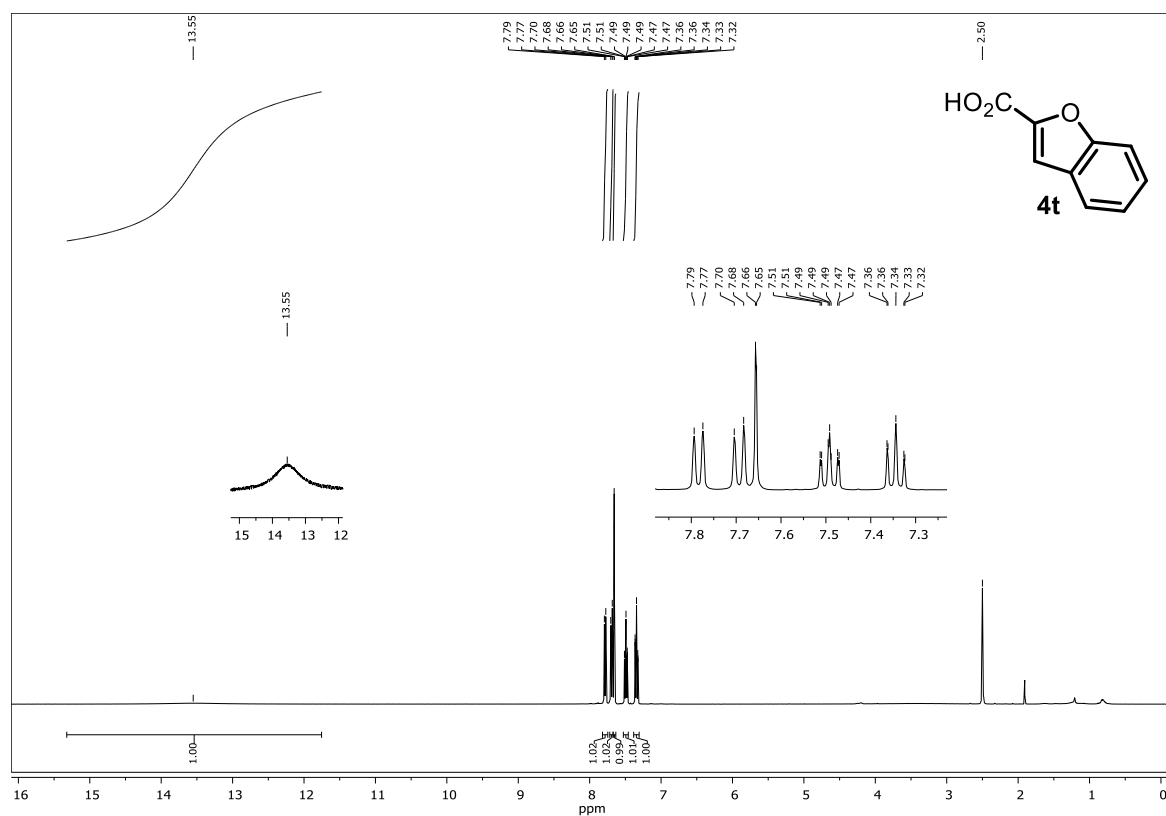


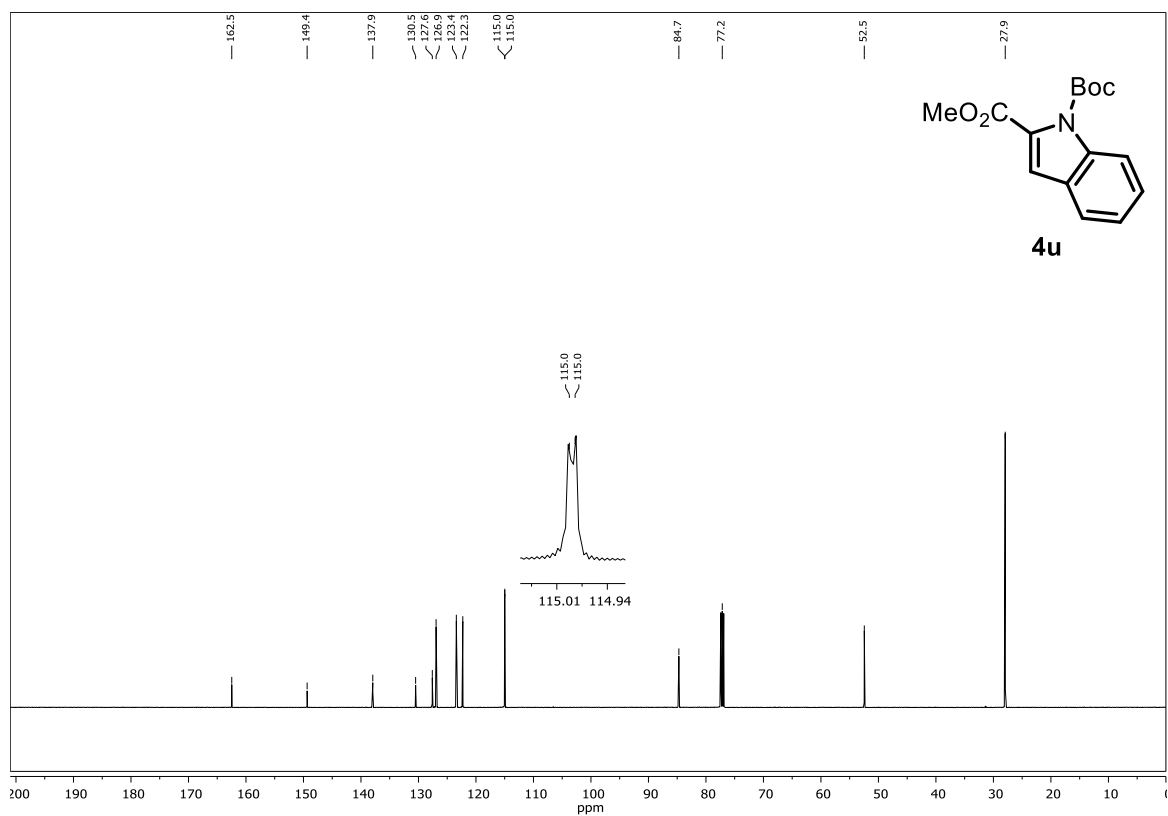
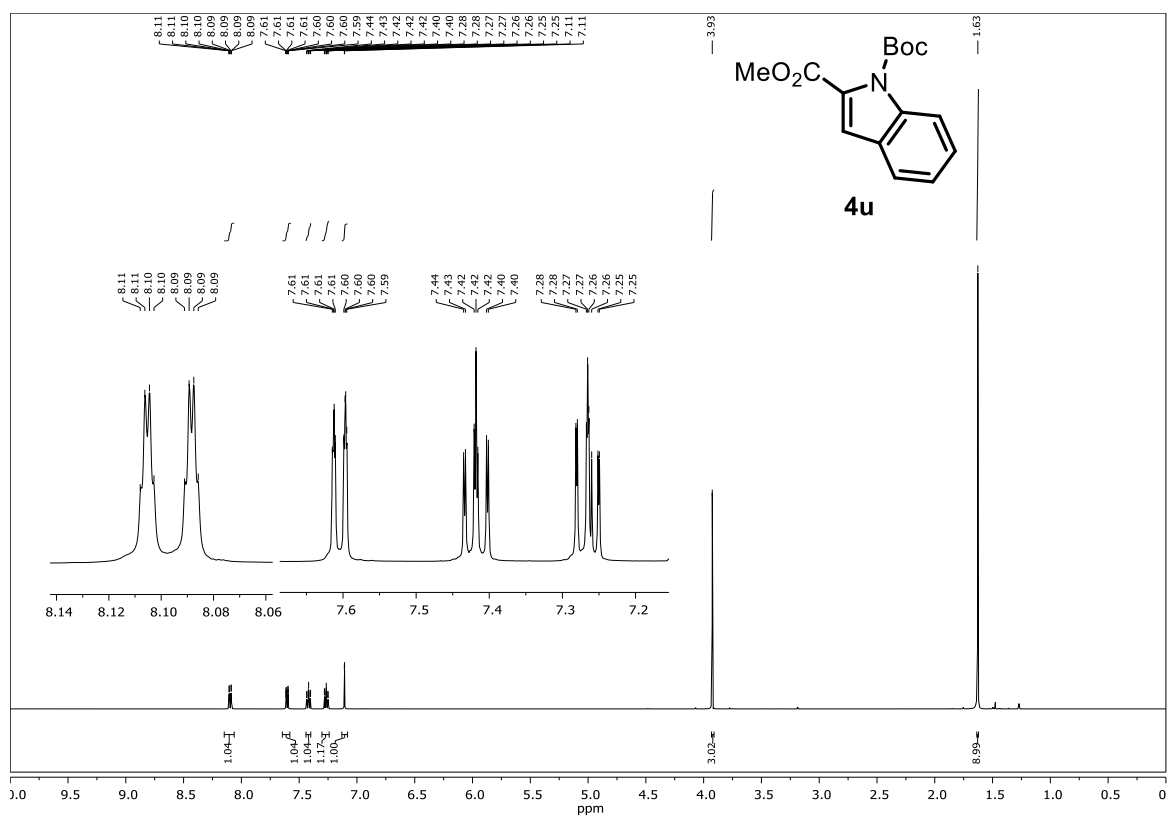


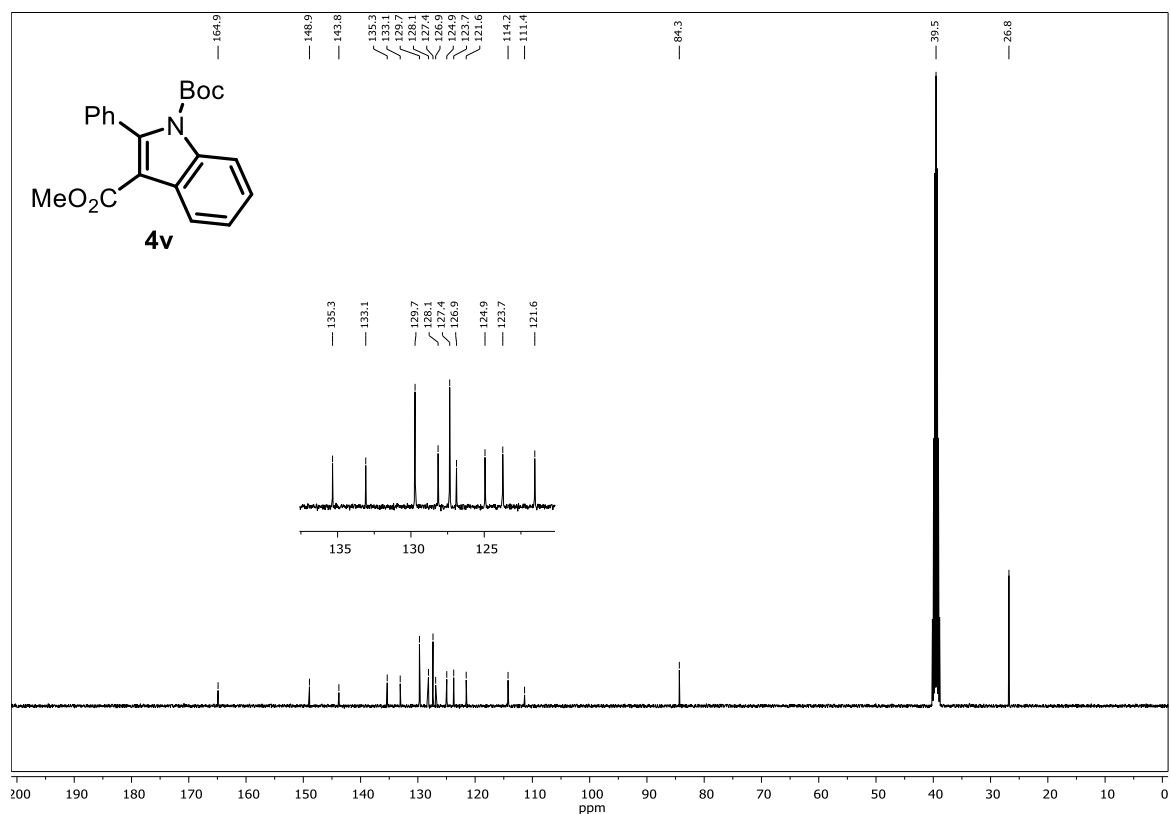
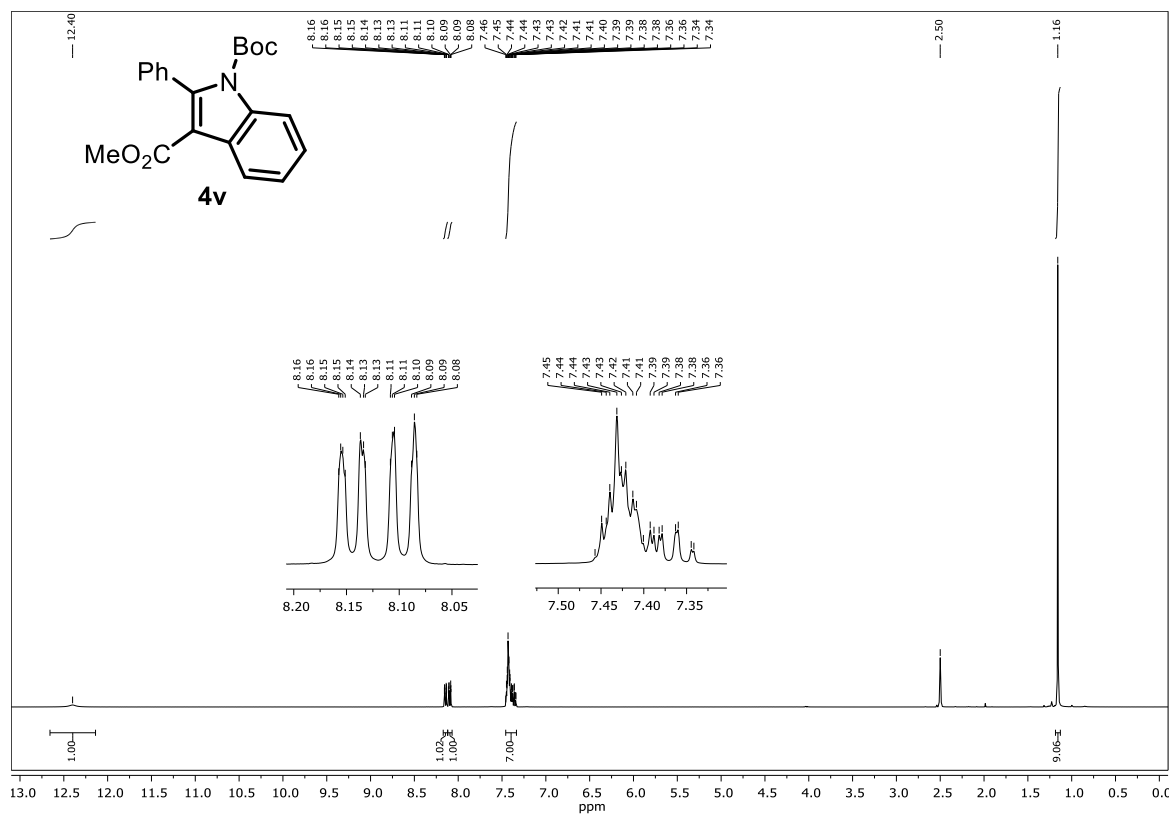


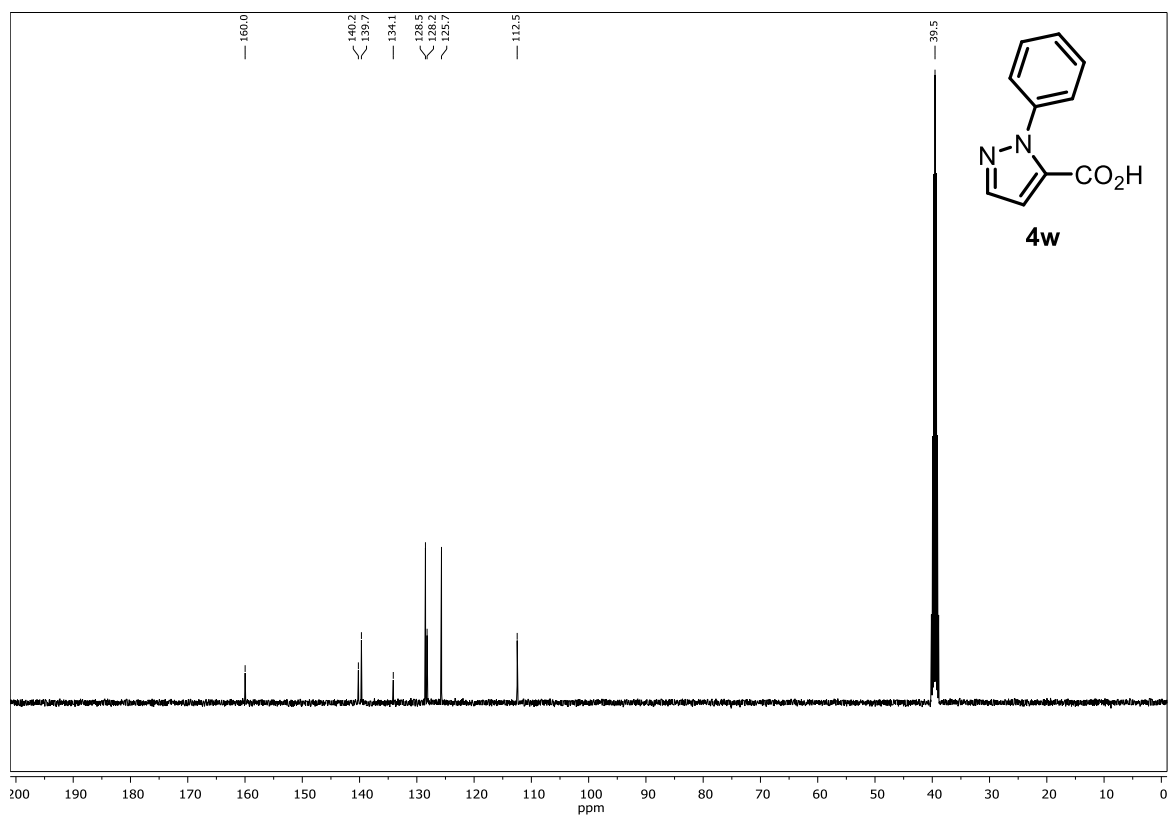
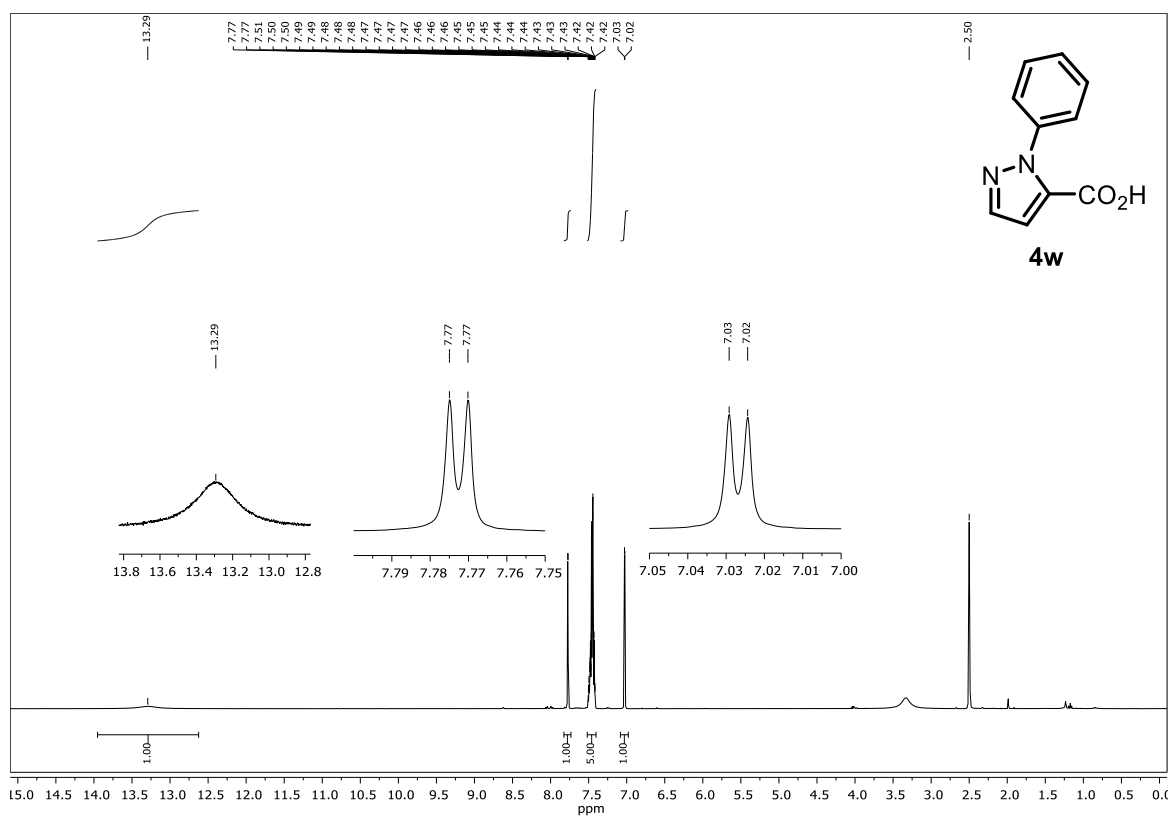


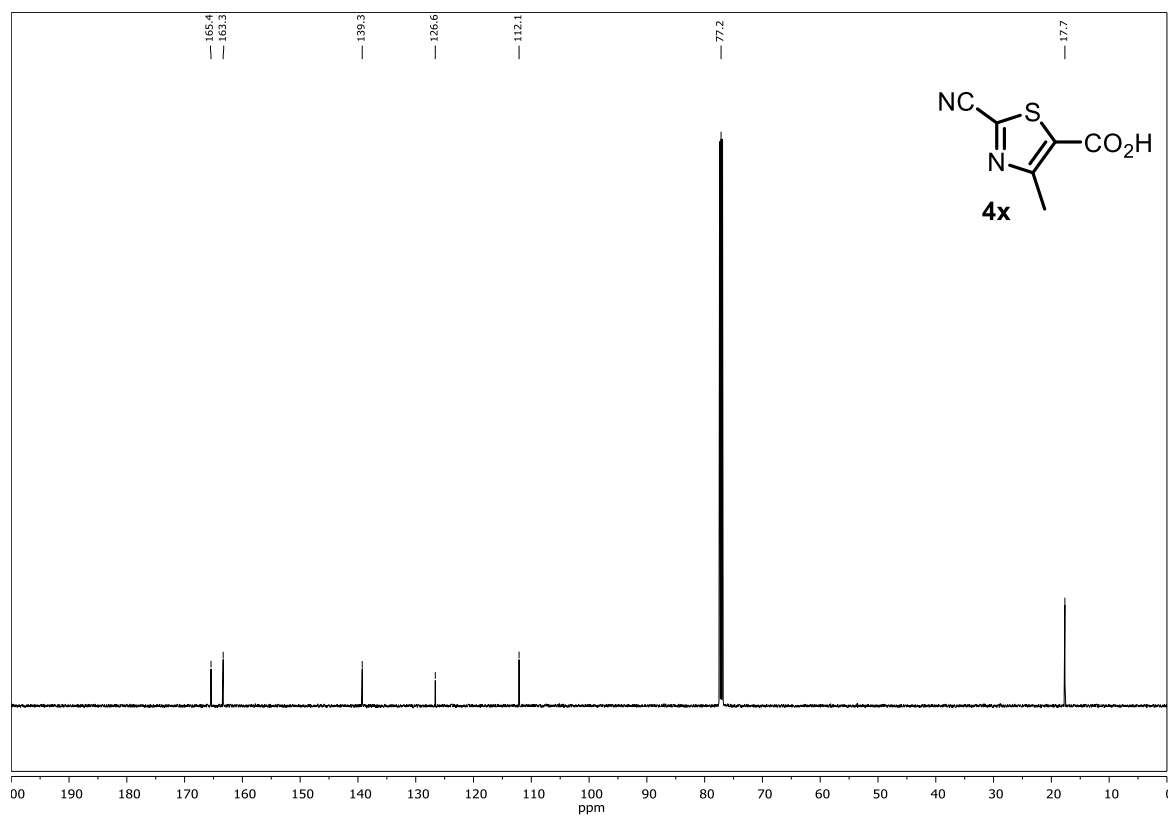
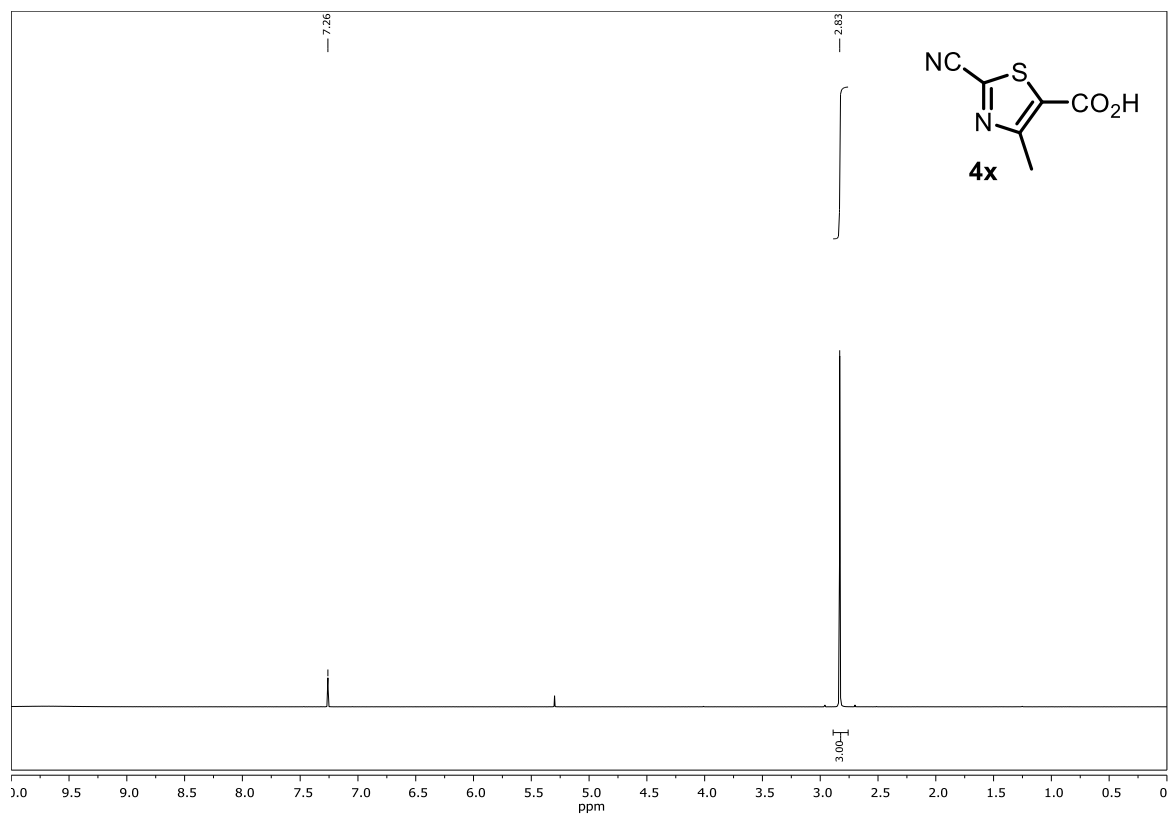


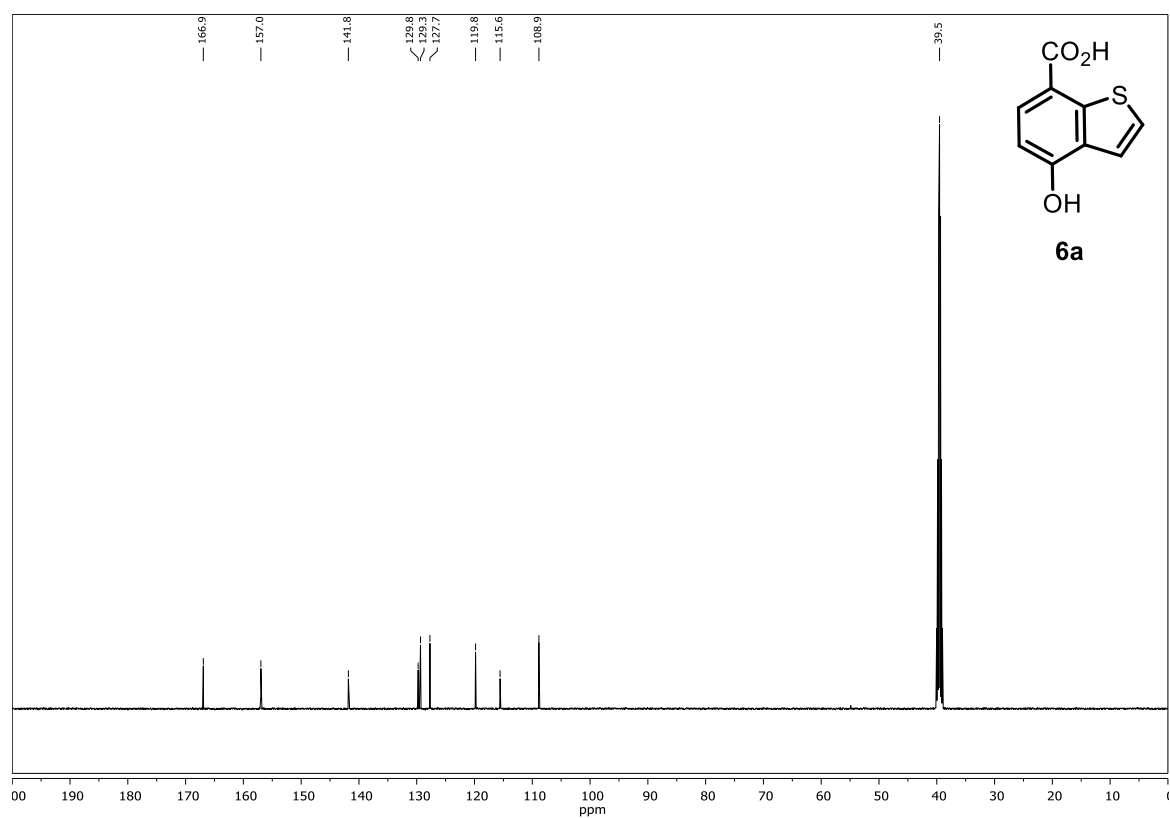
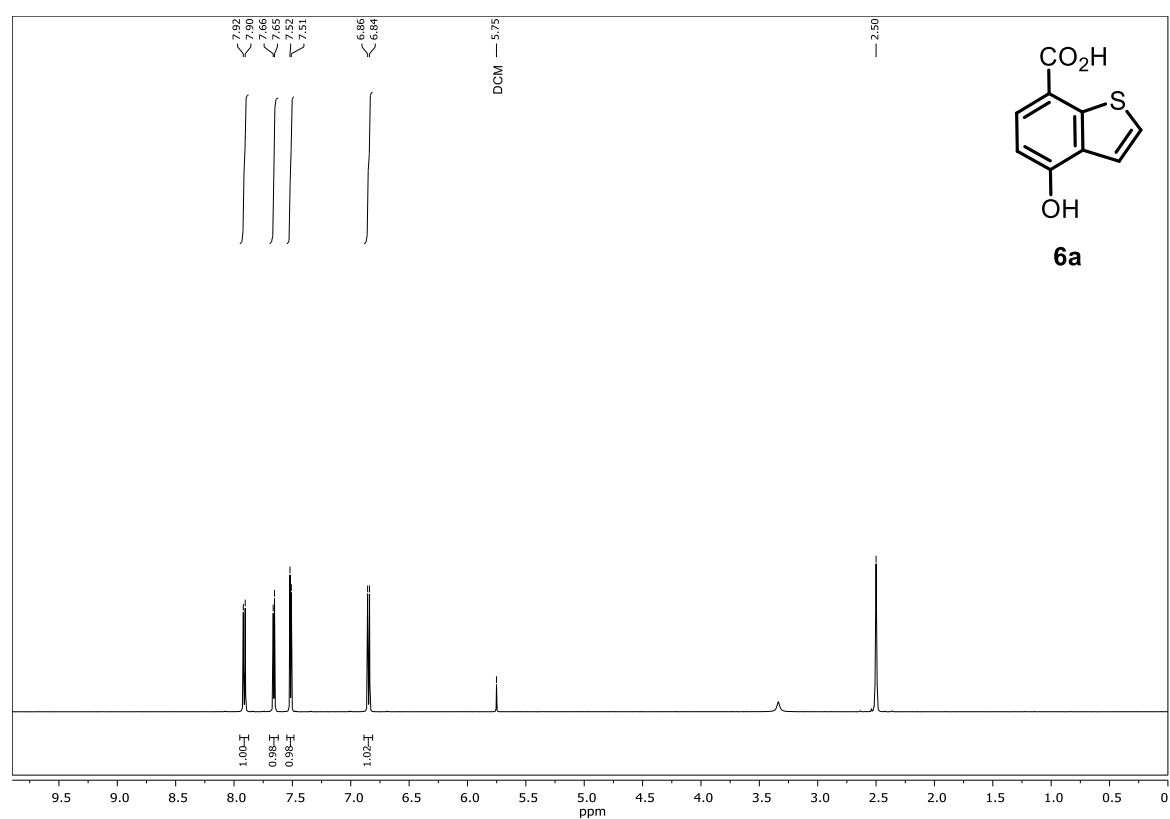


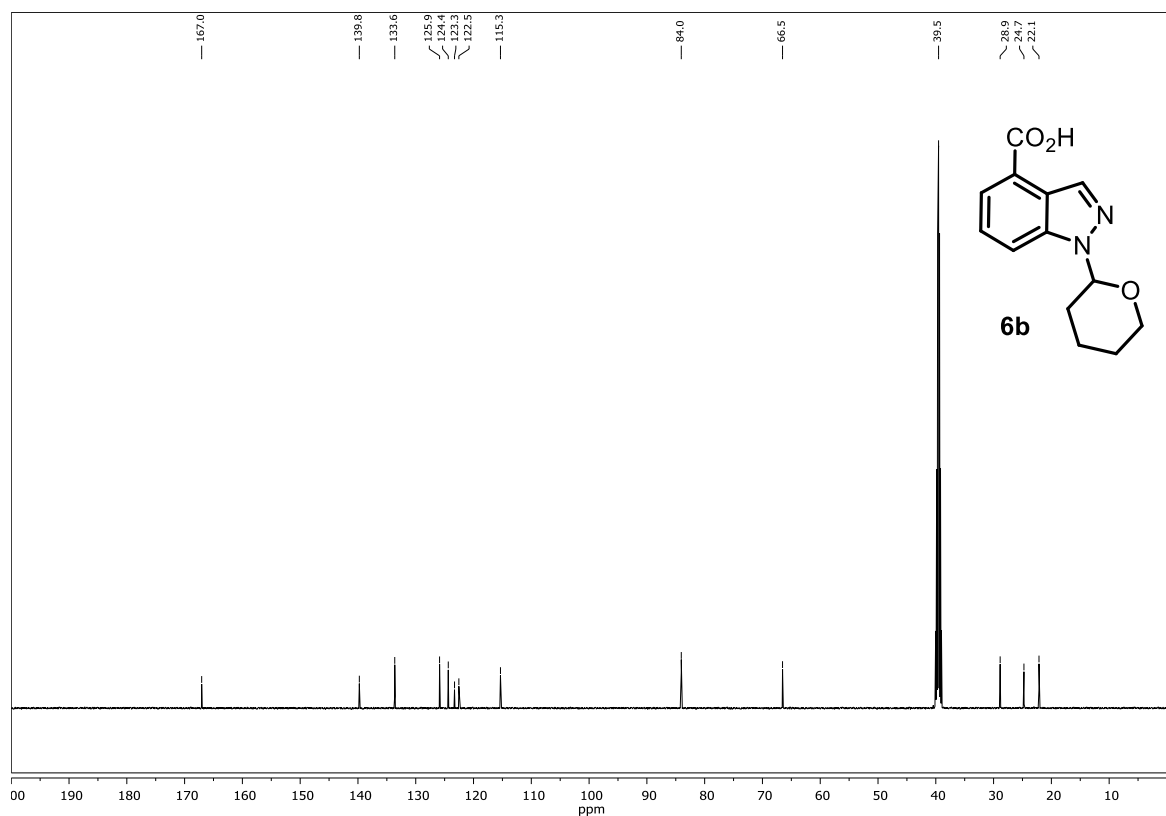
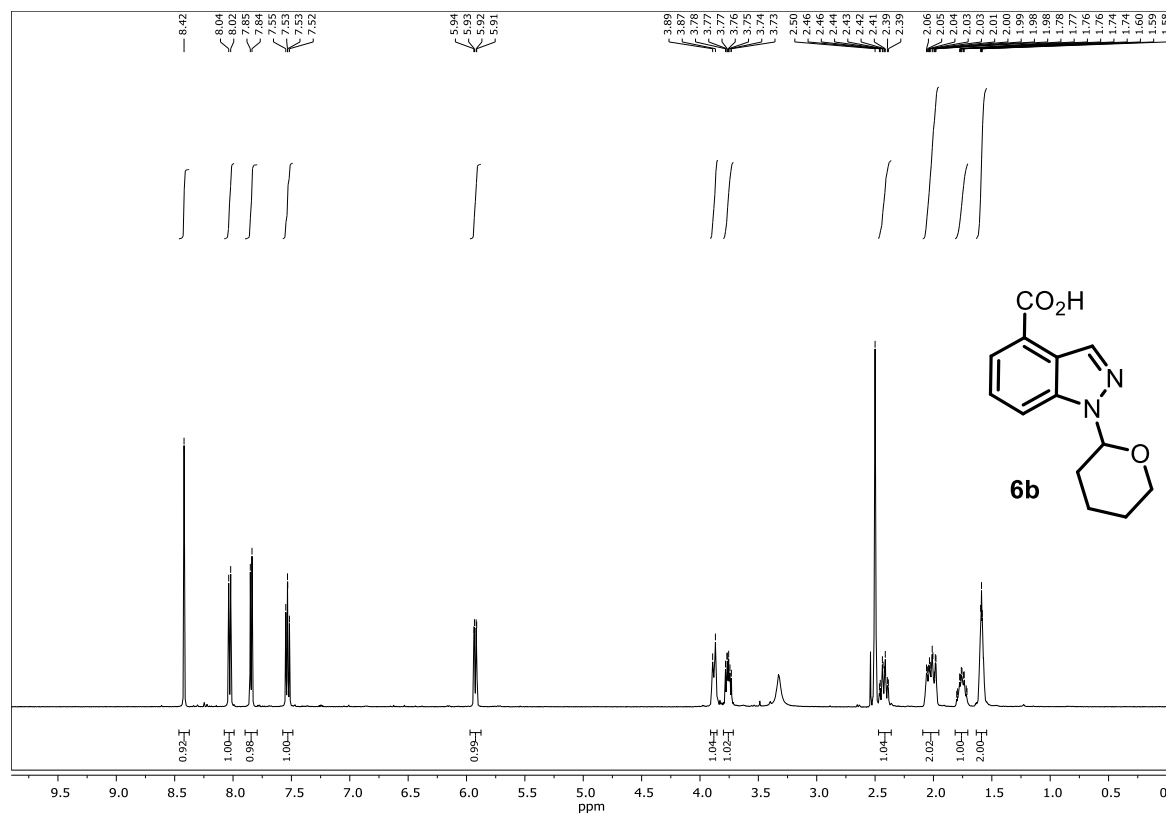


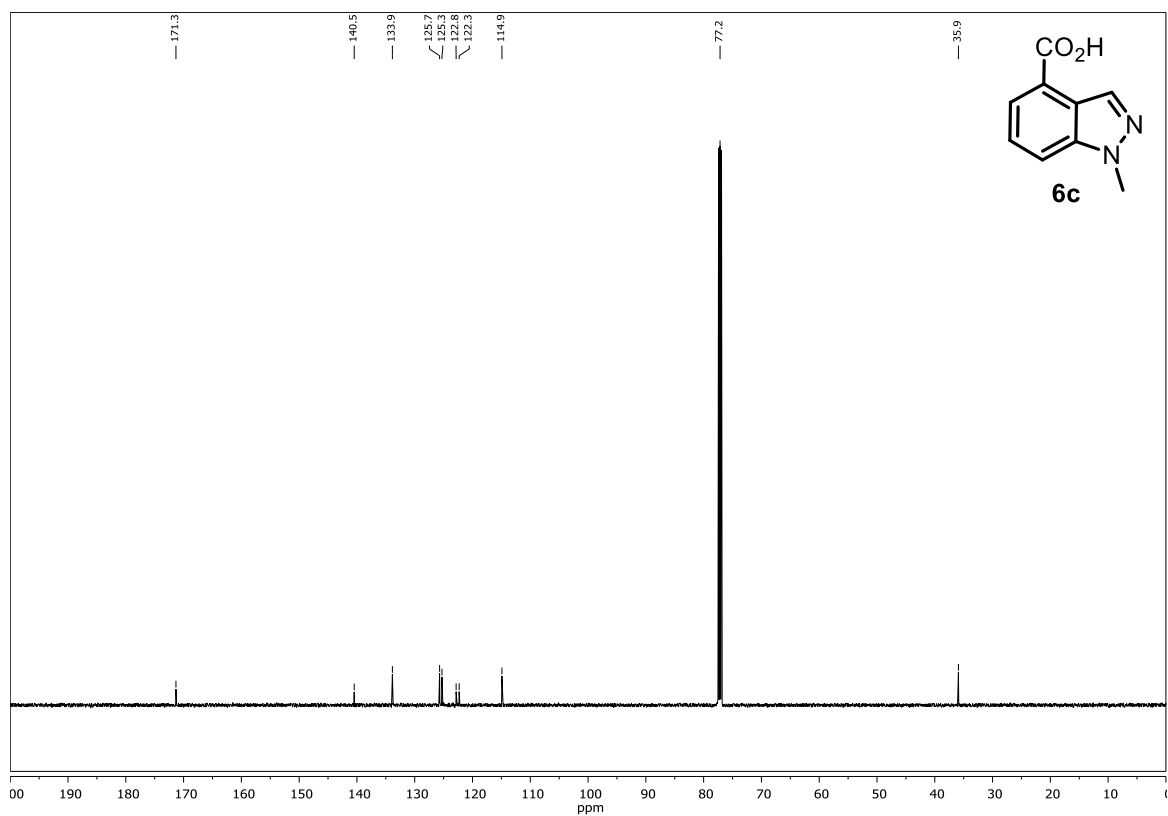
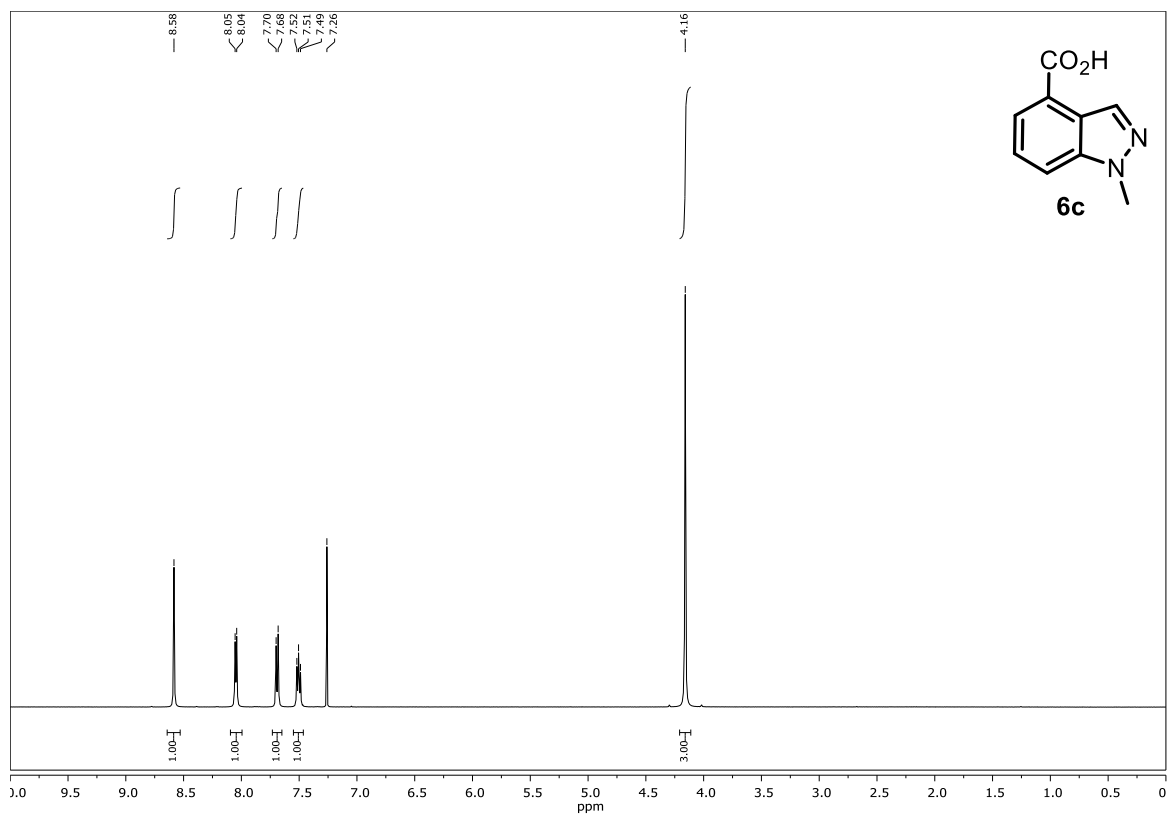


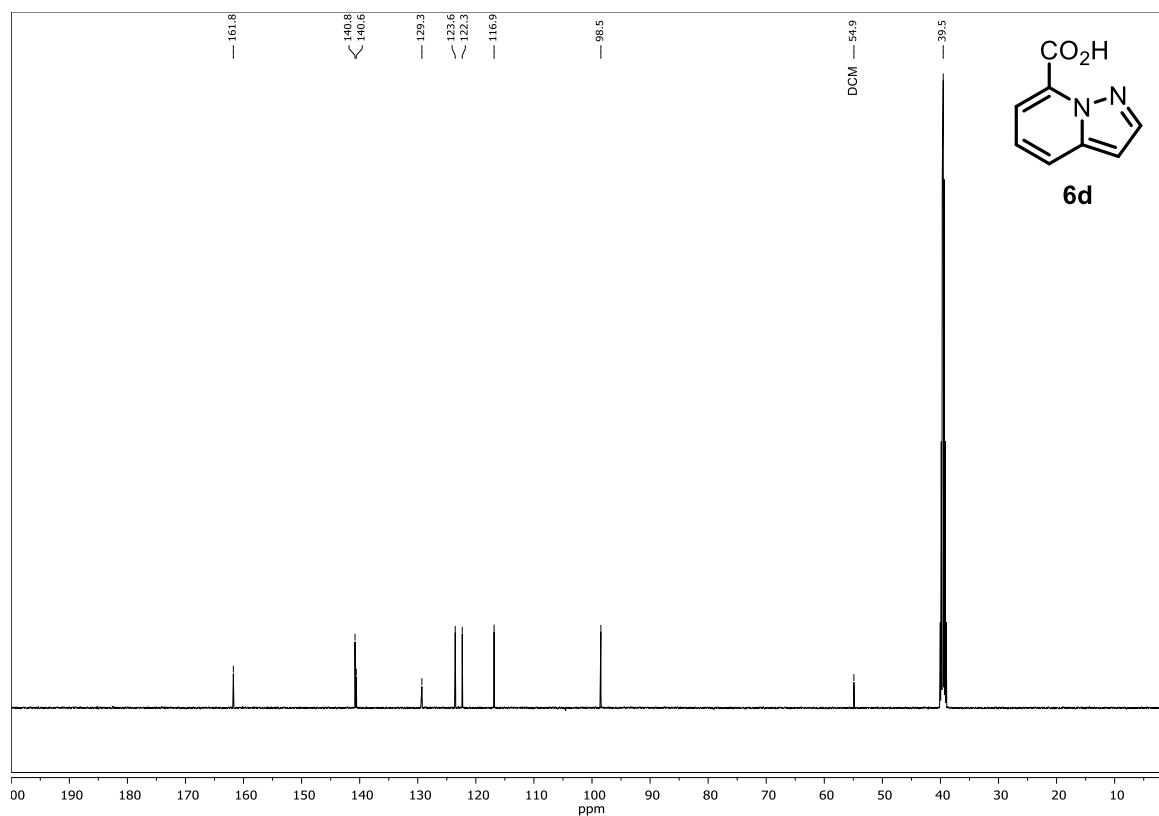
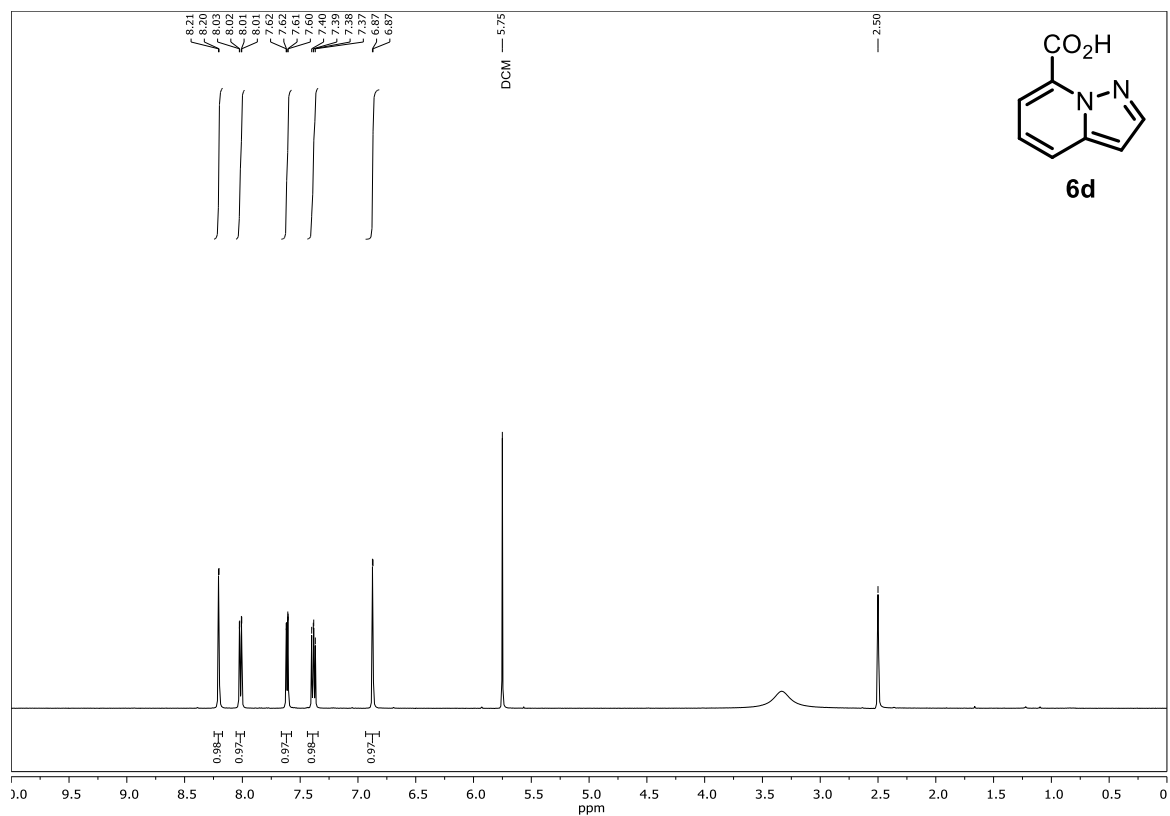


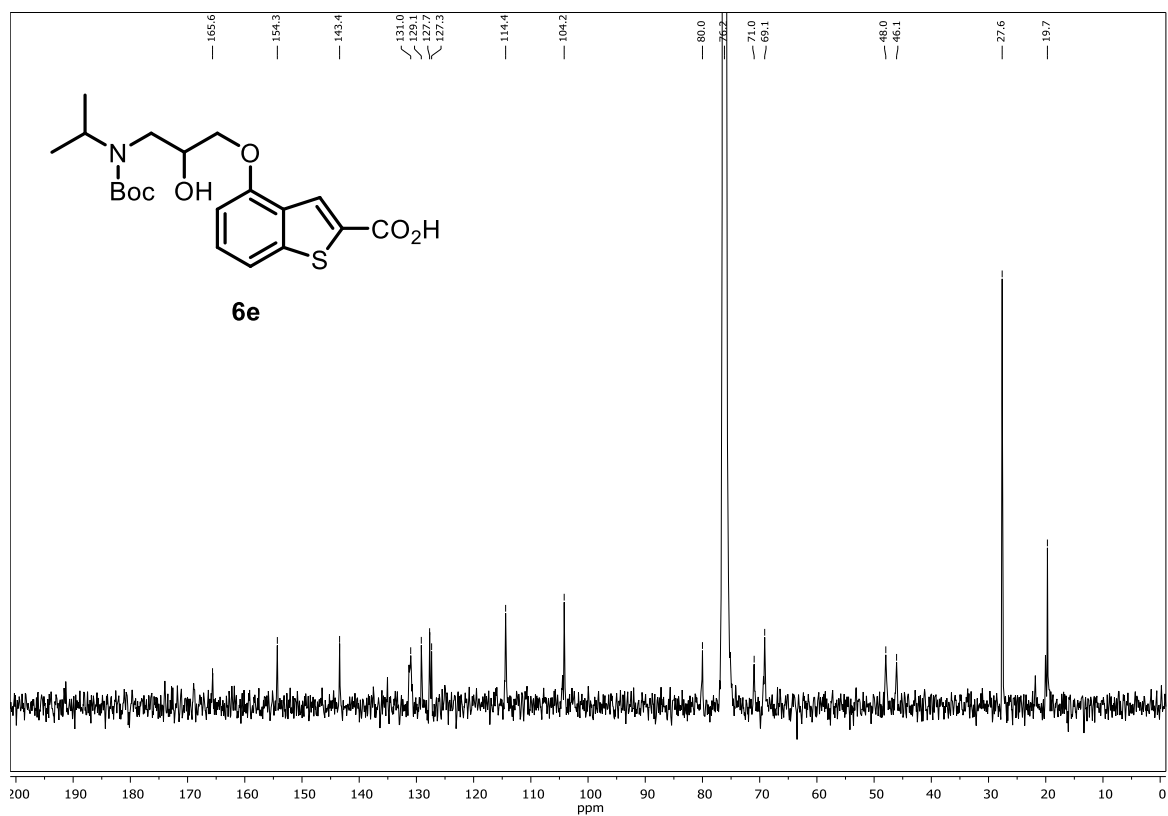
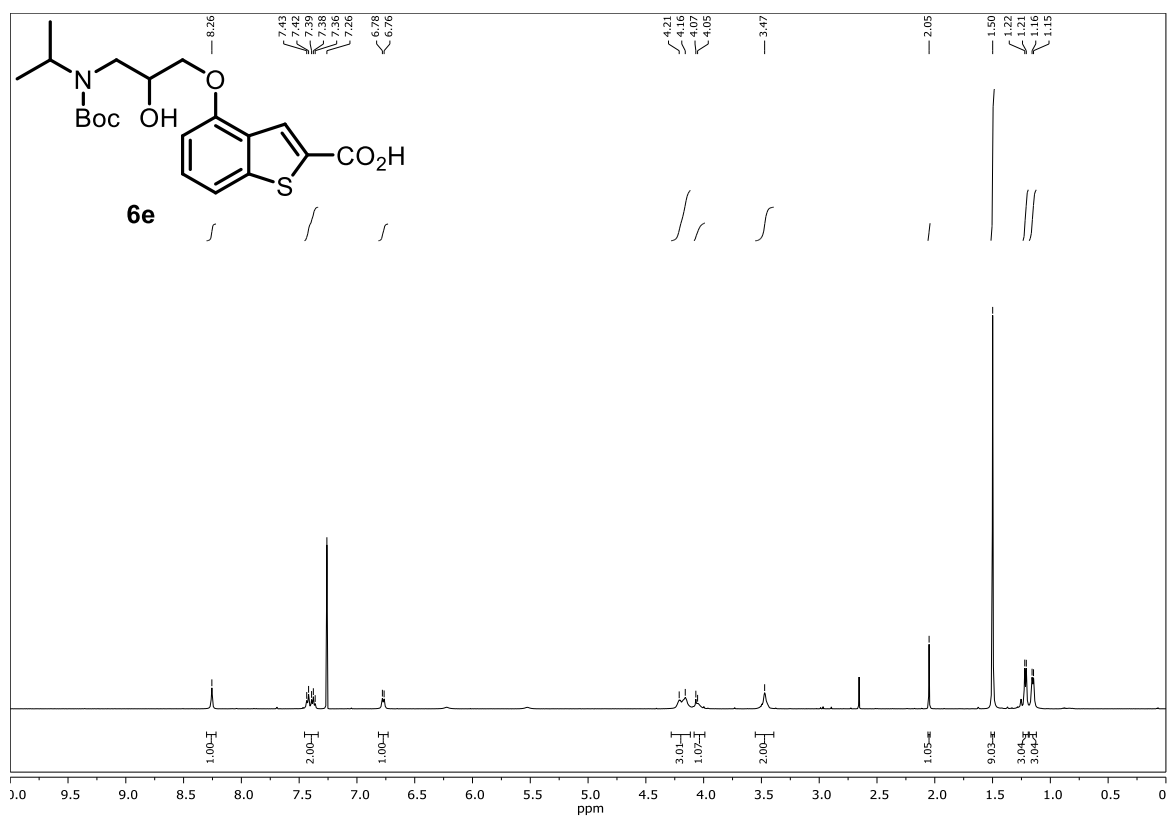


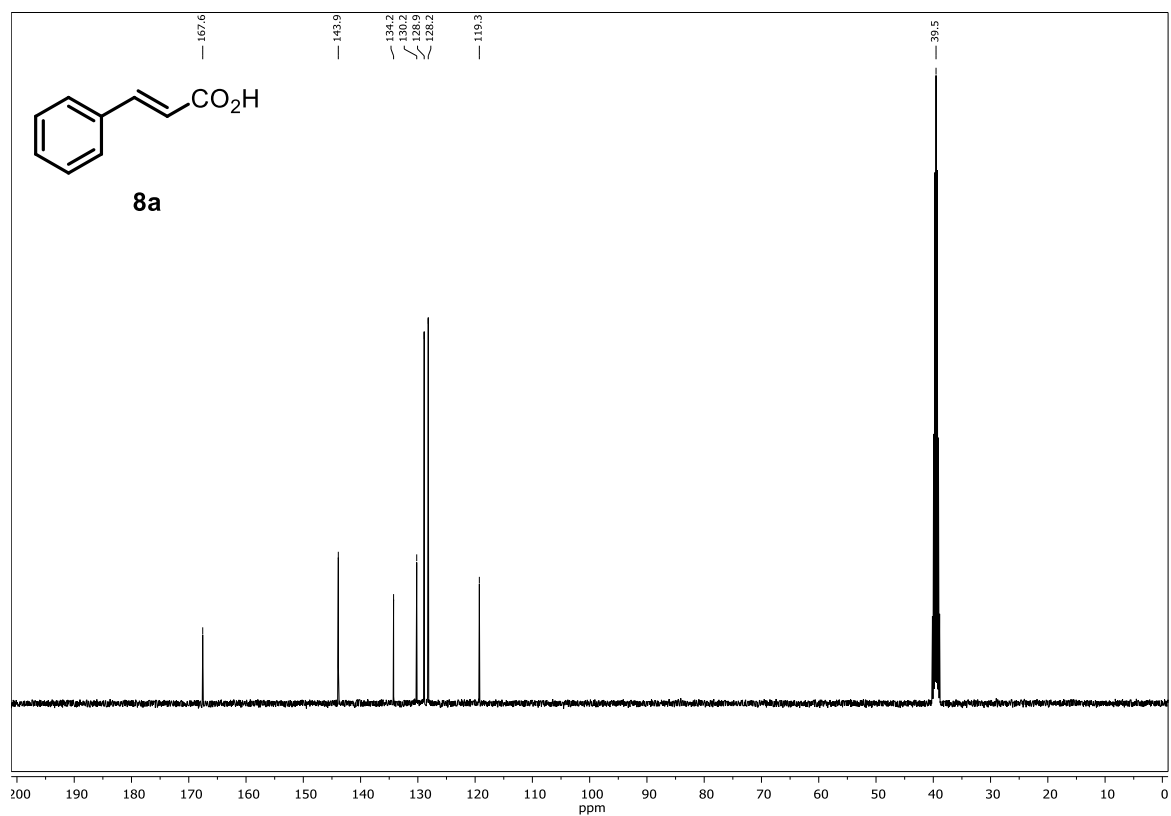
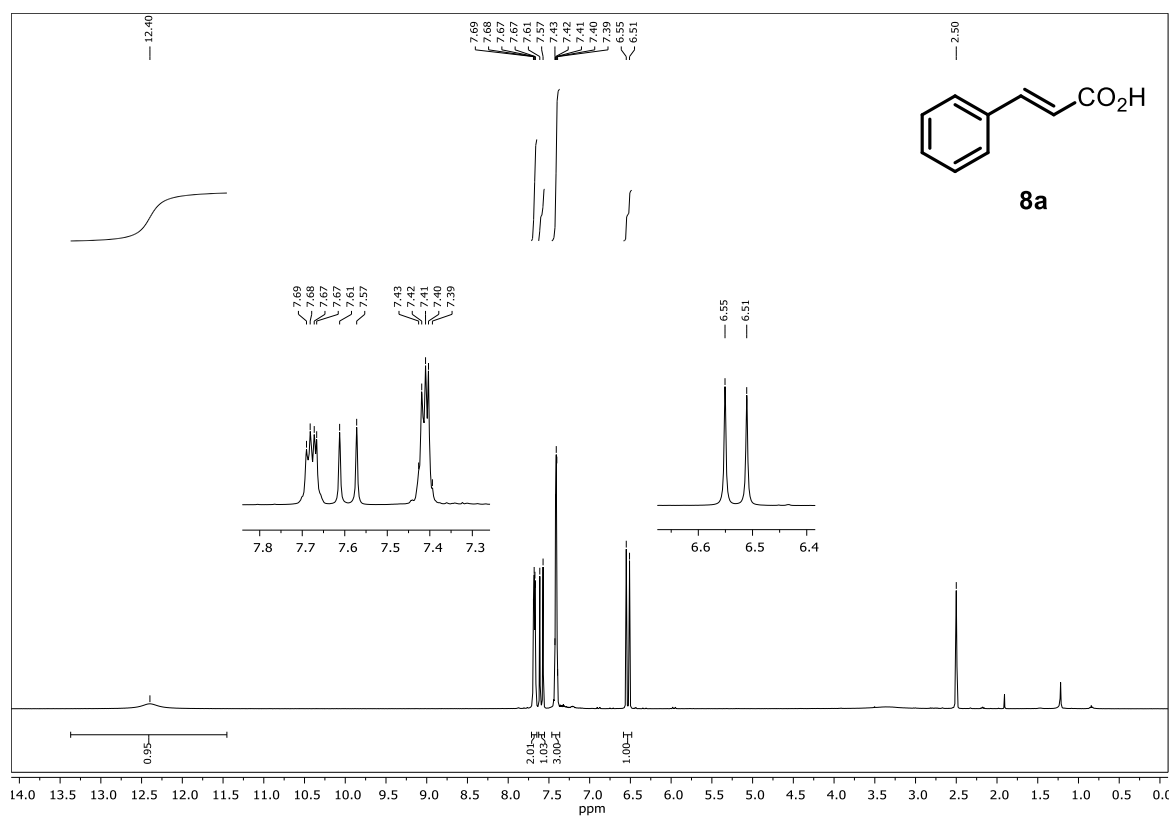


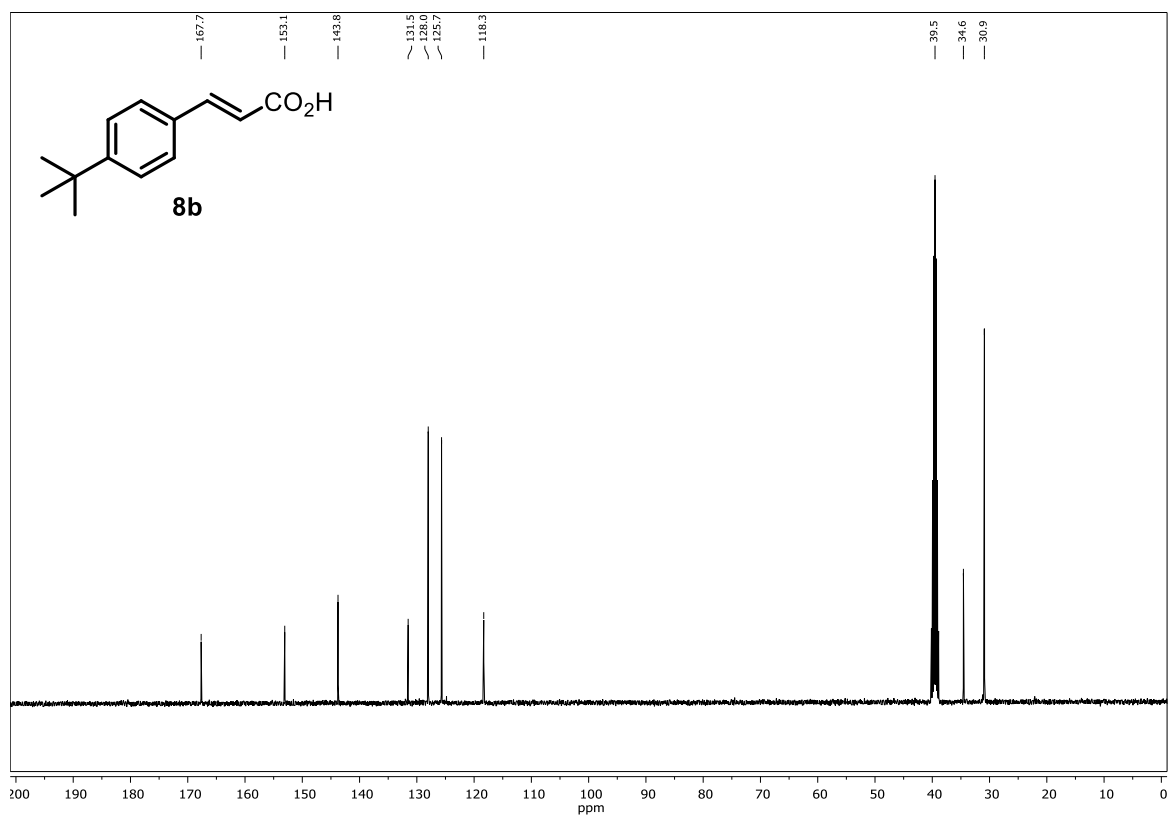
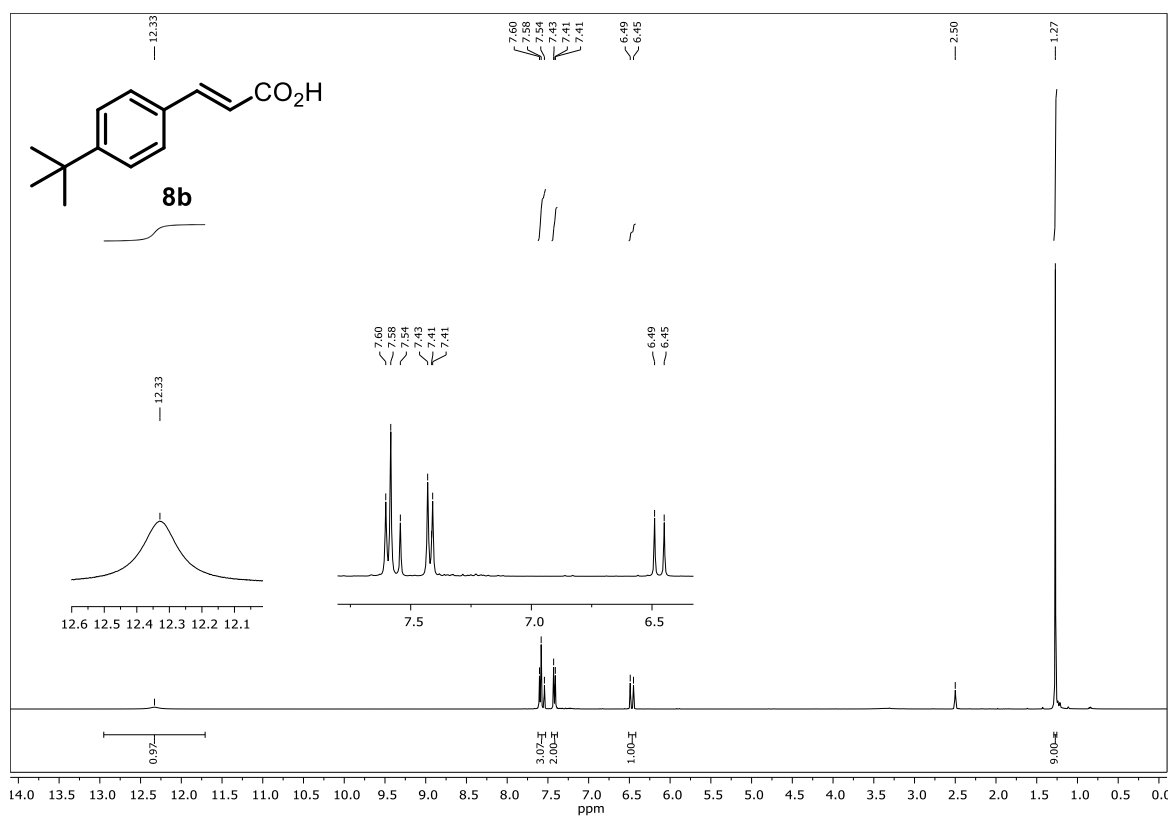


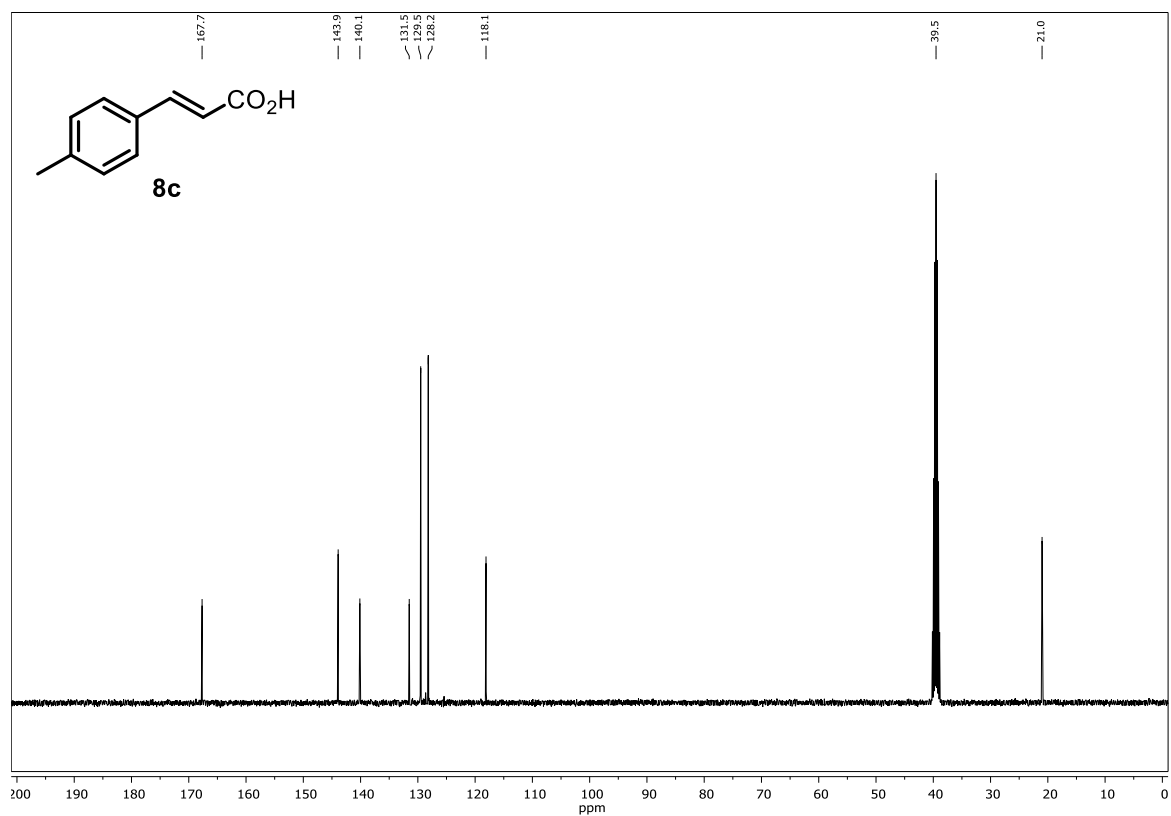
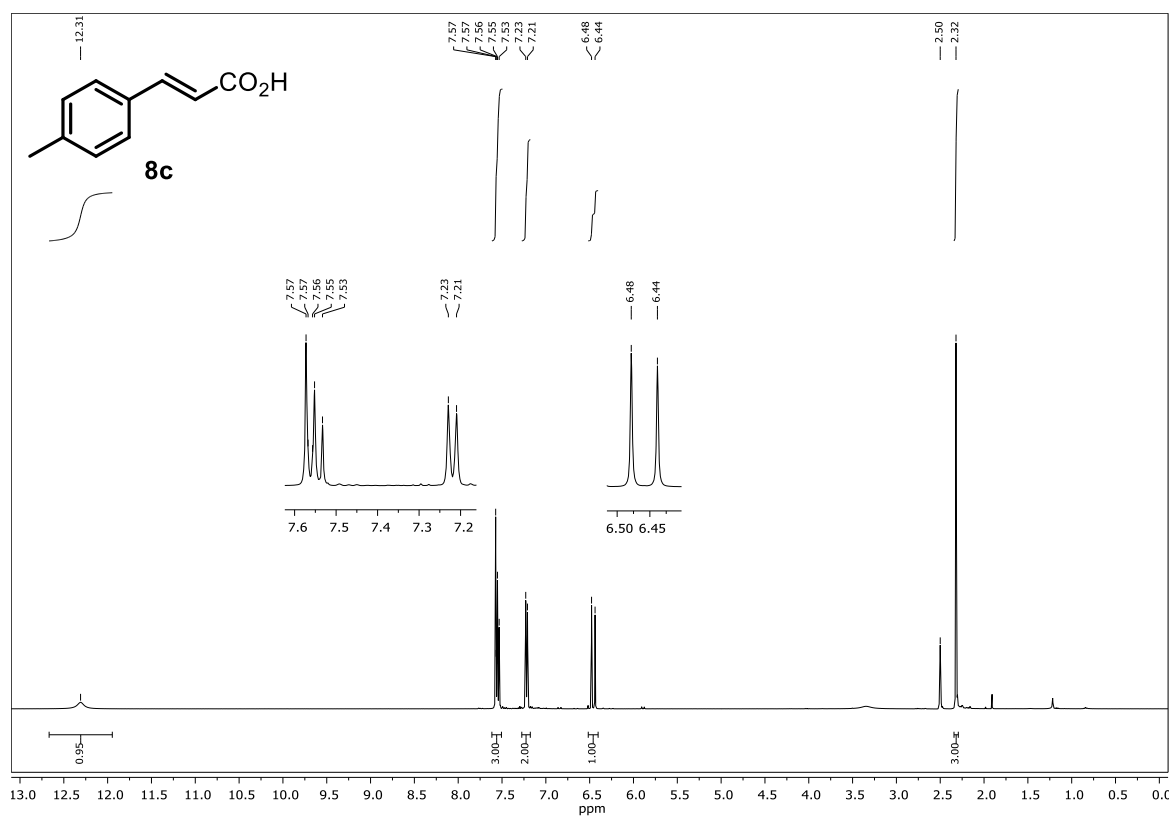


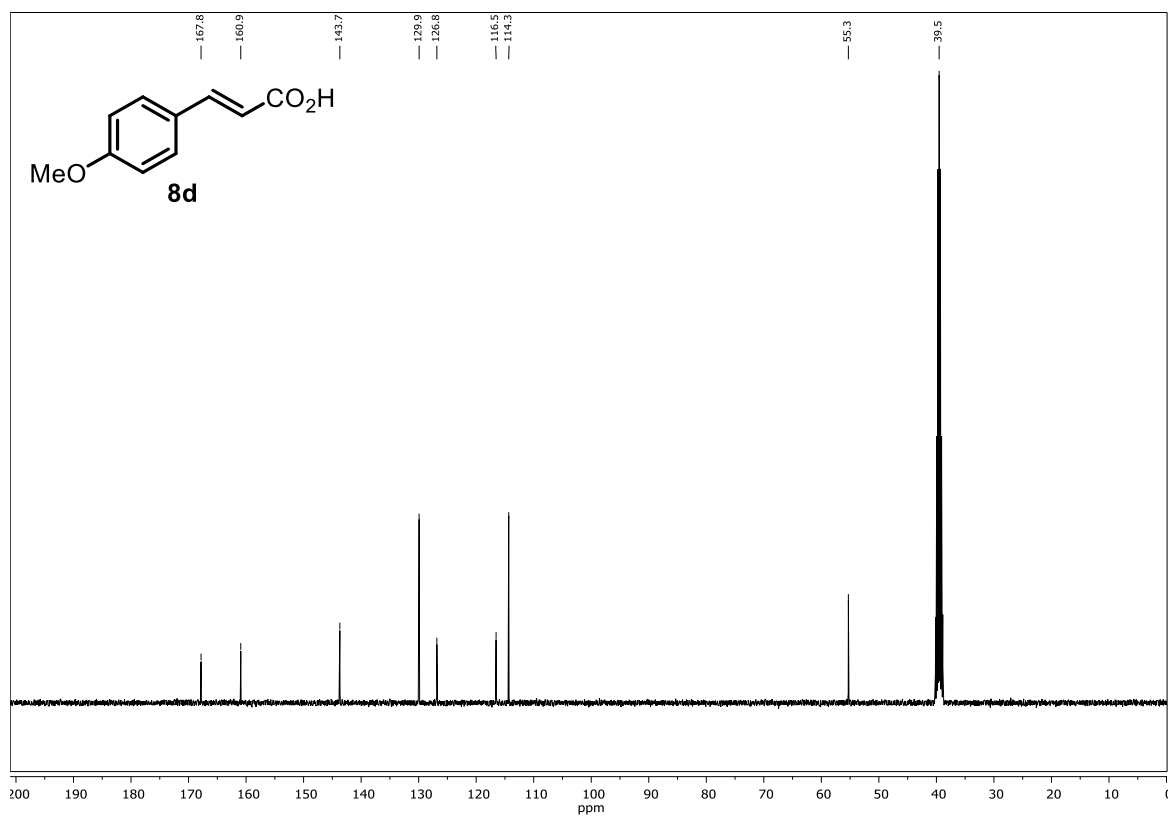
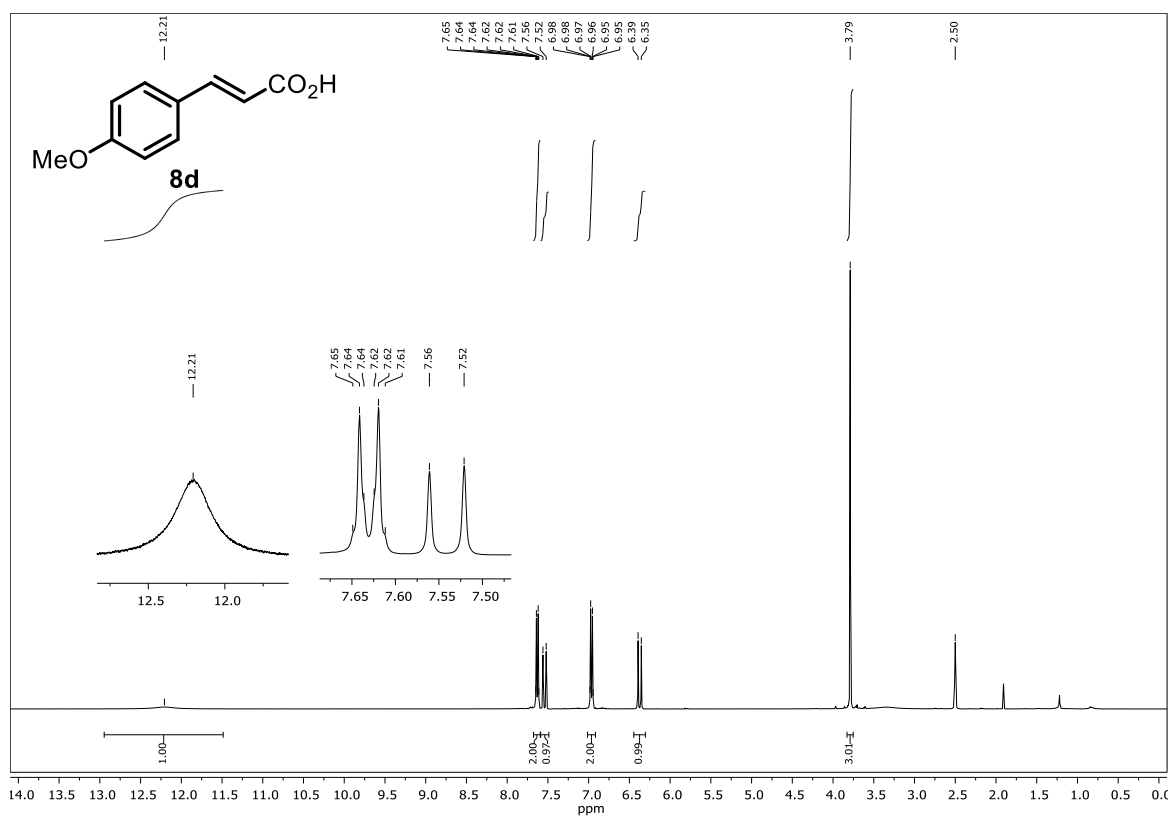


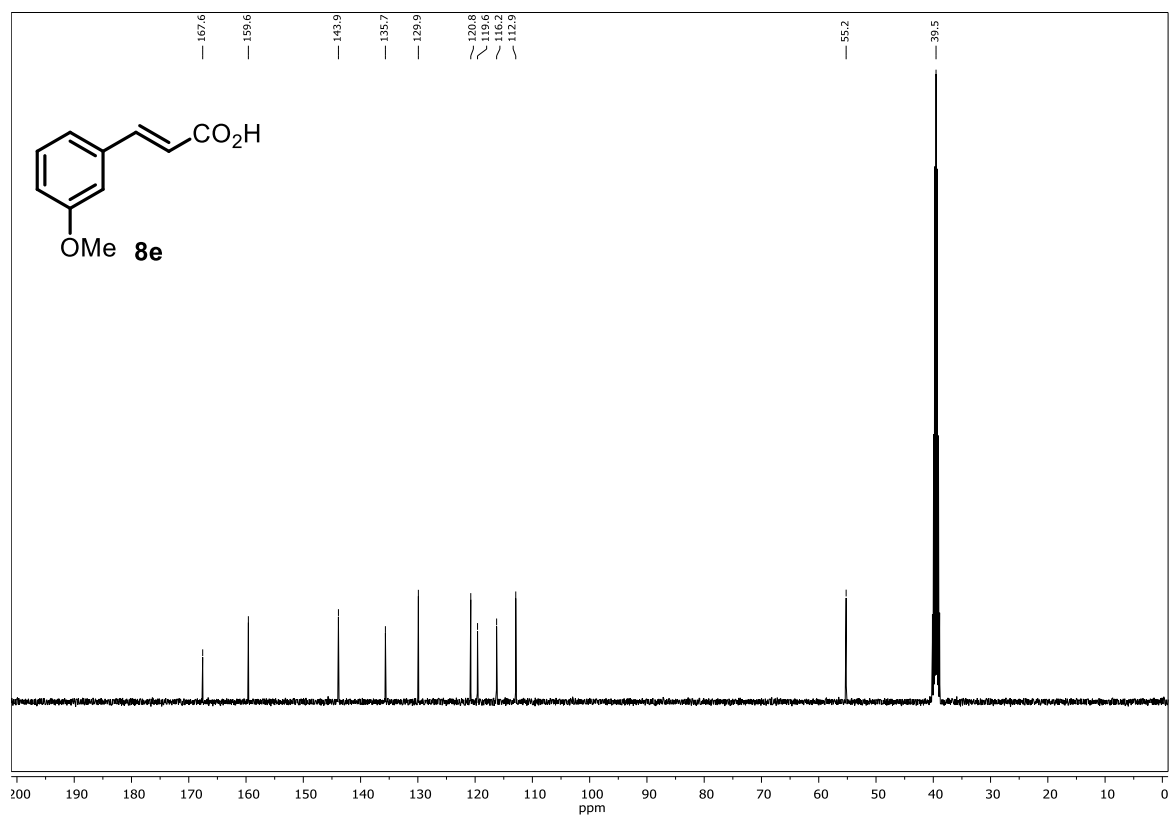
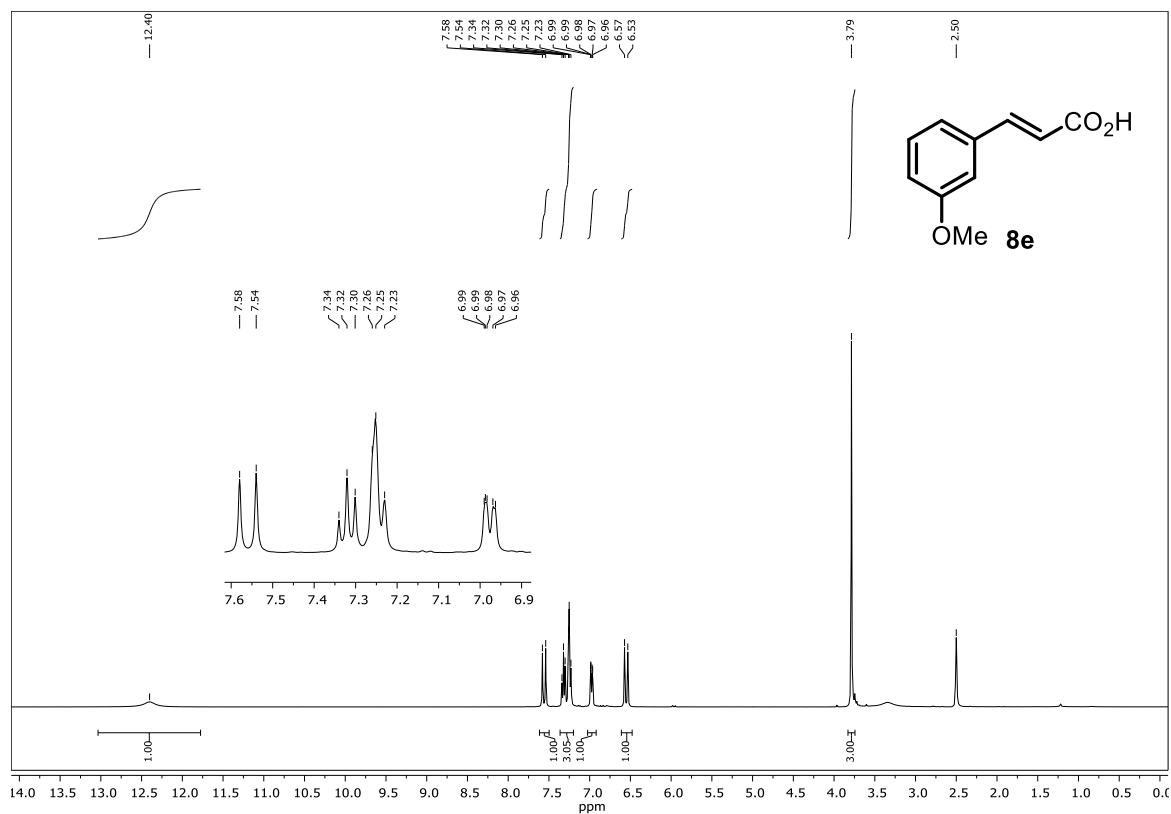


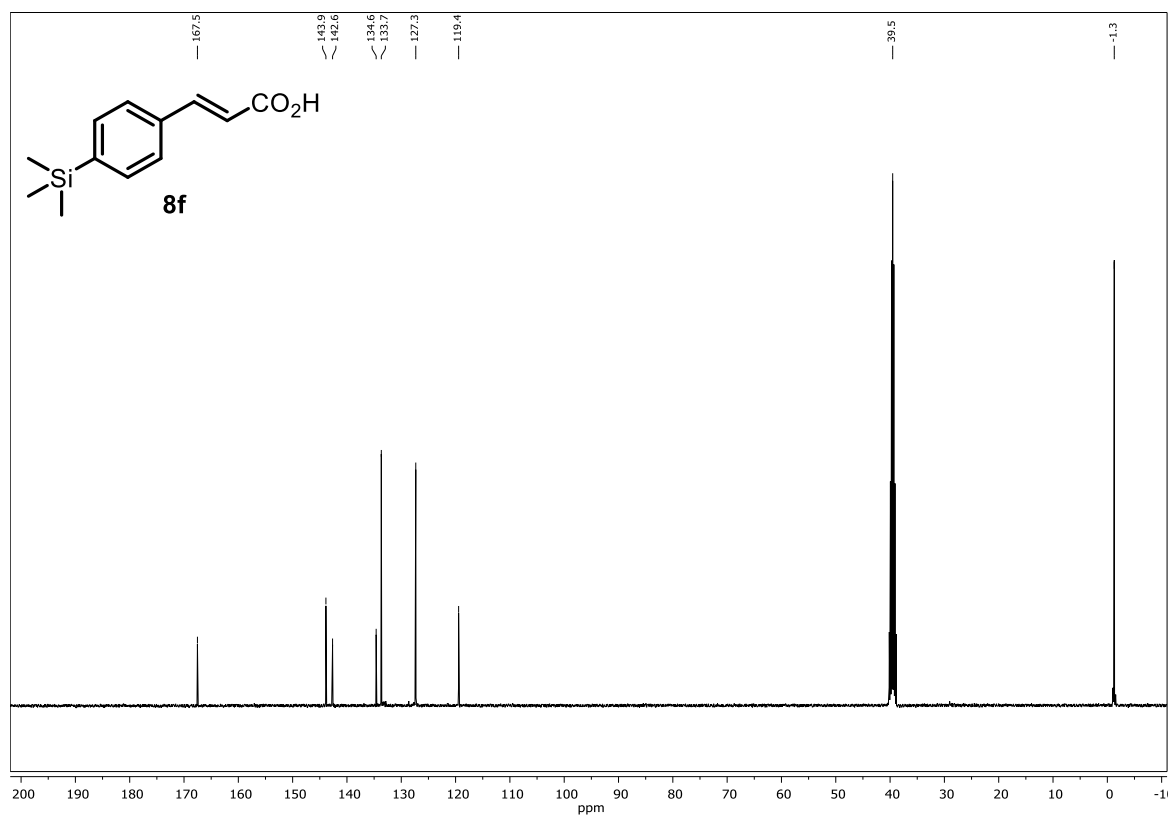
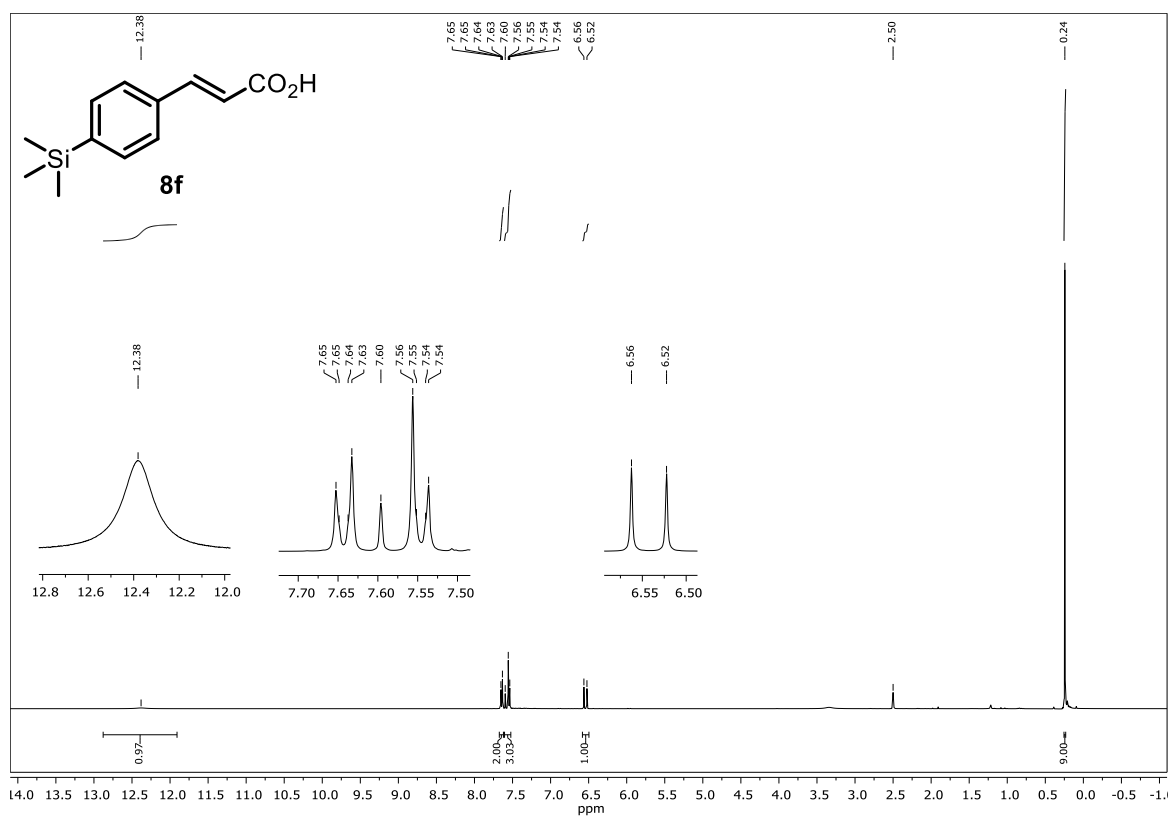


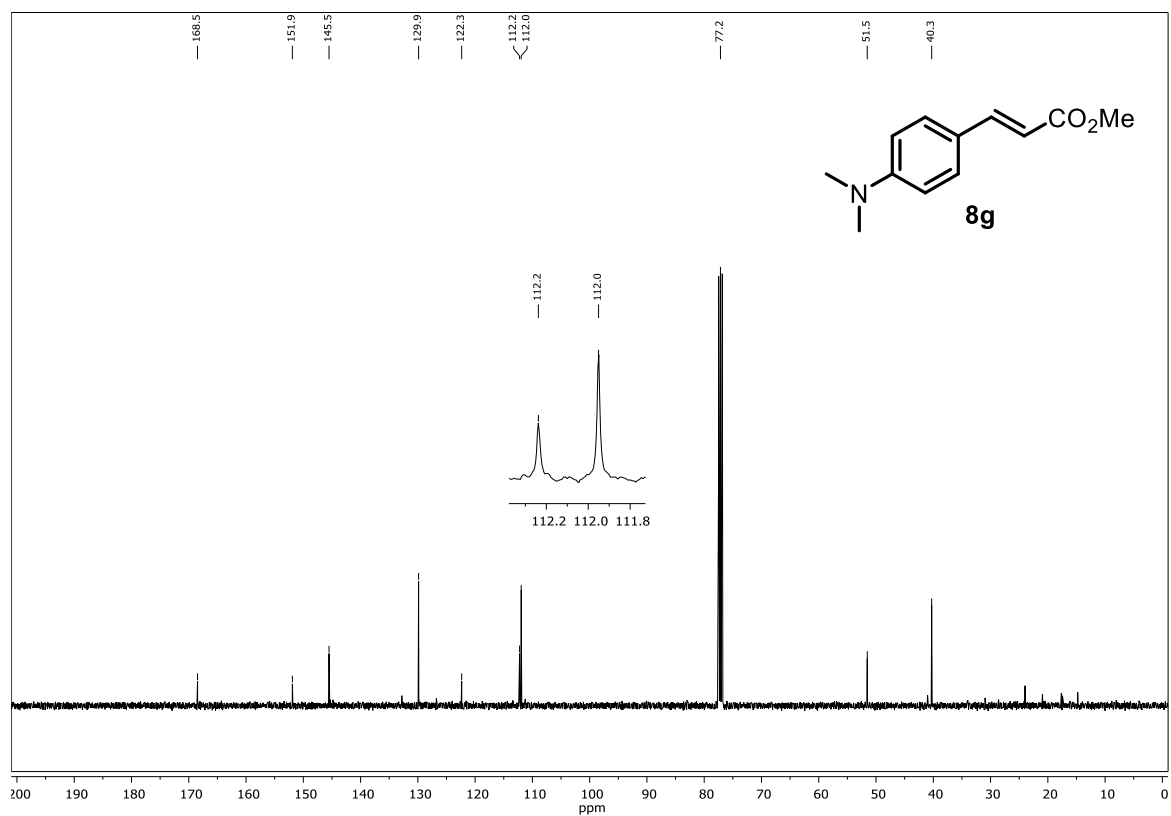
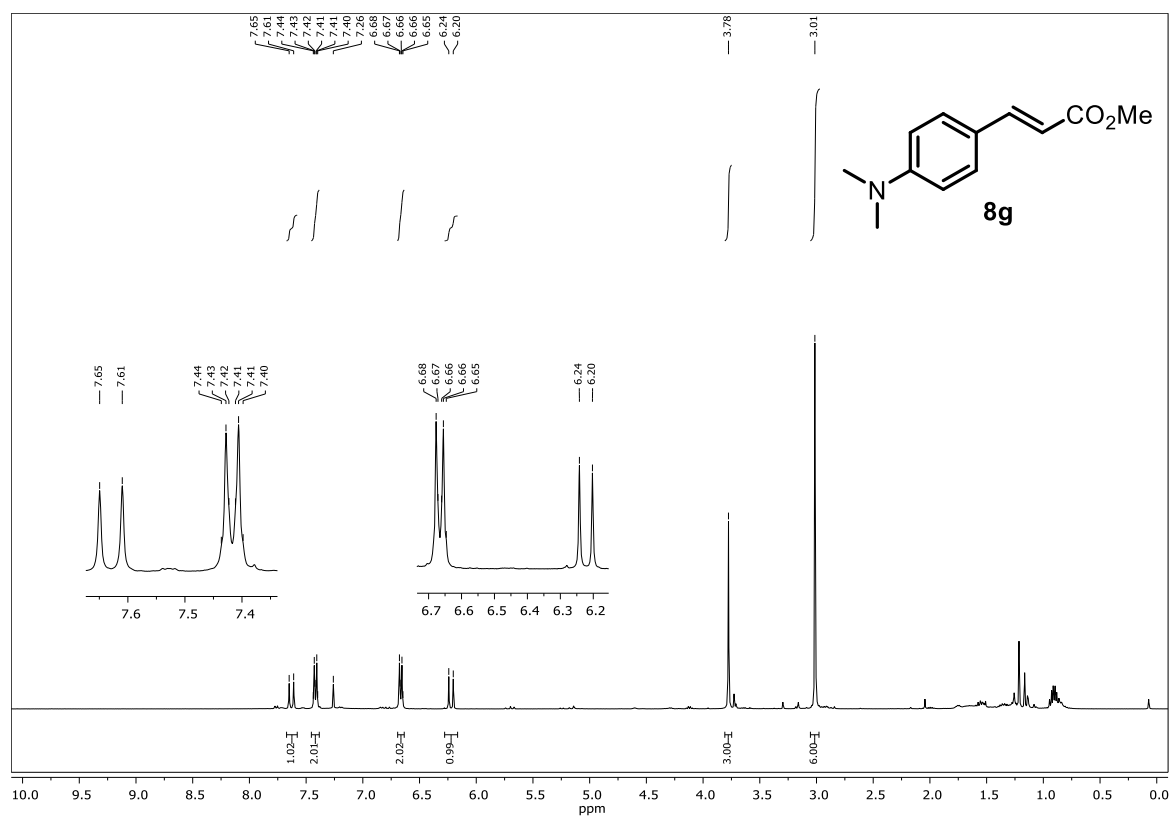


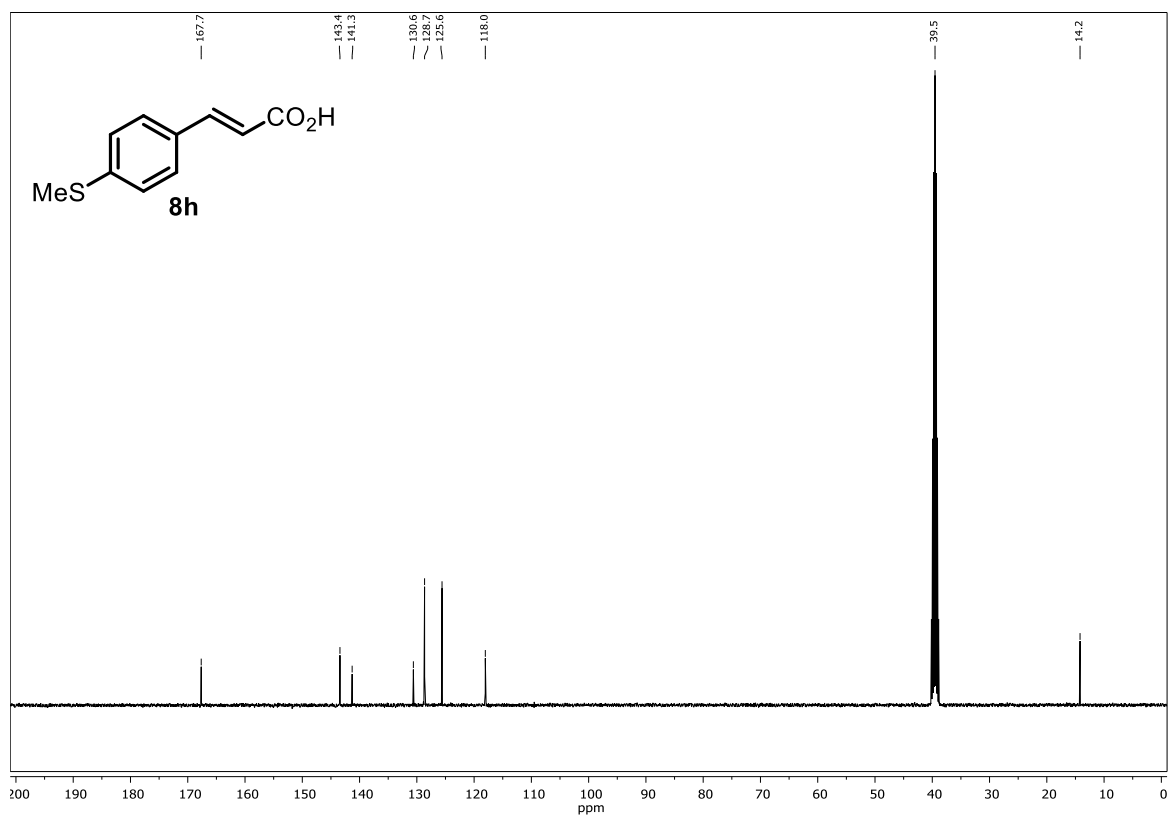
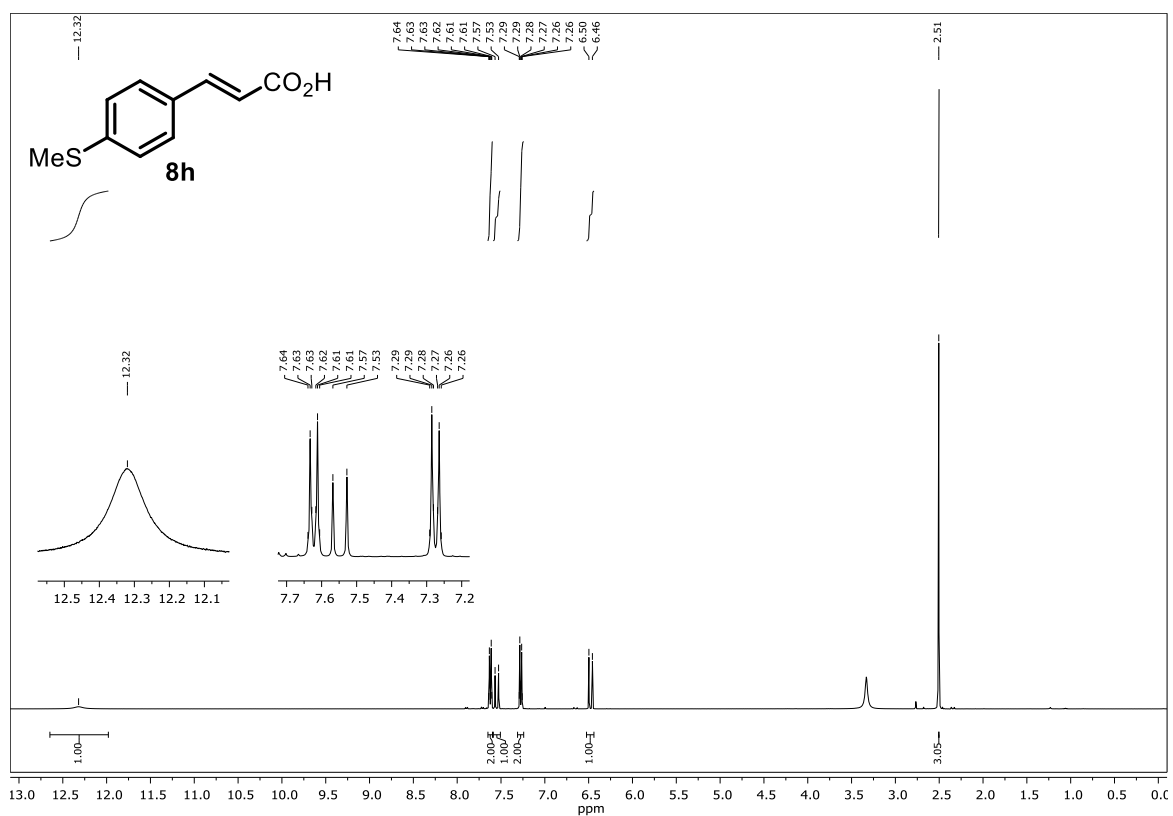


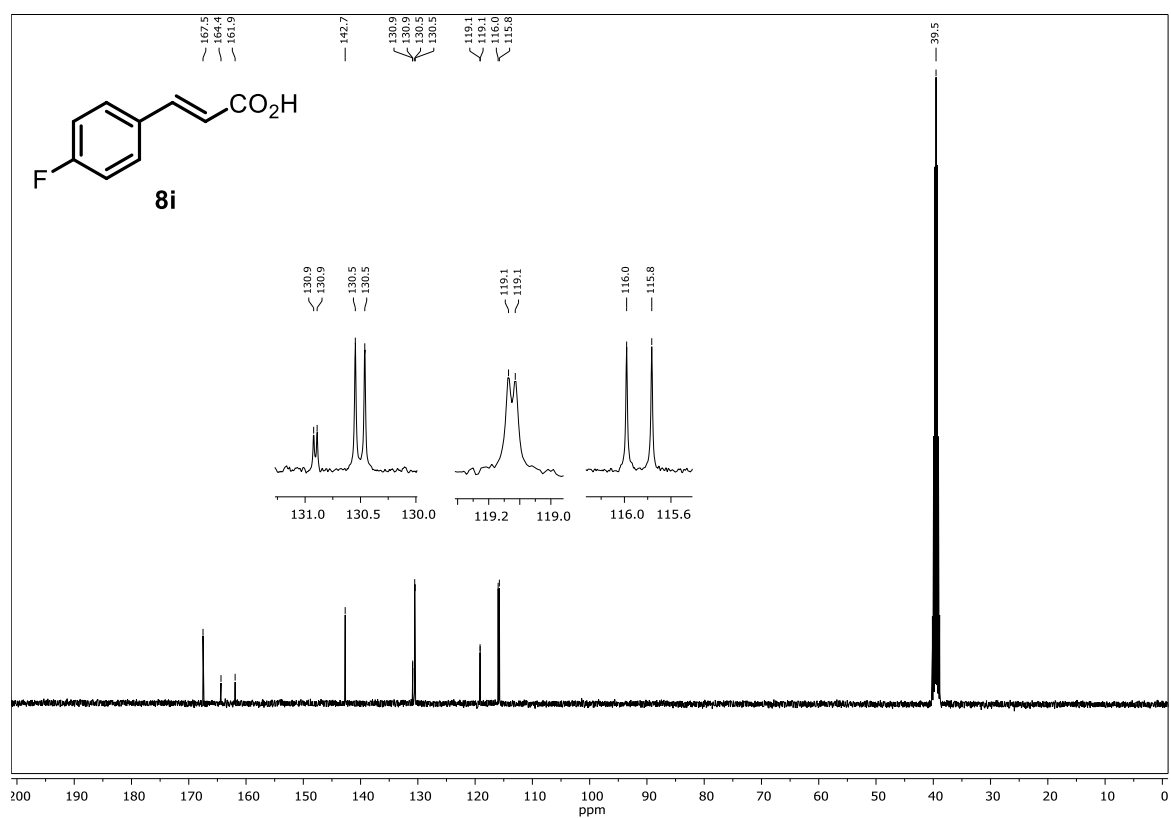
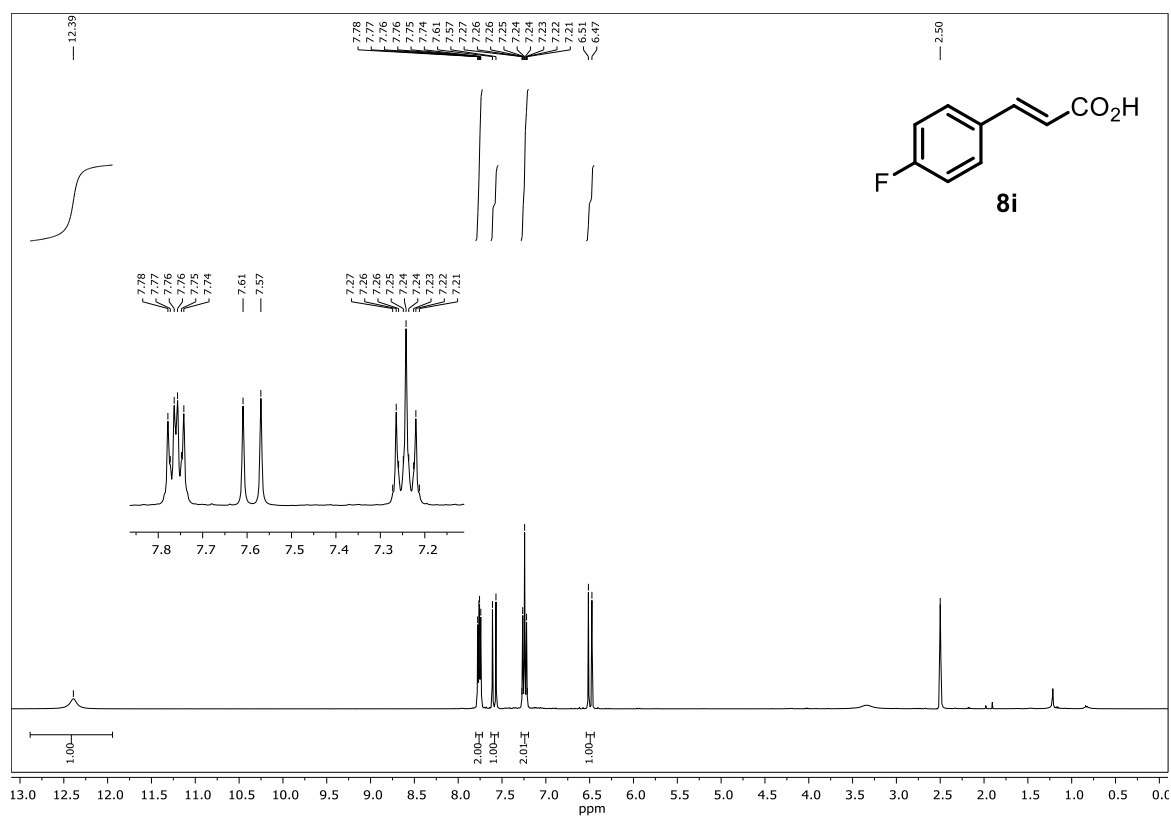


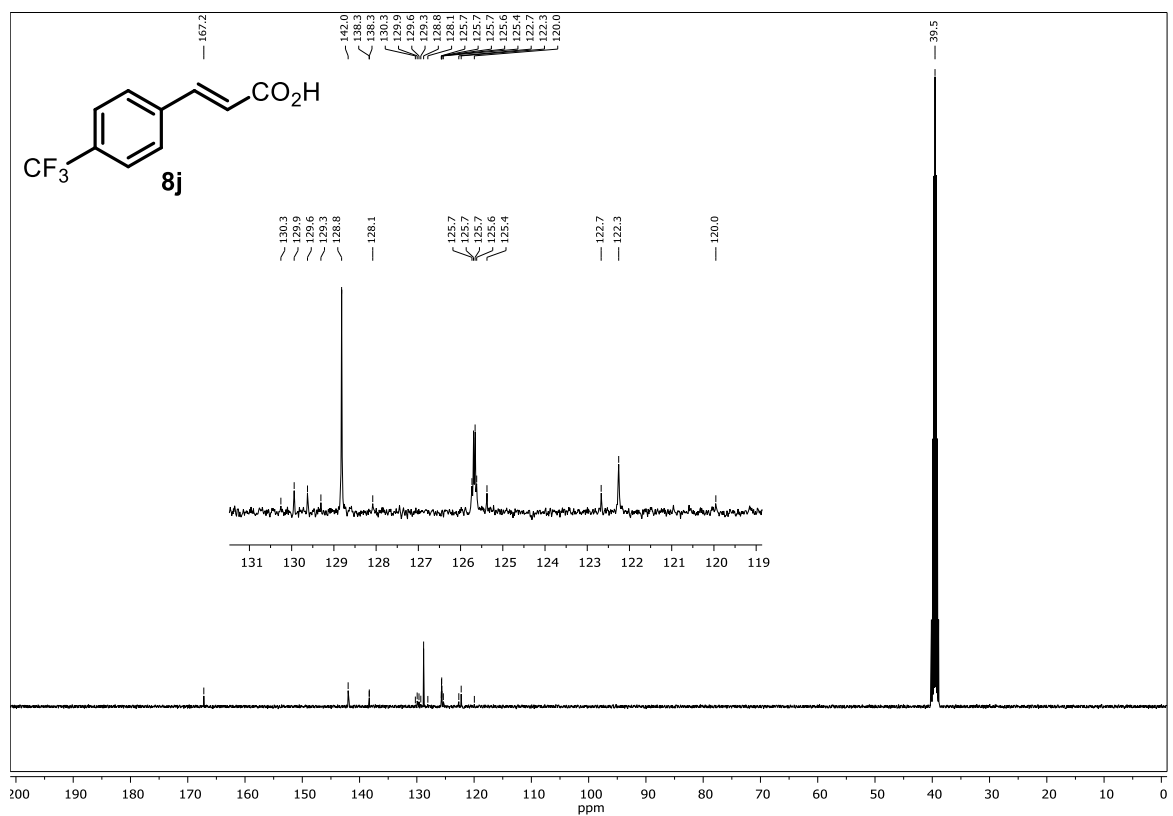
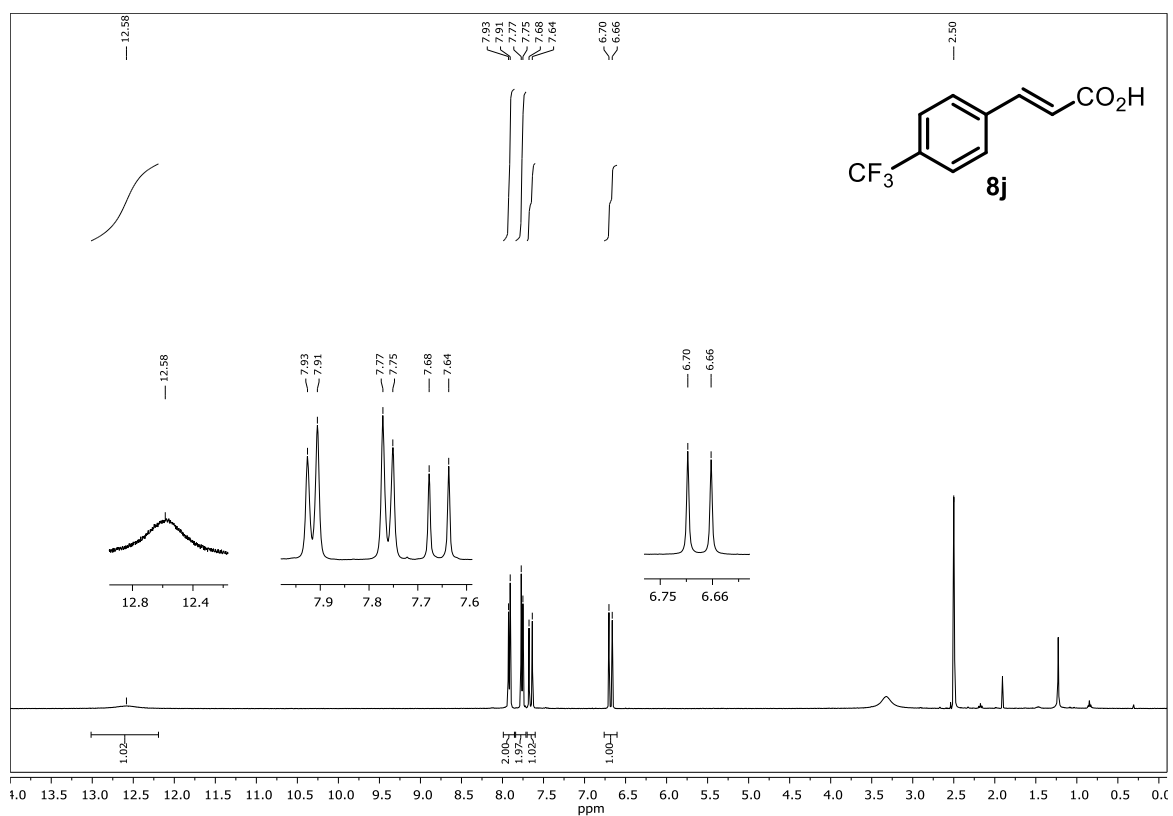


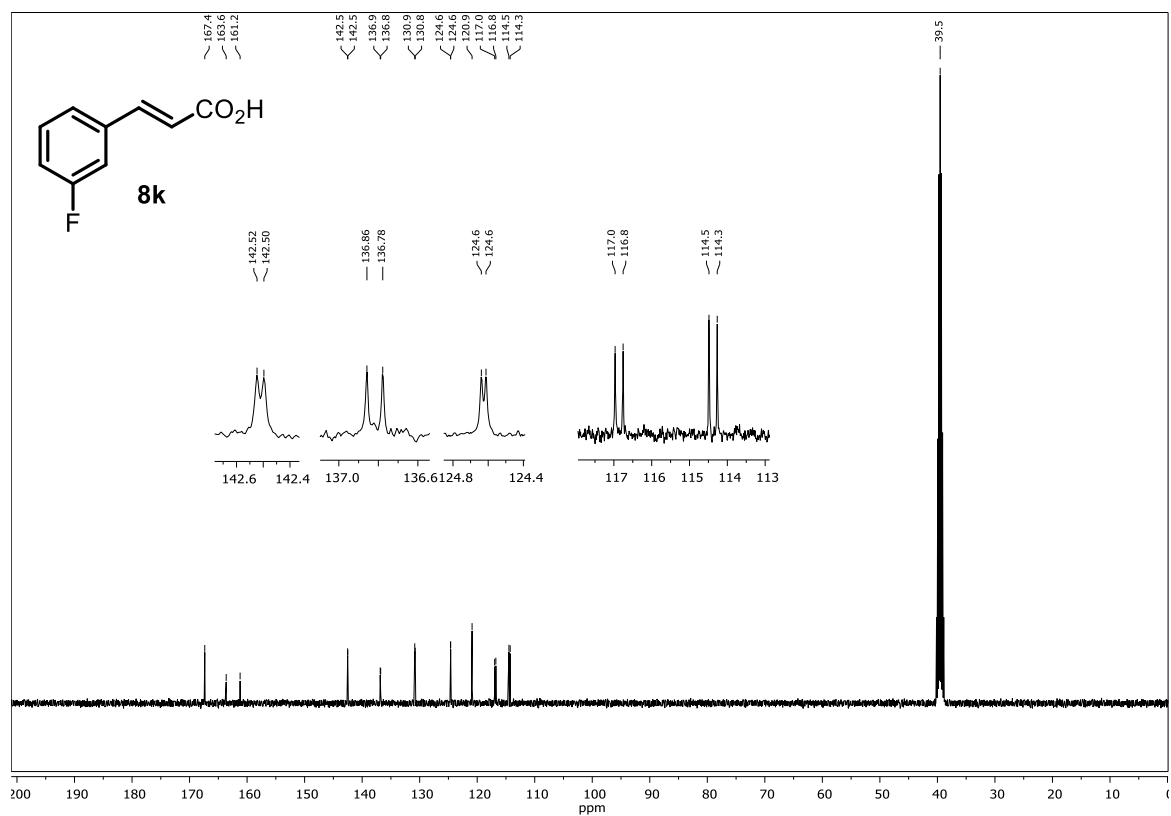
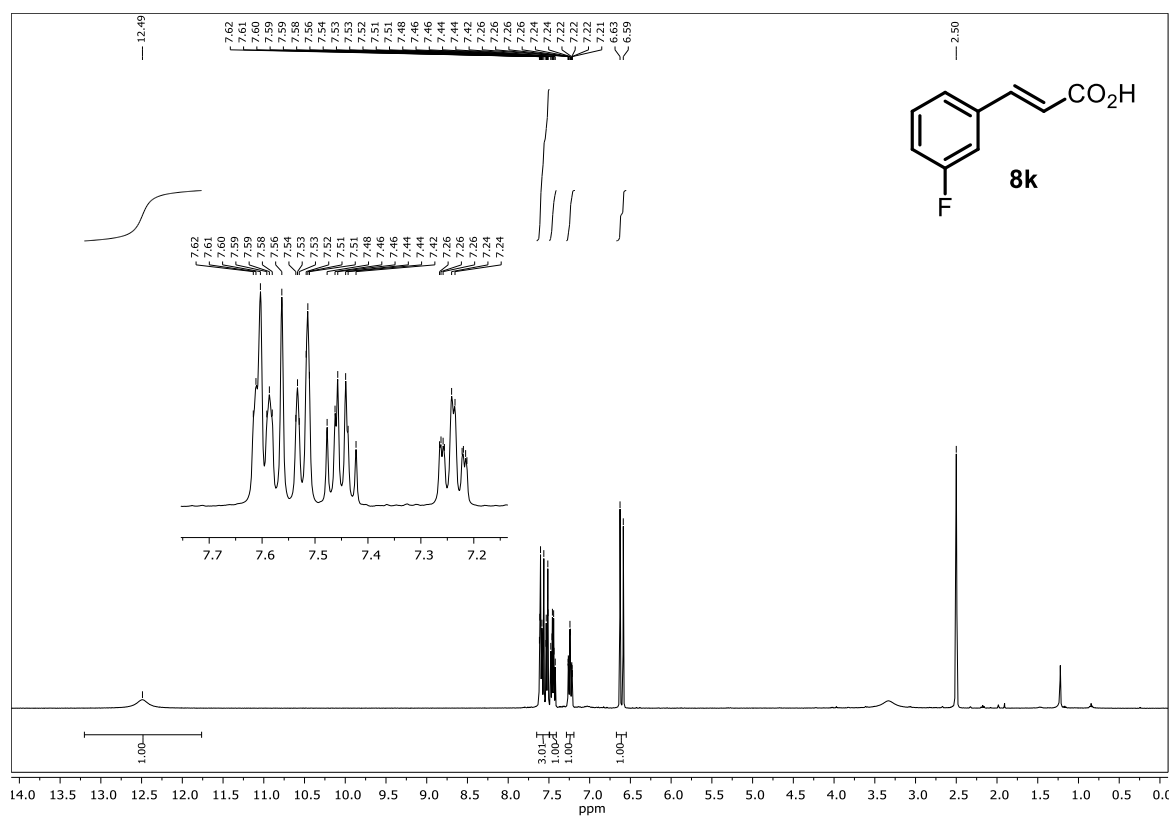


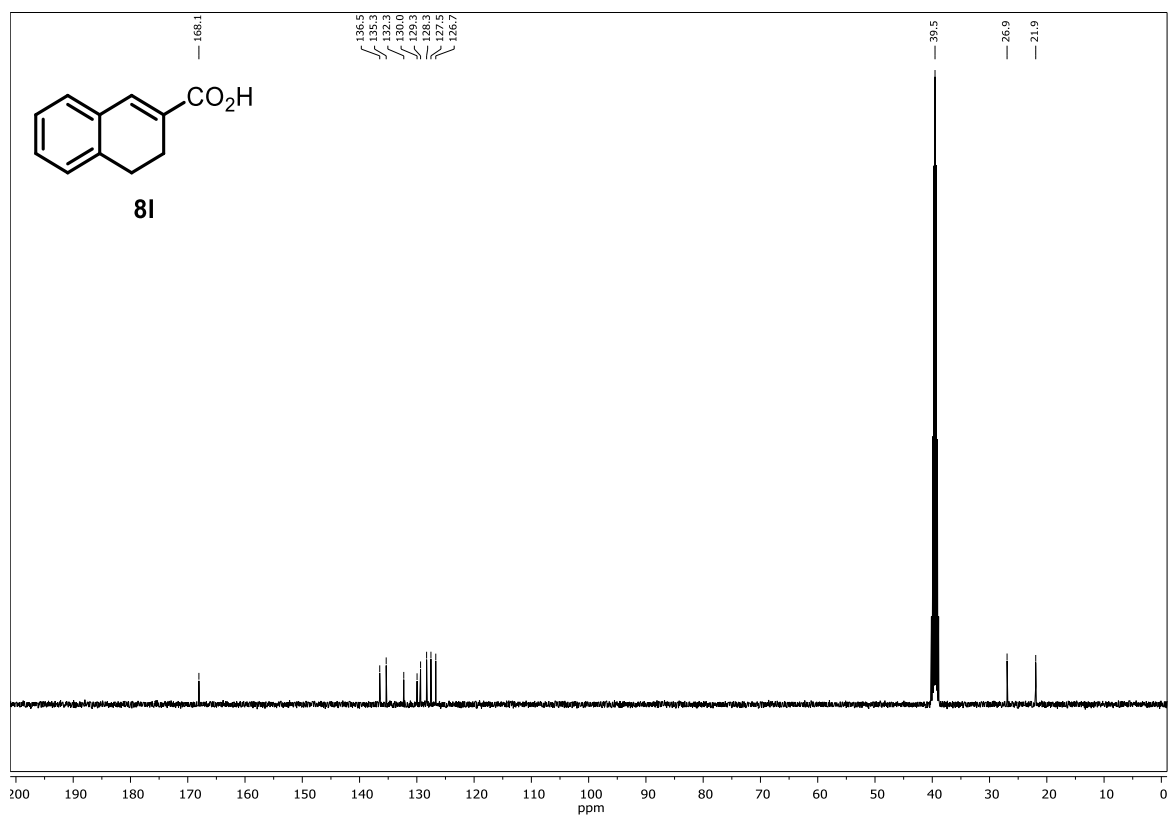
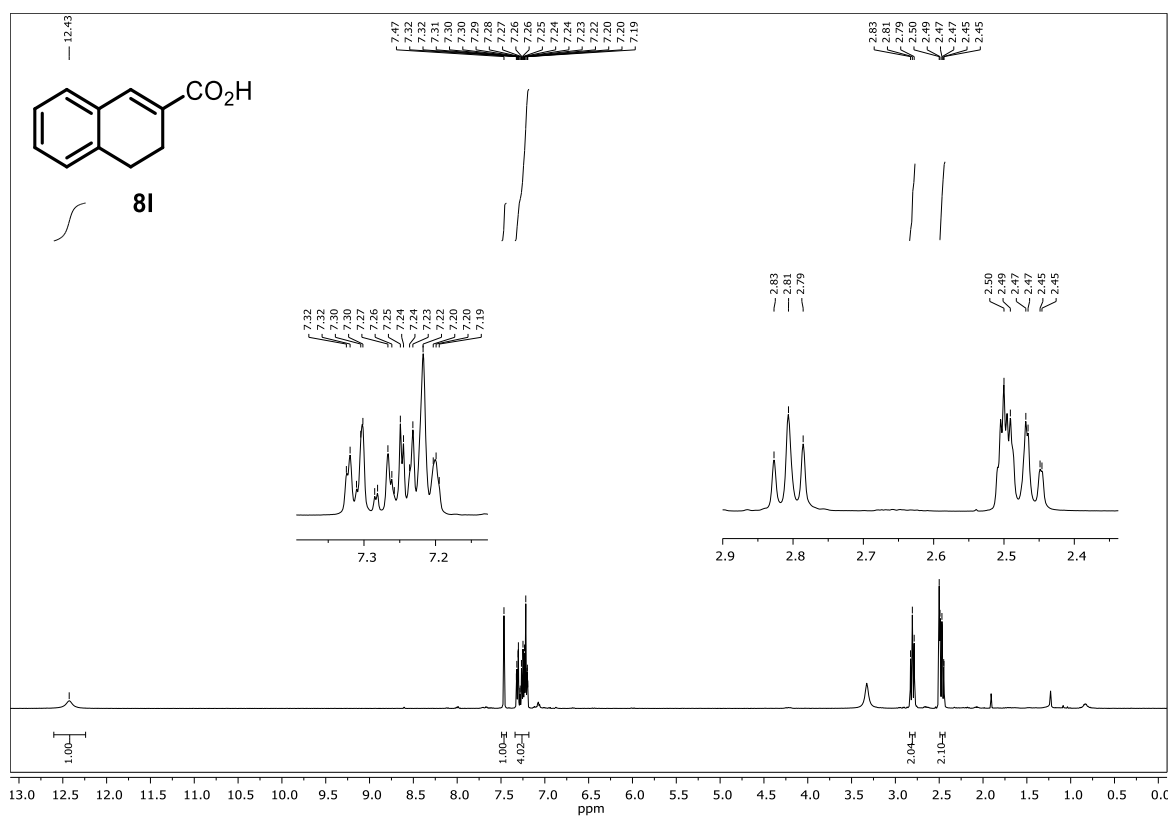


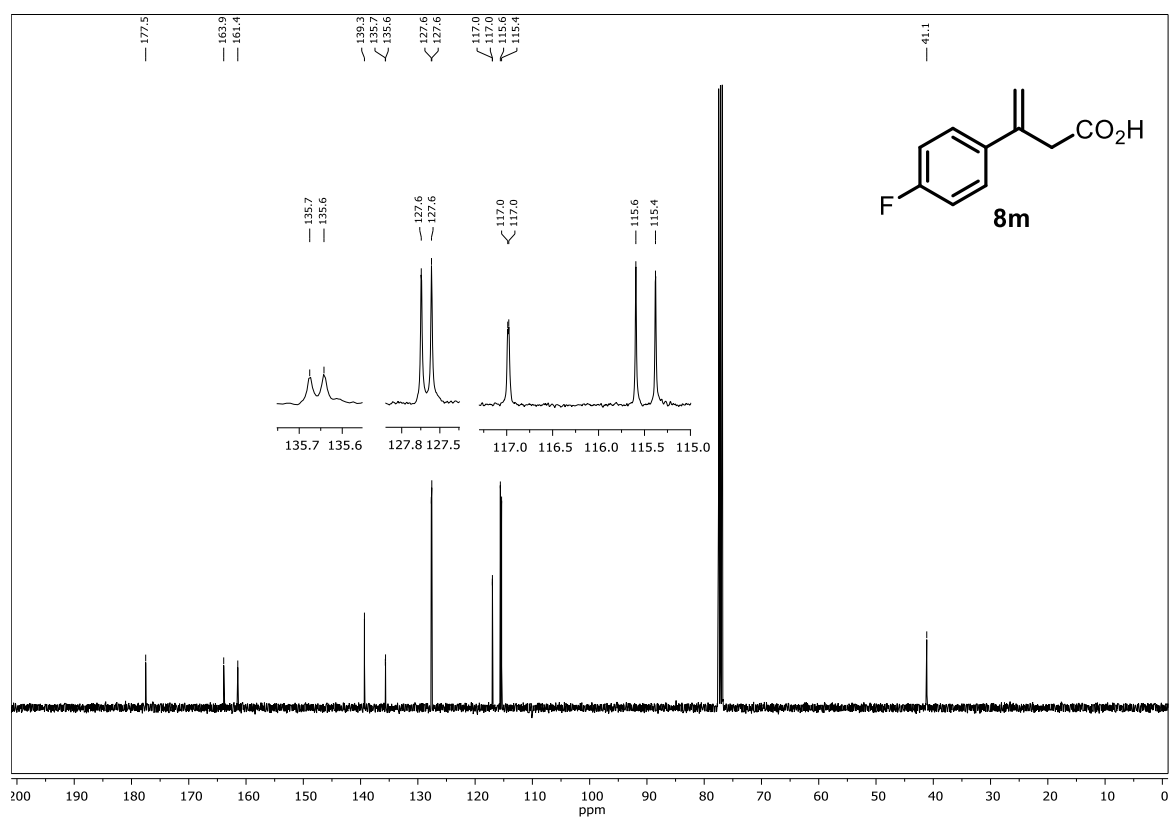
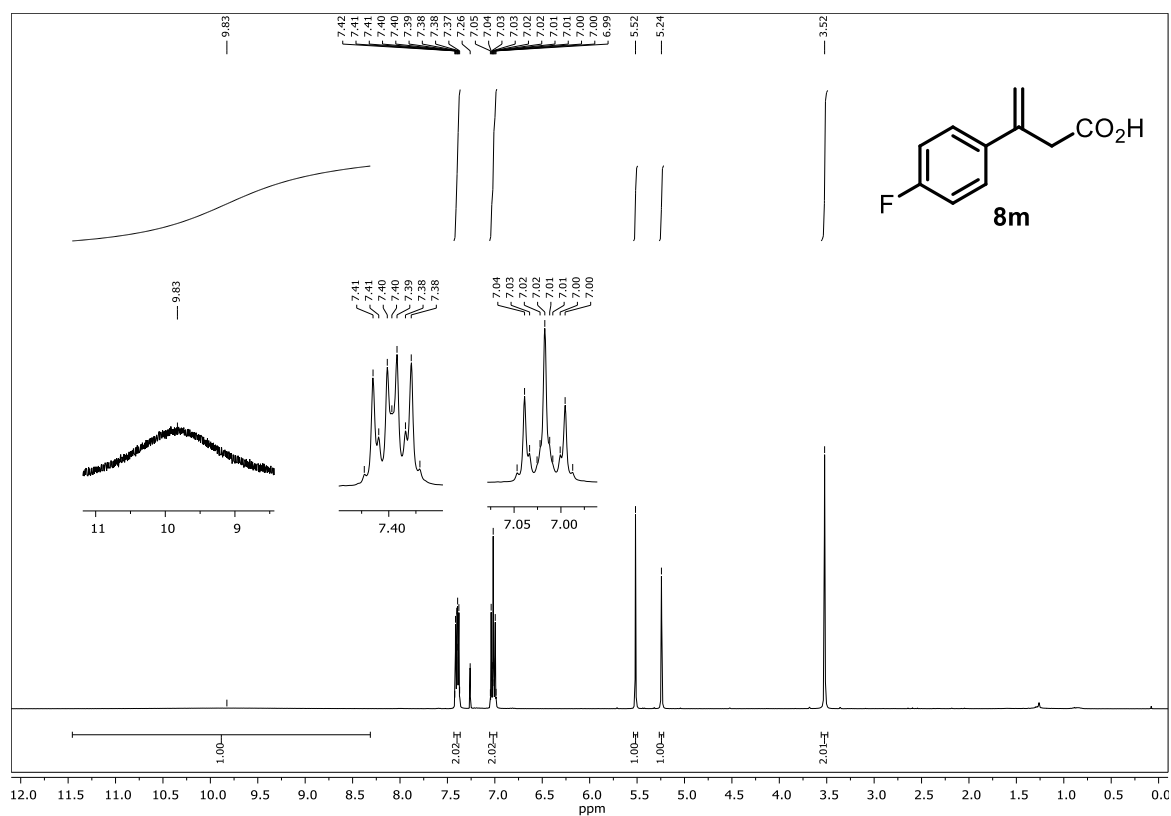


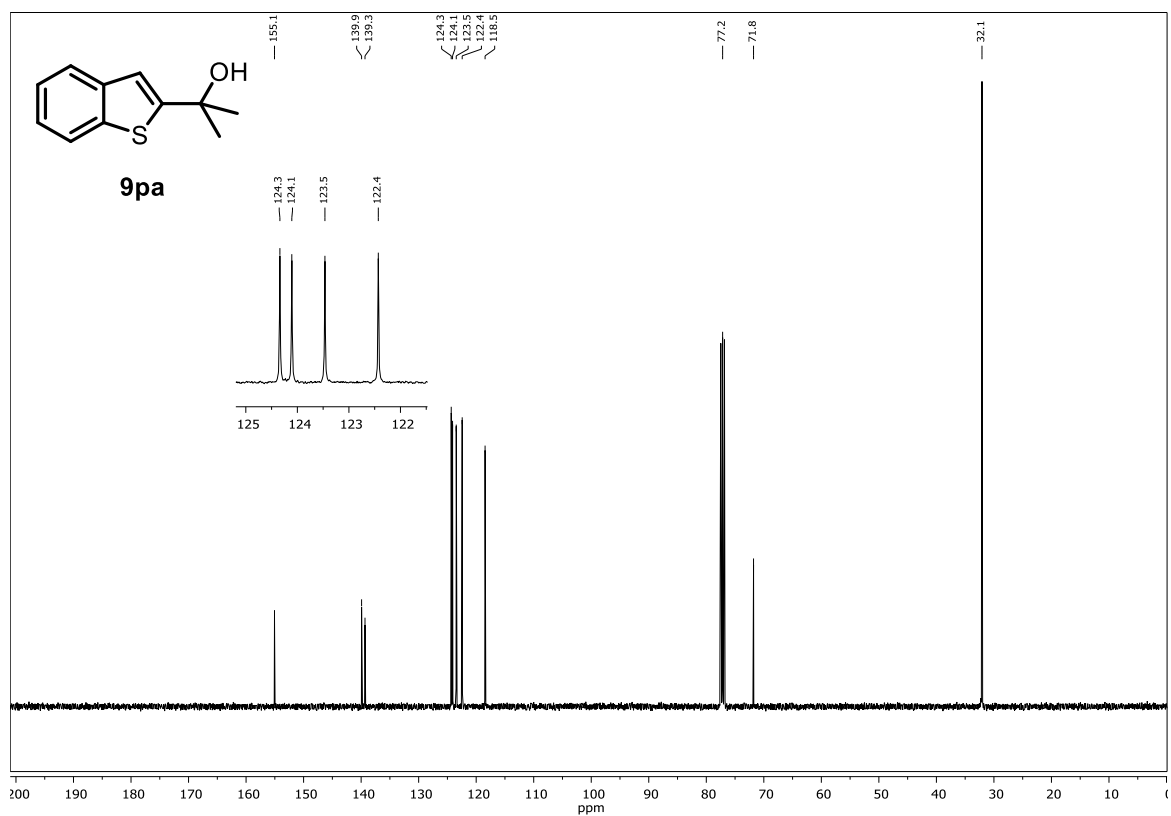
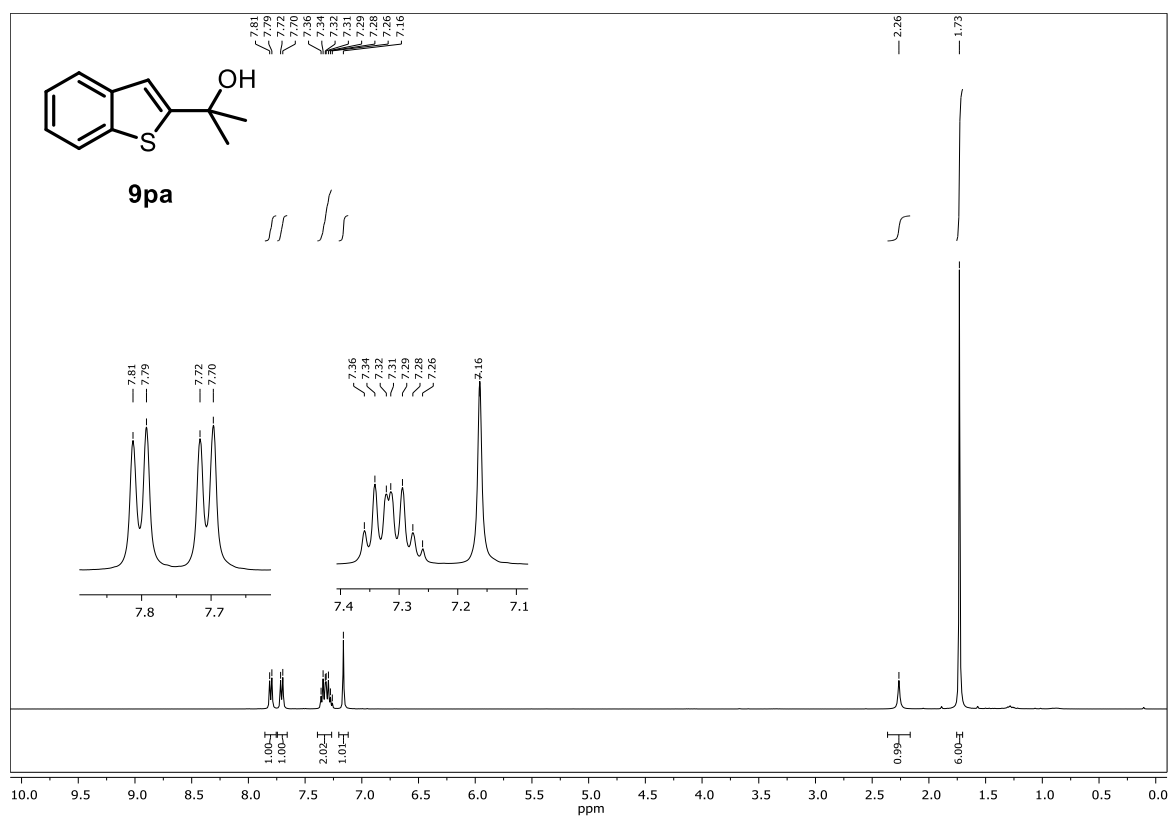




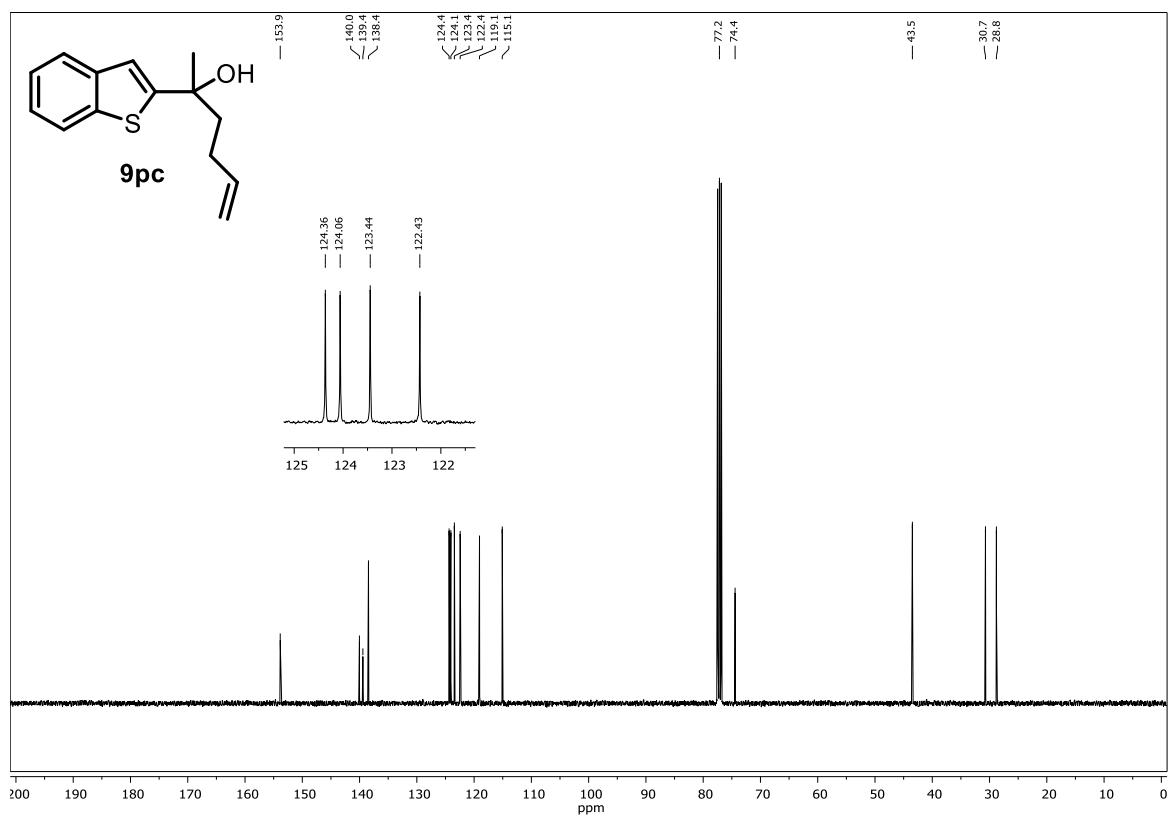
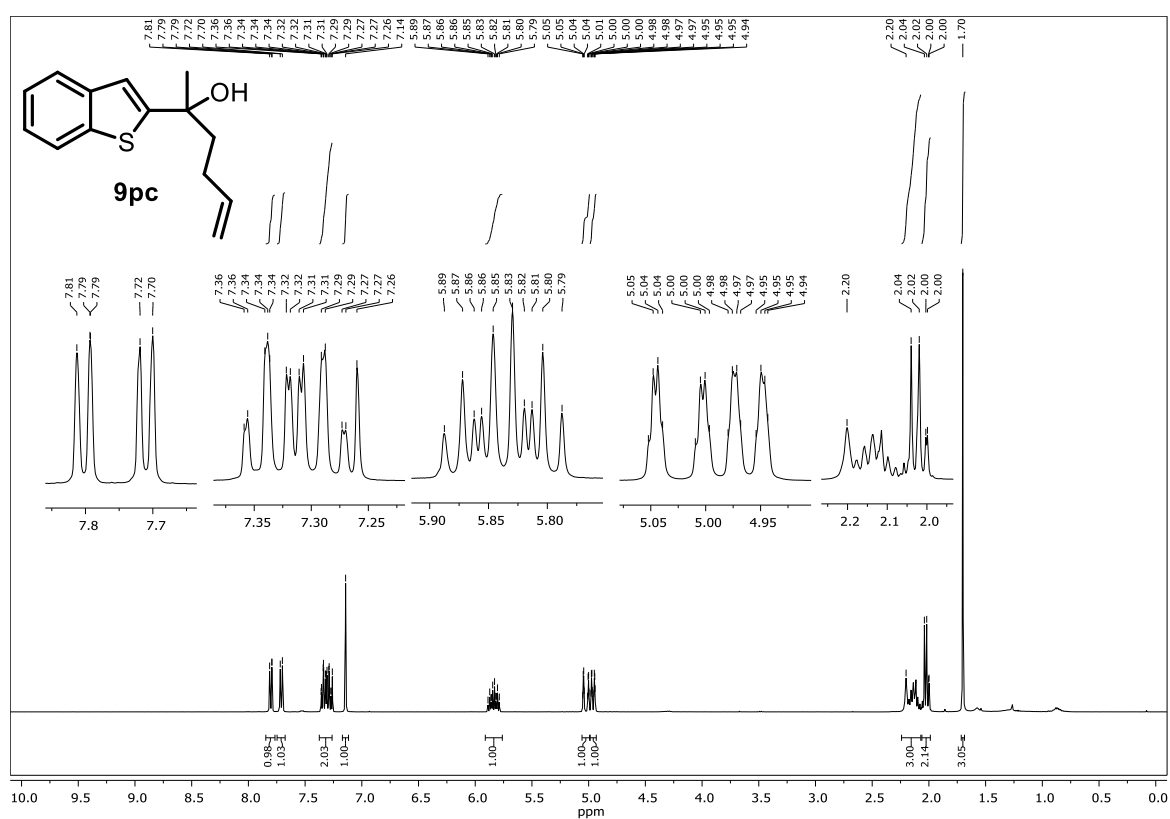












7.5 Curriculum Vitae

Personal Data

Name: Matthias Ludwig Schmalzbauer
 Date of birth: 05.06.1990
 Place of birth: Burglengenfeld
 Nationality: German

Education

11/2016 – 07/2020	Ph.D. in Organic Chemistry Institute of Organic Chemistry, University of Regensburg <i>“Photoinduced Electron Transfer Reactions of Organic Anions”</i> Supervisor: Prof. Dr. Burkhard König
10/2014 – 09/2016	Master of Science in Chemistry Institute of Organic Chemistry, University of Regensburg & Facultad de Ciencias Químicas, Universidad Nacional de Córdoba, Argentina Master thesis: <i>“Visible light mediated anthraquinone catalyzed inter- and intramolecular C-H arylation using aryl halides”</i> Supervisors: Prof. Dr. Burkhard König (Regensburg), Prof. Dr. Roberto A. Rossi (Córdoba)
10/2011 – 07/2014	Bachelor of Science in Chemistry Institute of Inorganic Chemistry, University of Regensburg Title of thesis: <i>“β-Prolin Derivate in der Organokatalyse”</i> Supervisor: Prof. Dr. Oliver Reiser
09/2009 – 06/2011	Allgemeine Hochschulreife (A-Levels) Berufliche Oberschule Regensburg
09/2006 – 02/2009	Apprenticeship as IT system electronics engineer
02/2009 – 08/2009	Employed as IT system administrator KRONES AG, Neutraubling

Memberships

11/2016 – present	Gesellschaft Deutscher Chemiker (GDCh, German Chemical Society)
11/2016 – 04/2019	DFG – Graduate Training Group GRK 1626 “Chemical Photocatalysis”

Conferences

07/2019	The 29th International Conference on Photochemistry Boulder, Colorado, USA (poster presentation)
03/2019	Artificial Photosynthesis Faraday Discussion Cambridge, United Kingdom (poster presentation)
09/2018	26. Lecture Conference on Photochemistry Garching/Munich, Germany (poster presentation)
06/2018	EuCHEMS conference on Organic Free Radicals (ECOFR 2018) Marseille, France (poster presentation)
09/2017	26th ISHC Congress (International Society of Heterocyclic Chemistry, Regensburg, Germany)
2016 – 2019	24th – 35th Seminar Days of the GRK 1626 oral contributions and poster presentations

Publications

- Matthias Schmalzbauer, Michela Marcon and Burkhard König, “Excited State Anions in Organic Transformations”, manuscript in preparation.
- Matthias Schmalzbauer, Thomas D. Svejstrup, Florian Fricke, Peter Brandt, Magnus J. Johansson, Giulia Bergonzini and Burkhard König, “Redox-neutral Photocatalytic C-H Carboxylation of Arenes and Styrenes with CO₂”, manuscript submitted.
- Matthias Schmalzbauer, Indrajit Ghosh and Burkhard König, “Utilising excited state organic anions for photoredox catalysis: activation of (hetero)aryl chlorides by visible light-absorbing 9-anthrolate anions”, *Faraday Discuss.* **2019**, 215, 364-378.
- Javier I. Bardagí, Indrajit Ghosh, Matthias Schmalzbauer, Tamal Ghosh and Burkhard König, “Anthraquinones as Photoredox Catalysts for the Reductive Activation of Aryl Halides”, *Eur. J. Org. Chem.* **2018**, 34-40.

DANKSAGUNG

8 Danksagung

Mein erster Dank gilt Prof. Dr. Burkhard König für das in mich gesetzte Vertrauen und die Möglichkeit, die vorliegende Arbeit unter seiner Aufsicht anfertigen zu dürfen. Des Weiteren bedanke ich mich für seine kontinuierliche Unterstützung in allen Belangen und die gegebenen Freiheiten um eigene Ideen verfolgen zu können. Die etlichen hilfreichen Diskussionen und Überlegungen haben wesentlich zum Erfolg der Arbeit beigetragen. Darüber hinaus möchte ich mich für die Gelegenheit bedanken, dass ich meine Arbeit auf verschiedenen Konferenzen präsentieren konnte.

Für die Übernahme des Zweitgutachtens danke ich Prof. Dr. Oliver Reiser. Weiterhin danke ich Prof. Dr. Patrick Nürnberger dafür, dass er als Drittprüfer eintritt. Prof. Dr. Joachim Wegener danke ich für die Übernahme des Prüfungsvorsitzenden.

Für die gute Zusammenarbeit, geprägt von zahlreichen Ideen und Ratschlägen sowie für das Korrekturlesen des Manuskripts zu Anthron-katalysierten Arylierungsreaktionen möchte ich mich bei Indrajit Ghosh bedanken. Darüber hinaus danke ich Javier Bardagi für seine Beiträge und die Koordination des Projekts zur lichtvermittelten Arylierung in Gegenwart von Anthrachinon. In diesem Zusammenhang gilt mein Dank auch Indrajit und Tamal Ghosh. Thomas Svejstrup, Peter Brandt und Giulia Bergonzini von unserem Kooperationspartner AstraZeneca danke ich für ihre Beiträge zur photokatalysierten C–H Carboxylierung. Ein großes Dankeschön geht an Michela Marcon für die Hilfe bei der Anfertigung des einleitenden Reviews zu angeregten Anionen in organischen Reaktionen.

Weiterhin bedanken möchte ich mich bei den festangestellten Mitarbeitern des AK Königs, Britta Badzura, Simone Strauß, Julia Zach und Dr. Petra Hilgers für ihre Hilfe bei Problemen aller Art. Mein besonderer Dank gilt Ernst Lautenschlager, der bei auftretenden technischen Schwierigkeiten immer mit Rat und Tat zur Seite stand, Regina Hoheisel für ihre große Sorgfalt und Geduld bei CV-Messungen und Dr. Rudolf Vasold für die GC/MS Messungen. Ganz herzlich bedanken möchte ich mich bei unserer ehemaligen Sekretärin Katharina Nickl für die große Hilfe bei bürokratischen Angelegenheiten.

Ebenfalls bedanken möchte ich mich bei meinen Forschungspraktikanten Marie-Sofie Dürr, Johannes Graumüller, Sascha Grotjahn und Andreas Ratzenböck sowie bei unserer Auszubildenden Selina Eichinger.

Bedanken möchte ich mich auch bei den Mitarbeitern der Zentralen Analytik und der NMR-Abteilung für den tollen Service und die schnelle Bearbeitung von Messaufträgen.

Für die Finanzierung von Teilen meiner Promotion, Konferenzbesuchen und Seminartagen danke ich dem „GRK 1626 Chemische Photokatalyse“.

Mein ganz besonderer Dank gilt meinen Laborkollegen Alexander, Anna, Karin und Karsten für die schöne Zeit, die wir gemeinsam verbringen durften. Vielen Dank für die stets lustigen Mittags- oder Kaffeepausen, die freundschaftliche Atmosphäre und eure Unterstützung in allen Belangen.

Bei allen ehemaligen Weggefährten und aktuellen Mitgliedern des AK König möchte ich mich für die Hilfsbereitschaft untereinander und die immer gute Stimmung im Team bedanken. Für die vielen geselligen Runden beim Grillen oder Grölen, beim Weißwurstfrühstück oder bei bayerischer Brotzeit, an der Uni oder in der großen weiten Welt möchte ich mich vor allem bei Ali, Alex, Andi, Anna, Daniel, Javier, Johanna, Karin, K-Boi, Ranit, Rok, Tobi und Uli bedanken.

Bei Thomas Weinbender, der mir vom ersten Tag des Studiums an zur Seite stand, möchte ich mich ganz besonders für die Freundschaft bedanken. Für die schöne gemeinsame Zeit möchte ich mich auch bei meinen ehemaligen Kommilitonen Lukas, Kauze, Nele, Verena und Weini bedanken.

Weiterhin möchte ich mich bei meinen Freunden Christian, Sebastian und Julian, bei Jana & Sebastian, bei Doris & Christian, der ganzen Schwallhalla- und TeamTurban-Truppe und bei allen Spillers, Röschs, Preßls und Schiekofers für die schönen geselligen Stunden bedanken, in denen ich immer viel Kraft tanken konnte.

Zu Guter Letzt danke ich von ganzem Herzen meiner lieben Maria, meinen Eltern Regina und Reinhard, meiner Schwester Maria mit Robert und meinen Brüdern Michael und Martin mit Xenia und Emma. Ohne eure großartige Hilfe und euren unermüdlichen Zuspruch wäre ich nicht so weit gekommen.

Danke

Eidesstattliche Erklärung

- (1) Ich erkläre hiermit an Eides statt, dass ich die vorliegende Arbeit ohne unzulässige Hilfe Dritter und ohne Benutzung anderer als der angegebenen Hilfsmittel angefertigt habe; die aus anderen Quellen direkt oder indirekt übernommenen Daten und Konzepte sind unter Angabe des Literaturzitats gekennzeichnet.
- (2) Bei der Auswahl und Auswertung folgenden Materials haben mir die nachstehend aufgeführten Personen in der jeweils beschriebenen Weise unentgeltlich geholfen:
 1. Das Manuskript zu Kapitel 1 wurde in Zusammenarbeit mit Michela Marcon verfasst.
 2. Gekennzeichnete Experimente und die Ausformulierung des Manuskripts zu Kapitel 2 wurden von Javier I. Bardagí und Indrajit Ghosh durchgeführt.
 3. Gekennzeichnete Experimente in Kapitel 3 wurden von Thomas D. Svejstrup und Florian Fricke durchgeführt.
- (3) Weitere Personen waren an der inhaltlich-materiellen Herstellung der vorliegenden Arbeit nicht beteiligt. Insbesondere habe ich hierfür nicht die entgeltliche Hilfe eines Promotionsberaters oder anderer Personen in Anspruch genommen. Niemand hat von mir weder unmittelbar noch mittelbar geldwerte Leistungen für Arbeiten erhalten, die im Zusammenhang mit dem Inhalt der vorgelegten Dissertation stehen.
- (4) Die Arbeit wurde bisher weder im In- noch im Ausland in gleicher oder ähnlicher Form einer anderen Prüfungsbehörde vorgelegt.

Regensburg, 23.06.2020